

# **EUROTHERM SEMINAR #116**

## **Innovative solutions for thermal energy storage deployment**

**24-26 May 2023**  
**University of Lleida**  
**Lleida, Spain**



© Edicions i Publicacions de la Universitat de Lleida, 2023  
© Eurotherm Seminar #116 Innovative solutions for thermal energy storage deployment  
© of the text: authors of each contribution  
© of images, tables and figures: authors of each contribution

ISBN 978-84-9144-439-8  
DOI 10.21001/eurotherm.seminar.116.2023

## Preface

It was a pleasure for Prof. Luisa F. Cabeza and the GREiA research group full team at the University of Lleida (Spain) to organize the ***Eurotherm Seminar #116 “Innovative solutions for thermal energy storage deployment”*** from May 24th to 26th, 2023, in Lleida (Spain).

This seminar did bring together researchers and practitioners from academia and industry, who are working in the rapidly expanding field of thermal energy storage (TES).

The most recent trends in such areas as novel storage materials, advanced storage concepts and configurations, TES for renewable energy systems, TES in buildings and industry, use of advanced techniques such as artificial intelligence in TES, and social, environmental, and educational aspects.

Theoretical, numerical, and experimental approaches will be presented for the entire range of applications, from material characterization to complete storage systems.

We want to thank all participants to the conference.





## **Committees**

### **Conference chairs**

- Prof. Luisa F. Cabeza, University of Lleida, Spain
- Prof. Gennady Ziskind, Ben-Gurion University of the Negev, Israel
- Prof. Michel de Paepe, Ghent University, Belgium

### **Organizing committee**

GREiA research group at University of Lleida (Spain)

- Prof. Luisa F. Cabeza
- Dr. Gabriel Zsembinszki
- Dr. Emiliano Borri
- Dr. David Vérez
- Rodrigo Martinez
- Edgar Rojas
- Nadiya Mehraj
- Alessandro Ribezzo
- Omais Rehman
- Pablo Tagle



## Sponsors

We would like to thank very warmly the contribution from the sponsors to the conference:

**ANALISIS-DSC**  
DYNAMIC & SECURITY COMPUTATIONS



**ЯPOW**

**:KREUM**

Sorption  
Technologies



**atlas**  
energia

**TES**  
THERMAL ENERGY STORAGE

**energianufri**

**Enginyers**  
Industrials de Catalunya  
Demarcació de Lleida

**PLUS<sup>®</sup>**  
TECHNOLOGY FOR  
A BETTER WORLD



**E3G** ENGINYERIA  
I ENERGIA

**CIMENTS**  
**MOLINS**  
INDUSTRIAL

**VEOLIA**

# THANK YOU VERY MUCH

## Keynote speakers

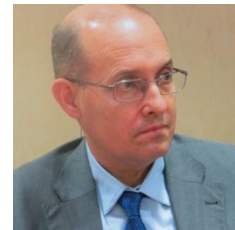
**Dr. Antonio Marco Pantaleo** - EIC Programme Manager for energy systems and green technologies

He has twenty years of experience in multidisciplinary research on renewable and clean energy technologies (solar, wind, biomass, and hybrid), energy systems integration, biosystems engineering, energy use in agricultural sector and food processing. He holds a first degree in electric engineering from Politecnico of Bari and a PhD in process systems engineering from Imperial College London, where he is affiliated as research fellow to the Clean Energy Processes Lab (CEP) and Centre for Process Systems Engineering (CPSE) of the Department of Chemical Engineering. He is an associate professor of clean energy technologies at the Department of Agro-environmental Sciences of the University of Bari. Before becoming professor, he co-founded an energy service company, joined Edison Energie Speciali and the strategic planning division of GSE (Gestore dei Servizi Energetici). He also worked as scientific expert and consultant for public and private organisations, including the Italian Ministry of Research, and was vice-Rector for energy policy of University of Bari. Marco authored over hundred scientific papers, and he is member of IEA working group on energy storage, ASME technical committee on clean fuels, and is delegate for energy at the Italian Sustainable Universities Network. At the European Innovation Council, he is responsible for the Pathfinder Challenges portfolio on Green Hydrogen generation (2021), mid to long duration energy storage (2022), CO<sub>2</sub> and Nitrogen management and valorisation (2022), clean cooling technologies (2023); for the transition challenge on systems integrated energy systems (2021), energy storage (2022); and for the accelerator challenge on Green Deal (2022), Fit for 55% (2022) and energy storage (2023).



**Dr. Julian Blanco** – Director of CIEMAT – Plataforma Solar de Almeria

Dr. Julian Blanco (Industrial Engineer by Seville Univ., 1985 and PhD by the Univ. of Almeria, 2003) has more than 30 years of experience having worked at different sectors. He works at the PSA since 1990 and he has been involved in 26 EU and 18 National R&D+i projects (respectively coordinating 7 and 3) related to the development of solar energy and water-related technologies (public calls). Previous professional positions included: Associate Director of PSA; Head of Research Unit (Envir. Appl. of Solar Energy) of CIEMAT; Operating Agent of the Int. Energy Agency SolarPACES Program – Task VI (Solar Energy & Water Processes and Applications), Spanish alternate member of Executive Committee of IEASolarPACES Program, and coordinator of Joint Program on CSP of the European Energy Research Alliance (EERA). Author of 1 book and co-author of 10 books as well as 24 chapters in others. He has also co-authored more than 90 publications in indexed international journals, more than 60 articles in technical journals, more than 250 contributions to more than 200 different International Congress and Symposia and 5 patents. Honorary/guest editor of Books/Journals/Conference Proceedings 5 times, giving more than 80 invited talks (around 20 keynotes) and participating in more than 50 international courses. He has directed 2 PhD Thesis. Among other appointments, he has been visiting Professor at King Saud University (Riyadh, Saudi Arabia). Member of international Steering Committee of Solar Energy Research Center (SERC), Chile; the Academic Committee of the “Instituto de Investigación e Ingeniería Ambiental” (3iA); Univ. Nacional de San Martín (Argentina); and the International Committee to the Scientific Audit Panel of the Mexican program “Sea and brackish water desalination with renewable energies” (Mexico). In addition to Spain he has developed projects and professional activities in 32 additional world countries.



**Dr. Harald Mehling** – Consultant (R&D), Thermal Energy Storage and Thermal Analysis

Dr. Harald Mehling started working on energy related R&D in 1994 with his diploma thesis on radiative heat transfer, then worked additionally on heat transport and storage in materials for his PhD thesis. Afterwards, in 1999, he focussed on heat storage with Phase Change Materials (PCM), from material development and characterization to applications, working as group leader and later as senior scientist at the ZAE Bayern. Since 2013 he works as consultant on Thermal Energy Storage, with focus on PCM. In parallel to consulting companies and R&D institutions, he works as author and sometimes as lecturer. As a physicist, his expertise starts with basic material properties, and from his work at the ZAE Bayern then extended to material characterization, material development, design and testing of heat storages, and their integration into systems. His experience covers a wide range of applications, and includes also quality control as consultant for the RAL Quality Association PCM. Dr. Harald Mehling is author of more than 100 publications. Widely known is “Heat and Cold Storage with PCM – An up-to-date introduction into basics and applications”, together with Prof. L.F. Cabeza. His latest books are focussed on energy related education, published in 2016 “Technologies of energy conversion, storage, and transport in the energy system – A brief introduction”, and then in 2018 «Understanding the basics of energy – An introduction from simple to complex situations».

**Dr. Gennady Ziskind** – Department of Mechanical Engineering, Ben-Gurion University of the Negev, Beer-Sheva, Israel

Dr. Gennady Ziskind is Anne Tanenbaum Professor in Engineering Thermodynamics and Head of Department of Mechanical Engineering at Ben-Gurion University of the Negev (BGU) in Beer-Sheva, Israel. He earned his M.Sc. and D.Sc. degrees from the Faculty of Mechanical Engineering at the Technion–Israel Institute of Technology, in the field of aerosol mechanics. His present activities deal with various aspects of heat and mass transfer and multiphase systems, including solid-liquid phase-change, latent heat energy storage and thermal management. His work presents a unique combination of original theoretical and numerical modeling with inventive experimentation. His research has been sponsored by the European Union, DARPA, Israeli Ministry of Energy, Israeli Ministry of Science, ONR, Israeli Atomic Energy Agency, CEA, Israeli Innovation Authority, Pazy Foundation, BIRD, BSF and various industries. Dr. Ziskind has co-authored more than 80 journal articles and more than 100 conference papers. His recent publications include a book, Phase-Change Materials for Thermal Management of Electronic Components, published by World Scientific Publishers in 2019, as a volume in the Encyclopedia of Thermal Packaging. Dr. Ziskind is a frequent invited speaker on thermal energy storage at important professional events, including 16th International Heat Transfer Conference (Beijing, 2018), 7th Swiss Symposium on Thermal Energy Storage (Lucerne, 2020) and 5th Thermal and Fluids Engineering Conference (New Orleans, 2021). Among other international activities, Dr. Ziskind has served as Associate Editor of Journal of Heat Transfer (ASME, two terms 2015-2021, awarded “Special Recognition for Exemplary Service”) and Associate Editor of International Journal of Thermal Sciences (Elsevier, since 2019). He is Delegate to the Assembly of International Heat Transfer Conferences, Member of the ASME Safety Standards Committee for Thermal Energy Storage (TES) Systems, and an active participant of several European research frameworks, including INPATH-TES. Dr. Ziskind co-chaired Eurotherm Seminars 99 (2014) and 112 (2019) in Spain, both entitled Advances in Thermal Energy Storage, and organized INNOSTORAGE–Advances in Thermal Energy Storage International Conference in Israel in 2016.

## Abstracts

The extended abstract of all the contributions that participated in the project, either in oral or poster form, are included next.



CAMPUS CAPFONT, UNIVERSITAT DE LLEIDA



EUROTHERM2023-1105

## Contribution of thermal storage to the energy efficiency of the building

Lluís Grau i Molist

Liberal Architect. Camí Ral 45-47 Bx 2<sup>a</sup>, 08393 Caldes d'Estrac Spain. Phone: 34-629722641, e-mail: lgm@coac.net

### Abstract

When climate change begins showing the characteristics of the future climate and in a complex climate environment throughout the year, the use of thermal storage in buildings, separate from specifically electrical storage, is inevitable in the general energy efficiency strategies for buildings with a positive energy balance. Along with other more general provisions (orientation, compactness, ...) thermal storage in certain strategic elements, both in the positive and negative sense of the term, is one of the passive systems that can most contribute to energy savings and make sufficient, together with very efficient active systems, the available renewable inputs (solar, for example) that would otherwise be insufficient. The aim is to highlight the interest in an economic thermal accumulation, adapted to short-cycle (daily or weekly) renewable energy replacements and for any type and use of the building.

**Keywords:** thermal mass, renewable energy replenishment, short cycle, density, specific heat, conductivity

### 1. Introduction

Legend has it that, in the last third of the 20th century, when an architect from Barcelona who was building a new central building with the main facade oriented to the South, almost exactly, with a glass curtain wall, he was asked if he was aware that he was making a real oven. He answered yes because the increase in the useful area represented by going from a conventional facade to a curtain wall not only compensated for the extra cost that this entailed with respect to the conventional solution but also the energy expenditure that it entailed during the useful life of the building.

Beyond whether the story is true or not, it exemplifies what the traditional arguments have been to justify the big decisions when designing a building. The economic argument that here covers the main concepts of the economic balance of the building (construction cost, efficient ratio between useful surface / built surface and cost of maintaining comfort conditions) is what, definitively, makes a good solution novel from which part of the problems it will entail is explicitly ignored just because there is an economic compensation. The environmental argument simply did not exist, nor did the one derived from the interior conditions of comfort and health (asymmetrical radiation, anomalous stratification of temperatures, annoying air renewal, excessive glare, etc.).

Today we cannot ignore the arguments historically ignored or avoid the fulfilment of the economic argument and, in this context, thermal storage has an important role to play in meeting the requirements of all of them.

The final objective of the proposal is the achievement of the building with a positive energy balance and, to achieve this, the combination of reducing energy demand by passive measures, the use of highly efficient active systems and the production own renewable energy.

In many places with a temperate climate, the average outdoor temperature condition is comfortable. It may be too hot during the day or too cold at night but is nevertheless more comfortable on average. There are also temporary heat loads resulting from high occupancy or strong solar radiation that may quickly raise the indoor temperature. If heat gains are accumulated when present and restituted when

needed, the energy used for heating or cooling could be largely reduced or even not needed. Thermal inertia is an efficient and passive way to take this task.

## 2. Materials and method

Conceptually, accumulation is the only technique that allows us to efficiently take advantage of the available renewable energies defined by low powers at the local level and their temporal discontinuity both in the short cycle -hourly/daily- and in the long -seasonal- of the 'solar energy, night cooling, etc... or more random ones like wind power. It allows us to adjust the energy capture/shine cycle to needs regardless of local energy availability and its cycles. In our case, the formats of the elements with which we want to work allow us to deal with guarantees from hourly to weekly cycles [1] compared to other modalities of a larger scale or with larger devices that allow us to deal with longer cycles.

It is intended to mark the position of thermal storage in the reduction of thermal demand and with the efficient benefit of renewable ports in a climate that allows renewable port in relatively short cycles. In general terms, the main strategy will be, in the first place, to discriminate between thermal uses and specifically electrical ones, each with its specific accumulation system. In particular, the thermal storage elements will be conventional constructive components of the building (structural elements, interiors full of exteriors, interior distribution elements, etc.) that do not generate economic costs or involve a loss of useful surface of the building building, its solids and that exchange heat, essentially, by radiation and convection. Therefore, other systems are considered which, being able to be more efficient (water tanks, stone beds, materials that change state, etc.), imply an alteration, in many aspects, of the work and are not easy to install nowadays.

We take it for granted that the most general overall characteristics such as the orientation, compactness or the number, format and location of the facade openings, ...which begin to regulate the thermal flows between the interior and the exterior already foresee that will work with thermal accumulation.

The concept of thermal accumulation is closely linked to that of internal thermal mass with sufficient inertia as the main passive system which, by itself:

- reduces the indoor temperature fluctuations caused by outdoor climate variations and indoor peak loads, for power calculation purposes, allow the use of average temperatures instead of absolute maximum or minimum temperatures
- is essential to passive air conditioning in summer (especially by having, partially, in the enclosures) and, in winter, take advantage of the passive contributions (solar, internal gains,...)
- distribute -or take away- the heat through the radiation system working with large radiant surfaces (floors, ceilings, etc.)
- allow its energy activation/accumulation/transfer with the cadence that interests you according to calculation and
- facilitate the adaptation of the building's operation, for summer comfort
- 
- All of the above will not be possible without thermal insulation placed, systematically, on the external face of the main sheet of the enclosures that is part of the thermal mass and which must achieve:
  - that the thermal mass interacts, only, with the interior
  - a high level of insulation that minimizes losses in winter and
- achieve a first energy class building according to the applicable regulations

When the implementation of active systems is necessary, it must be taken into account that accumulation leads to a drop in power supplies directly proportional to the accumulation cycle (to the number of operating hours, for example).

Another concept that must accompany the accumulation is that of the efficient internal transmission of energy (in both senses of the term) so it must be associated with the radiation transmission system (they are solid elements), to the large radiant surfaces (perfectly available indoors) and to water as a heat-carrying fluid compared to air.

Moving from the convection system to the radiation system leads to a load forecast with a 40% decrease and a 66% decrease in powers to go from CoP 2.5 to CoP > 4 in efficient active systems that are sensitive to these parameters [2]. This final efficiency derived from the accumulation of the partial efficiencies of both passive and active systems will lead, in many cases, to a decrease in the supplying powers (for example, solar) which will make them sufficient, when under normal conditions, they would not be. This is particularly important in urban environments where buildings grow in height and roofs do not usually have a sufficient surface area.

### 3. Results and discussion

The materials that can provide the described properties are those that bring together three characteristics simultaneously: a high Density ( $\rho \geq 700 \text{ Kg/m}^3$ ), a good Conductivity ( $\lambda > 5 \text{ W/m K}$ ) and a high Specific Heat ( $c = \sim 1000 \text{ J/Kg K}$ ), that is to say, materials that require a lot of energy to change their temperature (in both entities) but in which heat moves easily. The thermal accumulation capacity of a material is quantified by its thermal effusivity (b) [1]

$$b = \sqrt{\lambda c \rho} \quad \text{Ws}^{1/2} / \text{m}^2 \text{ K} \quad (1)$$

And the amount of heat accumulated in a material since its surface is heated is proportional to  $b \sqrt{t}$

$$\text{Ws} / \text{m}^2 \text{ K} \quad (2)$$

where  $t$  is the time the heating lasts [1].

On the other hand, *thermal diffusivity* (a) expresses the ease with which energy penetrates a material

$$a = \frac{\lambda}{c \rho} \quad \text{m}^2/\text{s} \quad (3)$$

from which the depth reached ( $\delta$ ) is obtained after a time  $t$  of energy application

$$\delta = \sqrt{at} \quad \text{m} \quad (4)$$

Formula (2) is valid as long as  $\delta$  is smaller than  $d$  (piece thickness). When  $\delta$  approaches  $d$ , then is greater than  $d$ , one tends towards an accumulated maximum which is the heat capacity  $\times$  the temperature increase  $\chi \Delta T$ . In between, EN 13786 can be used. In general, to work with accumulation, high effusivities ( $> 700 \text{ Ws}^{1/2}/\text{m}^2\text{K}$ ) and low diffusivities are suitable.

The following concepts are also of interest:

Areal Thermal Capacity ( $\chi$ ) of a constructive element, which is the ability of the element to regulate the internal thermal loads to which it is exposed

$$\chi = d c \rho \quad \text{J/m}^2\text{K} \quad (5)$$

where  $d$  is the thickness of the element and  $c$  and  $\rho$  are the aforementioned properties.

The dynamic thermal capacity, which depends on the materials, their arrangement in the element and the rate of change of the external conditions, is the dynamic heat capacity of the surface described in EN 13786.

Given that many common materials have a thermal diffusivity (a) close to  $0,6 \times 10^{-6} \text{ m}^2/\text{s}$  the conclusion is reached that the minimum thicknesses for maximum efficiency for energy variations of a day are 10 cm and of a week are 25 cm [1]. These thicknesses are perfectly normal in conventional construction elements and it is convenient to have them directly exposed inside a minimum of 50% of the surfaces of the storage elements.

Thinking about summer comfort, Italian regulations [3] put the so-called Periodic Thermal Capacity of an enclosure in an inverse relationship with its Periodic Thermal Transmittance (defined in the ISO 13786 standard [4]) which regulates the behaviour of the closures in the summer and which obliges buildings with non-residential uses to a minimum Periodic Thermal Capacity of  $40 \text{ kJ/m}^2\text{K}$ . This feature designed for summer also works satisfactorily in winter.

The second concept of interest is that of the Thermal Capacity of a space or a building (C) which is the sum of the thermal capacities of all the elements in contact with the interior environment:

$$C = \sum_i A_i \chi_i \quad \text{J/K} \quad (6)$$

where  $A$  is the surface of each element and  $\chi$  its thermal capacity

For a given space this thermal capacity can vary by a factor of 6 depending on the materials used in its construction, according to their apparent areas and whether they are light or heavy [1]

A third concept that indicates the behaviour of the accumulation is the Time Constant ( $\tau$ ) also characteristic of the thermal inertia of a heated interior space that relates the thermal capacity of this space and its heat loss coefficient

$$\tau = C / H \quad \text{s} \quad (7)$$

Where  $C$  is the effective interior Thermal Capacity and  $H$  the heat loss coefficient of this interior which is the power to be supplied to maintain a degree of temperature difference between the interior and exterior. For a space in certain conditions given the concept varies from 8 hours if it is a greenhouse (light elements) up to 10 days if it is made of concrete (heavy element) and very well insulated [1].

#### 4. Conclusions

The use of the thermal inertia or so-called internal thermal mass of the elements that make up buildings for thermal storage significantly increases energy efficiency because:

It stabilises the internal temperature and therefore improves the comfort conditions when internal or external heat loads vary

- it adapts very easily to climates with short-cycle renewable energy replenishment (less than or equal to weekly) saving these temporary discontinuities
  - it is sensitive to both internal and external passive energy contributions of different signs
  - it is complementary and compatible with all those provisions that provide partial efficiencies
  - it is particularly suitable when there is continuous use of the building;
  - it is compatible with efficient energy transport from surplus areas to deficit areas
  - allows for efficient and healthy transfer/absorption of heat and
- allows it to be integrated into a larger-scale thermal accumulation strategy, being able to be complementary to seasonal accumulation, if applicable.

#### Acknowledgements

I appreciate the collaboration of Claude-Alain Roulet in addition to his bibliographic contributions.

#### References

- [1] Roulet, Claude- Alain. *Santé et qualité de l'environnement intérieur dans les bâtiments*. Presses Polytechniques et Universitaires Romandes. Lausanne 2008
- [2] Ricci, Manolo i Gros, Joan Ramon. *Climatización Radiante: Una alternativa a los Sistemas Convectivos*. Ponencias UPC 060103
- [3] *Normativa sull'efficienza energetica* DM 26/06/2015 i el Decret de 24 de desembre de 2015 *Adozione dei criteri ambientali minimi per l'affidamento di servizi di progettazione e lavori per la nuova costruzione, ristrutturazione e manutenzione di edifici per la gestione dei cantieri della pubblica amministrazione e criteri ambientali minimi per le forniture di ausili per l'incontinenza*.
- [4] Norma ISO 13786:2007 (UNE-EN ISO 13786:2007). *Prestaciones térmicas de los productos y componentes para la edificación. Características Térmicas dinámicas. Métodos de cálculo*. AENOR. Madrid 2011

EUROTHERM2023-H106

## Energy stored in terminal units of building heating systems. Dynamic modeling of radiators in building performance simulation tools.

J.F. Belmonte<sup>1,2\*</sup>, J.A. Almendros-Ibáñez<sup>1,2</sup>

<sup>1</sup>Universidad de Castilla-La Mancha, Renewable Energy Research Institute, Section of Solar and Energy Efficiency, Avda. de la Investigación, 1, 02071, Albacete, Spain

<sup>2</sup>Universidad de Castilla-La Mancha, E.T.S. de Ingenieros Industriales de Albacete, Campus Universitario, 02071, Albacete, \*Corresponding author e-mail: juanf.belmonte@uclm.es

### Abstract

This work compares the dynamic thermal behavior of four commercially available radiators with high differential thermal masses (capacitance), from light to very heavy units, against those exhibited by steady-state models usually used in Building Performance Simulation (BPS) tools. The conducted TRNSYS simulations using a dynamic model (Type 362) able to capture radiator capacitance effects, revealed that the modeling of heavy cast-iron radiators using conventional static models is not appropriate for building load estimation and heating equipment control, reporting underestimations in the heating energy emitted between 12 and 20 %. Energy and load estimation errors associated with capacitance can be minimized using dynamic models, process facilitated by manufacturer's sheets, as they usually provide reliable input data for characterizing radiators' capacitance, namely, metal weight and fluid content per radiator element.

**Keywords:** Thermal capacitance; dynamic radiator model; TRNSYS; BPS tools; building heating system; air-source heat pump.

### 1. Introduction

Radiators and baseboards are terminal-units widely used in building heating systems for many years, especially in Europe. These units are typically installed attached to a wall and below windows (i.e., surfaces with high heat losses), providing heating to the conditioned spaces by radiation and natural convection mechanisms. Standard modeling of radiators in Building Performance Simulation (BPS) tools, such as EnergyPlus and TRNSYS [1, 2], historically omits dynamic models for radiators and baseboards (usually only steady-state models) within their standard libraries, neglecting the effects of thermal capacitance of these units (thermal mass or inertia) on the heat rate delivered by the fluid, and that emitted into the zones, although in some cases (i.e., heavy cast-iron radiators) the energy that these terminal units can store can be significant. In this line, although some research interest has been paid to properly account the share of radiation and natural convection of radiator's total heat emission [3], little attention has been put on thermal inertia effects, even when it is known that warm-up and cool-down periods may be long (i.e., cast-iron radiators), during which the radiator thermal mass is gradually heated up (heat storage period), receiving hot water from the heating loop but providing a low heat emission into the zone, and latterly, when the heating system is switch off, important amounts of residual heat are available to be emitted to the zones, until radiators finally achieve room temperatures (heat recovery period). In a time in which many building owners are planning to substitute in their heating system combustion-based boilers by air-source heat pumps, accurate modeling of radiators' capacitance effects becomes critical, as contrary to boilers these equipment's efficiencies and heating capacities are very sensitive to ambient temperatures. In addition, the energy stored provided by radiators may be utilized as a zone delayed heat gain, as lower heating loads occur at higher ambient temperatures. Circumstance that favors a better match of the heating load by shifting the energy stored in radiators at midday, which can be emitted into the zone at late afternoon when ambient temperature drops and heating load rises.

This situation is clearly depicted in Figure 1, showing the typical “M-shaped” of building’s heating load, in which a 100 m<sup>2</sup> apartment located in Madrid (complying with energy code requirements) is evaluated using a BPS tool over 5 days in January.

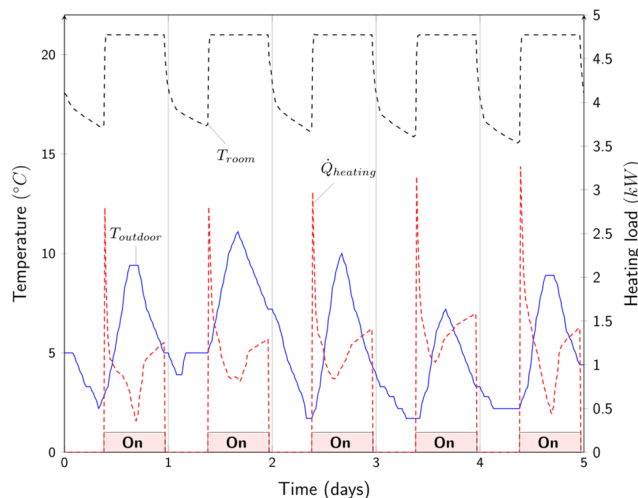


Figure 1. Typical M-shaped of a house heating load for a discontinuous operation (active from 9:00-23:00 h) during 5 days in January for weather conditions of Madrid. Simulation results using EnergyPlus [1].

## 2. Materials and method

Four commercially available radiator models with highly differential capacitances, from light (aluminum) to extremely heavy (cast-iron), but similar nominal heating power (170-190 W/element) have been simulated in the TRNSYS environment. The differential performance provided by a dynamic model (the non-standard TRNSYS component model, Type 362 [4]) versus a static model that mimics all emission characteristics but has no thermal mass, has been evaluated for a complete heat storage/recovery cycle, receiving during the loading period (8 hours) a hot fluid with different inlet temperatures (namely, 90, 80, 70, 60, and 50 °C), and flow rates (those producing a fluid temperature drop as it passes through, of 5, 10, and 20 °C, respectively). Table 1 summarizes the most relevant characteristics of radiators according to manufacturer’s data sheets [5].

Table 1. Radiators characteristics. Data reported for a radiator of 10 elements.

Radiator Reference Model [5]	Material	Nominal Power for a temp. difference of 60°C (kW)	Emission exponent, n (-)	Metal Weight (kg)	Fluid content (kg)	Thermal capacitance (kJ/°C)
Dubal 80	Aluminum	1.899	1.34	18.3	5	37.736
Astral 80	Aluminum	1.779	1.31	16.1	3.8	30.696
Condal 80	Aluminum	1.875	1.31	16.9	4	32.268
Epoca 90	Cast-iron	1.717	1.27	125.4	29.5	180.994

Figure 2 compares the heating rate curves for a complete heat storage/recovery process under the operating conditions indicated in the caption of the figure, distinguishing that delivered by the hot fluid, from that emitted by the radiator into zone, for a light and an extremely heavy radiator (both constituted of 10 elements). The indicated areas below the curves correspond to the energy stored (equal to the energy released during later hours) by each radiator, which greatly vary.

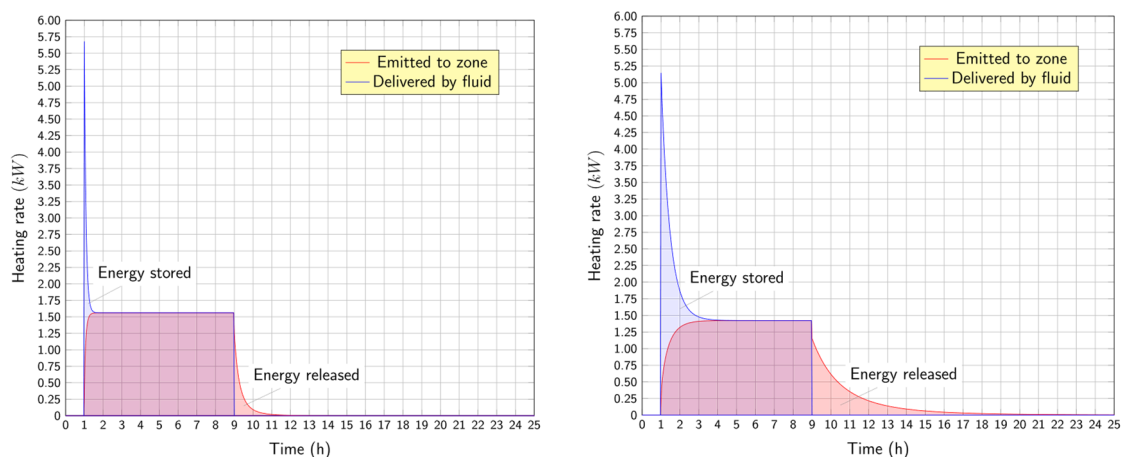


Figure 2. Energies stored by a light (left, model Dubal 80) and an extremely heavy (right, model Epoca 90) radiator, considering for both an inlet temperature of 80°C, and a temperature fluid drop of 20°C.

The heat emissions provided by static models are additionally included in figure 3, highlighting the heating energy underestimations that the use of static models yields compared to dynamic models, which have an effect in both: heating equipment demands, and zone loads actually met.

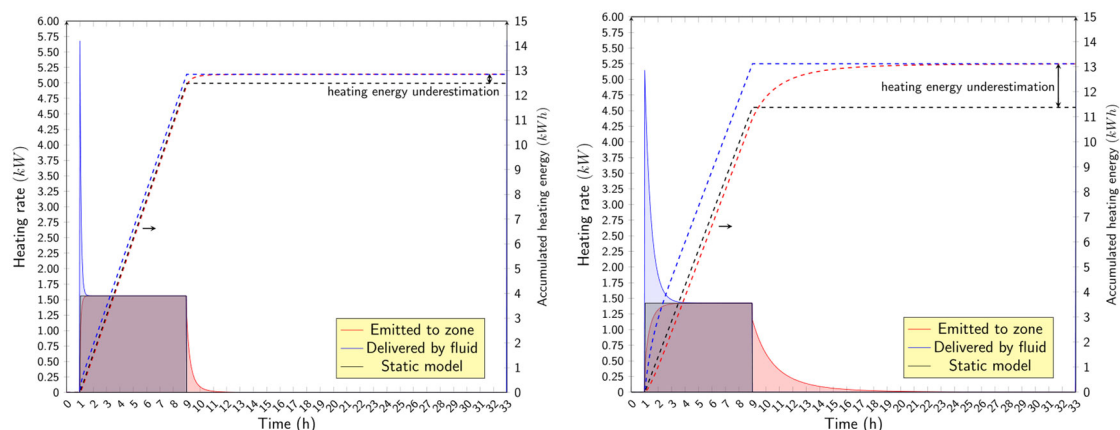


Figure 3. Heating energy underestimations for a complete heat storage/recovery cycle when a steady-state radiation model (no mass) is considered. Left: Dubal 80, right: Epoca 90, considering for both an inlet hot fluid temperature of 80°C, and a temperature drop of the fluid as it passes through of 20°C.

### 3. Results and discussion

Table 2 collects the most relevant results from the TRNSYS simulations, which correspond to those exhibited for the lighter and heavier radiator under study. The maximum thermal energy stored in radiators, and heating energy underestimations observed for static model conducting a complete heat storage/recovery cycle, were chosen as the most relevant variables.

Table 2. Energy stored and heating energy underestimation of a static model in a complete heat storage/recovery process under different operating conditions for the lighter (Astral 80) and heavier (Epoca 90) radiator analyzed. Results obtained for 10 elements (min. and max. values are highlighted).

		Astral 80 radiator model		Epoca 90 radiator model	
Inlet fluid temp (°C)	Fluid temp. drop (°C) at nom. conditions	Total energy stored in a heat storage/recovery cycle (kWh)	Heating energy underestimation of a static model (%)	Total energy stored in a heat storage/recovery cycle (kWh)	Heating energy underestimation of a static model (%)
90	5	<b>0.565</b>	3.021	<b>3.237</b>	15.927
	10	0.519	2.756	2.977	14.751
	20	0.442	<b>2.320</b>	2.527	<b>12.638</b>

80	5	0.485	3.171	2.784	16.547
	10	0.448	2.915	2.569	15.384
	20	0.384	2.460	2.194	13.266
70	5	0.438	3.371	2.360	17.300
	10	0.376	3.098	2.156	16.146
	20	0.325	2.657	1.855	14.038
60	5	0.326	3.629	1.871	18.244
	10	0.303	3.348	1.740	17.118
	20	0.264	2.889	1.510	15.021
50	5	0.245	<b>3.972</b>	1.410	<b>19.530</b>
	10	0.229	3.686	1.319	18.420
	20	<b>0.202</b>	3.230	<b>1.171</b>	16.352

#### 4. Conclusions

The conducted TRNSYS simulations have revealed that steady-state models generally used in BPS tools may greatly underestimate the heating requirements of heavy cast-iron radiators, exhibiting discrepancies between 12 and 20 % against dynamic models. These discrepancies are much smaller in the case of light radiators (aluminum), not exceeding for any operating condition considered values beyond a 4 %. The four commercially available 10 element-radiators considered in this study, have shown a great ability to store significant amounts of energy, ranging from approximately 0.5 to 3.2 kWh (from lighter to heavier radiator), being recommended the use of dynamic models (particularly for cast-iron radiators) to accurately model their heating performance in BPS tools.

#### Acknowledgements

This work was partially funded by the project PID2021-127322OB-I00 (Ministerio de Ciencia e Innovación MICIN/AEI/10.13039/501100011033 and NextGenerationEU/PRTR); Project TED2021-131046B (Ministerio de Ciencia e Innovación MCIN/AEI /10.13039/501100011033 and NextGenerationEU/PRTR). Project SBPLY/21/180501/000017 (Regional Government of Castilla-La Mancha); Project RED2018-102431-T, (Ministerio de Ciencia, Innovación y Universidades); and Project 2020-GRIN-28725 (Universidad de Castilla-La Mancha).

#### References

- [1] EnergyPlus. Energy Simulation software. U.S. Department of Energy's (DOE). Building Technologies Office (BTO), National Renewable Energy Laboratory (NREL). 2022.
- [2] TRNSYS 18. A TRaNsient SYStem Simulation program. Klein, S. and Beckman, J.M. University of Wisconsin-Madison. 2022.
- [3] A New model for calculating the convective and radiant impact of radiators and baseboards in EnergyPlus. Kang, D. and Strand, R.K. SimBuild2010. IBPSA-USA. New York City, 2010.
- [4] TRNSYS-Models for Radiator Heating Systems. Types 361, 362 and 320. Holst S. 1996. Transsolar Software Engineering. Available at <https://trnsys.de/en/addons-en>.
- [5] BAXI CLIMATIZACIÓN. Data available at <https://www.baxi.es/productos/radiadores>.



EUROTHERM2023-M107

## Experimental determination of characteristic curves of zeolites for sorption heat storage

Henri Schmit<sup>1</sup>, Tobias Schubert<sup>1</sup>, Eberhard Lävemann<sup>1</sup>, Stefan Hiebler<sup>1</sup>

<sup>1</sup>ZAE Bayern, Walther-Meissner-Str. 6, 85748 Garching, Germany, Phone: 49-89-32944222, Fax: 49-89-32944212, e-mail: [henri.schmit@zae-bayern.de](mailto:henri.schmit@zae-bayern.de)

### Abstract

Thermal energy storage based on adsorption and desorption of water on zeolites promises high energy storage densities. The so-called characteristic curve of an adsorbent links the adsorbed water volume to the adsorption potential. With a characteristic curve available, the heat of adsorption of an adsorbent can be calculated for different conditions encountered in specific applications. Thus, the maximum storable amount of thermal energy can be assessed at a material level. In this work, the feasibility to use an existing hydrothermal test setup to determine the required equilibrium data for the construction of characteristic curves is checked on zeolites 13XBFK and NaYBFK, both from Chemiewerk Bad Köstritz GmbH (CWK). For the two zeolites, characteristic curves were determined for an adsorption potential ( $\Delta F$ ) between  $81 \text{ kJ kg}^{-1} \leq \Delta F \leq 2192 \text{ kJ kg}^{-1}$ . The determined characteristic curve for 13XBFK is valid for an adsorbed water volume ( $W_{\text{ads}}$ ) between  $0.030 \text{ cm}^3 \text{ g}^{-1} \leq W_{\text{ads}} \leq 0.336 \text{ cm}^3 \text{ g}^{-1}$ . For NaYBFK the validity is between  $0.009 \text{ cm}^3 \text{ g}^{-1} \leq W_{\text{ads}} \leq 0.323 \text{ cm}^3 \text{ g}^{-1}$ . The obtained characteristic curves are in good agreement with existing ones from other sources. Therefore, the hydrothermal test setup can be used to reliably determine characteristic curves of zeolites.

**Keywords:** Thermal energy storage, Water sorption, Zeolite, Characteristic Curve

### 1. Introduction

Thermal energy storage based on adsorption and desorption of water on adsorbents promises high energy storage densities (ca.  $180 \text{ kWh m}^{-3}$ ) [1]. Zeolites are well-known adsorbents and those with high water adsorption capacities are potentially interesting for application in thermal energy storage systems [2]. The so-called characteristic curve of an adsorbent links the adsorbed water volume to the adsorption potential. With a characteristic curve available, the adsorption potential and, hence, the heat of adsorption of an adsorbent can be calculated for different conditions encountered in specific applications. Thus, the maximum storable amount of thermal energy can be assessed at a material level. However, it is notoriously difficult to obtain the required equilibrium data over a large range of sample temperatures and water vapour pressures.

At ZAE Bayern, a multiple sample setup, with relatively large sample masses up to 5 g, was built to test the hydrothermal stability of adsorbents [3]. The 16 samples can be exposed to a temperature range between  $30 \text{ }^\circ\text{C}$  and  $350 \text{ }^\circ\text{C}$ , and dew point temperatures between  $5 \text{ }^\circ\text{C}$  and  $70 \text{ }^\circ\text{C}$ . Due to these wide ranges, the existing test setup has potential to acquire the equilibrium data for the construction of characteristic curves. The aim of this work is to check its feasibility.

### 2. Materials and methods

The development of the theory behind the characteristic curve is commonly attributed to Dubinin [4]. It is based on the assumption that in microporous adsorbents like zeolites, the water vapour adsorption can be described as filling up of the microporous volumes. The adsorbate, in this case water, is thereby described as a liquid, that, for a given temperature, can fill a certain volume in the adsorbent (here zeolite). The adsorption potential  $\Delta F$  corresponds to the isothermal change of the free energy between

unbound water vapour at saturation pressure and the adsorbed water vapour with a certain relative pressure. In the case of an isothermal adsorption, the adsorption volume is a function of the water vapour pressure. The latter, in return, at constant temperature, is only dependent on  $\Delta F$ . Hence, the adsorption potential is a function of the adsorption volume. For many adsorbents, the points of different adsorption isotherms coincide on one curve, the so-called characteristic curve.

Two well-known zeolites with known characteristic curves were selected to check the feasibility of determining characteristic curves with the hydrothermal stability setup: 13XBFK and NaYBFK, both from Chemiewerk Bad Köstritz GmbH (CWK). The two zeolites, although pelletised, are so-called “binderless” or “binder-free”, since the binder itself acts as active zeolite.

At ZAE Bayern, a multiple sample setup was built to test the hydrothermal stability of adsorbents [3]. The setup shown in Figure 1 has 4 temperature-controlled sample blocks, each containing 4 sample containers. 4 sample containers of each sample block are connected orthogonally to each other and to 1 of 4 temperature-controlled water reservoirs. With this configuration, samples can be exposed to a total of 16 different conditions of temperature and water vapour pressure by setting 4 different temperatures and 4 different dew point temperatures. Thereby, the temperature range of each sample block is between 30 °C and 350 °C, while that of each water reservoir is between 5 °C and 70 °C.

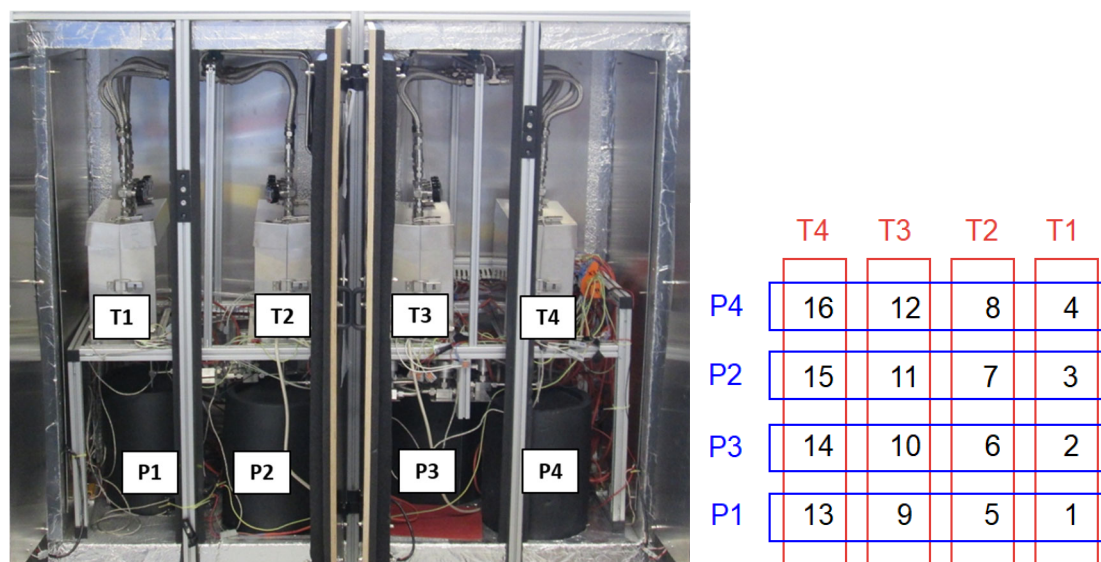


Figure 1. The picture on the left hand side shows the temperature-controlled cabinet of the hydrothermal test setup with 4 temperature-controlled water reservoirs (P1 to P4) and 4 sample blocks (T1 to T4). The schematic on the right hand side shows the orthogonal interconnection of the water reservoirs and sample blocks, through which it is possible to subject the samples to 16 different hydrothermal conditions [3].

A measuring procedure starts with introducing around 3 g of a sample into each of the 16 sample containers. The samples are then placed into the sample blocks and gradually dried for around 20 hours at temperatures up to 350 °C under constant evacuation. To determine the dry sample masses, the manual valve on top of each sample container is first closed. Subsequently, the samples are removed from the sample blocks. They are weighted manually after a cooling period at room temperature. The measured equilibrium data necessary for the construction of the characteristic curve is subsequently determined in adsorption. Technically, it is feasible to determine 16 data points in one measurement run. However, in practice, it has proven advantageous to determine 8 data points in one measurement run. Thereby, each data point consists of the arithmetic mean value of the results obtained for 2 samples. Hence, the data points become more reliable and outliers can be identified more easily, while the downside is a longer measurement time. In three measurement runs, 24 data points are determined in adsorption. Before each measurement, the samples are dried under the aforementioned conditions.

For both zeolites, dew point temperatures,  $T_p$ , were varied between 25 °C and 34 °C for the 3 measurement runs in adsorption. In the same 3 measurement runs, the temperatures,  $T$ , were varied between 43 °C and 315 °C. The fit from equation (1), proposed by Fischer [2], was used to obtain the characteristic curves based on the 24 data points for each zeolite.

$$W_{ads} = \frac{a+c\cdot\Delta F+e\cdot\Delta F^2+g\cdot\Delta F^3}{1+b\cdot\Delta F+d\cdot\Delta F^2+f\cdot\Delta F^3} \quad (1)$$

### 3. Results and discussion

For the two zeolites CWK 13XBFK and NaYBFK equilibrium data was obtained with the hydrothermal test setup. For each zeolite, 24 data points were determined, each one corresponding to a mean adsorption volume,  $W_{ads,mean}$ . The mean adsorption volumes of 13XBFK in function of the adsorption potential  $\Delta F$  are shown on the left hand side in Figure 2. Since the calculated standard deviations are small (maximum  $0.002 \text{ cm}^3 \text{ g}^{-1}$ ) compared to the absolute values of  $W_{ads,mean}$ , they are not visible. The small standard deviations show a good agreement between the two different samples exposed to the same conditions.

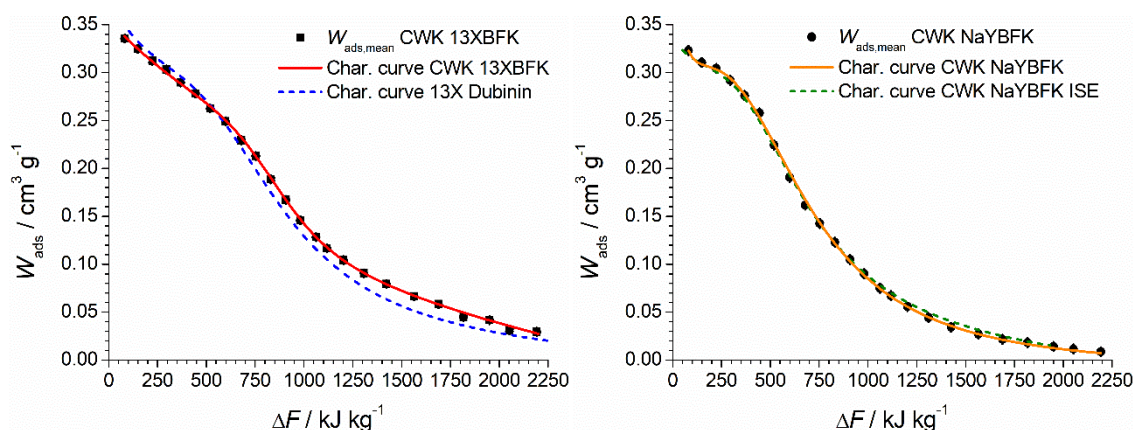


Figure 2. Left hand side: experimentally determined mean adsorption volumes,  $W_{ads,mean}$ , for CWK 13XBFK (black squares). The characteristic curve fitted to this data is shown as red line. The blue dotted line is the characteristic curve of 13X based on experimental data from Dubinin ([2][5]). Right hand side:  $W_{ads,mean}$  for CWK NaYBFK (black circles). The characteristic curve fitted to this data is shown as orange line. The green dotted line shows the characteristic curve of CWK NaYBFK based on unpublished experimental data from the Fraunhofer ISE.

The characteristic curve of 13XBFK is represented by the fit (red line) through the points representing the adsorption volumes in Figure 2. It is valid for an adsorption potential between  $81 \text{ kJ kg}^{-1} \leq \Delta F \leq 2192 \text{ kJ kg}^{-1}$  and an adsorbed water volume between  $0.030 \text{ cm}^3 \text{ g}^{-1} \leq W_{ads} \leq 0.336 \text{ cm}^3 \text{ g}^{-1}$ . The parameters with 4 significant digits, used to construct the characteristic curve of 13XBFK in Figure 2, are listed in Table 1.

Table 1. Parameters with 4 significant digits for equation (1) to obtain the characteristic curves of CWK 13XBFK and NaYBFK.

Zeolite	parameter						
	a	b	c	d	e	f	g
13XBFK	0.3550	$-1.467 \cdot 10^{-3}$	$-7.444 \cdot 10^{-4}$	$2.992 \cdot 10^{-7}$	$5.730 \cdot 10^{-7}$	$5.739 \cdot 10^{-10}$	$-1.262 \cdot 10^{-10}$
NaYBFK	8.590	1.734	0.4093	$-2.393 \cdot 10^{-3}$	$-5.323 \cdot 10^{-5}$	$4.554 \cdot 10^{-6}$	$-3.395 \cdot 10^{-8}$

The characteristic curve of 13XBFK determined with the hydrothermal test setup is thereby in good agreement with the characteristic curve of 13X (blue dashed line) based on experimental data from Dubinin ([2][5]). It has to be noted, that the 13X measured by Dubinin was likely not formed into pellets, but under the form of powder. A comparison with the CWK 13XBFK is thus meaningful, since the 13XBFK, as mentioned before, is a binderless zeolite. Hence, it can be expected, that its adsorption capacity is nearer to a 13X powder than to 13X as pellets containing a non-active binder.

On the right hand side of Figure 2,  $W_{ads,mean}$  determined for CWK NaYBFK are plotted in function of the adsorption potential. Again, the standard deviations are small (maximum  $0.001 \text{ cm}^3 \text{ g}^{-1}$ ) compared to the absolute values of  $W_{ads,mean}$ . The characteristic curve of NaYBFK is represented by the fit (orange line) through the adsorption volumes in Figure 2. It is valid for an adsorption potential between  $81 \text{ kJ kg}^{-1} \leq \Delta F \leq 2192 \text{ kJ kg}^{-1}$  and an adsorbed water volume between  $0.009 \text{ cm}^3 \text{ g}^{-1} \leq W_{ads} \leq 0.323 \text{ cm}^3 \text{ g}^{-1}$ . The parameters with 4 significant digits, used to construct the characteristic curve of NaYBFK in Figure 2, are listed in Table 1. The green dashed line in Figure 2 represents the characteristic curve of CWK NaYBFK based on unpublished experimental data from the Fraunhofer ISE. The agreement between both characteristic curves is very good.

From the above results, it can be concluded, that the determination of characteristic curves with the existing hydrothermal test setup was successful for the two investigated zeolites 13XBFK and NaYBFK. It can thus be used in the future to reliably determine the characteristic curves of further zeolites and potentially of other adsorbents.

#### 4. Conclusions

In this work, the feasibility to use an existing hydrothermal test setup to determine the required equilibrium data for the construction of characteristic curves was checked on zeolites 13XBFK and NaYBFK, both from CWK. For each zeolite, the necessary equilibrium data for the construction of the characteristic curve was determined in three measurement runs in adsorption, each one preceded by a drying of the 16 samples. 24 data points were obtained for the construction of the characteristic curve of each zeolite. For both zeolites, characteristic curves were determined for an adsorption potential ( $\Delta F$ ) between  $81 \text{ kJ kg}^{-1} \leq \Delta F \leq 2192 \text{ kJ kg}^{-1}$ . The determined characteristic curve for 13XBFK is valid for an adsorbed water volume ( $W_{ads}$ ) between  $0.030 \text{ cm}^3 \text{ g}^{-1} \leq W_{ads} \leq 0.336 \text{ cm}^3 \text{ g}^{-1}$ . For NaYBFK the validity is between  $0.009 \text{ cm}^3 \text{ g}^{-1} \leq W_{ads} \leq 0.323 \text{ cm}^3 \text{ g}^{-1}$ . The obtained characteristic curves are in good agreement with existing ones from other sources. Hence, the hydrothermal test setup can be used to reliably determine characteristic curves of zeolites.

#### Acknowledgements

The work of ZAE Bayern was part of the project AMThES and supported by the Federal Ministry for Economic Affairs and Climate Action under the project code 03EN6006. The authors would like to thank Mr. Philipp Hügenell from the Fraunhofer ISE for providing the data on CWK NaYBFK. The responsibility for the content of this publication is with the authors.

#### References

- [1] E. Lävemann et al., Mobile Sorptionsspeicher zur industriellen Abwärmenutzung Grundlagen und Demonstrationsanlage – MobS II, FKZ 0327383B, TIB Hannover, 2015
- [2] F. Fischer, Hydrothermale Stabilität von 13X-Zeolithen: Experimentelle Untersuchung und Modellierung, PhD thesis, TU München, 2018
- [3] F. Fischer and E. Lävemann, Meas. Sci. Technol. 26 (2015) 065603
- [4] B. P. Bering, M. M. Dubinin and V. V. Serpinsky, J. Colloid. Interface Sci. 21(1966) 378-393
- [5] M. M. Dubinin, J. Colloid. Interface Sci. 23(1967) 487-499

EUROTHERM2023-D108

## Development of a software tool for performance analysis of CSP plants in tower configuration with molten salt TES system

Pablo Tagle-Salazar<sup>1</sup>, Cristina Prieto<sup>2</sup>, Luisa F. Cabeza<sup>1</sup>

<sup>1</sup>GREiA Research Group, Universitat de Lleida, Pere de Cabrera s/n, 25001, Lleida, Spain, e-mail: pablo.tagle@udl.cat, luisaf.cabeza@udl.cat

<sup>2</sup>University of Seville, Department of Energy Engineering, Camino de los Descubrimientos s/n, 41092, Seville, Spain, e-mail: cprieto@us.es

### Abstract

Concentrating solar power is a technology with a growing market potential for decarbonized power generation using solar thermal resources. Thermal energy storage systems are key components of solar power plants that improve the dispatchability of the energy generated. Two-tanks with molten salts is the most deployed thermal energy storage system for solar power plants. This study presents a developed simulation tool for annual performance analysis of a solar power plant coupled with a two-tank storage system with molten salts. Main contribution of this tool is the implementation of a fully transient model that estimates heat losses of thermal storage. This model considers variation due to wind speed, ambient temperature, and other effects. Implementing these kind of models into long-term performance analysis tools improves assessment of round-trip efficiency of thermal energy storage systems.

**Keywords:** Concentrating solar power (CSP); sensible heat thermal energy storage; molten salt; transient modeling; performance analysis; Modelica.

### 1. Introduction

Solar energy is a renewable and sustainable source of energy that can be used to generate electricity, heat water and buildings, and power other devices. It is considered as one of the key solutions against global warming, as it produces no greenhouse gas emissions and can reduce the dependence on fossil fuels. Installed capacity using solar resources has grown in recent years, and it is expected to continue this trend in the future. However, it still represents a small fraction of total energy generation capacity [1].

Besides solar photovoltaics, concentrating solar power (CSP) is another technology for power generation using solar resource. CSP uses mirrors or lenses to concentrate solar radiation from a large area to focus it onto a receiver. A heat transfer fluid (HTF) flows inside the receiver and then it is heated. Later, the energy in the HTF is used to power a turbine connected to a generator, either by direct steam generation (water as HTF) or via heat exchange (molten salts or thermal oils as HTF). The advantage of CSP plants is its capability to integrate thermal energy storage (TES), which allows to generate energy even with low or non-existing solar resource (at nights, i.e.), and also performs load shifting. This makes CSP technology a reliable and dispatchable source of energy.

Sensible heat, latent heat, and thermochemical heat are the main ways to store energy. Sensible heat systems store energy by a temperature gradient. Heat is stored by a change of phase (solid-liquid, or liquid-vapor) in latent heat storage. Energy is stored by endothermal/exothermal chemical reactions for thermochemical heat TES. From these, sensible heat storage using molten salts is the most deployed TES technology, using a two-tank system. Here, one tank contains the “hot” salt, and the other stores the “cold” salt. Figure 3 shows a CSP plant in tower configuration with a direct two-tank molten salt TES system. Typical operation of this kind of plants consists of that the cold salt flows from the cold tank to the receiver, then it is heated and stored in the hot tank. Later, the hot salt flows to the heat

exchanger and produces the steam to power the turbine in the thermal cycle. Then, the salt is cooled and stored in the cold tank.

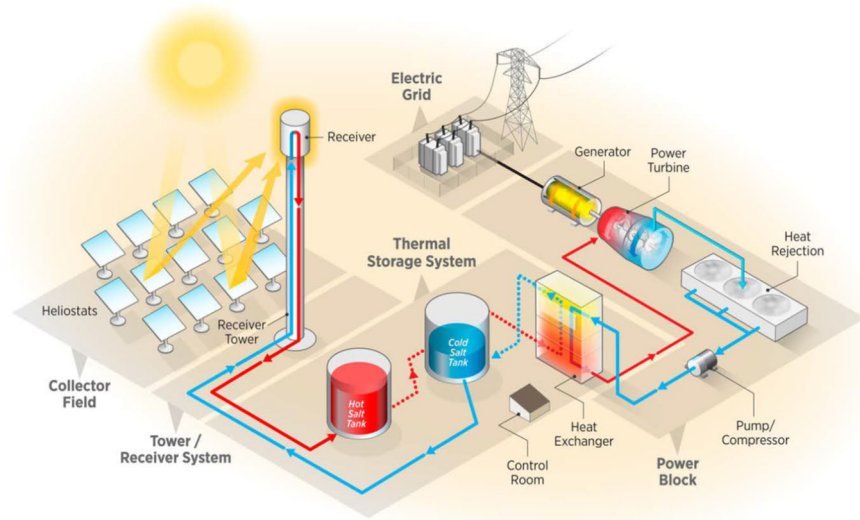


Figure 3. Typical CSP plant with tower configuration [2]

In order to simulate CSP plants, there is an open-access library called “SolarTherm” [3]. This package was developed by the Australian National University using OpenModelica. Here, heat losses of thermal storage are modeled as  $U \cdot A \cdot \Delta T$ , where  $A$  is the area of the tank exposed to the ambient,  $\Delta T$  the temperature difference between the salt in the tank and the external ambient, and  $U$  is the heat transfer coefficient. Most of software available in the market also use this thermal model. Main disadvantage of this mathematical model is that it considers  $U$  as constant during the whole simulation. This assumption neglects the effect of other parameters (such as wind speed) which make heat losses varies all along a day. Then, models that can predict transient thermal behavior of heat losses are needed. The intention of this paper is to present a simulation tool where there was implemented a transient heat transfer model for heat losses estimation of thermal energy storage system. This is the main contribution on research since there is no available software in the market with fully transient heat losses model for long-term simulations.

## 2. Methodology

OpenModelica is the software used to develop the simulation tool. It is an open-source software that allows users to perform modeling of complex dynamic systems using the Modelica language. Main advantages of this language are that it performs acausal modeling of continuous and/or discrete events, and it can solve systems of non-linear algebraic and differential equations.

The new software tool developed in this paper uses a transient heat transfer model for thermal losses of the two-tank molten salt TES system. Main assumptions of the model are the following.

1. It is based on one-dimensional and transient heat transfer analysis.
2. The mathematical model is focused on one isolated tank since both hot and cold tanks have a similar heat transfer behavior. They only interact with each other by unmixed mass flow of both molten salts and gas.
3. The boundary of the heat transfer analysis are the external air of the tank and the soil.
4. Inside the tank, both molten salts and the inert gas above the salt are considered as ideally mixed (uniform temperature), single-phase fluids, and open control volumes. They do not interact with each other except via heat exchange through the interface surface (contact surface of both fluids).
5. All surfaces of the metal jacket inside the tank exchange heat with fluids by natural convection.

6. Conduction heat transfer through a layer is modeled as a 1-D multiple serial  $\Pi$ -element thermal resistance-capacitance network.
7. Natural and mixed convection is modeled by Newton cooling law as function of the Nusselt number.
8. Inside the tank, radiation heat transfer is modeled as a three gray-surfaces cylindrical enclosure (inner dry surfaces of the tank and the free surface of the salts). Outside the tank, a surface in a large isothermal hemisphere is the model for radiation heat transfer.
9. Mixed convection and incoming solar radiation are considered in the outer surface of the tank.

This thermal model was implemented into OpenModelica environment for performance analysis of TES systems. In addition, in order to simulate a CSP plant, models for other components (such as receiver and power block) were adapted from SolarTherm library for the needs of this study. A CSP plant with a 110 MWe of gross output is simulated using the tool. Later, the results are compared with solution given by Solar Model Advisor (SAM) for the same power plant. Transient response of key parameters (such as heat flows, temperatures, etc.) are also compared. Similarities and differences of both tools are also mentioned.

### 3. Results

Simulations from a typical summer day with high solar resource, high wind speed and low temperature (as possible) was selected. Figure 4 shows the weather data from the reference day. Figure 5 shows the transient response for the thermal losses of the TES system and the net power output for both OpenModelica (OM) using the model described in section 20 and SAM. Notice that SAM does not show any transient response of thermal losses, but OpenModelica does. This behavior is principally because of the model from SAM does not consider any other variable than the difference temperature between the salts and the ambient. Notice that most visible changes in thermal losses occurs when there is a high variation in wind speed for the OpenModelica simulation (around 13 h, 19 h, and 22 h). Other important change occurs around 7 h, when the solar field starts to operate. At this point, hot salt from the receiver goes to the hot tank, so it acts like a “heat gain”, making heat losses goes down. Modeling the influence of these and other effects on thermal losses on the tanks are the key advantage of the developing tool over others software. For the case of the output power, transient response is similar from both tools.

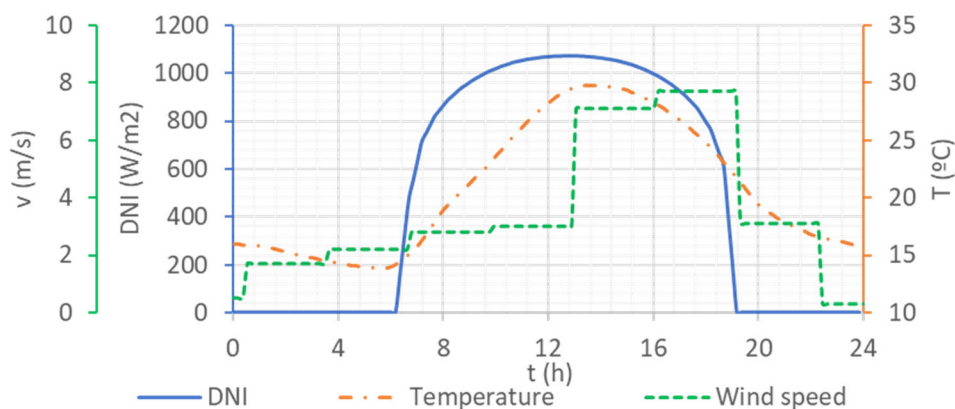


Figure 4. Weather data from the reference day

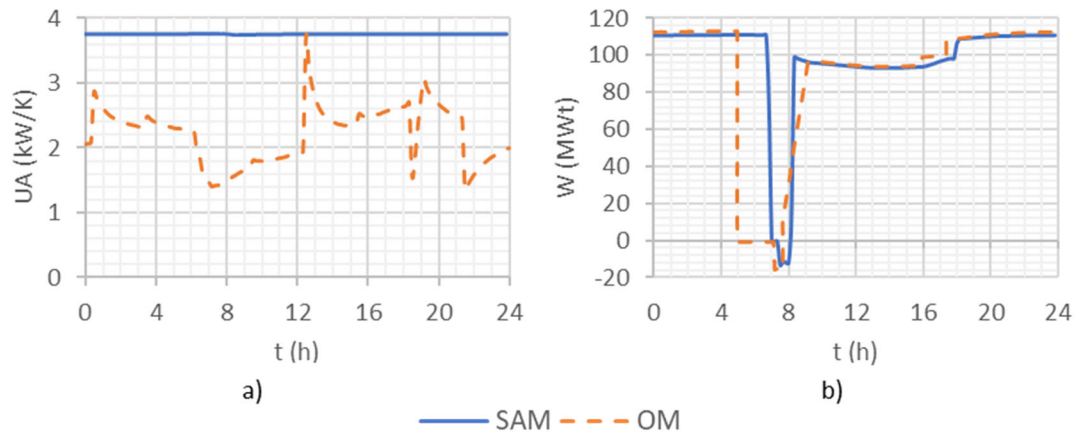


Figure 5. Comparison of transient response at reference day. (a) Thermal losses of TES system, (b) Net power output to grid

#### 4. Conclusions

A software tool for long-term simulation of CSP plants is developed. The key contribution is the mathematical model for thermal losses in the TES system implemented in OpenModelica. This model, in combination with modules from SolarTherm library, were used to simulate a CSP plant with accurate results. It was shown that the tool can model transient behavior of the thermal losses of the TES system, including effects by wind speed, temperature, and others. Furthermore, transient behavior of other parameters of the plant shows good agreement when compared with other software tools in the market (i.e., SAM).

#### Acknowledgements

This work was partially funded by the Ministerio de Ciencia e Innovación - Agencia Estatal de Investigación (AEI) - NextGeneration EU (PCI2020-120695-2 - MCIN/AEI/10.13039/501100011033/NextGenerationEU/PRTR). The authors would like to thank the Catalan Government for the quality accreditation given to their research group GREiA (2021 SGR 01615). GREiA is a certified agent TECNIO in the category of technology developers from the Government of Catalonia. This work is partially supported by ICREA under the ICREA Academia programme.

#### References

1. Ritchie H, Roser M, Rosado P. Energy [Internet]. 2022 [cited 2023 Jan 26]. Available from: <https://ourworldindata.org/energy>
2. Mehos M, Turchi C, Vidal J, Wagner M, Ma Z, Ho C, et al. Concentrating Solar Power Gen3 Demonstration Roadmap. NREL/Tp-5500-67464 [Internet]. 2017;1–140. Available from: [www.nrel.gov/docs/fy17osti/67464.pdf](http://www.nrel.gov/docs/fy17osti/67464.pdf)
3. SolarTherm [Internet]. [cited 2022 Nov 4]. Available from: <https://build.openmodelica.org/Documentation/SolarTherm.html>



EUROTHERM2023-B109

## Comparative study on the passive cooling of electronic devices using metallic and organic phase change materials via latent heat storage

Elad Koronio, Ayelet Lecker, Gennady Ziskind

Ben-Gurion University of the Negev, P.O.B 635, Beer-Sheva 84105, Israel, E-mail: gziskind@bgu.ac.il

### Abstract

Phase change materials (PCMs) are gaining significant attention in the field of thermal management due to their high latent heat capacity and the ability to absorb heat nearly isothermally during phase change. As a result, they can reduce component temperatures during transient operations. In this study, we compare PCM-based heat sinks made of plate fins and PCM compartments, using two types of PCMs: n-Octacosane, an organic paraffin, and Field's metal, a eutectic metal alloy. These PCMs undergo a solid-liquid transition at a similar temperature, but have differing thermal properties, with Field's metal having a higher thermal conductivity (by two orders of magnitude). Results show that Field's metal stores a larger portion of generated power as latent heat due to its superior thermal properties, leading to lower maximum temperatures.

**Keywords:** Phase change materials, Transient thermal management, Numerical modeling

### 1. Introduction

Phase change materials (PCMs) are promising in the field of thermal energy storage and thermal management due to their latent heat capacity. This enables them to store (or release) a considerable amount of energy during the phase transition process. In terms of thermal energy storage, this energy could be utilized for later use [1]. In terms of electronics thermal management, where high heat fluxes, generated by high energy density components, result in very high temperatures, utilization of phase change materials as a sort of thermal buffer can prevent damage due to overheating [2].

For electronic cooling applications, paraffins were extensively studied due to their high heat capacities (sensible and latent), adequate transition temperatures and low densities, which are key properties for transient operation of volume-limited systems. Nevertheless, their storing capability in a transient process is impeded by their low thermal conductivity ( $\sim 0.2$  W/m K), and they are therefore usually integrated within extended surfaces such as fin arrays or porous media to promote heat dissipation [3].

The effects of extended surfaces topology on the effectiveness of the heat sink are well established. Numerous studies have qualitatively and quantitatively investigated the effects of system parameters (e.g., fin geometries, fin distributions or pore size) on the overall performance of the heat sink (e.g., [4,5]). Nevertheless, a proper comparison between materials and their properties for a certain application has not been thoroughly explored, though these properties are significant for the efficiency of heat transport through the system.

There are three main parameters that determine the effectiveness of PCMs in transient operations: latent heat per unit mass,  $L$ , density,  $\rho$ , and thermal conductivity,  $k$ . To weigh out the contribution of these properties, a figure of merit (FOM) was proposed, so that  $FOM = \rho \times L \times k$  [6]. For higher values, the PCM is considered more effective. The value of  $\rho \times L$  is simply the volumetric latent heat capacity. The higher it is, a given volume can store more energy in the form of latent heat, which is key especially for cooling of small-scale electronic devices. The addition of high thermal conductivity ensures higher heat dissipation rates. When comparing paraffins and metal alloys for example, the higher thermal conductivity of metallic elements and alloys results in greater figures of merit.

In the present study, a comparative investigation of two types of PCMs is conducted to evaluate their performance for passive cooling of electronics. The first is n-Octacosane (chemical formula  $C_{28}H_{58}$ ), an organic paraffin, and the second is Field's metal, a eutectic metallic alloy (weight composition of 51% In, 32.5% Bi and 16.5% Sn). The two were selected due to similar melting temperatures ( $T_m \sim 60^\circ\text{C}$ ), but distinctively different figures of merit. A numerical model of a heat sink comprised of parallel plate fins with PCM compartments was constructed and several key parameters, such as maximum temperature and accumulated heat, were extracted. An experimental setup was designed and built to validate the numerical scheme and investigate the heat sink performance in real conditions.

## 2. Methodology

### 2.1. Numerical investigation

Comparison of the PCM-based heat sinks performance was based on a detailed numerical study where a generic design of parallel-plate fins heat sink integrated with PCM was modeled. A CAD model is depicted in figure 1 with the relevant dimensions. The selected geometric features are based on a geometry inspected in previous research from our group [4]. This was chosen not as the most efficient one, but as an appropriate basis for a comprehensive parametric study. Moreover, it was chosen such that natural convection due to density variations in the liquid PCM could be neglected (small corresponding Rayleigh number for both PCMs in this configuration). Thus, we could isolate the effects of material properties without considering other complex phenomena.

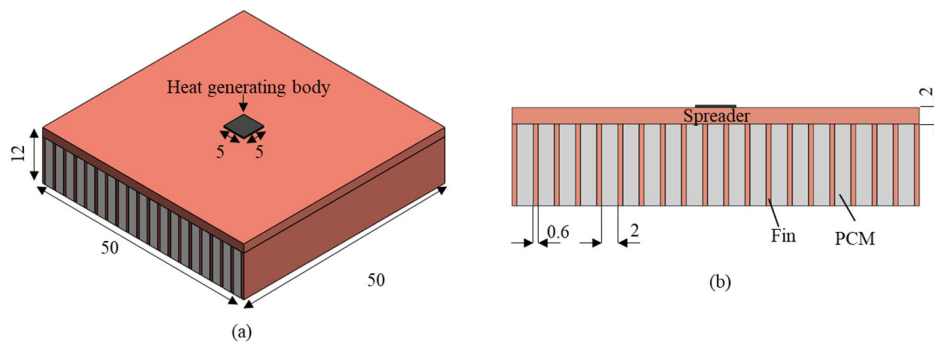


Figure 6. CAD model for the numerical parametric study. Dimension given in mm.

Here, a localized heat source is generating constant power  $q$ , and a spreader is used to reduce the high heat fluxes and spread the heat to all areas of the heat sink. On the other side, fins are found, with the PCM filling the spaces between them. Numerical computations were carried out in Ansys Fluent, a commercial CFD software which utilizes the enthalpy method [4] for modeling of the melting process. The initial temperature was selected as  $55^\circ\text{C}$ , so that melting of the PCMs would start after a brief heating period. Other than the boundary of the heat generating body, where a constant heat flux was set, all other boundaries were considered adiabatic. Table 1 summarizes the thermal and physical properties of the selected PCMs (as gathered from the literature [7,8], where  $c_p$  is the specific sensible heat capacity). In this study, all material properties were considered temperature-invariant. Both copper and aluminum were used as the sink materials.

Table 2. Phase change material properties examined in the numerical parametric study.

Material	$T_m$ $^\circ\text{C}$	$k$ $\text{W/m K}$	$\rho$ $\text{kg/m}^3$	$c_p$ $\text{J/kg K}$	$L$ $\text{kJ/kg}$
n-Octacosane	61.6	0.2	807	2310	253
Field's metal	60.0	18.5	7880	285	27.4

## 2.2. Experimental validation

To validate the numerical approach, experiments in laboratory conditions were held for both PCMs and heat sink materials. An off-the-shelf heat sink with similar geometric properties was acquired for the experimental study. Since in real conditions, leakage and heat transfer to the environment cannot be neglected, a custom insulating encasing was manufactured. A chip resistor was attached to the bottom side of the spreader to simulate a working electronic device supplying constant power. Photos of the experimental system are depicted in figure 2, where copper heat sinks with n-Octacosane (figure 2a) and with Field's metal (figure 2b) are shown.

Experiments were held in ambient conditions at a temperature of  $22 \pm 1^\circ\text{C}$ , which was also the initial temperature. To validate the simulations, a computational model of the experimental setup was designed as viewed in figure 2c, where only a quarter of the domain was considered due to symmetry. The computational model included all relevant properties of the components. In the experiments, a thermocouple was inserted into the chip resistor cover to monitor the temperature. In the computational model, temperature was recorded in the same location. Results from the experiments and corresponding simulations are shown in figure 2d for three input powers supplied by the chip, for a representative case of copper with n-Octacosane. The temperature measurements and computational predictions show good agreement over the examined operation time. In addition, the curves for powers of 8W and 10W are up to full melting of the PCM, meaning that the simulation was also able to predict the melting time.

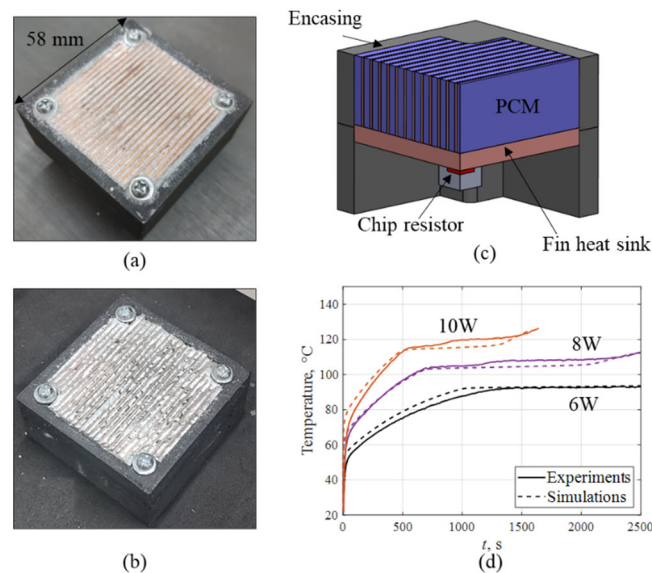


Figure 2. Experimental setup and numerical validation: (a) encased copper heat sink with n-Octacosane, (b) encased copper heat sink with Field's metal, (c) computational model for numerical validation, and (d) comparison of chip temperatures as a function of time between experiments and simulations, for a copper heat sink with n-Octacosane and three different power inputs.

## 3. Results and discussion

The parametric numerical study involved several cases with four combinations of materials (as mentioned in section 2) and four power inputs: 20, 40, 60 and 80W. As a representative case, results will be presented for a copper heat sink with Field's metal and n-Octacosane for all examined power inputs and an operation time of 60s. Two main parameters were extracted to evaluate the effectiveness of the materials: maximum temperature ( $T_{max}$ ), shown in figure 3a, and melt fraction of the PCM ( $MF$  – the relative amount of PCM that transitioned from solid to liquid), shown in figure 3b. The results indicate a great advantage for the Field's metal (dashed line) vs. n-Octacosane (solid line) for all power inputs in terms of maximum temperature.

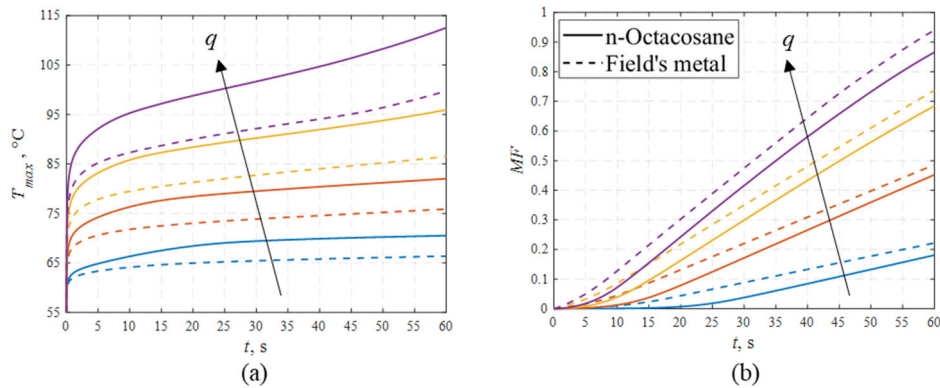


Figure 3. Simulation results for the parametric study for increasing power inputs of 20, 40, 60 and 80W, with a copper heat sink and both PCMs as a function of time: (a) maximum temperature and (b) melt fraction.

The lower temperature in the systems with Field's metal is an indication for its higher thermal conductivity and thermal diffusivity ( $\alpha = k/\rho c_p$ ). This observation is also attributed to the higher melt fraction of the Field's metal as viewed in figure 3b. This indicates that the stored latent heat,  $Q_{lat} = \rho V \cdot MF \cdot L$  (where  $V$  is the volume of the PCM), in the system is greater. According to the properties in table 1, the volumetric latent heat of the Field's metal is slightly larger than the paraffin's (but practically the same), so that for a given volume its storage rate capacity is larger. With the addition of higher thermal conductivity, i.e., higher figure of merit, the heat is dissipating at a faster rate in the metallic PCM so that it undergoes melting faster. Since more heat is accumulated in the form of latent heat, the sensible heating of the overall system is subsequently lowered.

#### 4. Conclusions

In this study, a comparison between two types of phase change materials - organic and metallic - for use in a heat sink for passive transient cooling of electronic devices was conducted. The numerical results were validated through experiments. The findings showed that although both materials have similar volumetric latent heat capacities, Field's metal has a higher thermal conductivity which leads to faster heat dissipation and results in a faster melting rate, greater latent heat storage rate capacity and thus lower maximum temperatures in the system. The results presented in the study are a part of a more comprehensive examination of relevant configurations through numerical and experimental analyses.

#### References

- [1] Prieto, C., Cabeza, L.F., Thermal energy storage (TES) with phase change materials (PCM) in solar power plants (CSP). Concept and plant performance, *Applied Energy*, 254, 113646, (2019).
- [2] Bianco, V., Rosa, M.D., Vafai, K. Phase-change materials for thermal management of electronic devices, *Applied Thermal Engineering*, 214, 118839, (2022).
- [3] Ziskind, G., Enhancing heat transfer in phase change materials, *Proceeding of the 16th International Heat Transfer Conference*, Beijing, China, August 10-15, (2018).
- [4] Shatikian, V., Ziskind, G., Letan, R., Numerical investigation of a PCM-based heat sink with internal fins: constant heat flux, *Int. J. Heat Mass Tran.*, 51(5-6), 1488-1493, (2008).
- [5] Saha, S.K., Dutta, P., Heat transfer correlations for PCM-based heat sinks with plate fins, *Applied Thermal Engineering*, 30, 2485-2491, (2010).
- [6] Shamberger, P.J., Cooling capacity figure of merit for phase change materials, *ASME J. Heat Transfer*, 138, 024501-1, (2016).
- [7] Hale, D.V., Hoover, M.J., O'Neill, M.J., Phase change materials handbook, Technical Report NASA-CR-51363, NASA, (1971).
- [8] Lipchitz, A., Harvel, G., Sunagawa, T., Thermophysical characteristics of liquid metal In-Bi-Sn Eutectic (Field's metal) as a similarity coolant, *ASME J of Nuclear Rad. Sci.*, 8(3), 031301, (2022).

EUROTHERM2023-T110

## Reaction kinetics of the hydration of potassium carbonate including the influence of metastability

Bram Kieskamp<sup>1</sup>, Amirhoushang Mahmoudi, Mina Shahi<sup>2</sup>

<sup>1</sup>University of Twente, Drienerlolaan 5, Enschede, The Netherlands, Phone: +31534898046, e-mail: b.m.kieskamp@utwente.nl

<sup>2</sup>University of Twente, Drienerlolaan 5, Enschede, The Netherlands, Phone: +31534892362, e-mail: m.shahi@utwente.nl

### Abstract

Effective energy storage technologies have an increasingly important purpose in the energy transition due to their capacity to limit the gap in supply and demand of renewable energy. Thermochemical energy storage (TCES) is one of these technologies and a promising one to store heat for domestic space heating and hot tap water. This can occur through the repeated de- and rehydration of salt hydrates. To model the performance of such a system an accurate reaction kinetic data considering the influence of reaction metastability is desired. In this study the reaction kinetics for the hydration of  $K_2CO_3$  are characterized near-equilibrium conditions using STA analysis. The result is an extension of the Arrhenius- $f(\alpha)$  equation that accounts for a rate reduction due to reaction metastability.

**Keywords:** Potassium carbonate, thermochemical heat storage, reaction kinetics, metastable zone

### 1. Introduction

The world is increasingly employing the use of renewable energy sources to mitigate the effects of climate change. For residential heating applications, such sources are solar thermal collectors, industrial waste heat and heat pumps powered with green electricity. Renewable heat sources are however typically intermittent in nature, resulting in a temporal mismatch between supply and demand. Effective heat storage solutions are desired to bridge this gap, both for the short term (day-night) and the long term (seasonal). Thermochemical energy storage (TCES) can be used for both.

In TCES a thermochemical material (TCM) stores heat through a reversible reaction. Heat is stored through an endothermic reaction, which can be released on-demand through an exothermic reaction. The salt hydrate potassium carbonate ( $K_2CO_3$ ) is one such TCM, which has been identified as a strong candidate for residential heating applications due to its high energy density, suitable operating conditions, and economic viability (Donkers et al., 2017). The anhydrate form reacts with water vapor to form the sesquihydrate, releasing heat in the process (Equation 1). This process can be reversed to dehydrate and thus store energy.



The direction of this reaction depends on the pressure compared to the equilibrium pressure as given by the Van 't Hoff equation:

$$\ln \frac{p_{eq}}{p_0} = \frac{\Delta S}{R} - \frac{\Delta H}{RT} \quad (2)$$

The rate of this reaction depends on the temperature, conversion state and water vapor pressure. Although previous studies have characterized the hydration kinetics (Gaeini et al. 2019, Fisher et al. 2021), these studies did not include the influence of reaction metastability (Sögütoglu et al., 2019) and

thus overestimate the reaction rate when operating close to equilibrium conditions. In this study the reaction kinetics for the hydration of  $K_2CO_3$  are characterized at near-equilibrium conditions.

## 2. Materials and methods

For the characterization of the powdered  $K_2CO_3$  (Acros Organics, 98.5% purity) a combination of Thermo-Gravimetric Analysis (TGA) and Differential Scanning Calorimetry (DSC) is used: Simultaneous Thermal Analysis (STA). The STA device (Netzsch STA 449 F3 Jupiter) is connected to a humidifier and a nitrogen gas supply. This way the mass change and the heat of reaction can be measured during the hydration and dehydration. The direction of the reaction is controlled by setting the relative humidity and the temperature of the inlet gas.

A powder sample of around 10mg is placed in an alumina crucible ( $\phi 6.8\text{mm}$ ,  $85\mu\text{L}$ ). At this amount, vapor transport inside the crucible and heat conduction to the thermocouple are efficient, and the influence of sensor noise is low. The sample is first subjected to repeated hydration ( $35^\circ\text{C}$ , 30% RH, 3 hours) and dehydration cycles ( $120^\circ\text{C}$ , 0%RH, 2 hours) until the reaction rate has stabilized and there is no observable difference between consecutive cycles (7-10 cycles). Afterwards four more hydration cycles are performed at 17.7%RH, 10.5%RH, 6.2%RH, and 3.6%RH.

## 3. Results and discussion

In order to characterize the rate of this reaction the general kinetic equation is used (Vyazovkin et al., 2011):

$$\frac{d\alpha}{dt} = k_r \cdot k(T) \cdot f(\alpha) \cdot h(p) \quad (3)$$

With  $k_r$  an unknown rate constant [1/min],  $k(T)$  the Arrhenius equation,  $f(\alpha)$  the reaction model and  $h(p)$  the driving force. Each function will be discussed separately.

### 3.1. Reaction model

A general form of the reaction model for decelerating type reactions is the reaction-order model:

$$f(\alpha) = (1 - \alpha)^q \quad (4)$$

with  $\alpha$  the molar conversion and  $q$  a fitting constant. This is obtained by calculating the reaction rate from the TGA and DSC data and fitting it to the following equation:

$$\log\left(\frac{d\alpha}{dt}\right) = q \log(1 - \alpha) + C \quad (5)$$

In which  $C$  is an unknown constant. The resulting value for  $q$  is  $0.38 \mp 12.6\%$ . The quality of the fit at  $30^\circ\text{C}$  and 30%RH is shown in Figure 1. The initial 10% conversion is neglected for this fit to exclude the effect of induction time (Sögütoglu et al., 2019) and sensor delay.

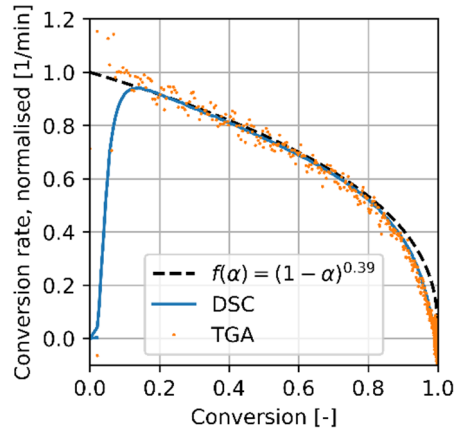


Figure 7. Reaction model  $f(\alpha)$  at 35°C and 30%RH

### 3.2. Driving force

For the driving force of the reaction various forms have been employed in literature (Gaeini et al. 2019, Fisher et al. 2021). However, these relations do not consider the metastable region close to the equilibrium conditions, which leads to near-zero reaction rates even after sufficient induction time (Sögütöglu et al., 2021). To account for this, the following relation is proposed based on Figure 2:

$$h(p) = \left(\frac{p}{p^*} - 1\right), \text{ with: } p^*(T = 35^\circ\text{C}) = p_{eq} + 0.76 \quad (7)$$

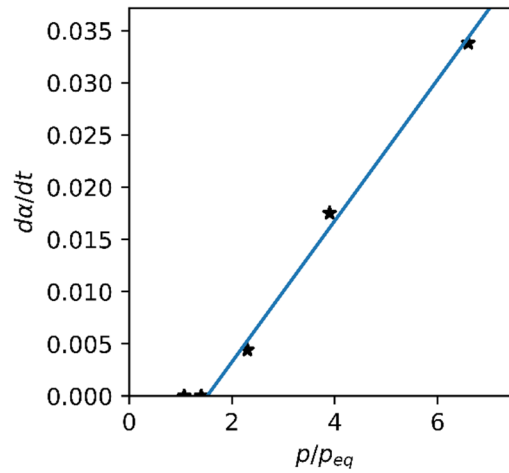


Figure 8. Driving force  $h(p)$  at 35°C with experimental values (stars) and linear fit (line) given by Equation 7

### 3.3. Kinetic equation

Inserting the obtained relations back into Equation 2 and using the Arrhenius equation as obtained by Mahmoudi et al. (2021), the reaction kinetic model for hydration will be as follows:

$$\frac{d\alpha}{dt} = 0.038 \cdot \exp\left(-\frac{9266.2}{RT}\right) \cdot (1 - \alpha)^{0.38} \cdot \left(\frac{p}{p^*} - 1\right)$$

## 4. Conclusions

In this research a reaction kinetic equation is presented for the hydration of potassium carbonate powder which takes into account the influence of metastability at near-equilibrium conditions. This result is a

linear driving force with a slight offset. Furthermore, the presented reaction order model shows a more consistent reaction rate with less drop-off as the TCM approaches full saturation. As a result, the obtained kinetic equation provides a basis for future numerical studies.

The following steps can still be taken to further improve the kinetic equation: (I) Find a relation for  $p^*(T)$  that covers a wide range of temperature conditions. (II) Include an additional factor to model the induction period which is present during the start of hydration when operating close to equilibrium conditions.

## References

- Donkers, P. A. J., Sögütöglu, L. C., Huinink, H. P., Fischer, H. R., & Adan, O. C. G. (2017). A review of salt hydrates for seasonal heat storage in domestic applications. *Applied Energy*, *199*, 45–68. <https://doi.org/10.1016/j.apenergy.2017.04.080>
- Vyazovkin, S., Burnham, A. K., Criado, J. M., Pérez-Maqueda, L. A., Popescu, C., & Sbirrazzuoli, N. (2011). ICTAC Kinetics Committee recommendations for performing kinetic computations on thermal analysis data. *Thermochimica Acta*, *520*(1–2), 1–19. <https://doi.org/10.1016/J.TCA.2011.03.034>
- Gaeini, M., Shaik, S. A., & Rindt, C. C. M. (2019). Characterization of potassium carbonate salt hydrate for thermochemical energy storage in buildings. *Energy and Buildings*, *196*, 178–193. <https://doi.org/10.1016/j.enbuild.2019.05.029>
- Fisher, R., Ding, Y., & Sciacovelli, A. (2021). Hydration kinetics of  $K_2CO_3$ ,  $MgCl_2$  and vermiculite-based composites in view of low-temperature thermochemical energy storage. *Journal of Energy Storage*, *38*, 102561. <https://doi.org/10.1016/J.EST.2021.102561>
- Sögütöglu, L.-C., Steiger, M., Houben, J., Biemans, D., Fischer, H. R., Donkers, P., Huinink, H., & Adan, O. C. G. (2019). Understanding the Hydration Process of Salts: The Impact of a Nucleation Barrier. *Crystal Growth & Design*, *19*(4), 2279–2288. <https://doi.org/10.1021/acs.cgd.8b01908>
- Mahmoudi, A., Donkers, P. A. J., Walayat, K., Peters, B., & Shahi, M. (2021). A thorough investigation of thermochemical heat storage system from particle to bed scale. *Chemical Engineering Science*, *246*, 116877. <https://doi.org/10.1016/j.ces.2021.116877>
- Sögütöglu, L. C., Birkelbach, F., Werner, A., Fischer, H., Huinink, H., & Adan, O. (2021). Hydration of salts as a two-step process: Water adsorption and hydrate formation. *Thermochimica Acta*, *695*, 178819. <https://doi.org/10.1016/J.TCA.2020.178819>



EUROTHERM2023-P111

## Model-based analysis of a dual thermal storage system in the district heating system

Chung-Yu Yeh, Amirhoushang Mahmoudi, Abhishek Singh, Mina Shahi

Department of Thermal and Fluid engineering, University of Twente, Netherlands, e-mail: [c.yeh@utwente.nl](mailto:c.yeh@utwente.nl),  
[m.shahi@utwente.nl](mailto:m.shahi@utwente.nl)

### Abstract

In order to effectively address the problem of peak load demand, short-term and long-term thermal storage can be combined in a district heating system. High (dis)charge rates of sensible heat storage system are advantageous for meeting quick fluctuations in daily and weekly heat demand, however self-discharging loss is the main drawback of such system. Thermochemical heat storage (TCS) is suitable for long-term storage since it offers a high volumetric energy density and low standby heat losses. In this study, a district heating system model was created on Openmodelica to examine the impact of connection and operational conditions of TCS deployment. The results suggest that TCS's low (dis)charging rate is the key challenge in using it for peakload reduction. Different connections and controls could have an effect on TCS's (dis)charging rate.

**Keywords:** Thermal energy storage (TES), Thermochemical energy storage (TCES), District heating system (DHs), Peak-load shaving, Two storage systems, Model-based analysis.

### 1. Introduction

For many European countries, including the Netherlands, district heating systems (DHs) have been viewed as a crucial feature of the heat transition plan<sup>[1]</sup>. DH is a centralized method of providing heat services, and it typically consists of three subsystems: the heat generation subsystem, which is made up of various heat sources; the heat distribution subsystem, which is in charge of delivering the heat carrier via underground pipe systems toward buildings or homes; and the heat consumption subsystems, which represent the dynamic heat demand required from the connected facilities. Along with the previously listed key components, other add-ons like thermal energy storage are implemented to increase demand management flexibility.

To accelerate the heat transition, DHs will be used to meet a larger portion of the heat demand. As a result, the expansion of DHs would raise the pressure on DHs due to the imbalance between supply and demand. A simple way to fix the mismatch problem was to scale up the already-existing short-term thermal storage (STS) capacity, for example, by installing an additional water storage tank. However, having a large volume of water in the tank will have the unavoidable effect of increasing standby heat losses. Thus, a possible alternative is the addition of long-term thermal storage to DHs. The fundamental difficulty in combining STS and long-term thermal storage (LTS) in DHs is their incompatibility in terms of response time and nominal power. The key to a successful LTS implementation is understanding how to effectively combine the two types of storage strategies and take advantage of each one's individual strengths<sup>[2]</sup>.

Low self-discharge, high energy efficiency, and large volumetric density are advantages of thermochemical heat storage (TCS). It is an appropriate method for the use of LTS. At the district level, implementing sensible heat storage on a big scale is very challenging due to the need for a vast space and particular geographic requirements, such as those in pits or boreholes. In terms of system operation, TCS offers more flexibility. TCS can adapt to various temperature environments by modifying its operating conditions. TCS can also be employed for cooling and heating purposes. TCS, therefore is a viable storage option for district-level systems, which are typically built in urban areas<sup>[3]</sup>.

## 2. Modeling district heating system and TCS

Figure 1 shows the district heating model and the baseload heat generation profile. A heat substation divides the primary and secondary networks so they can run at different temperature levels. A cogeneration heat and power plant (CHP) in the primary network will provide the baseload heat source, of which the monthly variation profile is illustrated in Figure 1. The natural gas-fired boiler is used as a peakload heat source because of its ability to ramp-up quickly. The boiler contributes to heat generation only when the baseload supply is insufficient to meet the heat demand. However, when there is overgeneration, which occurs when the baseload produced by CHP exceeds the need for heat, the excess heat will either be recycled or discarded. Peakload requirements from the boiler and wasted heat on the CHP are both important performance measures, and a storage solution can have an impact on them. Comparisons of the thermal power balance profile before and after the adaptation of thermal storage in Figure 2 clearly show the effect of thermal energy storage.

The supply-demand imbalance is crucial for figuring out the suitable range of storage capacity. The maximum daily storage requirement in this case is 3,963 kWh (equivalent to 136 m<sup>3</sup> water volume of storage). The storage capacity for 3 to 6 consecutive days is determined to be 400 to 800 m<sup>3</sup> of water volume.

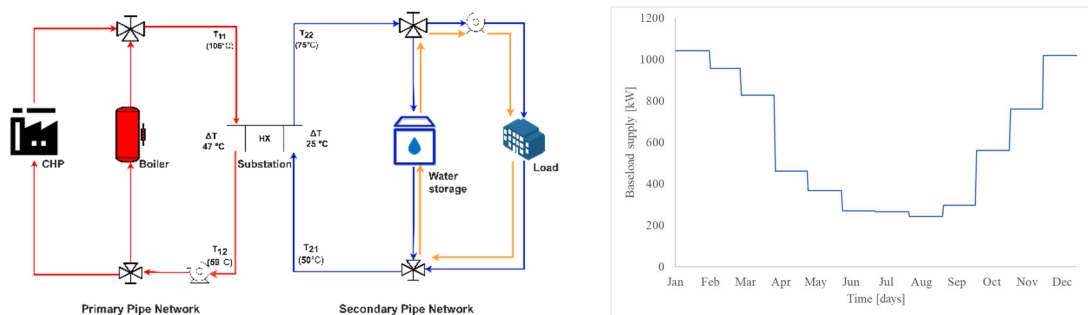


Figure 1. (Left) A schematic of the district heating system, showing the CHP and boiler used for heat generation, the primary and secondary networks used for heat distribution, the load-bearing heat consumers, and the water storage tank. (Right) The CHP's heat generation profile. It is assumed that the value for each month represents the average heat demand for that month.

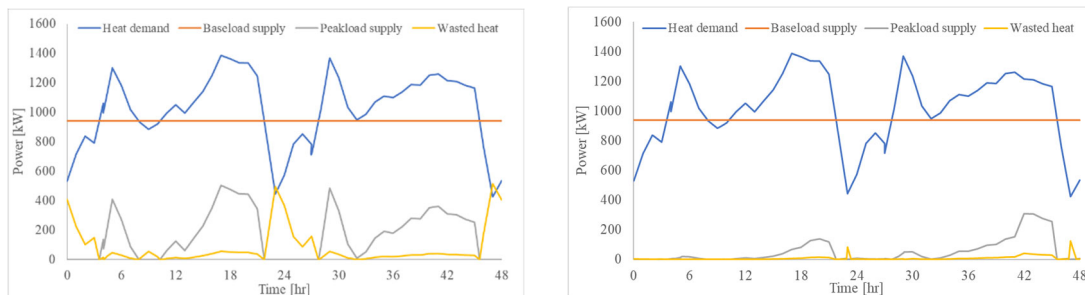


Figure 2. Energy balance profiles for two days in a row in February for DHs without thermal storage implementation (Left) and DHs with a water tank of 400m<sup>3</sup> (Right).

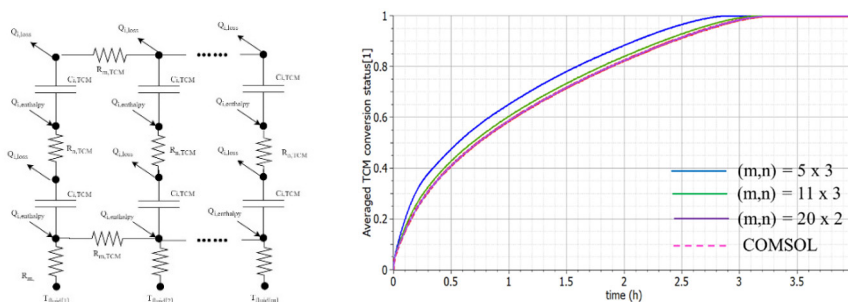


Figure 3. (Left) Heat transfer, kinetic reaction, and convective fluid heat transfer are components of the discrete matrix TCS (m,n). (Right) A small reactor volume (4e<sup>-5</sup> m<sup>3</sup>) and a finer discrete number in the reactor's depth direction are used to validate the TCS model.

Table 1. The operational condition of the TCS system

Evaporator pressure [mbar]	15	Max. hydration temp. [ °C]	64
Condenser pressure [mbar]	12	Min. dehydration temp. [ °C]	60.6

In this study a closed fixed bed reactor is considered. Potassium carbonate ( $K_2CO_3$ ) is used as the energy medium in TCS due to its high reaction enthalpy (91.32 kJ/mol), high system energy density (0.96 GJ/m<sup>3</sup> in the closed system), and suitable discharge temperature for the built environment as shown in Table 1.

In order to take into account the spatial gradient of temperature, a two-dimensional discrete matrix is included in the model to capture the heat transmission inside the reactor of various volumes, as illustrated in Figure 3. The heat capacitor and heat conductance elements are used to model heat accumulation and heat conduction inside the reactor. According to the kinetic model in Equation 1, the reaction enthalpy is transferred to each heat capacitor. Heat transfer fluid in contact with the heat capacitor provides (extracts) the heat source (reaction heat). In a closed system, it is assumed that the pressure distribution within the fixed bed is uniform.

$$\frac{d\alpha}{dt} = K e^{\frac{-E}{RT}} (1 - \alpha) \left(1 - \frac{p_{eq}}{p}\right); p_{eq} = 4.228 \times 10^{12} e^{\frac{-7337}{T}} \quad (1)$$

### 3. Results and discussion

Figure 4 displays three different scenarios which we considered in our DH model. In the first scenario, only a water tank is considered as the heat storage system while in the second and third scenarios, a TCS is also added. In Scenario 2, TCS is connected to the water tank. In Scenario 3, TCS is connected to the return line of DHs to have a high driving force for energy conversion due to low fluid temperature in DHs.

According to the modeling results of three scenarios, peakload shaving depends on preserving enough energy in water storage. It is advised that water storage be given first priority during daily charging to ensure enough energy for the next peakload. TCS can use the remaining heat when there is an excess of heat or when the water storage is nearly full. Water storage is the first to discharge during peak load requests; TCS only steps in once the energy level of the water storage drops below a predetermined level. This strategy is advantageous for DHs because it requires less water storage, which is good for saving space and reducing standby heat losses. Figure 5 (Left) demonstrates that in the first scenario when the water volume rises above 600 m<sup>3</sup>, the decline in peak load generation becomes less apparent. Thus, in this scenario, a total storage capacity of 600 m<sup>3</sup> water is regarded as the ideal storage capacity for DHs.

To compare the performance of the dual storage system with the single storage system that only has one water storage. The total storage capacity was kept the same, which was equivalent with 400 m<sup>3</sup> of water and 30 m<sup>3</sup> of  $K_2CO_3$ . In Figure 5 (Left) you can see the annual boiler generation in Scenario 3 is less than in Scenario 2 and very close to Scenario 1. It can conclude that the dual storage system is further improved in Scenario 3, and it performs similarly to 600 m<sup>3</sup> of water in Scenario 1 in terms of peakload shaving. However, the operational power of TCS is incompatible with water storage as seen in Figure 5 (right). Enhancing the TCS nominal power therefore is the main goal of further advancement.

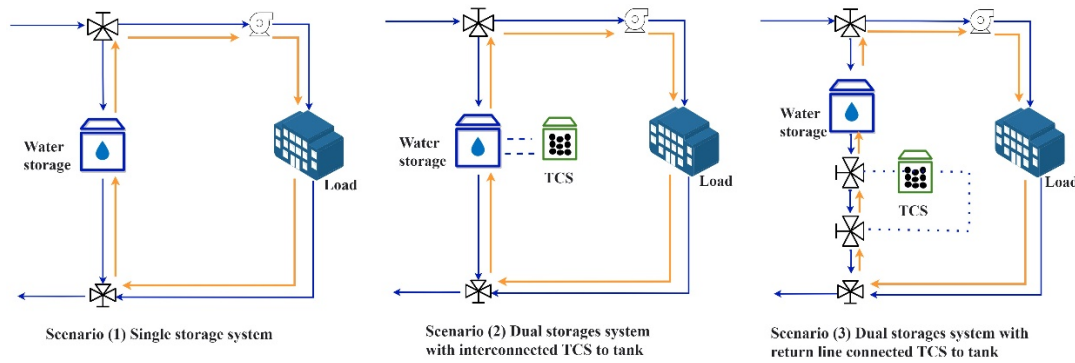


Figure 4: Setup of the storage system for each of the three scenarios.

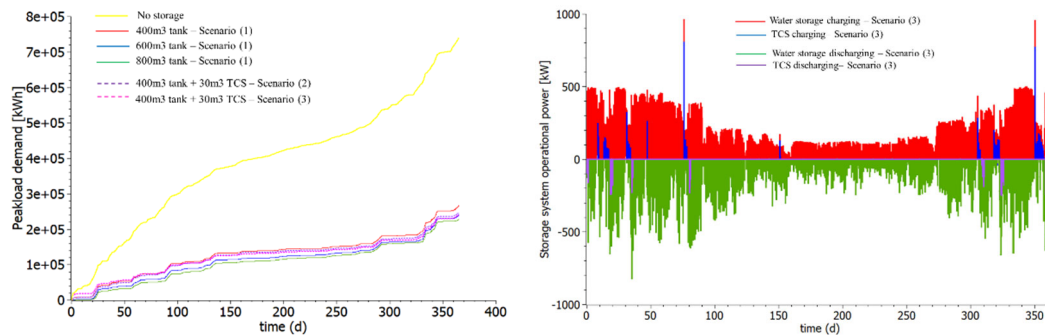


Figure 5: (Left) Annual accumulative boiler generation for all three scenarios. (Right) Storage operational power of water storage and TCS in Scenario (3).

## 4. Conclusions

To assess storage effectiveness with regard to peak load reduction, a district heating system with a dual thermal storage system of a water tank and TCS is simulated. Two types of connection and operation of the TCS system are analyzed using a two-dimension discrete TCS model. Results indicate that TCS's (dis)charging rate is the bottleneck for the performance of peak load shaving. Through optimizing the connection of TCS to water storage, it is possible to increase the TCS (dis)charging rate.

## Acknowledgments

This research work has been supported and funded by the Netherlands' TKI Urban Energy, Project HeatLand with project number 1921402.

## References

- [1] The Hague. Climate agreement, 2019.
- [2] Rosato, A. et al. Dynamic simulation of a solar heating and cooling system including seasonal storage serving a small Italian residential district. *Thermal Science* 24 (2020): 3555–3568.
- [3] Clark, A. et al. "State of the art on salt hydrate thermochemical energy storage systems for use in building applications." *Journal of Energy Storage* 27 (2020): 101145.

EUROTHERM2023-Y112

## Close-contact melting of phase change material on two inclined surfaces for latent heat thermal energy storage

Tomer Shockner<sup>1</sup>, Inon Salman<sup>1</sup>, Dmitry Portnikov<sup>1</sup>, Gennady Ziskind<sup>1</sup>

<sup>1</sup>Ben-Gurion University of the Negev, Beer-Sheva 84105, Israel, e-mail: gziskind@bgu.ac.il

### Abstract

Phase change materials (PCM) are widely investigated for latent heat thermal energy storage (LHTES) due to their ability to absorb and release large amounts of thermal energy during solid-liquid phase transitions. However, the low thermal conductivity of PCM can make it challenging to achieve efficient storage of thermal energy, due to limited time periods. Close-contact melting (CCM) is a known approach to enhance the melting of PCM, but little is known about the behavior of CCM on inclined asymmetric hot surfaces, which may occur inside LHTES storage units. In this study, we investigate CCM of PCM on asymmetric surfaces using a newly designed and built experimental device. Experiments were performed at different orientations to reveal the melting rate dependence on orientation. The results provide insights into the melting dynamics of PCMs in the device and may inform the design of LHTES systems for improved thermal energy storage.

**Keywords:** Thermal energy storage, Phase change materials, Close-contact melting

### 1. Introduction

Development of alternative means to harvest energy, especially from renewable sources, still poses a great challenge to the scientific community. A possible remedy is thermal energy storage (TES), which is currently considered by experts a grand challenge in thermal science and engineering for deep decarbonization [1]. The present work is focused on latent heat thermal energy storage (LHTES) which is considered a promising solution for thermal energy storage [2].

The key disadvantage of PCM is their low inherent thermal conductivity [3]. Thus, heat transfer augmentation is the priority for PCM-based systems, and numerous approaches have been suggested [3-5]. In our study we aim to incorporate the advantageous close-contact melting (CCM), see Ref. [3] for in-depth discussion. Due to its merits, CCM gained a lot of popularity in recent years [6-9]. Melting in CCM studies mostly occurs on a single hot surface, while only one attempt to study CCM with two non-symmetric hot surfaces has been made [10].

Close contact melting on two asymmetric surfaces could be observed, for example, in shell and tube storage unit with longitudinal fins for a so-called ‘Mercedes’ configuration, see Ref. [10]. The two upper thirds of such system exhibit an intriguing melting sequence: the solid on each side is melting on two hot surfaces, inclined and vertical, causing a nontrivial solid motion, which probably includes both translation and rotation. This is unlike the common CCM scenario where the solid motion is only downward, or where the solid is rotating while melting only on one (vertical) hot surface [5]. Since the experimental apparatus was relatively small in that experiment [10], visualization difficulties arose and no definite conclusions were made from the experimental investigation.

Thus, in the current work an original experimental device is designed, built and tested to understand heat transfer modes in it. The conducted experiments have a demonstrative nature, aiming at revealing the possible melting patterns and solid-bulk motion in such installation. This work is thus an initial effort, and it is envisioned that additional experiments will be conducted during the first half of 2023. The experimental results will be used later to validate an advanced numerical method being developed by the leading author, as a part of his ongoing Ph.D. research.

## 2. Experimental methodology

The experimental device has two major purposes: (1) to allow CCM on two asymmetric surfaces, such that the melting patterns and solid motion could be observed; (2) validate our novel numerical approach being developed nowadays. Thus, it was decided that the arrangement should be an enlarged upper 1/3 of ‘Mercedes’ configuration with transparent boundaries, excluding the metal heated walls, built in one bent piece.

The designed device is shown in Fig. 1a, and its key parts are: two Perspex plates, a 120° section of a Perspex tube (inner diameter of 51.0 mm, outer diameter of 57.0 mm), and an aluminum plate (length of 121.6 mm, width of 28.0 mm, thickness of 5.0 mm) bent to 120°. The aluminum plate serves as the heated surface. The space between the above-mentioned parts forms the PCM chamber. Fig. 2b presents the assembled apparatus in the lab with a solid PCM inside.

Preliminary experiments were conducted to verify the newly built device. For example, special care was undertaken to prevent PCM leaking from the melting chamber. Another important matter is to create uniform initial conditions at the start of each experiment, to allow a possibility of comparison between the experiments and the numerical model later. The experiments were conducted inside an oven.

The PCM that was used during the study was Eicosane ( $C_{20}H_{42}$ ), with solid density of  $856 \text{ kg/m}^3$  and liquid density of  $775 \text{ kg/m}^3$ . This PCM is non-toxic and relatively easy to work with, and has a melting point of  $36.7 \text{ }^\circ\text{C}$ . The full thermal-physical properties of the PCM are provided in [5].

The experimental procedure includes the following steps. The solid-PCM filled device is taken from room temperature into the oven (temperature of  $1 \text{ }^\circ\text{C}$  below the melting temperature) for pre-heating period of one hour. Then, the device is placed at a given orientation. The oven is set to  $\sim 33.3 \text{ }^\circ\text{C}$  above the melting temperature, visualization of melting patterns is done, and each experiment ends with the melting of the entire PCM volume.



Figure 1. The experimental device: (a) design CAD model, and (b) photo of the laboratory installation.

## 3. Results and discussion

In the current stage of the study, two preliminary experiments, for orientations of  $30^\circ$  and  $15^\circ$ , are reported. The experiments are simply denoted according to the angle for convenience. The tests were conducted under the same controlled conditions, except for the angle variation. The melting behavior of the PCM is presented in Fig. 2. In the illustrations, the snapshots were taken after 15, 25, 30 and 35 minutes. As evident from the figures, the melting rate is faster for the case of  $30^\circ$  with total melting time of 55 minutes, whereas 70 minutes were required for  $15^\circ$ . The orientation of the system influences the hydrodynamic resistance in the flow “channels” next to the perimeter of the system, via which the molten PCM exits to the upper part of the system. These hydrodynamic resistances influence the thickness of the thin molten PCM layers (next to the heated surfaces) and by that affect the thermal resistance.

25 min



30 min



35 min



Figure 2. The experimental melting patterns for 30° (left column) and of 15° (right column).

#### 4. Conclusions

This study aimed to investigate the close-contact melting (CCM) of phase change materials (PCM) on asymmetric surfaces, in order to gain insights into the melting dynamics of PCMs in a latent heat thermal energy storage (LHTES) system. Two experiments were presented using a newly designed experimental device, and the results showed that the melting rate was significantly impacted by the orientation of the surfaces. There is a need for more accurate simulation tools to model the macro-scale melting process, including CCM on asymmetric surfaces. These findings have important implications regarding the focus of our efforts.

While this study provides valuable insights into the melting dynamics of PCMs on asymmetric surfaces, there are limitations that should be considered. For example, the study only examined two orientations, and further research is needed to understand the melting behavior of PCM on a wider range of orientations. This work is thus an initial effort, and it is envisioned that additional experiments will be conducted during the first half of 2023.

The findings of the present study are helpful in achieving reliable experimental results that will be used for validation of an advanced numerical model, which is being developed concurrently. This numerical tool will help us get a deeper understanding of melting in such systems of practical importance.

## Acknowledgements

This work is a part of project CSPplus, under the umbrella of CSP-ERA.NET supported by the European Commission within the EU Framework Programme for Research and Innovation HORIZON 2020 (Cofund ERA-NET Action, N° 838311). The BGU team is funded by Israeli Ministry of Energy within ERA-NET framework (contract #221-11-034).

The research work of Tomer Shockner is supported by a special scholarship from the Jewish National Fund (KKL-JNF).

## References

- [1] Majumdar, A., "Five grand challenges in thermal science and engineering for deep decarbonization", MIT InnoTherm, 2020. Retrieved Feb. 7 2023 from: <https://www.youtube.com/watch?v=aBM97efxHYs>.
- [2] Prieto, C., Cabeza, L.F., "Thermal energy storage (TES) with phase change materials (PCM) in solar power plants (CSP). Concept and plant performance", *Applied Energy*, 254, 113646, (2019).
- [3] Kozak, Y., G. Ziskind, G., Novel enthalpy method for modeling of PCM melting accompanied by sinking of the solid phase, *Int. J. Heat Mass Tran.*, 112, pp. 568-586, (2017).
- [4] Liu, C., Groulx, D., "Experimental study of the phase change heat transfer inside a horizontal cylindrical latent heat energy storage system", *Int. J. Therm. Sci.*, 82, pp. 100-110, (2014).
- [5] Rozenfeld, T., Kozak, Y., Hayat, R., Ziskind, G., "Close-contact melting in a horizontal cylindrical enclosure with longitudinal plate fins: demonstration, modeling and application to thermal storage", *Int. J. Heat Mass Tran.*, 86, pp. 465-477, (2015).
- [6] Shockner, T., Ziskind, G., "Combined close-contact and convective melting in a vertical cylindrical enclosure", *Int. J. Heat and Mass Transfer*, 177, 121492, (2021).
- [7] Shockner, T., Ziskind, G., "Experimental and numerical evaluation of phase-change material performance in a vertical cylindrical capsule for thermal energy storage", *Applied Thermal Engineering*, 219, 119519, (2023).
- [8] Fu, W., Yan, X., Gurumukhi, Y., Garimella, S.V., King, W.P., Miljkovic, N., "High power and energy density dynamic phase change materials using pressure-enhanced close contact melting", *Nat. Energy* 7, pp. 270-280, (2022).
- [9] Hu, N., Li, Z.R., Xu, Z.W., Fan, L.W., "Rapid charging for latent heat thermal energy storage: A state-of-the-art review of close-contact melting", *Renewable Sustainable Energy Reviews*, 155, 111918, (2022).
- [10] Hayat, R., Melting process in thermal storage unit based on phase change material, M.Sc. Thesis, Ben-Gurion University of the Negev, (2015).



EUROTHERM2023-J113

## Feasibility analysis of a seasonal sorption heat storage system under optimal control and different climatic conditions

Alicia Crespo<sup>1</sup>, Cèsar Fernández<sup>1</sup>, Álvaro de Gracia<sup>2</sup>, Andrea Frazzica<sup>3</sup>

<sup>1</sup>GREiA Research Group, University of Lleida, Pere de Cabrera s/n, 25001 Lleida, Spain, e-mail: alicia.crespo@udl.cat

<sup>2</sup>IT4S Research Group, Universitat de Lleida, Pere de Cabrera s/n, 25001, Lleida, Spain

<sup>3</sup>Instituto di Tecnologie Avanzate per l'Energia "Nicola Giordano", CNR-ITAE, Messina, Italy

### Abstract

Water-based sorption heat storage systems require heat at the evaporator above 0°C to prevent freezing of water. The performance of water-based sorption heat storage systems highly depends on climatic conditions when heat at the evaporator is obtained from solar energy or ambient air during winter. In this study, we analyze the feasibility of a water-based seasonal sorption heat storage system driven by solar collectors for three different European climates, represented by: Paris, Munich, and Stockholm. To avoid overestimating the size of the sorption storage at each location, the control is optimized aiming to minimize the operational costs. Energy densities around 117 kWh/m<sup>3</sup> are obtained when the sorption storage size is redesigned under optimal control scenario. Moreover, the sorption storage operated at minimum temperatures of - 15 °C, show independence from ambient temperature during its discharge in all the studied locations.

**Keywords:** seasonal sorption heat storage, simulations, control optimization, climatic zones

### 1. Introduction

The International Energy Agency (IEA) has set a net zero emissions building (nZEB) scenario by 2050. The use of seasonal thermal energy storage (TES) systems coupled with solar thermal collectors are a potential solution to reduce the greenhouse gas emissions in buildings in regions such as central and north Europe, where the solar irradiation during winter is low. In particular, the use of sorption heat storage systems is very promising since they present high energy density and low thermal losses at long-term.

Sorption storage systems require a low-temperature heat source to assist the evaporator, this temperature corresponds to 0°C for systems which operate with water at the evaporator. During winter days, “free energy” from ambient air or solar collectors can be used as heat source. In summer, ambient air can also be used as heat sink by the condenser of the sorption storage. To understand the impact of weather conditions on the sorption storage system and analyze its potential under different climates, a study of the system coupled to a dwelling thermal demand subjected to different climates must be carried out. In sorption TES, the thermal losses have high impact in the system performance since they cause a temperature decrease of the material inside the reactor. The longest the pause between two consecutive charges or discharges, the highest the thermal losses of the system. Hence, an optimal control of the system can contribute to minimize the heat losses between two consecutive charges and discharges by identifying which system states and weather conditions benefit its performance at each time step. Therefore, in this study, the performance of a seasonal sorption storage system filled by lithium chloride silica-gel (LiCl-Silica gel) [1] was studied under the climates of Paris (Atlantic), Munich (Continental) and Stockholm (Boreal). Moreover, the system rule-based control (RBC) strategy is optimized for the corresponding thermal demand, climatic conditions, and system states for each location to avoid overestimating the size of the sorption storage.

## 2. Materials and methods

### 2.1. Description of the system.

The analysed system consisted of a field of evacuated tube collectors, a stratified water tank, a seasonal sorption heat storage and a backup gas boiler. Moreover, the seasonal sorption heat storage is assisted by a heat storage and a dry-heater that act as low-temperature heat source to the evaporator. The goal of the system is to supply the domestic hot water (DHW) and space heating (SH) demand of a single-family house of 134 m<sup>2</sup> located in Central or North Europe. Figure 1 shows the configuration of the system.

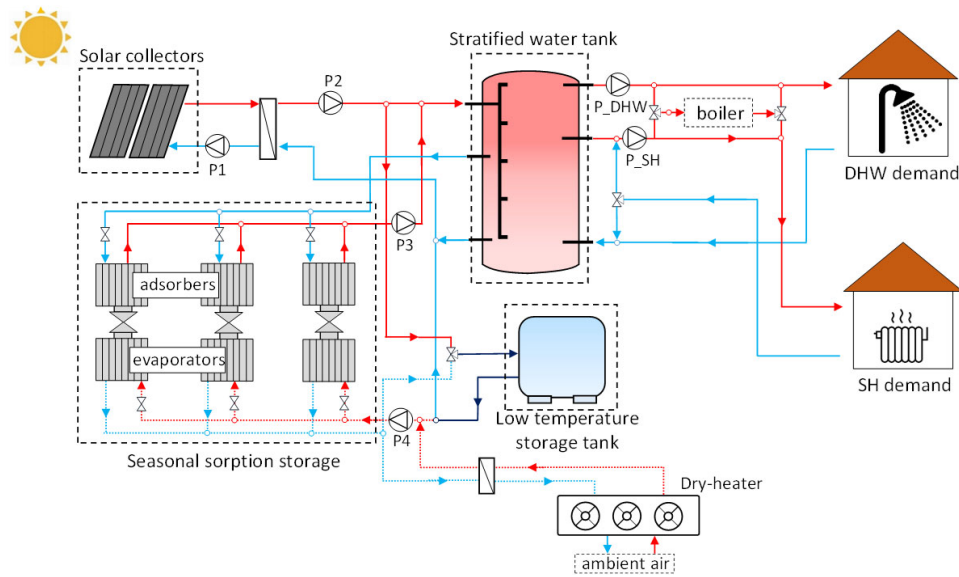


Figure 9. System configuration (connections represented for winter season)

The thermal resistance of building envelopes and SH temperature setpoints of the single-family house taken as reference were obtained from the deliverable report of SWS-Heating H2020 project [2]. The SH thermal demands were simulated using EnergyPlus [3].

The system was studied for three different locations: Paris, Munich and Stockholm, corresponding to Atlantic, Continental and Boreal biogeographical regions, respectively, according the European Environment Agency [4]. The simulations used meteorological data from Meteonorm [5] from Paris, Munich and Stockholm. The meteorological data consisted of average values of the period 1991-2010 with a time-step of 1 hour. Table 1 shows the climatic conditions for the different locations.

Table 3. Climatic conditions for the different locations

City	Annual average temperature [°C]	Annual E <sub>G</sub> [kWh/m <sup>3</sup> ]	Winter E <sub>G</sub> [kWh/m <sup>3</sup> ]
Paris	12.5	1069	309
Munich	9.4	1162	400
Stockholm	7.8	964	236

The system was simulated using a traditional rule-based control (RBC) strategy [6], whose control thresholds were optimized for each location by means of operational costs minimization. The authors used a cumulative reward function calculated based on the costs associated to run the system using different operational modes. The reward function also included a penalty in case not covering partially or totally the required thermal demand. Such reward ensures that the system tries to supply the largest amount of thermal demand considering that when both demands (SH and DHW) required the use of the gas boiler simultaneously, DHW demand was prioritized. Hence, it exists a scenario in which SH demand is not fully supplied. Both, the simulations and the control time step was set to 15 minutes, except for the stratified water tank whose simulation time step was set to 1 minute. The inputs to the control strategy were: solar irradiation, ambient temperature, state of the different system components and the DHW and SH demand profiles.

### 3. Results

The solar fractions of the solar-driven seasonal system under study were 44.5, 40.8 and 27.0 % in Paris, Munich, and Stockholm respectively, as presented in Figure . The highest solar fraction was reached for Paris due to its higher ratio between total annual solar irradiation (1069 kWh/m<sup>2</sup>) and thermal demand (6.4 MWh). Stockholm obtained the lowest solar fraction due to its lower annual solar resource (964 kWh/m<sup>2</sup>) and its higher thermal demand compared to Paris and Munich. Munich reached the highest amount of CO<sub>2</sub> emissions savings since the seasonal system delivered the highest amount of energy to the building in absolute terms (without back up boiler).

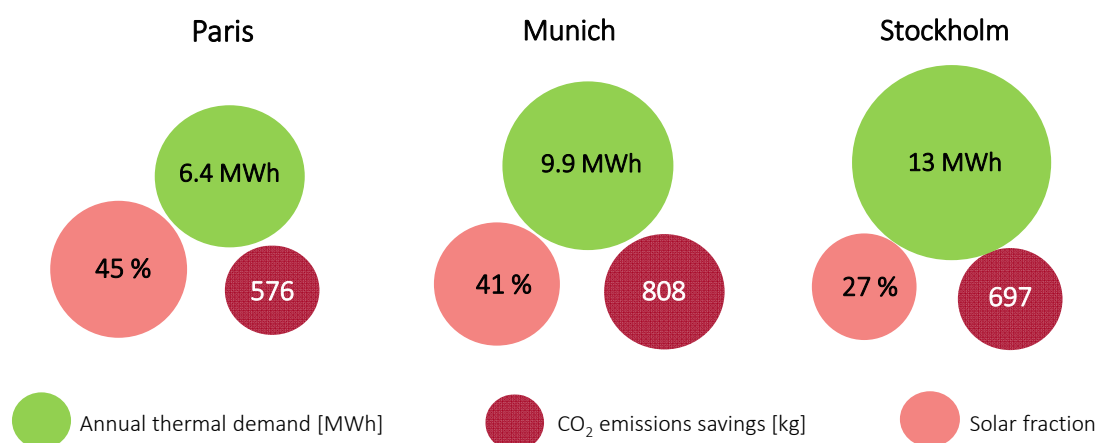


Figure 2. Performance indicators for the three studied locations

With respect to the sorption storage, the obtained energy densities were 106, 97 and 89 kWh/m<sup>3</sup> for Paris, Munich and Stockholm, respectively. These results were obtained considering a control scenario that minimized the operational costs for each location. Paris reached higher energy densities since the use of the dry heater (i.e. ambient heat) to discharge the sorption storage during winter allowed to employ a higher volume of the sorption storage and therefore increase the amount of stored energy.

The energy density of Stockholm may seem low. However, this energy density was calculated under a scenario that considered 100 % of the original volume of the sorption storage. Redesigning the size of the sorption storage based on the optimal size identified by the control optimization (78 % of the original size), the energy density increased up to 117 kWh/m<sup>3</sup>.

### 4. Conclusions

In this study, we analyzed a solar-driven seasonal sorption storage system under three different climates and optimal control. The results indicated that the system is suitable to operate in the three location in spite the low winter ambient temperatures. Energy densities around 117 kWh/m<sup>3</sup> are reached when the

sorption storage is redesigned based on the optimal volume that minimizes the operational costs. Hence, the system under study is feasible in the three studied climates from an operational and technical point of view.

### Acknowledgements

Alicia Crespo would like to acknowledge the financial support of the FI-SDUR grant from the AGAUR of the Generalitat de Catalunya and Secretaria d'Universitats i Recerca del Departament d'Empresa i Coneixement de la Generalitat de Catalunya. This project was funded by the European Union's Horizon 2020 Research and Innovation Programme under grant agreement No. 764025 (SWS-HEATING). The authors would like to thank the Catalan Government for the quality accreditation given to their research group GREiA (2021 SGR 01615). GREiA is a certified agent TECNIO in the category of technology developers from the Government of Catalonia.

### References

1. Frazzica, A.; Brancato, V.; Caprì, A.; Cannilla, C.; Gordeeva, L.G.; Aristov, Y.I. Development of “salt in porous matrix” composites based on LiCl for sorption thermal energy storage. *Energy* **2020**, *208*, 118338, doi:10.1016/j.energy.2020.118338.
2. University of Perugia *D5.3 Dynamic user-building interaction model predicting thermal-energy behaviour - Technical Report of SWS-heating project*; 2019;
3. Crawley, D.B.; Lawrie, L.K.; Winkelmann, F.C.; Buhl, W.F.; Huang, Y.J.; Pedersen, C.O.; Strand, R.K.; Liesen, R.J.; Fisher, D.E.; Witte, M.J.; et al. EnergyPlus: Creating a new-generation building energy simulation program. *Energy Build.* **2001**, *33*, 319–331, doi:https://doi.org/10.1016/S0378-7788(00)00114-6.
4. Biogeographic regions in Europe Available online: <https://www.eea.europa.eu/data-and-maps/figures/biogeographical-regions-in-europe-1>.
5. Meteonorm Software Available online: <https://meteonorm.com/en/> (accessed on Apr 1, 2022).
6. Crespo, A.; Fernández, C.; Vérez, D.; Tarragona, J.; Borri, E.; Frazzica, A.; Cabeza, L.F.; de Gracia, A. Thermal performance assessment and control optimization of a solar-driven seasonal sorption storage system for residential application - Accepted on 04/09/2022. *Energy* **2022**.

EUROTHERM2023-Y114

## Enhancement of the mechanical stability of $\text{Ca}(\text{OH})_2$ for application in thermochemical thermal energy storage

Hassan Agalit<sup>1</sup>, Yongliang Li<sup>1</sup>

<sup>1</sup>Birmingham Centre for Energy Storage (BCES) & School of Chemical Engineering, University of Birmingham, Birmingham B15 2TT, UK, Phone: +44 (0) 121 414 5135, e-mail: h.agalit@bham.ac.uk, y.li.1@bham.ac.uk

### Abstract

Thermochemical materials (TCMs) are considered a promising long-duration thermal energy storage technology to manage fluctuating renewables power generation. This thermal energy storage (TES) system, which is based on the use of reversible reaction, has a very high energy density and with almost zero loss of heat theoretically. Calcium hydroxide  $\text{Ca}(\text{OH})_2$  has very interesting heat storage properties but its mechanical strength is very questionable. In this paper, a novel porous composite  $\text{Ca}(\text{OH})_2$ /diatomite is synthesized which has superior enhanced mechanical stability compared to the pure material. An optimal synthesis process was designed using the Simultaneous Thermal Analysis (STA) apparatus. Furthermore, Scanning Electron Microscopy (SEM) coupled with Energy Dispersive Spectroscopy (EDS) has demonstrated that the obtained composite microstructure is porous and homogenous.

**Keywords:** Thermal Energy Storage, Thermochemical, Calcium Hydroxide.

### 1. Introduction

The growth in renewable energy sources has led to the need for long-duration energy storage (LDES) solutions to maintain a stable and flexible energy grid [1], [2]. Thermochemical heat storage (TCHS) is a promising candidate for LDES, with high energy densities, the potential for long-term storage, and low cost based on cheap raw materials. However, the technology is still in its early stages and faces challenges related to material stability and reactor design [3]. Cycles based on  $\text{CaO}/\text{Ca}(\text{OH})_2$  are of high interest for harvesting excess renewable energy [4]. The main challenge for these cycles is their reduced cyclic stability and poor mechanical stability, which are being addressed with the use of metal oxides and silicate binders [5], [6]. In this work, a novel porous composite of  $\text{CaO}/\text{diatomite}$  is formulated to enhance the mechanical stability of pure calcium oxide. Different formulations are synthesized to demonstrate the stabilizing effect of diatomite on  $\text{CaO}$ . Simultaneous Thermal Analysis (STA) was used to design an optimal heating program. Moreover, Scanning Electron Microscopy (SEM) was used to investigate the microstructure of the synthesized materials. Finally, Energy Dispersive Spectroscopy (EDS) was used to generate the chemical dispersion of each pellets in order to prove the homogeneity of their microstructure.

### 2. Materials and method

Calcium hydroxide  $\text{Ca}(\text{OH})_2$  was used as the precursor for  $\text{CaO}$ , and Ethyl Cellulose (EC) was used as the polymeric binder to generate the microporosity. Diatomite (Di) was used as the matrix for enhancing the mechanical stability of  $\text{CaO}$ . As illustrated in Simultaneous Thermal Analysis (STA) was used to define the optimal calcination temperature. Scanning Electron Microscopy (SEM) coupled with Energy Dispersive Spectroscopy (EDS) were used to investigate the synthesized pellets microstructure and chemical dispersion.

Table 4, four formulations were synthesized to investigate the stabilizing effect of diatomite on pure calcium oxide. For each formulation containing  $\text{CaO}$ , calcium hydroxide was calcined firstly at 500 °C before mixing it with the other materials in adequate proportions.

The powder was mixed respecting the different proportions mentioned in Simultaneous Thermal Analysis (STA) was used to define the optimal calcination temperature. Scanning Electron Microscopy (SEM) coupled with Energy Dispersive Spectroscopy (EDS) were used to investigate the synthesized pellets microstructure and chemical dispersion.

Table 4, then they were compacted into pellets of a diameter of 10 mm. Finally, the obtained green bodies were calcined firstly at 450 °C to eliminate the polymeric binder (EC), then flowed by two isothermals at 800 °C and 1000 °C consecutively to sinter the composite material.

Simultaneous Thermal Analysis (STA) was used to define the optimal calcination temperature. Scanning Electron Microscopy (SEM) coupled with Energy Dispersive Spectroscopy (EDS) were used to investigate the synthesized pellets microstructure and chemical dispersion.

Table 4. Formulations of the investigated materials.

Samples	CaO/EC	CaO/Di	CaO/Di/EC	Di
Formulation (wt. %)	70:30	50:50	35:35:30	100

### 3. Results and discussion

#### 3.1. Thermal analysis

As illustrated in Figure 10, the CaO/EC (wt. % 70:30) powder mixture loses most of its polymeric binder (around 18%) between 200 °C and 368 °C. Followed by a small loss of mass between 368 °C and 450 °C which might be related to the remaining water in the Ca(OH)<sub>2</sub>. Finally, the last stage of mass losses (around 14%) is between 450 °C and 700 °C, which is related to the elimination of any remaining EC. Consequently, based on this thermal analysis the previous heating program was proposed to eliminate all the carbonaceous matters using two isothermals at 400 °C and 800 °C consecutively. Then, the last isothermal at 1000 °C was used to sinter the microstructure of the different materials.

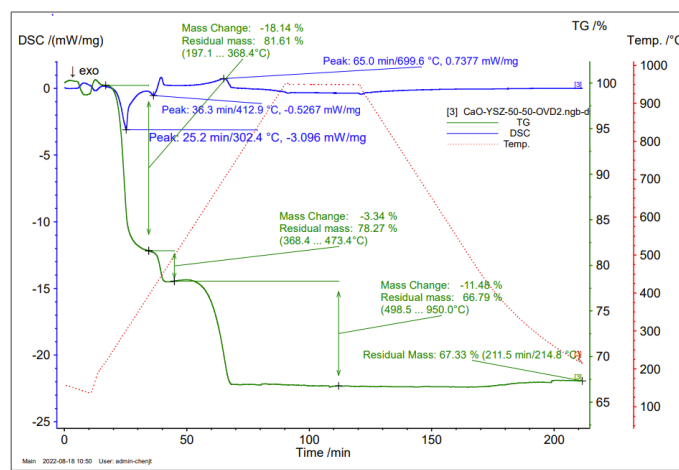


Figure 10. Simultaneous Thermal Analysis (STA) of CaO/EC mixture (wt. % 70:30).

#### 3.2. Microstructure and chemical dispersion

The microstructures of the different synthesized materials are illustrated in Figure 11. All four pellets have a porous microstructure and the average pore sizes fall in the range of 1-2 μm. In Figure 11 (b), CaO is homogeneously distributed in the diatomite matrix as can be seen from the chemical mapping. The microstructures in Figure 11 (b) and (d) seem to be similar which means that the inclusion of EC

does not have any evident effect on increasing the porosity of the composite material as it was expected. This might be explained by the fact that diatomite is already very porous as shown in Figure 11 (c). Consequently, it can be concluded that no polymeric binder is needed to produce the microporosity as the CaO is impregnated in the micropores of diatomite.

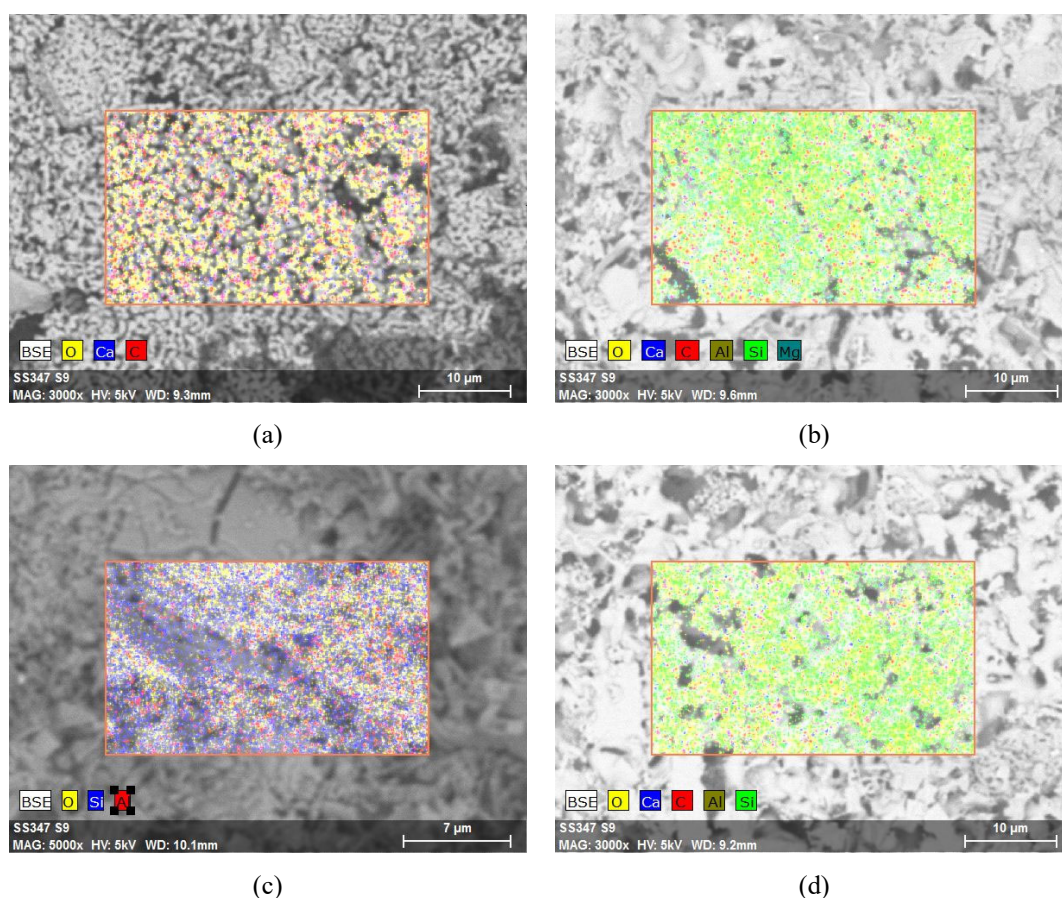


Figure 11. SEM/EDS analysis of (a) CaO/EC, (b) CaO/Di, (c) Di (d) CaO/Di/EC

### 3.3. Stability under ambient conditions

As far as it concerns the apparent stability of the produced four pellets, the CaO/EC was very fragile after the heating program and it disintegrated after being left in an ambient atmosphere. This is due to the absorption of the water in the surrounding humid air. On the contrary, all the pellets incorporating diatomite matrix have much superior mechanical stability even after being left in ambient conditions. These promising results show that the CaO was well-impregnated inside the diatomite matrix which acted as a shield against the infiltration of ambient air. Furthermore, diatomite has enhanced significantly the mechanical stability of  $\text{Ca}(\text{OH})_2$ .

## 4. Conclusions

In this work, the effect of diatomite on the mechanical stability of  $\text{Ca}(\text{OH})_2$  was investigated through the synthesis of four formulations via an optimal heating program. It was demonstrated that diatomite has significantly improved the mechanical stability of the CaO under ambient conditions when compared to the reference material CaO/EC, which was disintegrated into powder after several hours. Another interesting finding was that diatomite can act as a supporting matrix as well as a microporosity template. Hence, in that case, no polymeric binder is needed.

These promising results should be investigated further under hydration/dehydration conditions at higher temperatures, in order to check the stability of the proposed composite materials in those conditions.

## Acknowledgements

The research leading to these results has received funding from the Engineering and Physical Sciences Research Council (EPSRC) under grant No. [EP/V041665/1].

## References

- [1] I. Irena, “Renewable energy technologies: Cost analysis series,” Concentrating solar power, 2012.
- [2] “Net-zero power: Long-duration energy storage for a renewable grid | McKinsey.” <https://www.mckinsey.com/capabilities/sustainability/our-insights/net-zero-power-long-duration-energy-storage-for-a-renewable-grid> (accessed Nov. 15, 2022).
- [3] A. J. Carrillo, J. González-Aguilar, M. Romero, and J. M. Coronado, “Solar energy on demand: a review on high temperature thermochemical heat storage systems and materials,” *Chemical reviews*, vol. 119, no. 7, pp. 4777–4816, 2019.
- [4] K. Wang, T. Yan, R. Li, and W. Pan, “A review for Ca (OH) 2/CaO thermochemical energy storage systems,” *Journal of Energy Storage*, vol. 50, p. 104612, 2022.
- [5] Y. A. Criado, M. Alonso, and J. C. Abanades, “Enhancement of a CaO/Ca (OH) 2 based material for thermochemical energy storage,” *Solar Energy*, vol. 135, pp. 800–809, 2016.
- [6] M. Gigantino, S. Sas Brunser, and A. Steinfeld, “High-temperature thermochemical heat storage via the CuO/Cu2O redox cycle: From material synthesis to packed-bed reactor engineering and cyclic operation,” *Energy & Fuels*, vol. 34, no. 12, pp. 16772–16782, 2020.



EUROTHERM2023-T116

## Thermodynamic analysis and optimization of a liquid air energy storage system integrated with a high-temperature thermal energy store

Yixuan Huang<sup>\*</sup>, Tongtong Zhang, Yulong Ding<sup>\*\*</sup>

Birmingham Centre for Energy Storage & School of Chemical Engineering, University of Birmingham, Birmingham, B15 2TT, UK, e-mail: Y Huang: yxh058@student.bham.ac.uk; Y Ding: Y.Ding@bham.ac.uk

### Abstract

Liquid air energy storage (LAES) technology can use off-peak electricity or renewable energy to produce liquid air (i.e. charging process) and convert the stored cryogenic energy back to high-quality electricity during peak time (i.e. discharging process). Compared with other large-scale energy storage technologies, such as compressed air energy storage and pumped hydro energy storage, the LAES has some outstanding advantages, including no geological constraint, high energy density and its potential for multi-energy-vector services. However, the round-trip efficiency of the stand-alone LAES is usually below 55%, or even 50%. To improve the performance of the LAES further, we propose to integrate the LAES system with a high-temperature thermal energy store (HTES) which can be charged via direct resistive heating. The stored heat in the HTES is released to improve the air temperature before expansion during the LAES discharging process for power generation enhancement. In this way, the round-trip efficiency of the LAES system can be improved by ~30%.

**Keywords:** Liquid air energy storage, high-temperature thermal energy storage, thermodynamic analysis, efficiency enhancement

### 1. Introduction

As known, as an energy storage technology, the LAES system consists of charging and discharging processes. During the charging process, the purified air is liquified by consuming off-peak electricity or renewable energy and is finally stored in a liquid air tank at a temperature of ~-190 °C and near ambient pressure. This liquefaction process involves air compression, and the compression heat is usually recovered and stored in a thermal storage medium, such as thermal oil, molten salt or pressurized water. During the discharging process, the stored liquid air is pumped to a high pressure, firstly evaporated by ambient heat and then superheated by the stored compression heat, before finally expanding in air turbines for power generation.

Currently, RTE is the most commonly used indicator to assess the performance of an energy storage technology, which is defined as the ratio of the work output during discharging to the work input during charging over a complete cycle [1]. The RTE of a standalone LAES system is around 50-60%, which is a disadvantage compared to other energy storage technologies. Therefore, much effort has been made in recent years to improve the RTE of the LAES. Examples for such efforts include the integration of LAES system with external heat sources such as waste industrial heat and solar heat, and external cold sources such as the LNG (liquified natural gas) cold. Peng et al. [2] proposed to recover and store the cold energy released from the LNG regasification process, and reutilise this high-grade cold energy to increase the liquid air yield of the air liquefaction process of the LAES. The RTE of this hybrid system can be significantly improved to 78~89%. Cetin et al. [3] proposed the integration of the LAES with a single-flash geothermal power plant, where the geothermal water is used in the LAES discharging process to superheat the air and the compression heat recovery is removed from the LAES charging process. The hybrid system can achieve an RTE of 46.7%. In addition, the heat from the nuclear power plant (NPP) is also proposed to be reused in the LAES system for the RTE enhancement for the LAES

and the peak-shaving capacity improvement for the NPP [4]. Although the RTE of the LAES can be enhanced by these integration methods, the operational flexibility of LAES is reduced.

Due to the high operational flexibility, the standalone LAES is still the one with the most promising applications. To improve the RTE of the standalone LAES, the recovery, storage, and reutilization of the compression heat is one of the keys. In previous studies, a two-tank thermal store is the most used compression heat recovery design in the LAES system, with thermal oil (<360°C), molten salt (220°C~600°C), and pressurised water (<180-200°C) being the three most studied heat transfer fluids/thermal storage mediums [5–7]. Given the cost, pressurised water is the most suitable, however, the maximum temperature of the recovered compression heat is limited and hence the RTE of the LAES. Although the temperature range of the thermal oil is optimal for compression heat recovery, the short lifespan of the thermal oil reduces its feasibility. Therefore, to solve this compression heat storage problem for the standalone LAES system, we propose a LAES system that includes a high-temperature thermal energy store (denoted as LAES-HTES). In this LAES-HTES, during the charging process, the LAES uses off-peak/renewable electricity to produce liquid air while generating high-temperature heat (300-1000°C) by direct resistive heating. This heat can be stored in the HTES, which can be a fluidised bed or some other low-cost method of sensible heat storage. During the discharging process, the stored heat can be used to superheat the air before expansion, which can improve the power generation significantly. At the same time, the compression heat (<150°C) recovered from the LAES charging process can be used directly for heat supply to end-users (e.g., space heating).

## 2. System description

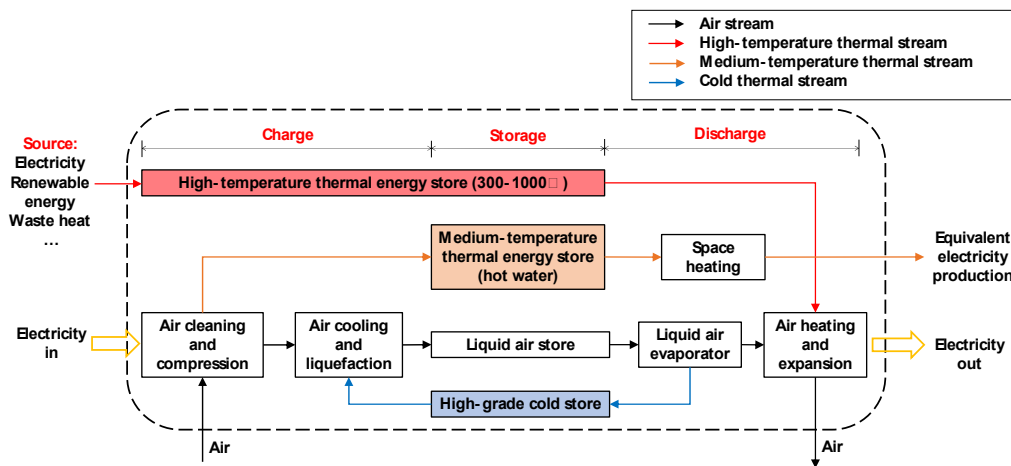


Fig. 1. The basic working principle for LAES-HTES system

Fig.1 shows the basic principle for the proposed LAES-HTES system. Air is compressed and liquefied during the charging process and the compression heat is stored using pressurized water (max. 150°C). Meanwhile, the HTES is charged as well to a relatively high temperature (300~1000°C). During discharging process, the stored liquid air is used for power generation as the normal LAES system. The difference is that the heat used to superheat the air before expansion comes from the HTES and not from the stored heat of compression. Instead, the stored compression heat is used for direct space heating.

## 3. System performance indexes

According to the system description above, the electricity is consumed by the air liquefaction process and the resistive heating process to generate liquid air and the high-temperature heat during charging. And the liquid air and the heat are converted back to electricity during the discharging process. Therefore, in this study, the electrical round trip efficiency (i.e.,  $eRTE$ ) is defined as the ratio of total electricity generated during discharging to the total electricity consumed during charging:

$$eRTE = \frac{W_{turbine} - W_{cryo-pump}}{W_{compressor} + W_{HTES} - W_{cryo-turbine} - W_{turbo-expander}} \quad (1)$$

For this LAES-HTES system, the compression heat ( $Q_{COM}$ ) is used for space heating. Such amount of heat supply can also be provided by a heat pump by consuming electricity. Thus, in this study, to assess the value of the stored compression heat, it has been converted into the equivalent electricity consumption ( $W_{eqv}$ ) of the heat pump given an average COP of 3.06.

$$W_{eqv} = \frac{Q_{com}}{COP} \quad (2)$$

To evaluate the overall performance of the LAES-HTES system, the nominal-electrical round trip efficiency ( $neRTE$ ) is defined as the ratio of the sum of actual electricity generation and the equivalent electricity generation from the space heating during discharging to the total power consumption during charging.

$$neRTE = \frac{W_{turbine} - W_{cryo-pump} + W_{eqv}}{W_{compressor} + W_{HTES} - W_{cryo-turbine} - W_{turbo-expander}} \quad (3)$$

#### 4. Results and discussion

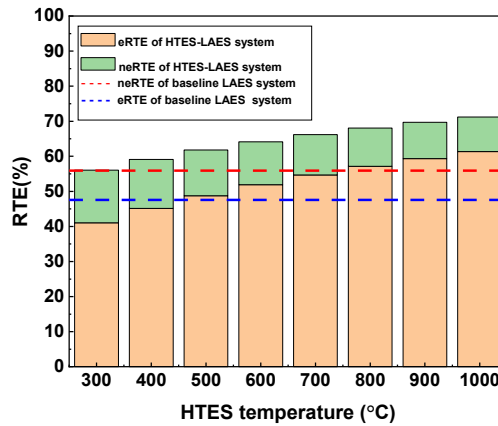


Fig. 2.  $eRTEs$  and  $neRTEs$  of the baseline LAES and the LAES-HTES at different HTES temperatures

In this paper, the baseline LAES system and the LAES-HTES system are thermodynamically analysed and compared. Fig.2 shows the RTEs ( $eRTEs$  and  $neRTEs$ ) of the baseline LAES system and the LAES-HTES system under different HTES storage temperature. In the LAES-HTES system, the turbine inlet temperature, which is determined by the HTES temperature, can significantly influence the power output and thus the RTE. As shown in Fig.2, both the  $eRTE$  and  $neRTE$  of the LAES-HTES system increase as the HTES temperature increases. One can also see that, when the HTES temperature is above 500°C, the  $eRTE$  of the LAES-HTES system is higher than that of the baseline LAES. However, the  $neRTE$  of the LAES-HTES system is always higher than that of the baseline LAES system.

The compression stage can also affect the operating performance of LAES-HTES system. Fig. 3 (a) shows that the  $eRTE$  of the LAES-HTES system continuously increases as the number of compression stages increases. However, the  $neRTE$  of the LAES-HTES system comes with a maximum value when a four-stage compression configuration is utilized.

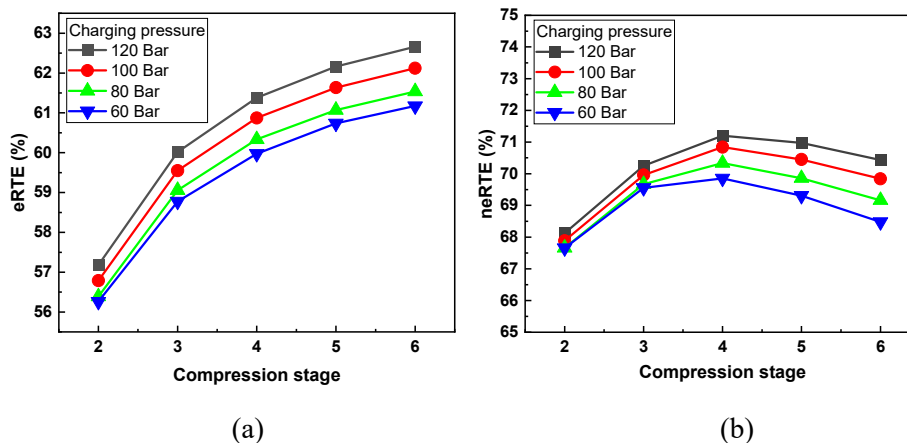


Fig. 3. Effect of compression stage on RTE of LAES-HTES system

## 5. Conclusion

In this paper, a LAES system combined with a HTES has been proposed. This proposed LAES-HTES system can significantly improve the working performance compared with the baseline LAES system. The eRTE and neRTE of the baseline system (charging and discharging at 120 bar) are 47.6% and 55.9%, respectively. By integration with HTES, both the eRTE and neRTE of the LAES system can be improved by ~30%, reaching 62.7% and 71.2%, respectively under the same operating parameters (HTES temperature at 1000 °C).

## Reference

- [1] Vecchi A, Li Y, Ding Y, Mancarella P, Sciacovelli A. Liquid air energy storage (LAES): A review on technology state-of-the-art, integration pathways and future perspectives. *Adv Appl Energy* 2021;3. <https://doi.org/10.1016/j.adapen.2021.100047>.
- [2] Peng X, She X, Li C, Luo Y, Zhang T, Li Y, et al. Liquid air energy storage flexibly coupled with LNG regasification for improving air liquefaction. *Appl Energy* 2019;250:1190–201. <https://doi.org/10.1016/J.APENERGY.2019.05.040>.
- [3] Cetin TH, Kanoglu M, Yanikomer N. Cryogenic energy storage powered by geothermal energy. *Geothermics* 2019;77:34–40. <https://doi.org/10.1016/J.GEOTHERMICS.2018.08.005>.
- [4] Li Y, Cao H, Wang S, Jin Y, Li D, Wang X, et al. Load shifting of nuclear power plants using cryogenic energy storage technology. *Appl Energy* 2014;113:1710–6. <https://doi.org/10.1016/J.APENERGY.2013.08.077>.
- [5] Ryu JY, Alford A, Lewis G, Ding Y, Li Y, Ahmad A, et al. A novel liquid air energy storage system using a combination of sensible and latent heat storage. *Appl Therm Eng* 2022;203:117890. <https://doi.org/10.1016/J.APPLTHERMALENG.2021.117890>.
- [6] Guo H, Xu Y, Chen H, Zhou X. Thermodynamic characteristics of a novel supercritical compressed air energy storage system. *Energy Convers Manag* 2016;115:167–77. <https://doi.org/10.1016/J.ENCONMAN.2016.01.051>.
- [7] Zhang T, Zhang X, Xue X, Wang G, Mei S. Thermodynamic analysis of a hybrid power system combining Kalina cycle with liquid air energy storage. *Entropy* 2019;21. <https://doi.org/10.3390/E21030220>.

EUROTHERM2023-P117

## Enthalpy determination of phase change material objects by mixing calorimeter

Rajkumar Yadav<sup>1</sup>, Nidhi Agrawal<sup>1</sup>, Harald Mehling<sup>2</sup>, Samit Jain<sup>1</sup>

<sup>1</sup>Pluss Advanced Technologies Ltd., B-205, Pioneer Urban Square, Sector 62, Gurugram 122101, India, Phone: +91-124-4309490-2, Fax: +91-124-4824214, e-mail: rajkumar.yadav@pluss.co.in

<sup>2</sup>Consultant, Weingartenstr, 37, 9702 Würzburg, Germany, Phone: +49 (0)152 03806387, e-mail: harald.mehling@gmail.com

### Abstract

Phase change materials (PCMs) store heat/cold by changing phase in a narrow temperature range and with high storage density. They are therefore used in many applications for heat/ cold storage, also called thermal energy storage (TES). Many applications use the PCMs encapsulated in pouches made of polymeric film or in solid containers made of plastic or metals. Regarding characterization, encapsulated PCM e.g., a pouch is a PCM object that has a storage capacity per object. The heat stored by a PCM object could be calculated from the amount of PCM contained in it, but more reliable is a direct measurement as the PCM could change with time by phase separation, or show less supercooling due to larger mass. The heat stored in different types of PCM objects was determined directly using the mixing calorimeter method. The PCMs are water (to test the setups), organic PCMs of 46 °C and 65 °C temperatures, and inorganic PCMs of 48 °C and 72 °C, and the encapsulations are stainless steel balls and HDPE tabs.

**Keywords:** Phase Change Material (PCM), PCM Object, Thermal Energy Storage (TES), Mixing Calorimeter

### 1. Introduction

Thermal energy storage, often also called heat and cold storage depending on the application, plays a crucial role in the energy system and many common situations. PCMs are used today in a wide range of applications: in buildings for space heating and cooling as well as to prepare domestic hot water, in logistics, specifically the cold chain, for heating or cooling of the human body, even in medical applications, in mobility, in electronics, as well as industrial processes (Mehling et al., 2022).


The capacity to store heat is the main property of macro-encapsulated PCM. It can simply be calculated from the material properties of the PCM and its amount, and respectively the same for the encapsulation material. However, the properties of the PCM could change with the amount of PCM encapsulated, specifically the degree of supercooling, they could change with time, e.g., by phase separation, or its amount could change by leakage. Further on the PCM, and with it its properties, might not be known at all if macro-encapsulated PCM is bought. Direct measurement of the stored heat on macro-encapsulated PCM is thus more reliable than simple calculation, sometimes even the only option. Doing direct measurements is part of quality control, and crucial when buying.

Here, we describe the setup of a mixing calorimeter for measurements on macro-encapsulated PCM, results on measurements on four different PCMs in two different encapsulations, and a comparison of the results with calculations from measurements by the T-history/3-layer calorimeter and the differential scanning calorimeter (DSC).

## 2. Materials/Samples

Altogether, 4 different PCMs were encapsulated in 2 different encapsulations; this means in total 8 samples (all PCMs and encapsulations are commercial products of Pluss Advanced Technologies). The four PCMs investigated are the two inorganic, hydrated salt (HS) PCMs HS48 and HS72, and the two organic mixture (OM) PCMs OM48 and OM65. The two macro-encapsulations are ThermoTab600 and Stainless Steel (SS) ball. The SS ball encapsulation is shown in Figure 1a. It has a diameter of 80 mm, a weight of 132 g (empty), and a volume of 235 ml (internal). The ThermoTab600 is shown in Figure 1b. It has dimensions of 190mm · 120mm · 35mm, a weight of 114 g, and a volume of 548 ml. *savE* and other trademarks are the property of respective companies.

PCM	Mass (g)
<i>savE</i> OM 46	208
<i>savE</i> OM 65	194
<i>savE</i> HS 48	270
<i>savE</i> HS 72	327



PCM	Mass (g)
<i>savE</i> OM 46	446
<i>savE</i> OM 65	451
<i>savE</i> HS 48	640
<i>savE</i> HS 72	824




Figure 1. PCM objects; SS ball (a), and ThermoTab600 (b)

## 3. Experimental method

### 3.1. Method

In a mixing calorimeter, the sample exchanges heat with a reference medium, commonly a liquid. The heat stored by the sample between the initial and final temperature is calculated from the same for the reference liquid, for which also its amount and specific heat capacity must be known (Walcher, 1985, Zheng et al., 2013). Ideally, a measurement setup is an adiabatic environment; for a real setup, a well-insulated container can be used (Figure 2a).

For preconditioning, a PCM object was put in a water bath, set at a temperature of a minimum of 10 °C higher than the phase change temperature ( $T_{PC}$ ) of the PCM for the freezing enthalpy determination, and lower for the melting enthalpy determination. A measured quantity of water as a reference liquid was put in the insulated box. The amount of the reference medium, water, was taken as approximately 10 times the weight of the PCM object to result in well-detectable temperature changes. Two ThermoTab600 and four SS Balls PCM objects were used in the experiments to keep the ratio of reference to PCM at approximately 10. Two temperature sensors were put in the reference medium, diagonally opposite in corners. The starting temperature of the medium ( $T_{medium}$ ) was selected 25 °C higher and lower than the  $T_{PC}$  in the case of melting and freezing enthalpy analysis, respectively. Ambient temperature ( $T_{ambient}$ ) was selected 20 °C lower than  $T_{medium}$ . The temperature sensors were connected to the datalogger. Then, stirring the reference medium, water, in the box with the pump was started. Finally, the PCM objects were immersed in the medium to allow heat exchange. The experiment was completed when the thermal equilibrium between the medium and the PCM object was achieved in the box i.e.,  $T_{object}$  became equal to  $T_{medium}$ , an equilibrium temperature ( $T_{equil}$ ).  $T_{object}$  is the starting temperature of the PCM objects.

Water was tested first as a PCM sample in the mixing calorimeter. The trials were performed for 2 hours. The temperature of the medium was recorded as an output from the set-up. Figure 2b shows the temperature profiles of the medium and the PCM objects.

The enthalpy of the PCM was calculated based on the energy balance between the object tested, the reference medium, and a correction by heat loss to the ambient.

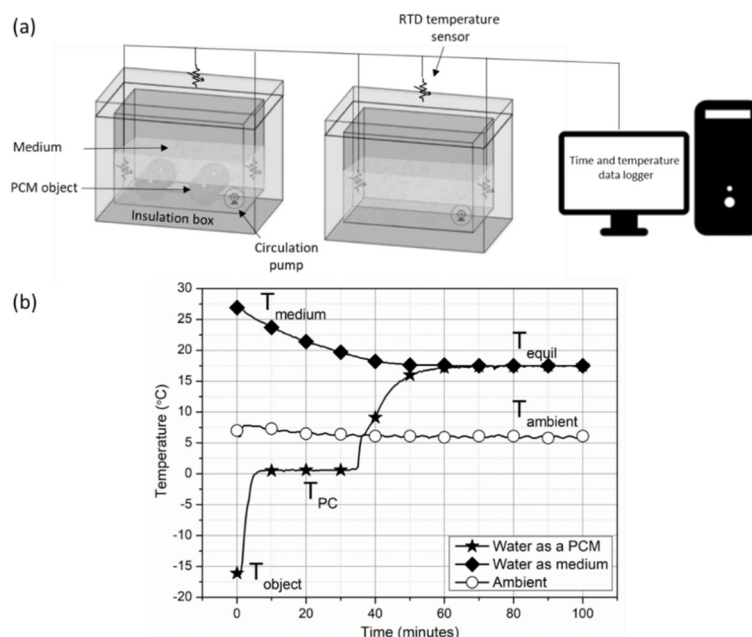


Figure 2. Schematic diagram of the mixing calorimeter set-up (a), and an output graph from a measurement (b) where water was also the PCM in the encapsulation (as indicated by  $T_{PC}$  at about  $0^{\circ}\text{C}$ )

### 3.2. Heat stored by encapsulated PCM, determined by the mixing calorimeter

Table 1 details the enthalpy ( $Q_{\text{object}}$ ) obtained for the PCM objects in a temperature range from  $T_{\text{object}}$  at the start of the measurement to  $T_{\text{equil}}$  at the end (Figure 2b).

Table 1. Enthalpy data of the 4 PCMs in 2 encapsulations, as determined by the mixing calorimeter

PCM object		$T_{\text{object}} (^{\circ}\text{C})$	$T_{\text{equil}} (^{\circ}\text{C})$	$Q_{\text{object}} (\text{kJ})$
SS Ball (4 numbers)	OM46	70.0	38.0	226
	OM65	90.0	40.5	213
	HS48	67.0	49.0	246
	HS72	90.0	41.3	354
ThermoTab600 (2 numbers)	OM46	70.0	33.4	241
	OM65	90.0	35.5	311
	HS48	73.5	38.0	366
	HS72	90.0	42.0	432

Hydrated salts (HS) based PCMs showed comparatively higher enthalpy than organic PCMs. The higher enthalpy of HS PCMs can be attributed largely to their higher volumetric density as compared to organic ones.  $T_{\text{object}}$  and  $T_{\text{equil}}$  can be adjusted according to the requirement of the temperature range of the PCM object used in a TES application. For a cooling measurement,  $T_{\text{object}}$  should be kept above the phase change temperature of the PCM ( $T_{PC}$ ) used in the PCM object and  $T_{\text{equil}}$  should be a lower value than  $T_{PC}$ , for a heating measurement reverse. This will allow a better phase change of the PCM inside the PCM object.

Enthalpy profiles of the four PCMs from DSC, 3LC measurement, and mixing calorimeter ( $Q_{PCM}$ ) are shown in Figure 3; compared with the enthalpy difference of the PCM alone as determined from the measurement on the encapsulated PCM, taking into account the heat stored in the encapsulation. The results of all methods are given for the PCMs cooling/solidification phase. The PCM object tests for HS48 in SS Ball encapsulations were repeated three times, which showed a variation of 3%. The variation in the repeatability is minimal and is considered highly precise keeping the experimental

accuracy in mind. Generally, the enthalpy difference as predicted by the mixing calorimeter method is in well agreement with the enthalpy profiles of the DSC and 3LC methods.

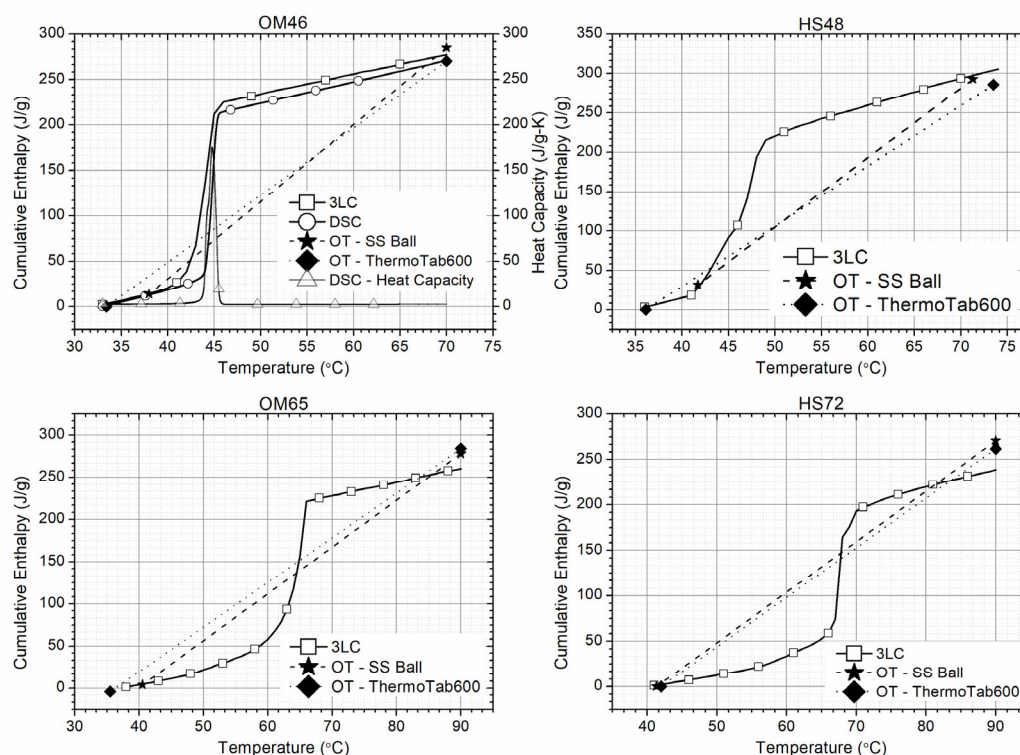


Figure 3. Enthalpy profiles of PCMs only from 3LC and enthalpy differences from mixing calorimeter

#### 4. Conclusions

The enthalpy of PCM objects was determined by the mixing calorimeter method. The method was successfully tested on 4 PCMs, from two main types of PCMs; organic and inorganic. The enthalpy calculated from the mixing calorimeter matched the value from the DSC and 3LC measurements, confirming a reliable enthalpy measurement from the method. The method determines the enthalpy of a PCM object in a temperature range. The temperature range can be selected as per the object’s working temperature in a TES application. The study proved that the method is applicable across PCM types, temperatures, and encapsulations geometries. The method duration was much less as compared to the T-history/3LC method.

#### Acknowledgments

The authors are thankful to Pluss Advanced Technologies Ltd., Gurugram, India for the research facilities.

#### References

Mehling, H., Brütting, M., Haussmann, T. 2022. PCM products and their fields of application - An overview of the state in 2020/2021. *Journal of Energy Storage* (51)

Walcher, W., 1985. *Praktikum der Physik*. Teubner, 1985, 5th ed.

Zheng, Y., Zhao, W., Sabol, J.C., Tuzla, K., Neti, S., Oztekin, A., Chen, J.C., 2013. Encapsulated phase change materials for energy storage – Characterization by calorimetry. *Solar Energy* 87 (2013) 117–126



EUROTHERM2023-Y118

## Enhancing the Efficiency of Solar District Heating with Seasonal Thermal Energy Storage Systems through Machine Learning Controller

Youssef Elomari<sup>1</sup>, Carles Mateu<sup>1,2</sup>, Marc Marín-Genescà<sup>1</sup>, Manel Vallès<sup>1</sup>, Dieter Boer<sup>1,\*</sup><sup>1</sup> Departament d'Enginyeria Mecànica, Universitat Rovira i Virgili, Av. Paisos Catalans 26, 43007 Tarragona, Spain<sup>2</sup> GREiA Research Group, Department of Computer Science and Industrial Engineering, University of Lleida, Jaume II, 69, 25001 Lleida, Spain

\* Correspondence: dieter.boer@urv.cat

### Abstract

This study presents a deep reinforcement learning control strategy for enhancing the efficiency of solar district heating systems (SDHS) with thermal energy storage. The application of the methodological approach has been applied to an SDHS in Madrid (Spain) to provide for the heating demands of a neighborhood that consists of 280 apartments in order to more effectively illustrate the abilities of the proposed control strategy. The present work focuses on the development of a co-simulation framework based on TRNSYS (transient system simulation) and Python for offline training of a control strategy based on deep reinforcement learning algorithms for a smart agent that will control the integrated heat pump into SDHS with a seasonal storage system. The work will consider the life cycle cost analysis for the techno-economic evaluation of the proposed control strategy.

**Keywords:** solar district heating systems, thermal energy storage, heat pump, deep reinforcement learning, life cycle cost analysis

### 1. Introduction

District energy systems provide a variety of alternatives for incorporating energy storage and renewable energy sources into residential and commercial buildings [1]. Among these, solar communities with seasonal thermal energy storage [2] and solar thermal systems [3] can support the development of fourth and fifth-generation district heating systems [4], [5]. Systems for district heating powered by solar energy help in the deployment of large-scale solar energy-based solutions. In fact, several successful large-scale solar district heating systems (SDHSs) are currently in use in Austria, Canada, China, Germany [6], and Denmark [7]. Tian et al. [7] highlighted two successful instances of big SDHSs. Even though the modeling and design of these systems have been thoroughly studied recently [8], [9], further study is still necessary to develop advanced control techniques for solar district heating systems.

Techniques for controlling HVAC (heating, ventilation, and air conditioning) are complex due to the way the system's components interact with one another and with the thermal dynamics of buildings. The continuous adjustment of the heating or cooling system while maintaining the comfort levels set by the occupants is one technique to reduce the amount of energy used for space conditioning. The traditional rule-based control (RBC) formulations are often implemented as simple hysteresis loops, which reheat or cool the building each time a temperature threshold is reached.

Model predictive control (MPC) enhances the control method by incorporating the ability to use the predictions of external factors such as weather, electricity price, etc. This leads to a wider range and more efficient control compared to RBC. The primary aim is to the control building temperature, with cost optimization being a secondary goal. While MPC outperforms RBC regarding its operation capability, it complicates the system and requires the availability of a model that accounts for the system dynamics. Due to the complexity of building thermal dynamics and heterogeneous environment

disturbances, the classical rule-based and model-based approaches are frequently ineffective in practice [10].

Another control method is reinforcement learning (RL) which is a model-free approach where the agent learns the optimal action to take by "trial and error" without the need for previous knowledge of the system or process. Model-free methods can operate without a model of the environment [11]. RL techniques can learn by interacting with its environment and do not require any supervision. In recent years and within many fields, RL has become a strong alternative to MPC. The fundamental idea behind RL is that the optimal behavior or action is encouraged by way of a positive reward, while the least desirable action is punished by a negative reward [12], [13]. The drawbacks of conventional RL can be overcome by deep reinforcement learning (DRL), which enhances RL with deep neural networks to approximate the value function and policy function when those are hard to model due to the dimensionality of the problem. Therefore, the DRL approach is more suitable and flexible in terms of control strategies than traditional control approaches. DRL has been utilized extensively in both the business and academic fields, such as, in robotics [14], gaming [15], industrial systems [16], and autonomous vehicles [17].

The present work focuses on the development of a co-simulation framework based on TRNSYS (transient system simulation) and Python for offline training of a control strategy based on deep reinforcement learning algorithms for a smart agent that will control the integrated heat pump and seasonal storage system of a SDHS. The work will consider the life cycle cost analysis for the technical economic evaluation of the proposed control strategy.

## 2. Materials and method

This section describes the system's details and the methodology used for system modeling and control.

### 2.1. Energy system description

An overview of the analyzed systems is presented in Figure 1. The main components of the system are COL, the domestic hot water storage tank (DHWT), a half-buried sensible seasonal storage tank (SST), an auxiliary natural gas heater (AUX), and a water-to-water heat pump unit (HP). This SDHS model was designed and based on the system proposed by Abokersh et al. [18] and Tulus et al. [19].

### 2.2. Co-simulation TRNSYS-Python framework

TRNSYS program is a tool, for simulating an energy system's dynamic behavior. In the simulation studio, TRNSYS's components are linked graphically to solve algebraic and differential equations. The TRNSYS simulation environment's dynamic nature helps to introduce the SHDS model in a more realistic manner. This software does, however, have significant limitations when it comes to the development and optimization of HVAC system control. Some intelligent control algorithms, such as DRL-based control approaches, are inconvenient and difficult to use directly in the built-in software [20].

In order to address this issue, a co-simulation testbed with a SDHS TRNSYS model and DRL-based control approach has been built in order to enable dynamic data transfer and interaction between these two systems as depicted in Figure 2b. As DRL-based training requires a large amount of training data, (i.e. of simulations), those simulations would have to be done in parallel to maximize computational resources usage and to reduce the required time for the experimentation. In order to control such simulations and to be able to train the DRL control software, they have been developed, following the de facto standard for DRL training, as a Gym environment [21].

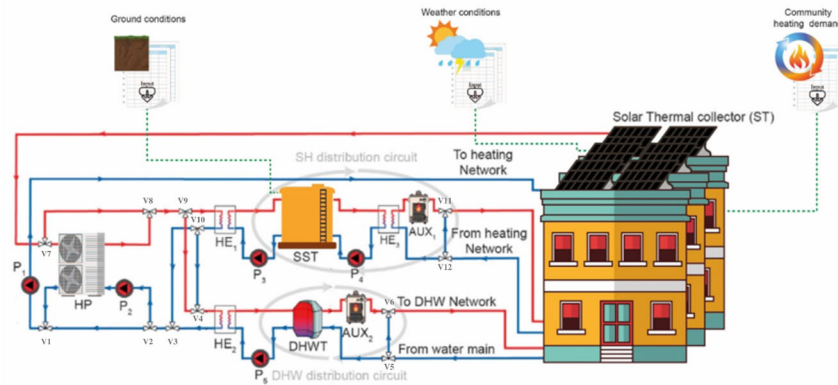


Figure 12. An overview of the HP with SDHS integration's design

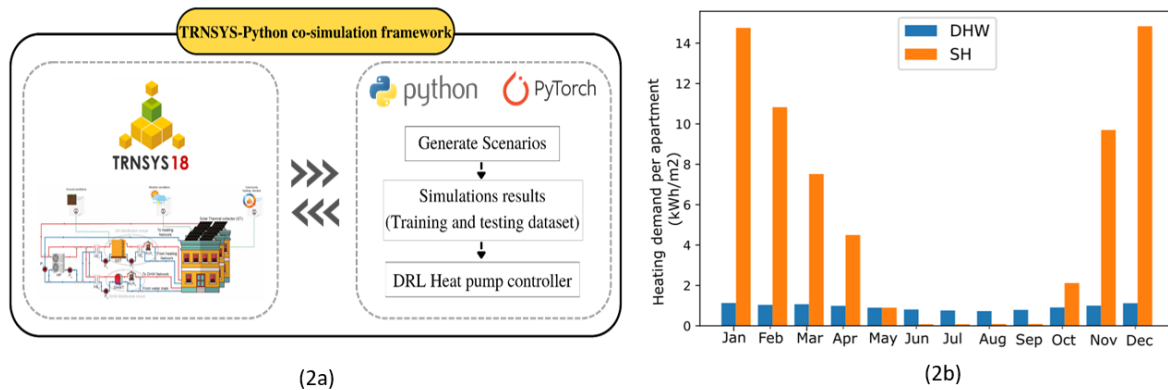


Figure 13. TRNSYS-Python co-simulation framework (Figure 2a), and the demand profiles (Figure 2b) for domestic hot water and space heating per month for a neighborhood of 10 buildings in Madrid.

### 2.3. Case study

The methodological approach has been applied to an SDHS in Madrid (Spain) to provide for the heating demands of a neighborhood that consists of 10 buildings in order to more effectively illustrate the abilities of the proposed framework. This case study has already been described in a former article where more details can be found [18]. Each building has 28 apartments, each of which has 90 m<sup>2</sup> of usable space [22] and is equipped with a DHW system and radiant underfloor heating system to meet the requirement for space heating (SH) and domestic hot water (DHW) at 50 °C and 60 °C, respectively. Each building requires yearly 191.34 MWh of heating. Based on Tulus et al. [19] and Abokersh et al. [18], the proposed SDHS was previously validated.

#### 2.3.1. Heating demand profiles

In order to compare the proposed DRL-based control strategy to the rule-based control strategy in Abokersh's study [18] the SH and DHW inputs will remain the same. Figure 2b shows the monthly DHW and SH demand for a neighborhood in Madrid that consists of 10 residential buildings. The Energy Plus database is used to gather the weather data for Madrid. This includes the incident solar radiation, ambient temperature, relative humidity, and other pertinent information. We are currently starting the model training and hope to have the results ready when the conference will take place.

### 3. Conclusions

The current work aims to develop a co-simulation framework that will allow for the offline training of a deep reinforcement learning-based control strategy for a smart agent that will control the integrated heat pump into SDHS with a seasonal thermal storage system. The work will consider the life cycle cost analysis for the technical economic evaluation of the proposed control strategy. The results of the study will indicate whether the proposed heat pump control strategy offers significant advantages over traditional methods, in terms of both technical performance and cost-effectiveness.

## Acknowledgments

The authors acknowledge financial support from the “Ministerio de Ciencia, Innovación y Universidades” Spain [PID2021-127713OA-I00, PID2021-123511OB-C31, PID2021-123511OB-C33, PID2021-124139NB-C22 - MCIN/AEI / 10.13039/ 501100011033 / FEDER, UE&TED2021-129851B-I00].

## References

- [1] D. Olsthoorn, F. Haghighat, and P. A. Mirzaei, “Integration of storage and renewable energy into district heating systems: A review of modelling and optimization,” *Solar Energy*, vol. 136, pp. 49–64, 2016, doi: 10.1016/j.solener.2016.06.054.
- [2] F. M. Rad and A. S. Fung, “Solar community heating and cooling system with borehole thermal energy storage - Review of systems,” *Renewable and Sustainable Energy Reviews*, vol. 60, pp. 1550–1561, 2016, doi: 10.1016/j.rser.2016.03.025.
- [3] C. Winterscheid, J. O. Dalenbäck, and S. Holler, “Integration of solar thermal systems in existing district heating systems,” *Energy*, vol. 137, pp. 579–585, 2017, doi: 10.1016/j.energy.2017.04.159.
- [4] H. Lund *et al.*, “The status of 4th generation district heating: Research and results,” *Energy*, vol. 164, pp. 147–159, 2018, doi: 10.1016/j.energy.2018.08.206.
- [5] S. Buffa, M. Cozzini, M. D’Antoni, M. Baratieri, and R. Fedrizzi, “5th generation district heating and cooling systems: A review of existing cases in Europe,” *Renewable and Sustainable Energy Reviews*, vol. 104, no. June 2018, pp. 504–522, 2019, doi: 10.1016/j.rser.2018.12.059.
- [6] D. Tschopp, Z. Tian, M. Berberich, J. Fan, B. Perers, and S. Furbo, “Large-scale solar thermal systems in leading countries: A review and comparative study of Denmark, China, Germany and Austria,” *Appl Energy*, vol. 270, no. January, p. 114997, 2020, doi: 10.1016/j.apenergy.2020.114997.
- [7] Z. Tian *et al.*, “Large-scale solar district heating plants in Danish smart thermal grid: Developments and recent trends,” *Energy Convers Manag*, vol. 189, no. October 2018, pp. 67–80, 2019, doi: 10.1016/j.enconman.2019.03.071.
- [8] L. Mesquita, D. McClenahan, J. Thornton, J. Carriere, and B. Wong, “Drake Landing solar community: 10 years of operation,” *ISES Solar World Congress 2017 - IEA SHC International Conference on Solar Heating and Cooling for Buildings and Industry 2017, Proceedings*, no. August, pp. 333–344, 2017, doi: 10.18086/swc.2017.06.09.
- [9] R. Renaldi and D. Friedrich, “Techno-economic analysis of a solar district heating system with seasonal thermal storage in the UK,” *Appl Energy*, vol. 236, no. October 2018, pp. 388–400, 2019, doi: 10.1016/j.apenergy.2018.11.030.
- [10] L. Yu, S. Qin, M. Zhang, C. Shen, T. Jiang, and X. Guan, “A Review of Deep Reinforcement Learning for Smart Building Energy Management,” *IEEE Internet Things J*, vol. 8, no. 15, pp. 12046–12063, 2021, doi: 10.1109/IIOT.2021.3078462.
- [11] V. Mnih *et al.*, “Human-level control through deep reinforcement learning,” *Nature*, vol. 518, no. 7540, pp. 529–533, Feb. 2015, doi: 10.1038/nature14236.
- [12] V. Mnih *et al.*, “Playing Atari with Deep Reinforcement Learning”
- [13] L. Yu, S. Qin, M. Zhang, C. Shen, T. Jiang, and X. Guan, “Deep Reinforcement Learning for Smart Building Energy Management: A Survey.” [Online]. Available: <https://www.researchgate.net/publication/343626535>
- [14] O. Kotevska *et al.*, “Methodology for Interpretable Reinforcement Learning Model for HVAC Energy Control,” in *Proceedings - 2020 IEEE International Conference on Big Data, Big Data 2020*, Dec. 2020, pp. 1555–1564. doi: 10.1109/BigData50022.2020.9377735.
- [15] A. Chen, T. Dewan, M. Trivedi, D. Jiang, A. Aditya, and S. Mohammed, “The Use of Reinforcement Learning in Gaming The Breakout Game Case Study.pdf,” no. April, 2020, doi: 10.36227/techrxiv.12061728.
- [16] J. Zhao, C. Yang, W. Dai, and W. Gao, “Reinforcement Learning-Based Composite Optimal Operational Control of Industrial Systems with Multiple Unit Devices,” *IEEE Trans Industr Inform*, vol. 18, no. 2, pp. 1091–1101, 2022, doi: 10.1109/TII.2021.3076471.
- [17] J. Kober, J. A. Bagnell, and J. Peters, “Reinforcement learning in robotics: A survey,” *International Journal of Robotics Research*, vol. 32, no. 11, pp. 1238–1274, 2013, doi: 10.1177/0278364913495721.
- [18] M. H. Abokersh, M. Vallès, K. Saikia, L. F. Cabeza, and D. Boer, “Techno-economic analysis of control strategies for heat pumps integrated into solar district heating systems,” *J Energy Storage*, vol. 42, 2021, doi: 10.1016/j.est.2021.103011.
- [19] V. Tulus, M. H. Abokersh, L. F. Cabeza, M. Vallès, L. Jiménez, and D. Boer, “Economic and environmental potential for solar assisted central heating plants in the EU residential sector: Contribution to the 2030 climate and energy EU agenda,” *Appl Energy*, vol. 236, no. November 2018, pp. 318–339, 2019, doi: 10.1016/j.apenergy.2018.11.094.
- [20] H. Zhang, D. Wu, and B. Boulet, “A review of recent advances on reinforcement learning for smart home energy management,” in *2020 IEEE Electric Power and Energy Conference, EPEC 2020*, Nov. 2020. doi: 10.1109/EPEC48502.2020.9320042.
- [21] G. Brockman *et al.*, “OpenAI Gym,” Jun. 2016, [Online]. Available: <http://arxiv.org/abs/1606.01540>
- [22] IDAE Secretaría General Departamento de Planificación y Estudios, “Análisis del consumo energético del sector residencial en España INFORME FINAL,” 2011.

EUROTHERM2023-W119

## Development of a Predictive Model for Thermal Characteristics of Thermal Energy Storage Materials

Ana Carolina Rosa<sup>1,2</sup> Alejandro Calderón<sup>3</sup>, Carles Mateu<sup>4</sup>, Assed Haddad<sup>1</sup>, and Dieter Boer<sup>2</sup>

<sup>1</sup> Programa de Engenharia Ambiental, UFRJ, Universidade Federal do Rio de Janeiro, Rio de Janeiro, 21941-901, Brazil, e-mail: carolinarosa@poli.ufrj.br, assed@poli.ufrj.br

<sup>2</sup> Department of Mechanical Engineering, University Rovira i Virgili, Av. Països Catalans, 26, 43007 Tarragona, Spain, e-mail: dieter.boer@urv.cat

<sup>3</sup> Department of Materials Science and Physical Chemistry, Universitat de Barcelona, Martí i Franquès 1-11, Barcelona 08028, Spain, e-mail: acalderon@ub.edu

<sup>4</sup> Department of Computer Science and Industrial Engineering, University of Lleida, Lleida, Spain, e-mail: carles.mateu@udl.cat

### Abstract

Thermal energy storage (TES) materials are crucial for improving energy efficiency. Its features of storing and releasing heat allow the management and use of thermal energy in various applications, like building heating and cooling systems or thermal energy storage at high temperatures for energy conversion. Concrete is a commonly used TES material due to its unique features and good thermal properties. Still, its effectiveness and thermal properties depend on the ideal composition that meets project specifications. Researchers have already applied artificial intelligence (AI) techniques like artificial neural networks (ANNs) to find this ideal composition. However, few papers use ANN to predict thermal properties, and there is a lack of a general model to predict different types of concrete. The novelty of this study is to fill this gap and develop a methodology to predict concrete's thermal conductivity using ANN algorithms with an extensive database.

**Keywords:** TES materials, machine learning, neural networks, concrete, thermal properties, thermal conductivity

### 1. Introduction

Thermal energy storage (TES) materials are of utmost importance in the energy efficiency of many applications due to their specific characteristic mitigating intermittent availability of energy [1]. They play an essential role in energy storage and management, as they can store the thermal energy generated during periods of low demand and release it during periods of high demand. They balance out fluctuations in energy demand and variable availability, leading to improved energy efficiency and reduced energy costs.

The utilization of TES materials in the construction sector is necessary as it aids in preserving indoor thermal comfort, despite fluctuations in the outdoor environment conditions. Regarding building materials, concrete, masonry, and specific stones, among others, can also be used as thermal energy storage materials. As the energy storage system's effectiveness relies on TES materials' thermal properties, an accurate prediction of their thermal properties is vital for optimizing their performance in thermal applications. Therefore, a predictive model that can accurately estimate the thermal behavior of these materials would be beneficial in optimizing their use.

Artificial Intelligence (AI) techniques such as machine learning can be used to develop such predictive models by learning from large datasets and finding patterns that can be used to make predictions. By incorporating AI, the predictive models can adapt to varying conditions and continuously improve their accuracy, making them a valuable tool in optimizing the performance of thermal energy storage systems [2].



## 2. Methodology

Selecting a TES material for a project is challenging, and the material's thermal properties influence this choice. Among these properties, thermal conductivity is one of the most studied, which presents a reliable database in the literature, and it is essential to determine the materials' heat transfer behavior. However, predicting the thermal conductivity of concrete is crucial since it is a composite material composed of different constituents, such as water, cement, fine aggregate, coarse aggregate, and other admixtures [4]. Hence, the thermal conductivity value changes according to the composition of these constituents. To avoid time-consuming experiments and provide a reliable model to predict the concrete's thermal conductivity, some ANN models have been employed to determine its value based on the experimental database and data found in published papers. This work presents a general methodology to build an ANN model to predict thermal conductivity.

The methodology framework adopted in this study is depicted in Figure 2. As an initial step, it was performed the data collection and preprocessing. Then, a group of a large dataset of concrete compositions and the corresponding thermal conductivity values were gathered and split into three groups: training, validation, and testing. In this first step, it should be guaranteed that the data is diverse, including different types of aggregates, cement, and other binders. The second step is the selection of an appropriate neural network architecture for the prediction task, i.e., the definition of a neural network algorithm of the hidden layers number and neurons in each layer to find the best model for the dataset. Following the third step is the model training level, where it is trained using the training data. Additionally, the loss function is optimized, and the model parameters are updated. The fourth step encompasses the model validation with a different dataset to evaluate its performance. Some metrics can be used to check the model performance, such as Mean Absolute Error (MAE), Root Mean Squared Error (RMSE), and correlation coefficient. Finally, the last step is the fine adjustments of the hyperparameters, adding or removing the hidden layers or swapping the activation function.

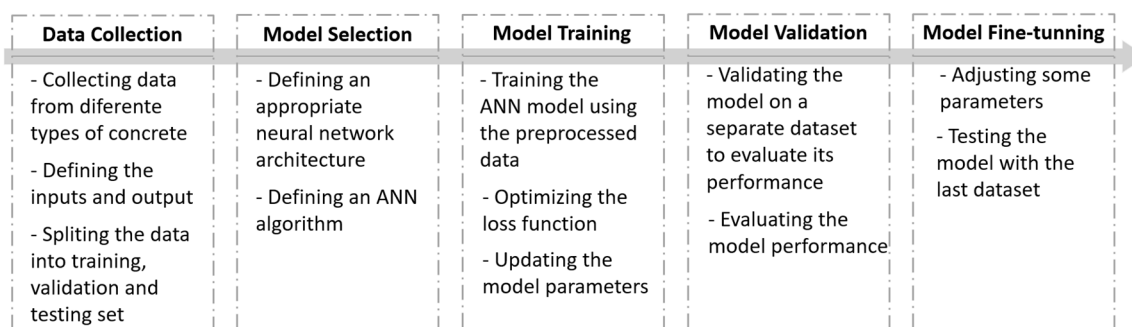


Figure 2. Methodology framework

## 3. Case study

This case study demonstrates the potential for ANNs to improve the accuracy and efficiency of TES material property predictions, with important implications for energy-efficient building construction. The case study explores the use of ANNs to predict the thermal conductivity of different types of concrete. By training an ANN around 200 data of concrete, the model can accurately predict the thermal conductivity of concrete based on its composition and density.

This paper uses feed-forward neural networks based on a backward propagation algorithm for network learning. To train the ANN with thermal conductivity as the output, this research utilized experimental data reported by previous researchers with thirteen parameters: the water-cement ratio, the unit water weight, the unit cement weight, the unit of ceramic powder, the unit fine aggregate weight, the unit coarse aggregate weight, the unit natural aggregate weight, the unit fly ash weight, the unit silica fume weight, the unit slag weight, the unit fiber weight, the unit superplasticizer weight, and density.

## 4. Conclusions

This work is part of a broader effort to develop a methodology for predicting the thermal properties of TES materials using ANN. The ultimate goal of this research is to extend the model developed for concrete to other TES materials, thereby advancing the field of energy efficiency and enabling the development of new energy storage solutions that can meet the growing demands of the future. Additionally, integrating artificial intelligence techniques enhances the intelligence and feasibility of TES systems. By developing models that can predict the thermal properties of TES materials, researchers can improve the performance and efficiency of these materials, making them more effective and cost-efficient. Besides that, the ability to predict the thermal properties of TES materials will also facilitate the development of new energy storage solutions that can meet energy demands, ensuring a more sustainable and energy-efficient future for the next generations.

## Acknowledgments

The authors would like to acknowledge financial support from the Coordenação de Aperfeiçoamento de Pessoal de Nível Superior (CAPES) - Finance Code 001, Conselho Nacional de Desenvolvimento Científico e Tecnológico (CNPq), Fundação de Amparo à Pesquisa do Estado do Rio de Janeiro (Faperj) 2019-E-26/202.568/2019 (245653), and "Ministerio de Ciencia, Innovación y Universidades" of Spain [PID2021-127713OA-I00, PID2021-123511OB-C32, PID2021-123511OB-C33, PID2021-124139NB-C22 - MCIN/AEI/10.13039/501100011033/FEDER, UE & TED2021-129851B-I00].

## References

- [1] H. Zhang, J. Baeyens, G. Cáceres, J. Degreè, and Y. Lv, Thermal energy storage: Recent developments and practical aspects, *Progress in Energy and Combustion Science*, vol. 53, 1-40, 2016. ISSN 0360-1285. doi:10.1016/j.pecs.2015.10.003.
- [2] Z. He, W. Guo, and P. Zhang, Performance prediction, optimal design and operational control of thermal energy storage using artificial intelligence methods, *Renewable and Sustainable Energy Reviews*, vol. 156, 2022. doi: 10.1016/j.rser.2021.111977.
- [3] N. N. Htun, S. Sukchai and S. Hemavibool, Properties of concrete material for thermal energy storage, 2014 International Conference and Utility Exhibition on Green Energy for Sustainable Development (ICUE), Pattaya, Thailand, 1-5, 2014. ISBN:978-1-4799-2627-5
- [4] Lee, JH., Lee, JJ. and Cho, BS. Effective Prediction of Thermal Conductivity of Concrete Using Neural Network Method. *Int J Concr Struct Mater*, vol. 6, 177–186, 2012. doi: 10.1007/s40069-012-0016-x



EUROTHERM2023-K122

## Effects of Eccentricity on the Melting Performance of the PCM within L-shaped Shell-and-Tube Latent Heat Thermal Energy Storage Units

Wenwen Ye<sup>1</sup>, J.M. Khodadadi<sup>2</sup>

<sup>1</sup>Department of Mechanical Engineering, 1418 Wiggins Hall, Auburn University, AL 36849-5341, USA; Phone: 01-334-524-8171; e-mail: wzy@auburn.edu

<sup>2</sup>Department of Mechanical Engineering, 1418 Wiggins Hall, Auburn University, AL 36849-5341, USA; Phone: 01-334-844-3333, Fax: 01-334-844-3307; e-mail: khodajm@auburn.edu

### Abstract

A numerical study is conducted to study the melting performances of the enclosed phase change material (PCM, n-octadecane) in L-shaped shell-and-tube latent heat thermal energy storage (LHTES) systems. The L-shaped units were composed of horizontal, elbow-shaped, and vertical parts connected continuously. The hot heat transfer fluid (water) was circulated through the inner copper tube serving as the heat source. The numerical results showed that increasing the radial eccentricity led to a great heat transfer enhancement, due to greater amount of PCM being subjected to natural convection. However, when the eccentricity was further raised from 11.43 to 15.24 mm, the improvement was insignificant. The portion of the PCM featuring high-speed melting was found within the region above the hot inner tube where intense activity of natural convection-induced upwelling plumes was observed.

**Keywords:** L-shaped shell-and-tube latent heat thermal energy storage system, Melting, Natural convection, Phase change materials.

### 1. Introduction

Latent heat thermal energy storage (LHTES) systems which utilize phase change materials (PCM) as the energy storage medium have attracted the researchers' attention for many decades due to their high heat storage density and the capability of absorbing and releasing of heat over a small temperature range. Although extensive research has been conducted on the topic of LHTES, low thermal conductivity of the PCM has obstructed their commercialization and further widespread applications. Metallic fins and foams and carbon/graphite fibers of high conductivity have been highly favored thermal conductivity enhancers, as reported in the series of reviews of Fan and Khodadadi [1], Dhaidan and Khodadadi [2] and Ye et al. [3].

The most investigated geometries of LHTES units are classified as rectangular [4], spherical [5] containers and shell-and-tube configurations. Among the aforementioned enclosures, horizontal- and or vertically-positioned shell-and-tube LHTES units have been analyzed broadly due to their potential ability of storing heat and also their ease of construction. Addressing thermal performance limitations of shell-and-tube LHTES units, some authors studied the effects of the eccentricity of the inner tube on the melting performance. It was observed that while the inner tube was moved closer to the bottom shell, the melting performance was effectively enhanced since the volume of the PCM influenced by natural convection was enlarged [6]. So far, L-shaped LHTES units that combine horizontal, elbow and vertical components have not been investigated, which could function as transition junction in practical installation when necessary.

Melting of the PCM (n-octadecane) within the L-shaped shell-and-tube LHTES units were analyzed computationally. Five (5) cases were simulated to analyze the effects of the radial eccentricity of the inner tube on the melting performance of the PCM.

## 2. Physical model

The benchmark case of the L-shaped cylindrical shell-and-tube LHTES unit (with no eccentricity) is introduced schematically by Fig. 1(a), incorporating horizontal, elbow-shaped bend, and vertical parts connected continuously. Five test cases were simulated to examine the effects of radial eccentricity of the inner tube ( $\epsilon$ ). Two side views of a test case with eccentric inner tube are shown in Fig. 1(b), where  $R_o = \frac{R_c + R_s}{2}$ ,  $R_{ec} = R_o + \epsilon = \frac{R_{to} + R_{ti}}{2}$ .

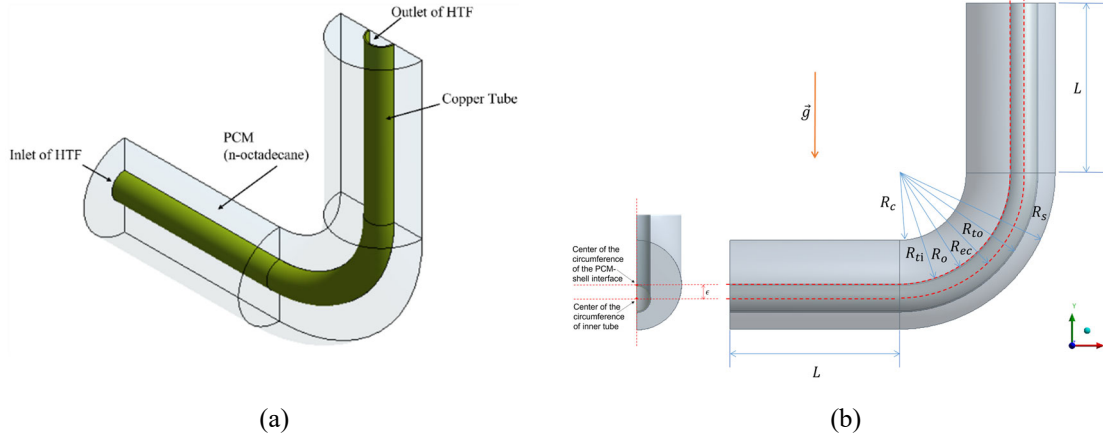


Fig. 1. Schematic diagrams of the (a) computational domain (half of the physical model) of the benchmark L-shaped shell-and-tube LHTES unit and (b) side view of a test case with eccentric inner tube.

## 3. Formulations of the Problem

The enthalpy-porosity method was employed to simulate the melting of the PCM. To simplify the simulation, the flow of liquid PCM and HTF are assumed to be Newtonian and incompressible. The time-dependent governing equations of the simplified model are as follows.

$$\frac{\partial(\rho u_i)}{\partial x_i} = 0 \quad (1)$$

$$\frac{\partial(\rho u)}{\partial t} + \frac{\partial(\rho u u)}{\partial x} + \frac{\partial(\rho v u)}{\partial y} + \frac{\partial(\rho w u)}{\partial z} = -\frac{\partial P}{\partial x} + \frac{\partial}{\partial x} \left( \mu \frac{\partial u}{\partial x} \right) + \frac{\partial}{\partial y} \left( \mu \frac{\partial u}{\partial y} \right) + \frac{\partial}{\partial z} \left( \mu \frac{\partial u}{\partial z} \right) + S_x + S_{bx} \quad (2)$$

$$\frac{\partial(\rho v)}{\partial t} + \frac{\partial(\rho u v)}{\partial x} + \frac{\partial(\rho v v)}{\partial y} + \frac{\partial(\rho w v)}{\partial z} = -\frac{\partial P}{\partial y} + \frac{\partial}{\partial x} \left( \mu \frac{\partial v}{\partial x} \right) + \frac{\partial}{\partial y} \left( \mu \frac{\partial v}{\partial y} \right) + \frac{\partial}{\partial z} \left( \mu \frac{\partial v}{\partial z} \right) + S_y + S_{by} \quad (3)$$

$$\frac{\partial(\rho w)}{\partial t} + \frac{\partial(\rho u w)}{\partial x} + \frac{\partial(\rho v w)}{\partial y} + \frac{\partial(\rho w w)}{\partial z} = -\frac{\partial P}{\partial z} + \frac{\partial}{\partial x} \left( \mu \frac{\partial w}{\partial x} \right) + \frac{\partial}{\partial y} \left( \mu \frac{\partial w}{\partial y} \right) + \frac{\partial}{\partial z} \left( \mu \frac{\partial w}{\partial z} \right) + S_z + S_{bz} \quad (4)$$

$$\frac{\partial(\rho h)}{\partial t} + \frac{\partial(\rho u h)}{\partial x} + \frac{\partial(\rho v h)}{\partial y} + \frac{\partial(\rho w h)}{\partial z} = \frac{\partial}{\partial x} \left( k \frac{\partial T}{\partial x} \right) + \frac{\partial}{\partial y} \left( k \frac{\partial T}{\partial y} \right) + \frac{\partial}{\partial z} \left( k \frac{\partial T}{\partial z} \right) - S_h \quad (5)$$

The temperature of PCM is obtained by iteration between the energy equation and the liquid fraction equation. The total enthalpy  $H$  of the PCM is computed as the sum of the sensible enthalpy  $h$  (kJ/kg) and latent enthalpy  $\Delta H$  (kJ/kg), i.e.  $H = h + \Delta H$ , with:

$$h = h_{ref} + \int_{T_{ref}}^T C_p dT \quad (6)$$

$$\Delta H = f_l \mathcal{L}_{PCM} \quad (7)$$

$$f_l = \begin{cases} 0 & T < T_{solidus} \\ \frac{T - T_{solidus}}{T_{liquidus} - T_{solidus}} & T_{solidus} < T < T_{liquidus} \\ 1 & T > T_{liquidus} \end{cases} \quad (8)$$

where  $h_{ref}$ ,  $T_{ref}$ ,  $C_p$ ,  $\mathcal{L}_{PCM}$ , and  $f_l$  refer to reference sensible enthalpy at the reference temperature, reference temperature, specific heat at constant pressure, latent heat of the PCM, and melt fraction of the PCM, respectively. The liquid-solid mushy zone is treated as a porous medium with porosity considered as the liquid fraction. The liquid fraction lies between 0 and 1 in the mushy zone.

## 4. Computational Procedures and Validation

The discretized governing equations are solved numerically by using the commercial software ANSYS® FLUENT [7] which is based on the the finite-volume-method. The effective numerical study was validated with the experimental temperature data reported by Longeon et al. [8].

## 5. Results and Discussions

Temperature field on the planes normal to curved symmetry axis of the shell that include the inlet and outlet planes of the units in addition to the  $z=0$  plane at 30 minutes are shown in Fig. 2. One can observe that the PCM were almost molten above the horizontal part of the HTF tube in the cases of  $\epsilon=0$  and 0.15 inches by 30 minutes, however there are still blue region existing in the case of  $\epsilon=0.45$ , signifying the remaining solid phase still was subjected to natural convection. As observed in Fig. 3(a), the melting rate was enhanced during the initial fast melting period. The duration of the slow melting stage was also greatly reduced. Consequently, the complete melting time of the unit decreased dramatically for greater values of radial eccentricity as illustrated in Fig. 3(b). Based on the melt fraction profile, while the eccentricity increased from 0 to 0.45 inches, the improvement of the melting rate was remarkable. However, the reinforcement became feeble after the radial eccentricity jumped from 0.45 to 0.6 inches. One can find the liquid fraction profile for the cases of  $\epsilon=0$  and 0.45 were similar, especially during the initial 34 minutes. By increasing the radial eccentricity, a greater fraction of the volume of PCM above the HTF tube was then subjected to natural convection and upwelling thermal plumes and less amount of PCM was subjected to slower conduction. In effect, faster melting within the unit was induced.

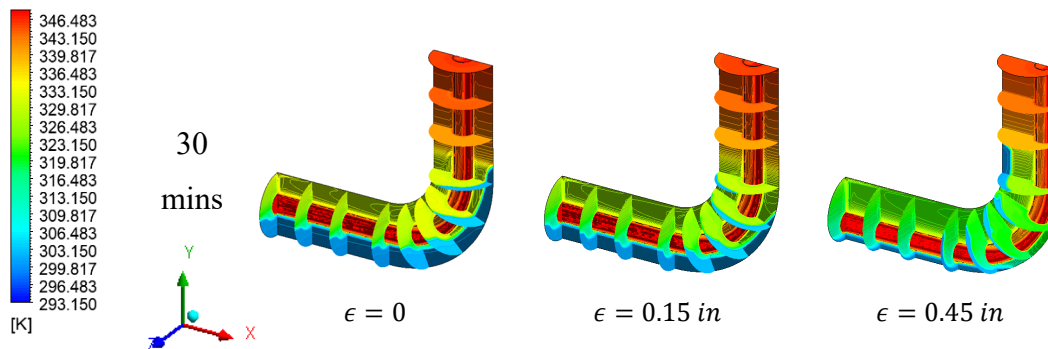


Fig. 2. Temperature contours on various surfaces for cases 3 and 5 with different radial eccentricity.

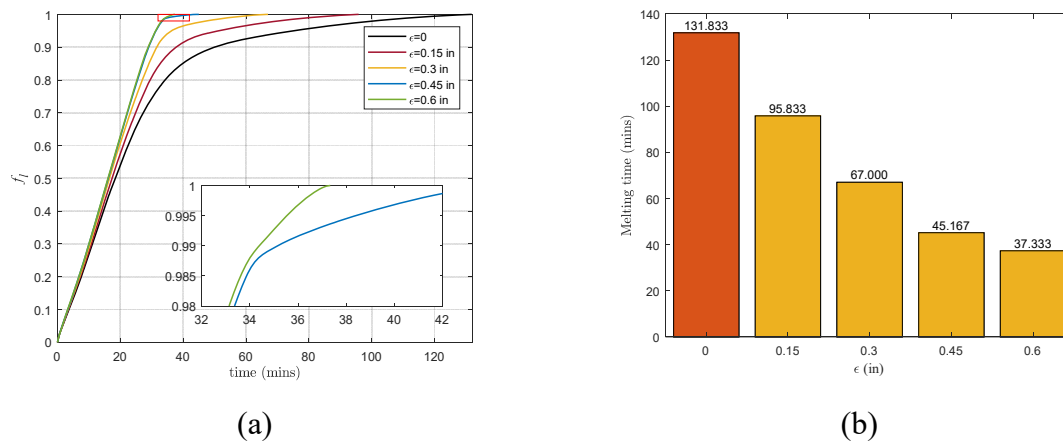


Fig. 3. Dependence of the (a) instantaneous liquid fraction and (b) the total melting time on variations of the radial eccentricity.

## 6. Conclusions

In the present work, a mathematical model combining the HTF, HTF carrying tube, and PCM was developed to investigate the thermal characteristics of L-shape shell-and-tube LHTES systems with different radial eccentricity of the inner tube  $\epsilon$  during the melting process. Incrementing the radial eccentricity of the inner HTF tube could effectively improve the overall melting rate and reduce the required melting time. However, when the eccentricity was further increased from 0.45 to 0.6 inches, the improvement was insignificant.

## References

- [1] Liwu Fan, J.M. Khodadadi, 2011. Thermal conductivity enhancement of phase change materials for thermal energy storage: a review, *Renew. Sustain. Energy Rev.* 15 24–46.
- [2] Dhaidan, N.S. and Khodadadi, J.M., 2017. Improved performance of latent heat energy storage systems utilizing high thermal conductivity fins: A review. *Journal of Renewable and Sustainable Energy*, 9(3), p.034103.
- [3] Ye, W., Jamshideasli, D. and Khodadadi, J.M., 2023. Improved Performance of Latent Heat Energy Storage Systems in Response to Utilization of High Thermal Conductivity Fins. *Energies*, 16(3), p.1277.
- [4] Tian, L.L., Liu, X., Chen, S. and Shen, Z.G., 2020. Effect of fin material on PCM melting in a rectangular enclosure. *Applied Thermal Engineering*, 167, p.114764.
- [5] Tan, F.L., Hosseinizadeh, S.F., Khodadadi, J.M. and Fan, L., 2009. Experimental and computational study of constrained melting of phase change materials (PCM) inside a spherical capsule. *International Journal of Heat and Mass Transfer*, 52(15-16), pp.3464-3472.
- [6] Yazici, M.Y., Avci, M., Aydin, O. and Akgun, M., 2014. On the effect of eccentricity of a horizontal tube-in-shell storage unit on solidification of a PCM. *Applied Thermal Engineering*, 64(1-2), pp.1-9.
- [7] ANSYS® FLUENT, 2012: User's Guide, Release 14.5, ANSYS Inc., USA.
- [8] Longeon, M., Soupart, A., Fourmigué, J.F., Bruch, A. and Marty, P., 2013. Experimental and numerical study of annular PCM storage in the presence of natural convection. *Applied Energy*, 112, pp.175-184.

EUROTHERM2023-D123

## Effects of the Angle between Split Annular Fins on the Melting Performance of the PCM within Vertical Shell-and-Tube Latent Heat Thermal Energy Storage Units

Wenwen Ye<sup>1</sup>, J.M. Khodadadi<sup>2</sup>

<sup>1</sup>Department of Mechanical Engineering, 1418 Wiggins Hall, Auburn University, AL 36849-5341, USA; Phone: 01-334-524-8171; e-mail: wzy@auburn.edu

<sup>2</sup>Department of Mechanical Engineering, 1418 Wiggins Hall, Auburn University, AL 36849-5341, USA; Phone: 01-334-844-3333, Fax: 01-334-844-3307; e-mail: khodajm@auburn.edu

### Abstract

A numerical study is conducted to study the melting performances of the enclosed phase change materials (PCM, n-octadecane) in vertical shell-and-tube latent heat thermal energy storage (LHTES) systems. The hot heat transfer fluid (water) was circulated through the inner copper tube originating from the bottom inlet of the unit. The annular fins were uniformly spaced axially. The charging performance of the cases with 4 split annular fins were compared with the cases with non-split annular fins with the volume of fins unchanged for all cases. It was observed that melting time was reduced for  $\phi = 15^\circ$  and  $30^\circ$ , but it was extended when  $\phi = 45^\circ$ .

**Keywords:** Melting, Natural convection, Phase change materials, Vertical shell-and-tube latent heat thermal energy storage system.

### 1. Introduction

Phase change materials (PCM) are utilized as promising thermal energy storage medium due to their high heat storage density and the capability of absorbing and releasing of heat over a small temperature range. The critical bottleneck associated with extensive utilization of PCM is their low thermal conductivity which results in low heat transfer rate and extended time duration required for completing phase transition. Metallic fins and foams and carbon/graphite fibers of high conductivity have been considered as promising thermal conductivity enhancers, as reported in the reviews of Fan and Khodadadi [1] Dhaidan and Khodadadi [2] and Ye et al. [3]. The most investigated geometries of LHTES units are classified as rectangular [4], spherical [5] containers and shell-and-tube configurations. Shell-and-tube LHTES units have been analyzed broadly due to their potential ability of storing heat and also their ease of construction. Longitudinal [6] and annular fin [7] designs are the mostly investigated fin structures.

Split annular fins are proposed here to improve the interchange of the fluid flow between the neighboring compartments through the split openings. Melting of the PCM (n-octadecane) within the vertical shell-and-tube LHTES units with split annular fins were analyzed computationally. Cases with split annular fins and the case with non-split annular fins were compared.

### 2. Physical model

The physical model of the vertical shell-and-tube LHTES unit with split angle  $\phi = 30^\circ$  is introduced schematically by Fig. 1(a). In order to reduce the computational cost, a quarter of the physical model was simulated due to symmetry Fig. 1(b). The fins' thickness and the axial distance between neighboring fins were invariant. The split angle  $\phi$  increased from  $0^\circ$  to  $45^\circ$  with an interval of  $15^\circ$ , thus the corresponding radial length of the fins ( $w$ ) was increased to maintain constant PCM volume.

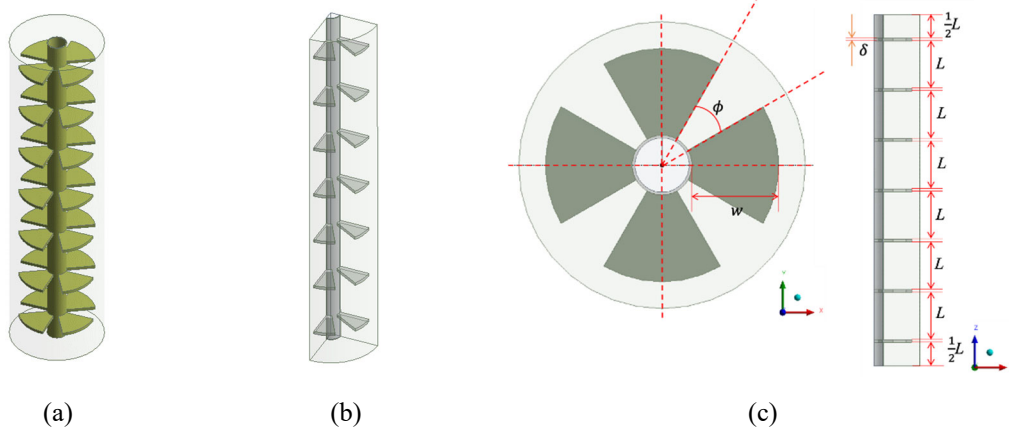


Fig. 1. Schematic diagrams of the (a) physical model (b) computational domain (a quarter of the physical model) of the vertical shell-and-tube LHTES unit and (c) arrangement of the unit and split fins.

### 3. Formulations of the Problem

The enthalpy-porosity method was employed to simulate the melting of the PCM. To simply the simulation, the flow of liquid PCM and HTF are assumed to be Newtonian and incompressible. The time-dependent governing equations of the simplified model are as follows.

$$\frac{\partial(\rho u_i)}{\partial x_i} = 0 \quad (1)$$

$$\frac{\partial(\rho u)}{\partial t} + \frac{\partial(\rho u u)}{\partial x} + \frac{\partial(\rho v u)}{\partial y} + \frac{\partial(\rho w u)}{\partial z} = -\frac{\partial P}{\partial x} + \frac{\partial}{\partial x} \left( \mu \frac{\partial u}{\partial x} \right) + \frac{\partial}{\partial y} \left( \mu \frac{\partial u}{\partial y} \right) + \frac{\partial}{\partial z} \left( \mu \frac{\partial u}{\partial z} \right) + S_x + S_{bx} \quad (2)$$

$$\frac{\partial(\rho v)}{\partial t} + \frac{\partial(\rho u v)}{\partial x} + \frac{\partial(\rho v v)}{\partial y} + \frac{\partial(\rho w v)}{\partial z} = -\frac{\partial P}{\partial y} + \frac{\partial}{\partial x} \left( \mu \frac{\partial v}{\partial x} \right) + \frac{\partial}{\partial y} \left( \mu \frac{\partial v}{\partial y} \right) + \frac{\partial}{\partial z} \left( \mu \frac{\partial v}{\partial z} \right) + S_y + S_{by} \quad (3)$$

$$\frac{\partial(\rho w)}{\partial t} + \frac{\partial(\rho u w)}{\partial x} + \frac{\partial(\rho v w)}{\partial y} + \frac{\partial(\rho w w)}{\partial z} = -\frac{\partial P}{\partial z} + \frac{\partial}{\partial x} \left( \mu \frac{\partial w}{\partial x} \right) + \frac{\partial}{\partial y} \left( \mu \frac{\partial w}{\partial y} \right) + \frac{\partial}{\partial z} \left( \mu \frac{\partial w}{\partial z} \right) + S_z + S_{bz} \quad (4)$$

$$\frac{\partial(\rho h)}{\partial t} + \frac{\partial(\rho u h)}{\partial x} + \frac{\partial(\rho v h)}{\partial y} + \frac{\partial(\rho w h)}{\partial z} = \frac{\partial}{\partial x} \left( k \frac{\partial T}{\partial x} \right) + \frac{\partial}{\partial y} \left( k \frac{\partial T}{\partial y} \right) + \frac{\partial}{\partial z} \left( k \frac{\partial T}{\partial z} \right) - S_h \quad (5)$$

The temperature of PCM is obtained by iteration between the energy equation and the liquid fraction equation. The total enthalpy  $H$  of the PCM is computed as the sum of the sensible enthalpy  $h$  (kJ/kg) and latent enthalpy  $\Delta H$  (kJ/kg), i.e.  $H = h + \Delta H$ , with:

$$h = h_{ref} + \int_{T_{ref}}^T C_p dT \quad (6)$$

$$\Delta H = f_l \mathcal{L}_{PCM} \quad (7)$$

$$f_l = \begin{cases} 0 & T < T_{solidus} \\ \frac{T - T_{solidus}}{T_{liquidus} - T_{solidus}} & T_{solidus} < T < T_{liquidus} \\ 1 & T > T_{liquidus} \end{cases} \quad (8)$$

where  $h_{ref}$ ,  $T_{ref}$ ,  $C_p$ ,  $\mathcal{L}_{PCM}$ , and  $f_l$  refer to reference sensible enthalpy at the reference temperature, reference temperature, specific heat at constant pressure, latent heat of the PCM, and melt fraction of the PCM, respectively. The liquid-solid mushy zone is treated as a porous medium with porosity considered as the liquid fraction. The liquid fraction lies between 0 and 1 in the mushy zone.

### 4. Computational procedures and validation

The discretized governing equations are solved numerically by using the commercial software ANSYS® FLUENT [8] which is based on the the finite-volume-method. The numerical study was validated with the experimental temperature data reported by Longeon et al. [9].

## 5. Results and discussions

Temperature contours on the planes normal to vertical axis of the LHTES unit (some cut through the fins) in addition to the  $x=0$  and  $y=0$  planes at various time instants (10-40 minutes) are shown in Fig. 2. One can observe that the PCM close to the inner tube melts faster for the cases without split angle ( $\phi = 0^\circ$ ), thus the upwelling thermal plumes induced by natural convection from the top surface of the annular fins is more intense. However, the PCM farther from the inner tube melts faster for the cases with  $\phi = 30^\circ$ . This could be attributed to the length of the split fins ( $w$ ) extended with increased  $\phi$ , in order to keep constant PCM volume. As observed in Fig. 3, the fastest melting rate and shortest melting time was obtained for the case of  $\phi = 15^\circ$ . While  $\phi$  was increased to  $30^\circ$ , the increment of melting rate was weakened but still higher than the case of non-split annular fins. However, it was observed that melting time was increased while  $\phi$  was further raised to  $45^\circ$ , and the melting rate was remarkably reduced. By incrementing the split angle  $\phi$ , natural convection was enhanced further from the inner tube but suppressed close to the inner tube.

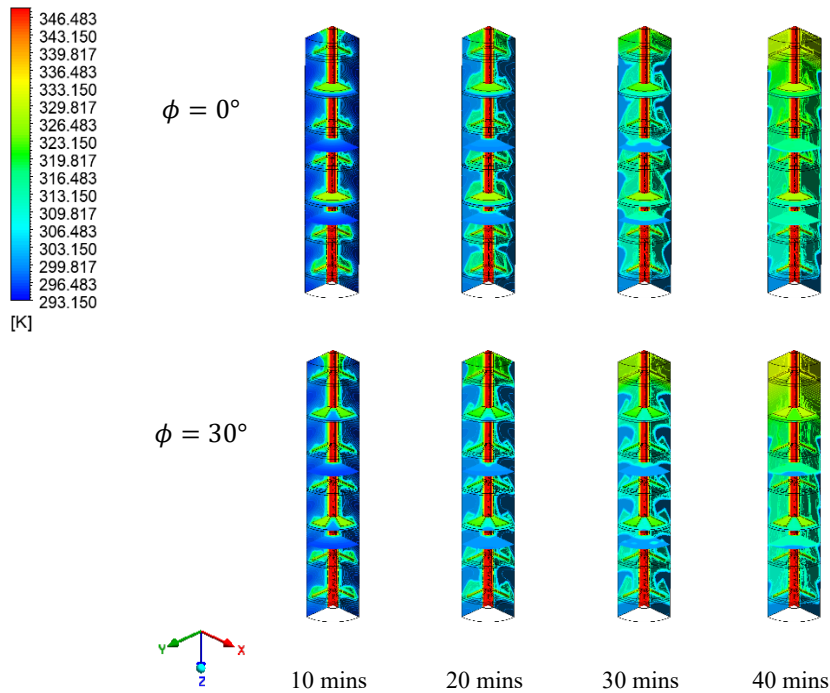


Fig. 2. Temperature contours on various surfaces for cases with different split angle.

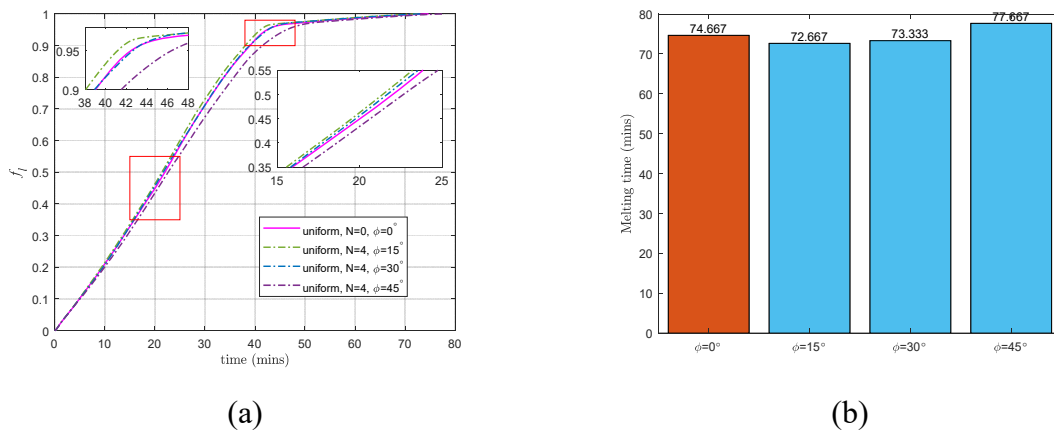


Fig. 3. Dependence of the (a) instantaneous liquid fraction and the (b) total melting time on variations of the split fin angle.

## 6. Conclusions

In the present work, a numerical model of vertical shell-and-tube LHTES systems was developed. The melting characteristics of the PCM enclosed in the LHTES systems were explored under the influence of the various split angles. Melting rate was increased with split fin angles  $\phi = 15^\circ$ , and  $30^\circ$ , but then reduced for  $\phi = 45^\circ$ . The presence of upwelling thermal plumes close the inner tube is more intense for the case without split angle.

## References

- [1] Liwu Fan, J.M. Khodadadi, 2011. Thermal conductivity enhancement of phase change materials for thermal energy storage: a review, *Renew. Sustain. Energy Rev.* 15 24–46.
- [2] Dhaidan, N.S. and Khodadadi, J.M., 2017. Improved performance of latent heat energy storage systems utilizing high thermal conductivity fins: A review. *Journal of Renewable and Sustainable Energy*, 9(3), p.034103.
- [3] Ye, W., Jamshideasli, D. and Khodadadi, J.M., 2023. Improved Performance of Latent Heat Energy Storage Systems in Response to Utilization of High Thermal Conductivity Fins. *Energies*, 16(3), p.1277.
- [4] Tian, L.L., Liu, X., Chen, S. and Shen, Z.G., 2020. Effect of fin material on PCM melting in a rectangular enclosure. *Applied Thermal Engineering*, 167, p.114764.
- [5] Tan, F.L., Hosseinizadeh, S.F., Khodadadi, J.M. and Fan, L., 2009. Experimental and computational study of constrained melting of phase change materials (PCM) inside a spherical capsule. *International Journal of Heat and Mass Transfer*, 52(15-16), pp.3464-3472.
- [6] Li, H., Hu, C., He, Y., Tang, D. and Wang, K., 2021. Influence of fin parameters on the melting behavior in a horizontal shell-and-tube latent heat storage unit with longitudinal fins. *Journal of Energy Storage*, 34, p.102230.
- [7] Yang, X., Guo, J., Yang, B., Cheng, H., Wei, P. and He, Y.L., 2020. Design of non-uniformly distributed annular fins for a shell-and-tube thermal energy storage unit. *Applied Energy*, 279, p.115772.
- [8] ANSYS® FLUENT, 2012: User's Guide, Release 14.5, ANSYS Inc., USA.
- [9] Longeon, M., Soupart, A., Fourmigué, J.F., Bruch, A. and Marty, P., 2013. Experimental and numerical study of annular PCM storage in the presence of natural convection. *Applied Energy*, 112, pp.175-184.



EUROTHERM2023-T124

## Numerical Investigation on Melting of Direct-Contact Storage of Thermal Energy Utilizing Phase Change Materials

Onyedika V. Mbelu<sup>1</sup>, J.M. Khodadadi<sup>2</sup>

<sup>1</sup>Department of Mechanical Engineering, 1418 Wiggins Hall, Auburn University, AL 36849-5341, USA; Phone: 01-334-559-4775; e-mail: ovm0002@auburn.edu

<sup>2</sup>Department of Mechanical Engineering, 1418 Wiggins Hall, Auburn University, AL 36849-5341, USA; Phone: 01-334-844-3333, Fax: 01-334-844-3307; e-mail: khodajm@auburn.edu

### Abstract

A 2-dimensional numerical model is designed to study the dynamic characteristics of the discharging process of a direct-contact thermal energy storage (TES) system. The classical problem of a system that consists of air laying on top of phase change material (PCM) at initial stage is analyzed. The system is made up of three inlet heat transfer fluid (HTF) nozzles. The HTF used is water and the PCM is octadecane. As the simulation starts, HTF flows into the TES system from the top at a constant temperature higher than the melting temperature of the PCM, exchanging heat with solid PCM. The HTF system was cut off at exactly 46 secs in-order to avoid mass imbalance in the system. Due to density differences between the liquid and solid PCM, the molten PCM emerging from the solid PCM floats through the sinking hot water to the top of unit.

**Keywords:** Direct-contact heat exchange, Melting, Multi-phase flow, Natural Convection; Phase Change Materials; Thermal Energy Storage.

### 1. Introduction

Since solar energy and waste heat are erratic heat sources, there is a critical need to develop advanced thermal energy storage (TES) technologies that can quickly and compactly store or release huge amounts of heat. Among various forms of energy, thermal energy constitutes a major portion of losses that are encountered in a variety of energy conversions systems. Storage of thermal energy through utilization of phase change materials (PCM) is widely practiced considering its operation at a desired constant temperature, ease of tailoring to low- to high-temperature applications, etc. In the past, there has been a lot of studies as regarding indirect contact TES systems, where heat flows through a heat transfer wall set between the HTF and the PCM increasing the thermal resistance of the system, thus the time to complete the charging and discharging process of the TES system increases [1]. The direct-contact heat transfer and storage system, in contrast to the indirect-contact TES system, has a wider heat transfer surface in which the PCM combines directly with a heat transfer medium, such as water/paraffin. Because of this, direct-contact TES systems with the proper PCM have higher efficiency and more energy storage, e.g. [2]–[4].

This study aims to investigate the melting rate of a direct-contact thermal storage system. The overall objectives are to investigate the effects of HTF inlet flow rate and temperature on liquid PCM volume fraction, complete discharging time and discharging capacity of the unit.

## 2. Physical model and methodology

A 2-D model was developed with the aid of computer-aided design (CAD) called Spaceclaim tool in workbench Fluent ANSYS. The geometry is made up of a rectangular system of dimensions 0.12 m x 0.22 m for the air zone and 0.43 x 0.22 m for the PCM zone. Three inlet nozzles at the top are placed on the top of the unit with dimension of 0.02 m for the heat transfer fluid coming into the system to melt the PCM.

As the simulation starts, HTF is introduced from the top of the tank during discharging process to melt the PCM, whereas the air layer was allowed to discharge to the atmosphere from two ports on the top corners of the unit. The HTF flowed into the tank from the inlet nozzles at a constant temperature higher than the melting temperature of the PCM, exchanging heat with the solid PCM. The melting starts slowly initially due to dominance of conduction. To verify mass balance of the three phases (air, PCM, water), calculations were performed to determine exactly the time to cut off the flow at the inlet. The system was cut off at exactly 46 secs in-order to avoid discharge of hot water from the air exit ports. Due to density differences between the liquid and solid PCM, the molten PCM released from the solid-liquid interface floats through the hot sinking water to the top of unit.

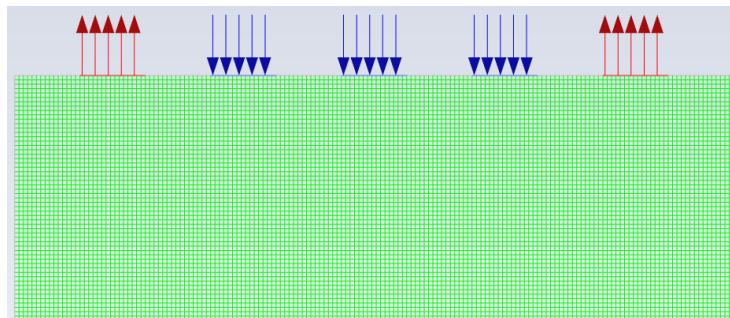


Figure 1. CFD model (grid) of the direct-contact system showing the three water inlets and two air outlets

The volume-of-fluid approach was used to keep track of each phase's volume fraction across the entire domain. Through Navier-Stokes equations, the finite-volume formulation was resolved. The phase transition (melting) processes were simulated using a solidification and melting model with the enthalpy-porosity approach. The melt interface is not specifically tracked in this technique. Instead, each cell in the domain relates to a quantity known as the liquid fraction, which shows the fraction of the cell volume that is in liquid form. Based on an enthalpy balance, the liquid fraction is determined at each iteration. The mushy zone is defined as a region with a liquid fraction between 0 and 1. The mushy zone is represented as a "pseudo" porous medium, with porosity decreasing from 1 to 0 as the material solidifies. When the material in a cell has totally solidified, the porosity is zero, and the velocities are also zero.

## 3. Results and discussion

At  $t = 0$ , the system is at steady-state with air at the top and the solid PCM is at the bottom. The HTF at a high temperature flow in through the 3 inlets nozzles into the domain to melt the PCM. Air jets out through the two outlets at the top to the atmosphere. The HTF gets in at a flow rate of 0.18 kg/s and a Reynolds number of 500. Figure 2 below shows contours of water volume fraction and PCM volume fraction. At 10 secs, water drips slowly into the system to melt the PCM by convection. As it gets to the surface of the solid PCM, it melts the PCM due to its high temperature. This gradually generates some molten PCM at the top of the solid PCM. The HTF inlets nozzles are shut-off at 46 secs and the air discharge ports are also blocked to stop water from getting into the system thus preventing undesirable discharge of hot HTF from the air exit ports. From this instance forward, the hot HTF that is already in the system now continues to melt the PCM. In figure 2 below, the red region on the left signifies HTF

seated on top of solid PCM, while the other image shows molten PCM that has floated to the top of water due to density differences.

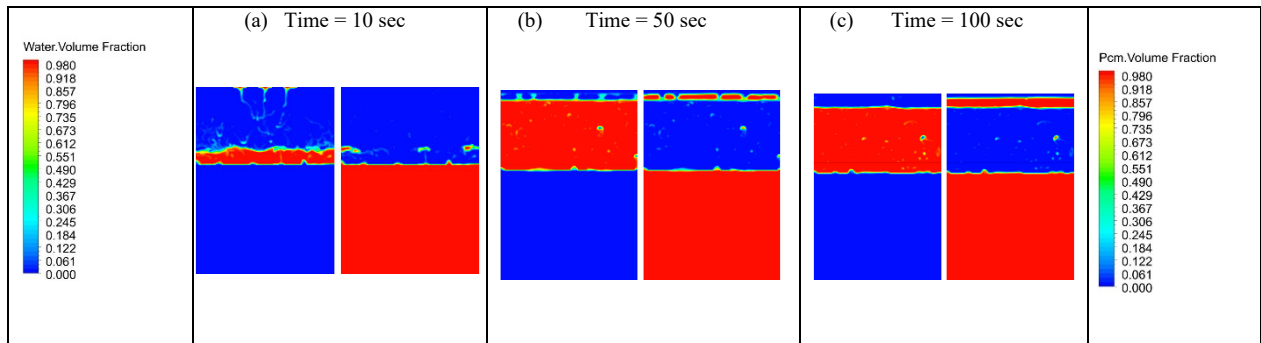


Figure 2. Contour plots of water volume and PCM volume fractions at time instants of (a) 10 secs, (b) 50 secs and (c) 100 secs.

Figure 3 shows the temperature contours during the discharging process of the PCM in the storage unit. At 10 secs, the HTF flows through the inlet channels, gets cooled by the air layer and upon reaching the solid PCM block transfers heat to the solid PCM. When the inlet is shut off at 46 secs, it is noticed that HTF starts to lose sensible heat. At 50 secs, the temperature drops by 15 K and drops further at 100 secs, but this energy lost by the HTF is gained by the PCM in form of latent heat as it changes from solid to liquid.

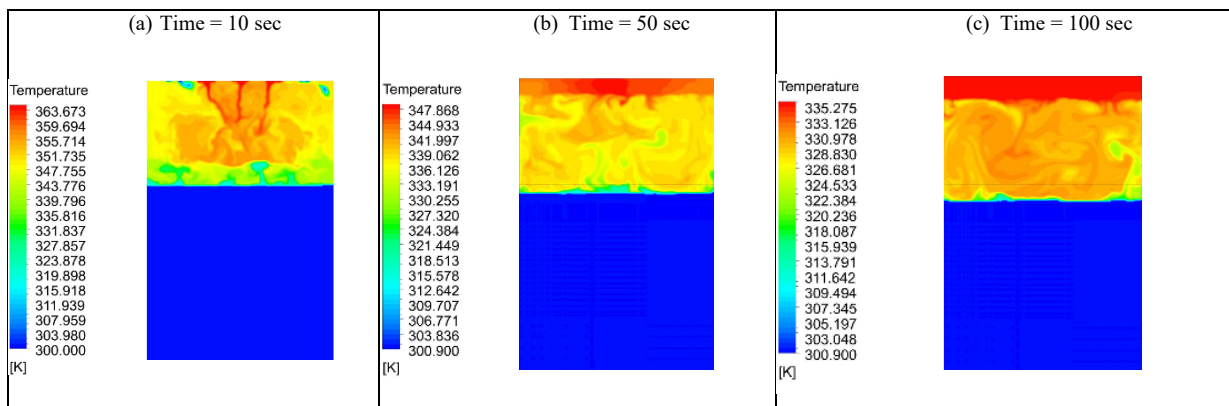


Figure 3. Contour plots of temperature at time instants of (a) 10 secs, (b) 50 secs and (c) 100 secs.

After shutting off the HTF ports at 46 secs, conduction heat transfer purely dominates the system and it is left to run for 1450 secs. As the melting continues, more molten PCM is formed, while the temperature of the system keeps decreasing. At 1450 secs, 27% of liquid PCM is formed which is shown in the volume fraction plot in Fig. 4a. Figure 4b shows the amount of energy in form of sensible heat gained by water from 0 to 46 secs before shutdown. After shutdown at 46 secs, the energy starts to reduce due to the fact that the energy is lost to PCM as it melts from solid to liquid.

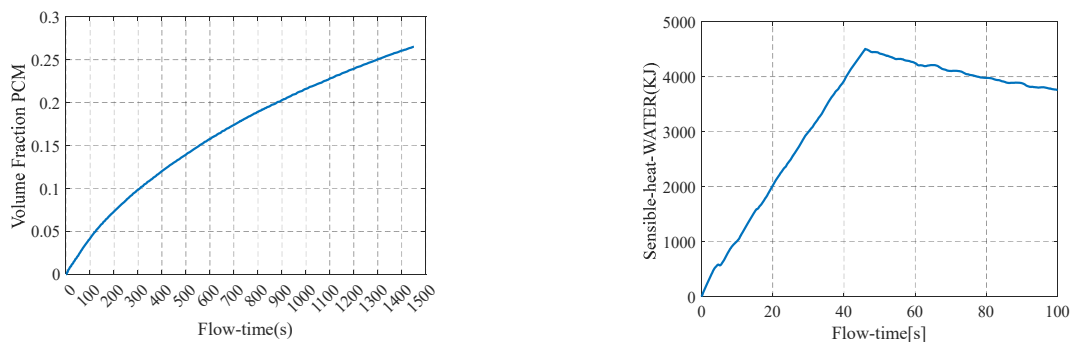


Figure 4. Time-dependent variations of (a) the volume fraction of liquid PCM and (b) Sensible heat of Water.

## 4. Conclusions

Based on findings presented in this study, the following concluding remarks are drawn:

1. Discharging capacity increases with HTF flow rate when HTF inlet temperature is constant. The increase of flow rate leads to a larger heat transfer coefficient of convection, which is beneficial to heat transfer. The higher the HTF flow rate, the shorter the time to complete discharging process.
2. Increasing the HTF inlet temperature before shutting off the inlet results in a higher liquid PCM volume fraction (melting rate).

## References.

- [1] S. Wu, G. Fang, and X. Liu, "Dynamic discharging characteristics simulation on solar heat storage system with spherical capsules using paraffin as heat storage material," *Renew. Energy*, vol. 36, no. 4, pp. 1190–1195, Apr. 2011.
- [2] S. Guo, J. Zhao, W. Wang, J. Yan, G. Jin, and X. Wang, "Techno-economic assessment of mobilized thermal energy storage for distributed users: A case study in China," *Appl. Energy*, vol. 194, pp. 481–486, May 2017.
- [3] T. Nomura, N. Okinaka, and T. Akiyama, "Technology of Latent Heat Storage for High Temperature Application: A Review," *ISIJ Int.*, vol. 50, no. 9, pp. 1229–1239, 2010.
- [4] W. Wang, S. He, S. Guo, J. Yan, and J. Ding, "A combined experimental and simulation study on charging process of Erythritol–HTO direct-blending based energy storage system," *Energy Convers. Manag.*, vol. 83, pp. 306–313, Jul. 2014.

EUROTHERM2023-L126

## Experimental investigation on the CO<sub>2</sub> hydrate formation using a hollow shaft stirrer for cold thermal energy storage

Dacheng Li<sup>1</sup>, Tiejun Lu<sup>1</sup>, Yulong Ding<sup>1</sup>, Yongliang Li<sup>1\*</sup>

<sup>1</sup>Birmingham Centre for Energy Storage, School of Chemical Engineering, University of Birmingham, Edgbaston, Birmingham B15 2TT, UK, Phone: 44- 07925877010, email: d.li.6@bham.ac.uk

### Abstract

To improve the performance of the CO<sub>2</sub> hydrate formation process, a hollow shaft stirrer was adopted and tested in this paper. An experimental system was built to learn the variation of the temperature and pressure during the reaction and validate the effectiveness of proposed research. The influence of different stirring speeds on the dissolution rate, subcooling, and gas uptake was investigated. The outcome of this study could contribute to accelerating the hydrate formation using an enhanced stirring function and can improve the capacity of the cold thermal storage system.

**Keywords:** CO<sub>2</sub> hydrate; stirring; hollow shaft; speed; formation; uptake

### 1. Introduction

Gas hydrates are becoming one of the promising cold thermal storage media owing to the high formation/dissociation enthalpy and melting/freezing temperature [1]. Additionally, the fluidity of the hydrate natural refrigerants provides more flexibility to the operation of the storage systems. Recently, carbon dioxide (CO<sub>2</sub>) is becoming one of the popular guest gases because the formed hydrate has attractive properties including no Ozone Depletion Potential, very low Global Warming Potential, non-flammable, non-toxic, and low-cost [2]. However, low formation rate and subcooling are the main challenges that hinder the application of this technology. Using the mechanical way to stir and mix the gas phase and liquid water is a straightforward method to solve the problem [3]. Compared to adding promoters (surfactants) and additives into the aqueous solution [4], this technology is easy to operate and can extend its application to the medical department and the food applications. Traditional stirrer normally has a poor mixing rate for gas-liquid, and this will lead to excess unreacted gas inside the reaction. The activation of stirring needs energy and the improvement of the agitation effects on the hydrate formation per unit energy is a key issue that needs to be discussed. In this paper, a stirrer with a hollow shaft impeller that can not only mix the reactants but also generate bubbles is adopted and tested. The effects of the rotation speed on the hydrate formation are studied experimentally and the corresponding influence on the gas uptake is also investigated.

### 2. Experimental section

#### 2.1. Materials

Carbon dioxide with a purity of 99.8 % was supplied by the BOC Ltd and used as guest molecules. On the other hand, distilled water was prepared in the laboratory using a water distiller from Stuart and used as host molecules.

#### 2.2. Facility

As shown in Figure 1, an experimental facility was built in the current study. The reactor, which is made of SS316 material, has a volume of 10 litres and can withstand a pressure of 10 MPa. Two glass windows

are designed at the outer wall of the reactor aiming to observe the reaction processes. A stirrer which consists of a hollow shaft and a gas induction impeller is equipped in the reactor to homogenise the aqueous solution. When the impeller rotates, the gas phase in the reactor can be sucked into the hollow shaft through the opened holes. Then the gas passes to the bottom and escapes through the impeller into the solution thereby increasing the mixing characteristics of the reactants. The stirring action was driven by a three-phase AC motor and the rotation speed can be regulated from 0 rpm to 700 rpm. To achieve the desired temperature for the reaction, thermal oil from a thermostat is adopted as heat transfer fluid (HTF) and circulates through the helical coil located inside the reactor. To minimise the heat loss to the outside, the reactor was enclosed with insulation. Four platinum resistance thermometers with an accuracy of  $\pm 0.1$  K are installed inside the reactor to measure the temperature of the gas phase and liquid phase (Top, Middle, and Bottom). The ambient temperature and the inlet and outlet temperature of the HTF are measured via three thermocouples with an accuracy of  $\pm 1.5$  K. On the other hand, three pressure gauges are used to measure the pressure change over the reaction process. The measured temperature and pressure were recorded by a data acquisition system.

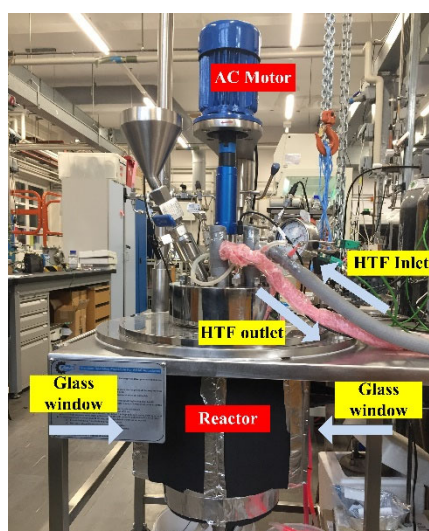


Figure 1. Real diagram of the facility for CO<sub>2</sub> hydrate

### 2.3. Procedures

Before inputting the reactants, the inside of the reactor was washed thoroughly using distilled water. Then the reactor was loaded with 5 L of distilled water and vacuumed by a rotary vane pump (pressure reached -0.8 bar). Hereafter, the stirrer started to rotate at an initial speed of 200 rpm, and carbon dioxide was continuously injected into the reactor until an initial dissolution equilibrium state, where the temperature and pressure were 295.15 K and 4 MPa, was achieved. Then, the temperature of the HTF was set at 268.15 K to cool the reactants and the stirrer was regulated to a desired rotation speed to implement the hydrate formation process. The process lasted for 3 hours and a half under the guarantee that the temperature of the water was always above the freezing point. The experiment was repeated at the rotation speed of 250 rpm, 400 rpm, 500 rpm, and 600 rpm.

## 3. Results and discussion

### 3.1. Effect of stirring speed on the hydrate formation

The processes of hydrate formation were obtained, and the corresponding P-T curves were depicted in Figure 2. A downward shift of the dissolution curves (approaching the equilibrium) can be observed with the increase of stirring speed before the rupture of metastability occurred. At a certain temperature, a higher dissolution degree of CO<sub>2</sub> in the water can be achieved when the speed increases. Besides, the degree of subcooling can be improved significantly by increasing the rotation speed of the impeller. The induction time was 7890 s, 5250 s, 1420 s, and 235 s, respectively, corresponding to the stirring speed of 250 rpm, 400 rpm, 500 rpm, and 600 rpm.

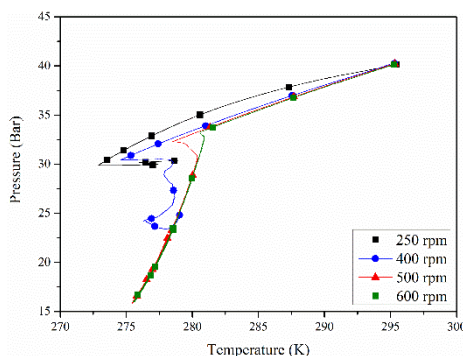


Figure 2. P-T curve for CO<sub>2</sub> hydrate formation under the different stirring speeds

The dynamic performance inside the reactor is given in Figure 3. According to the sudden increase in temperature and drop in pressure, it can be learned that the hydrate formation occurred in sequence from high to low speed. The enhanced effects of agitating and bubbling with the acceleration of the stirring can not only enlarge the heat transfer coefficient but also reinforce the mass transfer between the gas phase and liquid phase.

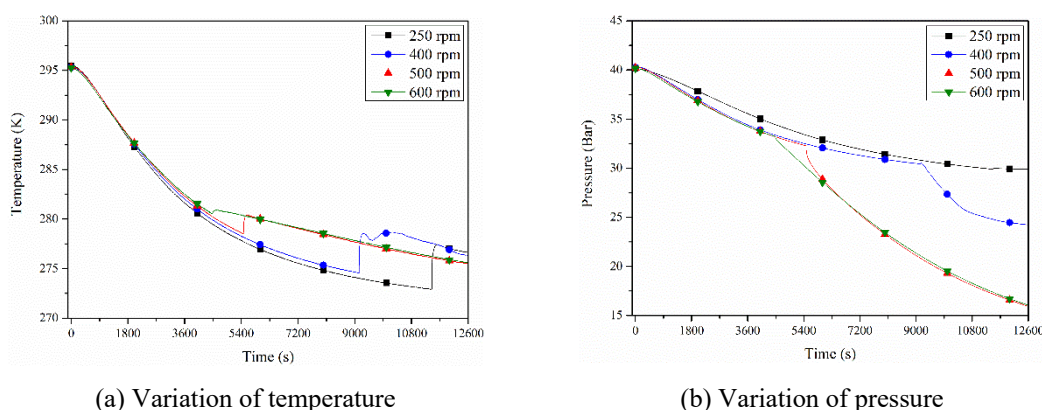


Figure 3. Dynamic characteristics of CO<sub>2</sub> hydrate formation

### 3.2. Effect of stirring speed on gas uptake

The volume changes of the gas phase during the phase transformation were neglected. Then the amount of CO<sub>2</sub> gas consumed can be calculated using the following equation:

$$\Delta n_t = (\rho_0 - \rho_t)V/N \tag{1}$$

where  $\rho$  is the density of gas phase which is obtained by REFPROP [5]; Subscripts 0 and  $t$  represent conditions of the reactor at time  $t=0$  and  $t$ ;  $V$  is the volume of the gas phase; and  $N$  is the mole mass of the gas.

The variation of the gas uptake into the aqueous solution under different stirring speeds is depicted in Figure 4. It can be learned that, before the hydrate formed, the amount of gas consumption was similar under different rotation speeds. Then a sudden surge of the gas uptake can be observed when the CO<sub>2</sub> molecule started to be trapped by the cage of water molecules. The total gas consumption at 600 rpm is 2.4 times that under 250 rpm.

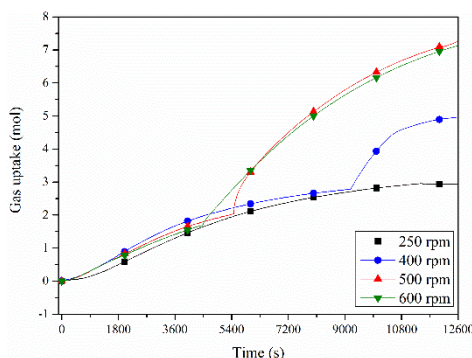


Figure 4. Effect of stirring speed on the CO<sub>2</sub> uptake

## 5. Conclusions

According to the experimental results, the following conclusion can be made:

(1) The hollow shaft stirrer is effective for improving the CO<sub>2</sub> hydrate formation and the dissolution rate increases with the stirring speed; (2) The acceleration of the rotation speed can greatly contribute to reducing the subcooling degree; (3) The amount of gas uptake can be boosted by using higher stirring speeds that are benefited from the faster hydrate formation.

## Acknowledgements

This project has received funding from the European Union's Horizon 2020 research and innovation programme under the Marie Skłodowska-Curie grant agreement No. 101007976. The authors also express their sincere gratitude to the Engineering and Physical Sciences Research Council (EPSRC) for the funding provided to this project (EP/V041665/1 and EP/T022701).

## References

- [1] Ziad Youssef, Anthony Delahaye, Li Huang, François Trinquet, Laurence Fournaison, Clemens Pollerberg, Christian Doetsch, State of the art on phase change material slurries, *Energy Conversion and Management*, 65, 2013, 120-132.
- [2] Nan Hua, Tiejun Lu, Liwei Yang, Andrew Mckeown, Zhibin Yu, Bing Xu, Adriano Sciacovelli, Yulong Ding, Yongliang Li, Thermodynamic analysis and economic assessment of a carbon dioxide hydrate-based vapor compression refrigeration system using load shifting controls in summer, *Energy Conversion and Management*, 251, 2022, 114901.
- [3] Tulluru Bhavya, Burla Sai Kiran, Pinnelli S. R. Prasad, The Role of Stirring and Amino Acid Mixtures to Surpass the Sluggishness of CO<sub>2</sub> Hydrates, *Energy & Fuels*, 35, 2021, 13937-13944
- [4] Shidong Zhou, Kun Jiang, Yongli Zhao, Yuandao Chi, Shuli Wang, Guozhong Zhang, Experimental Investigation of CO<sub>2</sub> Hydrate Formation in the Water Containing Graphite Nanoparticles and Tetra-n-butyl Ammonium Bromide, *Journal of Chemical & Engineering Data*, 63, 2018, 389-394.
- [5] E.W. Lemmon, I.H. Bell, M.L. Huber et al., NIST Standard Reference Database 23: Reference Fluid Thermodynamic and Transport Properties-REFPROP, Version 10.0, National Institute of Standards and Technology, Standard Reference Data Program. Gaithersburg. 2018.



EUROTHERM2023-M127

## A test rig for component testing for high-temperature thermal energy storage with liquid metals

Klarissa Niedermeier<sup>1</sup>, Martin Lux<sup>2</sup>, Markus Daubner<sup>3</sup>,  
Franziska Müller-Trefzer<sup>4</sup>, Thomas Wetzel<sup>5</sup>

<sup>1</sup>Karlsruhe Institute of Technology (KIT), Institute for Thermal Energy Technology and Safety (ITES),  
Hermann-von-Helmholtz-Platz 1, 76344 Eggenstein-Leopoldshafen, Germany,  
Phone: +49-721-60826902, e-mail: klarissa.niedermeier@kit.edu  
<sup>2</sup>KIT, ITES, e-mail: martin.lux@kit.edu  
<sup>3</sup>KIT, ITES, e-mail: markus.daubner@kit.edu  
<sup>4</sup>KIT, ITES, e-mail: franziska.mueller-trefzer@kit.edu  
<sup>5</sup>KIT, Institute of Thermal Process Engineering, Kaiserstr. 12, 76131 Karlsruhe,  
e-mail: thomas.wetzel@kit.edu

### Abstract

Thermal energy storage systems for high temperature  $> 600^{\circ}\text{C}$  are currently mainly based on solid storage materials that are thermally charged and discharged by a gaseous heat transfer fluid. Usually, these systems benefit from low storage material costs but suffer from moderate heat transfer rates from the gas to the storage medium. Therefore, at the Karlsruhe Liquid Metal Laboratory, liquid metals are investigated as alternative heat transfer fluids for heat storage systems, making use of the broad temperature range, in which they are in a liquid state, and their efficient heat transport capabilities. In this work, the design of a high-temperature liquid lead test rig is presented. The goal of the experiments is to demonstrate the operability of a pump, valves and the measurement equipment at  $700^{\circ}\text{C}$  in a challenging corrosive environment.

**Keywords:** thermal energy storage, high temperature, component tests, corrosion, liquid metals

### 1. Introduction

For the use in power-to-heat-to-power systems, high temperatures are desired in the thermal energy storage for high energy conversion efficiencies [1]. For that purpose, thermal energy storage systems with liquid metal as heat transfer fluids are being investigated at the Karlsruhe Liquid Metal Laboratory (KALLA) at the Karlsruhe Institute of Technology (KIT) [2, 3]. The liquid metals offer a broad liquid range and can transport heat more efficiently than conventional fluids such as gases or salts [4]. In the recent past, a packed-bed storage system with liquid metals being used as heat transfer fluid has successfully been tested at KALLA at lab scale and a demo-scale system is currently under construction [5].

However, for high temperatures of  $700^{\circ}\text{C}$ , compatible key components such as pumps and valves are not available yet due to the corrosive nature of the liquid metals at elevated temperatures. This is why at KIT, in a current joint project with the company KSB SE & Co. KGaA and the German Aerospace Center (DLR) funded by the German Federal Ministry for Economic Affairs and Climate Actions (BMWK), a test rig is being set up that will allow to test pumps and valves at  $700^{\circ}\text{C}$ . This paper will give an overview of the status regarding the materials and the design of the components of the test rig.

### 2. Materials and methods

The test rig LIMELIGHT (liquid metal loop for high temperature) will use lead as liquid metal, which has a melting temperature of  $327.5^{\circ}\text{C}$  [6]. The thermo-physical properties (at  $700^{\circ}\text{C}$  and 1 bar) are listed in Table 5.

Table 5. Properties of liquid lead (Pb) at 700°C and 1 bar [6]

Density	kg/m <sup>3</sup>	10196
Thermal conductivity	W/(m K)	19.9
Dynamic viscosity	mPa s	1.5
Specific heat capacity	J/(kg K)	142.1

The material of the pipes of the liquid metal test loop heated up to 700°C is a high-temperature chromium-nickel alloy (1.4958). To improve its corrosion resistance, a protective alumina layer is added to the inner wall of the pipes. This is done in a pre-treatment by the generation of aluminium in a pack-cementation process with a subsequent oxidation. Previous works have shown that alumina-forming metals and coating show a high resistance to liquid metals [7].

The loop will allow isothermal tests of the components at 700°C to assess the material compatibility over time. For comparison, the compatibility of the material is tested in non-moving liquid lead at the same temperature. Within the scope of the project, further materials are tested in non-moving lead.

### 3. Results and discussion

#### 3.1. Design of the test rig

The design of the high-temperature test rig is shown in Figure 14. It can be divided into two parts: the liquid metal loop (with main loop and sump tank) and the auxiliary systems (gas system and instrumentation).

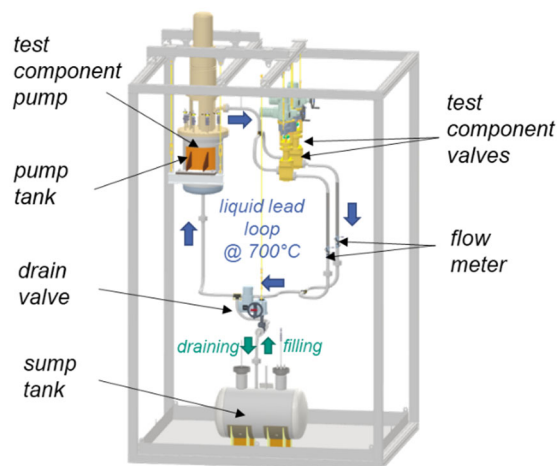


Figure 14. Simplified 3D design of the liquid lead containing parts of the test rig (blue arrows: flow direction of main 700°C loop; green arrows: flow direction during draining/filling of the loop); additional auxiliary gas systems not displayed here

The blue arrows indicate the flow direction of the liquid lead in the high-temperature loop. At the top, the pump and valves of the project partner KSB SE & Co. KGaA, which are to be tested, are shown. The pump is a centrifugal pump and will be realized as an immersion pump. Upstream of the test valves, the liquid metal flow is determined by flow meters that are based on the venturi effect and are designed according to ISO 5167-4. All pipes are inclined so that in case of emergency all components and pipes can be drained via the drain valve into the sump tank (green arrows). The sump tank also holds the liquid if the test rig is not in operation. At the start of operation, gas pressure is used to force the liquid metal into the upper part of the loop. In order to keep the lead in a liquid state at all times, trace heating is installed at the outer surface of all liquid-metal containing parts of the test rig. The trace heating is also used to heat up the medium and keep it at 700°C for the high-temperature component test. During operation, the drain valve is closed and approximately 60 l of liquid lead are in the upper part of the test

rig (blue arrows). For thermal insulation to the environment, a combination of layered Insulfrax mat and ProRox are used.

An argon gas system is used to ensure an inert atmosphere in the loop to prevent the formation of lead oxide. Argon is also used as the sealing gas for the rotating mechanical seal of the pump. The absolute gas pressure in sump and pump tank will be measured with FESTO SPTW pressure transmitters as well as the differential pressure of both valves and both venturi nozzles with Siemens pressure-transducers and measuring instruments. The level of the liquid metal in the tanks will be determined with BERU ZE 18-12 electrodes, which close an electric circuit once the electrically conductive liquid metal reaches the sensor. Bulk temperatures and surface temperatures are measured with thermocouples (type K).

### 3.2. Main components of the liquid metal test rig

The sump tank (Figure 15) is made of 1.4571 without an additional coating, as it is not experiencing the maximum temperature of the test rig (700°C), but only keeping the liquid lead inside above melting temperature in case of standstill and in case of an emergency only having a short-time temperature rise to 550°C. The volume of the sump tank is 170 l. The 3D drawing in Figure 15 (left) shows the DN25 connections for the instrumentation (temperature, level, pressure). Additionally, a 20mm pipe is installed to connect the safety valve (pressure relief valve), which opens in case of overpressure and a DN25 pipe (filling pipe), which is used for filling and draining the upper part of the loop with liquid lead at the start of operation and connects the sump tank to the drain valve, which opens in case of emergency.

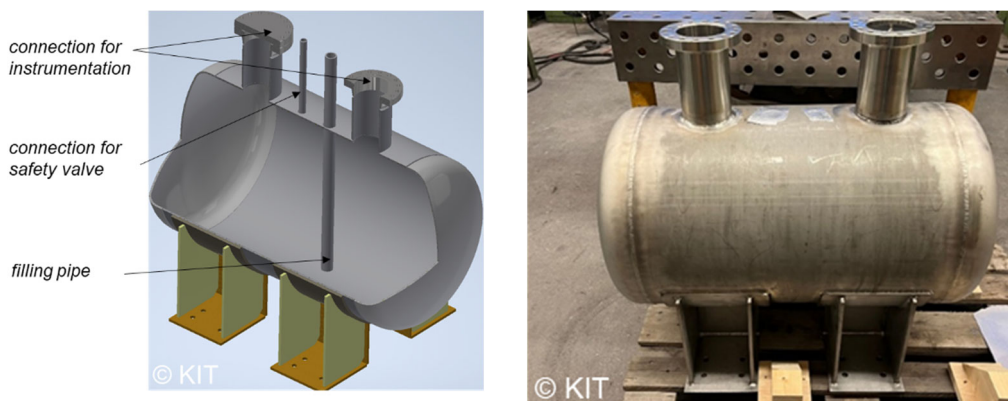


Figure 15. Sump tank for liquid lead loop (left: 3D drawing, right: photo after construction)

The 3D design for the pump tank for the immersed pump is shown in Figure 16 (left). At the DN400 flange, connections for temperature, level and pressure are provided as well as connections for the inert gas stream and the safety valve, which opens in case of an overpressure. The volume of the pump tank is approximately 70 l. From the pump tank the circular flow of liquid lead passes the valves, the venturi nozzles and goes back into the pump tank through a DN25 pipe.

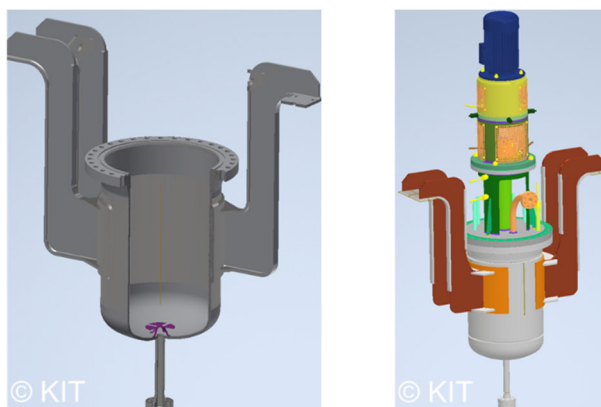


Figure 16. Pump tank for the liquid lead loop (left: 3D drawing, right: 3D drawing including immersed pump)

#### 4. Conclusions

A new liquid lead test loop is designed and currently under construction in the Karlsruhe Liquid Metal Laboratory (KALLA) at KIT. The goal is to test key components for the operation of heat storage systems (pump and valves) in 700°C flowing liquid lead to gain important insights in the material compatibility and measurement experience regarding temperature, pressure, flow and level in such challenging conditions. In combination with the parallel demonstration of a packed-bed heat storage solution with liquid metal as the heat transfer fluid, this shall close one important gap to enable the facilitation of high-temperature heat storage with liquid metal.

#### Acknowledgements

The authors would like to acknowledge the funding of the project LIMELISA (03EE5050C) by the German Federal Ministry for Economic Affairs and Climate Actions (BMWK) and the fruitful collaboration with the project partners KSB SE & Co. KGaA and German Aerospace Center (DLR).

#### References

- [1] Dumont, O.; Frate, G. F.; Pillai, A.; Lecompte, S.; De paepe, M.; Lemort, V. Carnot battery technology: A state-of-the-art review (2020). *J. Energy Storage* 32. 101756. doi: 10.1016/j.est.2020.101756
- [2] Niedermeier, K.; Flesch, J.; Marocco, L.; Wetzel, T. Assessment of thermal energy storage options in a sodium-based CSP plant (2016). *Applied thermal engineering*, 107, 386–397. doi:10.1016/j.applthermaleng.2016.06.152
- [3] Laube, T.; Marocco, L.; Niedermeier, K.; Pacio, J.; Wetzel, T. Thermodynamic Analysis of High-Temperature Energy Storage Concepts Based on Liquid Metal Technology (2020). *Energy technology*, 8 (3), 1900908. doi:10.1002/ente.201900908
- [4] Boerema, N.; Morrison, G.; Taylor, R.; Rosengarten, G. Liquid sodium versus Hitec as a heat transfer fluid in solar thermal central receiver systems (2012). *Solar Energy* 86, 2293–2305. doi: 10.1016/j.solener.2012.05.001
- [5] Müller-Trefzer, F.; Niedermeier, K.; Daubner, M.; Wetzel, T. Experimental investigations on the design of a dual-media thermal energy storage with liquid metal (2022). *Applied Thermal Engineering*, 213, 118619. doi:10.1016/j.applthermaleng.2022.118619
- [6] Handbook on Lead-bismuth Eutectic Alloy and Lead Properties, Materials Compatibility, Thermal-hydraulics and Technologies – 2015 edition (2015). OECD/NEA
- [7] Shi, H.; Azmi, R.; Han, L.; Tang, C.; Weisenburger, A.; Heinzl, A.; Maibach, J.; Stüber, M.; Wang, K.; Müller, G. Corrosion behavior of Al-containing MAX-phase coatings exposed to oxygen containing molten Pb at 600°C (2022) *Corrosion Science* 201, 110275. doi: 10.1016/j.corsci.2022.110275

EUROTHERM2023-H129

## Investigating the Influence of the Aspect Ratio on the Exergetic Performance of a Large Thermal Energy Storage System using a High-Resolution CFD model

Krüger Benno<sup>1</sup>, Dammel Frank<sup>1</sup>, Stephan Peter<sup>1</sup><sup>1</sup>Institute for Technical Thermodynamics, Department of Mechanical Engineering, Technical University of Darmstadt, Alarich-Weiss-Straße 10, 64287 Darmstadt, Germany, e-mail: krueger@ttd.tu-darmstadt.de

### Abstract

Sensible thermal energy storages play a large role in the transition towards more sustainable district heating networks. A core question in this regard is the influence of the aspect ratio of height to diameter on the storage performance. To provide reliable answers for large storage systems, a two-dimensional, high-resolution, FEM-based model has been developed and validated using temperature and mass flow data from a reference storage under real operating conditions. Based on this model, a variation of the aspect ratio has been performed. Results show, that a higher aspect ratio provides a benefit in the exergetic performance of the storage system, presumably due to the lower cross-sectional area; thus benefitting thermal stratification.

**Keywords:** Thermal energy storage, Stratified Storage, CFD, Exergy, Aspect Ratio

### 1. Introduction

In the transition towards renewable energy sources, thermal energy storage (TES) systems with water as storage material are important to manage the increased volatility associated with these sources. Additionally, they allow to decouple heat generation and demand and therefore facilitate systems that are more efficient. This is especially useful for co-generation systems [1]. When considering sensible TES systems, stratified storage systems are generally more efficient than fully mixed systems, as their significantly increased exergy provides usable temperature levels for a longer time [2]. Therefore, destratification should be avoided if possible [3]. To model TES and thus study the mechanisms of destratification and possible prevention measures, simple one-dimensional models are not sufficient and more detailed high-resolution models in two or three dimensions are needed [4-6].

High-volume TES systems have not yet been modeled extensively using high-resolution models, but some work does exist. Streckiene et al. [7] developed a two-dimensional numerical model of a TES using the finite volume method as provided by the commercial software package PHOENICS. The TES at the CHP plant in Hvide Sande, Denmark, with a gross volume of 1960 m<sup>3</sup>, provided validation data. Numerical modeling proved superior in accuracy to analytical analyses of the same storage. Further work of the same authors implemented of a three-dimensional model and focused on charge and discharge operation [8]. However, no significant differences were found when comparing the two- and three-dimensional models.

One important parameter of TES is their Aspect Ratio (AR), the ratio of storage tank height to diameter. There exists some work on the impact of the AR on small TES; Ievers and Lin conclude that a higher AR leads to a higher degree of thermal stratification. Most of the associated gains can be realized with an AR of three; further increases show diminishing returns [5]. Other studies come to a similar conclusion regarding small TES. Karim et al. found that storage tanks with higher AR result in reduced mixing and heat loss, as the contact area between layers of different temperatures are smaller [9]. Bai et al. concluded from their studies, that a higher AR is beneficial for stratification, whereas a smaller AR

is better in regard to energy efficiency. However, no significant amount of work exists concerning the influence of the AR in large TES systems [10].

## 2. Materials and method

A high-resolution two-dimensional axisymmetric FEM model was chosen for this work. It is implemented using COMSOL Multiphysics 6.0. The geometry of the existing TES, with a volume of 4300 m<sup>3</sup>, constructed by the company ENTEGA AG at a waste incineration plant in Darmstadt is simplified to reduce computational complexity and increase robustness of the model. No turbulence modeling is used. The boundary conditions are modeled in accordance with the existing TES – heat loss to the outside via the outer walls is modeled using the ambient temperature from weather measurement data [11]. Losses via the bottom of the storage are modeled using a constant heat flux, as the focus of this work is not on the interaction between the soil and storage as in works by other authors [12]. The steam cushion on top of the water in the tank is represented by a constant temperature boundary condition of 100°C. For this study, a period of 24 hours is modeled, during which charging, standby and discharging phases are represented. Mass flow, and its temperature, to the upper and lower radial diffusers is modeled using measurement data from the original TES.

The existing TES is equipped with temperature measurement equipment, providing temperature data at 144 spots in the TES. For this work, this is used to accurately calculate the enthalpy content of the storage. The enthalpy derived from measured temperatures is first used to validate the model. At this point, three meshes are evaluated. All meshes use triangular elements and solely differ in their resolution. The first mesh, called “normal”, is comprised of 122272 elements; the second mesh, called “fine”, is comprised of 154329 elements and the third mesh, called “extra fine” is comprised of 206626 elements.

In a second step, the exergy evolution of the TES is compared for three different AR over the same period of charging, standby and discharging phases. To facilitate an accurate assessment, the volume of all tanks is identical and the initial temperature distribution modified such that it is as similar as possible while possessing the same exergy content for all cases at  $t=0$ .

## 3. Results and discussion

Firstly, the formulated model is validated against the measurement data and its mesh dependency tested.

### 3.1. Model Validation

The enthalpy content of all three models tracks the enthalpy content derived from measurements very closely. The “normal” mesh performs marginally worse than the other two meshes, as can be seen in figure 1. The difference between the “fine” and the “extra fine” mesh seems to be negligible. Therefore, the “fine” mesh is used for all further simulations, and meshes of a comparable resolution are used when changes in the model geometry require a modification of the mesh.

### 3.2. Aspect Ratio

The reference TES has an AR of 1.39. Models of two comparable TES are simulated; one with an AR of 1.00 and one with an AR of 2.00. The results can be seen in figure 2. It can be seen that the TES with an AR of 1.00 shows worse performance. It inhibits both a faster decay of exergy when in the standby phase and it shows a lower charging and discharging efficiency, as the wider storage has a larger contact area between the high and low temperature volumes. In a similar way, the thermocline also occupies a larger relative volume fraction of the usable volume, thus leading to higher exergy losses. Accordingly, lower losses can be seen for the TES with an AR of 2.00.

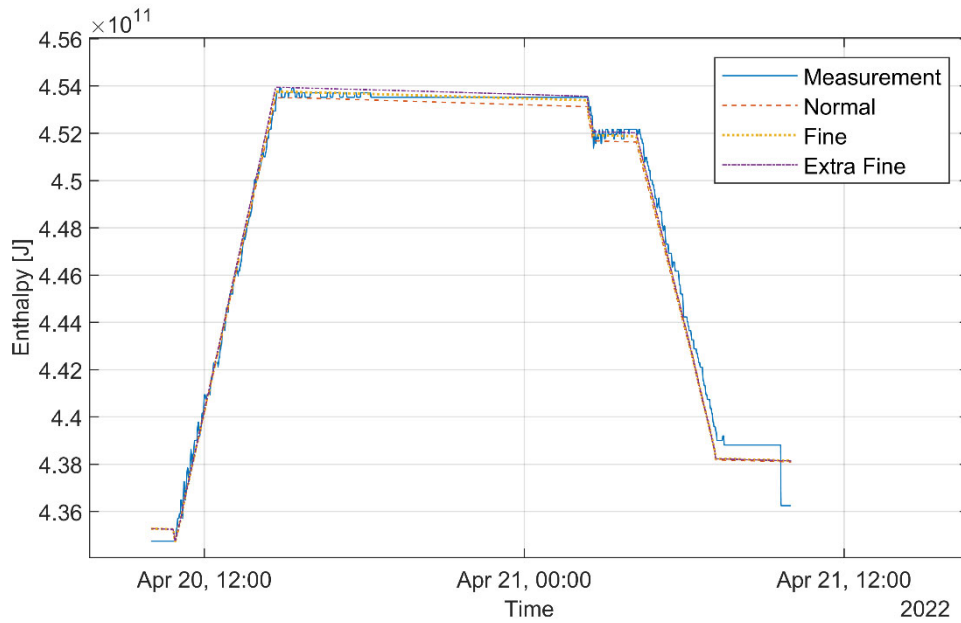


Figure 1. Enthalpy content of the TES over time. Measurement data and numerical model on three different mesh resolutions.

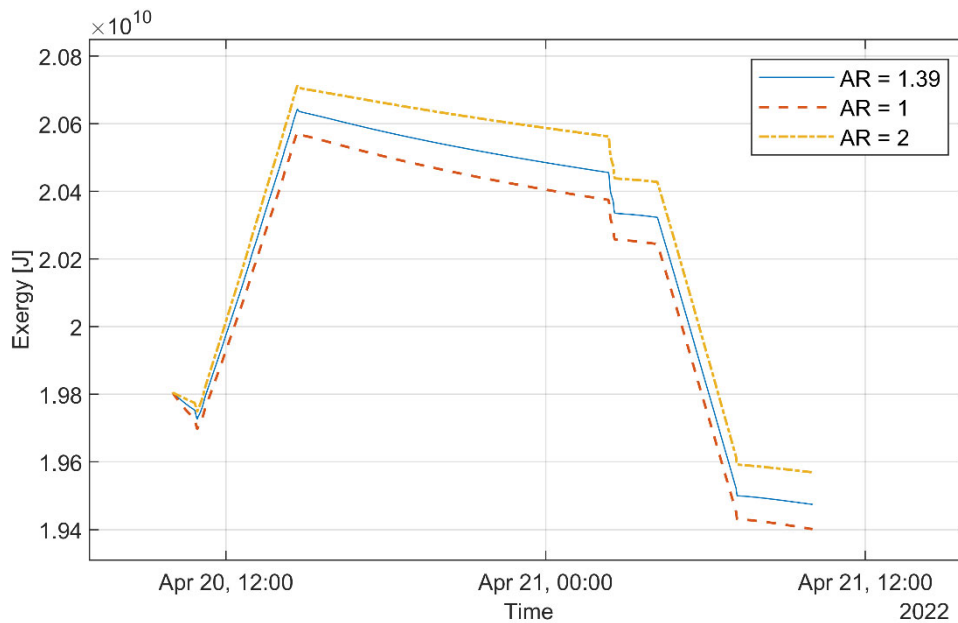


Figure 2. Comparison of the exergy content of three TES with different AR over time.

#### 4. Conclusions

A model of a large TES has been successfully developed and validated. The model performs well over a time span of 24 hours and shows only small deviations. A mesh convergence study was conducted. Derived models of TES with different AR and the same volume were developed and tested. The results show that a higher AR provides a higher exergetic efficiency, as destratification processes due to mixing and conduction are slower than in TES with a lower AR. These do not seem to be mitigated by the higher heat losses to the environment, which are due to the higher surface area, as these are comparatively small for a large TES. When constructing a TES of this size, practical concerns such as the permissible height most likely limit the maximum AR.

## Acknowledgements

Financial support was provided by EFRE Hessen (Europäischer Fonds für Regionale Entwicklung Hessen).



Europäische Union  
Investition in Ihre Zukunft  
Europäischer Fonds  
für regionale Entwicklung

## References

- [1] A. Arteconi *et al.*, “Thermal energy storage coupled with PV panels for demand side management of industrial building cooling loads,” *Applied Energy*, vol. 185, pp. 1984–1993, 2017, doi: 10.1016/j.apenergy.2016.01.025.
- [2] M. A. Rosen and I. Dincer, “Exergy methods for assessing and comparing thermal storage systems,” *International Journal of Energy Research*, no. 27, pp. 415–430, 2003.
- [3] M. A. Rosen, R. Tang, and I. Dincer, “Effect of stratification on energy and exergy capacities in thermal storage systems,” *International Journal of Energy Research*, vol. 28, no. 2, pp. 177–193, 2004.
- [4] O. Abdelhak, H. Mhiri, and P. Bournot, “CFD analysis of thermal stratification in domestic hot water storage tank during dynamic mode,” *Build. Simul.*, vol. 8, no. 4, pp. 421–429, 2015, doi: 10.1007/s12273-015-0216-9.
- [5] S. Ievers and W. Lin, “Numerical simulation of three-dimensional flow dynamics in a hot water storage tank,” *Applied Energy*, vol. 86, no. 12, pp. 2604–2614, 2009, doi: 10.1016/j.apenergy.2009.04.010.
- [6] R. de Césaró Oliveski, A. Krenzinger, and H. A. Vielmo, “Comparison between models for the simulation of hot water storage tanks,” *Solar Energy*, vol. 75, no. 2, pp. 121–134, 2003, doi: 10.1016/j.solener.2003.07.009.
- [7] G. Streckiene, V. Martinaitis, and P. Vaitiekunas, “Simulation of Thermal Stratification in the Heat Storage For CHP Plant,” in vol. 2, *Selected papers / The 8th International Conference Environmental Engineering, May 19 - 20, 2011, Vilnius, Lithuania*, Vilnius: VGTU Press "Technika", 2011, pp. 812–819.
- [8] G. Streckiene and V. Miseviciute, “Research of Operation Modes of Heat Storage Tank in CHP Plant Using Numerical Simulation,” *Scientific Journal of Riga Technical University. Environmental and Climate Technologies*, vol. 6, no. -1, 2011, doi: 10.2478/v10145-011-0013-3.
- [9] A. Karim, A. Burnett, and S. Fawzia, “Investigation of Stratified Thermal Storage Tank Performance for Heating and Cooling Applications,” *Energies*, vol. 11, no. 5, p. 1049, 2018, doi: 10.3390/en11051049.
- [10] Y. Bai, M. Yang, Z. Wang, X. Li, and L. Chen, “Thermal stratification in a cylindrical tank due to heat losses while in standby mode,” *Solar Energy*, vol. 185, pp. 222–234, 2019, doi: 10.1016/j.solener.2018.12.063.
- [11] DWD Climate Data Center (CDC), “Historische tägliche Stationsbeobachtungen (Temperatur, Druck, Niederschlag, Sonnenscheindauer, etc.) für Deutschland: Version v21.3,” 2021.
- [12] A. Dahash, F. Ochs, A. Tosatto, and W. Streicher, “Toward efficient numerical modeling and analysis of large-scale thermal energy storage for renewable district heating,” *Applied Energy*, vol. 279, p. 115840, 2020, doi: 10.1016/j.apenergy.2020.115840.



EUROTHERM2023-P130

## Organic salt hydrates as innovative materials for thermochemical energy storage

Emanuela Mastronardo<sup>1</sup>, Elpida Piperopoulos<sup>1</sup>, Luigi Calabrese<sup>1</sup>, Edoardo Proverbio<sup>1</sup>,  
Candida Milone<sup>1</sup>

<sup>1</sup>Engineering Department, University of Messina, C.da di Dio, Messina, Italy,  
e-mail: emastronardo@unime.it; epiperopoulos@unime.it; lcalabrese@unime.it; eproverbio@unime.it;  
cmilone@unime.it

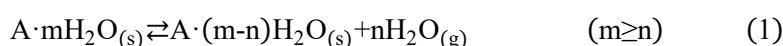
### Abstract

In order to overcome the issues caused by deliquescence in inorganic salt hydrates for thermochemical heat storage applications, it is here proposed and investigated the use of organics salts hydrates, specifically calcium ceftriaxone (CaCf) and calcium lactate (CaL). As main difference among the two salts CaCf presents a bulky organic ligand with different heteroatoms (C<sub>18</sub>H<sub>16</sub>N<sub>8</sub>O<sub>7</sub>S<sub>3</sub><sup>-</sup>) while CaL has a smallest ligand and oxygen as unique heteroatom (C<sub>6</sub>H<sub>10</sub>O<sub>6</sub><sup>-</sup>). Both are characterized by low water solubility, thus more resistance to deliquescence, a tendency to coordinate a high number of water molecules, and stability under operating conditions. The materials' heat storage capacities (595 and 1021 kJ/kg for CaCf and CaL, respectively) are comparable with that of other inorganic salt hydrates, without appreciable efficiency losses in terms of energy as cycles are performed due to unconverted material. These results support the idea of considering hydrated organic salts for effective TCS applications.

**Keywords:** organic salt hydrates, calcium ceftriaxone, calcium lactate, thermochemical heat storage

### 1. Introduction

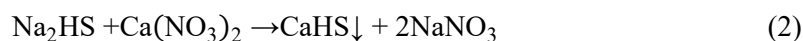
In order to shift towards carbon-free renewable energy sources, which are inherently intermittent, the use of an energy storage technology is essential. In this regard, thermochemical heat storage (TCS) with salt hydrates offers a viable solution for storing heat and re-use it on demand through a reversible reaction [1]:



The solid hydrated salt is converted (endothermic charging step), to the products that consist of a totally or partially dehydrated solid salt and water vapor. The reverse hydration reaction of the salt with water vapor, being exothermic, releases the stored heat when required. These systems, however, suffer of several drawbacks due to their tendency to undergo deliquescence phenomena. Indeed, the hydration reaction often leads to a saturated salt solution rather than a salt hydrate. Hence a deliquescence phenomenon occurs. This can imply chemical instability, mass transfer hindering, and high-pressure drops that would lead eventually to the system failure, but also corrosion issues due to the dripping of the salt solution to other metal components of the systems [2,3]. For moving TCS systems toward a higher technology readiness level, more efforts should be focused on the materials innovation. In this regard, this work aims to explore innovative materials based on highly insoluble organic hydrated salts in order to reduce and/or avoid deliquescence phenomena under operating conditions, able to coordinate a high number of water molecules, and stable under operation conditions [4]. Specifically, calcium ceftriaxone (CaCf) and calcium lactate (CaL) were selected as model compounds for investigation.

### 2. Materials and methods

CaCf was prepared by precipitation using disodium ceftriaxone hemiheptahydrate as the precursor:



While CaCL was purchased from Sigma Aldrich, (purity >98%,  $[\text{CH}_3\text{CH}(\text{OH})\text{COO}]_2\text{Ca} \cdot 5\text{H}_2\text{O}$ ) in form of fine powder. The initial water content and thermal stability were evaluated by thermogravimetric analysis coupled with a mass spectrometer. The heat storage capacity was also estimated from Differential Scanning Calorimetric (DSC) analysis. A full hydration/dehydration cycle in a controlled (temperature, relative humidity) and measurable (mass change) environment has been performed through a thermogravimetric dynamic vapor sorption system (DVS Vacuum Surface Measurement Systems) to verify the salts dehydration/hydration reversibility. The structural integrity of the molecules was verified by X-ray diffraction and Fourier-Transform Infrared Spectroscopy. Morphological observation of the salts and in their dehydrated and re-hydrated forms was carried out by an environmental scanning electron microscope (ESEM, FEI Quanta 450) operating with an accelerating voltage of 2 kV under low vacuum conditions.

### 3. Results and discussion

As deduced from TG-MS analysis (not reported here from brevity), the initial water content is 7 and 5  $\text{H}_2\text{O}$  molecules for CaCf and CaL, respectively. Both investigated materials begin to release water from 35 °C and are thermally stable up 150 °C, when the dehydration is concluded. Despite the smaller water content, the estimated heat storage capacity for CaL (1021 kJ/kg) is almost double than that of CaCf (595 kJ/kg). The materials undergo a significant structural modification during the dehydration/hydration cycle. The fresh salts, with their initial water content, have a crystalline structure, while after dehydration they became amorphous (Figure 1).

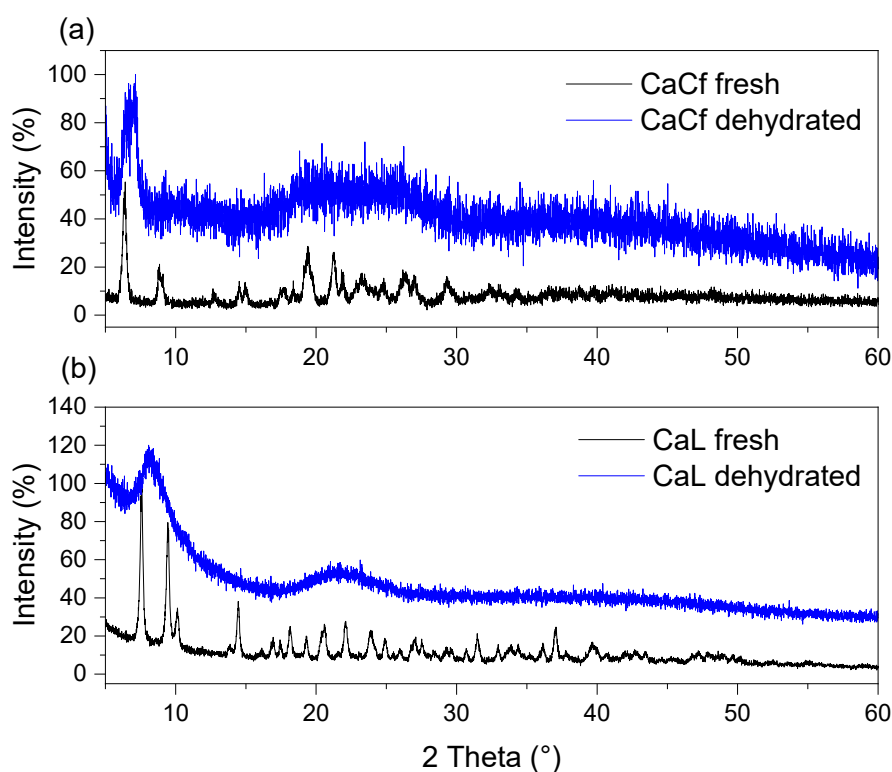


Figure 1. XRD analysis of fresh and dehydrated (a) CaCf and (b) CaL.

This structural modification in case of CaL is also accompanied by a substantial morphological modification, as inferred by SEM micrographs. From the DVS dehydration/hydration cycle (Figure 2) is evident that for both salts the re-hydration reaction is fully reversible, despite a broad hysteresis between dehydration and hydration phases thus indicating a kinetic barrier. Indeed, generally, the presence of hysteresis between the sorption and desorption isotherms indicates that the water diffusion through the material structure is slower when the lattice re-arranges upon hydration [5].

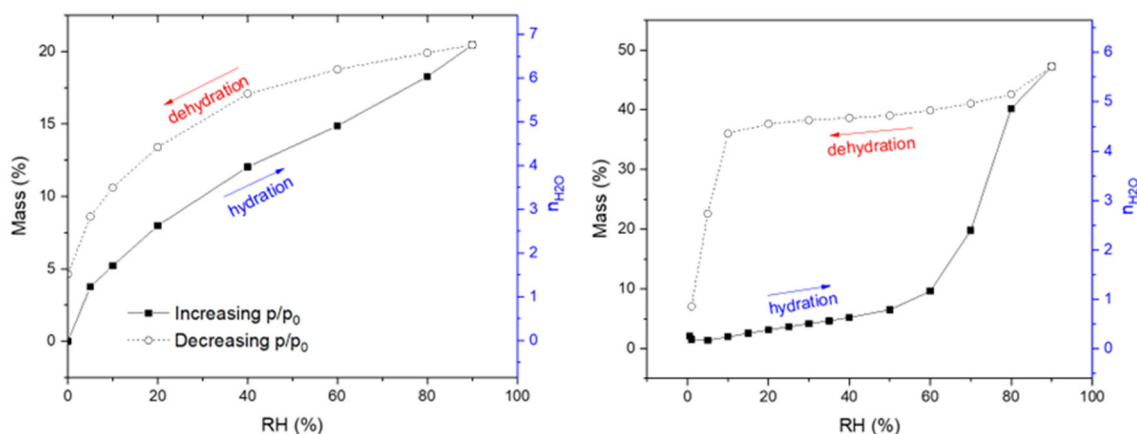


Figure 2. DVS analysis of (a) CaCf and (b) CaL.

This is applicable to both CaCf and CaL, which, as already observed, transform from a completely amorphous structure to a more ordered one when they convert from the dehydrated to the hydrated form. Due to this hysteresis, it can be deduced that at equal temperatures, the difference in the relative humidity conditions under which the heat storage occurs and those at which the release phase takes place is extreme, thus avoiding the dispersion of the accumulated heat in the case of required intermediate operating conditions.

What is more, both investigated salts do not exhibit deliquescence even at 90% of relative humidity (RH) and 30 °C. FT-IR analyses carried out on the fresh salts as well as on their dehydrated and rehydrated forms do not show any decomposition.

#### 4. Conclusions

The investigated organic salts hydrate, CaCf and CaL, in contrast to their inorganic counterparts, are stable upon exposure at an RH of 90% at 30 °C, assuring no drawbacks related to deliquescence and, at the same time, fully rehydrating at low temperature. No decomposition is observable under the operating conditions. The materials' heat storage capacities are comparable with that of other inorganic salt hydrates, without appreciable efficiency losses in terms of energy as cycles are performed due to unconverted material. Such encouraging results support the idea of considering hydrated organic salts for effective TCS applications, breaking new ground for this field of research. Further studies are ongoing for a better understanding of the materials' kinetic behavior and their stability upon several hydration/dehydration cycles.

#### Acknowledgments

This study was conducted as part of the project PON "Ricerca e Innovazione 2014 e 2020", Project ARS01\_00334 NAUSICA—NAvi efficienti tramite l'Utilizzo di Soluzioni tecnologiche Innovative e low Carbon and "Thermochemical materials for heat storage: development and characterization" sponsored by INSTM (Consorzio Interuniversitario Nazionale per la Scienza e Tecnologia dei Materiali), in the framework of the IEA SHC Task 67 "Compact Thermal Energy Storage Materials"

#### References

- [1] P.A.J. Donkers, L.C. Sögütöglu, H.P. Huinink, H.R. Fischer, O.C.G. Adan, A review of salt hydrates for seasonal heat storage in domestic applications, *Appl. Energy*. 199 (2017) 45–68. <https://doi.org/10.1016/j.apenergy.2017.04.080>.
- [2] K.E. N'Tsoukpoe, T. Schmidt, H.U. Rammelberg, B.A. Watts, W.K.L. Ruck, A systematic multi-step screening of numerous salt hydrates for low temperature thermochemical energy storage, *Appl. Energy*. 124 (2014) 1–16. <https://doi.org/10.1016/j.apenergy.2014.02.053>.



- [3] T. Kohler, T. Biedermann, K. Müller, Experimental Study of  $\text{MgCl}_2 \cdot 6\text{H}_2\text{O}$  as Thermochemical Energy Storage Material, *Energy Technol.* 6 (2018) 1935–1940. <https://doi.org/10.1002/ente.201800042>.
- [4] E. Mastronardo, E. La Mazza, D. Palamara, E. Piperopoulos, D. Iannazzo, E. Proverbio, C. Milone, Organic Salt Hydrate as a Novel Paradigm for Thermal Energy Storage, *Energies*. 15 (2022) 1–8. <https://doi.org/10.3390/en15124339>.
- [5] E. Tieger, V. Kiss, Studies on the crystal structure and arrangement of water in sitagliptin l-tartrate hydrates, *CrystEngComm*, (2016) 3819–3831. <https://doi.org/10.1039/c6ce00322b>.

EUROTHERM2023-J131

## ***In-situ* Studies on Sulfonate Polyether Ether Ketone (SPEEK)-based Composite Coatings for Thermochemical Heat Storage**

Emanuela Mastronardo<sup>1</sup>, Emanuele Previti<sup>1</sup>, Lucio Bonaccorsi<sup>2</sup>, Elpida Piperopoulos<sup>1</sup>, Luigi Calabrese<sup>1</sup>, Edoardo Proverbio<sup>1</sup>, Candida Milone<sup>1</sup>

<sup>1</sup>Engineering Department, University of Messina, C.da di Dio, Messina, Italy, e-mail: [emastronardo@unime.it](mailto:emastronardo@unime.it); [emanuele.previti@studenti.unime.it](mailto:emanuele.previti@studenti.unime.it); [epiperopoulos@unime.it](mailto:epiperopoulos@unime.it); [lcalabrese@unime.it](mailto:lcalabrese@unime.it); [eproverbio@unime.it](mailto:eproverbio@unime.it); [cmilone@unime.it](mailto:cmilone@unime.it)

<sup>2</sup>Department of Civil, Energy, Environment and Material Engineering, University Mediterranea of Reggio Calabria, 89124 Reggio Calabria, Italy e-mail: [lucio.bonaccorsi@unirc.it](mailto:lucio.bonaccorsi@unirc.it)

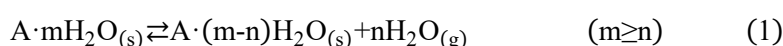
### **Abstract**

Innovative Calcium Lactate/Sulfonate Polyether Ether Ketone (CaL/SPEEK) composite coatings were synthesized and characterized for investigating their structural and morphological modification during hydration/dehydration cycles through *in-situ* techniques. These studies can certainly provide an in-depth understanding of the reaction mechanism and materials changes during the charging/discharging operations, thus leading to valuable information for the advancement of TES materials. The SPEEK, being water vapor permeable, allowed the mass transfer during the CaL hydration and dehydration steps. What is more, the flexibility of the matrix allows the volume shrinkage/expansion of the salt caused by the cyclic dehydration/hydration reactions without significant damages. Such encouraging results support the idea of considering the coating technology for effective TCS applications.

**Keywords:** sulfonate polyether ether ketone (SPEEK), organic salt hydrates, calcium lactate, thermochemical heat storage, composite coatings, *in-situ* characterization

### **1. Introduction**

Low-grade waste heat can be recovered through thermochemical heat storage (TCS) systems operating with salt hydrates through the following reversible reaction [1]:



Heat is transferred from a selected source to the salt hydrate, and the dehydration reaction takes place (storage step). The heat is stored for as long as the salt and kept in the dehydrated form. When heat is required, water is made accessible to the salt, the reversible hydration takes place, and heat is released (release step). Nevertheless, these materials suffer of severe issues caused by their tendency to undergo deliquescence, such as chemical instability, mass transfer hindering, and high-pressure drops that would lead eventually to the system failure, but also corrosion issues due to the dripping of the salt solution to other metal components of the systems [2,3]. Recently, a poorly soluble organic salt hydrated, calcium L-lactate pentahydrate (CaL), has been proposed as a novel TCS material in order to reduce and/or avoid deliquescence phenomena under operating conditions, albeit able to coordinate a high number of water molecules and stable under operation condition. Indeed, CaL can operate under conditions typical for low-temperature heat storage systems (20-120°C) with a heat storage capacity of ~1021 kJ/kg. In order to enhance the diffusion of vapour during the hydration process while increasing also the heat transfer efficiency with the heat exchanger, an innovative Calcium Lactate/Sulfonate Polyether Ether Ketone (CaL/SPEEK) composite coating was synthesized. We here investigated the structural and morphological modification during hydration/dehydration cycles of the coatings through *in-situ* studies. Specifically, a characterization protocol coupling temperature scanned X-ray diffraction (XRD), environmental scanning electron microscopy (ESEM) and thermogravimetric dynamic vapor sorption analysis was proposed. These studies can certainly provide an in-depth understanding of the reaction

mechanism and materials changes during the charging/discharging operations, thus leading to valuable information for the advancement of TES materials.

## 2. Materials and methods

CaCl was purchased from Sigma Aldrich, (purity >98%,  $[\text{CH}_3\text{CH}(\text{OH})\text{COO}]_2\text{Ca} \cdot 5\text{H}_2\text{O}$ ) in form of fine powder. For the coating preparation SPEEK was solubilized in dimethylformamide (DMF), and then the organic hydrated salt is added, in different proportion (50-80% wt.). The coating deposition of the resulting solutions was performed, using drop casting technique, on aluminium strips. Morphological observation of CaL/SPEEK coatings while hydrating was carried out by an environmental scanning electron microscope (ESEM, FEI Quanta 450) operating with an accelerating voltage of 5 kV. Initially, the material was dehydrated in oven at 80 °C for 2h and then placed in the ESEM chamber for acquiring the micrographs under controlled water vapor atmosphere. The relative humidity (RH) has been varied between 0-90% by tuning the temperature and water vapor pressure in the ranges of 5-40 °C and 10-800 Pa. A full hydration/dehydration cycle in a controlled (temperature, relative humidity) and measurable (mass change) environment has been performed through a thermogravimetric dynamic vapor sorption system (DVS Vacuum Surface Measurement Systems). The coating structure was investigated by temperature scanned X-ray diffraction (XRD). Water vapor permeability was also investigated.

## 3. Results and discussion

The as prepared coatings, regardless the CaL content, appear as a transparent layer on the aluminum lamina (Figure 1a) and, due to final drying after deposition, CaL is in its dehydrated form as can be inferred from XRD analysis (Figure 1b, black curve). The CaL is fully dissolved into the polymeric matrix. After hydration the material turns in its crystalline phase structure (Figure 1b, red curve).

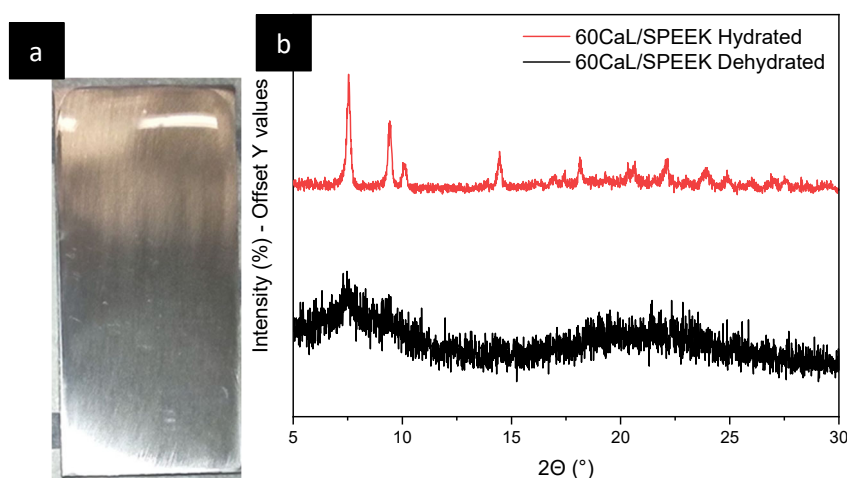


Figure 17. (a) CaL/SPEEK coating on aluminum lamina with 60% wt. of CaL (code: 60CaL/SPEEK). (b) XRD analysis on

The ESEM analysis conducted on the CaL/SPEEK coating simulated the hydration/dehydration reaction conditions. This approach allowed to visually evaluate the morphological modification while hydrating and dehydrating the CaL salt embedded in the water vapor permeable SPEEK. The dehydration and hydration conditions were obtained varying temperature and water vapor pressure in the ranges of 5-40 °C and 10-800 Pa, respectively, in order to vary the chamber RH at which the material is exposed. For brevity, *in-situ* ESEM micrographs of only 60%CaL/SPEEK are shown in Figure 2. The material in its initial state (Figure 2a) shows a smooth surface with the CaL finely dispersed in the polymeric matrix. After hydration for 2h at 95% RH a needle-like particles still embedded in the SPEEK appear on the analysed surface. The final step of the dehydration carried out for 2h at 60 °C and 0% RH brings to the formation of some cracks on the coating surface, albeit the structural integrity is still preserved.

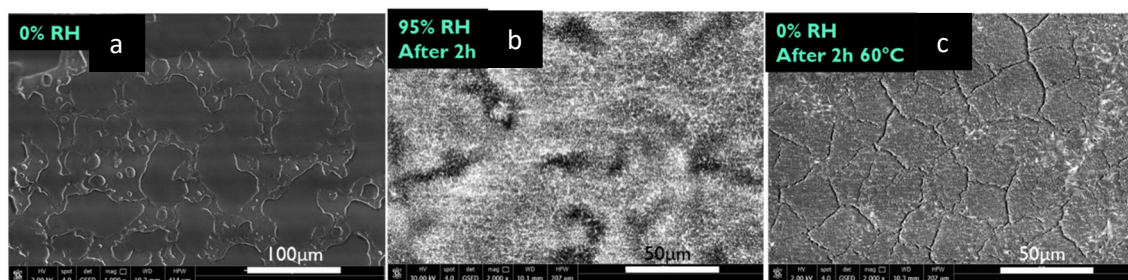


Figure 18. ESEM analysis simulating the hydration/dehydration cycle by varying the RH: (a) RH=0% initial state; (b) after 2h at 95% RH – hydration state; (c) after 2h at 60°C and 0% RH – dehydration state.

#### 4. Conclusions

Innovative Calcium Lactate/Sulfonate Polyether Ether Ketone (CaL/SPEEK) composite coatings were synthesized and characterized for investigating their structural and morphological modification during hydration/dehydration cycles through *in-situ* techniques. The environmental SEM analysis simulated the hydration/dehydration reaction conditions, thus allowing the evaluation of the interaction between the salt and the water vapor environment in the SPEEK. The results show the complete dissolution of the salt into the polymeric matrix. SPEEK, being water vapor permeable, allowed the mass transfer during the CaL hydration and dehydration steps. Additionally, despite some cracks are visible on the coating surface after a hydration/dehydration cycle, the flexibility of the matrix allows the volume shrinkage/expansion of the salt caused by the cyclic dehydration/hydration reactions without significant damages. These encouraging results paved the way for breaking new ground on CaL/SPEEK composite coatings for TCS applications. The hydration/dehydration kinetics are still object of investigation and as well as their stability upon several hydration/dehydration cycles.

#### Acknowledgments

This study was conducted in the framework of the IEA SHC Task 67 “Compact Thermal Energy Storage Materials”, and financially supported by P.O. FESR SICILIA 2014/2020 project “SMART-ART” CUP G79J18000620007.

#### References

- [1] F. Trausel, A.J. De Jong, R. Cuypers, A review on the properties of salt hydrates for thermochemical storage, *Energy Procedia*. 48 (2014) 447–452.
- [2] K.E. N’Tsoukpoe, T. Schmidt, H.U. Rammelberg, B.A. Watts, W.K.L. Ruck, A systematic multi-step screening of numerous salt hydrates for low temperature thermochemical energy storage, *Appl. Energy*. 124 (2014) 1–16.
- [3] T. Kohler, T. Biedermann, K. Müller, Experimental Study of  $MgCl_2 \cdot 6 H_2O$  as Thermochemical Energy Storage Material, *Energy Technol.* 6 (2018) 1935–1940.

EUROTHERM2023-P132

## Experimental demonstration of a novel dispatchable high temperature latent heat storage system

Asem Alemam<sup>1</sup>, Nicolas Lopez Ferber<sup>1</sup>, Valerie Eveloy<sup>1</sup>, and Nicolas Calvet<sup>1</sup>

<sup>1</sup>Mechanical Engineering Department, Khalifa University, Masdar Institute Solar Platform, P.O. Box 127788, Abu Dhabi, United Arab Emirates. e-mail: nicolas.calvet@ku.ac.ae

### Abstract

The issue of supply-demand mismatch in renewable energy systems highlights the importance of energy storage systems in microgrids. This study offers an experimental validation of a state-of-the-art full-scale electrical thermal energy storage (ETES) system, also called Carnot battery. It includes a solar-powered high temperature latent heat thermal energy storage system connected to a Stirling engine developed by Azelio AB (Sweden) and commercially called TES.POD<sup>®</sup> (Thermal energy storage power on demand). Based on the experimental data obtained from the TES.POD<sup>®</sup> system, the input power, output power, and system efficiency are reported over 10 days. Results show that this prototype can produce electricity at a nearly constant rate of 10.5 kW for 13 hours with an average cycle efficiency of 23%. The tested system performed well indicating promising potential for latent heat storage to be used for long duration energy storage applications.

**Keywords:** Electrical thermal energy storage (ETES), Carnot battery, Phase change material (PCM), Al-Si metal alloy, Stirling engine.

### 1. Introduction

Solar energy is abundant worldwide; however, it is intermittent and not accessible during the night or cloudy/dusty weather. Energy storage systems can be used to offset the variable production of renewable energy sources and provide uninterrupted or on-demand energy generation for consumers. One solution is to use a phase change material (PCM) in a thermal energy storage (TES) system. Following a previous research collaboration on corrosion preventive validation [1], Khalifa University, Masdar, and Azelio AB (Sweden) signed a collaborative research agreement in January 2022 to install and test Azelio's Thermal Energy Storage-Power on Demand (TES.POD<sup>®</sup>) technology at the Masdar Institute Solar Platform (MISP) [2]. The novelty of the project is the utilization of a metal alloy as the PCM, which has a high thermal conductivity. The Aluminum-Silicon (Al-Si) alloy was chosen due to its melting temperature around 575°C, which is suitable for power generation using a Stirling engine. TES.POD<sup>®</sup> is one of the first modular commercial high temperature electric TES systems that can be suitable for microgrid stabilization and providing long duration energy storage in remote photovoltaic (PV) or wind turbines connected areas.

Azelio's TES.POD<sup>®</sup> has a specified long lifespan of 30 years with no degradation [3]. Each TES.POD<sup>®</sup> unit consists of four main parts; the heating system, storage tank, the heat transfer fluid (HTF) loops (liquid sodium), and the power block. For the heating system, a 100 kW<sub>e</sub> electric heater powered by either renewable energy (PV or wind) or grid electricity is used to heat the HTF. Subsequently, the HTF carries thermal energy to melt the Al-Si material inside the PCM storage tank, this process is called storage charging phase. In the discharge phase, another HTF loop collects heat from the PCM tank, causing PCM solidification, and supplies it to the power block, that is a Stirling engine connected to a generator producing a maximum electric power of 13 kW. Figure 19 shows one of the two TES.POD<sup>®</sup> units operated and tested at the MISP.



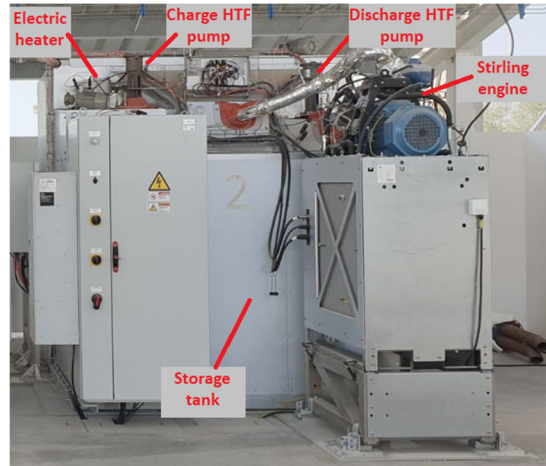


Figure 19. TES.POD<sup>®</sup> unit at the MISF.

There are three possible operating modes that the TES.POD<sup>®</sup> follows, with only one mode at a time: charging, discharging, and idle. In charging mode, energy is stored in the TES and in discharging mode, released from the TES. In idle mode, neither charging nor discharging takes place and the system is completely switched off; this mode might be beneficial for proper scheduling of the system operation. Figure 20 represents a schematic diagram of the basic idea of the TES.POD<sup>®</sup>. The system consumes power during the charging phase to heat the HTF, while electrical power is produced by the Stirling engine and electrical generator during the discharging phase.

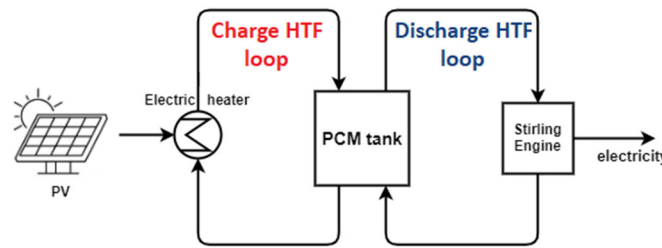


Figure 20. Main components in a TES.POD<sup>®</sup> unit.

## 2. Methods

The performance of the TES.POD<sup>®</sup> system is experimentally characterized. Data of interest such as electric heater power consumption for sensible heating of the HTF, and electrical power generated by the generator connected to the Stirling engine, are measured using high-resolution sensors. The energy supplied by the heater and energy produced by the Stirling engine are calculated from the area enclosed by the power curve. The net TES.POD<sup>®</sup> first-law efficiency (electrical to electrical) over a single operating cycle including one charge and one discharge is derived from the above measured quantities as the ratio of electricity generated by the Stirling engine, over the electricity consumed by the electric heater taking into consideration the auxiliary components consumption during both charge and discharge cycles:

$$\eta_{cycle} = \frac{\int_0^t P_{engine} dt - \int_0^t P_{AUX_D} dt}{\int_0^t P_{heater} dt + \int_0^t P_{AUX_C} dt} \quad (1)$$

Each daily cycle consists of a single charge cycle and a discharge cycle, which simulate a real-world operation scenario of such systems. The power consumption and production data were measured over 10 consecutive days of operation (i.e., 10 daily cycles) between Sep 26<sup>th</sup> and Oct 6<sup>th</sup>, 2022. Each daily cycle commenced at 9:00 am with 24 hours duration. While in this initial experimental characterization phase the TES.POD<sup>®</sup> electrical power input was supplied by the grid, the system will be driven using a 450 kW<sub>p</sub> solar PV farm currently under installation after TES.POD<sup>®</sup> commissioning.

### 3. Experimental results

Figure 21 depicts the power inflow and outflow to/from the TES.POD<sup>®</sup> unit for the 10-day period under analysis. Several operation scenarios were tested over the study period, the average duration of charge, discharge and idle phases were 7, 13 and 4 hours, respectively. During the first 3 days, the electric heater power increased and decreased steadily to imitate the power production profile of PV to some extent. However, the heater power profile increases and decreases sharply during the rest of the days.

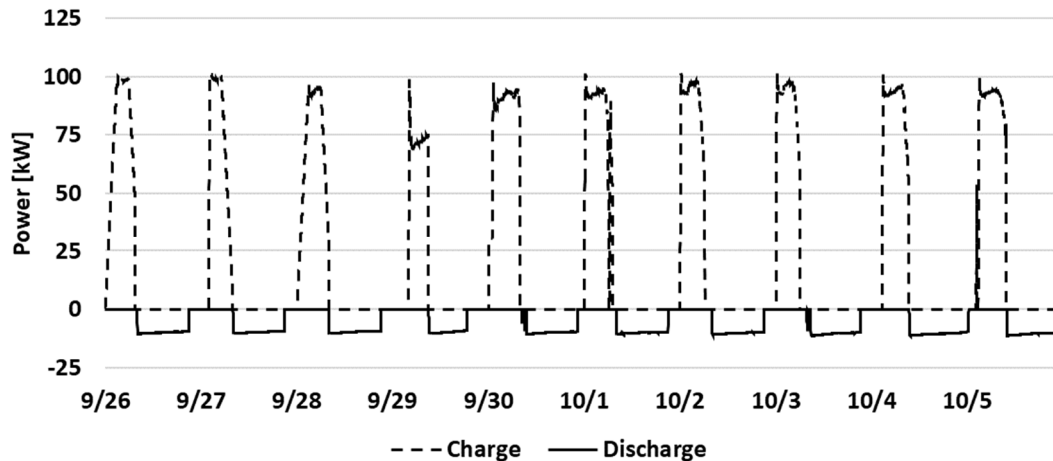


Figure 21. Charge and discharge power profile from 10 consecutive days from Sep. 26<sup>th</sup> to Oct 6<sup>th</sup> at the MISP.

The measurements in Figure 21 show that the TES.POD<sup>®</sup> can generate near constant power at  $10.5 \pm 1$  kW<sub>e</sub> rate over the 13 hours of discharge. This is attributable to the use of a highly conductive PCM as storage medium, which results in almost constant heat rate supplied by the storage tank to the power block.

The TES.POD<sup>®</sup> cycle first-law efficiency derived using equation 1 over the testing duration is represented in Figure 22. The net cycle efficiencies range between 19.2% and 26.6% with an average of 23%. This variation is explained by the different operation scenarios tested these days. For instance, the electric heater worked for less than 6 hours with 35% of the time at power less than the rated power while the Stirling engine operated near the nominal power for 13 hours, resulting in the highest net cycle efficiency of 26.6%, which was recorded on Sep. 27<sup>th</sup>. On the other extreme, the lowest net cycle efficiency was 19% on Sep. 30<sup>th</sup> due to the long electric heater operation period of 8 hours with the highest energy input over the testing duration. Other than these cycles, the TES.POD<sup>®</sup> net efficiency varied around its average value with a slight deviation of less than 7.5%, which can be justified by the variation of the day-to-day input and output power and duration.

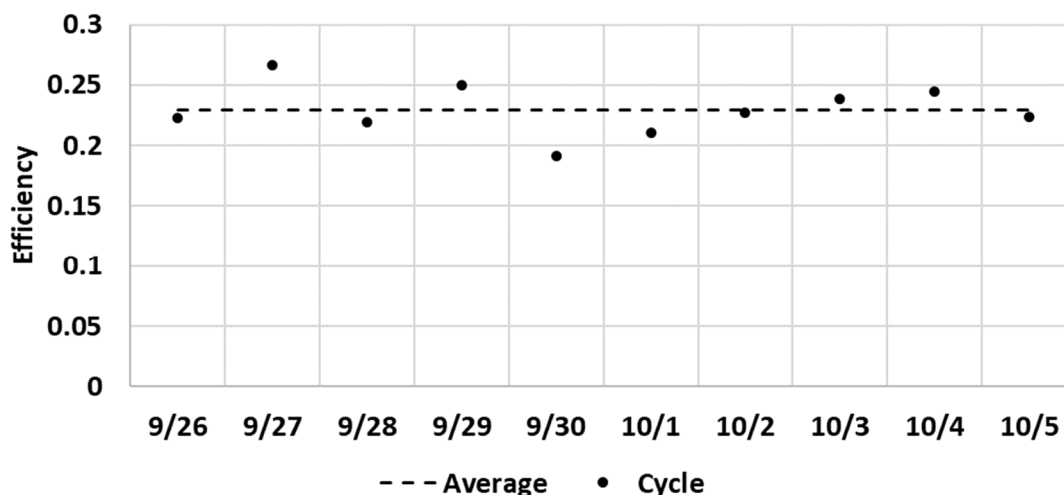


Figure 22. TES.POD<sup>®</sup>'s net cycle efficiency over 10 cycles from Sep. 26<sup>th</sup> to Oct 6<sup>th</sup>.

#### 4. Conclusions

Azelio's TES.POD<sup>®</sup> technology was successfully experimentally demonstrated at the MISP, indicating its potential for long duration energy storage applications, with the ability to produce an average 10.5 kW<sub>e</sub> over 13 hours with an average net cycle efficiency of 23%.

#### Acknowledgment

This work is funded by Azelio AB through the Research grant number 8434000329 and ASPIRE Virtual Research Institute Task 2 Grid Scale Energy Storage funding number 8434000442.

#### References

- [1] A. Dindi, N. Lopez Ferber, D. Gloss, E. Rilby, and N. Calvet, "Compatibility of an Aluminium-Silicon metal alloy-based phase change material with coated stainless-steel containers," *J Energy Storage*, vol. 32, no. September, pp. 1–18, 2020, doi: 10.1016/j.est.2020.101961.
- [2] "Khalifa University, Masdar and Azelio launch electrical thermal energy storage system technology that enables 24/7 clean energy utilization, at Masdar City." <https://www.ku.ac.ae/khalifa-university-masdar-and-azelio-launch-electrical-thermal-energy-storage-system-technology-that-enables-247-clean-energy-utilization-at-masdar-city> (accessed Feb. 20, 2022).
- [3] Azelio AB, "Azelio Annual Report 2021," Gothenburg, Sweden, 2021. doi: 10.3934/allergy.2022001.

EUROTHERM2023-H133

## Development of the solid/liquid phase change materials library - sIPCMLib

Tilman Barz<sup>1</sup>, Fabrizia Giordano<sup>1</sup>, Adam Buruzs<sup>1</sup>

<sup>1</sup>AIT Austrian Institute of Technology GmbH, Center for Energy, Giefinggasse 2, 1210 Vienna, Austria, e-mail: tilman.barz@ait.ac.at

### Abstract

We give an overview about ongoing activities for the development of a library for solid/liquid phase change materials (PCM) – sIPCMLib, which is available at <https://slpcmlib.ait.ac.at/>. The purpose of the library is to provide computer code for the calculation of PCM thermal and rheological properties. These properties can be used for the numerical modeling of heat transfer in PCM and the analysis of the thermal performance of PCM enhanced materials and components. Most commercial PCM included in sIPCMLib are materials and mixtures with a non-isothermal phase change behavior, showing multi-step transitions and thermal hysteresis. It is discussed how to account for these complex phenomena in numerical modeling in Matlab, Python and Modelica/Dymola.

**Keywords:** Solid/liquid phase change materials; phase transition models; Modelica/Dymola; apparent and effective material properties; numerical library; thermal hysteresis

### 1. Introduction

Solid/liquid PCM are usually characterized not only by their calorific properties, but also by the thermal conductivity in the solid and liquid phases, viscosity of liquid phase and density as a function of temperature [1]. Pressure dependence is mostly neglected.

Currently there does not exist a database which provides relevant material properties for commercial PCM in a format and syntax which allows linking to numerical models of heat transfer with phase change. sIPCMLib aims at closing this gap and to support the workflow for model-based analysis of PCM enhanced materials and components, see **Error! No s'ha trobat l'origen de la referència..**

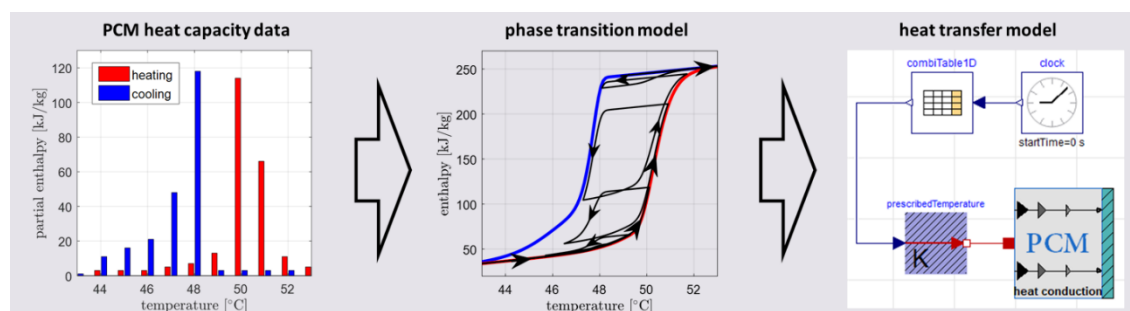


Figure 23. The workflow in sIPCMLib: Starting from heat capacity data of a selected PCM (left); identify the effective phase transition behavior and model relevant material properties (middle); use the properties for the modeling of heat transfer in PCM (right).

### 2. General features of sIPCMLib

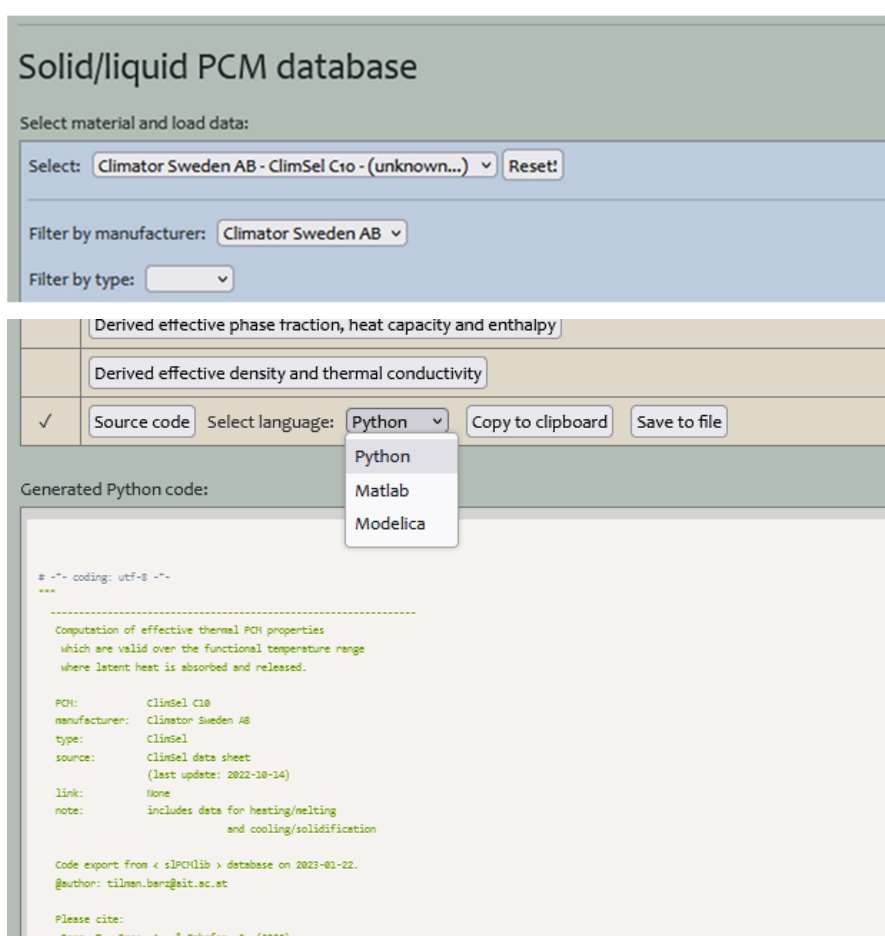
sIPCMLib provides data, correlations and models for the computation of so-called "effective" material properties of solid/liquid PCM showing a non-isothermal phase transition behavior:

- data: single phase solid and liquid properties

- correlations: temperature dependent functions to predict
  - the progress of the phase change during complete melting and solidification processes: liquid mass, and liquid volume phase fraction functions
  - effective properties within the phase transition temperature range: density, thermal conductivity, specific heat capacity and enthalpy
- models: (macroscale phenomenological) phase transition models to account for temperature shifts in latent transition changes, e.g. due to multi-step transitions and thermal hysteresis

To date, 79 commercial paraffin-based and hydrated salt-based PCM are included in the database of sPCMLib covering commercial products from Rubitherm GmbH, Climator Sweden AB and Knauf Gips KG. Work is in progress to add materials from more manufacturers.

The source code (Python, Matlab, Modelica/Dymola) for correlations is available (via copy to clipboard or save to file), see **Error! No s'ha trobat l'origen de la referència.** for an example. Modelica/Dymola source code for phase transition models is included in the repository <https://github.com/AIT-TES/sPCMLib>.



The screenshot shows the 'Solid/liquid PCM database' web interface. At the top, there's a section 'Select material and load data:' with a dropdown menu set to 'Climator Sweden AB - ClimSel C10 - (unknown...)' and a 'Reset!' button. Below that, 'Filter by manufacturer:' is set to 'Climator Sweden AB' and 'Filter by type:' is empty. There are three tabs: 'Derived effective phase fraction, heat capacity and enthalpy', 'Derived effective density and thermal conductivity', and 'Source code'. The 'Source code' tab is active, showing a 'Select language:' dropdown with 'Python' selected, and buttons for 'Copy to clipboard' and 'Save to file'. A dropdown menu is open over the language selection, showing 'Python', 'Matlab', and 'Modelica'. Below the menu, the 'Generated Python code:' section shows a code preview with the following content:

```

# -*- coding: utf-8 -*-
...
-----
Computation of effective thermal PCM properties
which are valid over the functional temperature range
where latent heat is absorbed and released.

PCM:      ClimSel C10
manufacturer: Climator Sweden AB
type:     ClimSel
source:   ClimSel data sheet
          (last update: 2022-10-14)
link:     None
note:     includes data for heating/melting
          and cooling/solidification

Code export from < sPCMLib > database on 2023-01-22.
@author: tilman.banz@it.ec.ut

Please cite:
Banz, T., Gres, A., & Enhofer, J. (2022).

```

Figure 24. Web-interface where the generated source code for the computation of effective properties is available in different programming languages.

### 3. On the conversion of heat capacity data given as partial enthalpies to smooth functions and the derivation of effective material properties

Heat storage capacity of PCM is usually tabulated as scalar values for the phase change enthalpy and melting temperature. For some PCM also apparent heat capacity data is available. According to recommendations by Mehling and Cabeza [2], most manufacturers publish heat capacity data as stored

heat in 1.0 K intervals (partial enthalpies), see **Error! No s'ha trobat l'origen de la referència.** for an example.

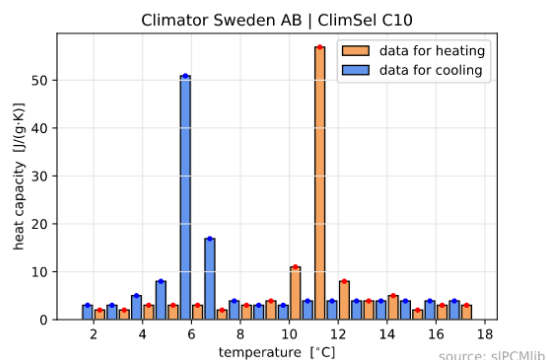


Figure 25. Heat capacity data for heating (melting) and cooling (solidification) of the commercial PCM ClimSel C10 as available in the manufacturer datasheet from Climator Sweden AB (Skövde, Sweden).

As pointed out e.g. by Kosny [1], a real PCM with a non-isothermal phase change behavior should be represented by a temperature dependent function, e.g. enthalpy as function of temperature. For efficient numerical solution it is advisable to use smooth functions, such as interpolation splines or smooth analytical fitting functions. Relevant material properties are effective (or apparent) specific heat capacity, enthalpy, density, thermal heat conductivity and viscosity.

Non-isothermal behavior means that the phase change occurs in a temperature range with co-existing solid and liquid material, not at a single temperature. The effective properties describe the material behavior in solid and liquid state, and within this temperature range. The properties are modelled by a weighting of solid and liquid contributions, see [3] for details. The weighting is realized by temperature dependent phase transition functions. They describe the portion of solid and liquid material and thus, the phase change progress. The functions are defined either on a mass or on a volume basis, i.e. liquid mass fraction and liquid volume fraction. In Differential Scanning Calorimetry (DSC) analysis of heat capacity data, the baseline construction method is used for the determination of the liquid mass phase fraction [4] and the phase change enthalpy. The baseline connects solid and liquid heat capacities in the phase transition temperature range and represents the effective heat capacity, see **Error! No s'ha trobat l'origen de la referència.** left for an example.

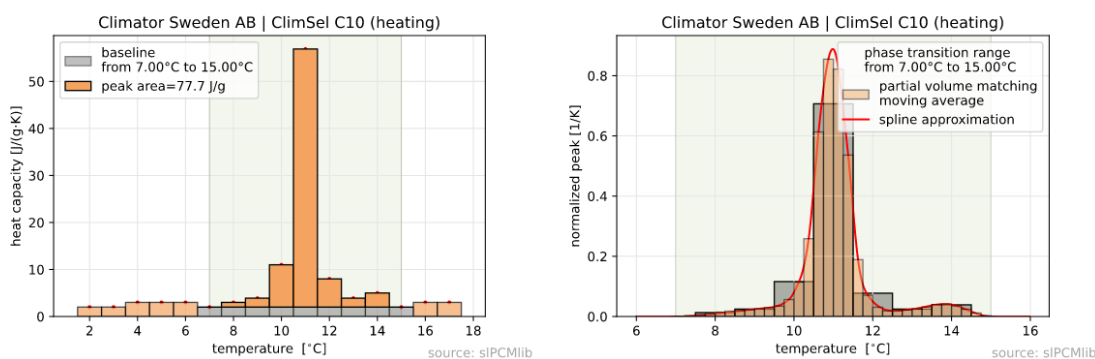


Figure 26. LEFT: Results from the baseline construction for the data for heating in **Error! No s'ha trobat l'origen de la referència.** RIGHT: Smoothed and interpolated heat capacity peak for the data in **Error! No s'ha trobat l'origen de la referència.** left.

In **Error! No s'ha trobat l'origen de la referència.** left the baseline construction is applied to data given as partial enthalpies on a 1 K grid. The data is usually obtained from (continuous) heat capacity measurements generated by e.g. T-history method or three-layer-calorimetry. The calculation of partial enthalpies means averaging of data, thus, some details of the curve shape of the original heat capacity data might be lost. A heuristic approach to reverse this process, to partially recover the original shape and to smooth the staircase graph (partial enthalpies) is the so-called partial volume matching moving average method proposed in [5]. The method produces partial enthalpy values on a (more) dense grid,

see **Error! No s'ha trobat l'origen de la referència.** right. The important feature of this method is the mean preservation, i.e. the total area under the curve (i.e. the enthalpy) does not change. In sIPCMlib we have obtained reasonable results using a 0.25 K grid. The moving average method realizes a first transformation. The second transformation is done by spline interpolation. We use cubic hermite basis functions and Akima method [6], see **Error! No s'ha trobat l'origen de la referència.** right. The normalized integral peak function is then the (liquid mass) phase fraction function. Monotonic increasing phase fraction functions are obtained if the peak functions are non-negative. This is accomplished by consideration of corresponding non-negativity conditions in Akima interpolation method, see [7]. As an example, **Error! No s'ha trobat l'origen de la referència.** shows the identified smooth (and monotone increasing) phase fraction functions for heating and cooling (left) and corresponding enthalpy (right).

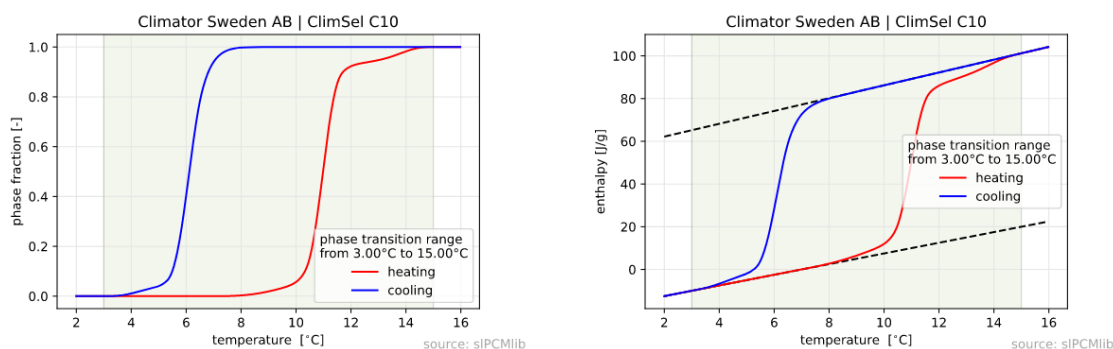


Figure 27. LEFT: Smooth liquid mass phase fraction functions for heating and cooling for the data in **Error! No s'ha trobat l'origen de la referència.** RIGHT: Corresponding enthalpy.

## 4. Conclusions

sIPCMlib, available at <https://slpcm.lib.ait.ac.at/>, allows for a detailed analysis of the thermal performance of PCM enhanced materials and components. Compared with property models considering an isothermal phase change behavior the phase transition models in sIPCMlib may be more realistic and accurate. sIPCMlib generated computer code can be easily included in Matlab, Python and Modelica/Dymola software. Example numerical models and applications are available at <https://github.com/AIT-TES/sIPCMlib> and will be also covered in the presentation.

## Acknowledgements

This project has received funding from the European Union Horizon Europe Programme under grant agreement No 101096789 (HYSTORE).

## References

- [1] Kosny. PCM-Enhanced Building Components. Engineering Materials ... Springer, 2015.
- [2] Mehling, Cabeza. Heat And Cold Storage With PCM. Springer: Cham, Switzerland, 2008.
- [3] Barz, Bres, Emhofer. (2022). Asian Modelica Conference 2022 (pp. 63-74). Linköping Press.
- [4] Hemminger, Sarge. Journal of Thermal Analysis and Calorimetry, 37(7):1455–1477, 1991.
- [5] Rymes, Myers, (2001). Solar Energy, 71(4), 225-231.
- [6] Akima (1970). Journal of the ACM (JACM), 17(4), 589-602.
- [7] Butt, Brodli (1993). Computers & Graphics, 17(1), 55-64.



**Eurotherm Seminar #116**  
Innovative solutions for thermal energy storage deployment





EUROTHERM2023-B134

## **Volume variation in a thermochemical material- An experimental study**

Aastha Arya<sup>a,\*</sup>, Max Beving<sup>b</sup>, Amirhoushang Mahmoudi<sup>a</sup>, Mina Shahi<sup>a,\*</sup>

<sup>a</sup>University of Twente, Department of Thermal and Fluid Engineering, P.O. Box 217, 7500AE Enschede, the Netherlands; email: a.aastha@utwente.nl, m.shahi@utwente.nl, a.mahmoudi@utwente.nl

<sup>b</sup>Eindhoven University of Technology, Department of Mechanical Engineering, P.O. Box 513, 5600MB, Eindhoven, the Netherlands, email: M.A.J.M.Beving@tue.nl

### **Abstract**

The research focuses on swelling and shrinkage during cycling of a thermochemical material. Potassium carbonate has been cycled and the change in size has been monitored over subsequent cycles with the help of in-situ measurement in the micro-climate chamber. The experiments have been performed for different operating conditions and the resultant images were processed to calculate the equivalent diameter of the salt grains. Micro -CT scans were performed for both the samples to compare the two-dimensional results from in-situ experiments to a complete three-dimensional analysis.

**Keywords:** Thermochemical material, Potassium Carbonate, Micro-Computed X-Ray Tomography (Micro-CT), Thermochemical Energy Storage

### **1. Introduction**

Nearly half of the energy consumed globally is used for heating, mostly for industrial processes and heating of buildings. Much of this energy, around 90%, is sourced from fossil fuels. A significant amount of energy is consumed in the residential sector, with 70% of it being used to produce hot tap water and heating homes [1]. Thermochemical energy storage is an energy-saving technique that can preserve primary energy sources and decrease greenhouse gas emissions [2]. This method involves temporarily storing energy in a material for later use. Among the various thermochemical materials (TCM) under investigation for low-temperature thermal energy storage applications, salt hydrates have been identified as particularly promising. These materials undergo an exothermic reaction during formation, resulting in the release of heat which can be harnessed for heating purposes. The reverse reaction is endothermic, and sustainable heat sources such as waste heat, solar thermal or PV+ heat pumps can be utilized for the drying of the TCM. Once dried, the material can be stored until such time as the heat is required, at which point the hydration reaction can be initiated to release the stored energy in accordance with demand.

For a thermochemical material (TCM) to be suitable for practical use, the material must be able to withstand the hydration process and maintain chemical and mechanical stability to be used in multiple cycles. During hydration and dehydration, the material swells and shrinks due to intake and release of water vapor.

Swelling is the enlargement of a solid caused by the absorption of water and occurs when the chemical potential between the absorbing solid and absorbed fluid reaches equilibrium. A state of imbalance produces a pressure that causes swelling to occur. Swelling is influenced by factors such as the properties of the material and environmental conditions like temperature and pressure. Swelling during hydration of TCM is a consequence of exposure of salt to humid conditions. Horabik and Molenda [3] examined the relationship between the moisture content in grains and the pressure on the walls of a model silo. They discovered that when the moisture content increased by 22%, the pressures on the walls, both vertical and lateral, also rose by 49% and 80% respectively. Individual hydrated grains often crack when they are dehydrated. Cracking can hinder the application of TCM. It increases the porosity of individual grains but the damage in internal structure over repeated cycles can lead to pulverisation and poor mechanical stability[4]. The powdered material will agglomerate or fill the void space in the bed thus

decreasing the permeability and the void space in bed. Furthermore, shrinkage that occurs during the drying process is determined by the chemical and physical properties of the compounds, the initial moisture content, and the specific conditions under which the dehydration is taking place [5].

The internal structure of pores in granular materials is determined by the configuration of the particles, their sizes, and shapes. This means that the properties of the particles and how they are packed together both contribute to determining the material's overall mechanical properties, porosity levels, and fluid flow characteristic [6]. For instance, the ability of a granular material to allow fluid to flow through it decreases as the particle size becomes smaller and the porosity becomes lower. This phenomenon forms the foundation of the Kozeny-Carman equation, which links the particle size, porosity and permeability of the material [7]. Swelling of TCM in a packed bed is restricted by the reactor wall and thus swelling of grains imposes extra pressure on the reactor wall. When it comes to granular materials that do not change shape, the internal structure of the pores and the corresponding fluid flow properties can be determined through experimentation. This can be done by using column experiments to measure various hydraulic properties, and by using techniques such as X-ray tomography or micro-CT to visualize the internal pore structure. However, measuring these properties becomes challenging or impossible when the granular material is undergoing deformation over a period of time. Thus, to observe and quantify the volume variation, an in-situ measurement has been performed in a micro-climate chamber with one layer of TCM. Measurement of volume variation is further accompanied by Micro-CT experiments to measure change in porosity during cycling as well a three-dimensional analysis of change in volume of the particles when cycled individually and a comparison when they are cycled in a reactor.

## 2. Material and experimental method

A composite material made of potassium carbonate has been created as part of CREATE project[8] making it possible to produce it at low cost and on a large scale. The material shown in Figure 28 has been designed to be used in granular form in large-scale reactors.



Figure 28. Potassium carbonate grains placed inside a ring in climate chamber. A sample image used for image processing.

The in-situ experiment has been performed in a climate chamber coupled with an optical microscope. A sketch of the set-up is shown in Figure 29. The climate chamber has been connected to a humidifier to supply dry and humid air for dehydration and hydration step. The experiment has been repeated for different temperature and humidity values. Size change has been quantified with the help of image processing for different operating conditions.

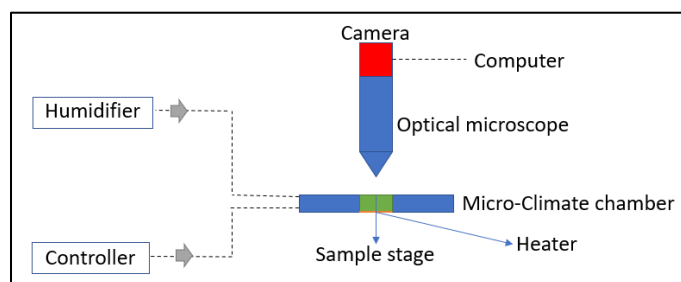


Figure 29. In-situ experiment set-up. The sample is placed inside the stage and the stage acts as microclimate chamber for facilitating hydration and dehydration.

Both uncycled and cycled samples were analysed using the Zeiss Xradia Context Micro CT. The samples were examined under normal conditions, but the environment can be modified if needed.

### 3. Results

Images were taken every five minutes with the help of microscope coupled with a camera. The obtained images were processed via edge detection algorithm to calculate the equivalent diameter. The images after the end of every hydration and dehydration cycle were analysed. The change in equivalent diameter with respect to time has been plotted in Figure 30. Approximately 27% increase in equivalent diameter has been noted at the end of first hydration step for an uncycled sample. Similar trend was observed for different operating conditions of cycling. The increase in equivalent diameter after first hydration step was limited between 27-30% and the grain did not return to its original size after the end of eight cycles of hydration and dehydration. The significant increase in size has been observed only for first cycle.

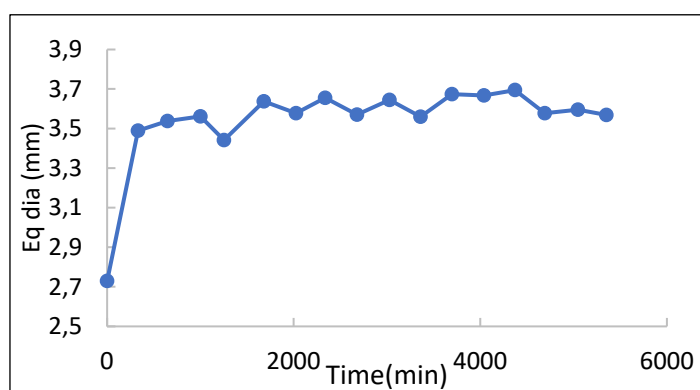


Figure 30. Variation of equivalent diameter with time during cycling

Apart from this 2D analysis, the volume variation has been quantified using Micro-CT scans of the uncycled and cycled sample. The volume of uncycled sample is  $15.93\text{mm}^3$  which increased to  $22.30\text{mm}^3$  after one cycle of hydration and dehydration. The pores and solid part of the grain visualized using Micro-CT are shown in Figure 31. The increase in the grain size is almost 39% when an individual grain is cycled. 2D analysis was limited to measurement of increase in size in one plane but Micro-CT helped in quantifying it for entire volume. This study will be further extended to find a correlation between the operating conditions, the effect of number cycles and volume variation.

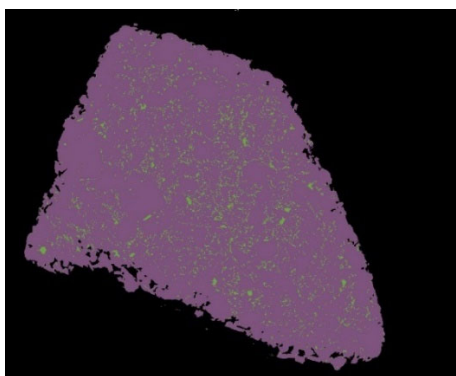


Figure 31. A 2D view of the uncycled grain with green coloured pores and pink colour representing solid part of the salt.

### 4. Conclusions

Quantifying the swelling and shrinkage helps in comprehending the creation of empty spaces within the bed caused by individual swelling and shrinkage of the grain. This in turn, can indicate the amount of stress experienced by the surrounding and impact on the mechanical stability of the grain. To minimize the formation of voids and preserve the thermal conductivity of the bed, it is beneficial to select a salt

that has minimal volume changes. It is difficult to numerically evaluate the contribution of controlling parameters thus, an experimental study at particle and reactor scale is necessary.

## Acknowledgements

This research is executed with the support of MMIP (Meerjarige Missiegedreven Innovatie Programma) 3&4 grant from the Netherlands Ministry of Economic Affairs and Climate policy as well as the Ministry of the Interior and Kingdom Relations. The authors would like to thank Pim Donkers from Cellcius for providing the material for experiments.

## References

- [1] T. Gilbert *et al.*, “Article Heat source and application-dependent levelized cost of decarbonized heat Heat source and application-dependent levelized cost of decarbonized heat,” *Joule*, pp. 1–22, 2022, doi: 10.1016/j.joule.2022.11.006.
- [2] M. A. J. M. Beving, A. J. H. Frijns, C. C. M. Rindt, and D. M. J. Smeulders, “Effect of cycle-induced crack formation on the hydration behaviour of K<sub>2</sub>CO<sub>3</sub> particles : Experiments and modelling Thermochemica Acta Effect of cycle-induced crack formation on the hydration behaviour of K<sub>2</sub>CO<sub>3</sub> particles : Experiments and modelling,” *Thermochim. Acta*, vol. 692, no. November, p. 178752, 2020, doi: 10.1016/j.tca.2020.178752.
- [3] J. Horabik and M. Molenda, “Grain pressure in a model silo as affected by moisture content increase,” pp. 385–392, 2000.
- [4] P. A. J. Donkers, L. C. Sögütöglu, H. P. Huinink, H. R. Fischer, and O. C. G. Adan, “A review of salt hydrates for seasonal heat storage in domestic applications,” *Appl. Energy*, vol. 199, pp. 45–68, 2017, doi: 10.1016/j.apenergy.2017.04.080.
- [5] M. Rungsiyopas and T. Ruiz, “Modelling of the shape effect on the drying shrinkage of wet granular materials,” *Chem. Eng. Res. Des.*, vol. 132, pp. 295–302, 2018, doi: 10.1016/j.cherd.2018.01.038.
- [6] S. Leszczynski, “The effect of particle shape on porosity of swelling granular materials- Discrete element method and the multi sphere approximation,” *Powder Technol.*, 2019, doi: 10.1016/j.powtec.2019.09.036.
- [7] J. Bear, “Dynamics of fluids in porous media.”
- [8] “EU H2020 CREATE Project. EeB-06-2015 - Google Scholar.” <https://scholar.google.com/scholar?inst=5726176096060060532&q=EU H2020 CREATE Project. EeB-06-2015> (accessed Feb. 06, 2023).

## **Territorial specialization and competitiveness project**

Edgar F. Rojas Cala<sup>1</sup>, Carles Mateu<sup>1</sup>, Mercè Teixidó<sup>2</sup>, Francesco Guarino<sup>3</sup>, Luisa F. Cabeza<sup>1</sup>

<sup>1</sup> GREiA Research Group, Universitat de Lleida, Pere de Cabrera s/n, 25001 Lleida, Spain, Phone: +34 973 003 704, e-mail: edgar.rojas@udl.cat, carles.mateu@udl.cat, luisaf.cabeza@udl.cat

<sup>2</sup> GRIHO Research Group, Universitat de Lleida, Pere de Cabrera s/n, 25001 Lleida, Spain, Phone: +34 973 003 704, e-mail: merce.teixido@udl.cat

<sup>3</sup> Dipartimento di Energia, Ingegneria dell'Informazione e Modelli Matematici, Università di Palermo Viale delle Scienze 90128 Palermo, Italy, e-mail: francesco.guarino@unipa.it

### **Abstract**

The University of Lleida is one of the entities that promote the energetic and competitive development of the Lleida region in Spain. As an example, it is currently carrying out a project in the city of Balaguer that seeks to reduce the energy consumption of the city's public buildings by monitoring the behaviour of the buildings. The data obtained from sensors that detect changes in temperature and humidity inside the building. This information is then matched with other information from the building or the external city environment in order to optimise a portion of the building energy consumption. The project is currently in the data acquisition stage, with the aim of subsequently implementing a control stage on the buildings.

**Keywords:** PECT; energy consumption; building monitoring; temperature; Balaguer; data acquisition

### **1. Introduction**

The Territorial Specialisation and Competitiveness Projects (PECT) are initiatives driven by territorial actors and led by public entities of the region. Financed by the European Union Fund (ERDF2014-2020), these projects aim to consolidate and strengthen the territorial structure through the economic and energy transformation of the region, generating positive environmental and economic impacts on the region. In this framework, the Generalitat de Catalunya has promoted the PECT Project- Green & circular b. Ponent project, in which the University of Lleida, through the GREIA research group, will carry out several tasks that will influence the economic and energetic development of the Lleida region.

Among the tasks entrusted to the University of Lleida is the monitoring of several public buildings in the city of Balaguer (Spain) to assess the behaviour, demand, and actual use of energy by services in the buildings. And then, through the use of artificial intelligence, propose measures and actions to reduce the energy consumption that these buildings currently generate.

The monitoring work started at the end of 2019 and is currently at a stage where the amount of data obtained has grown to a point where we can now start creating the initial artificial intelligence models that will allow the proposed work to be carried out.

### **2. Materials and method**

Thanks to the Paeria de Balaguer and the Ministry of Education, the University of Lleida has gained access to several public buildings in the city of Balaguer in order to monitor the behaviour inside these buildings and thus be able to model the energy consumption. The selected buildings are: the municipal library, the city theatre, the modernist house, the museum and the public school of the city; each of these buildings has a unique shape and a unique use by the inhabitants of the city, which can help to make later a more resilient and optimal artificial intelligence.

In each of the five buildings to be monitored, it was decided to measure the energy consumption of the building by measuring the temperature and humidity. To accomplish this task, and to satisfy one of the project requirements that the application be easy to replicate and extend to other locations, COTS (Components Off The Shelf) sensors were chosen because they are inexpensive, based on well-known standards, and readily available. For that, Xiaomi® zigbee brand temperature sensors were placed in strategic locations of the buildings as well as modelling the energy used by light fixtures and appliances by inspecting energy. These sensors are designed to take humidity and temperature measurements and, whenever a change is detected, send this information using the zigbee communication protocol to a main receiver per building. These receivers are Raspberry Pi single-board computers with a Zigbee plug-in. Each receiver is housed in a box modelled by 3D printing that protects the computer and allows its implementation in the building.

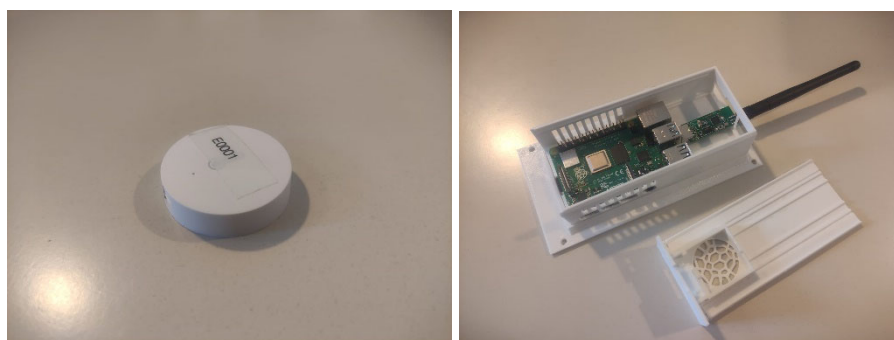


Figure 1. Devices implemented in the monitored buildings

Each building has a receiver and a number of sensors depending on the size and design of the building, which send all the information to a database in order to be processed with other data acquired from other sources. One of these sources is a meteorological station located in the city of Balaguer which shares its data publicly; the owner of the station has given permission to the project to use the information on his site in order to monitor meteorological features of the city.

All the stored data must be further processed and prepared to be able to work with it, through artificial intelligence in order to start the development stage of improving the energy performance of the different buildings.

### 3. Results and discussions

During the first period of the project a considerable amount of data from the sensors and the weather station has acquired. A database has been built to schematize the annual behaviour of the city of Balaguer and most of the buildings measured. The data not only refers to meteorological measurements of the city or the behaviour of the buildings, but also to the behaviour of the different measuring devices that have been installed. Below is a schematic of each of the sources of data with the respective type of data acquired, which are organized temporally.

The data is stored on an Influxdb time series database, and managed through the use of the Grafana tool that allows the optimal visualization of these data and the ability to be shared for use in other stages of the PECT Green & circular b. ponent project. We are also currently analyzing these data and their possible uses for implementation with artificial intelligence for energy optimization applications in the different buildings of the city.

Table 1. data acquired during the course of the project

Devices		Data						
Meteo Webpage		Temperature	Humidity	UV	Rain	Solar	Wind speed	Time
Buildings	Library			Device Data	Voltage	Battery		
	Theatre							
	Modernist house							
	Museum							
	school							

#### 4. Conclusions

The data acquisition process has provided a good database for future exploitation through artificial intelligence; the next step to be taken is the use of these data to reduce the energy consumption of the buildings, so it will be evaluated whether it is necessary to acquire more data or a different type of data to achieve this goal.

#### Acknowledgements

This work was partially funded by the Generalitat de Catalunya and the European Union Fund under the project ERDF2014-2020. The authors thank the Generalitat de Catalunya for the quality accreditation granted to the GREiA research group (2021 SGR 01615) and GRIHO research group (2021 SGR 01620). GREiA is a TECNIO-certified agent in the category of technological development of the Gobierno de Cataluña. This work is partially supported by ICREA inside the program ICREA Academia.

EUROTHERM2023-F136

## Evaluation of the social impact during the life cycle of an energy system based on seasonal thermal energy storage

Emiliano Borri, Luisa F. Cabeza

GREiA Research Group, University of Lleida, Pere de Cabrera s/n, 25001-Lleida, Spain, Phone: +34 973 003576, e-mail: luisaf.cabeza@udl.cat

### Abstract

The EU-funded project SWS-Heating aims to develop a heating system for residential buildings integrating a novel seasonal thermal energy storage based on selective water sorbents able to increase the share of renewables. This study evaluates the social impact of the developed system using a social life-cycle assessment (S-LCA) approach. Results showed that the system has a medium-high social impact which shows a great potential of improvement especially in the manufacturing and end-of life stage.

**Keywords:** Social life cycle assessment; S-LCA; seasonal thermal energy storage

### 1. Introduction

Thermal energy storage (TES) is one of the key technologies of the current energy transition. The integration of TES into energy systems based on renewable sources helps to balance the thermal energy supply and demand thus increasing the generation capacity of systems having both economic and environmental benefits. In recent years a lot of effort was put into the research of novel, efficient and compact TES technologies to be integrated into different applications. In the built environment TES is mainly integrated with energy systems which provides heating and cooling [1]. Storing thermal energy for long-term can be one of the solutions to the share of renewables. The development of seasonal TES attracted in recent years several researchers. In this context the EU-funded project SWS-Heating (Grant Agreement 764025) aim to develop a novel seasonal thermal energy storage (STES) based on selective-water sorbent (SWS) materials to store the heating energy provide by renewables in summer to be used in winter when space heating is needed. In the framework of the project a generic heating system was developed to integrate the novel STES in a potential residential building (single family house). The system developed include evacuated-tube solar collectors, a vacuum combi-storage water tank, a latent heat TES to support the STES and a back-up gas/electric boiler. The system able to operate in several operational modes integrates an advanced control to optimize the system efficiency and reduce the operating cost. Although novel technologies and energy systems are developed by researchers to reduce the energy consumption from fossil fuels and thus carbon emission, sustainability aspects during the whole life-cycle from the production of components to the end of life are often overlooked. In this case life-cycle sustainability assessment (LCSA) methodologies can be applied following the principles developed in International Organization for Standardization (ISO) 14040 and 14044 [2,3]. LCSA methodologies includes environmental life cycle assessment (LCA), life-cycle costing (LCC) and social life-cycle assessment (S-LCA) [4]. Few studies related the life-cycle assessment of energy systems integrating renewables were published in literature [5–7]. Nevertheless, a research gap can be found in social LCA studies especially in the field of thermal energy storage. The main objective of this paper is to evaluate the social impact of the generic heating system developed within the SWS-Heating project during the life-cycle using S-LCA methodology. Results will provide an additional information to the product in a commercial future perspective giving and indication on the socio-economic effect on people and communities.



## 2. Methodology

### 2.1 Description of the SWS-Heating concept and system

A schematic of the system concept developed within the project SWS-Heating is shown in Figure 32.

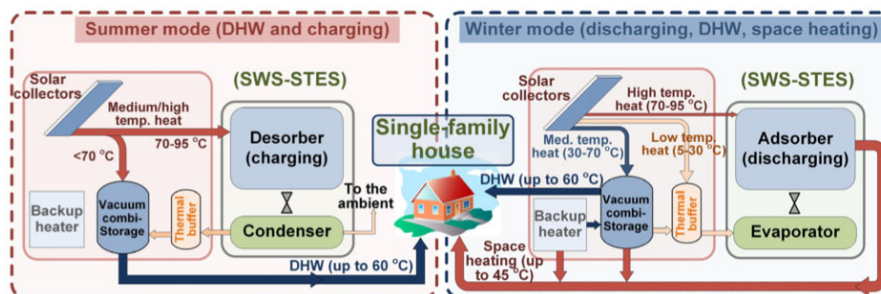


Figure 32. SWS-Heating system concept

The system includes the main components:

- Novel STES based on selective water sorbents material.
- Evacuated tubes solar collectors.
- Water storage combi-tank with vacuum insulation.
- Latent heat TES.
- Back-up gas boiler.
- System controller.
- Auxiliary components (i.e., heat exchangers).

As shown in Figure 1 during summer, solar heat is used to provide domestic hot water (DHW) by charging the combi-tank and to charge the STES. During winter mode, the STES is discharged into the combi-tank to provide space heating. In order to increase the efficiency of the STES, low-grade heat from the solar collectors can be used directly or stored in the latent heat TES to increase the conversion efficiency of the STES. The back-up boiler can be used in all seasons to support both heating and DHW demand.

### 2.2 S-LCA methodology

The S-LCA performed in this study follows the are reported by the “Guidelines for Social Life Cycle Assessment of products” in 2009, developed by UNEP and SETAC following the steps defined in the standards ISO 14040 and 14044 including:

- The definition of the goal and scope.
- The inventory phase (i.e., definition of the questionnaire and data collection).
- The impact assessment.
- Interpretation of results.

The life cycle of the SWS-Heating considers for each of the main components a cradle-to-gate approach with the following phases: extraction of raw materials and manufacturing of components; installation; operation and maintenance; and dismantling and disposal of waste. The stakeholders considered to evaluate the social impact were workers, local community, society, consumers, and value chain actors. For each stakeholder different sub-categories corresponding to the item if interest, were identified. The questionnaire was done to collect data based on different indicators for each sub-category selected from the S-LCA methodological sheets. Indicators, and the related collected data, can be quantitative, semi-quantitative and/or qualitative, and are generally collected through questionnaires. The questionnaire was filled by companies involved in the project and some external ones. General data at country level regarding social aspects were also collected from available sources. Once all data were collected, impact assessment was performed following two main steps: Performance Assessment (PA) and the Impact

Assessment (IA). In the first step the performance of the company and of the country related to the company works was assessed in form of Performance Reference Points (PRP) assigning a score based on the data provided to each indicator for each subcategory of each stakeholder. The PRP for the site-specific assessment were retrieved from different sources. The score assigned for each indicator ranged from 1 (very good performance) to 6 (very bad performance). The impact assessment was assessed following the quantitative approach reported on Caruso et al. [8]. In this case the scores given during the PA were assessed considering the strength of correlation between sub-categories and different of social impact categories (Working Conditions (WC); Health & Safety (HS); Human Rights (HR); Socio-Economic Repercussions (SER); Indigenous Rights (IR); Governance (G)). The results Impact Assessment will be, similarly to the PA, a number ranging from 1 (positive effect) to 6 (very negative effect).

## 2. Results

The results of the S-LCA performed in this study are shown in Table 1. The results shows that the total social impact of the SWS-Heating system in all the life cycle has a score of 4 over 6 indicating a medium/high negative impact. During the manufacturing stage (A1-A3), the components which has the highest negative effect are the solar collectors. This could be attributed to the fact that the companies interviewed are medium or small size companies that lack of social aspects to some the stakeholders considered. The same conclusion can be done for the social impact generated from the PCM tank and the water tank.

Table 1. Results of the social LCA for different stages

Component	A1-A3 stages	A4-A5 stages	B2-B4 stage	C1 stage	C2 stage	C3 stage	C4 stage
STES	3	2.75	3.5	4	4.5	5	5
PCM tank	4						
Water Tank	4						
Solar Collectors	5						
Controller	2.7						
Gas Boiler	4						
Heat exchangers	3						
<b>Total</b>	<b>4</b>						

The gas boiler which are mainly produced by big companies has a high negative effect mainly due to the risk of corruption in this sector. The STES and the heat exchangers have a medium impact. In these medium-size companies some aspect can be improved including the engagement with local community, promote the social responsibility with value chain actors. The controller has the lowest impact. However also in this case big companies which are involved in the production of controller components can be affected to high risk of corruption. The lowest social impact during the life cycle is during the life-cycle is during the installation (A4-A5 stages) nevertheless improvements can be done especially in the engagement with local communities. From this study highest negative effects are the demolition in the use stage which includes maintenance and repair (B2-B4) and the end-of life stage (C1-C4). Social aspect that can be improved involves the society in the commitment to sustainability issues and technological deployment and in the engagement with local community. However, it is worth to mention that since the questionnaire includes general data related to the different countries on where the companies are located, some of the aspects has to be improved as national level.

### 3. Conclusions

In this study, the social impact of the system developed within the SWS-Heating project which aim to develop a heating system for building applications integrating a novel seasonal storage based on selective water sorbents to maximize the share of renewables. The social impact was evaluated from internal and external companies collecting data through a questionnaire based on different indicators defined for different stakeholders (workers, local community, society, consumers, and value chain actors) and collecting general data about the country where the company are located. The result showed that effect on the social environment has a medium high negative effect. In this case small companies have the greatest potential to reduce the impact on society improving the involvement within local communities and with relation with value chain actors and suppliers. Lowest social impact was found in the installation stage. Future works will aim to provide a detailed analysis on the social impact to find the hot spots of improvement that could increase the social acceptance of the developed system.

### Acknowledgments

This project was funded by the European Union's Horizon 2020 Research and Innovation Programme under No. 764025 (SWS-HEATING). This work is partially supported by ICREA under the ICREA Academia programme. The authors would like to thank the Catalan Government for the quality accreditation given to their research group GREiA (2021 SGR 01615). GREiA is a certified agent TECNIO in the category of technology developers from the Government of Catalonia.

### References

- [1] Borri E, Zsembinszki G, Cabeza LF. Recent developments of thermal energy storage applications in the built environment: a bibliometric analysis and systematic review. *Appl Therm Eng* 2021;189.
- [2] ISO 14040:2006(en), Environmental management — Life cycle assessment — Principles and framework n.d.
- [3] ISO 14044:2006(en), Environmental management — Life cycle assessment — Requirements and guidelines n.d.
- [4] Guarino F, Cellura M, Traverso M. Costructural law, exergy analysis and life cycle energy sustainability assessment: an expanded framework applied to a boiler. *Int J Life Cycle Assess* 2020;25:2063–85. <https://doi.org/10.1007/s11367-020-01779-9>.
- [5] Buchmayr A, Verhofstadt E, van Ootegem L, Thomassen G, Taelman SE, Dewulf J. Exploring the global and local social sustainability of wind energy technologies: An application of a social impact assessment framework. *Appl Energy* 2022;312:118808.
- [6] Martín-Gamboa M, Quinteiro P, Dias AC, Iribarren D. Comparative social life cycle assessment of two biomass-to-electricity systems. *Int J Environ Res Public Health* 2021;18:4918.
- [7] Corona B, Bozhilova-Kisheva KP, Olsen SI, San Miguel G. Social life cycle assessment of a concentrated solar power plant in Spain: a methodological proposal. *J Ind Ecol* 2017;21:1566–77.
- [8] Caruso MC, Pascale C, Camacho E, Ferrara L. Comparative environmental and social life cycle assessments of off-shore aquaculture rafts made in ultra-high performance concrete (UHPC). *Int J Life Cycle Assess* 2022;27:281–300.

EUROTHERM2023-C137

## Environmental assessment of two configurations of CSP plants, in central tower and parabolic trough and with different thermal energy storage capacities

Gemma Gasa<sup>1</sup>, Antón Lopez-Roman<sup>2</sup>, Cristina Prieto<sup>2</sup>, Luisa F. Cabeza<sup>1</sup>

<sup>1</sup>GREiA Research Group, Universitat de Lleida, Pere de Cabrera s/n, 25001-Lleida, Spain, Phone: +34 973 003576, e-mail: luisaf.cabeza@udl.cat

<sup>2</sup>University of Seville, Department of Energy Engineering, Camino de Los Descubrimientos S/n, 41092, Seville, Spain, e-mail: cprieto@us.es

### Abstract

The objective of this study was to compare the life cycle analysis (LCA) of two types of configurations of concentrated solar power plants (CSP): the central tower and the parabolic trough. First, several CSP plants with central receiver technology were analysed, using as baseline a 110 MWe1 plant and 17.5 hours of molten salt thermal energy storage (TES) compared to a plant of equal power but without storage. Subsequently, the LCA of four plants with different TES capacities were compared. In the same way, the same TES capacities were compared in the parabolic trough configuration and finally, this study ends by comparing the environmental impacts of both configurations. The results show that TES is key for CSP plants, not only to guarantee dispatch capacity, but also to reduce their environmental impact. Regarding the comparison of the two types of configurations, at the time of submitting this abstract, the study is ongoing.

**Keywords:** Concentrating solar power (CSP) plant; tower plant; parabolic trough; thermal energy storage (TES); storage capacity; life cycle assessment (LCA)

### 1. Introduction

The use of renewable energies to replace fossil fuels seeks to implement sustainable energy development worldwide and contribute to the mitigation of climate change. Despite this, renewable energies represent a challenge in the programming required by the electrical system, where electricity can be dispatched on demand at the request of the electricity grid operators, according to market needs [1]. Renewable electricity dispatch capacity increases when storage is included in power supply systems. Thermal energy storage (TES) is one of the fundamental pillars on the road to decarbonization. Its introduction in solar thermal plants (CSP) seeks to improve its performance and flexibility to achieve better use of energy on demand. When TES is integrated, the CSP plant can run at full load for hours even in the absence of sunlight, and the operation of the CSP plant can be compared to conventional power generation plants [2]. The literature includes studies on the influence of storage capacity on the LCoE of CSP plants [3][4] but no studies on its environmental influence were found. Therefore, this work studies for the first time the impact of changing the storage capacity of a CSP plant, both in a tower configuration and in a parabolic trough, with the aim of evaluating whether the optimum found in the technical-economic analysis is equal to the environmental optimum and which of the two configurations generates less environmental impact.

### 2. Methodology

Life cycle assessment (LCA) is a methodology that allows evaluating the environmental loads associated with a product, process or activity, identifying and quantifying the energy, materials consumed and waste released into the environment throughout the entire life cycle. The LCA included in this study is

carried according to ISO 14040 and 14044. Thus, this LCA is based on the impact assessment method ReCiPe, in impact points, and IPCC2013 – GWP, in kgCO<sub>2</sub>eq, and the database used is Ecoinvent, which has positioned itself as a world leader in creating more transparent life cycle impact databases. Moreover, this work encompasses three distinct phases of evaluation: manufacturing, operational, and end of life.

### 3. Results and discussions

#### 3.1. Tower configuration

This study shows that storage is key for CSP plants, not only to ensure dispatchability, but to reduce their life cycle environmental impact. The CSP plant without storage has higher environmental impact than the plant with storage. As Figure 1 shows, when the total impact per kWh of net produced electricity is evaluated using the ReCiPe indicator, the CSP tower plant without storage generate 46% more impact than a plant with storage capacity of 17.5 h. When the climate change indicator per kWh of net produced electricity is considered, the impact is 67% higher without storage (31 gCO<sub>2</sub> eq/kWh) than with capacity storage of 17.5 h (9.8 gCO<sub>2</sub> eq/kWh). The operational phase impact determines the difference between the two plants and this can be attributed to the electricity consumption from the grid required by CSP plants without storage. Figure 2 shows that the systems with the greatest impact are the solar field and the TES systems.

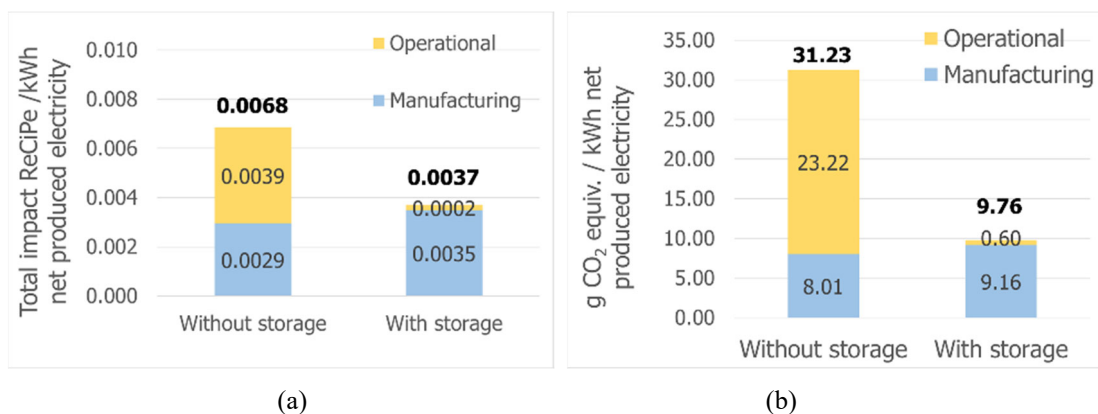


Figure 33. Impact of the manufacturing and operational phases per kWh of net produced electricity of a CSP tower plant with TES and one without TES: (a) ReCiPe indicator; (b) Climate change indicator

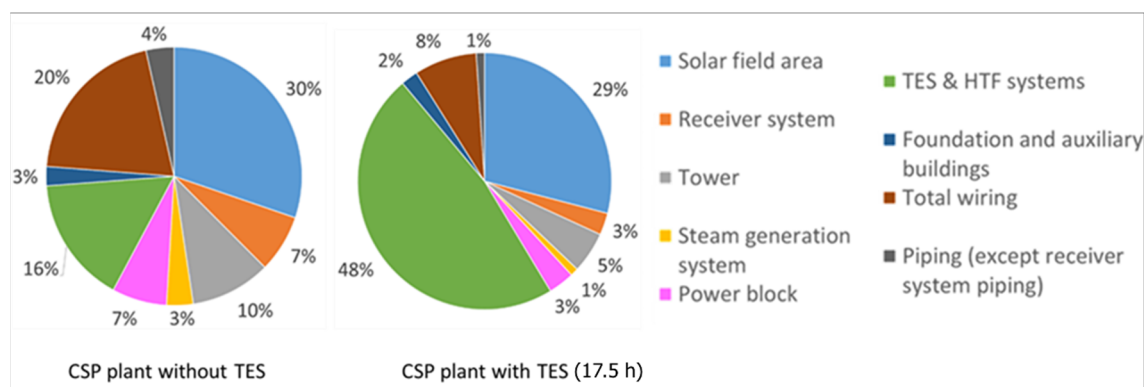


Figure 2. Contribution of each CSP component considered

Of the different energy storage capacities analysed (3 h, 6 h, 9 h, 17.5 h) the most environmentally efficient plant is the one with a storage capacity of 9 h (Figure 3).

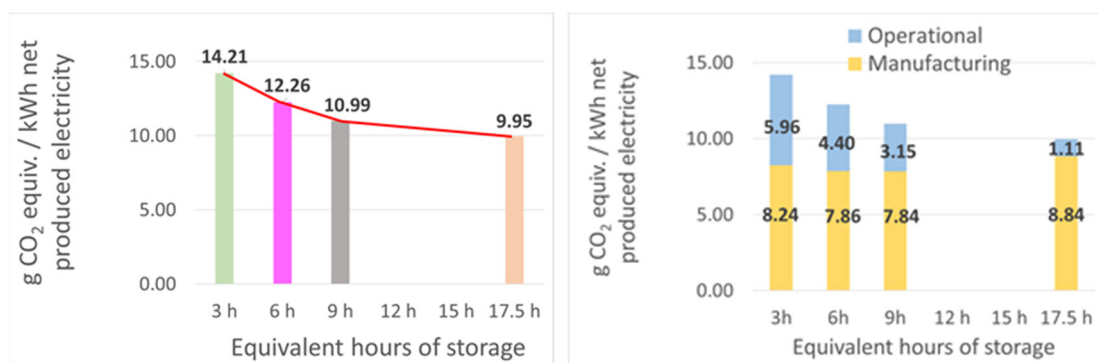


Figure 3. Impact of the manufacturing and operational phases per kWh of net produced electricity of different energy storage capacities: (a) ReCiPe indicator; (b) Climate change indicator

### 3.2. Parabolic trough

At the time of submitting this abstract, the study is ongoing.

## 4. Conclusions

The conclusions of the present study are:

a. For CSP tower plants:

- The CSP plant without storage has a higher environmental impact than the plant with storage.
- The impact of the operational phase determined the difference between the two plants, and this can be attributed to the consumption of electricity from the grid required by CSP plants without storage.
- The CSP tower plant systems that generated the highest impact were the solar field and the HTF and TES systems.
- When the storage capacity is increased in periods of 3 hours (3 h, 6 h and 9 h), the impacts generated throughout their useful life decrease, however, when the storage capacity increased from 9 h to 17.5 h, the impact generated is very similar.
- As the CSP plant increases its storage capacity, the impact generated during the manufacturing phase increase, however, the impact generated in the operation phase is reduced, since the increase in storage capacity reduces the contribution of the electricity required from the grid (used mostly for start-up procedures).

b. For CSP parabolic trough plants: At the time of submitting this abstract, the study is ongoing

## Acknowledgements

This work was partially funded by the Ministerio de Ciencia e Innovación - Agencia Estatal de Investigación (PID2021- 123511OB-C31 - MCIN/AEI/10.13039/501100011033/FEDER, EU).

The authors thank the Generalitat de Catalunya for the quality accreditation granted to the GREiA research group (2021 SGR 01615). GREiA is a TECNIO-certified agent in the category of technological development of the Gobierno de Cataluña. This work is partially supported by ICREA inside the program ICREA Academia.

## References

- [1] Papadopoulou, A. G.; Vasileiou, G.; Flamos, A., 2020. A comparison of dispatchable RES techno-economics: Is there a niche for concentrated solar power. *Energies* 13 (18), 4768.
- [2] Liu, M.; Steven, N.H.; Bell, S.; Belusko, M.; Jacob, R.; Will, G.; Saman, W.; Bruno, F., 2016. Review on concentrating solar power plants and new developments in high temperature thermal energy



storage technologies. *Renew Sustain Energy Rev* 53, 1411–1432.

[3] Gorman, B.T.; Lanzarini-Lopes, M.; Johnson, N.G.; Miller, J.E.; Stechel, E.B., 2021. Techno-Economic Analysis of a Concentrating Solar Power Plant Using Redox-Active Metal Oxides as Heat Transfer Fluid and Storage Media. *Front Energy Res* 9, 1–18.

[4] Guédez, R.; Spelling, J.; Laumert, B.; Fransson, T., 2014. Optimization of thermal energy storage integration strategies for peak power production by concentrating solar power plants. *Energy Procedia* 49, 1642–1651.

EUROTHERM2023-M138

## **Study on control optimization of a hybrid solar-biomass system for residential buildings using deep learning techniques**

Gabriel Zsembinszki, Cèsar Fernández, Emiliano Borri, Luisa F. Cabeza

GREiA Research Group, University of Lleida, Pere de Cabrera s/n, 25001-Lleida, Spain, Phone: +34 973 003576, e-mail: luisaf.cabeza@udl.cat

### **Abstract**

The EU-funded H2020 project SolBio-Rev aims to develop an energy system based on the use of solar energy and biomass to increase the share of renewable energy needed to meet heating, cooling, domestic hot water, and electricity demand in buildings. In this study, a smart control that used deep reinforcement learning techniques was applied to define an optimal control policy for a SolBio-Rev system installed in a standard multi-family house located in Madrid. The smart control aims at minimizing the operating cost during both summer and winter. Results show that the smart control achieved a cost reduction of 35% in winter, while no significant reduction was obtained in summer, compared to a standard rule-based strategy.

**Keywords:** Deep reinforcement learning, optimal control, modeling, residential buildings, hybrid energy systems, biomass

### **1. Introduction**

Deep reinforcement learning (DRL) proved to be successful for solving complex control problems that make it become a hot topic in the field of energy system control. Under this scope, it is possible to find DRL architectures approximating model predictive control (MPC) in complex systems, or DRL algorithms that successfully control an HVAC (heating, ventilation, and air conditioning) system for a given user comfort requirement [1]. A DRL architecture was successfully applied in a previous study by the authors [2] to deal with the complexity of an innovative hybrid energy storage system and to derive appropriate high-level control policies, able to minimize the operation cost of the system. The main contribution of this study is the use of DRL strategy for optimal control under demand response in another complex system, able to provide heating, cooling, and domestic hot water (DHW) to a multi-family residential building.

### **2. Methodology**

The system analyzed in this study is being developed within the EU Horizon 2020-funded project SolBio-Rev [3], which aims at developing a flexible energy system – suitable for building integration – and able to cover a large share of energy demand using renewable energy sources. A schematic of the SolBio-Rev system is shown in Figure 33. The system is composed of the following main subsystems: a field of solar thermal collectors with integrated thermoelectric generators (TEGs) connected to a short-term storage tank, a reversible heat pump connected in cascade with a sorption module, and a biomass boiler.



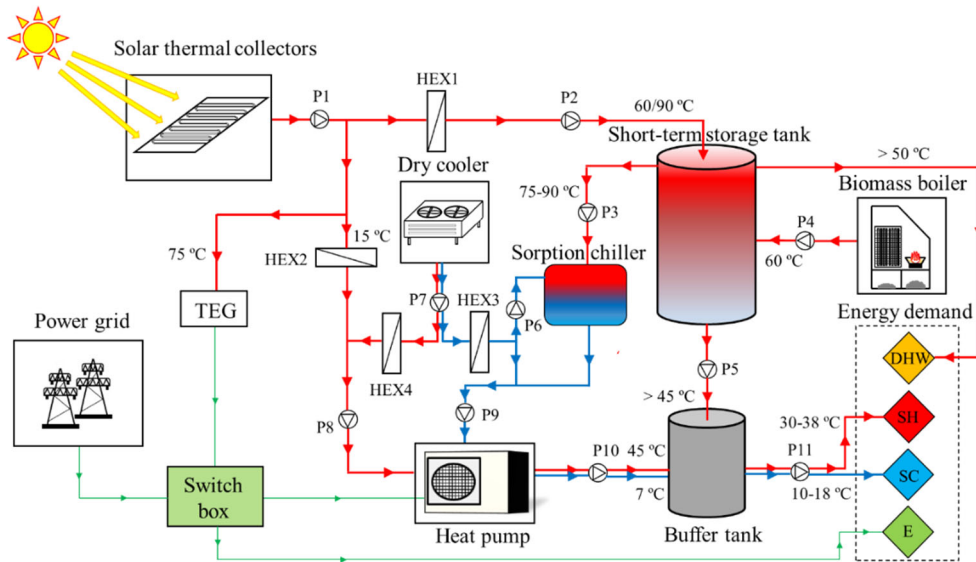


Figure 34. System components for the SolBio-Rev system

The components were sized based on the energy demand obtained through simulations of a multi-family house located in Madrid. In this case, the multi-family house taken as a reference was the one from the EU project iNSPIRe [4], with the U-values of a new/refurbished building according to the national building directive of Spain.

Based on models developed for the main system components, an approach using DRL policy gradient algorithms was applied. System modeling considered two different time scale slots: a finer time slot (3 minutes) to numerically compute the system behavior, not relevant for control purposes; and a second, longer time slot (15 minutes), to manage the high-level control system. Within the longer time slot, any action decided by the control system was not change until any of the subsystem limits was attained.

Control policies focused on minimizing operation costs are considered, using a cumulative reward function calculated based on the costs associated to running the system in different operation modes. The reward function also includes a penalty to ensure that the system is able to meet the energy demand of the building at any time. To evaluate the performance of the DRL control policy, a rule-based control (RBC) policy was first implemented for the different operation modes. The RBC policy is used as a reference to estimate the potential energy and cost savings that could be achieved due to the DRL control. The DRL algorithm was trained using the energy demand simulated for the reference multi-family house shown above using the weather data obtained from Meteonorm database [5] for Madrid. The results shown in the next section correspond to the validation set.

The input and system variables considered as an input to the control system include the level of solar irradiance, the ambient temperature, the status of the different subsystems, and the energy demand profile for heating, cooling, and DHW. The set of actions that are taken by the control algorithm are based on the combination of operational modes of each subsystem/component.

### 3. Results

In winter, when solar radiation is relatively low, the RBC (Figure 35) shows a high use of the biomass boiler to satisfy both DHW and space heating, and, during periods of highest solar radiation, solar energy is used to run the TEGs. The heat pump is never used in this case. However, the smart control using DRL algorithm (Figure 36) reduces the use of the biomass boiler. This is achieved by enhancing the use of the solar collectors and also of the heat pump. Moreover, the TEGs are never used. As a result, the DRL policy achieved a reduction of 35% in the operating cost in winter, from 37 € to 24 €, for 10 days of operation.

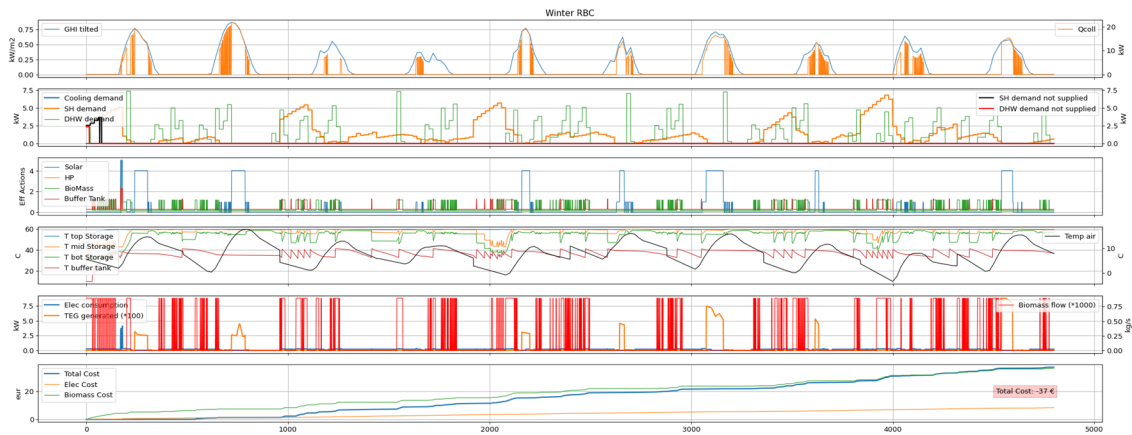


Figure 35. RBC policy for winter season

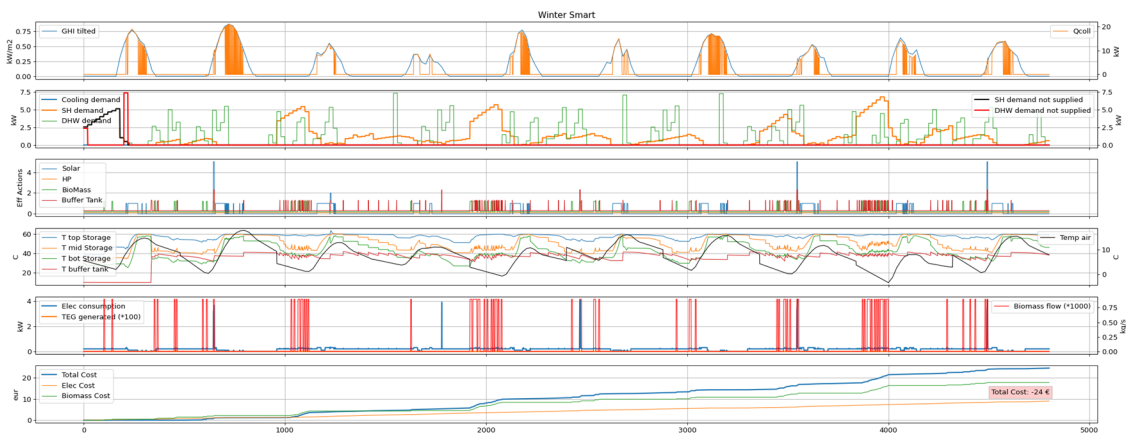


Figure 36. Optimal control for winter season

The effective actions decided by the RBC and DRL policies during summer are shown in Figure 37 and Figure 38, respectively. The results show that, in both cases, the biomass boiler is never used. Therefore, the total consumption is equal to the electricity consumption of the heat pump and circulation pumps. This means that the best control strategy is the one able to better manage the heat pump operation in cooling mode. Unlike the RBC strategy, the DRL strategy never used the heat pump in cascade with the sorption chiller, neither the TEGs. Contrary to what might be expected, the results show a very similar performance of both control strategies, being the DRL strategy able to reduce the operating cost by less than 2%, from 57 € to 56 €.

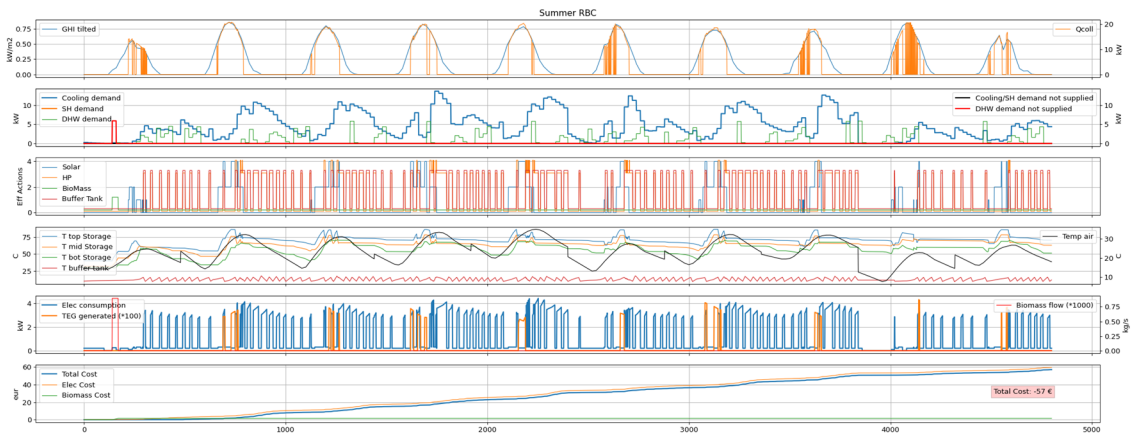


Figure 37. RBC policy for summer season

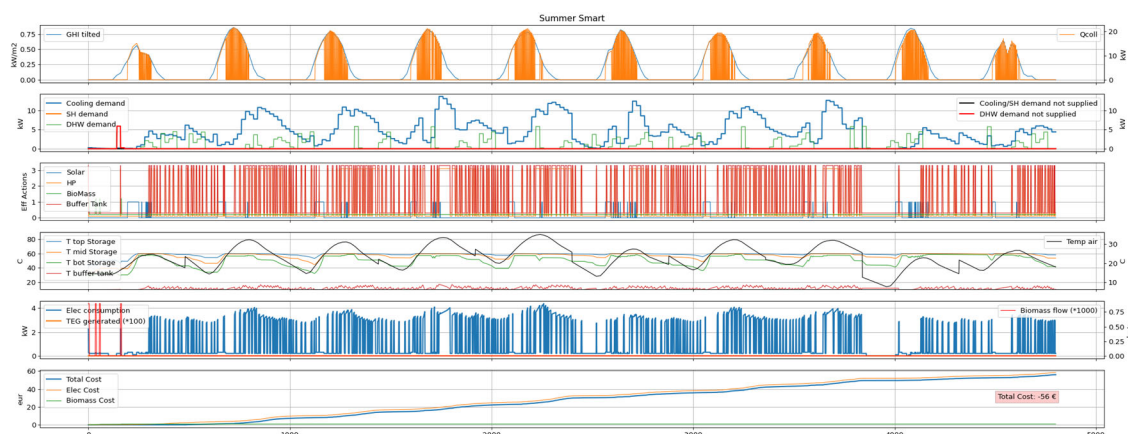


Figure 38. Optimal control for summer season

## 4. Conclusions

This study investigates the implementation of a smart control for a complex system developed within the project SolBio-Rev using a deep reinforcement learning policy. The system aims at reducing the energy consumption for heating, cooling, and domestic hot water of a standard residential building by enhancing the use of renewable energy sources, which is expected to be efficiently exploited by the implementation of an optimal high-level control system. The results showed that the smart control is able to reduce the total operating cost in winter by 35% due to a reduction in the use of the biomass boiler. However, the operating cost in summer could not be further reduced by the smart control with respect to the RBC strategy.

## Acknowledgements

This project was funded by the European Union's Horizon 2020 Research and Innovation Programme under No. 814945 (SolBio-Rev). This work is partially supported by ICREA under the ICREA Academia programme. The authors would like to thank the Catalan Government for the quality accreditation given to their research group GREiA (2021 SGR 01615). GREiA is a certified agent TECNIO in the category of technology developers from the Government of Catalonia.

## References

- [1] T. Wei, Y. Wang, Q. Zhu, Deep Reinforcement Learning for Building HVAC Control, Proceedings - Design Automation Conference. Part 12828 (2017). <https://doi.org/10.1145/3061639.3062224>.
- [2] G. Zsembinszki, C. Fernández, D. Vérez, L.F. Cabeza, Deep learning optimal control for a complex hybrid energy storage system, Buildings. 11 (2021). <https://doi.org/10.3390/buildings11050194>.
- [3] SolBio-Rev, (n.d.). <http://www.solbiorev.eu/> (accessed January 30, 2023).
- [4] C. Dipasquale, R. Fedrizzi, A. Bellini, M. D'Antoni, C. Bales, M. Gustafsson, F. Ochs, G. Dermentzis, S. Birchall, D2. 1c Simulation Results of Reference Buildings, EC FP7 Project INSPiRe, Grant Agreement. (2014).
- [5] Meteonorm, (n.d.). <http://www.meteonorm.com/>.

EUROTHERM2023-C139

## Comparison of different control strategies of an energy system thermal energy storage for building applications: an experimental study

Javier Fernández-Cantero<sup>1</sup>, Emiliano Borri<sup>1</sup>, Simone Arena<sup>2</sup>, David Verez<sup>1</sup>, Luisa F. Cabeza<sup>1</sup>

<sup>1</sup>GREiA Research Group, INSPIRES Research Centre, Universitat de Lleida, Pere de Cabrera s/n, 25001- Lleida, Spain

<sup>2</sup>Department of Mechanical, Chemical and Materials Engineering, University of Cagliari, Via Marengo 2, 09123, Cagliari, Italy

### Abstract

In this study, two identical experimental facilities that simulated a real-life building heating system with a thermal energy storage (TES) tank, photovoltaic (PV) panels, and a heat pump were tested through different rule-based control strategies optimization methods and the same external factors. One control strategy focused on minimizing the cost of operation while the second maximized the use of renewable energy. The final goal is to discern between two rule-based controls, the target strategy that can improve the use of the TES system the most and set a reference for future comparisons. The results showed that both control strategies can have periods when they are more efficient in cost due to the environmental values of the times assessed but the strategy used to minimize cost is always less energy efficient.

**Keywords:** Thermal energy storage; optimization; rule-based control.

## 1. Introduction

Climate change is already a reality that can be seen by the naked eye in our daily life. In the past years, most countries have seen record temperatures, droughts, floods, or wildfires in their territories [1]. To fight this, it is necessary that humanity stops CO<sub>2</sub> emissions and increases the use of renewable energy as the main generation source. This presents a problem due to the factor that even though these types of energy are clean and sustainable, they are not constant, so the best way to harness their power in full is to create storage equipment that can save the energy for when its more needed, achieving a balance between the demand and the supply of energy [2]. Thermal energy storage (TES) is one of the technologies that are capable of achieving this type of requirement, providing energy savings, energy conservation, and energy efficiency to the system [3] where its implemented. Even though the use of TES is a technology that has been explored in the literature [4], the optimization of its use by having a peak control strategy has not yet been fully explored or demonstrated. To this end, this paper establishes how the control strategy in the usage of a TES tank in a building prototype thermal system can impact the system efficiency and achieve energy savings.

## 2. Materials and methods

### 2.1. Experimental Setup

The experimental setup was located in a small area of the Agrifood Science and Technological Park in Lleida (Spain) currently used by the GREiA research group of the University of Lleida research group. The energy systems were installed in two metal containers with dimensions of 12.2 m × 2.43 m × 2.59 m. Inside both of them, there is identical equipment that will be used for the characterization of a building apartment thermal system. It is composed of a set of PV panels, a reversible heat pump (HP), a TES tank, an inertia tank, a fan-coil (FC), a small computer, and other electrical components for operational control. The PVs are a set of 4 Greenheiss GH-black panels with a maximum generation power of 1.5 kW, the reversible heat pump is a Kosner Aquaris V5 capable of supplying water between the temperature of 5 °C - 55 °C for a maximum heat power delivered of 5.5 kW, the TES tank is, a Kosner

500 L carbon steel tank, the inertia tank is, a Greenheiss 30 L stainless steel tank, the fan-coil is Kosner KFCI-CD30 2T with a capacity of transferring around 5.4 kW of thermal energy, the computer is an Intel NUC with a Core i7 10710U as processor and 8 GB of RAM that is in charge running the control strategies, reading and storing the values from all sensor and other equipment as well as controlling all the logical procedures that will secure the correct functioning of the entire system. Low-level communication is conducted by different software specialized in a specific task and then integrated to achieve the desired goal. Data will be collected using the software Telegraf and stored in a database using the program InfluxDB, while the platform that is in charge of the control is called Node-Red.

## 2.2. Rule-based control target strategies

### 2.2.1. Minimizing the cost of operation

A control strategy to minimize the system operating cost and maintain thermal comfort was developed and implemented in one of the containers. The main goal of the control system is to maintain thermal comfort, making the heating demand the key factor. If there is no demand, the algorithm will check the amount of energy supplied by the PV at the current moment to charge the TES (Mode B), or check the current price of the electricity of the grid to determine to charge or not the TES. To determine if the price of electricity is considered to be on peak time, the program will check all the prices of the electricity for the entire day and create an average measure to compare. On the other hand, if there is thermal demand, the program will check the amount of energy supplied by the PV. If the supplied energy is enough to turn the HP, then this will turn on to provide heating (Mode A). In case there is not enough energy generated, the algorithm will forecast the ambient temperature for the next three hours and compare this value with the set point for room comfort. If the values are in the range of  $\pm 3$  °C between each other the energy stored on the TES will be used (Mode C) In case the values are not close in range, the current price of the electricity and the state of charge of the TES will be checked to use the system in Mode C or Mode A. This program is runs every 10 seconds to evaluate possible changes in external and external factors during this period.

### 2.2.2. Maximizing the use of renewable energy

Another control strategy was created to use the TES to maximize the use of renewable energy and was integrated into container two. The most important feature of this targeted strategy is maintaining thermal comfort, so the key element is evaluating the presence of thermal demand. If there is none, the algorithm is set to check the values of the amount of energy supplied by the PV, if this value is high enough to turn on the HP then the set of rules will evaluate whether to charge the TES or not. On the contrary, if the energy delivered by the PV is low then the algorithm will evaluate the current share of renewable on the grid and compare it to the average values of the same month of last year. In this case of high share of renewables, TES will be charged. On the other hand, if there is thermal demand the program will monitor the amount of energy provided by the PV and if there is sufficient power to switch on the HP, the program will operate in Mode A, if there is not enough the algorithm will then look for information about the forecast of the ambient temperature over the following three hours to compare to the comfort room temperature set point. If the temperatures are close ( $\pm 3$  °C) the program will check if the TES can be used to provide heating and enter Mode C or Mode A. If the temperatures are not close the algorithm will check if the current share of renewable on the grid is high and decide to use the TES to deliver energy or use the HP. This program runs every 10 seconds to evaluate all possible changes in external and external factors during this period.

## 3. Results and discussion

The data compiled were retrieved over two-day periods of both systems being tested with a respective control strategy. The first test period shows (see (a) Minimum cost strategy; (b) Maximize the use of renewable strategy.) that both strategies can maintain thermal comfort most of the time except for when high solar radiation causes overheating in the containers. This demonstrates the correct functioning of the rule-based control operational modes. In comparison to each other in this first test period (see (a) First test period; (b) Second test period), the amount of energy used by the system of the container

implementing the maximized use of renewable energy presented 9% of energy savings while the cost of operation showed an 8% difference in saving to its favour. Another test period was established and, similar to the previous assessment, thermal comfort was achieved except for the eventual overheating during the mid-hours of the day. This time the results point out (see (a) First test period; (b) Second test period), that the maximized use of renewable energy strategy on container two can achieve a 3 % saving on energy spent compared to the minimization of the price of operation strategy in container one but is 8 % less efficient in operational cost.

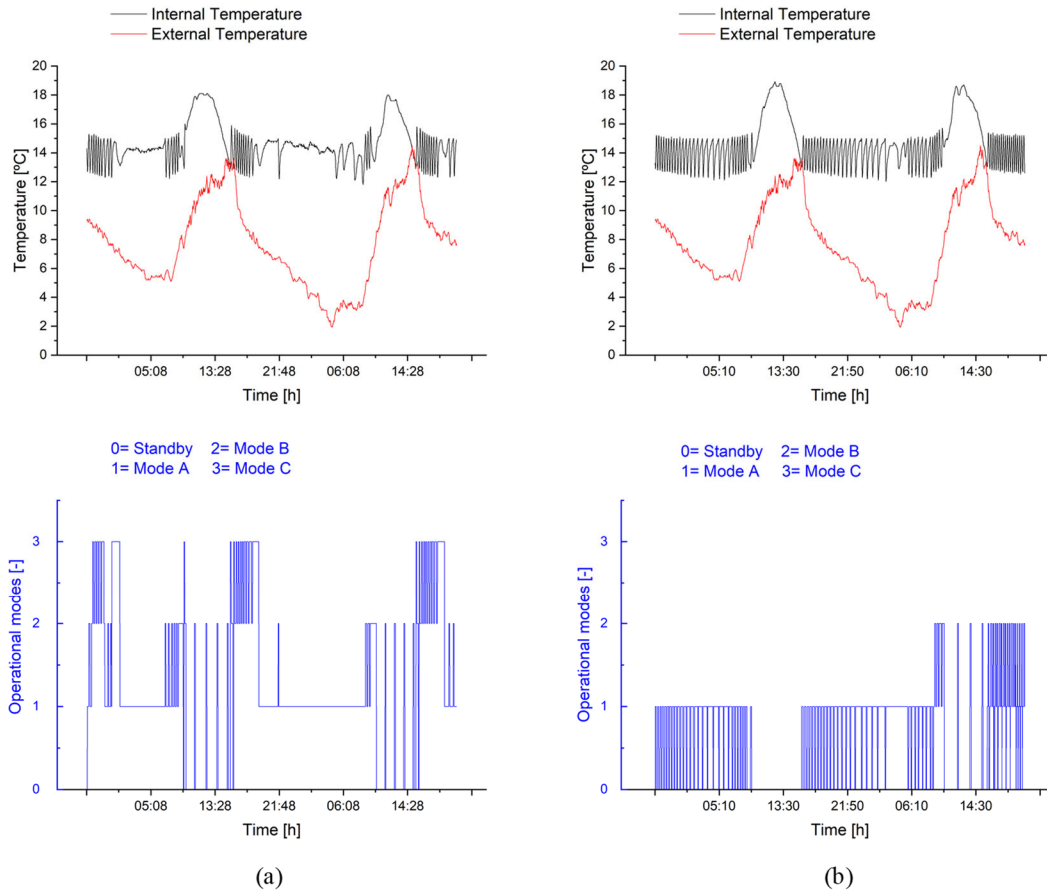


Figure 39. (a) Minimum cost strategy; (b) Maximize the use of renewable strategy.

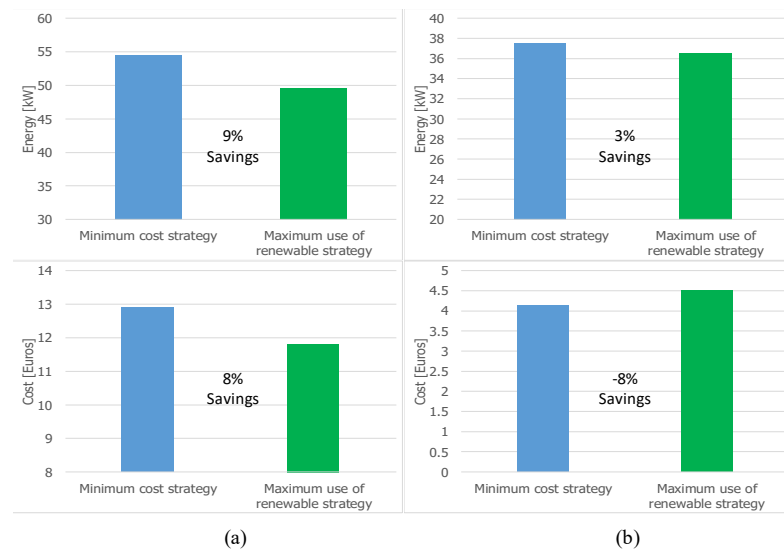


Figure 40. (a) First test period; (b) Second test period

## 4. Conclusions

In this paper, two rule-based control strategies were created with different targets that would optimize the use of thermal energy storage to achieve better efficiency in the thermal comfort of a building apartment. These approaches were both conducted in an experimental facility providing real-time data with almost identical internal and external factors between each other. The obtained data confirm that diverse approaches to the control strategy of thermal energy storage can offer an increase in the efficiency of the system without abandoning at any moment thermal comfort, providing even more relevance to exploring the use of smart control techniques that could further help with the optimization of the system and increase the amount of savings.

## Acknowledgments

This work was partially funded by the Ministerio de Ciencia e Innovación - Agencia Estatal de Investigación (PID2021- 123511OB-C31 - MCIN/AEI/10.13039/501100011033/FEDER, EU. The authors thank the Generalitat de Catalunya for the quality accreditation granted to the GREiA research group (2021 SGR 01615). GREiA is a TECNIO-certified agent in the category of technological development of the Gobierno de Cataluña. This work is partially supported by ICREA inside the program ICREA Academia.

## References

- [1] IEA, “Climate hazard assessment,” Paris, 2022. [Online]. Available: <https://www.iea.org/reports/climate-resilience-policy-indicator/climate-hazard-assessment>
- [2] L. Navarro *et al.*, “Thermal energy storage in building integrated thermal systems: A review. Part 1. active storage systems,” *Renew. Energy*, vol. 88, pp. 526–547, 2016, doi: 10.1016/j.renene.2015.11.040.
- [3] A. de Gracia and L. F. Cabeza, “Phase change materials and thermal energy storage for buildings,” *Energy Build.*, vol. 103, pp. 414–419, Sep. 2015, doi: 10.1016/j.enbuild.2015.06.007.
- [4] IRENA, *Innovation outlook: thermal energy storage*. 2020. [Online]. Available: [www.irena.org](http://www.irena.org)

EUROTHERM2023-L140

## Development of phase change materials in view of circular economy

Luisa F. Cabeza, Gabriel Zsembinszki, Emiliano Borri

GREiA Research Group, University of Lleida, Pere de Cabrera s/n, 25001-Lleida, Spain, Phone: +34 973 003576, e-mail: luisaf.cabeza@udl.cat

### Abstract

Circular economy is nowadays a key approach towards the valorization of resources by integrating them in production chain in the elaboration of a product or service. Circular economy is a step forward to the traditional ecological approach criteria, such as the recycling, reuse, and replacement of materials, and can be applied in different industry sectors. In the field of thermal energy storage, the use of materials that respond to the circular economy requirement can considerably contribute to the reduction of the environmental impact with respect to conventional materials derived from fossil fuel. BioPCMs are organic phase change materials that are ideal candidates to be used in latent thermal energy storage systems, especially those produced from wastes or by-products, not from natural sources. This study shows the potential and benefits of bioPCMs in residential applications compared to petroleum-derived traditional paraffins.

**Keywords:** Circular economy, phase change materials (PCMs), bioPCMs, thermal energy storage (TES), sustainability

### 1. Introduction

Circular economy is based on the concept of the valorization of resources by integrating them in production chain in the elaboration of a product or service. Therefore, new policies, product development, and research work towards overcoming the concept of end of life and wastes, enhancing the concept of developing new flows as cycles [1]. For example, the European Commission (EU) adopted the new circular economy action plan (CEAP) in March 2020 with the aim [2] to promote growth by transitioning to a modern, resource-efficient, and competitive economy.

Moreover, a circular economy approach benefits businesses and society with a better supply chain, low volatility of resource prices, better customer relations, and new job opportunities [3]. Circular economy is a step forward to the traditional ecological approach criteria, such as the recycling, reuse, and replacement of materials [4].

Literature shows that thermal energy storage (TES) is a promising technology to achieve the international environmental goals [5]. In particular, latent TES has a big role in buildings mitigation strategies [6]. But phase change materials (PCMs), the materials used in latent TES, come from fossil fuels (paraffin) or from natural resources (salt hydrates and salts). This is why, recently, bioPCM have attracted a lot of interest in the literature [7]. The advantages of using bioPCMs over other types of PCMs include, but are not limited to, minimization of environmental concerns, promotion of sustainability, and reduction of carbon footprint.

### 2. BioPCMs

BioPCMs, also called bio-based PCMs, are organic PCMs, therefore they have the same advantages and drawbacks. Organic PCMs are chemically and thermally stable, non-corrosive, they manifest insignificant subcooling, significant latent heat per unit mass, easy availability, and high workability [8]. Flammability, volume change corresponding to the phase transition, and low thermal conductivity



are their main shortcomings. A further advantage of bioPCMs is their low toxicity, which increases their use in different applications [9].

Sustainable and eco-friendly bio-sources such as palm kernel oil, coconut oil, palm oil, other tropical oils, and animal fat are the ones mostly used to produce bioPCMs [10–12]. Alcohols, fatty acids, glycols, and esters are the main types of bioPCMs [13,14]. Fatty acids that pertain to bioPCMs are usually derived from vegetable oils, fat esters, animal fat, etc., thus, their sources are mostly natural or bio-based [15].

But in view of circular economy, the most interesting bioPCMs are those produced from wastes or by-products, not from natural sources. An example of such is the production of fatty acids-based bioPCMs from renewable hydrolyzed waste cooking oil and feedstock waste using biocatalysts [16], or the use of non-edible fat waste from chicken and pig to produce stearic and palmitic acids that can be utilized as bioPCM (Figure 41) [17–19]. According to the literature, animal fats, such as chicken fat, lard, and tallow are the most commonly generated waste by-products from the agrifood industry [20].

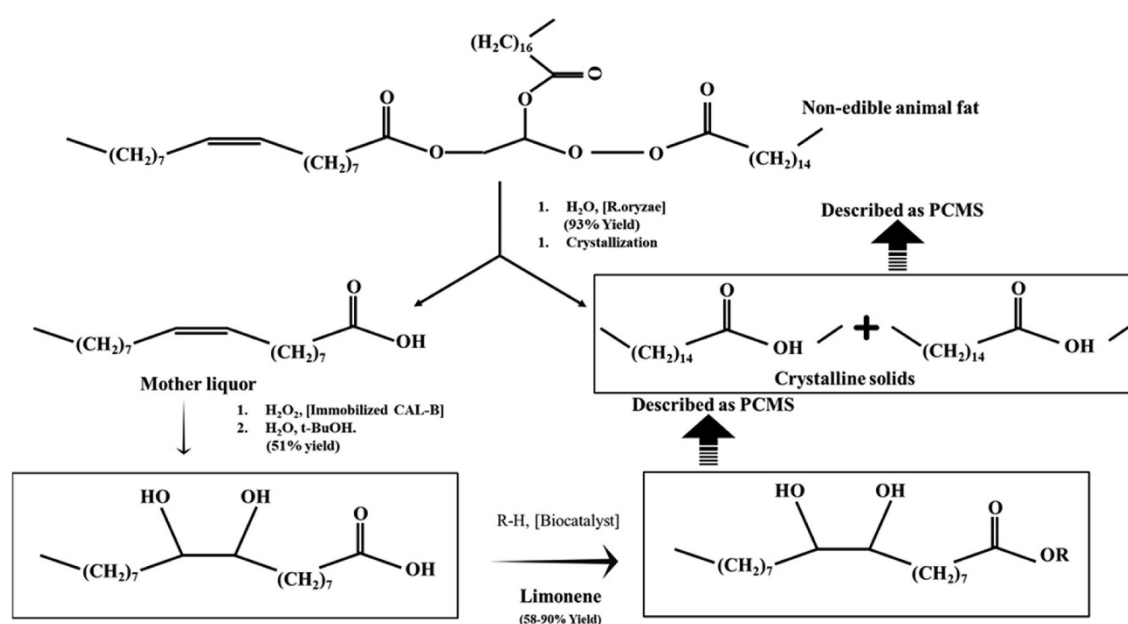


Figure 41. Syntheses of PCMs from non-edible animal fat [19]

### 3. Conclusions

Considering the comparable chemical-physical and superior environmental properties of bioPCMs composed of sustainable bio-sources as compared to conventional PCMs derived from fossil fuel, they have vast potential in TES applications in terms of sustainability, cost-effectiveness, resources conservation, and recycling. In addition, since no change in application method is required, their potential use in TES units for residential applications is as great as that of the market-leading petroleum-derived traditional paraffins [21–26].

Moreover, given that some so-called bioPCMs are in fact known materials, such as esters or fatty acids, other sources such as non-edible plant oils or other plant by-products should be assessed as raw material for PCM production.

### Acknowledgements

This project was funded by the European Union’s Horizon Europe Research and Innovation Programme under grant agreement No. 101096921 (THUMBS UP). Views and opinions expressed are however those of the author(s) only and do not necessarily reflect those of the European Union or CINEA. Neither the European Union nor the granting authority can be held responsible for them. The authors would like to thank the Catalan Government for the quality accreditation given to their research group (2021 SGR

01615). GREiA is certified agent TECNIO in the category of technology developers from the Government of Catalonia. This work is partially supported by ICREA under the ICREA Academia programme.

## References

- [1] A.M.M. Nunes, L.M. Coelho Junior, R. Abrahão, E.P. Santos Júnior, F.J. Simioni, P. Rotella Junior, L.C.S. Rocha, Public Policies for Renewable Energy: A Review of the Perspectives for a Circular Economy, *Energies* (Basel). 16 (2023) 485. <https://doi.org/10.3390/en16010485>.
- [2] European Commission, Circular economy action plan, [https://Environment.Ec.Europa.Eu/Strategy/Circular-Economy-Action-Plan\\_en](https://Environment.Ec.Europa.Eu/Strategy/Circular-Economy-Action-Plan_en). (2022).
- [3] T. Galkina, International ECOpreneurship: Environmental commitment and international partner selection of Finnish firms from the energy sector, *Journal of International Entrepreneurship*. 19 (2021) 300–320. <https://doi.org/10.1007/s10843-021-00286-8>.
- [4] V. Koval, I.W.E. Arsawan, N.P.S. Suryantini, S. Kovbasenko, N. Fisunencko, T. Alosyna, Circular Economy and Sustainability-Oriented Innovation: Conceptual Framework and Energy Future Avenue, *Energies* (Basel). 16 (2022) 243. <https://doi.org/10.3390/en16010243>.
- [5] L.F. Cabeza, *Advances in Thermal Energy Storage Systems*, Elsevier, 2021. <https://doi.org/10.1016/C2019-0-00061-1>.
- [6] L.F. Cabeza, M. Chàfer, Technological options and strategies towards zero energy buildings contributing to climate change mitigation: a systematic review, *Energy Build.* 219 (2020) 110009 (1–46). <https://doi.org/10.1016/j.enbuild.2020.110009>.
- [7] M.F. Junaid, Z. ur Rehman, N. Ijaz, M. Čekon, J. Čurpek, A. Babeker Elhag, Biobased phase change materials from a perspective of recycling, resources conservation and green buildings, *Energy Build.* 270 (2022) 112280. <https://doi.org/10.1016/j.enbuild.2022.112280>.
- [8] Y. Kang, S.-G. Jeong, S. Wi, S. Kim, Energy efficient Bio-based PCM with silica fume composites to apply in concrete for energy saving in buildings, *Solar Energy Materials and Solar Cells*. 143 (2015) 430–434. <https://doi.org/10.1016/j.solmat.2015.07.026>.
- [9] S.-G. Jeong, O. Chung, S. Yu, S. Kim, S. Kim, Improvement of the thermal properties of Bio-based PCM using exfoliated graphite nanoplatelets, *Solar Energy Materials and Solar Cells*. 117 (2013) 87–92. <https://doi.org/10.1016/j.solmat.2013.05.038>.
- [10] F. Frota de Albuquerque Landi, C. Fabiani, A.L. Pisello, Palm oil for seasonal thermal energy storage applications in buildings: The potential of multiple melting ranges in blends of bio-based fatty acids, *J Energy Storage*. 29 (2020) 101431. <https://doi.org/10.1016/j.est.2020.101431>.
- [11] E. Reyes-Cueva, J.F. Nicolalde, J. Martínez-Gómez, Characterization of Unripe and Mature Avocado Seed Oil in Different Proportions as Phase Change Materials and Simulation of Their Cooling Storage, *Molecules*. 26 (2020) 107. <https://doi.org/10.3390/molecules26010107>.
- [12] S. Kahwaji, M.A. White, Edible Oils as Practical Phase Change Materials for Thermal Energy Storage, *Applied Sciences*. 9 (2019) 1627. <https://doi.org/10.3390/app9081627>.
- [13] A. Sharma, V. v. Tyagi, C.R. Chen, D. Buddhi, Review on thermal energy storage with phase change materials and applications, *Renewable and Sustainable Energy Reviews*. 13 (2009) 318–345. <https://doi.org/10.1016/j.rser.2007.10.005>.
- [14] M. Duquesne, C. Mailhé, K. Ruiz-Onofre, F. Achchaq, Biosourced organic materials for latent heat storage: An economic and eco-friendly alternative, *Energy*. 188 (2019) 116067. <https://doi.org/10.1016/j.energy.2019.116067>.
- [15] D. Li, B. Zhuang, Y. Chen, B. Li, V. Landry, A. Kaboorani, Z. Wu, X.A. Wang, Incorporation technology of bio-based phase change materials for building envelope: A review, *Energy Build.* 260 (2022) 111920. <https://doi.org/10.1016/j.enbuild.2022.111920>.
- [16] S. Kumar, S. Negi, Transformation of waste cooking oil into C-18 fatty acids using a novel lipase produced by *Penicillium chrysogenum* through solid state fermentation, *3 Biotech*. 5 (2015) 847–851. <https://doi.org/10.1007/s13205-014-0268-z>.

- [17] P. Gallart-Sirvent, M. Martín, G. Villorbina, M. Balcells, A. Solé, C. Barrenche, L.F. Cabeza, R. Canela-Garayoa, Fatty acid eutectic mixtures and derivatives from non-edible animal fat as phase change materials, *RSC Adv.* 7 (2017) 24133–24139. <https://doi.org/10.1039/C7RA03845C>.
- [18] C. Fabiani, A. Pisello, M. Barbanera, L. Cabeza, F. Cotana, Assessing the Potentiality of Animal Fat Based-Bio Phase Change Materials (PCM) for Building Applications: An Innovative Multipurpose Thermal Investigation, *Energies (Basel)*. 12 (2019) 1111. <https://doi.org/10.3390/en12061111>.
- [19] P. Gallart-Sirvent, M. Martín, A. Solé, G. Villorbina, M. Balcells, L.F. Cabeza, R. Canela-Garayoa, Combining biocatalysts to achieve new phase change materials. Application to non-edible animal fat, *Molecular Catalysis*. 444 (2018) 76–83. <https://doi.org/10.1016/j.mcat.2017.10.037>.
- [20] S.A.A. Ghani, S.S. Jamari, S.Z. Abidin, Waste materials as the potential phase change material substitute in thermal energy storage system: a review, *Chem Eng Commun.* 208 (2021) 687–707. <https://doi.org/10.1080/00986445.2020.1715960>.
- [21] E. Douvi, C. Pagkalos, G. Dogkas, M.K. Koukou, V.N. Stathopoulos, Y. Caouris, M.Gr. Vrachopoulos, Phase change materials in solar domestic hot water systems: A review, *International Journal of Thermofluids*. 10 (2021) 100075. <https://doi.org/10.1016/j.ijft.2021.100075>.
- [22] M.K. Koukou, G. Dogkas, M.Gr. Vrachopoulos, J. Konstantaras, C. Pagkalos, V.N. Stathopoulos, P.K. Pandis, K. Lymperis, L. Coelho, A. Rebola, Experimental assessment of a full scale prototype thermal energy storage tank using paraffin for space heating application, *International Journal of Thermofluids*. 1–2 (2020) 100003. <https://doi.org/10.1016/j.ijft.2019.100003>.
- [23] G. Dogkas, M.K. Koukou, J. Konstantaras, C. Pagkalos, K. Lymperis, V. Stathopoulos, L. Coelho, A. Rebola, M.Gr. Vrachopoulos, Investigating the performance of a thermal energy storage unit with paraffin as phase change material, targeting buildings' cooling needs: an experimental approach, *International Journal of Thermofluids*. 3–4 (2020) 100027. <https://doi.org/10.1016/j.ijft.2020.100027>.
- [24] A. de Gracia, L.F. Cabeza, Phase change materials and thermal energy storage for buildings, *Energy Build.* 103 (2015) 414–419. <https://doi.org/10.1016/j.enbuild.2015.06.007>.
- [25] E. Borri, G. Zsembinszki, L.F. Cabeza, Recent developments of thermal energy storage applications in the built environment: a bibliometric analysis and systematic review, *Appl Therm Eng.* 189 (2021).
- [26] G. Zsembinszki, A.G. Fernández, L.F. Cabeza, Selection of the Appropriate Phase Change Material for Two Innovative Compact Energy Storage Systems in Residential Buildings, *Applied Sciences*. 10 (2020) 2116. <https://doi.org/10.3390/app10062116>.

EUROTHERM2023-V141

## Experimental evaluation at high temperatures of the corrosive behaviour of PCMs based on inorganic salts

Franklin R. Martínez Alcocer<sup>1,2</sup>, Emiliano Borri<sup>1</sup>, Svetlana Ushak<sup>2,3</sup>, Cristina Prieto<sup>4</sup>, Luisa F. Cabeza<sup>1</sup>

<sup>1</sup> GREiA Research Group, University of Lleida, Pere de Cabrera s/n, 25001-Lleida, Spain, Phone: +34 973 003576, e-mail: luisaf.cabeza@udl.cat

<sup>2</sup> Center for Advanced Research in Lithium and Industrial Minerals, University of Antofagasta, Avenue Universidad de Antofagasta 02800, Antofagasta, Chile. e-mail: svetlana.ushak@uantof.cl

<sup>3</sup> Departamento de Ingeniería Química y Procesos de Minerales University of Antofagasta, Avenue Universidad de Antofagasta 02800, Antofagasta, Chile.

<sup>4</sup> University of Seville, Department of Energy Engineering, Camino de los Descubrimientos s/n, 41092, Seville, Spain, e-mail: cprieto@us.es

### Abstract

Thermal energy storage (TES) is recognized as a key technology for the implementation in CSP plants productive process. Phase change materials are the materials used in latent TES, but they present corrosion to metals which are in contact, especially inorganic salts. In this study, four inorganic PCMs are tested against two stainless-steel fibres, to evaluate the corrosion effect of each PCM. Results show that hydroxide-based PCMs are more corrosive than nitrate-based salts. After one week, stainless-steel fibres, which were immersed in hydroxides, were destroyed and, fibres which were immersed in nitrates salts retained their integrity.

**Keywords:** Thermal energy storage (TES), corrosion test, inorganic PCMs

### 1. Introduction

In the last decades, CSP plants improved their technologies incorporating into their production process two molten salt tanks, storing energy in pure sensible way [1], which represents 12% of the installation costs [2]. However, replacing molten salt tanks with a tank composed of PCMs with different melting temperatures (cascade configuration) is more efficient, since latent heat is greater than sensible heat, which means that a greater amount of thermal energy can be stored with a smaller amount of material [1]. Moreover, to implement this technology it is necessary to develop PCMs with melting temperatures in the range of 300°C to 600°C (traditional operating temperature range of CSP plants) [3]. From an application point of view, inorganic salts are considered optimal for this aim, because they have high energy storage density. However, most authors agree that one of the main drawbacks of the use of PCM when high power is needed is the low thermal conductivity of the materials [4]. Furthermore, to overcome these problems, the addition of metal wool to PCM is an attractive option, since metal wools have high thermal conductivity and they are economically cheap. Nevertheless, inorganic salts are corrosive, which represented one of the most relevant phenomena to be considered for designing TES systems [5]. In this study, the corrosion effect of four different inorganic compounds, NaNO<sub>3</sub>, KNO<sub>3</sub>, NaOH and eutectic mixture NaOH-NaCl (80-20 wt.%) was evaluated, using two commercial stainless-steel fibres as substrate.

## 2. Materials and methodology

### 2.1. Materials

In this study, four different PCMs with similar melting temperatures, two nitrates and two hydroxides-based compounds, were selected to carry out this research. Thermal properties and details of the reagents were used to prepare PCMs are summarized in Table 6. Details and properties of selected PCMs [6]

Table 6. Details and properties of selected PCMs [6]

PCM	T <sub>melting</sub> (°C)	ΔH <sub>melting</sub> (J/g)	Source	Reference
NaNO <sub>3</sub>	310	172	Sigma-Aldrich	[1]
NaOH	318	165	Sigma-Aldrich	[7]
KNO <sub>3</sub>	335	95	VWR Chemicals	[8]
NaOH-NaCl (80-20 wt.%)	370	370	Sigma-Aldrich – Pan Reac Applichem	[7]

Moreover, two commercial stainless-steel fibres were selected as a substrate. They were stainless steel 314 and 434. Their main characteristics are given in Table 7. Composition of commercial stainless-steel fibres [6]

Table 7. Composition of commercial stainless-steel fibres [6]

Substrate	Fibre 314		Fibre 434	
Chemical composition (%)	C	0.20	C	0.08
	Si	2.50	Si	1.00
	Mn	2.00	Mn	1.00
	P	0.045	P	0.04
	S	0.015	S	0.03
	Cr	24 -26	Cr	16 – 18
	Ni	19 - 22	Mo	0.90 – 1.30

### 2.2. Methodology

Briefly, four samples (0.30 g approx.) of each stainless-steel fibre were placed in tests tubs. After that, test tubs with the stainless-steel fibre samples were filled with 15 g of four solid PCMs (NaNO<sub>3</sub>, KNO<sub>3</sub>, NaOH and eutectic mixture NaOH-NaCl (80-20 wt.%)), as it can see in Figure 42. Immersion of stainless fibres in each PCM. Left: solid, right: liquid All the test tubes were placed in the muffle at 450°C (see Figure 42. Immersion of stainless fibres in each PCM. Left: solid, right: liquid, to ensure liquid state of the PCM. The stainless-steel fibres were immersed in liquid PCM for one week. In addition, the corrosion tests were carried out in duplicate.



Figure 42. Immersion of stainless fibres in each PCM. Left: solid, right: liquid

### 3. Results

From the samples assessed it was possible to observe that both of studied stainless-steel fibres present corrosion at naked eye after immersion into  $\text{NaNO}_3$ ,  $\text{NaOH}$ ,  $\text{NaOH-NaCl}$  (80-20 wt.%) and  $\text{KNO}_3$  during the entire experimental period (Figure 2). These results are in accordance with the literature [5], where it was previously shown that one of the disadvantages of using inorganic PCM is their high corrosive effect. Furthermore, nitrates showed to be less corrosive than hydroxides, as shown in Figure 2, stainless-steel fibres that were immersed in hydroxides were completely destroyed compared to stainless-steel fibres that were immersed in nitrates, which despite showing corrosion retained their integrity.











Fibre 314				
Before tests	$\text{NaNO}_3$	$\text{NaOH}$	$\text{NaOH-NaCl}$ (80-20 wt%)	$\text{KNO}_3$
				
Fibre 343				
Before tests	$\text{NaNO}_3$	$\text{NaOH}$	$\text{NaOH-NaCl}$ (80-20 wt%)	$\text{KNO}_3$
				

Figure 43. Corrosion of stainless-steel fibres in contact with  $\text{NaNO}_3$ ,  $\text{NaOH}$ ,  $\text{NaOH-NaCl}$  (80-20 wt.%) and  $\text{KNO}_3$

#### 4. Conclusions

Corrosion experiments were carried out amongst two stainless-steel fibres immersed in four different PCMs, two nitrates and two hydroxides. The degradation phenomena were analysed qualitatively after the immersion of stainless-steel fibres in PCMs for one week. Considering the visual changes of the immersed stainless-steel, hydroxides showed to be more corrosive than nitrates.

#### Acknowledgements

Franklin R. Martinez Alcocer thanks the National Doctorate Scholarship for foreign students ANID 2021 Folio 21211932 for the financial support in the research. This project was funded by the European Union's Horizon Europe Research and Innovation Programme under grant agreement 101084182 (HYBRIDplus). Views and opinions expressed are however those of the author(s) only and do not necessarily reflect those of the European Union or CINEA. Neither the European Union nor the granting authority can be held responsible for them. This work is partially supported by ICREA under the ICREA Academia programme. The authors would like to thank the Catalan Government for the quality accreditation given to their research group (2021 SGR 01615). GREiA is certified agent TECNIO in the category of technology developers from the Government of Catalonia.

#### References

- [1] C. Prieto, L.F. Cabeza, Thermal energy storage (TES) with phase change materials (PCM) in solar power plants (CSP). Concept and plant performance, *Appl. Energy*. 254 (2019) 113646. <https://doi.org/10.1016/j.apenergy.2019.113646>.
- [2] IRENA (2021), Renewable capacity statistics 2021, Abu Dhabi, 2021.
- [3] B. Banerjee, S. Chatterjee, J. Datta, S.D. Saha, Application of phase changing materials in a CSP plant for thermal energy storage: A review on recent developments, *Mater. Today Proc.* (2022). <https://doi.org/10.1016/j.matpr.2022.04.306>.
- [4] C. Prieto, A. Lopez-Roman, N. Martínez, J.M. Morera, L.F. Cabeza, Improvement of phase change materials (PCM) used for solar process heat applications, *Molecules*. 26 (2021). <https://doi.org/10.3390/molecules26051260>.
- [5] P.E. Marín, S. Ushak, A. de Gracia, M. Grageda, L.F. Cabeza, Assessing corrosive behaviour of commercial phase change materials in the 21–25 °C temperature range, *J. Energy Storage*. 32 (2020). <https://doi.org/10.1016/j.est.2020.101711>.
- [6] STAX metal fibres, (n.d.). <https://www.stax.de/en/> (accessed January 23, 2023).
- [7] M. Liu, W. Saman, F. Bruno, Review on storage materials and thermal performance enhancement techniques for high temperature phase change thermal storage systems, *Renew. Sustain. Energy Rev.* 16 (2012) 2118–2132. <https://doi.org/10.1016/j.rser.2012.01.020>.
- [8] H. Michels, R. Pitz-Paal, Cascaded latent heat storage for parabolic trough solar power plants, *Sol. Energy*. 81 (2007) 829–837. <https://doi.org/10.1016/j.solener.2006.09.008>.

EUROTHERM2023-K143

## Optimizing Geopolymer Concrete Thermal Energy Storage: A Parametric Study of Key Design Parameters for High-Temperature Applications

Mohammad Rahjoo<sup>1</sup>, Guido Goracci<sup>1</sup>, Juan J Gaitero<sup>2</sup>, Pavel Martauz<sup>3</sup>, Esther Rojas<sup>4</sup>, Jorge S Dolado<sup>5</sup>

<sup>1</sup>Centro de Física de Materiales, CSIC-UPV/EHU, Paseo Manuel de Lardizábal 5, 20018 Donostia-San Sebastián, Spain, e-mail: m.rahjoo@csic.es, guido.goracci@ehu.eus

<sup>2</sup>TECNALIA, Basque Research and Technology Alliance (BRTA), Parque Tecnológico de Bizkaia, Astondo Bidea, Edif. 700, 48160 Derio, Spain, e-mail: juanjose.gaitero@tecnalia.com

<sup>3</sup>Považská Cementáreň Cement Plant (PCLA), Ulica Janka Kráľa, 01863 Ladce, Slovakia, e-mail: martauz.p@pcla.sk

<sup>4</sup>Plataforma Solar de Almería (PSA-CIEMAT), Av. Complutense 40, 28040 Madrid, Spain, e-mail: esther.rojas@ciemat.es

<sup>5</sup>Donostia International Physics Center (DIPC), Paseo Manuel de Lardizabal 4, 20018 Donostia-San Sebastián, Spain, j.dolado@ehu.eus

### Abstract

This study presents a numerical evaluation of geopolymer concrete as a material for high-temperature thermal energy storage (TES) applications. Through a multi-objective comparative parametric study, the thermal performance of geopolymer concrete TESs was assessed. A 3D numerical model of a GEO TES module was developed, validated with experimental data, and served as a benchmark. Geometry shapes, sizes, tube sizes, and heat transfer fluid velocities were analyzed. The results indicate that TES modules without tubes exhibit superior thermal performance and that square geometry is more suitable for modular construction due to its higher storage capacity and ease of manufacturing.

**Keywords:** Geopolymer concrete, Thermal energy storage, High-temperature applications, Numerical modeling, Optimization, Sustainable energy

### 1. Introduction

This study examines the potential of geopolymer concrete as a material for high-temperature TES in concentrated solar power, solar process heat, and industrial waste heat applications. Geopolymer concrete has proven to be a promising alternative to Portland cement concrete due to its exceptional thermal properties. The authors conduct a comparative parametric analysis of different tube sizes, arrangements, and configurations to determine the scalability of a geopolymer TES prototype. Numerical modeling and simulation were used to assess the thermal energy storage capacity and performance of square, hexagonal, and circular GEO concrete geometries, with square being the most suitable for modular construction. The study also evaluates the impact of incorporating tubes in the TES module on thermal performance, finding that eliminating tubes may be a viable option in certain applications.

### 2. Materials and methods

The study focuses on a GEO module that studied experimentally. The GEO concrete has a thermal conductivity of 1.2 W/mK, a specific heat capacity of 1000 J/kgK, and a density of 2890 kg/m<sup>3</sup>. A 3D numerical model of the GEO TES module was developed using Comsol Multiphysics software and validated with experimental data, as shown in Fig. 2.



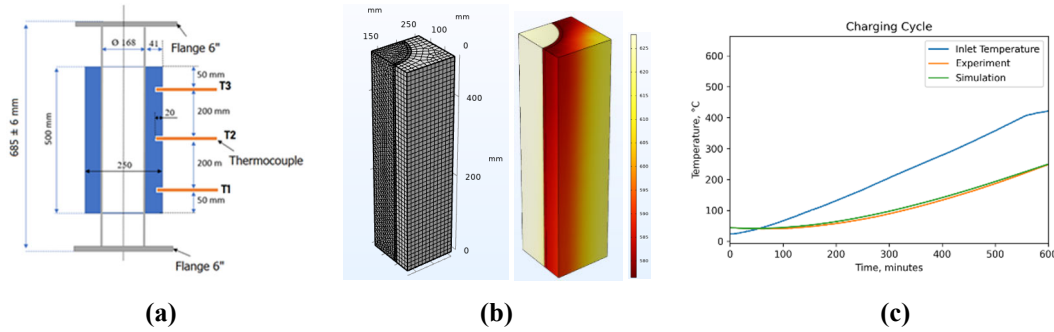


Fig. 1. (a) TES module configuration for thermal cycling test (b) Meshed view of the 3-D model result: charging processes for volume average temperature ( $T_{avg}$  °C). (c) Average temperature ( $T_{avg}$ ) of experiment vs simulation's volume average  $T_{avg}$ .

The numerical study aimed to determine the optimal design parameters for a thermal energy storage module using concrete as the storage material. It was conducted in two stages. Stage 1 evaluated the impact of pipe size and module size on thermal performance through computational fluid dynamics simulations, considering three different design schemes and evaluating each under a fixed inlet temperature boundary condition with the module boundary assumed to be insulated. Stage 2 proposed a modular design that addressed practical considerations such as working conditions, flow rate, and speed of the heat transfer fluid. The thermal energy storage capacity of the TES module was compared with and without metallic tubes in concrete, and the effect of tube walls on heat transfer performance was considered, as shown in Fig. 3(a)(b)(c). The results provide a clear comparison of different geometries and the impact of various parameters on thermal energy storage capacity. The study's results provide insight into how different geometries and parameters affect thermal energy storage capacity.

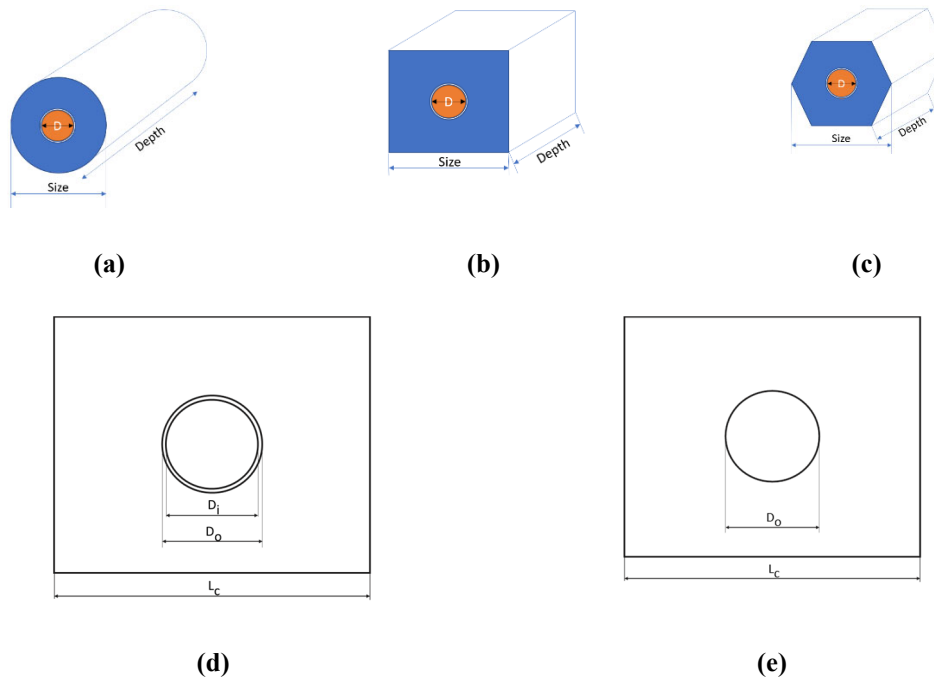


Fig. 2. (a) Circular surface geometry, (b) square surface geometry, (c) hexagonal surface geometry, (d) geometry used for parametric study of incorporating tube, (e) geometry used for parametric study without incorporating tube.

### 3. Results and discussion

The study aimed to identify key design parameters for a given energy storage requirement through a parametric analysis. The heat energy stored in the TES system was calculated using the equation  $Q =$

$m(\text{kg}) * C_p (\text{J/kg}^\circ\text{C}) * \Delta T (^\circ\text{C})$ . The results were presented using heatmaps, providing a clear comparison of different geometries and the impact of various parameters on thermal energy storage capacity. The size of the tube was found to significantly impact the output  $Q$  of the TES system, with the difference in thermal energy storage ranging from 29 to 75 MJ, while the difference in material mass ranged from 47 to 139 kg, indicating that mass is not the primary factor affecting TES capacity and selection criteria, as shown in Fig 4(b).

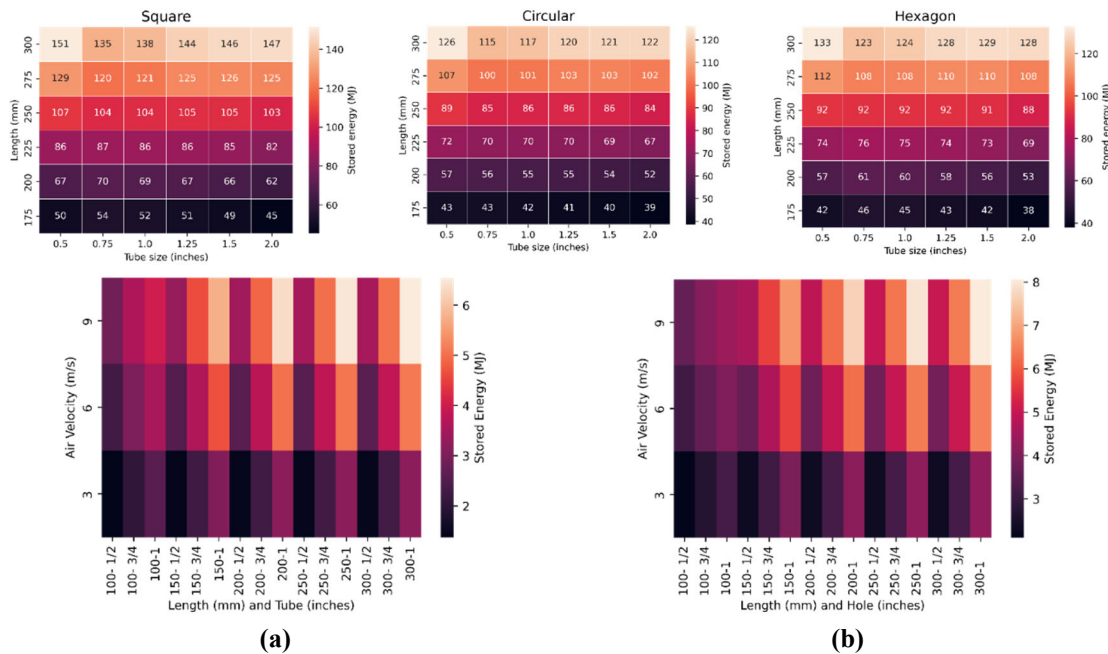


Fig. 3. Heatmap for the amount of energy storage per different lengths and tube sizes. Square, circular, and hexagon geometries. (a) and (b) Heatmap for the amount of energy storage per different lengths and tube sizes for Square geometry. (a) with tube implementation, (b) without tube implementation.

The simulation results showed that larger tube/hole sizes result in higher storage capacity, reaching up to  $\sim 8$  MJ for the largest hole size and 9 m/s velocity. The correlation matrix (Fig. 4) demonstrates the relationship between variables and two outcomes, Thermal Storage Amount ( $Q$ ) and  $T_{\text{avg}}$ . The variables with the strongest positive correlation with  $Q$  are  $T_{\text{inlet}}$ ,  $t_{\text{charging}}$ , and  $v_{\text{air}}$ , while  $T_{\text{avg}}$  has a moderate positive correlation with  $T_{\text{inlet}}$ . The variables with negative correlation with  $T_{\text{avg}}$  are  $L_c$ ,  $m_{\text{concrete}}$ , and  $V_{\text{concrete}}$ , while  $T_{\text{initial}}$  has a weak negative correlation with  $Q$ .

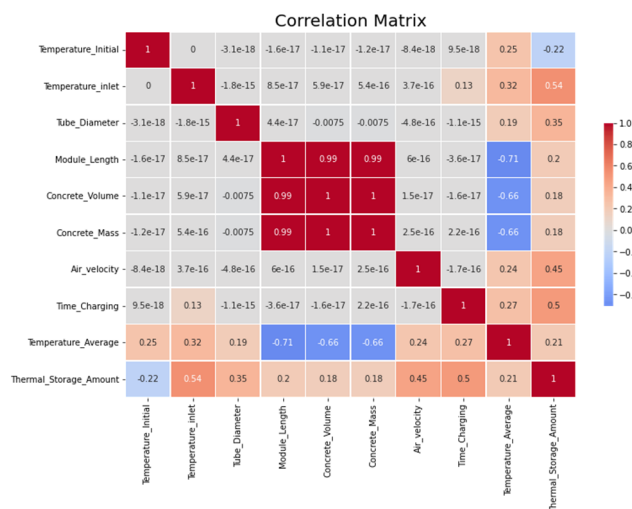


Fig. 4. Correlation matrix of different variables used in simulation.

#### 4. Conclusions

The study highlights the importance of having a validated numerical model and conducting parametric studies to predict key design parameters for thermal energy storage systems. The experimental validation of the numerical model ensures its accuracy and reliability, crucial for the future upscaling of the geopolymer concrete thermal energy storage (GEO) module. Eliminating tubes may lead to a more efficient and cost-effective system. The correlation matrix provides information on the relationships between variables and their impact on thermal energy storage amount and average temperature, useful for optimizing the design of future TES modules for specific applications.

#### Acknowledgements

The authors acknowledge the funding received from MCIN/AEI/10.13039/501100011033 and the European Social Fund under the 2019 call for predoctoral contracts. They also acknowledge the funding received from the Gobierno Vasco UPV/EHU and the computing resources and time provided by the Donostia International Physics Center (DIPC). The economic support from POVAZSKA is also acknowledged.

#### References

- L. F. Cabeza, *Advances in Thermal Energy Storage Systems*, Woodhead Publishing, 2021, pp. 37-54.
- L. F. Cabeza, D. Várez, G. Zsembinszki, E. Borri and C. Prieto, "Key Challenges for High Temperature Thermal Energy Storage in Concrete—First Steps towards a Novel Storage Design," *Energies*, vol. 15, no. 13, p. 4544, 2022.
- R. He, D. Nan and Z. Wang, "Thermal and mechanical properties of geopolymers exposed to high temperature: A literature review," *Adv. Civ. Eng.*, vol. 2020, pp. 1-17, 2020.
- M. Rahjoo, G. G. M. P. R. E. and J. Dolado, "Geopolymer Concrete Performance Study for High-Temperature Thermal Energy Storage (TES) Applications," *Sustainability*, vol. 14, no. 3, p. 1937, 2022.
- M. Rahjoo, G. Goracci, J. J. Gaitero, P. Martauz, E. Rojas and J. S. Dolado, "Thermal Energy Storage (TES) Prototype Based on Geopolymer Concrete for High-Temperature Applications.," *Materials*, p. 7086, 2022.
- COMSOL Multiphysics® v. 6.," COMSOL AB, 2020. [Online]. Available: [www.comsol.com](http://www.comsol.com). [Accessed 2022].

## The charging time energy fraction for describing different phases of charging a latent thermal storage heat exchanger

Kenny Couvreur<sup>1</sup>, Maité Goderis<sup>1</sup>, Wim Beyne<sup>1</sup>, Michel De Paepe<sup>1,2</sup>

<sup>1</sup>Department of Electromechanical, Systems and Metal Engineering – UGent, Ghent, Belgium,  
Kenny.Couvreur@UGent.be

<sup>2</sup>FlandersMake@UGent – Core lab EEDT-MP, Leuven, Belgium, www.flandersmake.be

### Abstract

Latent thermal energy storage (LTES) systems have great potential but the number of real-life applications are limited. The complex transient nature of LTES systems, the high cost of experimental set-ups, and the accompanying measurement uncertainty, makes it necessary to develop physics-based models to predict and evaluate the performance of a LTES heat exchanger. In this work, the charging time energy fraction method is further developed. A methodology is proposed which splits a full charging cycle into two relevant subprocesses. Charging time correlations for each of the two subprocesses are calibrated on simulation results. Then a methodology is proposed for combining the two charging time correlations and essentially predicting the HTF outlet temperature for a full charging cycle. Accurate predictions are obtained and a full characterization is possible of a LTES heat exchanger through the charging time energy fraction method.

**Keywords:** Latent thermal energy storage, Charging time energy fraction method, Predictive model, Charging behaviour

### 1. Introduction

Increasing the share of renewable energy in our total energy mix will require the deployment of innovative storage solutions. Latent thermal energy storage technologies are a class of thermal batteries given great potential. A wide variety of LTES systems have been described in literature [1]. The shell-and-tube design, with a phase changing material (PCM) at the shell side and a heat transfer fluid (HTF) flowing through the pipes in the center, is considered most promising for devices for commercial heat exchangers. Despite the potential of LTES, there are few commercial players offering standardized thermal storage units or providing expertise in designing application-specific storage solutions. This is partially attributed to missing knowledge on the thermal design and characterization of thermal energy storage systems.

The charging time energy fraction method (CTEFM) on the other hand is a method recently described by Beyne et al. [2]. This method can be used to obtain a predictive model of a LTES heat exchanger behaviour. The predictive models allows to estimate the dynamic HTF outlet temperature as function of the HTF inlet conditions and the initial battery conditions. The general correlation for the charging time is in the form of Eq. **Error! No s'ha trobat l'origen de la referència.** and used to estimate the efflux of energy and the HTF outlet temperature. The charging time is expressed as function of the energy fraction,  $\alpha$  which is a cumulative distribution function describing the stored energy. The energy fraction,  $\alpha$  is then the result of normalization with the maximum total internal energy change of the heat exchanger,  $\Delta U$  between the initial state and the HTF inlet temperature (Eq. 2).  $A(\alpha)$ ,  $B(\alpha)$ ,  $C(\alpha)$  and  $D(\alpha)$  are fitting coefficients which have to be fitted for each specific LTES heat exchanger.

$$t_c(\alpha) = \left( A(\alpha) + \frac{B(\alpha)}{\dot{m}} \right) \frac{1}{\Delta T} + \left( C(\alpha) + \frac{D(\alpha)}{\dot{m}} \right) \quad 1$$

$$\alpha(t) = \frac{J(t)}{\Delta U} \quad 2$$

The method as described in Beyne et al. [2] and Couvreur et al. [3] will fail to estimate the HTF outlet state for initial battery conditions different than what is used to calibrate the model. This is because the charging time correlation considers the charging time to be linear with the inverse of the temperature difference between the HTF inlet temperature and the phase change temperature and no information can be given on the initial temperature. The method thus needs to be adapted. Therefore this work further develops the CTEFM by proposing a methodology allowing to create a predictive model for the HTF outlet temperature for variable HTF inlet conditions and variable initial conditions.

## 2. Methodology

The LTES heat exchanger used in this work as a case to further develop the CTEFM is a shell-and-tube heat exchanger. Details of the set-up are described in the work of Couvreur et al. [3]. Since calibration of the predictive model used in the CTEFM requires a large experimental dataset, a finite volume model of the LTES heat exchanger is used to generate numerical datasets instead of experimental datasets. The model allows to output the HTF outlet temperature for given initial conditions and HTF inlet conditions.

Different phases are present during a charging cycle starting from a temperature lower than the phase change temperature: 1) The HTF present in the tubes are initially at a temperature equal to the initial temperature and are being pushed out of the tubes. 2) Heating of the solid PCM from the initial battery temperature to the phase change temperature. 3) Phase change of the PCM. 4) Heating of the liquid PCM from the phase change temperature to the HTF inlet temperature.

During the charging process at least one of these phases occur and often two or more are simultaneously occurring. The question is raised whether each of these phases can be characterized by a charging time correlation and whether a methodology can be developed to combine the correlations characteristic to the different phases back together and predict the charging time for a full charging process. Splitting the total charging process into the different subprocesses can be done by separating the total stored energy of the complete charging process into relevant pieces corresponding to the specific phase you want to describe as given in Eq. 3 where  $i$  stands for the number of different phases to be described. Completion of each of these phases contributes to a change in the total stored energy as further illustrated in Figure 1. For simplicity, the total charging process in this work is split into two relevant parts only: heating of the solid PCM and the phase change process with heating of the liquid PCM. Initial pushing of the HTF is neglected. Both melting and sensible liquid of the PCM are combined as a subprocess as it is difficult to consider melting and sensible heating of liquid PCM separately.

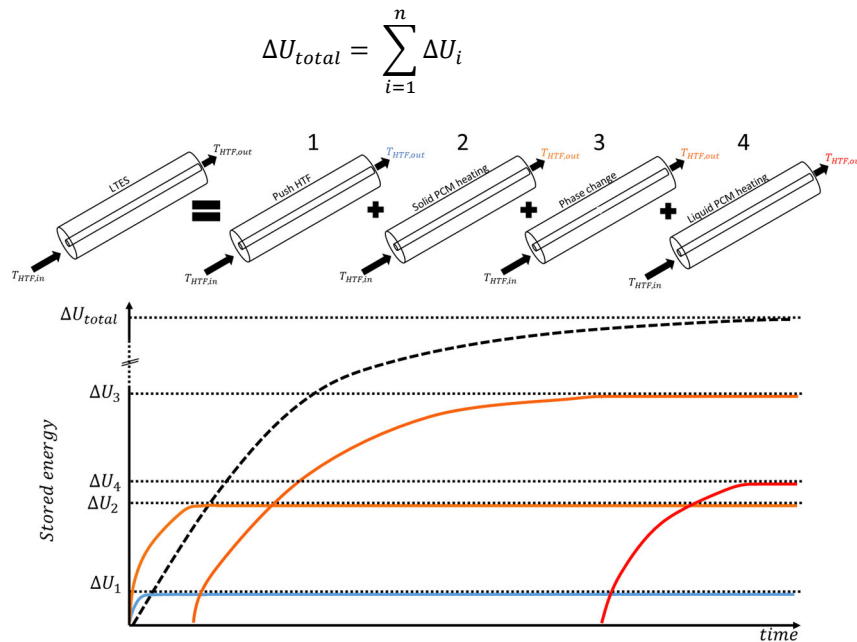


Figure 44. Decomposition of a LTES heat exchanger in 4 different subprocesses based and the respective evolution of the stored energy of each subprocess.

### 3. Method evaluation and results

LTES systems are mostly characterized by the temperature difference between the HTF inlet temperature and the PCM phase change temperature,  $\Delta T$  as the driving force for heat transfer. When no phase change is involved an alternative expression for the driving temperature difference is required. For a sensible storage system the driving temperature difference for heat transfer is the difference between the initial battery temperature and the HTF inlet temperature,  $\Delta T_s$ . For calibration of the charging time correlation (Eq. 1) two datasets of each 36 charging experiments with varying HTF mass flow rate and inlet temperature are created with the finite volume model. The charging process is strictly limited to a temperature range below the phase change temperature. It is found that sensible heating of the solid PCM is best described by Eq. 4 with  $\beta$  the energy fraction corresponding to the sensible heating phase. The melting process with sensible heating of the liquid PCM is still described by Eq. 2.

$$t_{c,s}(\beta) = C_s(\beta) + \frac{D_s(\beta)}{\dot{m}} \quad 4$$

### 4. The charging time correlation for a full charging cycle

Ideally, the correlations of the considered subprocesses can be combined to predict the behaviour of a full charging process without modifications to the original correlations. This would allow predicting the HTF outlet state for any given starting temperature. Splitting the total charging process into the two subprocesses based on separating the total stored energy and combining the two correlations describing each of the two subprocesses then requires complying with the conservation of energy and a smooth transition between the two subprocesses has to be realised. It is found that predicting the charging time for a full charging process for any given starting temperature, HTF inlet temperature and HTF mass flow rates is possible by Eq. 5. Eq. 5 is a combination of respectively Eq. 4 for the sensible heating process and Eq. 1 of the melting process, with  $\gamma$  the energy fraction related to the melting and the energy fraction of the total charging process remains  $\alpha$ .

$$t_c(\alpha) = \begin{cases} C_s(\beta) + \frac{D_s(\beta)}{\dot{m}}, & \beta \in [0 - \beta_T] \\ C_s(\beta_T) + \frac{D_s(\beta_T)}{\dot{m}} + \left[ \left( A_m(\gamma) + \frac{B_m(\gamma)}{\dot{m}} \right) \frac{1}{\Delta T} + C_m(\gamma) + \frac{D_m(\gamma)}{\dot{m}} \right], & \gamma \in [0 - 1] \end{cases} \quad 5$$

$\beta_T$ , is the threshold energy fraction which defines the endpoint of the sensible heating of the solid PCM and can be found by Eq. 6.

$$\beta_T = \frac{m_{pcm} c_{pcm,s} (T_{m,t,l} - T_{LTES,ini})}{m_{pcm} c_{pcm,s} (T_{m,t,l} - T_{LTES,ini}) + m_{pcm} c_{pcm,l} (T_{HTF,in} - T_{m,t,u})} \quad 6$$

Figure 2 shows the predictions of the HTF outlet temperature for the two subprocesses combined. The predictions for the sensible heating process are stopped once a temperature of 232 °C has been reached. This corresponds to the predicted HTF outlet temperature for starting the next phase change process.

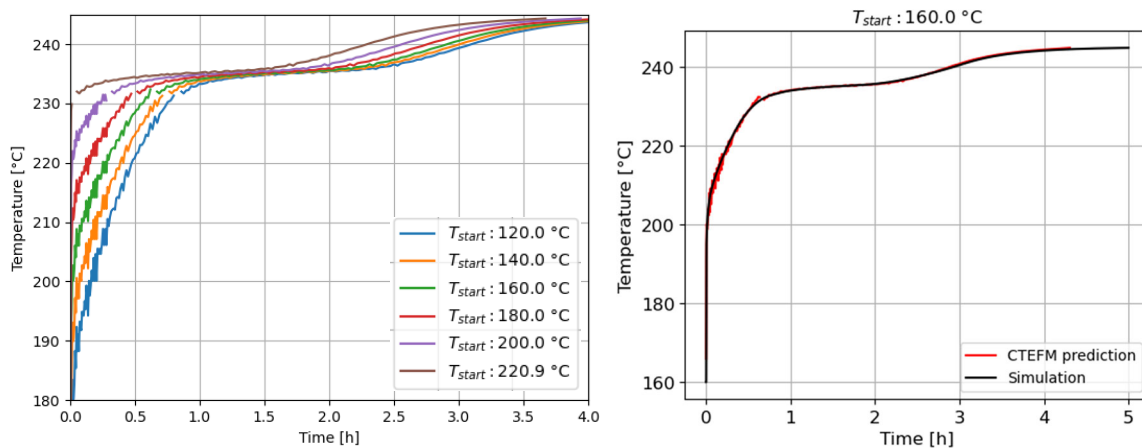


Figure 45. Left) HTF outlet temperature prediction with new methodology for a full charging cycle. Right) Comparison of the CTEFM prediction with the simulation data of one specific experiment.

## 5. Conclusions

This work proposes a methodology that splits a complete charging process into two subprocesses by splitting the total stored energy of a complete charging process into two relevant parts corresponding to the two subprocesses. Two predictive models, based on the charging time energy fraction method, for each subprocess are calibrated and show accurate HTF outlet predictions for the respective subprocess. Then a methodology is proposed for combining the resulting predictive models of each subprocess to a predictive model of a complete charging process. The predicted HTF outlet temperature based on this new methodology is compared to the simulated HTF outlet temperatures. All predictions have an integrated absolute temperature difference with the simulation data lower than 0.2 °C. The improved charging time energy fraction method has now been shown to be useful for an accurate characterization of a LTES system.

## References

- [1] Zalba, B., et al., *Review on thermal energy storage with phase change: materials, heat transfer analysis and applications*. Applied Thermal Engineering, 2003. **23**(3): p. 251-283.
- [2] Beyne, W., et al., *A charging time energy fraction method for evaluating the performance of a latent thermal energy storage heat exchanger*. Applied Thermal Engineering, 2021. **195**.
- [3] Couvreur, K., et al., *Characterization of a latent thermal energy storage heat exchanger using a charging time energy fraction method with a heat loss model*. Applied Thermal Engineering, 2023. **219**.

EUROTHERM2023-1146

## A simplified approach for simulating the discharging process in shell and tube heat exchangers with PCMs

Alessandro Ribezzo<sup>1</sup>, Emiliano Borri<sup>2</sup>, Matteo Morciano<sup>1</sup>, Luca Bergamasco<sup>1</sup>, Matteo Fasano<sup>1</sup>, Eliodoro Chiavazzo<sup>1</sup>, Luisa F. Cabeza<sup>2</sup>

<sup>1</sup>Department of Energy, Politecnico di Torino, Corso Duca degli Abruzzi 24, 10129 Torino, Italy, e-mail:

[eliodoro.chiavazzo@polito.it](mailto:eliodoro.chiavazzo@polito.it)

<sup>2</sup>GREiA Research Group, University of Lleida, Pere de Cabrera s/n, 25001 Lleida, Spain, e-mail:

[luisaf.cabeza@udl.cat](mailto:luisaf.cabeza@udl.cat)

### Abstract

Reliable numerical simulations of phase change materials (PCMs) are essential to overcome the limits of an extensive experimental campaign. However, the modeling and simulation of an entire heat exchanger containing a material undergoing phase transition are computationally demanding as they likely require fine mesh and long computational times. In this work, the properties of the application under study, which is a PCM-based shell and tube heat exchanger, were exploited to develop a simplified approach for the estimates of the time evolution during the discharging process of the heat exchanger. To achieve this, COMSOL simulations were performed, by taking into account the fluid flow of the heat transfer fluid (HTF), the heat transfer between the fluid, the pipe and the PCM, and the phase transition within the PCM. An acceptable compromise between the computational cost and the model accuracy can thus be demonstrated.

**Keywords:** Phase change material, CFD simulations, Heat exchanger, Apparent heat capacity method.

### 1. Introduction

The use of phase change materials (PCMs) represents one of the most promising solutions within the currently available thermal energy storage (TES) technologies, thanks to the achievable high stored energy density (as compared to sensible TES) and sufficient technological maturity [1]. However, the limited thermal conductivity of such materials may lead to incomplete phase transitions during the applications, thus reducing the effective energy capacities [2], [3].

In this context, numerical simulations may be exploited to overcome the drawback of developing extensive experimental campaigns for the testing of several design solutions – such as tank layouts, addition of fins, composite PCMs, nanocomposite PCMs – for establishing the best technology to achieve the complete phase transition in the specific applications under study. However, the numerical CFD simulations of a whole 3D heat exchanger containing are challenging, as they require a very fine mesh, which leads to very high computational cost [4].

In typical latent TES applications, the worst-case scenario is often experienced during the discharging process, which is mainly governed by the conductive heat transfer, thus leading to higher phase transition periods, as compared to the charging phase, in which the natural convection remarkably increases the heat transfer [5]. Therefore, the aim of the work is the development of a simplified approach in order to get reliable results (without expensive computational costs) of the discharging periods of a PCM-based shell & tube heat exchanger, which was experimentally validated in [6]. This approach consists in performing CFD simulations, by considering a subsystem of the whole heat exchanger, i.e. a simplified 3D single-tube geometry. Then, the whole geometry is modeled as a series of the tubes, thus obtaining the PCM temperature evolution during the discharging process by averaging the performed single-tube simulations. In each single-tube simulation, the coupling between the fluid flow of the heat transfer fluid (HTF), and the heat transfer between HTF, fluid pipe and PCM is modeled. The phase transition within the PCM is obtained by exploiting the effective heat capacity method, which



includes the latent heat within a modified value of the specific heat capacity [7]. Finally, the obtained temperature evolution during the discharging period numerically computed was compared to the experimental measurements performed.

## 2. Materials and methods

CFD numerical simulations of the PCM were performed by means of COMSOL to numerically estimate the experimental measurements of the work carried out by Gasia *et al.* [6]. The complete 3D model of the shell & tube heat exchanger and the subsystems taken into account in the numerical simulations are represented in Figure 1. The simulations of the subsystems were performed in series (from subsystem 1 to 10), by imposing the temperature of the HTF fluid of subsystem  $i+1$  as the outlet temperature of the previous one,  $i$ .

The PCM material under study is the n-octadecane, the HTF is distilled water, the case is made out of aluminum and the tubes out of copper. All the other parameters, such as the geometry and the temperature evolution of the HTF can be found in [6].

The numerical model of each subsystem considers the coupling between the fluid flow of the heat transfer fluid, the heat exchanges between the fluid, the tube pipe and the PCM, and the phase transition of the PCM. Therefore, the governing equations for the HTF fluid and the PCM are the continuity, the momentum, and the energy ones. Being the Reynolds number of the HTF equal to 4000 (mass flow rate = 0.05 kg/s), the fluid flow was simulated by means of the turbulent flow module of COMSOL, in which the k-epsilon model was adopted. The phase transition of the PCM was taken into account by using the apparent specific heat capacity [7], thus modifying the value of the heat capacity in the phase transition range. Pure conduction was considered in the PCM consistently with other works in literature [5]. A mesh refinement and a step size refinement study were performed to find the best compromise between computational costs and the reliability of the results, thus choosing a mesh containing 64440 elements. According to the position of the subsystem considered (1-10) symmetry or thermal insulations boundary conditions were imposed at the lateral faces of the subsystem. Therefore, i) the thermal losses towards the outside of the component have been neglected, due to the insulating material during the experimental measurements, and ii) the heat flux between adjacent subsystems was neglected. Therefore, the symmetry boundary condition considers the subsystems as if the tubes were in parallel, even if they actually are in series, thus neglecting the heat flux between adjacent subsystems. This simplified hypothesis was due to the high velocity of the HTF. Finally, the PCM mean temperature evolution during the discharging process has been computed by averaging the temperatures profile of the 10 subsystems taken into account and compared with the average PCM temperature experimentally measured.

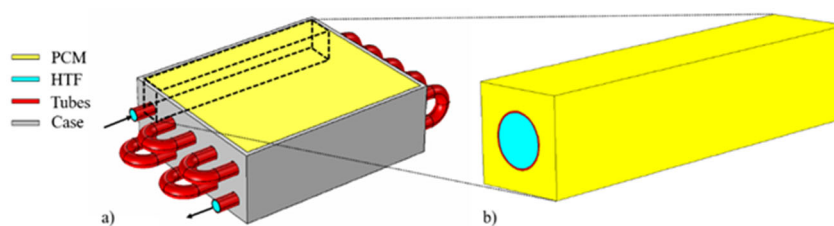


Figure 1. Complete 3D model of the shell & tube tank under study (a), and one of the ten subsystems exploited for the numerical simulations (b). It is worth noting that the insulating material is not shown here for a graphical reason, as it completely covers the heat exchanger.

### 3. Results and discussion

The comparison between the temperature evolution that was experimentally measured during the discharging period in [6] and the numerical simulations obtained by the simplified approach proposed in this work is shown in Figure 2. The experimentally measured temperatures depicted are obtained by averaging values obtained by seven thermocouples placed in different zones within the PCM during the experimental tests. On the other hand, the numerically predicted temperature evolution was obtained as the mean value of the average temperature of each subsystem considered. During the first 50 minutes, i.e., until the reaching of the start of the phase transition ( $T = 27.7\text{ }^{\circ}\text{C}$ ), the assumptions considered - no natural convection within the liquid phase of the PCM, negligible heat losses towards the environment and no heat flux between adjacent subsystems - resulted in a slower cooling down of the PCM as compared to the experimental measurements. Nonetheless, the overall discharging period is well predicted by the numerical simulations, as the computed temperature is always within the error bars since the start of the phase transition. Similar results were obtained in [5], in which a pure conduction model and a conductive+convective model were compared, thus denoting the neglect of the convection within the PCM as the most restrictive assumption of our work. The convection can be implemented in the model, without the requirement of an excessive increase in the computational cost. Finally, it is worth noting that the numerical results have been obtained with a total computational time of 2 hours, thus resulting in an acceptable compromise between preliminary reliable results and low computational costs.

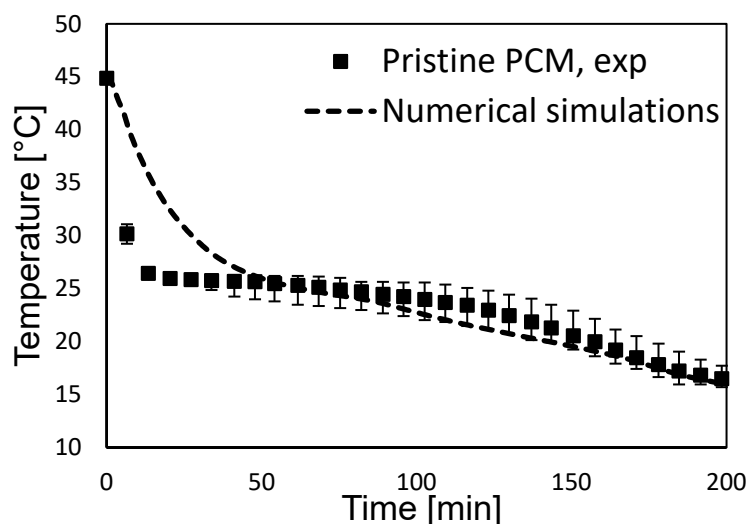


Figure 2. Comparison between the experimental measurements and the simplified numerical approach adopted in this work.

### 4. Conclusions

In this study, a simplified 3D approach (performed by COMSOL) was exploited to numerically estimate the temperature evolution of the PCM-based shell & tube tank that has been experimentally measured in [6]. As heat diffusion is assumed to be the dominant mechanism during the discharging process, only heat conduction was considered within the PCM. The coupling between the HTF fluid flow and the heat transfer between HTF and PCM was modeled. Besides an initial discrepancy between the numerical results and experimental measurements in the liquid region, the experimental temperature evolution of the PCM is well estimated by the simulations. These results have been obtained with a total computational cost of 2 hours (Intel Core i5-9400 CPU @ 2.90GHz and RAM 16 Gb), which is much lower than the one that would be required to model the whole heat exchanger and for the such discharging process. Future work will be performed by including a proper description of natural convection within the PCM liquid phase (e.g. by means of the enthalpy-porosity method [2]) to obtain good estimates of the PCM average temperature evolution also during the charging periods. Finally, this layout may be improved by including metallic wool, metallic foams or additives within the PCM [3] to

increase the effective thermal conductivity of the PCM composites, thus reducing the charging and discharging times.

## Acknowledgements

E.C. acknowledge the financial support of the Italian National Project PRIN Heat transfer and Thermal Energy Storage Enhancement by Foams and Nanoparticles (2017F7KZWS). This work was partially funded by the Ministerio de Ciencia e Innovación - Agencia Estatal de Investigación (PID2021-123511OB-C31 - MCIN/AEI/10.13039/501100011033/FEDER, EU. The authors from GREiA research group from University of Lleida would like to thank the Catalan Government for the quality accreditation given to their research group (2021 SGR 01615). GREiA is certified agent TECNIO in the category of technology developers from the Government of Catalonia. This work is partially supported by ICREA under the ICREA Academia programme.

## References

- [1] L. F. Cabeza, A. de Gracia, G. Zsembinszki, and E. Borri, “Perspectives on thermal energy storage research,” *Energy*, vol. 231, p. 120943, 2021, doi: 10.1016/j.energy.2021.120943.
- [2] M. Neri, E. Chiavazzo, and L. Mongibello, “Numerical simulation and validation of commercial hot water tanks integrated with phase change material-based storage units,” *J. Energy Storage*, vol. 32, no. September, p. 101938, 2020, doi: 10.1016/j.est.2020.101938.
- [3] A. Ribezzo, G. Falciani, L. Bergamasco, M. Fasano, and E. Chiavazzo, “An overview on the use of additives and preparation procedure in phase change materials for thermal energy storage with a focus on long term applications,” *J. Energy Storage*, vol. 53, no. April, p. 105140, 2022, doi: 10.1016/j.est.2022.105140.
- [4] C. Zauner, F. Hengstberger, M. Etzel, D. Lager, R. Hofmann, and H. Walter, “Experimental characterization and simulation of a fin-tube latent heat storage using high density polyethylene as PCM,” *Appl. Energy*, vol. 179, pp. 237–246, 2016, doi: 10.1016/j.apenergy.2016.06.138.
- [5] J. Sunku Prasad, P. Muthukumar, R. Anandalakshmi, and H. Niyas, “Comparative study of phase change phenomenon in high temperature cascade latent heat energy storage system using conduction and conduction-convection models,” *Sol. Energy*, vol. 176, no. November 2017, pp. 627–637, 2018, doi: 10.1016/j.solener.2018.10.048.
- [6] J. Gasia, J. M. Maldonado, F. Galati, M. De Simone, and L. F. Cabeza, “Experimental evaluation of the use of fins and metal wool as heat transfer enhancement techniques in a latent heat thermal energy storage system,” *Energy Convers. Manag.*, vol. 184, no. February, pp. 530–538, 2019, doi: 10.1016/j.enconman.2019.01.085.
- [7] R. Sciacovelli, A., Verda, V., & Borchiellini, *Numerical Design of Thermal Systems*. CLUT, 2013.

EUROTHERM2023-X147

## Describing conduction dominated sensible thermal energy storage heat exchangers using thermal quadrupoles

Wim Beyne<sup>1,2</sup>, Michel De Paepe<sup>1,2</sup>

<sup>1</sup>Ghent University, Sint-Pietersnieuwstraat 41, Ghent, Belgium, e-mail: wim.beyne@ugent.be  
<sup>2</sup>Flanders Make MIRO, Ghent Belgium <sup>2</sup>

### Abstract

Sensible thermal energy storage systems (STES) are commonly used in industry. However the operation of a TES system is inherently transient, and therefore the common design methods for heat exchangers are not applicable. The present paper proposes a novel method for describing STES system operation by describing fundamental heat transfer behavior using thermal quadrupoles. The predictions of the method are compared to a simplified numerical model of the system and obtain good agreement.

**Keywords:** sensible thermal energy storage, simplified model, thermal quadrupole

### 1. Introduction

Sensible thermal energy storage (STES) systems are the most commonly applied TES systems. The storage material can be liquid such as in water tanks or molten salt storage for concentrated solar power [1]. In other cases, the storage material is a solid such as concrete [2] or packed beds of solid modules [3]. In these cases, the only heat transfer mode in the storage material is conduction and this will be the topic of the present paper.

Designing and sizing is a key issue for the implementation of STES systems. Traditional design methods such as the effectiveness number of transfer units method are not applicable to transient storage systems [4]. Therefore, design methods are limited to conjugate heat transfer CFD (e.g. [5]) or lumped body approaches (e.g. [6]). Furthermore, there is no general method to reduce the behavior of an STES system to its fundamental heat transfer behavior at small scale.

For latent TES (LTES) systems, an integration method was recently developed which allows to extrapolate the fundamental heat transfer at small scale to full LTES heat exchanger performance [7]. The method uses the solution to the Stefan problem as small scale model and integrates the predicted stored energy over the surface area of the heat exchanger.

The present paper applies a similar integration as was used for LTES systems by using thermal quadrupoles as models for the fundamental heat transfer behavior in STES systems. Thermal quadrupoles allow to describe one-dimensional conductive heat transfer in basic geometries based on a transfer function in the Laplace domain [8].

### 2. Integrating thermal quadrupoles

A concrete slab STES heat exchanger is taken to understand how STES system can be reduced to fundamental small scale heat transfer behavior. Such a heat exchanger is shown schematically in Figure 1 with water as heat transfer fluid (HTF) flowing through a rectangular channel next to a slab of concrete which is the storage material. If the heat exchanger is divided in infinitesimal cross sections, the conduction in each of the slices is a one-dimensional conduction problem with an inner and outer surface area subject to an inner and outer temperature ( $T_{in}$  and  $T_{out}$ ) and heat flux ( $\dot{q}_{in}$  and  $\dot{q}_{out}$ ).

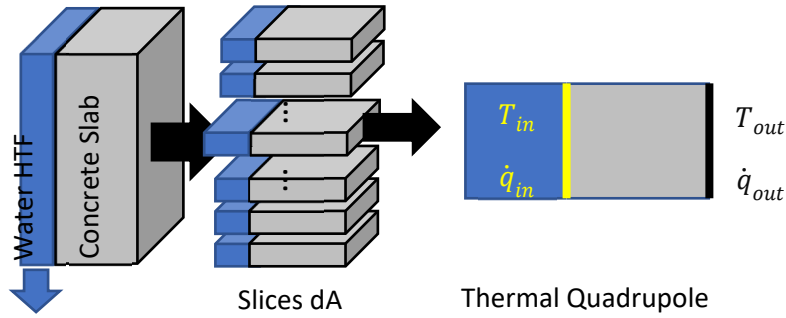


Figure 46. Schematic representation of the concrete slab STES heat exchanger, the division in slices with an infinitesimal Surface area and the thermal quadrupole describing heat transfer in each of the slices.

In a heat exchanger slice, the conservation of energy can be applied to the HTF. If the thermal mass of the HTF in the heat exchanger is neglected and the HTF is assumed to be at bulk temperature, the conservation of energy for a constant specific heat HTF corresponds to Equation 1. A model for the fundamental small scale heat transfer behavior would thus relate the temperature of the HTF  $T_{in}$  to the heat flux to the storage material  $\dot{q}_{in}$ . This would allow Equation 1 to be solved as an ordinary differential equation.

$$\dot{m}c_p \frac{dT_{HTF}}{dA} = -\dot{q}_{in} \quad (1)$$

Thermal quadrupoles are a representation of heat conduction through a solid body. In a thermal quadrupole, one part of the surface area has a surface average temperature and heat flux, while another part of the surface area has a different surface temperature and heat flux. This corresponds to the heat exchanger slice shown on Figure 1. The conductive heat transfer through the solid between these two surfaces results in a time-varying linear system. Therefore, the relation between the temperatures and heat fluxes on the two surfaces can be described by Equation 2 where  $\theta$  is the Laplace transform of temperature difference with the initial temperature and  $\varphi$  is the Laplace transform of the heat flux [8]. The coefficients  $A$ ,  $B$ ,  $C$  and  $D$  are functions of the Laplace transform variable and specific for the solid body geometry.

$$\begin{bmatrix} \theta_{in} \\ \varphi_{in} \end{bmatrix} = \begin{bmatrix} A & B \\ C & D \end{bmatrix} \begin{bmatrix} \theta_{out} \\ \varphi_{out} \end{bmatrix} \quad (2)$$

If the outside surface of the concrete slab is assumed adiabatic, then the outer surface heat flux is zero. The system of equations defined by Equation 2 can then be reformulated as a relation between temperature and heat flux on the water-concrete interface (Equation 3).

$$\varphi_{in} = \frac{C}{A} \theta_{in} \quad (3)$$

The ratio of coefficients  $C$  and  $A$  defines a function  $\beta$  which describes the heat transfer behavior. For the planar geometry shown in Figure 1, the  $\beta$  function is given by Equation 4 [8] with  $k$ ,  $\rho$ ,  $c$  and  $w$  respectively the thermal conductivity, density, specific heat capacity and width of the concrete pack. The convective heat transfer coefficient of the water is given by  $h$  and the Laplace transform variable of time is  $p$ .

$$\beta(p) = \frac{C}{A} = \frac{\frac{k}{h} \sqrt{\frac{p\rho c}{k}} \sinh\left(\sqrt{\frac{p\rho c}{k}} w\right)}{\frac{k}{h} \cosh\left(\sqrt{\frac{p\rho c}{k}} w\right) + \frac{k}{h} \sqrt{\frac{p\rho c}{k}} \sinh\left(\sqrt{\frac{p\rho c}{k}} w\right)} \quad (4)$$

Thermal quadrupoles have provided a relation between the temperature of the HTF and the heat flux to the storage material through the transfer function  $\beta(p)$ . However, the relation is in the Laplace domain.

Therefore, the Laplace transform is applied to Equation 1 and the resulting ordinary differential equation is solved as Equation 5 with  $\theta_{A=0}$  the Laplace transform of the inlet temperature of the heat exchanger.

$$\theta_{HTF} = \theta_{A=0} \exp\left(-\frac{\beta}{\dot{m}c_p} A_{tot}\right) \quad (5)$$

The inverse Laplace transform of  $\theta_{HTF}$  gives the outlet temperature of the HTF as a function of time. However, in general there is no analytical expression for the inversion of Equation 5. Therefore, a more robust approach is proposed by using a numerical inversion algorithm. In the present paper, the *Talbot* method implemented in the *mpmath* package in Python is used.

### 3. Comparison to a numerical solution

#### 3.1. Numerical model and case study

For the purpose of this paper, a numerical model is developed to predict the conductive heat transfer in the concrete slab. The numerical model neglects the thermal mass of the HTF and divides the concrete slab in  $n_x$  isolated slices as is done on Figure 1. Each of the slices is discretized in  $n_y$  equal parts with a temperature matrix  $T_j$  ( $j \in [0, n_x]$ ) describing the state of the slice. The temporal evolution of the temperature of each slice is estimated by Equation 6 and the HTF temperature of each slice is calculated based on heat transfer in the previous slice by Equation 7. Equation 8 defines the parameters of the model with  $A$  the heat transfer surface area (10 m<sup>2</sup>),  $w$  (0.1 m),  $\rho$  (800 kg/m<sup>3</sup>),  $c$  (2 kJ/kgK) and  $k$  (0.5 W/mK) the width, density, specific heat capacity and thermal conductivity of the concrete.  $h$  is the convective heat transfer coefficient (2500 W/m<sup>2</sup>K) and the product of HTF mass flow rate and specific heat capacity  $\dot{m}c_p$  is taken as 210 W/K. The simulated cycle is a concrete slab at an initial temperature of 10 °C which is subjected to a flow of HTF at an inlet temperature of 30 °C.

$$\frac{dT_j}{dt} = \frac{\Delta UA_C}{\Delta MC} \mathbf{M} T_j + \mathbf{b}_j \quad \forall j \in [0, n_x] \quad \text{with} \quad \begin{cases} \mathbf{M}_{1,1} = \frac{-\Delta \varepsilon \dot{m} c_p}{\Delta UA_C} - 1; \mathbf{M}_{1,2} = 1; \mathbf{b}_{j,1} = \frac{-\Delta \varepsilon \dot{m} c_p}{\Delta MC} T_{HTF}^j(t) \\ \mathbf{M}_{i,i} = 2; \mathbf{M}_{i,i-1} = -1; \mathbf{M}_{i,i+1} = -1; \forall i \neq 1 \text{ or } n_y \\ \mathbf{M}_{n_y, n_y} = 1; \mathbf{M}_{n_y, n_y-1} = -1 \end{cases} \quad (6)$$

$$\begin{cases} T_{HTF}^1 = \begin{cases} 0, & t < 0 \\ T_0, & t \geq 0 \end{cases} \\ T_{HTF}^j = T_{HTF}^{j-1} + \frac{\Delta MC}{\dot{m}c_p} \sum_{k=1}^{n_y} \frac{dT_k}{dt}; \quad \forall j \neq 1 \text{ and } \leq n_x \end{cases} \quad (7)$$

$$\Delta MC = \frac{w A \rho c}{n_y n_x}; \Delta UA = \left(\frac{w}{n_y} \frac{1}{2k} + \frac{1}{h}\right)^{-1} \frac{1}{\Delta MC} \frac{A}{n_x}; \Delta UA_C = \frac{n_y k A}{n_x w}; \Delta \varepsilon = (1 - \exp\left(\frac{-\Delta UA \Delta MC}{\dot{m}c_p}\right)) \quad (8)$$

#### 3.2. Model validation

Figure 47 compares the predictions of the numerical model with the predictions of the integrated thermal quadrupoles. The results show both the average concrete temperature (black) as the leaving water temperature (blue) and there is a clear agreement between both models.

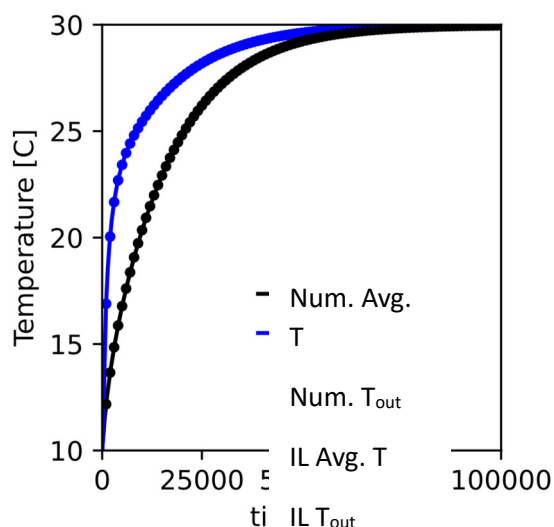


Figure 47: Comparison of average concrete temperature and HTF outlet temperature between numerical (num.) and inverted Laplace (IL) results for the test heat exchanger.

#### 4. Conclusions

The present paper describes a novel method to describe sensible thermal energy storage heat exchangers. The new method uses thermal quadrupoles to describe the heat conduction in the cross section and integrates it over the heat transfer surface. Through a numerical inverse Laplace transform, a prediction for average temperature and outlet temperature is obtained which corresponds well to numerical results.

#### References

- [1] C. Prieto and L. F. Cabeza, "Thermal energy storage (TES) with phase change materials (PCM) in solar power plants (CSP). Concept and plant performance," *Appl. Energy*, vol. 254, p. 113646, 2019/11/15/ 2019, doi: <https://doi.org/10.1016/j.apenergy.2019.113646>.
- [2] C. Liu and H. Yang, "Multi-objective optimization of a concrete thermal energy storage system based on response surface methodology," *Applied Thermal Engineering*, vol. 202, p. 117847, 2022/02/05/ 2022, doi: <https://doi.org/10.1016/j.applthermaleng.2021.117847>.
- [3] A. Gautam and R. P. Saini, "A review on sensible heat based packed bed solar thermal energy storage system for low temperature applications," *Sol. Energy*, vol. 207, pp. 937-956, 2020/09/01/ 2020, doi: <https://doi.org/10.1016/j.solener.2020.07.027>.
- [4] W. Beyne, I. T'Jollyn, S. Lecompte, L. F. Cabeza, and M. De Paepe, "Standardised methods for the determination of key performance indicators for thermal energy storage heat exchangers," *Renewable and Sustainable Energy Reviews*, vol. 176, p. 113139, 2023/04/01/ 2023, doi: <https://doi.org/10.1016/j.rser.2022.113139>.
- [5] L. Prasad and P. Muthukumar, "Design and optimization of lab-scale sensible heat storage prototype for solar thermal power plant application," *Sol. Energy*, vol. 97, pp. 217-229, 2013/11/01/ 2013, doi: <https://doi.org/10.1016/j.solener.2013.08.022>.
- [6] L. Doretto, F. Martelletto, and S. Mancin, "A simplified analytical approach for concrete sensible thermal energy storages simulation," *Journal of Energy Storage*, vol. 22, pp. 68-79, 2019/04/01/ 2019, doi: <https://doi.org/10.1016/j.est.2019.01.029>.
- [7] W. Beyne, R. Tassenoy, and M. De Paepe, "An approximate analytical solution for the movement of the phase change front in latent thermal energy storage heat exchangers," *Journal of Energy Storage*, vol. 57, p. 106132, 2023/01/01/ 2023, doi: <https://doi.org/10.1016/j.est.2022.106132>.
- [8] D. Maillet, S. Andre, J. C. Batsale, A. Degiovanni, and C. Moyne, *Thermal quadrupoles: solving the heat equation through integral transforms*. John Wiley & Sons Incorporated, 2000.

EUROTHERM2023-O148

## Topology optimization for multi-physics performance enhancement in thermochemical energy storage reactors

Gabriele Humbert<sup>1</sup>, Adriano Sciacovelli<sup>2\*</sup>,<sup>1,2</sup> School of Chemical Engineering, Birmingham Centre for Energy Storage, University of Birmingham, \*UK, e-mail: [a.sciacovelli@bham.ac.uk](mailto:a.sciacovelli@bham.ac.uk)

### Abstract

This paper proposes using topology optimization (TO) as a generative design method to improve the performance of thermochemical energy storage (TCS) reactors. The TO framework simultaneously optimizes fins geometry and enhancer material (highly conductive materials) while meeting requirements of discharge time, bed size, and bed porosity. The proposed method is tested on a reference TCS reactor using Strontium Bromide ( $\text{SrBr}_2$ ) with potential for applications in both industrial and domestic contexts. The TO designs achieve up to 200% performance enhancement compared to traditional configurations. The optimal amount of enhancer material varies depending on the targeted performance, and reducing the amount of  $\text{SrBr}_2$  may be beneficial. Furthermore, the paper discusses the benefits and limitations of the TO approach and provides guidelines for future development.

**Keywords:** thermal energy storage, thermochemical energy storage, topology optimization, decarbonisation, CFD

### 1. Introduction

Thermochemical energy storage systems use reversible chemical reactions to store and deliver thermal energy. Among the different thermal energy storage options, TCS devices present the advantages of the highest theoretical energy density, nearly negligible heat losses during the storage period and possible heat up-gradation between charging and discharging steps [1]. The existing reactors mainly adopt gas-solid reactions based on several solid thermochemical materials, such as salt hydrates, metal hydrides and metal oxides [2].

Research suggests that the performance attained by the existing TCS devices is far from their theoretical potential. Many studies have investigated host matrices to support the thermochemical material (TCM) and enhance heat and mass transport in the reactive bed [3]. In particular, host matrices are recommended to prevent the formation of compact blocks hindering reactants' transport and to improve cyclability. Alternative routes for performance enhancement are pursued also at device scale, typically through the integration of highly conductive inserts such as fins and metallic meshes to maximize heat transfer. A classic example is reported by Stengler et al. [4] who performed a numerical sensitivity analysis for a TCS device utilizing extended surfaces made of aluminium. The results showed the extended surface geometry to effectively mitigate the low thermal conductivity of the reactive bed and that improving device's overall performance. However, the design and optimization of TCS reactors still largely relies on traditional methods based (parametric optimization, lump-parameters models, effectiveness-NTU methods, etc). This present work takes an alternative and innovative routes by proposing Topology optimization (TO) as TCS design tool. Key novelty lies in the capability of TO in discovering new TCS reactor configuration starting with the minimal set of constraints and targeted performance. In this regard the proposed TO approach is a 'shape finding' approach that does not require any initial guess of reactor configuration. This is unique and the main novelty of the work here presented.

### 2. System Description and Topology Optimization Method

A reference closed-type TCS system increasingly adopted in the literature was considered in this work. The TCS system is depicted in Figure below. it is constituted of multiple TCS modules (representative



units) positioned inside a shell served with vapour through an evaporator/condenser component. The design is typical of closed systems and such modular configuration has been considered in a growing number of investigations; same dimension and operating conditions of [4][5] were adopted in the present study. Strontium Bromide was considered as the thermochemical energy storage material (TCM); the hydration-dehydration reaction of  $\text{StBr}_2$  has been identified as a attractive candidate reversible reaction for heat storage in domestic and industrial applications (depending on the hydration/dehydration step considered).

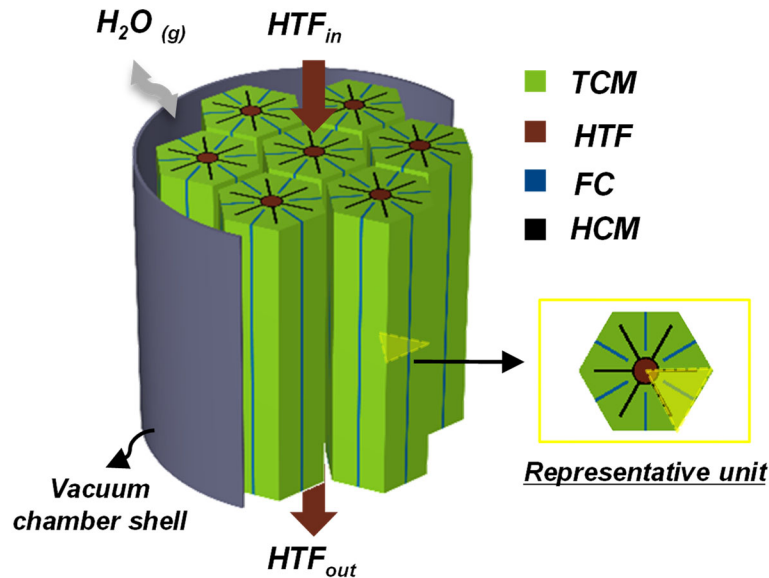


Fig 1. TCS reactor investigated in the present work.

### **Targeted performance objectives**

We optimized the HCM structures (fins) illustrated in Figure 1 with the aim of maximize two key performance indicators: i) maximization of reaction advancement for a desired discharge time  $t^*$  and for a maximum given amount of HCM materials  $V^*$ ; or ii) maximization of the discharged energy in a prescribed discharge time  $t^*$ . Both two objective functions thus targets maximization of discharge performance of the TCS reactor.

### **Governing equations**

The thermo-chemical behaviour of the TCS reactor was modelled through a multi-physics model comprising transport equations (partial differential equation) describing mass transfer, energy transfer and fluid-flow (vapour transfer) across the representative unit shown on the right-hand side of Figure 1 (2D cross section). Full details of the governing equations are available from in our prior work [5]. Governing equations were solved in un-steady state to simulate the discharge process and evaluate the targeted performance objectives. Both the governing equation and the evaluation of the performance were fully integrated in the TO algorithm, described hereafter, for optimization of the fins geometry.

### **Topology optimization algorithm**

The TO framework employs Solid Isotropic Material with Penalisation (SIMP) method in combination with Globally Convergent Method of Moving Asymptotes (GCMMA) optimization routines [6]. In such context, the geometry – i.e. the topology – to be optimized is described by the so-called indicator function  $s$  which takes a value between 0 and 1 *at each possible the position*  $x$  within the computational domain  $\Omega$  over which topological optimization is performed. Within the context of the present work,  $s = 1$  identifies the portion of the domain  $\Omega$  occupied by the HCM. Conversely,  $s = 0$  identifies the portion of the domain  $\Omega$  occupied by the TCM. The design, described by  $s(x)$ , is progressively updated by computing the sensitivity of the targeted performance objectives with respect of  $s(x)$ . For this purpose, the adjoint method is particularly convenient as it requires to solve one additional linear problem per each performance objective and constraints. Full details about the TO procedure and algorithm are presented in our prior work [7]. For illustrative purposes Figure 2 illustrates an example of how the TCS reactor design – i.e.  $s(x)$  – evolved throughout the TO optimization. It is worthy to

emphasize that no assumptions are made regarding the initial design (left plot). The optimal design emerges directly from the TO.

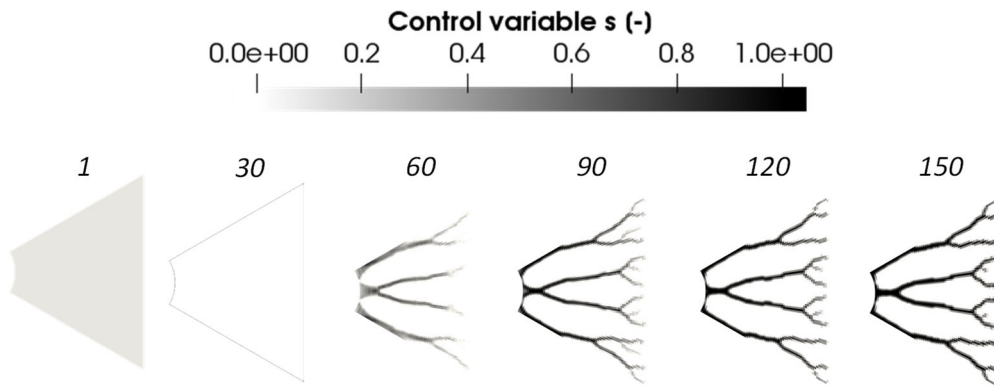


Fig 2. Example of design evolution during the iterations of the topological optimization.

### 3. Results and discussion

Figure 3 shows the optimal designs achieved through the proposed TO framework; the two district designs emerge depending on whether the maximum amount of HCM material, that is the amount of volume dedicated to the fins  $V^*$ , is either constrained or not. In the Figure 'EOM' identifies designs without constraints on  $V^*$ . Conversely, 'MUM' identifies the design for which  $V^*$  is constrained during the optimization. Interestingly, and counterintuitively, a larger amount of HCM and thus less TCM material, could lead to an *increase* in the *effective* energy storage density. That is can be appreciated by noticing that the quantity of reacted material ( $\alpha = 1$ ), is noticeably larger for EOM design.

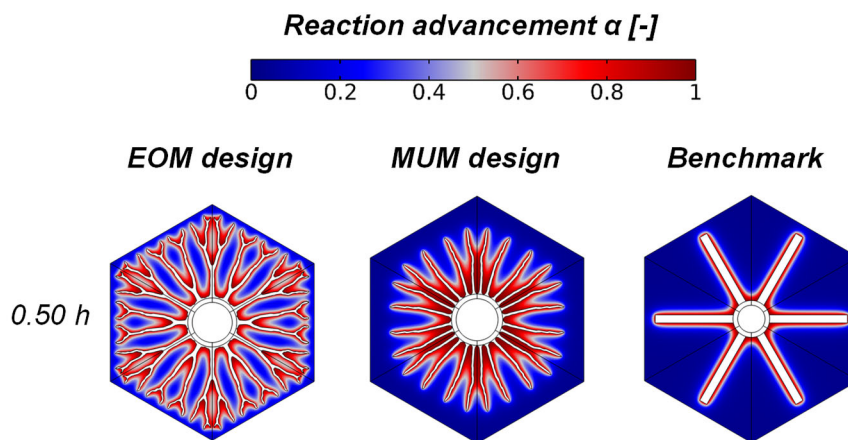


Fig 3. Reaction advancement contours for Topologically optimized designs and for benchmark design.

Further comparison between performance of TO designs and conventional ones currently employed ('benchmark' in Fig 3) is provided by Figure 4. Here, the history of the specific discharged energy,  $E$ , defined as the cumulative energy released at a given time  $t$  and per unit of volume of the reactor is presented. The trends demonstrate how the topologically optimized designs clearly outperform conventional designs. In the 'EOM' instance, the enhancement in discharged energy is  $\sim 250\%$ . Such design is therefore particularly suitable for applications where rapid discharge of the storage system are necessary. For example, in potential industrial applications requirement management of rapid fluctuations of process heat supply/demand.

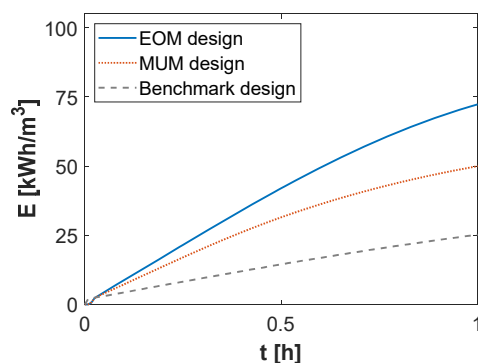


Fig 4. discharged energy history for topologically optimized designs and benchmark design.

## 4. Conclusions

In this work, the use of topology optimization (TO) for the effective design of thermochemical energy storage reactor was demonstrated. The optimal geometries were found to drastically outperform the conventional designs use so far. The performance increase unlocked by TO designs are particularly attractive: discharge performance are predicted to more than double. This is not a marginal gain as in most of traditional optimization analysis; but rather drastic increase worth to pursue further in the mission of making performance of thermo-chemical energy storage systems. Nonetheless, alongside the significant results presented in this paper a number of challenges to be addressed open up for what concerns TO in the specific field of thermo-chemical energy storage: firstly, application scenarios should be fully considered within the TO framework; indeed targeted performance, and thus ultimately design optimality, are likely to be highly depended on the specific application selected. Secondly, robustness of optimal TO design with respect of operating conditions requires further work; it is indeed well know that storage systems are expected to experience a rage of different conditions during their operational life. This should be factored in the development of optimal designs. Thirdly, optimization in three-dimensions might be pursued. Nonetheless, such decision should carefully weight the increase in computational complexity against the performance enhancement. Finally, manufacturability of TO design should be kept in consideration throughout the whole technology development cycle to ensure optimal design can be fabricated at scale and cost-effectively.

## Acknowledgments

Dr Sciacovelli would like to acknowledge the financial support from the UK Engineering and Physical Science Research Council (EPSRC) for the project ‘MIX-MOXes’ (EP/X000249/1)

## References

- [1] Cabeza LF, Solé A, Barreneche C. Review on sorption materials and technologies for heat pumps and thermal energy storage. *Renew Energy* 2017;110:3–39. <https://doi.org/10.1016/j.renene.2016.09.059>.
- [2] Aydin D, Casey SP, Chen X, Riffat S. Novel “open-sorption pipe” reactor for solar thermal energy storage. *Energy Convers Manag* 2016;121:321–34. <https://doi.org/10.1016/j.enconman.2016.05.045>.
- [3] Papakokkinos G, Castro J, López J, Oliva A. A generalized computational model for the simulation of adsorption packed bed reactors – Parametric study of five reactor geometries for cooling applications. *Appl Energy* 2019;235:409–27. <https://doi.org/10.1016/j.apenergy.2018.10.081>.
- [4] Stengler J, Linder M. Thermal energy storage combined with a temperature boost: An underestimated feature of thermochemical systems. *Appl Energy* 2020;262:114530. <https://doi.org/10.1016/j.apenergy.2020.114530>.
- [5] Humbert G, Ding Y, Sciacovelli A. Combined enhancement of thermal and chemical performance of closed thermochemical energy storage system by optimized tree-like heat exchanger structures. *Appl Energy* 2022;311:118633. <https://doi.org/10.1016/J.APENERGY.2022.118633>.
- [6] Pizzolato A, Sharma A, Ge R, Maute K, Verda V, Sciacovelli A. Maximization of performance in multi-tube latent heat storage – Optimization of fins topology, effect of materials selection and flow arrangements. *Energy* 2020;203:114797. <https://doi.org/10.1016/j.energy.2019.02.155>.
- [7] Pizzolato A, Sharma A, Maute K, Sciacovelli A, Verda V. Topology optimization for heat transfer enhancement in Latent Heat Thermal Energy Storage. *Int J Heat Mass Transf* 2017;113:875–88. <https://doi.org/10.1016/j.ijheatmasstransfer.2017.05.098>.

EUROTHERM2023-U149

## Innovative 3D adsorbent structures based on sa-po-34/S-PEEK composite materials for energy storage

Gabriele Marabello<sup>1</sup>, Emanuela Mastronardo<sup>1</sup> Andrea Frazzica<sup>2</sup> Luigi Calabrese<sup>1,2</sup>,

<sup>1</sup> Department of Engineering, University of Messina, Contrada di Dio Sant'Agata, 98166 Messina, Italy;  
[gmarabello@unime.it](mailto:gmarabello@unime.it); [emastronardo@unime.it](mailto:emastronardo@unime.it); [icalabrese@unime.it](mailto:icalabrese@unime.it)

<sup>2</sup> CNR - ITAE “Nicola Giordano”, Via Salita S. Lucia sopra Contesse 5, 98126 Messina, Italy,  
[andrea.frazzica@itaecnr.it](mailto:andrea.frazzica@itaecnr.it)

### Abstract

In this paper, the synthesis and characterization of an innovative three-dimensional lattice structure, based on a composite zeolite adsorbent material SAPO34 and sulphonated polyether ether ketone (S-PEEK), for thermal storage is evaluated. The structure was created with the aid of additive manufacturing technology which allowed to obtain a structure with a complex three-dimensional geometry, without a metal reinforcement support. The optimization of the technology has been developed in terms of sample geometry and composite material formulation. The three-dimensional structures thus obtained were morphologically and mechanically investigated in order to evaluate their structural integrity. To evaluate the adsorption/desorption capacity, the water vapor adsorption isobars at 11 mbar were measured at equilibrium in the temperature range 30-120°C, confirming that the matrix does not hinder the mass flow of water vapor and the zeolite filler participates in the adsorption/desorption process, indicating this material potentially suitable for thermochemical storage by sorption technology.

**Keywords:** zeolite, composite sorbent, sulfonated poly(ether ether ketone), additive manufacturing

### 1. Introduction

The growing need to propose more sustainable energy systems, based on a synergistic integration of different energy sources and the consequent development of technologies aimed at optimizing the recovery of waste heat has led to the investigation of innovative thermal energy storage technologies [1]. In this context, thermochemical heat storage represents a promising and viable technology, especially for long-term storage applications. However, its development on large-scale and realistic contexts has been partially limited by the need for more performing and suitable materials for fast and reliable storage design and tailoring.

Recent papers have shown that reactors consisting of coated heat exchangers (HEX) have multiple advantages in terms of heat transfer efficiency which make their applicability very promising [2]. However, limiting factors on the use of this technology are the low amount of adsorbent material present and a non-optimal mass transfer (due to the low porosity and the presence of the binder in the composite material) in a coated HEX. This reduces the storage performance of the reactor.

In previous works [3,4], a composite material was proposed consisting of a high content of zeolite (up to 90% by weight of SAPO-34) and a sulphonated poly(ether-ether-ketone) (S-PEEK) binder. The S-PEEK matrix has a high water vapor permeability, thereby minimizing mass diffusion limits within the adsorbent composite bulk. Furthermore, this composite material has shown promising results in terms of mechanical, thermal and ad/desorption stability.

Based on these promising results, the present paper aims to investigate the use of this material for the realization of three-dimensional lattice structures entirely made of adsorbent composite material (without metal support) with the aid of the additive manufacturing technique.

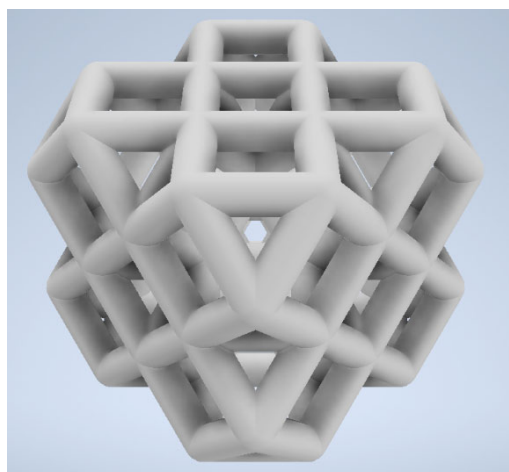
## 2. Materials and method

The sulfonation PEEK, used as matrix was prepared according to [5]. A SAPO 34 zeolite (AQSOA Z02) produced by Mitsubishi Plastics Inc. was used as an absorbent filler with main grain size of about 5-10  $\mu\text{m}$ . For the composite adsorbent, S-PEEK polymer was dissolved in N, N-Dimethylformamide (DMF) under magnetic stirring for 5 min. Then SAPO-34 powder was progressively added to the solution, under agitation at room temperature until a homogenous slurry is obtained. In parallel, a PVA negative shape of the attended 3D structure is obtained by additive manufacturing. The composite slurry was gently poured into the channels of the PVA mold until it is completely filled. Then the filled PVA mold has been dried at 60  $^{\circ}\text{C}$  for 12 h in a vacuum oven. Afterward, the negative PVA mold is dissolved in water by ultrasound until only the now solidified three-dimensional S-PEEK/zeolite composite structure is obtained.

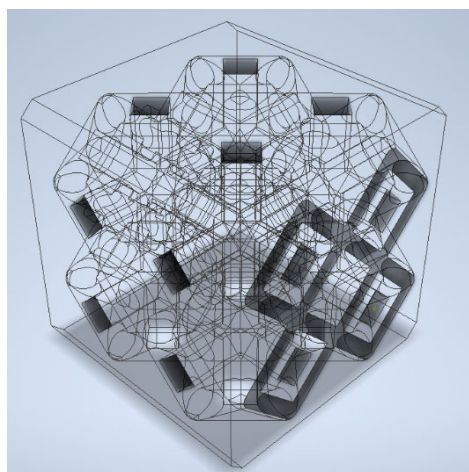
## 3. Results and discussion

Figure 48 shows the proposed steps for the manufacturing of the 3D printed lattice sorbent structure. In particular:

- *CAD Design*: Parametric design of the unitary lattice cell. Spatial replica 2x2x2 (Figure 48a).
- *Molding*: Design of the negative molding of the lattice structure (Figure 48b) and subsequent additive manufacturing by using PVA support.
- *Composite filling*: Preparation of the composite SAPO-34/S-PEEK slurry. The slurry is filled in the channel of the negative mold by using a micro-syringe. The slurry was added until the mold was fully filled (Figure 48c). The drying is performed in oven at 40 $^{\circ}\text{C}$  for 1 day.
- *Mold dissolution*. To remove the negative PVA mold a dissolution procedure in water was applied. In particular, the materials were placed un an ultrasonic bath at 70 $^{\circ}\text{C}$  for 5h until the complete dissolution of PVA support occurred. The residual material is the solid zeolite-S-PEEK sorbent material with the shape of the chosen lattice structure (Figure 48d).



a)



b)

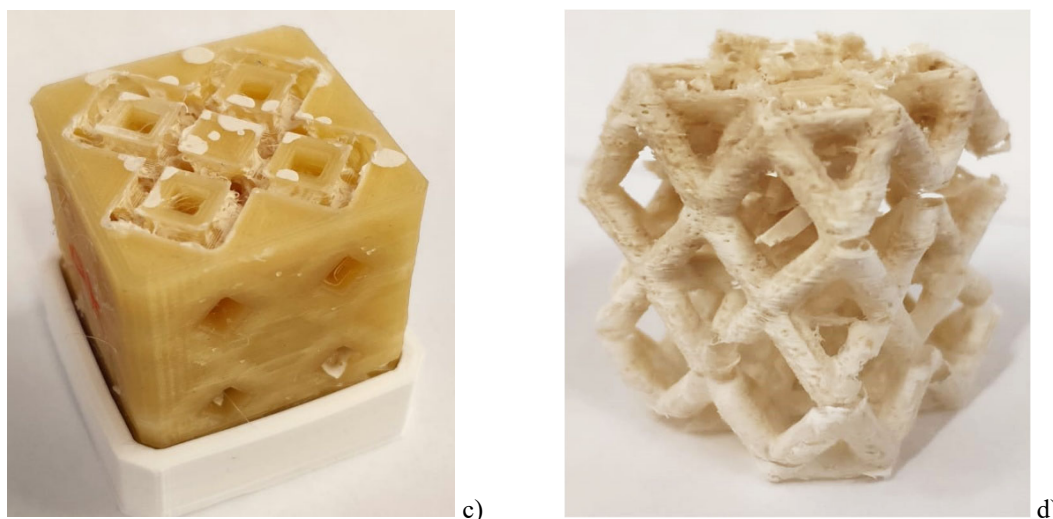


Figure 48. Manufacturing of the 3D printed lattice sorbent structure: a) parametric definition of the 3D cell; b) negative molding of the cell c) negative molding (PVA polymer) filled with composite SAPO-34/S-PEEK slurry; d) demolded lattice sorbent structure.

The 3D lattice structure thus obtained was morphologically and structurally assessed with the purpose to well define the synthesis characteristic, structural homogeneity and integrity. The adsorption/desorption capacity was performed by water vapor adsorption isobars at 11 mbar measured at equilibrium in the temperature range 30-120°C (by using a DVS equipment). The results reported in Figure 49, confirm that the matrix does not hinder the mass flow of water vapor and the zeolite filler participates in the adsorption/desorption process, indicating this material potentially suitable for thermochemical storage by sorption technology.

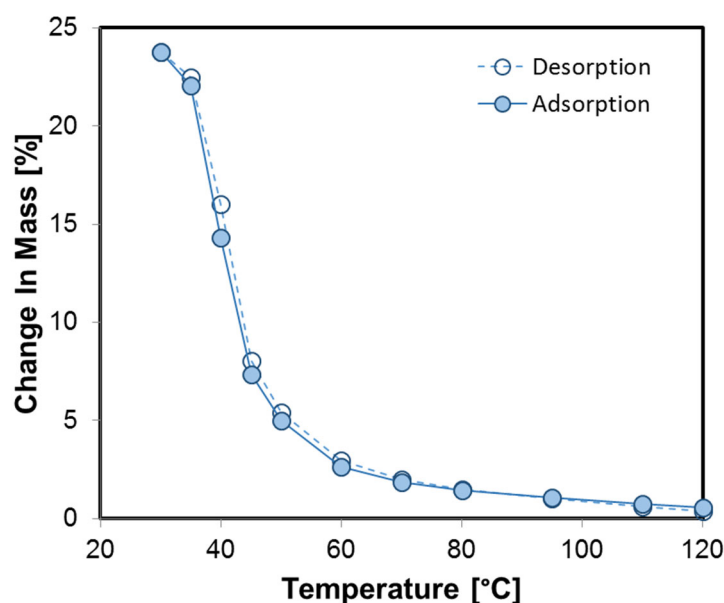


Figure 49. Water adsorption (filled marker) and desorption (empty marker) isobars at 11 mbar for 80% SAPO-34 zeolite filled in S-PEEK polymer material

#### 4. Conclusions

The present work investigated the synthesis and characterization of an innovative three-dimensional lattice structure, exclusively constituted by an adsorbent composite material (SAPO34 zeolite and S-PEEK as filler and matrix, respectively), for thermal storage. The results highlight that:

- The composite has an effective adsorption/desorption capacity, indicating that the polymeric matrix does not hinder the diffusion of water vapor towards the zeolite.
- The additive manufacturing, by using a negative PVA mold, is a suitable technology in order to procedure adsorbent tridimensional lattice structures.
- The 3D structure is structurally stable, regular, homogeneous and with a high surface area, indicating it as a promising solution for the construction of reactors for energy storage.

#### References

1. Sadeghi, G. Energy storage on demand: Thermal energy storage development, materials, design, and integration challenges. *Energy Storage Mater.* **2022**, *46*, 192–222, doi:<https://doi.org/10.1016/j.ensm.2022.01.017>.
2. Van Helden, W. Reactor Design for Thermochemical Energy Storage Systems. In *Advances in Energy Storage*; 2022; pp. 695–703 ISBN 9781119239390.
3. Palamara, D.; Palomba, V.; Calabrese, L.; Frazzica, A. Evaluation of ad/desorption dynamics of S-PEEK/Zeolite composite coatings by T-LTJ method. *Appl. Therm. Eng.* **2022**, *208*, doi:10.1016/j.applthermaleng.2022.118262.
4. Palamara, D.; Bruzzaniti, P.; Calabrese, L.; Proverbio, E. Effect of degree of sulfonation on the performance of adsorbent SAPO-34/S-PEEK composite coatings for adsorption heat pumps. *Prog. Org. Coatings* **2021**, *154*, 106193, doi:<https://doi.org/10.1016/j.porgcoat.2021.106193>.
5. Calabrese, L.; Palamara, D.; Bruzzaniti, P.; Proverbio, E. Assessment of high performance SAPO-34/S-PEEK composite coatings for adsorption heat pumps. *J. Appl. Polym. Sci.* **2021**, *138*, 50076, doi:<https://doi.org/10.1002/app.50076>.

EUROTHERM2023-R150

## **Rotating Wheel Recovery (RWR) system with PCM: proof of concept.**

J.A. Almendros-Ibáñez<sup>1,2,\*</sup>, M. Castro-García<sup>1,2</sup>, M. Díaz-Heras<sup>1,2</sup>, J.F. Belmonte<sup>1,2</sup>

<sup>1</sup>Universidad de Castilla-La Mancha, E.T.S. de Ingenieros Industriales de Albacete, Campus Universitario s/n, 02071, Albacete

<sup>2</sup>Universidad de Castilla-La Mancha, Renewable Energy Research Institute, Avda. de la Investigación 1, 02071, Albacete

\* Corresponding Author: jose.almendros@uclm.es, Phone: 926053229

### **Abstract**

In the recent years, one of the most recent proposals to reduce the energy consumption in buildings, is the use of Rotating Wheel Recovery (RWR) systems. These simple devices recover energy from the exhaust hot air stream, coming from the building, and is supplied to the cold stream before it is introduced in the building for ventilation purposes. This work explores the possibility of embedding a Phase Change Material (PCM) into the solid matrix of the RWR with a double objective: first, to increase the energy recovery capacity and second, to be able to maintain the supplied air into the building at the desired temperature for a longer period of time. In this way, a numerical model is developed and shows that with a mass fraction of PCM of 0.6, the RWR is able to maintain during 331 s a temperature higher than 18 °C when the same system without PCM only maintains the same temperature during 106 s.

**Keywords:** PCM, Rotating Wheel Recuperator, Building simulation, energy recovery, numerical modeling

### **1. Introduction**

During the last years, there is a notable interest in reducing the energy consumption of buildings due to the recent energy crisis, aggravated by the Ukraine war, and by the huge increase in the energy prices in Europe and Spain. In addition to this problem, after the Covid-19 pandemic, buildings designers pay special attention to the ventilation process of new buildings, with the aim of avoiding to maintain the air stagnant during long periods of time. In addition, national regulations requirements establish minimum ventilations air flows for different types of buildings.

Inherent to the ventilation process in climatic severe periods, either winter or summer, is the energy consumption to increase (in winter period) or reduce (in summer period) the temperature of the fresh ventilation air. The use of Rotating Wheel Recuperators (RWR) reduces the energy demand of the building, as it extracts energy from the exhaust air stream coming from the building during winter period which is stored typically in a solid matrix. Later, this energy is supplied to the fresh ventilation air to increase its temperature. The system can operate also during the summer period, reversing the energy flow direction.

The present proposal quantifies the expected improvement of embedding a PCM into the structure of the solid matrix of the RWR. With the possibility of storing energy in latent form, the energy recovery capacity increases, but the main advantage is that this energy is released at the desired temperature.

### **2. Numerical modeling**

In the numerical model of the RWR we have followed previous works published in the literature [1,2] for sensible energy recovery. In the heat transfer problem, it is assumed that the energy stored in the air is negligible compared with the energy stored in the solid matrix and the heat conduction in the direction perpendicular to the air flow is considered infinity [1], which permits to simplify the problem and assume a 1-D transient flow. The RWR operation is considered also discontinuous, i.e., the energy stored in the



solid matrix is readily available to the cold stream instantaneously. This assumption is reasonable if the rotating speed of the RWR is low.

For a sensible RWR, the air and solid energy equations for the matrix in contact with the exhaust hot stream are:

$$\rho_h \varepsilon c_{p,h} \frac{\partial T_h}{\partial t} = h_h a_p (\theta_h - T_h) - \rho_h \varepsilon u_h c_{p,h} \frac{\partial T_h}{\partial x} \quad (1)$$

$$\rho_s (1 - \varepsilon) c_{p,s} \frac{\partial \theta_h}{\partial t} = -h_h a_p (\theta_h - T_h) \quad (2)$$

where the subscript  $h$  indicates that it is the part of the solid matrix in contact with the *hot* stream. There are equivalent equations for the cold side. In these equations,  $T$  and  $\theta$  are the air and solid temperatures, respectively,  $h$  is the heat transfer coefficient between the air and the solid matrix,  $\varepsilon$  is the air voidage in the solid matrix, and  $a_p$  is the heat transfer area per unit of volume.

The solid energy equation (Equation (2)) should be modified to take into account the latent energy stored if a PCM is embedded in the solid matrix. In this case, the new equation is:

$$\rho_{s+pcm,h} (1 - \varepsilon) \frac{\partial i_{s+pcm,h}}{\partial t} = -h_h a_p (\theta_h - T_h) \quad (3)$$

where the subscript  $s+pcm$  refers to the solid matrix with embedded PCM, being  $i_{s+pcm}$  the average specific enthalpy defined as follows:

$$i_{s+pcm,h} = (1 - \alpha) i_s + \alpha i_{pcm} \quad (4)$$

with  $\alpha = m_{pcm} / (m_s + m_{pcm})$  is the mass fraction of the PCM in the solid matrix. Figure 1 shows the enthalpy-temperature curves (Equation (4)) for a solid matrix of aluminum with different values of  $\alpha = 0.2 - 0.4 - 0.6$ . The PCM selected for the simulation is RT18HC from Rubitherm, which has a transition temperature of 18 °C, which is an appropriated temperature for winter operation, and has an enthalpy change of approximately 200 kJ/kg according to the data provided by the manufacturer [3]. An ideal transition (isothermal) from liquid to solid at 18 °C is considered in the analysis.

The equations system formed by Equations (1) and (3) can further simplified neglecting the energy stored in the air (left hand side term of Equation (1)). Introducing non-dimensional variables, the equation system can be expressed as follows:

$$\frac{-1}{\frac{NTU_h}{c_h}} \frac{\partial i_{s+pcm,h}}{\partial \hat{t}} = \widehat{\theta}_h - \widehat{T}_h = \frac{1}{NTU_h} \frac{\partial \widehat{T}_h}{\partial \hat{x}} \quad (5)$$

where

$$NTU_h = \frac{h_p a_p}{\rho_h \varepsilon c_{p,h} \frac{u_h}{L}} \quad (6)$$

$$C_h = \frac{\rho_{s+pcm,h} (1 - \varepsilon) c_{p,s+pcm} \frac{1}{p_h}}{\rho_h \varepsilon c_{p,h} \frac{u_h}{L}} \quad (7)$$

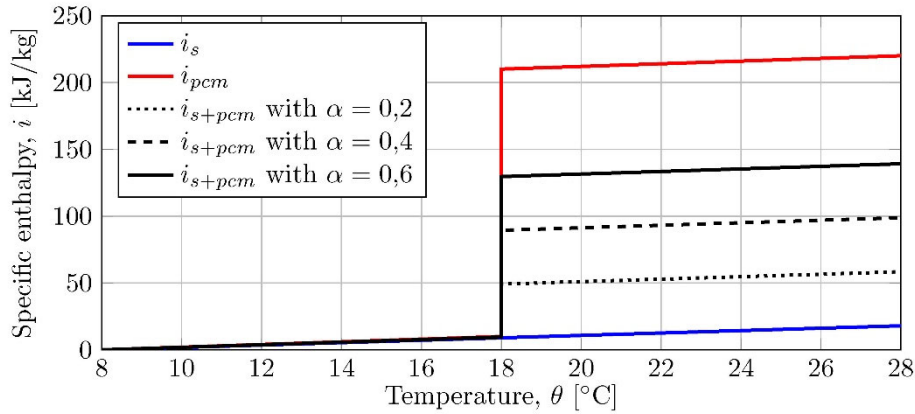


Figure 1. Enthalpy vs temperature curves for an aluminum solid matrix with different mass fractions of embedded PCM.

The equation system (Equations (5)) was numerically solved with finite difference scheme, using a RK4 discretization for the temporal derivative and an up-wind scheme for the spatial derivative. The time and spatial steps were properly chosen to assure the convergence and accuracy of the model.

### 3. Numerical results and discussions

The numerical results were obtained during the operation of the RWR under the design winter conditions in Madrid (Spain). The ventilation air flow rate used was imposed according to Spanish regulations for a house with 4 bedrooms. Table 1 indicates the operation conditions (air flow rate, temperatures) and the main dimensions of the proposed system.

Table 1. Air flow rate and hot and cold temperatures used in the simulations, obtained for winter period in Madrid (Spain) for a 4-bedroom house; main dimensions of the RWR (diameter and length) and air voidage.

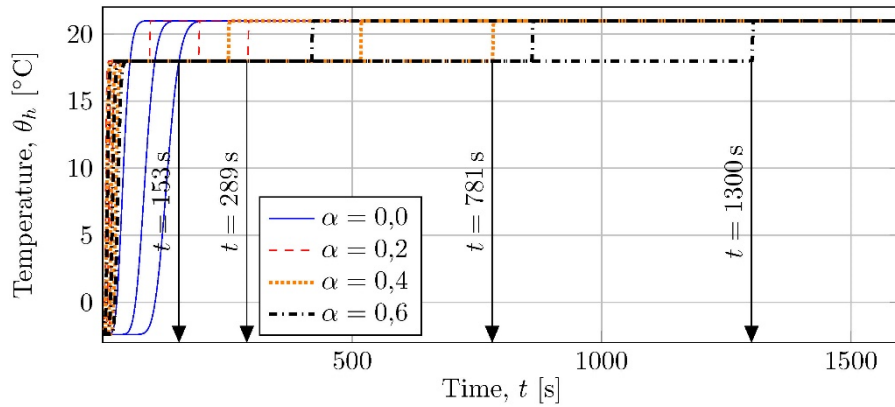
$\dot{V}$ [ $m^3/hr$ ]	$T_c$ [ $^{\circ}C$ ]	$T_h$ [ $^{\circ}C$ ]	$D$ [cm]	$L$ [cm]	$\varepsilon$ [-]
120	-2.4	21	15	20	0.4

Figure 2 shows the results obtained for the case studied for the RWR in contact with the exhaust air coming from the building (considered equal to building setpoint temperature). It is showed the temperature of the solid matrix at different axial positions of the RWR for different values of  $\alpha$  and the air temperature at the outlet. It is clearly observed how the front temperature advance axially. For  $\alpha = 0.6$  the solid matrix is fully charged at maximum temperature ( $T_h = 21^{\circ}C$ ) after 1300 s, approximately. During the recovery process of the energy by the cold stream, the cold air can be supplied to the building interior with a temperature higher than  $18^{\circ}C$  for 331 seconds.

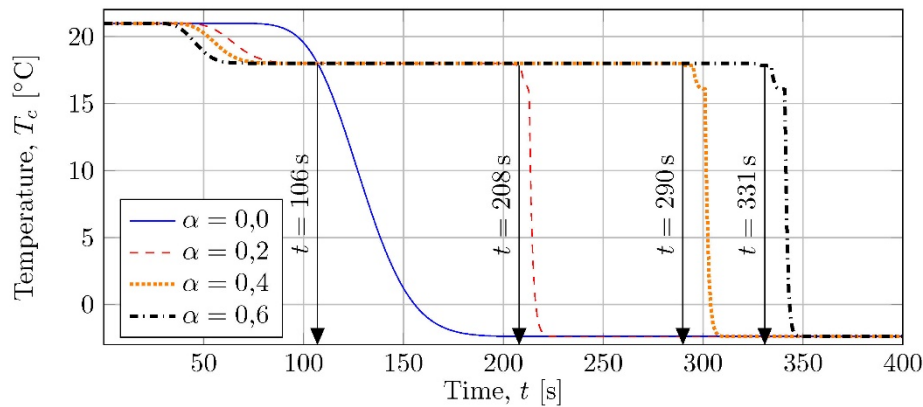
### 4. Conclusions and future works

The results presented in this work clearly indicates the potential of using PCM embedded in a RWR to improve the energy efficiency in buildings and to reduce their energy consumption. Under the conditions tested in this work for the design winter conditions of Madrid, the system permits to operate during 331 s with an air temperature higher than  $18^{\circ}C$  with a mass fraction of the PCM of  $\alpha = 0.6$ , while the same system without PCM only permits its operation for 106 s.

Future works will explore the possibility to fabricate a RWR based on additive manufacturing technologies. Fused Filament Fabrication (FFF) offers the possibility of generating complex geometries at relatively low cost [4] and permits to introduce pore formers in which the PCM will be embedded. The numerical results of the model will permit to optimize the geometry and PCM content of the RWR for the desired operating conditions.



(a) Temperature of the solid matrix at  $x/L = 1/3, 2/3, \text{ and } 1$



(b) Temperature of the cold stream at the outlet of the RWR

Figure 2. Temperatures curves of the RWR for different values of  $\alpha$ .

## Acknowledgements

This work was partially funded by the project PID2021-127322OB-I00 (funded by Ministerio de Ciencia e Innovación MICIN/AEI/10.13039/501100011033 and by NextGenerationEU/PRTR); Project TED2021-131046B (funded by Ministerio de Ciencia e Innovación MCIN/AEI/10.13039/501100011033 and by NextGenerationEU/PRTR). Project SBPLY/21/180501/000017 (funded by the Regional Government of Castilla-La Mancha); and Project 2020-GRIN-28725 (funded by Universidad de Castilla-La Mancha).

## References

- [1] Thulukkanam, K. (2000). Heat exchanger design handbook. CRC press.
- [2] Shah, R. K., & Sekulic, D. P. (2003). Fundamentals of heat exchanger design. John Wiley & Sons.
- [3] <https://www.rubitherm.eu/en/productcategory/organische-pcm-rt> (Last accessed, February 2023)
- [4] Marín Rueda et al., “Method for obtaining ceramic barbotine for the production of filaments for 3D-FDM printing, barbotine obtained using said method, and ceramic filaments”, WO2017191340A1

EUROTHERM2023-E152

## A novel machine-learning based framework for the optimal control of thermal storage integrated low-temperature heating network

Yangzhe Chen<sup>1</sup>, Thomas Ohlson Timoudas<sup>2</sup>, Boris Petkovic<sup>1</sup>, Qian Wang<sup>1,3</sup>

<sup>1</sup>Department of Civil and Architectural Engineering, KTH Royal Institute of Technology, Brinellvagen 23, Stockholm 100 44, Sweden

<sup>2</sup>RISE Research Institutes of Sweden, Division Digital Systems, Computer Science, Isafjordsgatan 22, 164 40, Kista, Sweden

<sup>3</sup>Uponor AB, Hackstavagen 1, Vasteras 721 32, Sweden

### Abstract

The mismatch between the building thermal demand and energy supply is a major impediment to achieve the demand flexibility, upon which, the effect of thermal storage equipment integrated with thermal management system can be significant. For such networks, it needs to be managed in a smart approach. Therefore, the smart control of integrated building energy systems associated with district heating and cooling networks has lately gained burgeoning attention due to its potential in synchronisation between grid, district heating networks and storages. The basic control architecture is managing the heat pumps' behaviour and the mismatches based on forecasting thermal demand of buildings, such as load shifting, and pre-storage. This paper proposes a novel control method which makes it possible to optimally control the thermal storage network integration.

**Keywords:** thermal storage, heat pump, demand flexibility, building control, district heating and cooling, operation strategy

### 1. Introduction

With the growing demand for reducing power stress of the grid, enabling thermal storage as a flexibility asset plays an increasing role for building energy management. However, the mismatch between the building energy demand and energy supply is a major impediment to achieve such flexibility. The applications of thermal storage in district heating networks have lately gained much attention in recent years due to its energy flexibility, which gives the possibility to reduce further carbon emission, utility cost and primary energy saving [1]. Research from Martínez-Lera et al. [2] demonstrated that combining thermal storage systems with district heating networks could help with reducing the negative effects of the variability of both electricity and thermal demands in buildings. Smith et al. [3] and Mago et al. [4] drew the same conclusion. According to Guelpa et al. [5], the integrated building energy infrastructure comprises energy vector distribution (e.g. gas, power, district heating and cooling), thermal energy storage, grid, renewable resources, and end users. Concluded by Costanza et al. [6], there are three main advantages, (i) higher flexibility and reliability, (ii) reduced waste resources, (iii) more rational exploitation of renewables and waste heat.

In this situation, developing optimal control strategy is the key to the operation of the whole system in the best way [7]. The most common classic control method aims to set the heat supply equal to the heat demand and control the supply water temperature, e.g., from heat pumps at a fixed point, which wastes much extra energy. Thus, a smart control strategy based on data-driven method and optimization

algorithm which simultaneously manages all resources based on the prediction of the future uncertainties will be the focus to develop.

## 2. Method

### 2.1. System description

A building energy system, shown in Fig. 1, connected to a district heating network was proposed to evaluate and validate the control strategy, which is from Ochsner Heat Pump, an AIT Austrian Institute of Technology. The system comprises multiple apartment units, each with its own independent heat pump to independently satisfy its thermal demand. A Phase Change Material (PCM) thermal storage tank integrated directly with the district heating network is directly connected to the heat pumps.

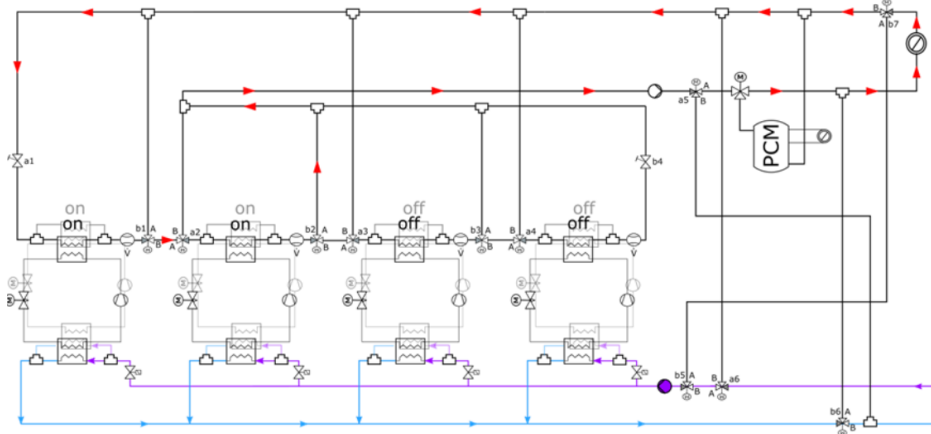


Figure 1. System Configuration

### 2.2. A new control framework

A novel integrated control framework was proposed for optimally managing the above energy network with the thermal storage tank. The proposed control framework is mainly based on fixed horizon optimization control and with the support of data-driven models. As shown in Fig. 2, the pre-built models are loaded and interact with the main optimization algorithm in every iteration. During the optimization process, the thermal demand prediction and corresponding weather state should be the input while the working state (on/off) and supply/return water temperature of the heat pumps and the charging/discharging action of the PCM storage tank will be the output with a resolution of 1h or less. Another optimization variable is the grid action (selling amount or purchasing amount). The objective function of the optimization process is set as the minimum cost in a whole day's operation, which comprises operation cost  $C_{operation}$  and carbon emission  $C_{carbon}$ , depending on the local energy mix. It is expressed as below, in which,  $n$  is the total planning time steps of the control horizon, 24 steps nominally. It is worth noting that heat pumps and PCM storage tank have their own maximum power and capacity, along with the energy balance of the target networks, and additionally, maximum charging and discharging rate are also an important constraint for the optimization. Finally the output control actions from the optimization algorithm are spreaded to the target devices, e.g. heat pumps, grid, and thermal storage devices.

$$\min J = \sum_{t=1}^n (C_{operation} + C_{Carbon}) \quad (1)$$

Within the framework, four models are developed, namely, indoor states prediction model, thermal load prediction model, heat pump model, and PCM storage model, in which, the former three models are through machine learning method. They are introduced as following:

- (1) Thermal load prediction model: in order to predict the thermal load, a large amount of building thermal load data is required, and the multivariate inputs are determined including outdoor temperature, outdoor humidity, day type, hour, solar irradiation. The historical values of the data mentioned above are also needed due to the building thermal inertia [7].
- (2) HP model: heat pump model is developed to predict the heating capacity and power consumption by means of COP value, which is the mechanical parameter of the heat pumps using real-life manufacturer's data.
- (3) Indoor states prediction model: the indoor state change is complex, and can be revealed by means of thermal-dynamic based model before, however, in this research, a machine learning model is adopted, aiming to predict the interaction between thermal energy provided and indoor states change. Besides, the resolution should be as small as possible to ensure the performance of the prediction model.
- (4) PCM model: through PCM model, charging and discharging, associated with energy dissipation, are the main target process that are simulated.

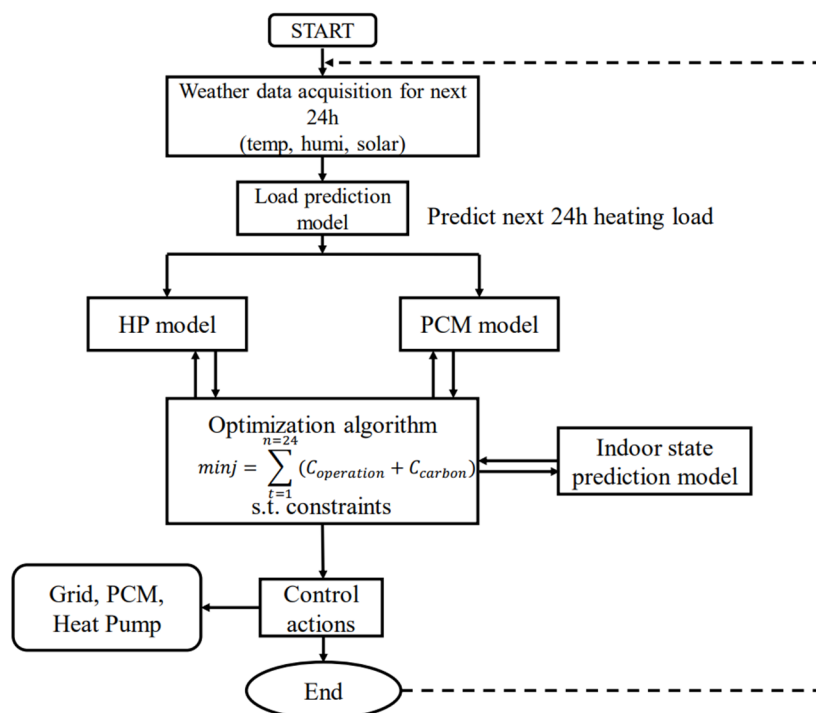


Figure 2. Proposed data-driven model based control framework

## References

- [1] Yang Zhao, Yuehong Lu, Chengchu Yan, & Shengwei Wang. MPC-based optimal scheduling of grid-connected low energy buildings with thermal energy storages Energy and Buildings, Energy and Buildings 86 (2015) 415–426.
- [2] S. Martínez-Lera, J. Ballester, J. Martínez-Lera, Analysis and sizing of thermal energy storage in combined heating, cooling and power plants for buildings, Applied Energy 106 (2013) 127–142.
- [3] A.D. Smith, P.J. Mago, N. Fumo, Benefits of thermal energy storage option combined with CHP system for different commercial building types, Sustainable Energy Technologies and Assessments 1 (2013) 3–12.
- [4] P.J. Mago, R. Luck, A. Knizley, Combined heat and power systems with dual power generation units and thermal storage, International Journal of Energy Research (2013).
- [5] Guelpa E, Bischi A, Verda V, Chertkov M, Lund H. Towards future infrastructures for sustainable multi-energy systems: a review, Energy 184 (2019) 2–21.



[6] Costanza Saletti, Mirko Morini, Agostino Gambarotta. Smart management of integrated energy systems through co-optimization with long and short horizons, *Energy* 250 (2022) 123748.

[7] Ziqing Wei, Fukang Ren, Bao Yue, Yunxiao Ding, Chunyuan Zheng, Bin Li, Xiaoqiang Zhai, Ruzhu Wang, Data-driven application on the optimization of a heat pump system for district heating load supply: A validation based on onsite test, *Energy Conversion and Management* 266 (2022) 115851

## Darkening sand particles for CSP applications

L. M. Cerutti-Cristaldo<sup>(1)</sup>; M. Díaz-Heras<sup>(1,2\*)</sup>; J.C. Pérez-Flores<sup>(1,2)</sup>, J. Canales-Vázquez<sup>(1,2)</sup>,  
J.A. Almendros-Ibáñez<sup>(1,2)</sup>

<sup>1</sup>Universidad de Castilla-La Mancha, Renewable Energy Research Institute, Avda. de la Investigación 1, 02071, Albacete

<sup>2</sup>Universidad de Castilla-La Mancha, E.T.S. de Ingenieros Industriales de Albacete, Campus Universitario s/n, 02071, Albacete

\*Corresponding author e-mail: Minerva.Diaz@uclm.es

### Abstract

Different recent works explored the possibility of using particles as heat transfer fluid and thermal storage system in the new generation of CSP plants, as they permit to reach higher temperatures than the actual CSP plants. The use of sand (a widely available material in arid or desert areas where CSP plants are usually located) has been limited due to its poor optical properties (low absorptivity). This work shows the preliminary results of an innovative chemically stable solid solutions that promote color changes in the sand particles. The mechanical properties of homogeneous particles is expected to be superior to those of coated or core-shell assemblies, presented in previous works of the literature. The X-Ray and SEM analysis of the two samples analysed suggest that they did not result in conventional coating, but in solid solutions or formation of novel phases, which will result in higher absorptivities and long-term stability than conventional coating.

**Keywords:** Thermal energy storage, fluidized beds, solar energy, radiation on particles, characterization.

### 1. Introduction

In the actual energy context, the development of renewable energies is becoming a key aspect for a fossil fuel-independent future in Spain and in Europe. The recent Ukraine war has shown the reality about the dependence of Europe on Russian gas, and the huge increase of the energy prices all around world, forces European countries to a real commitment to renewable energies. Among the different renewable sources, thermal solar energy has a huge potential to grow in Europe in the near future. According to the recent data published by the European Union [1], 37.5 % of the gross electricity consumption in Europe comes from renewable energy sources, being wind and hydropower more than two-thirds of the total electricity generated, whilst the electricity production by CSP is residual. According to [2], the CSP capacity installed in the EU 27 will grow from 2328.8 GW in 2021 up to 3000 GW in 2030.

CSP development will grow in the next years through the third generation of CSP plants [3], in which the use solid particles will be a key point to reach temperatures that exceed 800 °C and power conversion efficiencies greater than 50 % will be achieved with supercritical carbon dioxide (sCO<sub>2</sub>) Brayton cycle. Different particle CSP particle receivers have been explored: direct systems that use solar irradiation concentrated on the particles and indirect system, where the solar irradiation is concentrated on the external surface of a tube in which the particles are moving. In both systems, the use of cheap materials is a key point to reduce the Levelized Cost of Electricity (LCOE) to be competitive with conventional power plants. In addition, in direct systems, high absorptivity materials are mandatory to improve the energy effectively stored in the particles.

Among the different particles previously studied [4], SiC has the higher efficiency due to its higher absorptivity (around 0.9) which is double than the absorptivity of sand. In contrast, the high cost of SiC particles precludes its use in a large scale CSP plant, being the low-cost sand more competitive in this



aspect. Other works tried to explore the possibility of coating raw sand particles to darken its surface and augment the absorptivity [5-7]. Gimeno-Furio et al. [5] coated sand particles with two different substances: carbon black nanoparticles and glucose. In both cases the authors observed an increment of 140 % in the optical properties. García-Plaza et al. [6] experimentally tested the coated sand of Gimeno-Furio et al. [5] in a directly irradiated lab-scale fluidised bed. The carbon-black coated particles were successfully tested during 10 cycles without deterioration of the optical properties although the glucose coated particles were not properly fluidized because glucose reradiated at relative low temperatures, around 80 °C. More recently Chung and Chen [7] coated sand particles with black spinel nanoparticles and measured notably improvement in the solar absorptivity and thermal conductivity without degradation after being mechanically agitated in a rotatory drum with grinding balls.

The present work explores the possibility of a new staining processes for sand particles with the main objective of darkening the sand particles with cheap materials to maintain the low-cost advantage of sand compared to other materials, such as SiC [5].

## 2. Materials and method

To carry out this work, different sources of transition metals (Fe and Mn) were thermally treated in combination with raw silica sand. The main objective of this study is to produce chemically stable solid solutions that promote color changes in the sand particles. In a first stage, this strategy has been carried out by mixing sand samples in an agate mortar as follows:

- Sample 1:  $\text{MnCO}_3$  (Mn II) + raw sand. 1:10 w% ratio
- Sample 2:  $\text{Fe}(\text{NO}_3)_3 \cdot 9\text{H}_2\text{O}$  + raw sand. 1:10 w% ratio

Once mixed in the mortar, the two samples are introduced into a muffle furnace in the 500-1000°C temperature range to promote the diffusion in the solid state of Mn or Fe in the silica. In addition to demonstrating this color change visually, changes have been monitored with both X-Ray diffraction and Scanning Electron Microscopy (SEM).

## 3. Results and discussion

In all cases, the specimens obtained after thermal treatment of  $\text{MnCO}_3$  and  $\text{Fe}(\text{NO}_3)_3 \cdot 9\text{H}_2\text{O}$  with raw sand were apparently homogenous, with black and red-orange colour-scheme. Figures 1 and 2 show the X-ray diffraction patterns of raw sand mixed with  $\text{MnCO}_3$  and  $\text{Fe}(\text{NO}_3)_3$  and heated in the 500 to 900 °C temperature range. Raw sand material can be indexed as  $\text{SiO}_2$ , with trigonal structure and  $P_3121$  symmetry group. LeBail fitting renders the following cell parameters  $a=b=4.9415(4)$  Å,  $c=5.4361(3)$  Å, being  $V = 114.959(2)$  Å<sup>3</sup> in good agreement with the data previously described [8].

For raw sand mixed with  $\text{MnCO}_3$ , additional peaks are consistent with orthorhombic  $\alpha\text{-Mn}_2\text{O}_3$  [9] or cubic  $\beta\text{-Mn}_2\text{O}_3$  [10] coming from the thermal decomposition of the starting carbonate manganese at temperatures above 425 °C [11]. Similarly, for coated  $\text{Fe}(\text{NO}_3)_3 \cdot 9\text{H}_2\text{O}$  sample, secondary peaks of  $\text{Fe}_2\text{O}_3$  [12] appeared due to thermal decomposition above 150 °C.

Insets of both samples show a progressive shift of the  $\text{SiO}_2$  main diffraction peaks towards lower  $2\theta$  angles up to 700 °C. This can be considered as transition metal ions (Fe and Mn) entering the  $\text{SiO}_2$  lattice forming a solid solution according to Vegard's law. Above 700 °C, the evolution of the cell parameters apparently changes, and the diffraction peaks shift towards larger  $2\theta$  values that may imply further structural changes, including the formation of new phases as more transition metal ions diffuse into the silica-based sand grains.

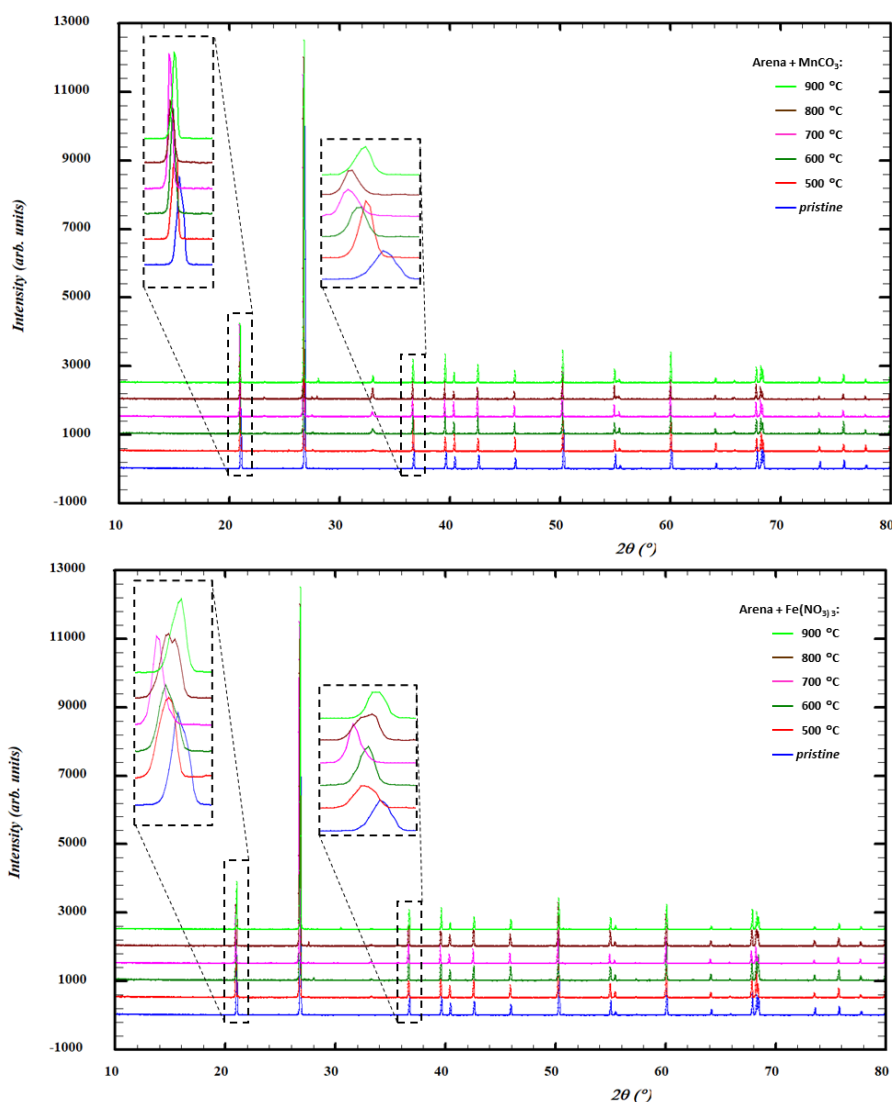


Figure 1. Diffraction patterns of raw sand mixtures with a)  $\text{MnCO}_3$  and b)  $\text{Fe}(\text{NO}_3)_3 \cdot 9\text{H}_2\text{O}$ .

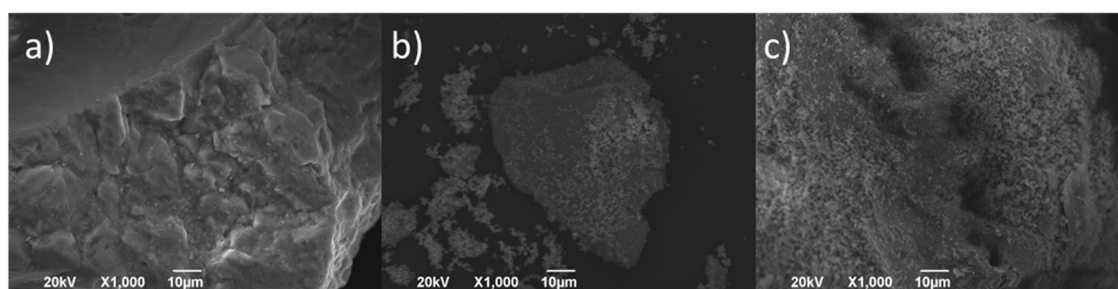


Figure 2. SEM images corresponding to a) raw sand, b) sand coated with  $\text{MnCO}_3$  and treated at  $500^\circ\text{C}$  for 6 hours and c) sand coated with  $\text{MnCO}_3$  and treated at  $900^\circ\text{C}$  for 6 hours.

In any case, the XRD results obtained reveal peak shifts in the main reflections of silica, which suggests that the strategies explored in the present work did not result in conventional coating, but in solid solutions or formation of novel phases. Such structural evolution is responsible for a dramatic darkening of the sand particles for both  $\text{MnCO}_3$  and Iron (III) nitrate.

SEM observation revealed also changes in the microstructure as a function of the thermal treatment. Coating with Mn oxide particles can be observed in the specimens treated at  $500^\circ\text{C}$  (figure 2b) and  $900^\circ\text{C}$  (figure 2c), though the adherence improves at higher temperatures and the particle size is larger.

EDS analysis revealed that a minor fraction of Mn has diffused into the SiO<sub>2</sub> grains, although further work is on-going to determine the limits of the solid solutions.

#### 4. Conclusions

The formation of solid solutions or novel phases may have important advantages over traditional coatings as the mechanical properties of homogeneous particles is expected to be superior to those of coated or core-shell assemblies. In other words, we believe this strategy may lead to higher absorptivities and stability in the long-term. Further work is on-going to evaluate the performance of chemically modified sands in CSP plants.

#### Acknowledgements

This work was partially funded by the project PID2021-127322OB-I00 (funded by Ministerio de Ciencia e Innovación MICIN/AEI/10.13039/501100011033 and by NextGenerationEU/PRTR); Project TED2021-131046B (funded by Ministerio de Ciencia e Innovación MICIN/AEI/10.13039/501100011033 and by NextGenerationEU/PRTR). Project SBPLY/21/180501/000017 (funded by the Regional Government of Castilla-La Mancha); and Project 2020-GRIN-28725 (funded by Universidad de Castilla-La Mancha).

#### References

- [1] <https://ec.europa.eu/eurostat> (Last accessed in February, 2023)
- [2] <https://www.eurobserv-er.org/solar-thermal-and-concentrated-solar-power-barometer-2021> (Last accessed in February, 2023)
- [3] Nie, F., Bai, F., Wang, Z., Li, X., & Yang, R. (2022). Solid particle solar receivers in the next-generation concentrated solar power plant. *EcoMat*, 4(5), e12207.
- [4] Díaz-Heras, M., Barreneche, C., Belmonte, J. F., Calderón, A., Fernández, A. I., & Almendros-Ibáñez, J. A. (2020). Experimental study of different materials in fluidized beds with a beam-down solar reflector for CSP applications. *Solar Energy*, 211, 683-699.
- [5] Gimeno-Furio, A., Hernandez, L., Martinez-Cuenca, R., Mondragón, R., Vela, A., Cabedo, L., ... & Jacob, M. (2020). New coloured coatings to enhance silica sand absorbance for direct particle solar receiver applications. *Renewable Energy*, 152, 1-8.
- [6] García-Plaza, J., Díaz-Heras, M., Mondragón, R., Hernández, L., Calderón, A., Barreneche, C., & Almendros-Ibáñez, J. A. (2022). Experimental study of different coatings on silica sand in a directly irradiated fluidised bed: Thermal behaviour and cycling analysis. *Applied Thermal Engineering*, 217, 119169.
- [7] Chung, K. M., & Chen, R. (2023). Black coating of quartz sand towards low-cost solar-absorbing and thermal energy storage material for concentrating solar power. *Solar Energy*, 249, 98-106.
- [8] Tucker, M.G. Dove, M.T. Keen, D.A., *Mineralogical Magazine* (1969-), 65 (2001), 489 – 507.
- [9] Bolzan, A. A. Fong, C. Kennedy, B. J. Howard, C. J. (1993), *Australian Journal of Chemistry*, 46, 939-944.
- [10] Hase, W. (1963) *Physica Status Solidi*, 3, 446-449.
- [11] L. Biernacki, S. Pokrzywnicki, J. (1999), *Thermal Analysis and Calorimetry*, 55, 227-232.
- [12] Pauling, L Hendricks, S.B., (1925) *Journal of the American Chemical Society*, 47, 781-790.

EUROTHERM2023-H155

## Role of Thermal Energy Storage in the coverage of seasonal energy mismatch and comparison with other technologies

Alice Tosatto<sup>1</sup>, Fabian Ochs<sup>1</sup>

<sup>1</sup>Unit of Energy Efficient Buildings, Department of Structural Engineering and Material Sciences, Universität Innsbruck, Innsbruck, Austria, Phone: +43 512 507-63617, e-mail: [alice.tosatto@uibk.ac.at](mailto:alice.tosatto@uibk.ac.at)

### Abstract

Seasonal energy storage systems are a key element for the full integration of volatile renewables (RE) in the energy system. The main challenges for their integration is related to their storage efficiency, that differs depending on the technology used, their effective coupling with the available RE and required load and their cost. This work focuses on large-scale thermal energy storage (TES) and its role in storing the seasonal energy surplus of RE: the storage is charged using a heat pump (HP) powered by the available surplus of photovoltaic (PV). This storage solution is compared to another path, which uses green H<sub>2</sub> produced by electrolysis and then used to produce electricity to power decentral HPs. The two paths are compared considering the size of PV field required to cover the same heating demand of the analyzed district and the overall conversion efficiency.

**Keywords:** renewable energy system, seasonal thermal energy storage, heat pump, photovoltaic, hydrogen storage

### 1. Introduction

In future renewable (RE) energy systems, energy storage plays a fundamental role for increasing the penetration of RE, enhancing the sector coupling and balancing the electrical network. The application of large-scale thermal energy storage (TES) systems was initially found in solar district heating (DH), to match the time shift between availability of solar thermal energy and heat demand [1]. However, TES systems can be effectively coupled with many technologies, such as heat pumps (HPs), whose high efficiency (coefficient of performance, COP) and flexibility, especially when coupled with TES, make them an important element to achieve a deeper sector coupling. Alongside the heating (and cooling) and the electricity distribution networks, the hydrogen (H<sub>2</sub>) network can also be effectively coupled through the use of conversion technologies (i.e. electrolysis, H<sub>2</sub> storage and fuel cell) to increase the flexibility of the energy system [2].

This work studies the ability of a large scale water-based TES to store seasonal energy surplus and provide it to the connected grid. The TES is charged with a large-scale HP when photovoltaic (PV) surplus is available. This solution is compared to another storage strategy based on green H<sub>2</sub> that is produced with PV surplus, stored and converted into electricity to power decentral HPs.

### 2. Methodology

#### 2.1 Large-scale TES modelling

Considering the large volumes required, for the large-scale TES, underground solutions are preferable. Both TES and surrounding ground are modelled with a finite-element discretization within COMSOL Multiphysics environment. A detailed description of the TES model is provided in [3].

The large-scale TES is charged with the surplus HP production at 95 °C to be able to provide heat to the local DH grid (return 65 °C). It is assumed that the analyzed DH distribution system has an efficiency of 85 %. A daily energy balance is considered between DH grid requirement and PV production. When

there is a surplus of PV production (i.e. in summer) high enough to cover the entire daily demand, the thermal energy required to cover the daily mismatch is stored in an ideal buffer TES (with an efficiency of 90 %), while the rest is stored in the large-scale TES. In winter days, in case, energy surplus is stored in the buffer TES, and the remaining load is covered by the large-scale TES.

## 2.2. Comparison of the TES and H<sub>2</sub> storage paths

The path efficiency of the large-scale TES strategy is compared to another seasonal storage strategy based on H<sub>2</sub>. In this second case, the daily surplus of PV is used to produce H<sub>2</sub> with an electrolyser, which is then stored and used to produce electricity when required. This electricity is used to power decentral HPs that provide the required heating load. When there is a surplus of PV production (i.e. in summer) high enough to cover the entire daily demand, the electric energy required to cover the daily mismatch is stored in a battery with an efficiency of 100 %, while the rest is used to produce H<sub>2</sub> with an electrolyser with an efficiency of 70 %. In winter days, PV surplus is stored in the battery and the remaining load is covered by the electric energy produced by the fuel cell with an efficiency of 50 % powered by the stored H<sub>2</sub>.

A visual schematic representation of the two studied paths is presented in Figure 1. The efficiencies of the elements considered are presented in Table 1: for sake of simplicity constant values are considered. The HPs and the electrolyser are assumed to be ideal, that is able to adapt to the load change. The same final heating demand is considered in both paths, which are compared considering the required amount of RE (in terms of PV fields) and their efficiencies.

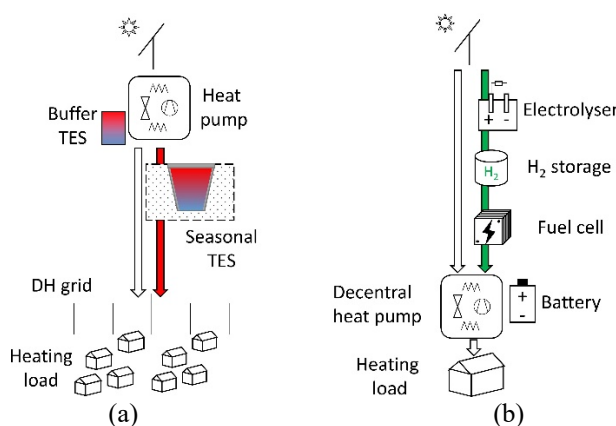


Figure 1. Schematic presentation of the two alternative paths of seasonal storage. (a) TES path with DH. (b) H<sub>2</sub> path with individual HPs in buildings.

Table 1. Efficiency ( $\eta$ ) and coefficient of performance (COP) of the technologies used in the two paths, based on [4].

	PV	TES path				H <sub>2</sub> path				
		Large HP	Large TES*	Buffer TES	DH grid	Electrolyser	H <sub>2</sub> Storage	Fuel Cell	Battery	Decentral HP
$\eta$ , COP	0.16	3	0.85	0.9	0.85	0.7	1	0.5	1	3

## 2.3. Case study

A specific case study is analyzed to compare the cycle efficiency of the two paths. From the climate data of the city of Innsbruck (Austria), the global radiation on a 45° tilted surface oriented towards south is derived to calculate the profile of PV electricity production. The heating load profile is derived based on the 24 h floating average of the ambient temperature, while in summer a constant heating demand is considered to account for domestic hot water production, for a total load of 15.8 GWh/a. The load profile and specific global solar radiation used in the calculation are shown in Figure 2.

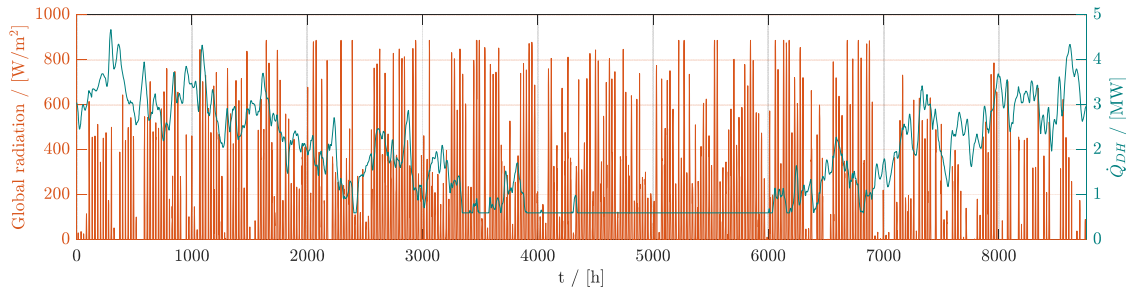


Figure 2. Hourly profiles of the district load demand and of the global solar radiation on a 45° tilted PV.

### 3. Results and discussion

#### 3.1. TES path

In order to size the large-scale TES, a daily evaluation of the heat demand and of the thermal surplus actually available to be stored is conducted, using the profiles presented in Figure 2 and considering different PV field sizes. As highlighted in Figure 1, the daily required thermal energy is primarily provided by the HP directly, then via the buffer storage, and then via the large-scale TES. The result is presented in Figure 3(a), from which it is possible to derive that the surplus of energy provided by a PV field of 50 000 m<sup>2</sup> is able to cover the required peak and can be stored in a TES volume of 260 000 m<sup>3</sup>. Figure 3(b) shows the resulting monthly balance for this pre-design phase.

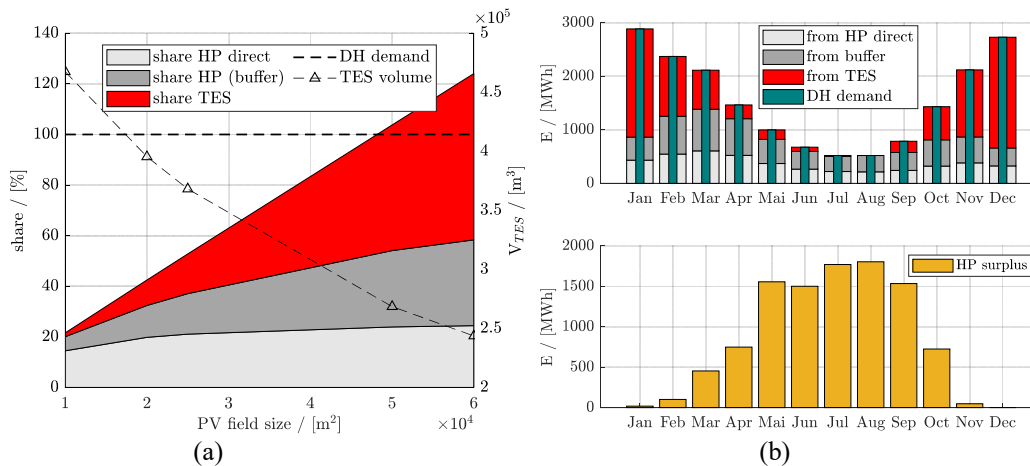


Figure 3. (a) Sizing of large-scale TES and PV field. (b) Monthly load shares for a PV field of 50 000 m<sup>2</sup>.

With this information, it is then possible to model the large-scale tank TES and to study precisely its thermal behavior over a period of one year. This step is particularly relevant since the effective storage volume of a TES depends largely on its geometry and envelope quality. The specific case of an insulated tank TES (diameter 81.5 m, height 50 m) is used as an example here: the 10<sup>th</sup> year of operation is considered to account for the ground pre-heating. The resulting TES thermal stratification is presented in Figure 4. The final TES energy efficiency in the analysed case (ratio between total energy extracted from the storage to total energy used to charge) is 85 % for 0.85 storage cycles. The path efficiency ranges between 2.5 and 2.16 (when using the large-scale TES).

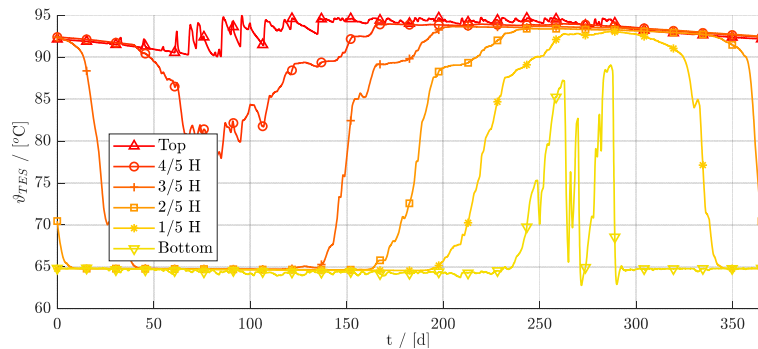


Figure 4. TES Thermal stratification from the numerical simulation during the last year of operation.

### 3.2. Hydrogen path

For the H<sub>2</sub> path, the decentral HPs are first powered by the available PV, then via the battery, and then via the re-electrification in a fuel cell of the stored H<sub>2</sub>. Considering the same profile, the required PV field size is more than 60 000 m<sup>2</sup>: the ratio between the PV electricity directly used in the HP (considering also the battery) and the electricity required to produce the H<sub>2</sub> is 0.67. Figure 5 shows the monthly profiles for different PV sizes and Figure 5(b) the respective share that can be covered by the H<sub>2</sub> storage. The path efficiency ranges between 3 and 1.05.

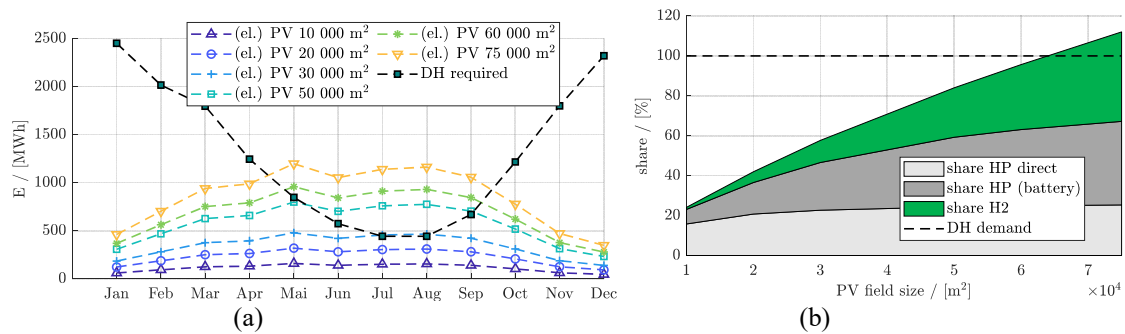


Figure 5. (a) Monthly profiles for different PV sizes. (b) Share available from the H<sub>2</sub>.

### 5. Conclusions

In this study, the methodology for comparing seasonal storage solutions was presented using a simple case study as an example. From the results, it was concluded that using large-scale TES in combination with a HP is the more efficient seasonal storage solution compared to the H<sub>2</sub> path. The TES path has a higher efficiency and requires significantly lower use of RE. Moreover, H<sub>2</sub> is a versatile energy carrier that will play a key role and is required in other sectors such as industry and mobility. It is noteworthy that, for the sake of simplicity, only PV has been considered here as RE source and in future work different future RE-Electricity systems should be investigated and also combinations of both paths.

### References

- [1] F. Ochs, “Modelling Large-Scale Thermal Energy Stores,” University of Stuttgart, 2009.
- [2] A. Lyden, C. S. Brown, I. Kolo, G. Falcone, and D. Friedrich, “Seasonal thermal energy storage in smart energy systems: District-level applications and modelling approaches,” *Renew. Sustain. Energy Rev.*, vol. 167, p. 112760, Oct. 2022, doi: 10.1016/J.RSER.2022.112760.
- [3] A. Dahash, F. Ochs, A. Tosatto, and W. Streicher, “Toward efficient numerical modeling and analysis of large-scale thermal energy storage for renewable district heating,” *Appl. Energy*, vol. 279, 2020, doi: 10.1016/j.apenergy.2020.115840.
- [4] Energistyrelsen, “Technology data for energy plants.,” 2022. .

EUROTHERM2023-U160

## Design and lab-scale testing of a mid-term thermochemical energy storage as a support to district heating networks

Valeria Palomba<sup>1\*</sup>, Omais Abdur Rehman<sup>1</sup>, Davide La Rosa<sup>1</sup>, Fabio Costa<sup>1</sup>, Vincenza Brancato<sup>1</sup>, Yannan Zhang<sup>1</sup>, Andrea Frazzica<sup>1</sup>, Gabriele Penello<sup>2</sup>, Walter Mittelbach<sup>2</sup>

<sup>1</sup>National Research Council of Italy – Institute for Advanced Energy Technologies (CNR-ITAE), Salita S.Lucia sopra Contesse 5, 98126 Messina, Italy. e-mail:valeria.palomba@itaecnr.it

<sup>2</sup>Sorption Technologies GmbH, Christaweg 52, 79114 Freiburg im Breisgau, Germany

### Abstract

This paper presents the design and first lab-scale testing of a thermochemical storage reactor that utilizes composite adsorbents, i.e. silica gel/CaCl<sub>2</sub>. The development activity included the preparation and characterization of the storage materials and the identification of the optimal packing ratio of the reactor. The lab-scale testing was performed to evaluate the performance of the reactor and the composite adsorbent under various conditions, in terms of operating temperature and dynamic response. The results show that the reactor is capable of efficiently storing and retrieving thermal energy, with high energy storage densities and fast response times. The reactor design and performance results presented provide a valuable foundation for future work aimed at developing practical, large-scale systems for integration into the district heating network.

**Keywords:** thermochemical storage; composite adsorbents; district heating; monthly storage

### 1. Introduction

The use of sorption storage for mid to long-term applications is gaining interest, not only for the residential areas but also in combination with district heating and cooling (DHC). Indeed, one of the most interesting fields of application is thermal-electric sector coupling. In this case, it is possible to use sorption storages as decentralized storages at district/substation levels or even at building levels, charging them directly from the main district heating/cooling ring or in combination with heat pumps. This is especially useful in the new generation of DHC, that approach the concept of “temperature neutral” network, in which the temperature is kept as close to ambient temperature as possible. At the same time, the new generation of DHC is intended to accommodate a larger share of renewables inside the grids (thermal and electric), which requires suitable storage systems for peak shaving and load shifting.

Sorption storage allows to answer to such challenges, thanks to its high flexibility (it can be operated for heating and cooling purposes), virtually lossless operation and possibility of being installed also in residential areas or in buildings (differently from underground storage or aquifer storage). The main challenges that sorption technology has to face for the specific application are: possibility of using non-toxic materials and refrigerants, that would hinder installation in buildings; the need for high energy density and a charging temperature lower than the state-of-art application of sorption system, usually intended for charging with solar heat or industrial heat at temperatures higher than 80°C.

Starting from such basis, the complete development of a thermochemical storage for the application in DHC was carried out, starting from the selection and preparation of the composite material and the lab-scale testing to evaluate its performance in terms of response time, power output and energy storage density. Results were also used for the calibration of an existing model of the storage.



## 2. Material selection and preparation

The material selection was carried out thanks to a dedicated preparation and characterization campaign at CNR-ITAE. Initially, 3 ionic liquids, namely [emim][Ac], EMIM DEP and DMIM DMP, and different salt hydrates,  $K_2CO_3$ ,  $FeCl_2$ ,  $LiCl$  and  $CaCl_2$  were selected. Experimental tests were carried out on the pure materials using the Dynamic gravimetric vapor sorption analyzer (DVS) equipment from Surface Measurement Systems. Results from the tests, highlighted that the ionic liquids show a higher sorption capacity at lower relative pressures (up to 0.9 kg/kg for a 40°C isotherm for the DMIM DMP and up to 0.6 kg/kg considering the application in heat pump-assisted operation), but their cost is still too high for large scale application. The salt hydrates showed up to 1.6 kg/kg of sorption capacity, but the vast majority of adsorption is shifted towards higher pressures (3 to 4 kPa for the  $K_2CO_3$  isotherm at 40°C), thus indicating that a higher charging temperature might be needed.

However, since salt hydrates showed leakage issues already during the small-scale testing, composite adsorbents using silica gel and  $LiCl$  and  $CaCl_2$  were prepared using the wet impregnation method. The composite prepared were tested in the DVS equipment and showed up to 0.6 kg/kg water adsorption.

Due to cost and corrosion issues, the silica gel/ $CaCl_2$  (25% wt) composites were selected for the lab-scale testing of the prototype.

## 3. Experimental testing of the lab-scale prototype

### 3.1. Testing facilities

The experimental testing was carried out in a testing rig dedicated to the testing of thermal systems. It includes a 36kW electric heater connected to a 1 m<sup>3</sup> water storage, and two air/water chillers connected to 0.75 m<sup>3</sup> storages that act as heat sinks/sources at different temperature levels. The temperature inside the 0.75 m<sup>3</sup> are also regulated by means of immersed heaters. Fast-response 3 way valves connected to a custom-made PID control in LabVIEW allow the continuous control of the inlet temperatures of the circuits. All circuits are thermally insulated. Temperature inlet/outlets are measured using Pt100 class 1/10 DIN sensors, temperatures inside the storage are measured using class A type T thermocouples, flow rates are measured using magnetic flow meters with  $\pm 2.5$  % full scale accuracy.

### 3.2. Heat exchanger preparation

The composite material prepared was used for filling a heat exchanger (HEX) with external dimensions of 266 x 132 x 445 (l x w x h) having aluminum fins and copper tubes coated with an epoxy resin to avoid possible corrosion from salt leakage. The heat exchanger was filled with a mixture of silica gel (Siogel® from Oker Chemie) and the composite, in 3 different ratios in volume: 50(siogel)-50(composite), 40(siogel)-60(composite), 30(siogel)-70(composite). As shown in Figure 50, the heat exchanger was subsequently closed by means of a metallic frame.



Figure 50. The heat exchanger with the composite material.

### 3.3. Testing methodology and results

The tests were carried out considering the possible operating boundaries for the system, listed in Table 8.

Table 8. Testing conditions.

CHARGE	DISCHARGE
Heat source: 85°C / Condensation: 30°C	Adsorption: 30°C / Evaporation: 15°C
Heat source: 75°C / Condensation: 30°C	Adsorption: 35°C / Evaporation: 15°C
Heat source: 85°C / Condensation: 35°C	Adsorption: 30°C / Evaporation: 10°C
Heat source: 75°C / Condensation: 35°C	Adsorption: 35°C / Evaporation: 10°C

An example of the results during the discharge of the prototype is shown in Figure 51. It is possible to notice that there is a  $\Delta T$  ranging between 6 and 2 K for about 2000 s, corresponding to a power of 0.5 till 2.5 kW. If the system is used for contemporary cooling provision, a useful effect is also available at the evaporator.

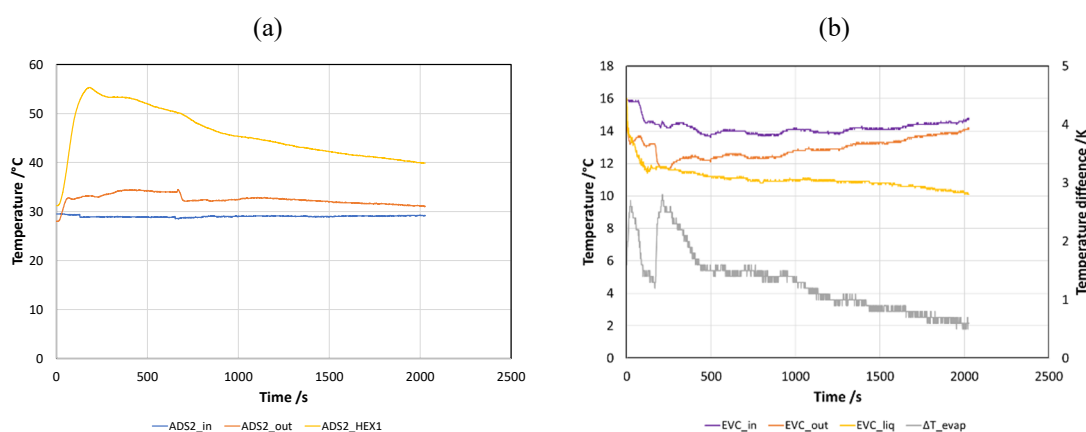


Figure 51. Results of a discharge test.

Results were also further analysed considering the achievable energy storage density in the various conditions. In the first preliminary tests carried out, up to 300 J/g<sub>adsorbent</sub> were achieved, which is about 30% less than the theoretical energy storage density of the material, but still represents a promising result.

## 4. Conclusions

In conclusion, this paper presents the design and initial lab-scale testing of a thermochemical storage reactor that utilizes composite adsorbents. The results show that the reactor is capable of efficiently storing and retrieving thermal energy. The study provides important insights into the potential of composite adsorbents for thermochemical energy storage and highlights the need for further efforts to get close to the theoretical energy density of the material. Overall, this work represents a significant step towards the development of sustainable and efficient energy storage solutions for the district heating sector.

## Acknowledgements

This project has received funding from the European Union's H2020 programme under Grant Agreement No. 101036656.

EUROTHERM2023-X161

## Iron, Aluminium and Magnesium: what is their potential for energy storage and conversion?

Tomasz Wronski<sup>1</sup>, Adriano Sciacovelli<sup>2\*</sup>

<sup>1</sup>University of Birmingham, School of Chemical Engineering, Birmingham Centre for Energy Storage, Birmingham B15 2TT, United Kingdom, Corresponding Author, e-mail: [t.m.wronski@bham.ac.uk](mailto:t.m.wronski@bham.ac.uk)

<sup>2\*</sup> University of Birmingham, School of Chemical Engineering, Birmingham Centre for Energy Storage, Birmingham B15 2TT, United Kingdom, Corresponding Author, e-mail: [a.sciacovelli@bham.ac.uk](mailto:a.sciacovelli@bham.ac.uk)

### Abstract

This paper investigates and quantifies the present potential, advantages and disadvantages of iron, aluminium and magnesium as materials for energy storage, clarifying the state of research on their conversion, the associated process concepts, and the obstacles to overcome before a deployment in real applications context. It focuses on the following criteria: energy storage potential, existing infrastructure and price, storage safety, pollutant formation during the discharge, which involves combustion, existence and efficiency of clean oxide reduction processes, and existence of power generating demonstrators. Despite its lower energy storage capacity, iron is deemed the most promising candidate because of its higher potential of zero-pollutant energy cycle. Magnesium's higher energy storage potential makes it a good candidate despite its higher price. The deciding factor will be future advancements in the prevention of nanoparticle formation.

**Keywords:** Metal combustion, Metal fuels, Energy carrier, Energy storage, Comparative review

### 1. Introduction

One of today's greatest challenges is the increasingly urgent need for zero-carbon energy. Although the development of renewable energies such as wind and solar has accelerated in the recent years, they present undeniable shortcomings when compared to fossil fuels. The main problem is the uneven geographical distribution of renewable resources combined with an absence of suitable energy storage and energy carriers. Many different energy storage systems have been developed in the recent years, starting with lithium-ion batteries and hydrogen fuel cells. Another route was proposed which relies on the storing of energy in metals and a subsequent discharge through combustion: they present a high energy density, produce no CO<sub>2</sub> during combustion, and can be regenerated from the oxides produced during combustion using renewable energies, making them a promising candidate for energy storage. Several reviews such as [1] have already been proposed in the recent years, showcasing the increasing interest in this domain and providing useful insights on fundamental characteristics of different metal candidates. As the interest grew, research has since progressed in many different directions. This paper focuses on iron, aluminium and magnesium, for which system-level investigation has been conducted in the recent years, and thus are deemed to be closest to a deployment in real applications. It takes a practical approach with the aim of providing a new academic or industrial actor with a clear overview of the current knowledge of the metal energy cycle as well as future prospects. A multiple criteria analysis has been conducted which considers all aspects of the metal energy cycle: energy storage potential, cost, storage safety, efficiency of the oxide reduction processes, pollutant formation during combustion, and the existence of system-level demonstrators. Figure 1 illustrates this approach.

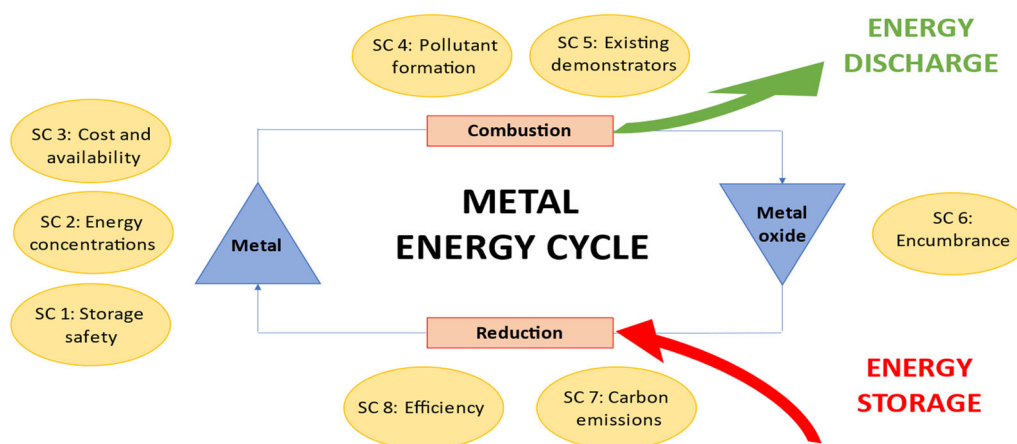


Figure 1. Schematic of the metal energy cycle and material selection criteria (SC)

## 2. Materials and methods

A multiple criteria analysis has been performed to rate each metal according to its likeliness to become a commercial energy carrier. The paper starts by comparing the intrinsic properties of the metal candidates which are energy storage capacity and safety. Economical and logistical parameters are then considered in the resource availability and price. Finally, the conversion processes are compared. Storage, or oxide reduction processes are considered based on current commercial practices and future prospects. The analysis of the energy discharge step through combustion, which is currently the limiting step of the metal energy cycle, was conducted based on fundamental and system-level research findings.

## 3. Results and discussion

### 3.1. Energy storage potential and safety (SC 1, 2 & 6)

One of the main advantages of using metals as an energy carrier is their high energy density and specific energy. Their energy density especially surpasses even that of fossil fuels, not to mention lithium-ion batteries or hydrogen. However, to fully utilize the energy storage potential of metals, the metal oxides formed during combustion need to be collected and stored. This is not the case for carbon-based fuels, whose products are released in the atmosphere. For this reason, the energy storage efficiency of the metal also depends on the volume and mass of oxide it will produce for a set amount of energy generated during combustion. Figure 2 compares the values for iron, aluminum and magnesium, also indicating energy concentrations of other commercial carriers.

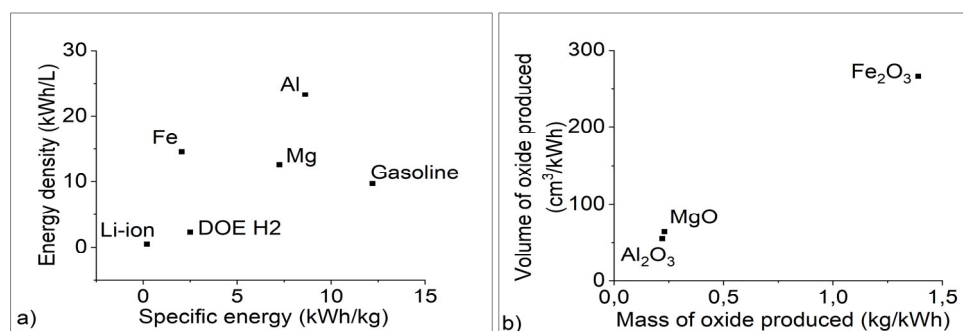


Figure 2. a) Energy density and specific energy of several energy carriers, adapted from [1][1]. b) Volume and mass of oxide formed per 1 kWh of energy released during metal combustion.

Aluminium thus presents the best energy storage potential, as it has both high volumetric and gravimetric energy concentrations and produces a relatively light and compact oxide in the form of Al<sub>2</sub>O<sub>3</sub>. Iron presents the lowest specific energy and produces over 5 times more volume and mass of oxide than the other two metals. Its high mass to energy ratio is a critical aspect that should prevent its usage for mobile applications, but stationary systems can still be considered. The storage of metal powders involves a

risk of explosion which was quantified by Jacobson et al. [2] who defined an explosibility index based on a materials explosion properties. All three metals considered here can present a moderate to severe risk (in the case of Mg and Al). The risk is also heavily dependent on the specific surface area of the powder, such as smaller particles or those with an irregular shaped presented a stronger risk. However, this risk remains very manageable as it is comparable to that of hydrocarbon fuels. On the other hand, the almost unlimited shelf life of metal powders when stored in hermetic containers is a great advantage.

### 3.2. Availability and prices (SC 3)

According to the US Geological survey[3], iron, aluminium and magnesium are among the most abundant elements on earth with world ore reserves being estimated in tens of billions metric tonnes (MT). The mining of these ores is relatively spread out across the globe; however, the smelting is conducted mainly in China, who is responsible for the production of 57% of Aluminium (world total: 78 million MT), 63% of pig iron (world total: 1.3 billion MT), and almost 80% of magnesium (world total: 1.15 million MT)[3]. This is in a large part due to its the cheap coal resources, which are used in processes relying on the carbo-thermal reduction of the metal oxides. This low diversity of producers in the case of magnesium can become a liability for the development of a global market. The limited use of this metal compared to iron and aluminium also means that the present logistical infrastructure is limited, making it harder to introduce magnesium as an energy storage material in a short time. It also results in a higher market price: as of January 2023, the prices of Rebar steel (99% iron), magnesium and aluminium per kWh generated through combustion, were respectively 0.34, 0.47 and 0.30 USD/kWh.

### 3.3. Oxide reduction processes (SC 7&8)

The oxide **reduction** processes need to be carbon free for a true zero-carbon energy cycle. Today, most of the iron and magnesium is produced using carbo- and silico-thermal processes which release large amounts of CO<sub>2</sub>. However, green alternatives exist such as electrolysis in molten salts (iron [4] and magnesium [5]) or direct reduction through hydrogen(iron [6]). The efficiency of electrolysis is highly dependent on the voltage used: although higher efficiencies are achieved in laboratory conditions, commercial processes need to compromise between time and energy costs and do not exceed energy efficiencies of 0.6 [4]. On the other hand, the efficiency of direct reduction of iron through hydrogen, reaching 0.71 [6], is dependent on the efficiency of water electrolysis for green hydrogen production. Aluminium is currently produced using the electrolytic Hall-Héroult process which produces CO<sub>2</sub> by consuming the carbon anode (or other green-house gases with biowaste-based alternatives). Research on appropriate inert anode replacement is still ongoing; and while it would prevent CO<sub>2</sub> emissions, it would also reduce the efficiency of the process.

### 3.4. Pollutant formation during combustion (SC 4)

Metals as energy carriers have the potential of zero-carbon energy storage and release, but the combustion process can still result in the formation of pollutants, such as nanoparticles and NO<sub>x</sub> emissions. The metal oxide formed during combustion should be recovered and recycled, but a fraction can form nanoparticles which are difficult to capture and represent both a material loss and an environmental and health hazard. The mode of combustion (gas phase or particle surface reaction) can affect the formation of nanoparticles. Iron was initially considered a prime candidate due to its predicted heterogeneous combustion mode, but recent experiments have shown that PM<sub>10</sub> emissions are still substantial [7]. High flame temperatures favor NO<sub>x</sub> emissions, but these can be mitigated or even eliminated through appropriate combustion conditions [4]. Research is still ongoing to prevent formation of pollutants, which might be easier to achieve with iron due to a lower flame temperature and a favored surface reaction mechanism.

### 3.5. System-level investigations of the discharge process through combustion (SC 5)

Most of the research on metal combustion is performed on a small scale, which is fundamental to the understanding of its fundamental mechanisms. However, only larger scale studies will allow for the development of commercial power generators. A first demonstration of a 100-kW iron-powered generator was developed in the Netherlands. The combustion of magnesium has been studied in a 20- 50 kW burner in France, providing data regarding flame stability and pollutant emissions. No such system has been developed for aluminium. However, different numerical studies showcased the feasibility of a water-aluminium combustor coupled to a hydrogen fuel cell and a gas turbine.

Combustion in air studied only at a smaller scale, and a similar system to the ones built for iron and magnesium should be possible, despite aluminium's higher ignition temperature. Whatever the choice of metal, a large part of the oxide particles tends to agglomerate on the system's walls, which will need to be addressed before any industrial application.

#### 4. Conclusions

This paper clarifies the current state of research surrounding iron, aluminum, and magnesium as potential energy storage materials, highlighting the advantages and disadvantages of each as well as the challenges that must be overcome before commercialization. Aluminum boasts the highest energy storage potential among the three metals considered but lacks zero-carbon regeneration processes. Magnesium has a high energy storage potential and has already been tested on a pilot scale, but the processes for reducing its oxide through electrolytic reduction are complex and not very efficient. Existing infrastructure surrounding its production is also limited, resulting in a higher price. Furthermore, its combustion in the gas phase makes it harder to prevent the formation of nanoparticles. Iron, on the other hand, has the lowest energy storage potential of the three, but its predicted surface combustion mechanism has attracted much attention. Its advantages include lower price, a wide existing infrastructure, a lower explosivity risk, a lower flame temperature which will make it easier to prevent NO<sub>x</sub> formation, and more efficient processes for reducing its oxide. However, nanoparticle formation is still substantial. Therefore, the focus of research should be on methods of preventing nanoparticle formation as this may be the determining factor for choosing between magnesium and iron as a future energy carrier.

#### Acknowledgments

The Authors would like to acknowledge the financial support from the UK Engineering and Physical Science Research Council (EPSRC) for the project 'MIX-MOXes' (EP/X000249/1)

#### References

- [1] J. M. Bergthorson *et al.*, "Direct combustion of recyclable metal fuels for zero-carbon heat and power," *Appl Energy*, vol. 160, pp. 368–382, Dec. 2015, doi: 10.1016/j.apenergy.2015.09.037.
- [2] M. Jacobson, A. R. Cooper, and J. Nagy, "EXPLOSIBILITY OF METAL POWDERS".
- [3] U. National Minerals Information Center, Mineral Commodity Summaries 2020.
- [4] H. Li, J. Lei, J. Liang, H. Yan, Z. Cai, and R. G. Reddy, "Study on the Direct Electrochemical Reduction of Fe<sub>2</sub>O<sub>3</sub> in NaCl-CaCl<sub>2</sub> Melt," *Int. J. Electrochem. Sci.*, pp. 11267–11278, Dec. 2019, doi: 10.20964/2019.12.68.
- [5] H. E. Friedrich and B. L. Mordike, Eds., *Magnesium technology: metallurgy, design data, applications*. Berlin ; New York: Springer, 2006.
- [6] J. Neumann, E. Corbean, F. Dammel, S. Ulbrich, and P. Stephan, "Energy and Exergy Assessment of Renewable Energy Storage using Iron as Energy Carrier."
- [7] H. Wiinikka, T. Vikström, J. Wennebro, P. Toth, and A. Sepman, "Pulverized Sponge Iron, a Zero-Carbon and Clean Substitute for Fossil Coal in Energy Applications," *Energy Fuels*, vol. 32, no. 9, pp. 9982–9989, Sep. 2018, doi: 10.1021/acs.energyfuels.8b02270.

EUROTHERM2023-B162

## Performance enhancement and manufacturing of form-stable $K_2CO_3$ -based thermochemical energy storage materials

Hongkun Ma<sup>1</sup>, Mengxiang Jiang<sup>2</sup>, Yi Wang<sup>2</sup>, Boyang Zou<sup>1</sup>, Li Wang<sup>2</sup>, Yulong Ding<sup>1\*</sup>

<sup>1</sup>Birmingham Centre of Energy Storage (BCES), University of Birmingham, Birmingham B15 2TT, United Kingdom, email: y.ding@bham.ac.uk

<sup>2</sup>School of Energy and Environmental Engineering, University of Science and Technology Beijing, Beijing 100083, China

### Abstract

Thermochemical energy storage (TCES) technology has attracted significant attention in recent years due to its high energy density and long-term storage with little energy loss. However, the superiorities of the technology are challenged by poor cyclability at the material scale, mainly due to structural stability degradation and agglomeration. This study aimed to address the technical challenges of TCES using salt hydrates, particularly  $K_2CO_3$  as an example, through formulating and fabricating form-stable composite thermochemical materials (CTCM). We used a novel direct mixing and compressing method and studied the scale-up of the CTCM manufacturing process. Thermal cycling tests with a humidity chamber were conducted to analyze the stability of CTCM. The effects of thermal performance, compressive strength, and microstructure of various CTCM candidates were evaluated.

**Keywords:**  $K_2CO_3$ , salt hydrate, thermochemical energy storage material, large-scale manufacturing, mechanical stability

### 1. Introduction

Heating accounts for around 50% of final energy consumption in 2021 but are mostly met by fossil fuels [1]. The net-zero target around the middle of this century requires urgent replacement of fossil fuels with clean renewable energy supply. Currently, renewable energy only represents around 2% of the energy needed for domestic heating [2]. This is mainly due to the intermittence and uneven distribution of renewable energy in both time and space. Thermal energy storage (TES) has the potential to address such a challenge. TES technologies can be broadly split into sensible, latent and thermochemical categories. Among the three TES technologies, the thermochemical-based technology using salt hydrates has received increasing attention due to its high energy density, negligible heat loss during long-term storage, non-toxicity, and suitable temperature range for domestic heating applications [3]. However, salt hydrates are prone to disintegrate and agglomerate during thermal cycling, leading to degradation in the reaction kinetics [4]. Recent efforts have been made to address such a challenge using composite thermochemical material (CTCM). This leads to an additional challenge in the manufacturing of the CTCM. Here, we present our recent work on  $K_2CO_3$ -based CTCM fabricated by a simple method of mixing and shaping. We studied the scale-up of such a manufacturing route and analyzed the thermal performance of the fabricated CTCM modules, their cyclability and mechanical stability.

## 2. Materials and methods

Expanded vermiculite is used as a supporting material purchased from Dupreminerals. The active material, Potassium carbonate ( $K_2CO_3$ ), was obtained from Fisher Scientific UK Ltd. These materials were used as received without purification.

In order to make CTCM modules,  $K_2CO_3$  (K) and vermiculite (V) were blended thoroughly to form a uniform mixture (K-V). Additional components (termed as additives) were found to be needed to aid the manufacturing process and enhance the CTCM mechanical properties. Four different additions were studied and the K-V mixtures thus formed are termed K-BCES1, K-BCES2, K-BCES3 and K-BCES4. These mixtures were fed to a tablet press machine (DX4, Bosch Packaging Technology) to manufacture CTCM pellets, which can produce tens of thousands of pellets. The energy storage performance of various pellets was characterised by their mass change and reaction enthalpy with an STA (STA 449 F3 Jupiter<sup>®</sup>, NETZSCH, Germany) at a dehydration temperature of 130 °C with a heating rate of 2 K/min. The K-BCES1 pellets were also subject to cycling tests in a humidity chamber (KBF115, Binder, Germany) at 40 °C and 40% RH for 2 hours and dehydration at 90 °C and 10% RH for 2 hours. The 3-D structure of the K-BCES1 was also studied with an X-ray Tomograph (XRT) device (Skyscanner 2211, Nano CT, Bruker, Kontich, Belgium). The compressive strength of the pellet samples was investigated by a compression tester (Microtester 5848, Instron, US).

## 3. Results and discussion

Fig. 1 (a) and (b) show the mass change and heat flow of the K-BCES1 sample during dehydration, respectively. One can see that the total mass losses of K-BCES1 before (C0) and after 20 cycles (C20) are very similar, which are around 16%. The K-BCES1 after 20 cycles has two mass change stages, one at 30-105 °C, and another at 105-130 °C. Part of the mass loss at 105 °C is likely related to the decomposition of  $KHCO_3$ , which is generated by a reaction of  $K_2CO_3$ ,  $CO_2$  and  $H_2O$  [5]. Similarly, the DSC curve of K-BCES1 after 20 cycles also has two peaks; the first (big) one is due to two reactions of the dehydration of  $K_2CO_3 \cdot 1.5H_2O$  and the decomposition of  $KHCO_3$ . The dehydration enthalpies of the K-BCES1 at zero cycle and after 20 cycles are close,  $\sim 515$  J/g. The STA results indicate that the K-BCES1 has good thermal stability and cyclability and was therefore used for subsequent study.

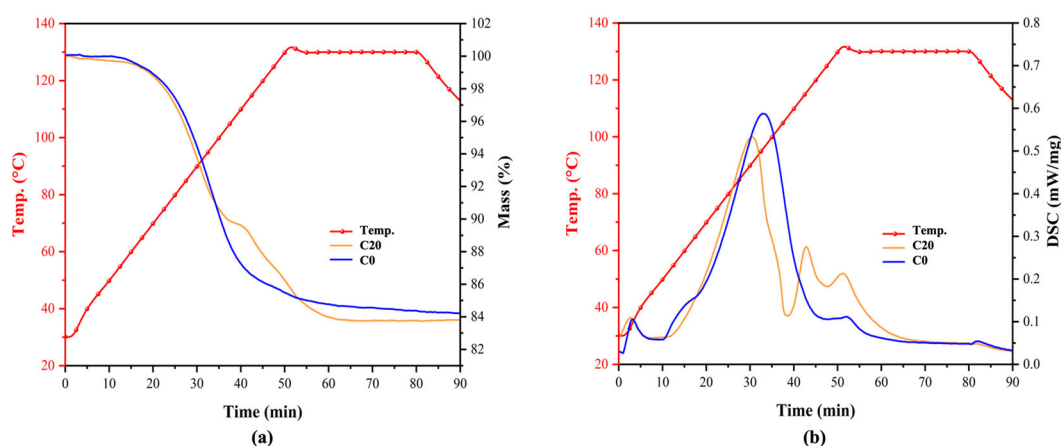


Fig. 1. The mass changes (a) and DSC curves (b) of the K-BCES1 before thermal cycling and after 20 cycles

Fig. 2 presents the cross-section XRT images of the K-BCES1 pellets after 30 cycles. The left color bar represents the density of the sample, whereas the black colour represents the lightest area and the white denotes the densest area. It can be easily observed that after 10 cycles and 20 cycles, the outer layer of the same pellet becomes porous and the mulberry color reveals that the outer layer density is lower than the interior density. Interestingly, the interior density of K-BCES1 after 20 cycles is higher than that of K-BCES1 after 10 cycles, which might be attributed to the rearrangement and agglomeration of the



particles after absorbing moisture in the interior. After 30 cycles, the porous outer layer is thicker and the interior density is lower, which indicates that the pellet is undergoing disintegration.

The total porosity distribution of K-BCES1 after 30 cycles calculated by the XRT images are displayed in Fig. 3, where the Z position varies with the XRT scanning stage position. The left side of the axis (Z position) represents the top of the pellet while the right side corresponds to the bottom of the pellet. The maximum porosity appears at the top or the bottom of the K-BCES1 ascribed to the porous outer layer shown in Fig. 2. However, the region of interest in the XRT scanning is affected by the sample shape. Sometimes, the true bottom of the pellet cannot be calculated and hence the porosity of the Z position on the right side is fairly low as in Fig.3 (a). The peak porosity of K-BCES1 C0 at the top surface is 22%, and the middle part is much denser compared to the top. With the increase in cycle number, the total porosity of both the top and bottom surfaces grows. After 30 cycles, the peak porosity of K-BCES1 C30 is more than 50% and all the porosity at any position is more than 20%, demonstrating that the porous layer becomes thicker. This change might adversely affect the compressive strength.

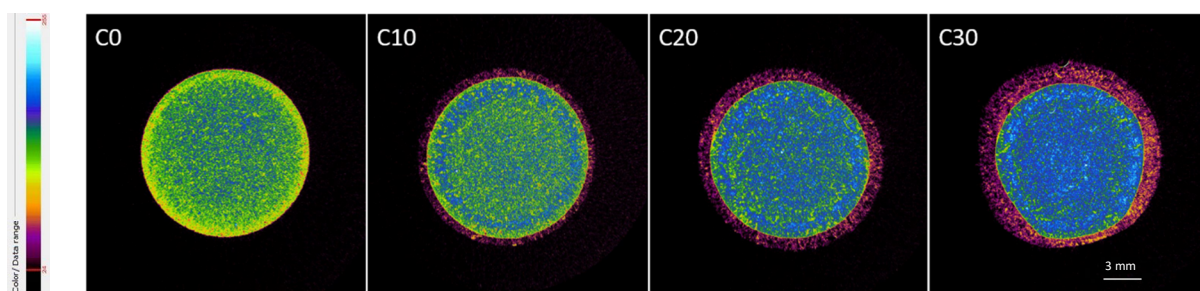


Fig. 2. The cross-section images of K-BCES1 over 30 cycles

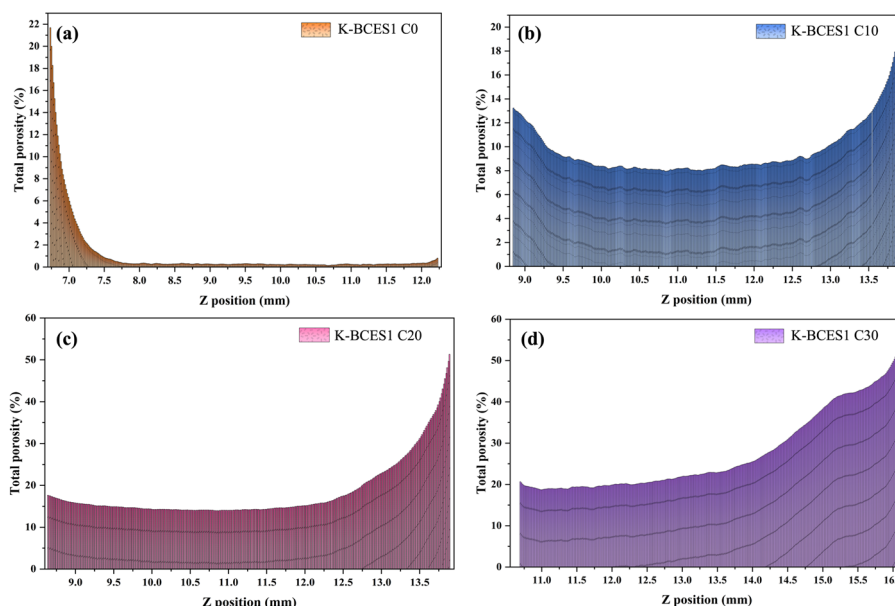


Fig. 3. The total porosity distribution of K-BCES1 over 30 cycles

As the K-CTCM pellets will be evaluated in the pilot reactor shortly, the mechanical strength of the pellets is an essential property for the evaluation of material lifespan in the reactor. To screen for the most reliable formulation, the compressive strength of the K-CTCM pellets were investigated using an Instron Microtester 5848. Table 1 summarises the compressive strength change of the K-CTCM pellets after different cycles. K-BCES3 disintegrated into pieces after 20 cycles. The K-BCES2 and K-BCES4 also disintegrated after 30 cycles. Only K-BCES1 has a sturdy structure over 30 cycles. However, after 50 cycles, the K-BCES1 could not maintain the mechanical strength with the final compressive strength dropping to 10.2 N (0.58 kPa). Work is underway to enhance the mechanical strength.

Table 1. The compressive strength of various K-CTCMs during 50 cycles

Samples		K-V	K-BCES1	K-BCES2	K-BCES3	K-BCES4
Compressive strength (N)	C0	5068.6	16276.0	3779.0	4431.3	13069.0
	C10	-	445.9	335.0	16.3	85.6
	C20	59.6	279.8	14.8	-	9.5
	C30	-	45.3	-	-	-
	C50	-	10.2	-	-	-

#### 4. Conclusions

Potassium carbonate-based composite thermochemical energy storage materials have been formulated and manufactured at scale. The thermal stability and cyclability of one of the formulations, K-BCES1, were studied by the STA results. A high energy density of 515 J/g was found to be maintained over 20 dehydration-hydration cycles. The XRT analyses show an increasingly thicker porous outer layer of the pellets during the cycling, which decreases compressive strength. K-BCES1 is the most robust and sturdy material compared to other candidates with different formulations.

#### Acknowledgements

The authors would like to thank UK Engineering and Physical Sciences Research Council (EPSRC) for partial support to this project under Grants EP/P003605/1, EP/V012053/1, EP/T022981/1 and EP/S0326221/1.

#### References

- [1] IEA (2022), Heating, IEA, Paris <https://www.iea.org/reports/heating>, License: CC BY 4.0.
- [2] V. Goodright, Estimates of heat use in the United Kingdom in 2013, DECC Statistics (2014).
- [3] P.A.J. Donkers, L.C. Sögütoglu, H.P. Huinink, H.R. Fischer, O.C.G. Adan, A review of salt hydrates for seasonal heat storage in domestic applications, Applied Energy 199 (2017) 45-68. <https://doi.org/https://doi.org/10.1016/j.apenergy.2017.04.080>.
- [4] R.-J. Clark, Salt hydrates for thermochemical energy storage, ResearchSpace@ Auckland, 2022.
- [5] L.C. Sögütoglu, P.A.J. Donkers, H.R. Fischer, H.P. Huinink, O.C.G. Adan, In-depth investigation of thermochemical performance in a heat battery: Cyclic analysis of K<sub>2</sub>CO<sub>3</sub>, MgCl<sub>2</sub> and Na<sub>2</sub>S, Applied Energy 215 (2018) 159-173. <https://doi.org/https://doi.org/10.1016/j.apenergy.2018.01.083>.

EUROTHERM2023-T163

## Ice-based thermal storage: impact of water-quality over metastability effects

Tommaso Reboli<sup>1</sup>, Marco Ferrando<sup>1</sup>, Stefano Barberis<sup>1</sup>, Alberto Traverso<sup>1</sup>

<sup>1</sup>University of Genoa – DIME, via Montallegro 1, 16145 Genova - Italy, e-mail: [tommaso.reboli@edu.unige.it](mailto:tommaso.reboli@edu.unige.it)

### Abstract

Ice storage systems have been always considered as one of the easiest and cost effective Latent Heat Thermal Energy Storage (LHTES), providing significant advantages in refrigeration and cooling systems for different applications in industrial, civil and power production applications, reducing cooling costs/consumptions, balancing energy supply and demand profiles, and shaving peak loads. Ice LHTES have been deeply investigated both from a modelling and experimental point of view, nevertheless the influence of water quality on ice LHTES behaviour in charging and discharging phases has not been investigated in detail, yet. Taking advantage of an integrated refrigeration system – LHTES experimental setup, this paper analyses the impact of different water quality levels on PCM metastability during charging and discharging phases, validating a Level-Ratio State of Charge (SoC) estimation approach.

**Keywords:** Thermal Energy Storage, State of Charge, Level Ratio, Metastability, Supercooled water, Ice storage

### 1. Introduction

Ice storage technology can be considered a proven PCM LHTES technology, particularly thanks to the easiness of its handling (high tank/pipes/HEX material compatibility) and its low CAPEX. Like all PCMs, an essential challenge for ice storage process is to enhance heat transfer performance of storage units [1], for instance by thermal conductivity augmentation[2], as well as to study their behaviour during charging and discharging phases [3]. Understanding the thermodynamic [4] and kinetic properties [5] of ice LHTES can facilitate/enhance their management and integration in different application. As an “easy to handle” PCM, water-based ice LHTES is studied to develop methodologies to model and predict thermodynamic properties of PCM [6], [7] and understand how kinetic processes, such as supercooling, impact the metastability of PCMs at different scales and how properties such as thermal conductivity influence the thermal power output, depending on State of Charge (SoC) [8]. Furthermore, it is relevant to highlight that i) LHTES performance analysis on large scale setups operating around the liquid density inversion temperature is still limited, and ii) the impact of water quality/water mixtures on ice LHTES has not been yet deeply investigated [9], [10]. Starting from previous works [11], [15]. in this field, in this paper a shell & tube, ice LHTES was studied in order to: 1) develop a SoC methodology based on the level ratio of LHTES compensator; 2) compare the behaviour of different water quality (tap water and demineralized water) as PCM, in both charge and discharge operations.

### 2. Materials and method

#### Experimental setup

The Thermal Energy Storage (TES) unit was created using a finned shell & tube design, where the Heat Transfer Fluid (HTF - made up of a blend of water and 47% ethylene glycol) circulates inside the tubes and the PCM is housed in the outer shell. The shell-side volume is close to 1.8 m<sup>3</sup> that in terms of energy corresponds to about 170 kWh by using water-ice as PCM. Further details on the system configuration and prior research can be found in [11]–[13]. A picture of the plant is reported in **Error! No s'ha trobat**

**l'origen de la referència.** (left). The PCM compartment on the shell side is connected to an external 500-liter compensator, that adjusts for the variation in volume resulting from the phase transition of the water to ice. In this plant a 10 kWel Heat Pump and a 30 kW Auxiliary Resistive Load (ARL) are also present, used during the charge and discharge operations of the TES rig. Figure 52 shows a scheme of the experimental setup. Through the three-way valve V it is possible to activate the “charge operation circuit” (HP-TES-ARL) or the “discharge operation circuit” (HP-ARL).

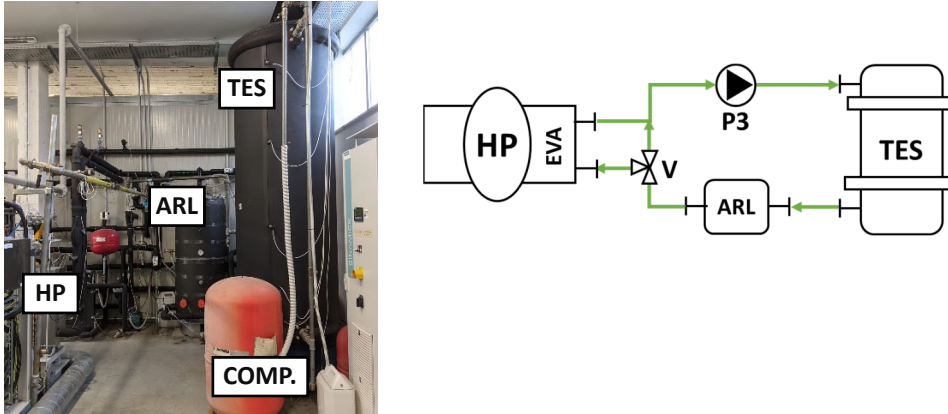


Figure 52. View of the plant (left) and experimental simplified circuit (right)

The pressure change due to expansion during the icing / melting process allows estimation of the amount of solid/liquid present in the TES. Thus, a pressure sensor is installed to monitor the pressure change providing an indication well correlated to the State of Charge [11]. Differently from the SoC estimation for sensible thermal storages [14], this approach can be applied to all those PCM characterized by a significant variation in density during the solidification / melting processes. In this work the PCM used was tap water instead demineralized water (used for previous publications)

### Level ratio and State of Charge

The SoC of the TES can be evaluated by monitoring the pressure of its compensator. The limits of this approach are that the trend of the pressure could depend on the initial pressure value (initial pressurization) and, more important, there could be no linear correlation between pressure and quantity of PCM already solidified / melted. For such reasons, the Level Ratio – LR is here introduced. Through some simple math, it is possible to link the normalized pressure of the compensator to the actual liquid level, and thus to the actual PCM volume - see Eq. (1):

$$LR = \frac{\Delta L_x}{\Delta L_{max}} = \frac{p_f}{p_x} \cdot \frac{p_x - p_{in}}{p_f - p_{in}} \quad (1)$$

where  $\Delta L_x$  is the current liquid level inside the compensator,  $\Delta L_{max}$  is the maximum variation in liquid level inside the compensator during a full charge / discharge operation,  $p_x$  is the current pressure of the compensator,  $p_{in}$  is the initial pressure of the compensator,  $p_f$  is the final pressure of the compensator. Theoretically, thanks to this approach it would be possible to link the LR to the current compensator pressure, with no need to know also the final pressure of the test. In fact, within the hypothesis that the  $\Delta L_{max}$  depends only on the PCM and the size of the vessel, it is possible to consider initial / final pressure values those found during any full charge-discharge operation considered as reference. From here on, the LR will be used as SoC indicator, as directly linked to the actual PCM volume and therefore more reliable.

### 3. Results and discussion

In this section a full-charge and a full-dicharge of the TES were done with “standard process conditions”, in accordance with what has already been highlighted in the previous works [11] (1.2 kg/s @ $T_{in} = -6^\circ\text{C}$  for charge operation and 1.2 kg/s @ $T_{in} = 9^\circ\text{C}$  for discharge operation). Then the results of these operations are compared to the ones already shown in [11] and [15]. It must be highlighted that the minimum pressures of the compensator were different: 0.28 bar(g) in these tests (tap water), and 0.41 bar(g) in the previous ones (demi water [11] and [15]).

The presence of a metastable phase preceding the incipient freezing phase during the Charge operation was verified through the analysis of the temperature trend, also using tap water as PCM. Even if the tap water contains salts that would encourage ice nucleation, all PCM thermal probes reached at least  $-1^{\circ}\text{C}$ , and then quickly raised up to  $0^{\circ}\text{C}$ .

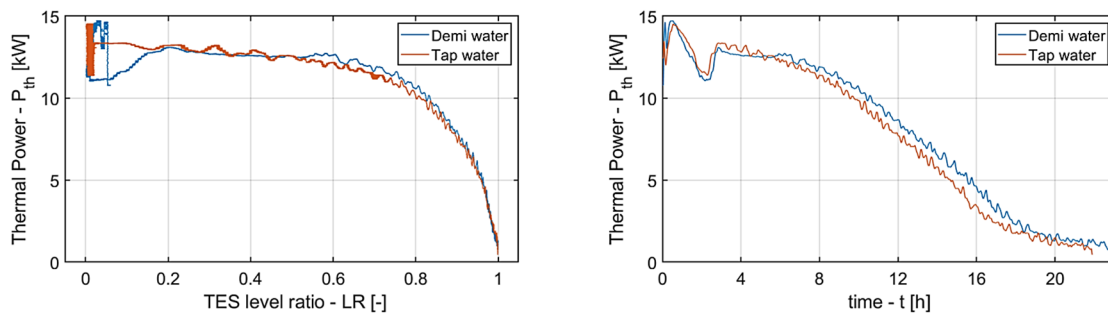


Figure 53. Demi VS Tap water in charge operation over LR (left) and time (right)

This behaviour directly affected the thermal power of the TES as clearly visible in Figure 53 – right (the discontinuity in the thermal power visible around 2nd hour): however, demineralised and tap water are impacted similarly, except for some minor differences immediately after the discontinuity. Anyway, looking at Figure 53 – left, an important difference between demineralized water and tap water is clearly visible: the presence of the metastable phase seems not to affect the TES pressure (and – thus – the LR) avoiding the discontinuity in the LR range 0-0.2 using tap water. This difference could be explained by a different behaviour of the tap water or by an effect of the initial pressurization of the compensator. Further tests need be carried out to properly explain this difference. Anyway, as expected the stored energy was almost the same in the two cases considering that tap water and demi water have very similar chemical characteristics.

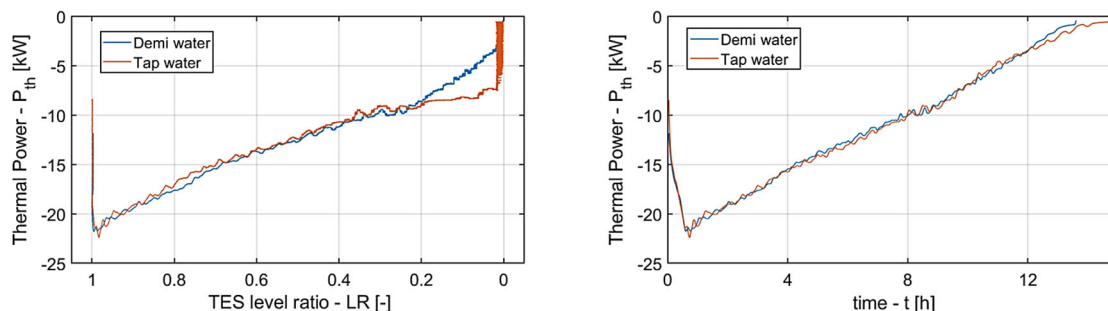


Figure 54. Demi VS Tap water in discharge operation over LR (left) and time (right)

Focusing on the analysis of the Discharge operation, it can be seen that the temporal trends of the thermal power for demi and tap water are practically the same (Figure 54 – right). Anyway, looking at Figure 54 – left for LR in the 0-0.2 range, the thermal power trend in the two cases follows different paths. Again, this difference is linked with a different trend of the compensator pressure, and this could be due to a different behaviour of the tap water or to an effect of the initial pressurization of the compensator.

#### 4. Conclusions

This paper shows the charging and discharging processes in an industrially-sized thermal energy storage. Performance was compared with two different fluids as PCM, demineralized water and tap water, using the Level Ratio parameter as SoC estimator. This parameter seems to be a good indicator of the amount of PCM that has changed phase. Therefore, it seems to be a convenient reference for determining the SoC for any initial condition. The comparison of tap water and demineralized water shows the same power profile with respect to time and a different profile with respect to Level Ratio. This could be related to the characteristics of the pressure compensator used in this experimental test-rig and to the initial pressure conditions in the two different cases. It seems that the composition differences between demineralized water and tap water are negligible for the case under consideration. This could be related to the difficulty of keeping water properly demineralized in an industrial setting such as the one covered

in this article, due to potential contamination with internal TES confinement (e.g. metal dust). However, further tests are needed to validate the goodness of the proposed approach.

## Acknowledgements

This project has received funding from the European Union's Horizon Europe research and innovation programme under grant agreement No 101096921, THUMBS UP. Views and opinions expressed are however those of the author(s) only and do not necessarily reflect those of the European Union or of CINEA.



## References

- [1] M. A. Rosen, I. Dincer, and N. Pedinelli, "Thermodynamic Performance of Ice Thermal Energy Storage Systems," *J. Energy Resour. Technol.*, vol. 122, no. 4, pp. 205–211, 2000.
- [2] L. J. Bonales, A. C. Rodriguez, and P. D. Sanz, "Thermal conductivity of ice prepared under different conditions," *Int J Food Prop*, vol. 20, pp. 610–619, 2017.
- [3] Y. Bi, M. Yu, H. Wang, J. Huang, and T. Lyu, "Experimental investigation of ice melting system with open and closed ice-storage tanks combined internal and external ice melting processes," *Energy Build*, vol. 194, pp. 12–20, 2019.
- [4] L. F. Cabeza, H. Mehling, S. Hiebler, and F. Ziegler, "Heat transfer enhancement in water when used as PCM in thermal energy storage," *Appl Therm Eng*, vol. 22, no. 10, pp. 1141–1151, 2002.
- [5] H. Bastida and et al, "Dynamic modelling of ice-based thermal energy storage for cooling applications," *IET Energy Syst. Integr.*, vol. 4, no. 3, pp. 317–334, 2022.
- [6] L. Bilir and Z. Ilken, "Total solidification time of a liquid phase change material enclosed in cylindrical/spherical containers," *Appl Therm Eng*, vol. 25, pp. 1488–1502, 2005.
- [7] S. Bellan, A. Cordiviola, S. Barberis, A. Traverso, J. González-Aguilar, and M. Romero, "Numerical analysis of latent heat storage system with encapsulated phase change material in spherical capsules," *Renewable Energy and Environmental Sustainability*, vol. 2, pp. 1–6.
- [8] S. N. Gunasekara, V. Martin, and J. N. Chiu, "Phase equilibrium in the design of phase change materials for thermal energy storage: State-of-the-art," *Renewable and Sustainable Energy Reviews*, vol. 73, pp. 558–581, 2017.
- [9] E. Chuvilin, B. Bukhanov, V. Cheverev, R. Motenko, and E. Grechishcheva, "Effect of Ice and Hydrate Formation on Thermal Conductivity of Sediments," *Impact of Thermal Conductivity on Energy Technologies, IntechOpen*, 2018.
- [10] E. Borri, J. Y. Sze, A. Tafone, A. Romagnoli, Y. Li, and G. Comodi, "Experimental and numerical characterization of sub-zero phase change materials for cold thermal energy storage," *Appl Energy*, vol. 275, 2020.
- [11] T. Reboli, M. Ferrando, A. Traverso, and J. N. W. Chiu, "Thermal energy storage based on cold phase change materials: Charge phase assessment," *Applied Thermal Engineering*, vol. 217, 2022.
- [12] T. Reboli, M. Ferrando, L. Gini, L. Mantelli, A. Sorce, and A. Traverso, "Gas Turbine Combined Cycle Range Enhancer - Part 2: Performance Demonstration," *J Eng Gas Turbine Power*, vol. 144, no. 12, 2022.
- [13] T. Reboli *et al.*, "Gas Turbine Combined Cycle Range Enhancer - Part 1: Cyber-physical setup," *Proceedings of ASME Turbo Expo, GT2022-82494*, 2022.
- [14] M. L. Ferrari, A. Cuneo, M. Pascenti, and A. Traverso, "Real-time state of charge estimation in thermal storage vessels applied to a smart polygeneration grid," *Appl Energy*, vol. 206, pp. 90–100.
- [15] T. Reboli, M. Ferrando, A. Traverso, and J. N. W. Chiu, "Thermal Energy Storage based on Cold Phase Change Materials: Discharge Phase Assessment," *Applied Thermal Engineering, Under Review*.

EUROTHERM2023-W164

## High temperature industrial thermal energy storage – Assessment of potential applications and benefits toward industrial decarbonisation

Pouriya H Niknam<sup>1\*</sup>, Stefano Barberis<sup>2</sup>, Adriano Sciacovelli<sup>3\*</sup>

<sup>1,3</sup> School of Chemical Engineering, Birmingham Centre for Energy Storage, University of Birmingham, UK, e-mail: p.niknam@bham.ac.uk, a.sciacovelli@bham.ac.uk \*Corresponding Authors

<sup>2</sup>University of Genova, Thermochemical Power Group, Department of Mechanical Engineering, Italy, email: stefano.barberis@unige.it

### Abstract

The energy transition in European industry should be viewed in the wider context of sectoral characteristics to identify the fundamental differentiators that underpin the potential of technological solutions. This study provides a deep dive into the opportunities for the uptake of thermal energy storage (TES) and the discussion includes three types of TES for waste heat recovery (WHR), steam storage (S2S), and power to heat (P2H). The plant-level process data and sector-level statistics are used to evaluate the TES contribution to EU-industry decarbonization. A link was observed between the process temperature and the opportunities for TES. It is demonstrated that the refinery sector, with a high plant-level process heat has the highest CapEx required for TES. Moreover, refinery, food and ceramic sectors have the highest potential for energy savings. Spain and Italy are identified as the top gainers from TES in these three sectors.

**Keywords:** Industrial decarbonisation, Thermal energy storage, steam storage, H2X

### 1. Introduction

The global industrial clusters emit around 8.8 Bt of CO<sub>2</sub> annually, equivalent to 24.2% of global emissions [1]. According to recent studies, there is an expected growth in energy demand by industry in the coming 20 years [1], coinciding with environmental concerns and the growing movement toward net-zero by 2050. One of the technological breakthroughs that can play a crucial role in industrial decarbonisation is TES system which can facilitate the management of industrial process heat by storing energy in the form of heat, enabling its use at a later time. TES enables intra-day or day-to-day charging and discharging to manage process heat fluctuations. It also increases the heat availability and avoids the system off-design operation. Moreover, the full potential of a TES is realised when it is used to receive different heat inputs and outputs.

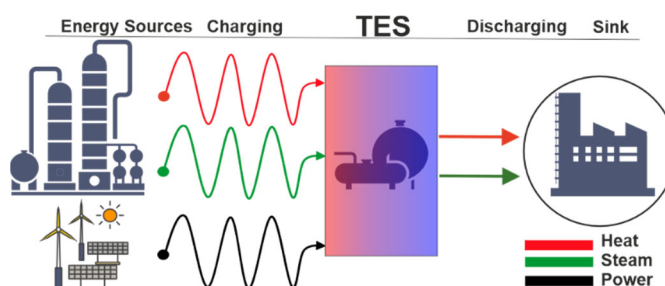


Fig 1. TES integration in industries for supplying heat and steam.

The potential sink and sources are illustrated in Figure 1. The inputs can be waste heat, excess steam, or low-cost renewable electricity, which all are often intermittently available in industrial sectors. The intermittency of the waste heat or steam stems from the process schedule, while that of the renewable arises from the inherent variability of wind, sunlight, or waves. The TES output can be either heat or steam when the demand exceeds the generation. Despite many studies analysed RES Heat and Waste

Heat integration potential in industrial sector as a whole, several studies discussed TES application in individual industrial sectors. Previous studies focused on specific industries like food, ceramics, or energy-intensive sectors [2]. The related research to date has tended to focus on a particular type of TES for a specific application or sector. Thus, the TES potential in the whole industrial sector is not so well addressed. The present aims to fill this gap and make a comparative analysis of all the EU industrial sectors and look at the industrial energy system as a whole. This holistic perspective enables us to prioritise the investments and deployment of TES systems benefiting both industry and society through energy transition and decarbonization.

## 2. Methodology

This study demonstrates sector-level analysis in the EU industries using statistical data from various sources [3] as well as process data, i.e., average heat and steam demands in various industries [4]. Process specifications for ten industrial sectors in the EU are extracted. The average energy consumption in the forms of heat and steam is assessed at plant, and sector levels. Three types of TES for the purposes of WHR maximisation (CASE 1), buffering of the steam supply by steam storage (CASE 2), and heat generation by low-cost electricity (CASE 3) are assumed to be integrated into industry, and their capacities are derived separately.

**CASE 1)** TES potential for WHR ( $Q_{TES,WHR}$ ) is subjected to the recovery of variable waste heat sources available in industrial processes. The recoverable heat percentage ( $Q_r$ ) is taken from the literature [5] as the maximum theoretical efficiency of WHR known as Carnot efficiency. A correction factor (CF), Eq. 1, accounts for the overlap between the TES operating temperature ( $T_{TES}$ ), assumes as 150 to 1000°C, and process heat temperature ( $T_p$ ). Therefore, the achievable heat by TES ( $Q_{TES,WHR}$ ) is calculated by Eq. 2:

$$CF_{TES} = \max(\min(T_{max,p}, T_{max, TES}) - \max(T_{min,p}, T_{min, TES}), 0) / (T_{max,p} - T_{min,p}) \quad (1)$$

$$Q_{TES,WHR} \text{ [MWh/day]} = Q_{plant} \times Q_r \times CF_{TES} \quad (2)$$

**CASE 2)** TES potential for steam supply purpose ( $Q_{TES,S2S}$ ) is defined as the recoverable heat by steam storage integrated into the industrial plant to balance steam supply/demand. This type of TES is able to store the excess of produced steam and shave peaks of steam loads. The recoverable steam by TES is assumed to be 5% of the steam used for process heating in each plant.

**CASE 3)** TES potential for power to heat ( $Q_{TES,P2H}$ ) is determined by the heat supplied by TES, exploiting low-cost electricity to fulfill 50% of the plant process heat demand. The plant scale TES capacity ( $C_{TES}$ ) is defined, as shown in Eq.3, for all types of TES as a function of cycle time (CT), including the charging and discharging.

$$C_{TES} \text{ [MWh]} = Q_{TES} \text{ [MWh/day]} / 24 \times (CT \text{ [hr]} / 2) \quad (3)$$

The emissions and the corresponding CO<sub>2</sub> costs are calculated based on energy and fuel saving from TES integration. Natural gas, with an emission reference of 230 gCO<sub>2</sub>/kWh, is assumed as the energy source. Electricity price, natural gas price (non-household consumers), and carbon price (EU ETS) from the EU 5-year average data (2017-2021) [6] are used in the assessment. Also, the electricity price includes a 64% night tariff discount in Germany.

Table 1. Assumptions for the technical, economic, and environmental assessments

Parameter		Unit	Value
TES	Number of cycles (NC)	1/yr	WHR 360; S2S 720; P2H 360
	cycle time (CT)	hr	WHR 6; S2S 3; P2H 12
	Reference cost ( $C_{TES,ref}$ )	€/Mwh	WHR 100; S2S 75; P2H 125
Steam / Electricity / NG price		€/kWh	0.034 / 0.082 / 0.027



The operating cost reduction is achieved by estimating the saving on cost of fuel ( $C_{f,sav}$ ) and cost of carbon ( $C_{C,sav}$ ):

$$C_{f,sav}^{plnt} = C_{TES} [MWh] \times NC \times \text{Gas Price} \quad (4)$$

$$C_{C,sav}^{plnt} = C_{TES} [MWh] \times NC \times \text{Emission [kgCO}_2\text{e/MWh]} \times \text{EUETS} \quad (5)$$

These parameters are calculated at plant-level for each TES type which can be scaled up to the sector level using the number of active sites ( $N_{sct}^{plnt}$ ). The economic viability is assessed by using the initial investment (CapEx). CapEx is given by Eq. 6 using the scaling exponent ( $\gamma = 0.75$ ).

$$\text{CapEx} = \text{CapEx}_{ref} \times (C_{TES,ref}/C_{TES})^\gamma \quad (6)$$

The cash flow for WHR and S2S approaches is the sum of saved fuel and CO<sub>2</sub> costs, while P2H cash flow also includes electricity cost. The payback period (PBP) is derived by dividing the investment required for each type of TES by the annual cash flow (F):

$$\text{PBP}_{TES} = \text{CapEx}_{TES}/F \quad (7)$$

The parameter which can be a basis for EU-level decision-makers in the EU industries decarbonisation is the total potential of emission abatement in the EU by all three types of TES, defined as the sum of the individual sector-level potential for each TES type. A dimensionless country-level potential index is also defined using the top three sectors with the highest potential.

$$PI_{sct,EU} = \sum_{sct} (N_{EU}^{plnt} \times C_{saving}^{plnt})_{WHR} + (N_{EU}^{plnt} \times C_{saving}^{plnt})_{S2S} + (N_{EU}^{plnt} \times C_{saving}^{plnt})_{P2H} \quad (8)$$

$$PI_{ctry} = \sum_{type} \sum_{sct} (N_{ctry}^{plnt} \times C_{sav}^{plnt})_{TES} / \sum_C \sum_{sct} (N_{EU}^{plnt} \times C_{sav}^{plnt})_{TES} \times 100 \quad (9)$$

( $\forall sct \in \{\text{Refinery, Ceramics, Food}\}, ctry \in \{\text{EU28}\}, type \in \{\text{WHR, S2S, P2H}\}$ )

### 3. Result and discussion

The calculation is conducted for all TES types using the plant-level process data and sector-level statistics. Figure 2a presents the plant-level demand estimation for the process heat and steam attributed to each sector, with refineries and paper sectors having the highest steam demand. The refinery, cement, and metal industries have the most process heat, followed by chemical plants. Comparing process heat temperatures across sectors (Figure 2b) provides insights into TES applicability. The food industry, for instance, has the least overlap with TES temperature.

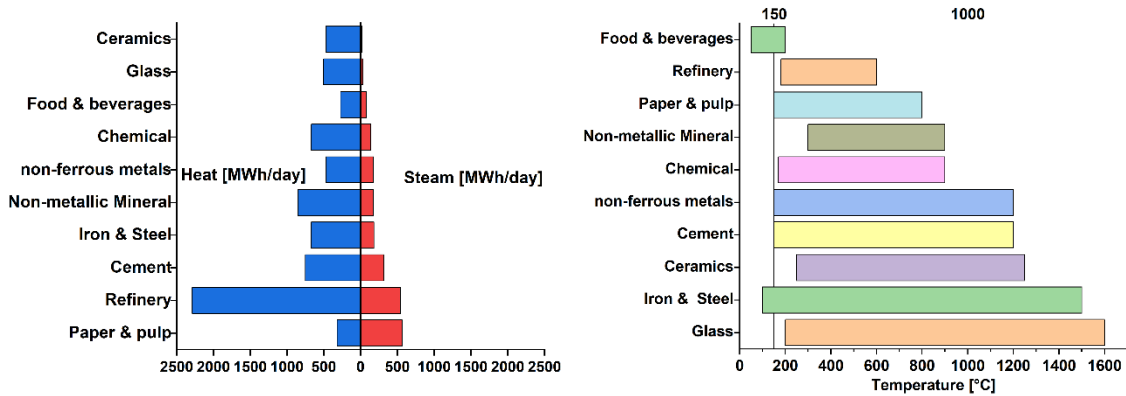


Fig 2. plant-level heat and steam demand (a: left); Process heat and TES temperature ranges (b: right)

The economic results, CapEx and PBP, are shown in Fig 3 at the plant-level sorted from lowest to highest. Due to the higher energy capacity foreseen in the P2H application, the CapEx and PBP are remarkably higher than the other two. The highest CapEx is identified for the refinery with the highest energy demand. This sector has the lowest PBP; making it suitable for TES investment. This potential ranking is conducted at the plant level, where only energy demands and temperature ranges are considered. Hence a sector-level analysis is required to see if refinery, the largest energy user in the EU industry, has the highest impact on energy transition.

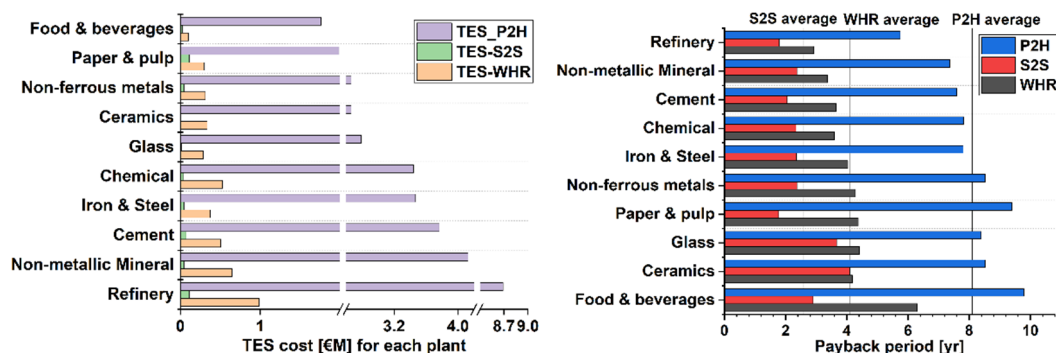


Fig 3. Plant-level CapEx (a: left) and payback period (b: right) with different TES types

Fig 4a shows the energy-saving potential of sectors, with the refinery, ceramics, and food industries showing the highest potential to reduce emissions by up to 7 MtCO<sub>2</sub>e. These sectors, with the highest impact on energy saving and emission reduction, are separately used for the country-level estimation. The PI<sub>ctry</sub> is demonstrated in Fig 4b, where Spain recorded the highest emission reduction potential (16%), followed by Italy (12%). By contrast, the lowest potential was found in countries with i.e. Estonia, Latvia, and Slovenia with less active sites in these sectors.

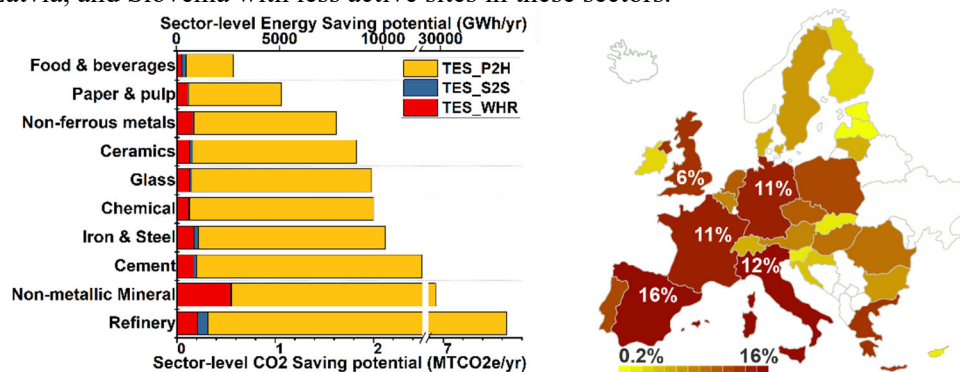


Fig 4. Sector-level potential energy and CO<sub>2</sub> saving (a: left), PI<sub>ctry</sub> across EU (b: right).

## 4. Conclusions

Hitting net zero entails rapid uptake of innovative energy solutions. Among energy transition enablers, TES has the potential to facilitate the transition, thanks to a flexible technology for different processes. This study informs the ongoing debate around the TES viability for EU industry decarbonization by quantifying the maximum TES potential at plant, sector, and country levels, identifying sectors of refineries, ceramics, and food with the highest impact on emission reduction. Spain and Italy are identified as countries expected to gain the most from TES implementation. These guidelines support the EU-level investment strategies in TES technology.

## 5. Acknowledgements

Dr Sciacovelli acknowledges the funding received from the EU Horizon Europe research innovation program (ZHENIT Project, GA 101056801) and the UK Research and Innovation (UKRI)

## 6. References

- [1] P Arnout, D Pinner, Decarbonization of industrial sectors: the next frontier, 2018 [Online].
- [2] P Niknam, A Sciacovelli, Hybrid PCM-steam TES for industries, Appl Energy 331, 2023.
- [3] R Quintana, Quantified potential of industrial symbiosis in Europe, 2020.
- [4] C McMillan, Generation and use of thermal energy in US Industrial sector, 2016.
- [5] C Paterson, First Release of So What Industrial Sectors Wh/C Recovery Potential, 2019.
- [6] Database - Eurostat - European Commission, europa.eu, 2021.

EUROTHERM2023-S165

## Athilea, a tool for the assessment of interior wall insulation solution

Rafael Monge Palma<sup>1a</sup>, Teresa Palomo Amores<sup>1b</sup>, MPaz Montero-Gutiérrez<sup>1c</sup>, MCarmen Guerrero Delgado<sup>1d</sup>, José Sánchez Ramos<sup>1e</sup>, Servando Álvarez Domínguez<sup>1f</sup>

<sup>1</sup>Grupo Termotecnia, Energy Engineering Dept., University of Seville, Spain, e-mail: <sup>a</sup>rmonge1@us.es ,  
<sup>b</sup>tplomo@us.es , <sup>c</sup>mmontero1@us.es , <sup>d</sup>mgdelgado@us.es , <sup>e</sup>jsr@us.es , <sup>f</sup>salvarez@us.es

### Abstract

Renovating a building can be a challenge when urban or architectural constraints do not allow the application of external thermal insulation systems. To fulfil the building code requirements and allow buildings to provide adequate levels of comfort and energy demand, the improvement of the thermal envelope needs to be carried out on the inside. This work presents an Excel® VBA tool to assess the impact of interior wall insulation on the loss of usable floor area and demand improvement. Based on a catalogue of six buildings representative of the Spanish building stock (three multi-family buildings and three single-family buildings), the user can define all the elements of the thermal envelope, as well as the climate zone or city, and insulation to be compared, making it possible to assess the expected cost of floor area loss and verify the compliance with regulatory requirements.

**Keywords:** Building renovation; Floor area loss; Energy efficiency; Insulation solutions; Residential buildings.

### 1. Introduction

Is not a novelty that the building sector represents a non-depreciable impact on the energy demand. Over the last years we have seen a refinement of the requirements for the building's thermal envelope [1], [2] to lead to buildings less energy-demanding without compromising the comfort of the occupants. However, most of the existing buildings are not energy-efficient [3], especially when 85% of the EU's building stock was built before the first Building Performance Directive [4]. Considering that, an effort is being done by the European Commission with the EU Renovation Wave program to the promotion renovation of the existing building stock [4]. Nevertheless, renovating a building, if not mandatory by law, is in most cases a voluntary decision. The main motivations for renovating a building rely on reducing energy bills and vulnerability to the energy market, increasing the property value and the ability to return the investment [5]. Yet, being a voluntary decision, the building owners need to have all the relevant information for their making-decision process. This information is more relevant when we are facing cases of a building where the urban or architectural constraints oblige a non-invasive technique of thermal insulation of the façade. For those cases, to fulfil the requirements of the minimum external wall transmittance value a loss of usable floor area will occur.

The studies of building thermal envelope refurbishment focus on finding the optimal cost solution [6], but the impact on the possibility of losing usable floor area is not considered. This work introduces a VBA Excel app tool to assess the impact of applying an internal insulation system on the usable floor area and energy demand. This tool was developed with industry experts and distributors, to provide quick and precise decisions for the deep renovation of buildings up to the nZEB or Passivhaus Standard level.

## 2. Materials and method

Applying insulation to the inner surface of a façade will lead to an improvement of the thermal envelope, but which insulation material will save more floor area? And how much will be the energy demand? Answering that two simple questions can rely on two paths for estimating the energy demand of a building: detailed and simplified. Although a detailed method based on building thermal simulation can produce more accurate estimations of the energy demand, the truth is a method that is time-consuming and requires a high level of expertise. A simplified method proposed by [7] is considered to compute the energy demand, due to simplicity can be easily integrated into a VBA Excel® environment. Nevertheless, this procedure requires a definition of adjusting coefficients that depends on the climate zone and building geometry. To overcome that limitation a building catalogue of six buildings was conceived (three multi-family buildings and three single-family buildings) considering the reference buildings of the building stock defined by the Spanish Directorate for Architecture, Housing and Planning [8], [9].

Making an understandable and user-friendly interface was the main objective during the development of this tool. For that, no external files are necessary to upload to compute a simulation. A dual weather database is available on the tool, where is included the twelve reference climates of the technical building code for peninsular Spain and the climates of each provincial capital. Also, all inputs necessary to the definition of the thermal envelope tool have pre-defined values. Figure 55 summarizes the steps and the input data required. On the building selection step, the user can access the geometrical characteristics of the reference buildings by pressing a help button.

**STEP 1: DATABASE**

Insulation thermal conductivity

Insulation material	Soilstone	Mineral Fibre	XPS	Other 1	Other 2
Thermal conductivity (W/m·K)	0.018			press to insert a value	press to insert a value

Energy and CO<sub>2</sub> emissions cost and conversion factors

vector energético	energy cost €/kWh	CO <sub>2</sub> emissions cost €/ton	CO <sub>2</sub> emissions conversion factor kg/kWh	primary energy conversion factor kWh/kWh	Total kWh/kWh	Non-renewable
Electricity						
Natural Gas						

**STEP 2: CLIMATE AND BUILDING**

Climate

City:

Climate Zone:

Building:  Building use:  Building type:

Building Elements

Avg. Roof U-value (W/m <sup>2</sup> ·K)	Avg. Floor U-value (W/m <sup>2</sup> ·K)	Avg. Window U-value (W/m <sup>2</sup> ·K)	Windows g-value, winter season (1)	Windows g-value, summer season (1)	Thermal Bridges (Q-value) (W/m <sup>2</sup> ·K)	Conditions

Air Leakage Rate (n<sub>50</sub> (h<sup>-1</sup>)) Summer Night Ventilation Rate (h<sup>-1</sup>) Conditions

**STEP 3: COMPARISON SCENARIO**

Select insulation materials

Insulation material	conductivity (W/m·K)	option	Thermal Resistance (m <sup>2</sup> ·K/W)	Insulation Material	Material Cost (€/m <sup>2</sup> )	Insulation Cost (€/m <sup>2</sup> )
Soilstone	0.018	<input type="radio"/>		Soilstone		
Mineral Fibre	0.035	<input type="radio"/>		XPS		
XPS	0.032	<input type="radio"/>		Other 1		
Other 1	0.048	<input type="radio"/>		Other 2		
Other 2	0.037	<input type="radio"/>				

Comparison value:

economic data

Insulation Material:  Material Cost (€/m<sup>2</sup>):  Insulation Cost (€/m<sup>2</sup>):

Soilstone:  XPS:

help floor market val. (€/m<sup>2</sup>):

- 1 Definition of insulators and their thermal conductivity
- 2 Energy and CO<sub>2</sub> emissions cost, and conversion factors
- 3 Selection of the climate
- 4 Selection of the building
- 5 Definition of the thermal envelope
- 6 Selection of the insulator material and thermal resistance for comparison
- 7 Definition of the material costs and property value

Figure 55. User interface and steps to compute a simulation.

## 3. Results and discussion

Figure 56 presents the results interface of the tool, where the user can overview the thermal envelope of the building, the energy demand, and the costs of each insulating system. Also, it is showed the net space saved as well as the economical savings.

Figure 57 presents two cases assessed by the tool for all Spanish winter zones. A comparison between two insulators and how the cost difference is influenced by the property value. This figure shows the impact of accounting for the lost usable floor area on the total cost of the renovation. When considered this variable it turns out that the property value has an impact on the definition of the choice of insulation system. Looking from a perspective of space savings potential, Figure 58 shows that the detached single-family home can save up to 9% of floor area by using a low thermal conductivity insulator instead of a

conventional solution. A lower savings potential is expected for multifamily buildings due to their higher compactness.

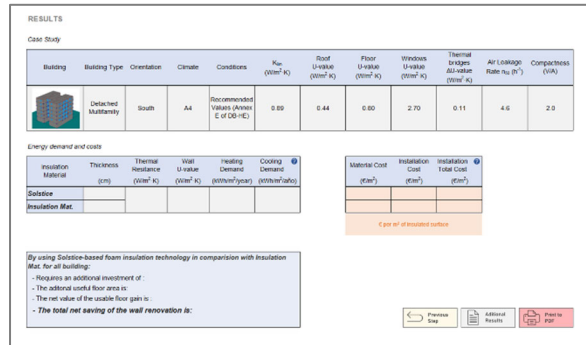


Figure 56. Results report interface.

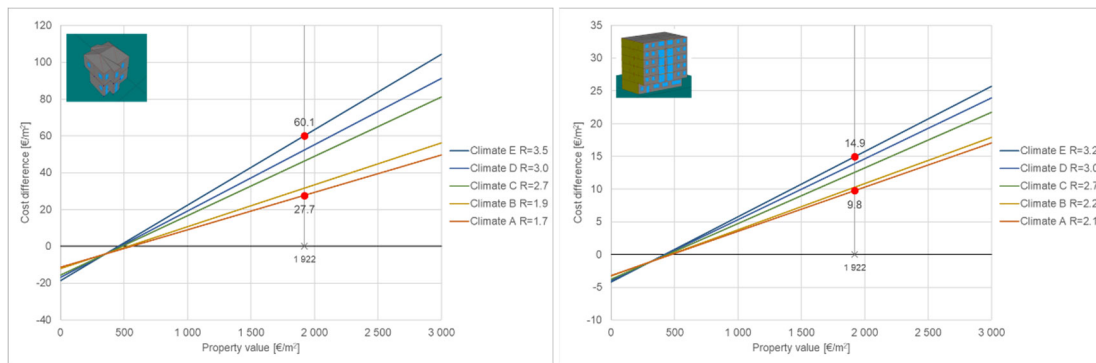


Figure 57. Comparison of a low thermal conductivity insulator and a mineral fibre board for a detached single-family home (left) and an attached multifamily building (right) across all Spanish winter zones. The average Spanish property value is highlighted [10].

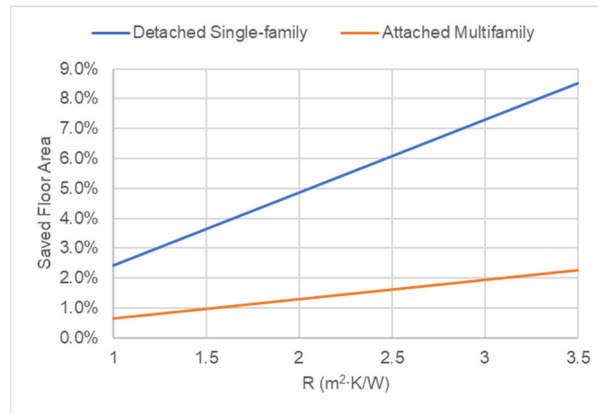


Figure 58. Low thermal conductivity insulator versus mineral fibre board: saved floor area potential example.

## 4. Conclusions

Applying interior insulation represents a non-neglectable effect on the loss of usable floor area, especially in climates with cold winters. The developed tool helps the building designers to estimate this impact as well as compliance with the building code and the expected energy demand of the renovated building. Athilea app is free and available on this [link](#).

## Acknowledgements

This study has been funded by the projects "CONSTANCY - Resilient urbanization methodologies and natural conditioning using imaginative nature-based solutions and cultural heritage to recover the street

life" (Grant Agreement PID2020-118972RB-I00) and the project "NATURBEAM - Lighting the way to a greener future to restore urban habitability through nature-based solutions" (Grant Agreement TED2021-130416B-I00) by the Science and Innovation Ministry of Spain. Also, this study has been co-financed by the European Regional Development Funds (ERDF).

## References

- [1] Ministerio de Fomento, "Real Decreto 732/2019, de 20 de diciembre, por el que se modifica el Código Técnico de la Edificación, aprobado por el Real Decreto 314/2006, de 17 de marzo," *Boletín Oficial del Estado*, vol. 311, pp. 140488–140674, Dec. 2019.
- [2] European Parliament and of the Council, "Directive (EU) 2018/844 of the European Parliament and of the Council of 30 May 2018 amending Directive 2010/31/EU on the energy performance of buildings and Directive 2012/27/EU on energy efficiency," *European Union. Official Journal of the European Union*, Strasbourg, Jun. 19, 2018.
- [3] E. Commission, J. R. Centre, F. Filippidou, and J. Jimenez Navarro, *Achieving the cost-effective energy transformation of Europe's buildings: combinations of insulation and heating & cooling technologies renovations: methods and data*. Publications Office, 2019. doi: doi/10.2760/278207.
- [4] European Commission, "A Renovation Wave for Europe - greening our buildings, creating jobs, improving lives. COM(2020) 662 final.," *Communication from the Commission to the European Parliament, the Council, the European Economic and Social Committee and the Committee of the Regions*. Official Journal of the European Union, Brussels, Oct. 14, 2020.
- [5] J. Friege and E. Chappin, "Modelling decisions on energy-efficient renovations: A review," *Renewable and Sustainable Energy Reviews*, vol. 39, pp. 196–208, Nov. 2014, doi: 10.1016/j.rser.2014.07.091.
- [6] J. Fernandes, M. C. Santos, and R. Castro, "Introductory Review of Energy Efficiency in Buildings Retrofits," *Energies (Basel)*, vol. 14, no. 23, p. 8100, Dec. 2021, doi: 10.3390/en14238100.
- [7] J. Sánchez Ramos, Mc. Guerrero Delgado, S. Álvarez Domínguez, J. L. Molina Félix, F. J. Sánchez de la Flor, and J. A. Tenorio Ríos, "Systematic Simplified Simulation Methodology for Deep Energy Retrofitting Towards Nze Targets Using Life Cycle Energy Assessment," *Energies (Basel)*, vol. 12, no. 16, p. 3038, Aug. 2019, doi: 10.3390/en12163038.
- [8] Directorate for Architecture Housing and Planning - Ministry of Development of Spain., "Report on cost optimal calculations and comparison with the current and future energy performance requirements of buildings in Spain." Ministry of Development of Spain, Dec. 2018.
- [9] Directorate for Architecture Housing and Planning - Ministry of Development of Spain, "Report on cost optimal calculations and comparison with the current and future energy performance requirements of buildings in Spain." Ministry of Development of Spain, Madrid, Jun. 07, 2013.
- [10] idealista/data, "Evolución del precio de la vivienda en venta en España," *Idealista informe de Precios*, Jan. 2023. <https://www.idealista.com/sala-de-prensa/informes-precio-vivienda/> (accessed Feb. 14, 2023).

EUROTHERM2023-N166

## How much can save a Spanish residential building by changing its thermostat?

Rafael Monge Palma<sup>1a</sup>, Teresa Palomo Amores<sup>1b</sup>, MPaz Montero-Gutiérrez<sup>1c</sup>, MCarmen Guerrero Delgado<sup>1d</sup>, José Sánchez Ramos<sup>1e</sup>, Servando Álvarez Domínguez<sup>1f</sup>

<sup>1</sup>Grupo Termotecnia, Energy Engineering Dept., University of Seville, Spain, e-mail: <sup>a</sup>rmonge1@us.es , <sup>b</sup>tplomo@us.es , <sup>c</sup>mmontero1@us.es , <sup>d</sup>mgdelgado@us.es , <sup>e</sup>jsr@us.es , <sup>f</sup>salvarez@us.es

### Abstract

Extending the set-point temperature have a direct impact on the building energy demand as well as on the occupant's thermal comfort. This measure is being promoted by European Commission to mitigate the effect of the current energy crisis. Therefore, how much a Spanish residential building can save by extending its set-point temperature? This study conducted a massive simulation covering six building models, 8 034 locations in peninsular Spain, 9 Koppen-Geiger climates and two construction periods, where 20°C and 25°C are the reference heating and cooling set-point temperatures, respectively. Results indicate on average, a demand reduction of 20% by lowering 1°C the heating set-point and a 25% cooling demand reduction by rising in 1°C the set-point temperature. Indicating that householders can contribute to mitigating the energy crisis without compromising their thermal comfort expectations and exceeding the IEA target.

**Keywords:** Energy policy; Thermostat; Potential energy savings; Residential buildings;

### 1. Introduction

Europeans are facing a natural gas supply crisis caused by the Russian-Ukrainian conflict. On July 2022 the European Commission proposed a gas demand reduction plan, which asks all Member States to reduce their dependence on gas by 15% [1]. That plan includes a wide range of measures that are suggested to the Member States, and one of them is the promotion of the reduction of heating and cooling demand [2]. According to the International Energy Agency (IEA) moving 1°C in our thermostats can lead to a reduction of 7% and 10% in heating and cooling demand, respectively, for the European residential building stock [2]. Nevertheless, the potential of savings in each country depends on their building stock characteristics and climate. So, asking citizens to adopt new indoor comfort levels should be based on data proper data.

This work will study the extension of the set-point temperature in Spain for a sample of six buildings representative of the Spanish building stock: three single-family buildings and three multifamily buildings. Also, are considered two periods of building regulation, the first and the latest implemented, to assess the possible range of potential savings and the relevance of the thermal envelope. This study covers all of Spain's peninsular municipalities being a reliable information source for the regulatory authorities in the decision-making process.

### 2. Materials and method

#### Buildings

A building catalogue of six buildings was conceived (three multi-family buildings and three single-family buildings) considering the reference buildings of the building stock defined by the Spanish Directorate for Architecture, Housing and Planning [3,4], for the cost-optimal calculations report under the Energy Performance Buildings Directive (Directive 2010/31/EU). The thermal envelope of the

buildings was defined according to the first (NBE-CT-79 [5]) and the latest (Royal Decree 732/2019 [6]) Spanish Technical Building Code. Each building's thermal envelope was defined to fulfil strictly the regulation requirements, i.e, each surface U-value and air permeability was defined to equal to the maximum allowed value by the building code. It also accounted for the lineal thermal bridge effect by incrementing the U-value of each surface. This increment corresponds to the average increment of the building's overall U-value. This effect was accounted for using the recommended values in the literature [7,8]. For the 1979 buildings, the lineal thermal bridges effect is not accounted in the definition of the maximum allowed surface U-values. The characteristics of considered building models are available in *Annex*.

### Climate

Coverage of all nine Koppen-Geiger climates of the Spanish peninsular is guaranteed by considering two free available weather databases to generate typical meteorological years (TMY) representative of the current climate for the 8 034 Spanish peninsular municipalities: Climate.OneBuilding.Org [9] and TMY generator of the PVGIS web-based tool [10]. 92 municipalities are covered by the Climate.OneBuilding.Org database and the remaining municipalities by the PVGIS TMY generator. The TMY files were created in .epw format to perform building thermal simulations with EnergyPlus.

### Temperature set-points

Table 9 presents the studied temperature set-points. The reference indoor range temperature was defined as 20-25°C, which corresponds to the definition of room temperature [11], as also the comfort range indicated in the Spanish Building Code [6]. The minimum heating set-point considered was defined as 17°C under the ASHRAE 55-2020 Standard [12]. The maximum cooling set-point considered was defined as 30°C. For the authors, a value above 30 °C is too high in conditioned spaces.

Table 9. Set-point temperatures (°C) for heating and cooling systems.

Heating	20	19	18	17		
Cooling	25	26	27	28	29	30

### Simulation

The simulation was performed using the EnergyPlus integrated into a developed VBA Excel® app. This app was able to generate an IDF file according to the building model and their location, run a simulation for each temperature set-point and save the results. An ideal load model was used to determine the heating and cooling load. This model simulates an ideal system to supply conditioned air to the zone that meets all the load requirements. The occupancy profile was defined according to Ahmed *et al.* [13]. Also was considered the suggested appliances and lighting usage profiles for residential buildings [13]. Regarding the last household survey in Spain [14], it was assumed for each dwelling a nominal occupancy of 3 persons. The ideal loads model considers the minimum outdoor airflow to ensure indoor air quality, which corresponds to 0.15 L/s·m<sup>2</sup> of floor area and 3.5 L/s·person [15].

## 3. Results and discussion

**Figure 59** indicates the expected energy savings potential by extending the set-point temperature. This figure presents the average savings and the variation range, in kWh/m<sup>2</sup>/year, for each building typology and construction year. Decreasing the set-point temperature by 1°C during the winter season has more impact on the demand than increasing by 1°C the set-point temperature during the summer season. Also, is observed a higher savings potential in the oldest building stock, being able the 1979's buildings save up to 2.9 times more on heating demand and 2.0 times more on cooling demand in comparison with the latest buildings.



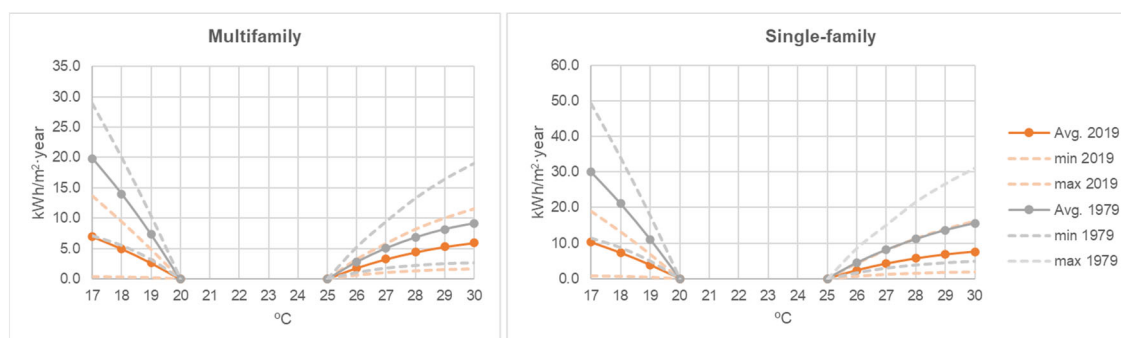


Figure 59. Annual demand savings for the studied set-point temperatures per building typology and construction year.

Looking at **Figure 60** the savings potential in percentage gives a different overview, especially because the percentages of savings have a slight variation between construction years and building typology. This is due to the fact of the building models are exposed to the same outdoor and indoor conditions. However, **Figure 60** shows that we can expect a demand reduction of 20% by lowering in 1°C the heating set-point, and rising in 1°C the cooling set-point by 25% of demand reduction is expected. Also, going to extreme set-point temperatures for heating or cooling, a huge reduction is obtained and for some locations that reduction can reach easily values above 90%.

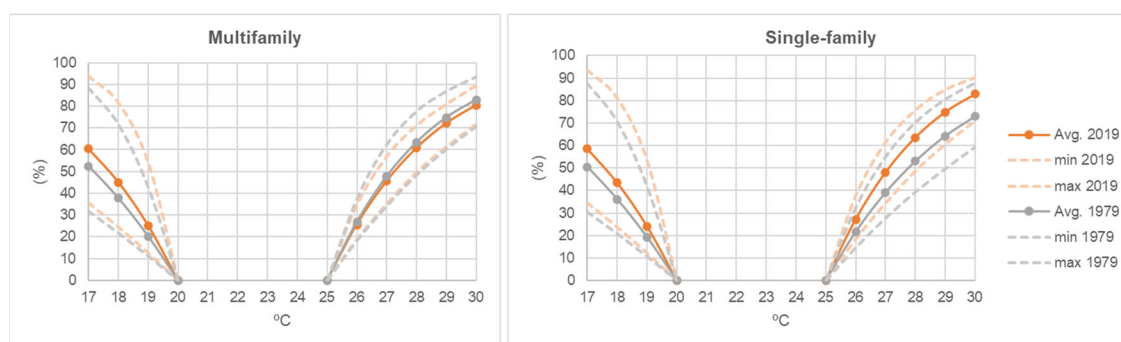


Figure 60. Percentage of demand savings for the studied set-point temperatures per building typology and construction year.

## 4. Conclusions

The percentage of demand reduction by extending the set-point temperature has a slight variation between building typologies and construction years, therefore is expected at least, on average, a demand reduction of 20% by lowering 1°C the heating set-point and 25% cooling demand reduction by rising in 1°C the set-point temperature. Although the similarity of the demand reduction percentages, the absolute savings vary with the building typology and construction year, where the oldest building stock shows a higher savings potential being able to save up to 2.9 times more than the latest buildings. Also, extending the heating set-point temperature have a higher relevance than rising the cooling set-point.

This work quantified a higher savings potential when compared with the International Energy Agency projections, indicating that householders can contribute to mitigating the energy crisis without compromising their thermal comfort expectations.

## Acknowledgements

This study has been funded by the projects "CONSTANCY - Resilient urbanization methodologies and natural conditioning using imaginative nature-based solutions and cultural heritage to recover the street life" (Grant Agreement PID2020-118972RB-I00) and the project "NATURBEAM - Lighting the way to a greener future to restore urban habitability through nature-based solutions" (Grant Agreement

TED2021-130416B-I00) by the Science and Innovation Ministry of Spain. Also, this study has been co-financed by the European Regional Development Funds (ERDF).

## References

- [1] European Commission, Communication from the Commission to the European Parliament, the Council, the European Economic and Social Committee and the Committee of the Regions. Save gas for a safe winter., COM(2022) 360 Final. (2022).
- [2] International Energy Agency, European Commission, Playing my part. How to save money, reduce reliance on Russian energy, support Ukraine and help the planet, IEA Publications. (2022). <https://iea.blob.core.windows.net/assets/cbc97c70-8bcf-4376-a8a9-4cd875195f6a/Playingmypart.pdf> (accessed September 16, 2022).
- [3] Directorate for Architecture Housing and Planning - Ministry of Development of Spain., Report on cost optimal calculations and comparison with the current and future energy performance requirements of buildings in Spain., (2018).
- [4] Directorate for Architecture Housing and Planning - Ministry of Development of Spain, Report on cost optimal calculations and comparison with the current and future energy performance requirements of buildings in Spain., (2013).
- [5] Presidencia del Gobierno, Real Decreto 2429/1979, de 6 de julio, por el que se aprueba la norma básica de edificación NBE-CT-79, sobre condiciones térmicas en los edificios, Boletín Oficial Del Estado. 253 (1979) 24524–24550. <https://www.boe.es/eli/es/rd/1979/07/06/2429> (accessed December 5, 2022).
- [6] Ministerio de Fomento, Real Decreto 732/2019, de 20 de diciembre, por el que se modifica el Código Técnico de la Edificación, aprobado por el Real Decreto 314/2006, de 17 de marzo, Boletín Oficial Del Estado. 311 (2019) 140488–140674.
- [7] Dirección General de Arquitectura Vivienda y Suelo, DA DB-HE / 3. Puentes Térmicos., Código Técnico de La Edificación. (2019).
- [8] International Standards Organization, EN ISO 14683:2020. Thermal bridges in building construction - Linear thermal transmittance - Simplified methods and default values., (2020).
- [9] L. Lawrie, D.B.C. K, Development of Global Typical Meteorological Years (TMYx), Climate.OneBuilding.Org. (2022). <http://climate.onebuilding.org> (accessed December 14, 2022).
- [10] Joint Research Centre. European Commission., PVGIS Photovoltaic Geographical Information System, (2022). [https://re.jrc.ec.europa.eu/pvg\\_tools/en/](https://re.jrc.ec.europa.eu/pvg_tools/en/) (accessed December 14, 2022).
- [11] The United States Pharmacopeial Convention, <659> Packaging and Storage Requirements. Revision Bulletin, Postponement., USP-NF Standards. (2017).
- [12] A. ASHRAE, Standard 55-2020: Thermal environmental conditions for human occupancy, American Society of Heating, Refrigerating, and Air-Conditioning Engineers, Inc. Atlanta. (2020).
- [13] K. Ahmed, A. Akhondzada, J. Kurnitski, B. Olesen, Occupancy schedules for energy simulation in new prEN16798-1 and ISO/FDIS 17772-1 standards, Sustain Cities Soc. 35 (2017) 134–144. <https://doi.org/10.1016/j.scs.2017.07.010>.
- [14] Instituto Nacional de Estadística, Continuous Household Survey, Year 2020., Press Releases. (2021).
- [15] ASHRAE, 2017 ASHRAE® Handbook - Fundamentals (SI Edition), American Society of Heating Refrigerating and Air-Conditioning Engineers Inc., 2017.

## Phase change microcapsule based composites for middle- to high-temperature thermal energy storage

Takahiro Kawaguchi<sup>1</sup>, Melbert Jeem<sup>2</sup>, Takahiro Nomura<sup>2</sup>

<sup>1</sup>Graduate School of Engineering, Hokkaido University, Japan, Phone: 81-11-7066842,  
e-mail: kawataka@eng.hokudai.ac.jp

<sup>2</sup>Faculty of Engineering, Hokkaido University, Phone: 81-11-7066842,  
e-mail: nms-tropy@eng.hokudai.ac.jp

### Abstract

Latent heat storage using alloy-based phase change materials (PCM) is expected to be applied to high-temperature heat utilization because of its ability to store heat at high density and constant temperature. Previously, to prevent corrosion of alloy PCMs, Microencapsulated PCM (MEPCMs) with stable oxide coatings on the surface of the alloy particles have been developed. By oxide coating of MEPCM, it is expected that composite PCM can be prepared by combined with sintering aids. In this study, the fabrication of composite PCM using Al-12 mass% Si MEPCM and the sintering aid was investigated. The composite PCM with a high latent heat capacity of 224.09 J g<sup>-1</sup> was successfully prepared under conditions containing 30 vol% of glass frit as a sintering aid. The composite PCM is expected to be applied to heat utilization systems because of its excellent performance.

**Keywords:** Latent heat storage, Microcapsule, Composite material

### 1. Introduction

In recent years, high-temperature thermal energy storage (TES) has become increasingly relevant for thermal systems application because of its ability to reduce output fluctuations from heat sources and storing renewable energies as heat. Latent heat storage (LHS) achieved by melting or solidification of phase change materials (PCMs) is suitable for high-temperature TES because it stores heat at a constant temperature and high density [1]. The storage temperature of LHS is determined by the melting point of the PCM, and alloys and molten salts have been proposed as the PCMs that operate at high temperatures. Owing to their high thermal conductivity, alloys systems are rather promising as PCMs, which capable to store and release heat quickly. However, alloy PCM is highly corrosive when melted and can corrode structural materials [2].

Therefore, microencapsulated PCMs (MEPCMs) were developed, in which the surface of the alloy PCM is covered with a chemically and thermally stable oxide coating [3]. Through its durable ceramic's coating, a composite of MEPCM mixed with other materials is feasible. In particular, complexing with sintering aids is expected to allow the fabrication of composite PCMs containing the MEPCM. In this study, we attempted to fabricate composite PCM by consisting of the Al-12 mass% Si eutectic alloy MEPCM and glass frit as a sintering aid.

### 2. Materials and method

Al-12 mass% Si alloy particle (average diameter: 31.7 μm) was used as a raw material for making the MEPCM. The sintering aid for the composite PCM preparation was glass frit (average diameter: 14.6 μm, composition: Al<sub>2</sub>O<sub>3</sub>, SiO<sub>2</sub>, MgO, ZnO, BaO, La<sub>2</sub>O<sub>3</sub> and B<sub>2</sub>O<sub>3</sub>).

The MEPCM that comprise composite PCM were obtained in two steps: a boehmite treatment to form a precursor coating of hydroxide on the alloy particles and a heat-oxidation treatment at high temperature to provide an oxide coating.  $333 \text{ g L}^{-1}$  of alloy particles were added to boiling water in which  $3.3 \text{ g L}^{-1}$   $\text{Al}(\text{OH})_3$  particles was suspended and pH9 was maintained with ammonia solution, and held for 3 h to perform the boehmite treatment. Thereafter, the particles were oxidized in air at  $1200 \text{ }^\circ\text{C}$  for 3 h to make the MEPCM.

For the fabrication of composite PCM, a powder mixture with MEPCM containing 20 vol% or 30 vol% of the glass frit was prepared. 0.5 g of the mixed powder was pressed at 20 MPa for 1 min at  $25 \text{ }^\circ\text{C}$  to produce a pellet-like compact. The compact was heat-treated in air at  $800 \text{ }^\circ\text{C}$  for 1 h. The composite PCMs were named GF20 or GF30 depending on the content of the glass frit.

### 3. Results and discussion

#### 3.1. Morphology of composite PCM

Figure 1 shows the overview of prepared composite PCM. GF20 and GF30 have the structure of the pellet shape. GF20 was found to have cracks on its surface, and its surface was so brittle that powder fell little by little just by touching it. However, GF30 held its shape well. The effect of sintering by the glass frit shows to work well with the addition of 30 vol%. In addition, XRD measurements on the composite PCM revealed peaks specific to the glass frit as well as Al and Si from the Al-12 mass% Si alloy. Therefore, the Al-12 mass% Si alloy inside the MEPCM is retained even after heat treatment at  $800 \text{ }^\circ\text{C}$  for fabrication of the composite PCM.

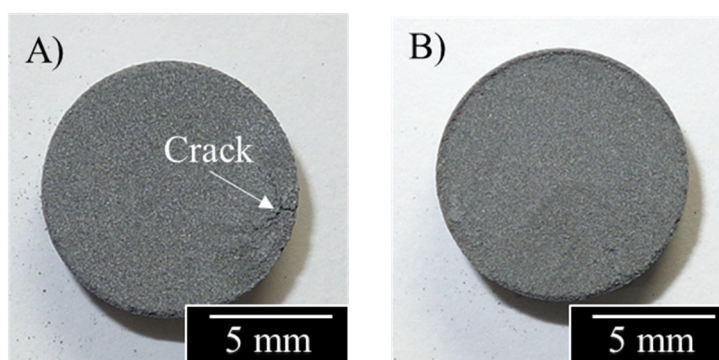


Figure 1. Overview of A) GF20 and B) GF30

#### 3.2. Latent heat capacity of composite PCM

Figure 2 shows DSC curve during heating of GF30. An endothermic peak was identified at  $576 \text{ }^\circ\text{C}$  as the onset temperature. Because of the eutectic temperature of the Al-12 mass% Si alloy of  $577 \text{ }^\circ\text{C}$  [4], the endothermic peak originates from the melting of the core alloy of the MEPCM. In addition, latent heat capacity corresponding to integrated value of the endothermic peak is  $224.09 \text{ J g}^{-1}$ . These values are 2.77 times of the heat storage capacity of a rock ( $\Delta T=100 \text{ K}$ ) as a typical sensible heat storage material [5]. Therefore, the composite PCM with high latent heat capacity was successfully fabricated using the Al-12 mass% Si alloy MEPCM and the glass frit.

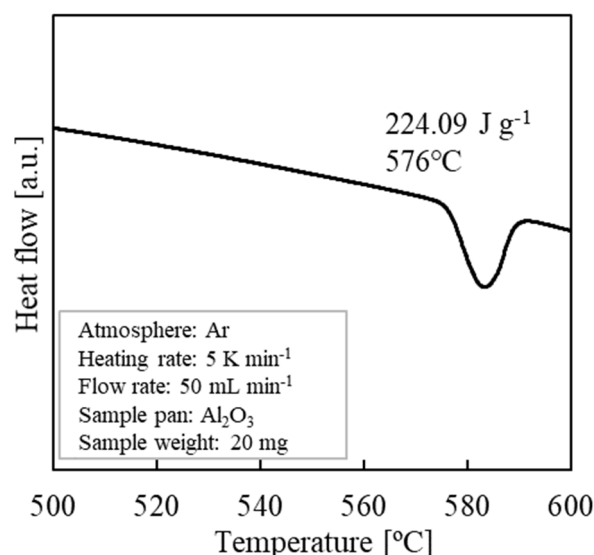


Figure 2. DSC curve during heating of GF30.

#### 4. Conclusions

In this study, to improve the latent heat capacity of the composite PCMs containing the MEPCMs, the preparation of the composite PCMs using the Al-12 mass% Si MEPCMs with high latent heat capacity and the glass frit as the sintering aid was investigated. The composite PCM was successfully prepared by mixing the glass frit of 30 vol% with the MEPCM. From cross-sectional observation of the composite PCM, it was confirmed that the shape of the MEPCM was retained. The latent heat capacity of the composite PCM was 224.09 J g<sup>-1</sup>. Therefore, we succeeded in fabricating the composite PCM with high latent heat capacity and high durability. Based on these research results, the fabricated composite PCM is expected to be applied to heat utilization systems at high temperatures.

#### Acknowledgements

The authors greatly appreciate the financial support from the New Energy and Industrial Technology Development Organization (NEDO). A part of this work was conducted at Hokkaido University, supported by the “Nanotechnology Platform” Program of the Ministry of Education, Culture, Sports, Science and Technology (MEXT), Japan.

#### References

- [1] M.M. Kenisarin, High-temperature phase change materials for thermal energy storage, *Renew. Sust. Energ. Rev.*, 14 (2010) 955-970, <https://doi.org/10.1016/j.rser.2009.11.011>.
- [2] P. Feng, B. Zhao, R. Wang, Thermophysical heat storage for cooling, heating, and power generation: A review, *Appl. Therm. Eng.*, 166 (2020) 114728, <https://doi.org/https://doi.org/10.1016/j.applthermaleng.2019.114728>.
- [3] T. Nomura, C. Zhu, N. Sheng, G. Saito, T. Akiyama, Microencapsulation of metal-based phase change material for high-temperature thermal energy storage, *Sci Rep*, 5 (2015) 9117, <https://doi.org/10.1038/srep09117>.
- [4] J. Murray, A. McAlister, The Al-Si (aluminum-silicon) system, *Bulletin of alloy phase diagrams*, 5 (1984) 74-84, <https://doi.org/10.1007/BF02868729>.
- [5] Japan Society of Thermophysical Properties, *Thermophysical properties handbook*, Yokendo, 2008, p118.

EUROTHERM2023-S169

## Exploring supercooling phenomena through extensive experimental method design

Fride Vullum-Bruer<sup>1</sup>, Magnus Rotan<sup>1</sup>, Jorge Salgado Beceiro<sup>1</sup>, Olai Brevik Mykland<sup>1</sup>, Ragnhild Sæterli<sup>1</sup>, Alexis Sevault<sup>1</sup>, José Lara Cruz<sup>2</sup>, Jawad Rabbi<sup>2</sup>, Jean-Pierre Bedecarrats<sup>2</sup>

<sup>1</sup>SINTEF Energy Research, Postboks 4761 Torgarden, 7465 Trondheim, Norway fride.vullum.bruer@sintef.no, Magnus.rotan@sintef.no, Jorge.beceiro@sintef.no

<sup>2</sup>Universite de Pau et des Pays de l'Adour, E2S UPPA, LaTEP, Laboratoire de Thermique, Énergétique et Procédés, 64000 Pau, France

jose.laracruz@univ-pau.fr, jawad.rabbi@univ-pau.fr, jean-pierre.bedecarrats@univ-pau.fr

### Abstract

For phase change materials (PCMs) one of the main challenges for industrial applications is the supercooling phenomena, leading to a hysteresis in the temperatures measured for melting and solidification of the material. Supercooling is however, a challenging property both to accurately measure and understand. There have been many attempts to model this phenomenon mathematically with various success. Most known models have been modified to fit specific experimental conditions and are thus not transferrable to other systems, neither small nor large scale. The current work has focused on designing a set of experiments where different parameters have been changed, particularly the sample size in order to understand the effect of container size on the supercooling behavior. This work sheds light on the effect that supercooling may impose on PCM-based industrial scale thermal energy storage.

**Keywords:** Supercooling, PCM, nucleation, sample size effects, thermal energy storage, hysteresis

### 1. Introduction

With the dramatic rise in energy prices in Europe and increased implementation of renewable intermittent energy sources, the need for energy storage in various forms is becoming ever more important. Thermal energy storage has gained significant attention recently and is expected to cover large market segments from private homes to large industrial scale applications in the coming years. Utilizing phase change materials (PCMs) to exploit the latent heat is one of the options currently available on the market. PCM-based energy storage technologies have great potential for providing high energy storage density within a narrow temperature range. And by altering the materials, the thermal storage can be tailored to suit applications from freezing temperatures down to -50 °C and up to several hundred degrees Celsius. Still, there are many challenges hampering the further development of this technology, one of which is supercooling (delay in crystallization due to the presence of a liquid state at a temperature below the solid-liquid equilibrium temperature). (1) Many researchers have attempted to understand the phenomenon of supercooling by both experimental and theoretical means. Thonon et al. have summarized a number of different studies where the modelling approach have been used. (2) One of the main take-aways from these studies is that it is very challenging to model supercooling on a general basis, and all the models existing in literature have tailored the models using experiment specific adjustments. Thus, the models are not transferrable to other setups and particularly not industrial scale applications. In this current research work, we have therefore attempted to understand supercooling by means of various experimental setups where sample size is one of the main parameters considered in addition to considering nucleation sites and heating/cooling rates.

## 2. Materials and methods

The materials tested in this study include CrodaTherm™ 37 (CT37) from Croda and savE® HS3N from PLUSS. CT37 has nominal melting and solidification temperatures of 36.8 °C and 35.0 °C, respectively and a latent heat of 204 kJ/kg (on melting) when measured by DSC. Values measured by 3LC were listed as slightly different, with melting and solidification temperature at 36 °C and total stored heat on melting was 216 kJ/kg. Nominal solidification and melting temperatures for HS3N are from the supplier listed as -3 °C and -2 °C, respectively. Latent heat is given as 346 kJ/kg.

**Error! No s'ha trobat l'origen de la referència.** shows one of the experimental setups used in this study. Here, a 1 liter beaker is used as the sample container and is filled with the PCM. 9 thermocouples are penetrated through an insulating lid, shown to the right in the figure below. The thermocouples are evenly spaced in the radial direction with varying distance from the bottom of the beaker (shown in

Table 10). The beaker is then placed in a glycol bath which can be ramped up and down in temperature

Thermocouple no.	6	7	8	9	5	4	3	2	1
Distance from bottom (mm)	5	13	21	29	37	45	53	61	69

while monitoring the temperature of the PCM through the different thermocouples.

Table 10. Distribution of thermocouples in setup shown in Fig. 1

Thermocouple no.	6	7	8	9	5	4	3	2	1
Distance from bottom (mm)	5	13	21	29	37	45	53	61	69

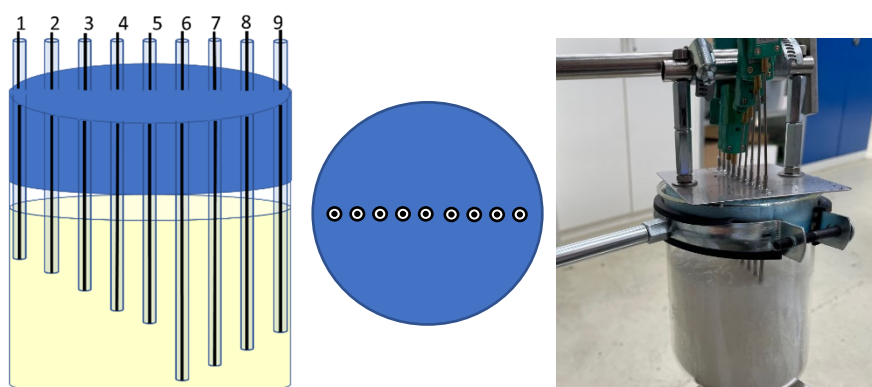


Figure 61. Experimental setup for measurements of phase change temperature of a material in a 1 litre container

A similar experimental set-up was carried out but using three polypropylene tubes (wall thickness  $t = 1$  mm, internal diameter  $D = 10$  mm, length = 75 mm) each filled with 1 mL of PCM. A single thermocouple is located in each tube directly in contact with the PCM.

For comparison, the PCMs analyzed using these setups have also been characterized using conventional differential scanning calorimetry (DSC) and 3-layer calorimetry (3LC) with sample sizes of approximately 40  $\mu$ L and 100 mL, respectively. The heating and cooling rates for the DSC measurements were set at 2 K/min. For the 3LC measurements the sample, which was placed in a specific 3LC container, was placed in a freezer at a set temperature and cooled until complete solidification of the material while performing measurements. For the heating, the sample was placed in room temperature and allowed to melt completely.

### 3. Results and discussion

Due to the limited space, only the results for HS3N are shown in this abstract. Fig. 2 (a) shows the heating and cooling curves using conventional DSC with a heating and cooling rate of 2 K/min, while Fig 2 (b) shows the results using 3LC. It is quite obvious that the results are significantly different. While a large hysteresis of approximately 17 K is observed in the DSC measurements, the 3LC data shows only minor differences between the onset for melting and solidification.

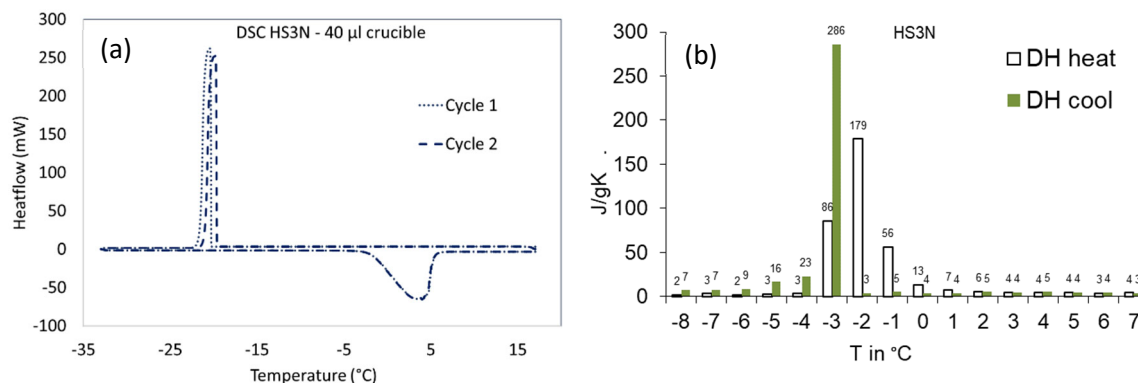


Figure 62. Figure (a) shows a conventional DSC measurement for HS3N, while the 3LC measurement is shown in (b).

Fig. 3 shows the results obtained with the experimental setup provided in Fig. 1. Here, the sample size is approximately 0.5 L compared to 100 mL and 40 µL for the 3LC and DSC, respectively. Although the temperature curves for the different thermocouple locations vary, it is quite clear that the degree of supercooling is very small compared to what is observed in DSC. From this data it seems obvious that the sample size potentially makes a big difference as to whether or not a material will experience large degree of supercooling. Fig. 4 showing the results for the three small tubes confirms the results. In the tubes, the sample size is 1 mL and the supercooling is about 13 K.

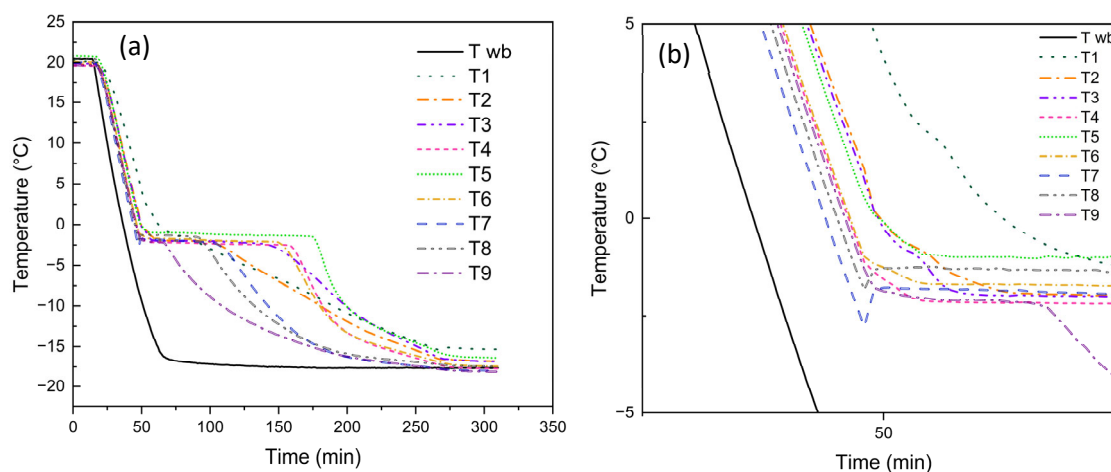


Figure 63. Solidification curves for HS3N measured using the experimental setup shown in Fig. 1. (b) is a zoom-in of the area just around the start of the crystallization, which shows very little supercooling.

It should however, be noted that there are also certain other differences between the characterization methods which cannot be entirely neglected. In the experimental setup in Fig. 1, the thermocouples will most certainly contribute as nucleation points, promoting nucleation at a higher temperature, and thus reducing the degree of supercooling. It can be the same for the small tubes where the thermocouple is in the PCM. For the 3LC on the other hand, there are no thermocouples located inside the PCM, which also shows considerably less supercooling than DSC measurements. Another variable which cannot be neglected is the cooling rate. For the DSC measurements the cooling rate can be controlled quite exact, while for the 3LC measurements, the tubes and the setup in Fig. 3, the temperature gradient is more



difficult to control and will most likely vary more. It is a known fact that the cooling rate will affect the degree of supercooling. However, it is not likely that this is the only reason for the significant differences observed here.

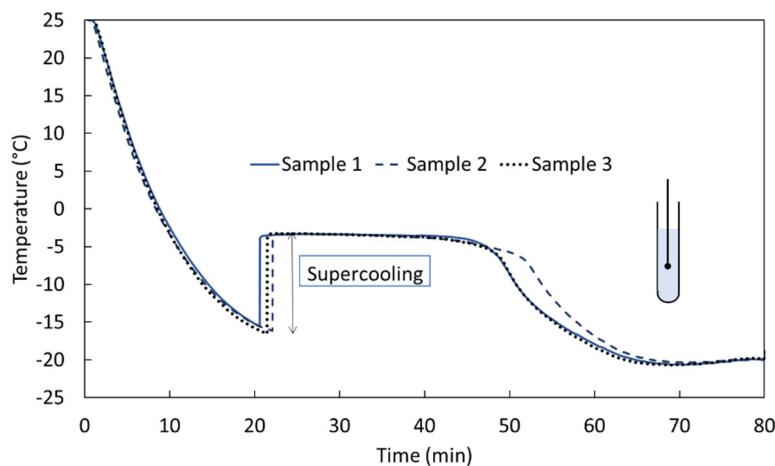


Figure 64. Solidification curves for HS3N in the small tubes (1 mL).

#### 4. Conclusions

The data presented shows melting and solidification behavior of a PCM measured with 4 different methods utilizing 4 significantly different sample sizes (40  $\mu$ L, 1 mL, 100 mL and 0.5 L). The results give a very clear indication that the degree of supercooling does indeed depend on the sample size and is much more pronounced for smaller samples. Although there are certain variables in these measurements that may affect the results, these will not account for the large difference observed between DSC, the tubes and the other two methods. When considering PCM for use in industrial applications, other measurement techniques should be considered in addition to DSC in order to evaluate suitability for a specific application.

#### Acknowledgements

This study was carried out through the research project KSP PCM-STORE (308847) supported by the Research Council of Norway and industry partners. PCM-STORE aims at building knowledge on novel PCM technologies for low- and medium temperature thermal energy storage systems.

#### References

1. *Numerical simulation and experimental research progress of phase change hysteresis: A review.* Longlei Que, Xuelai Zhang, Jun Ji, Liqiang Gao, Wenhao Xie, Lu Liu, Xingjiang Ding. 2021, Energy & Buildings, Vol. 253, p. 111402.
2. *Analytical modelling of PCM supercooling including recalescence for complete and partial heating/cooling cycles.* M. Thonon, G. Fraisse, L. Zalewski, M. Pailha. 2021, Applied Thermal Engineering, Vol. 190, p. 116751.

## Evaluation of the scraping forces in active latent heat thermal energy storages

Jonas Tombrink<sup>1\*)</sup> Alberto Egea Villarreal<sup>2)</sup>, Andrea Gutierrez<sup>1)</sup>

<sup>1)</sup> German Aerospace Center (DLR), Institute of Engineering Thermodynamics, Stuttgart, Germany

<sup>2)</sup> Polytechnic University of Cartagena, Department of Thermal and Fluid Engineering, Cartagena, Spain

\*Corresponding author e-mail: [jonas.tombrink@dlr.de](mailto:jonas.tombrink@dlr.de)

### Abstract

Low-cost Phase Change Materials (PCM) usually have a low thermal conductivity. During the discharge process, solidified PCM on the heat transfer surface acts as a thermal insulator, resulting in a reduction of the heat transfer between the PCM and the heat transfer fluid, thus the discharge power is reduced as the PCM solidifies. In active latent heat thermal energy storages (ALHTES), the solidified PCM layer is mechanically removed from the heat transfer surface by a scraper to maximize the heat transfer. In this study, this parasitic mechanical energy is quantified experimentally for the first time to optimize the design of future ALHTES. The required scraping force is measured for decanoic acid and paraffin, resulting in a value between 150 and 350 N·m<sup>-1</sup> depending on the angle of the scraper.

**Keywords:** Active Latent Heat Thermal Energy Storage, Phase Change Material, Heat Exchanger, Solidification

### 1. Introduction

With latent heat thermal energy storages (LHTES), thermal energy can be stored at an almost constant temperature by utilizing the phase change enthalpy released during the liquid to solid transition of a Phase Change Material (PCM) and vice versa. Due to the almost isothermal character, LHTES are mainly utilized in applications where a high thermal energy demand is required at a small temperature range. This includes residential applications due to the limited well-being temperature of humans within buildings [1], but also industrial processes that have an isothermal process, e.g. the evaporation and condensation of a fluid.

A wide range of materials has been characterized to be used as PCM so far. Thereby, all non-metallic PCM for medium to low temperature, namely organic and inorganic non-metallic PCMs, have a low thermal conductivity of usually less than 1 W·m<sup>-1</sup>·K<sup>-1</sup> [2,3]. During the discharge process of LHTES, a layer of solid PCM is growing at the heat exchanger wall. Since the phase change enthalpy is released at the boundary of liquid and solid PCM, the heat has to be transferred through the whole solid layer of PCM, which decreases the heat transfer. To overcome this decrease in the heat transfer, several approaches have been investigated in the past, which can be mainly divided into passive and active systems. Passive systems focus either on the increase of the heat transfer surface or in the modification of the PCM to increase the heat transfer. Active systems achieve a significantly high heat transfer by mechanically removing the solid phase of the PCM from the heat transfer area. These active systems can be further divided into four main principles: modification of the PCM to achieve a pumpable slurry after the solidification, transport of macro-encapsulated PCM, direct contact heat exchanger and scraped heat exchangers. Different types of scraped heat exchangers for latent heat storage have been previously studied [4,5]. To the best of our knowledge, the power required for the mechanical scraping of the PCM has not been detailed analysed yet. In this paper, an experimental test rig has been built to systematically

analyse and quantify the scraping forces and the required energy to separate two PCMs (decanoic acid and paraffin) from the heat transfer surface of an active heat exchanger.

## 2. Materials and method

Two PCM were investigated in this study, namely decanoic acid (98 %, supplied by Sigma Aldrich, melting point  $T_m = 31.5^\circ\text{C}$ ) and paraffin (RT44HC, supplied by Rubitherm GmbH, melting area  $T_m = 41 - 44^\circ\text{C}$ ). Both are well known PCMs for low temperature applications. The detailed properties of decanoic acid are summarized in [4], those of paraffin in [5].

To quantify the scraping forces, a linear moving test rig has been designed and built. A schematic drawing of the test rig is shown in Figure 65. In Figure 66, a picture of the real test rig in the lab is shown. Thereby, the molten PCM is placed on a stainless-steel metal sheet. Given that the ambient temperature is below the melting point of both, decanoic acid and the paraffin, the PCMs solidify afterwards on the surface of the metal sheet. The metal sheet is placed on a linear moving unit, driven by a controllable electrical engine by a gear drive. A scraper is placed on the top of the metal sheet, loosely connected by a rotary bearing. The angle of the scraper towards the metal sheet ( $\alpha$ ) can be adjusted (see Figure 65). A force sensor is placed behind the swing holding the scraper. The metal sheet with the solid PCM is moved towards the scraper. During the scraping process, the swing is pressed onto the force sensor by the scraping forces. The speed of the moving sheet ( $v$ ) is measured with a wheel speed sensor. The thickness of the PCM layer can be measured with a laser distance sensor. The temperature of the PCM layer shortly before the scraping process is measured with an infrared thermometer.

In this work, the scrapers width is 55 mm and the angle has been set to  $15^\circ$ ,  $45^\circ$  and  $60^\circ$  towards the metal sheet. The speed of the moving sheet was set in the range of 0.6 - 0.8 m/s. The temperature of decanoic acid during the scraping test was between  $30-31.5^\circ\text{C}$  and that of the paraffin between  $39-40.5^\circ\text{C}$ .

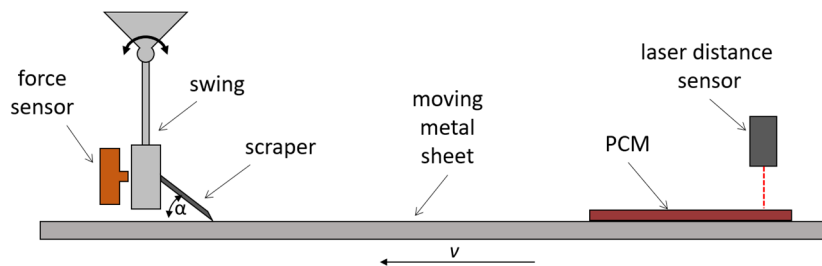


Figure 65. Schematic drawing of the linear moving scraper test rig.



Figure 66. Picture of the linear moving test rig.

### 3. Results and discussion

The results of the scraping test are shown in Figure 67. For decanoic acid, the values for the three tests varying the angle to 15°, 45° and 60° are presented. In the case of paraffin, only for the angles of 45° and 60° data are presented. In the tests carried out with an angle of 15°, no measurable values were obtained because the solid layer was scraped off with a force below the lower detection limit of the sensor.

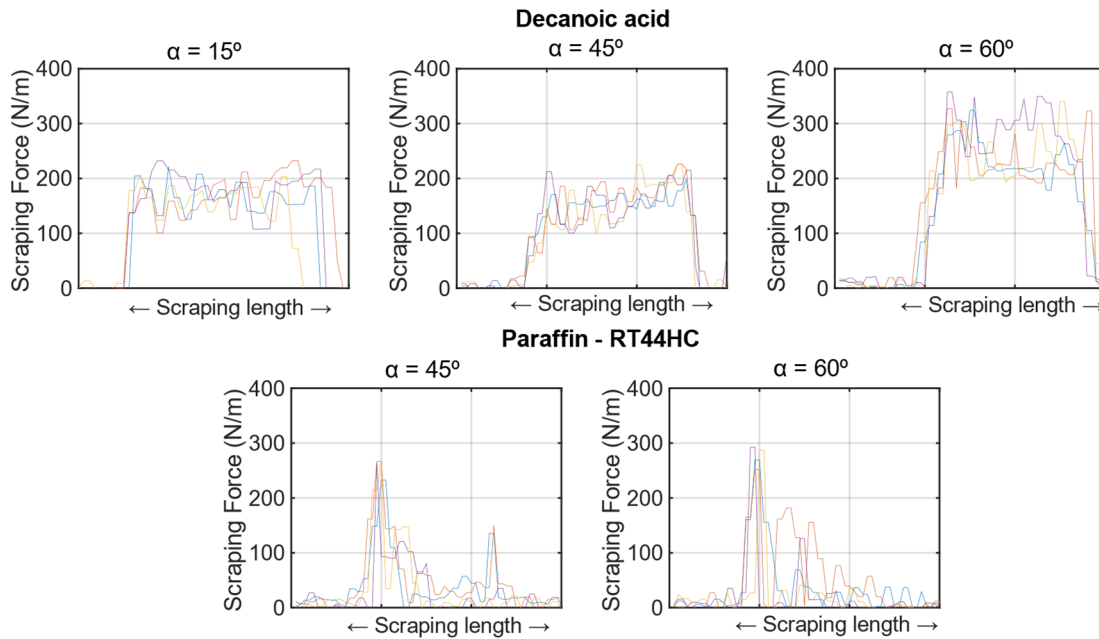


Figure 67. Scraping force of two PCM with different inclinations.

In the tests carried out with the decanoic acid, almost constant values were obtained throughout the entire length of the scrape. In addition, similar values were observed for the 15° and 45° angles, with an average scraping force of about 150 N·m<sup>-1</sup> and an increase of 66% for the 60° angle, obtaining an average force of about 250 N·m<sup>-1</sup>. In the tests carried out with paraffin, zones of high force of up to 300 N·m<sup>-1</sup> at the beginning of scraping followed by zones of low force of well below 100 N·m<sup>-1</sup> were observed for the two angles studied. The different behavior can be seen in Figure 68. While decanoic acid peels off as the scraper advances, paraffin peels off in larger portions. The reason for the different behaviour of the two materials when subjected to scraping forces needs to be investigated in detail based on material aspects, which is beyond the scope of this paper.

Finally, the required power  $P$  for the scraping process in real scraped active latent heat thermal energy storages can be calculated for linear moving scrapers using the force  $F$  and the velocity  $v$  by

$$P = F \cdot v \quad (1)$$

and for rotating scrapers via the torque  $M$ , meaning the distance  $r$  between the point of application of the force and the point of rotation multiplied by the force  $F$  and the angular velocity  $\omega$  by

$$M = F \cdot r \quad (2)$$

and

$$P = M \cdot \omega. \quad (3)$$

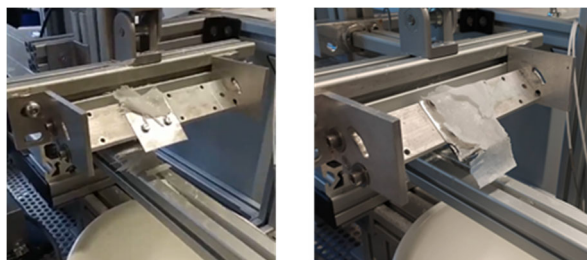


Figure 68. Picture of scraped PCM. Left: Decanoic acid. Right: Paraffin.

In [5] a latent heat thermal energy storage system based on a rotating drum heat exchanger is investigated, using decanoic acid as PCM. The solidified PCM is scraped off a drum with a diameter of 0.184 m and a length of 0.4 m with each rotation. In the experiments, the rotational speed was up to  $25 \text{ min}^{-1}$ . Applying an average scraping forces of  $200 \text{ N}\cdot\text{m}^{-1}$  to the dimensions of the rotating drum heat exchanger results in a required mechanical energy of 20 W, what is in the same order of magnitude as the values between 44 W and 79 W mentioned in [5]. Thereby, the quoted values have been obtained by comparing independent measurements of the heat transfer and no direct investigation of the required scraping force has been carried out.

#### 4. Conclusions

In this work, the scraping forces required to remove solid PCM from a metal sheet, which is necessary for the optimal design of future ALHTES, were investigated for the first time. Results were presented for two PCMs at different scraping angles. On the one hand, almost constant scraping forces have been obtained for decanoic acid associated with a gradual detachment of the PCM. On the other hand, the forces obtained for paraffin consist of punctual peaks associated with punctual detachment of large portions of PCM. Maximum values of  $350 \text{ N}\cdot\text{m}^{-1}$  have been obtained for decanoic acid and  $300 \text{ N}\cdot\text{m}^{-1}$  for paraffin, both with the highest inclinations studied.

#### Acknowledgements

The authors gratefully acknowledge to European Regional Development Fund and Ministerio de Ciencia e Innovaci3n - Agencia Estatal de Investigaci3n for the partial financial support of the project ALTES: “Active Latent Thermal Energy Storage”, Ref. PGC2018-100864-B-C21.

#### References

- [1] A. Sharma, A. Shukla, C.R. Chen, T.-N. Wu, Development of phase change materials (PCMs) for low temperature energy storage applications, *Sustain. Energy Technol. Assessments*. 7 (2014) 17–21. <https://doi.org/10.1016/j.seta.2014.02.009>.
- [2] M.M. Kenisarin, High-temperature phase change materials for thermal energy storage, *Renew. Sustain. Energy Rev.* 14 (2010) 955–970. <https://doi.org/https://doi.org/10.1016/j.rser.2009.11.011>.
- [3] S. Kahwaji, M.B. Johnson, A.C. Kheirabadi, D. Groulx, M.A. White, A comprehensive study of properties of paraffin phase change materials for solar thermal energy storage and thermal management applications, *Energy*. 162 (2018) 1169–1182. <https://doi.org/10.1016/j.energy.2018.08.068>.
- [4] J. Tombrink, H. Jockenh3fer, D. Bauer, Experimental investigation of a rotating drum heat exchanger for latent heat storage, *Appl. Therm. Eng.* 183 (2021). <https://doi.org/10.1016/j.applthermaleng.2020.116221>.
- [5] A. Egea, A. Garc3a, R. Herrero-Mart3n, J. P3rez-Garc3a, Experimental performance of a novel scraped surface heat exchanger for latent energy storage for domestic hot water generation, *Renew. Energy*. 193 (2022) 870–878. <https://doi.org/10.1016/j.renene.2022.05.057>.

EUROTHERM2023-Y171

## Crystal growth velocity of cold crystallizing long-term thermal energy storage material

Konsta Turunen

Department of Mechanical Engineering, School of Engineering, Aalto University, P.O. Box 16100, 00076 Aalto, Finland, e-mail: konsta.turunen@aalto.fi

### Abstract

Phase change materials can have large energy storage densities by using the latent heat of melting. The latent heat can be stored long-term and released when needed by exploiting supercooling, glass transition and cold crystallization. Crystallization behaviour of the material governs the storage and heat release abilities of this method, hence it should be thoroughly characterized. This work determines the crystal growth velocity of erythritol in a cross-linked sodium polyacrylate network (ErNa) during cold crystallization. ErNa samples were imaged with digital camera while they were cold crystallized at a constant temperature. The analysis revealed formation of metastable polymorph, which showed six times slower growth velocity than the apparently stable polymorph. The growth velocity of the stable polymorph exhibited a bell-shaped dependency with the cold crystallization temperature which can be used to design and optimize ErNa storages.

**Keywords:** Long-term thermal energy storage, phase change material, supercooling, cold crystallization, glass transition, erythritol

### 1. Introduction

Long-term thermal energy storage (TES) in a timescale of months can curtail the seasonal variations of renewable energy production. However, current long-term TES technologies rely on large underground storages, such as water-filled caverns [1]. If compact and efficient long-term TES emerged, it would enable a new way of implementing long-term TES in small and medium scale applications and heating systems.

Phase change materials (PCMs) can improve the energy density of TES by exploiting the latent heat of melting, but so far PCMs have remained inefficient in long-term TES. Use of supercooling, glass transition and cold crystallization offers a unique way to store and release the latent heat of melting: First, PCM is melted completely, which corresponds charging of the storage. Then, the material is supercooled to temperatures close to the glass transition region where the molecular movement slows down drastically. At these temperatures, even if the crystallization commenced, the crystallization rate is so slow that the latent heat of melting can be stored for months [2]. The discharge begins by re-heating the material to a cold crystallization temperature, which initiates crystallization. As crystallization releases heat, the temperature of the material increases towards the melting temperature, thus the stored latent heat is released.

Erythritol in cross-linked sodium polyacrylate network (ErNa) has demonstrated improved stability of the supercooled state, storage ability of several months [2] and feasible operation in a prototype storage of 6.5 kg [3]. Furthermore, cold crystallization rate of ErNa was analysed using DSC, which measures the heat flow during the crystallization, i.e. the overall crystallization rate [4]. However, nucleation and crystal growth velocity should be analysed individually, to determine their individual impact on the overall crystallization. This would improve the design and optimization of TES using ErNa and increase understanding of the cold crystallization process. Therefore, this work determines the crystal growth velocity of ErNa during cold crystallization at a constant temperature, by imaging ErNa samples with a digital camera.

## 2. Materials and methods

### 2.1. Material preparation

The analysed material is a mixture of erythritol and cross-linked sodium polyacrylate (ErNa). The preparation of ErNa follows the method presented in reference [5]. In summary, sodium hydroxide (assay  $\geq 99\%$ , VWR Chemicals), acrylic acid (assay  $\geq 99\%$ , Merck) and ethylene dimethacrylate (assay  $\geq 97.5\%$ , Merck) were mixed in aqueous erythritol (Food grade, Suomen Luontaistukku Ltd., Finland). After thorough mixing at  $60\text{ }^{\circ}\text{C}$  with a magnetic stirrer, potassium persulfate (assay  $\geq 98\%$ , VWR Chemicals) was added to initiate polymerization of the sodium polyacrylate. Polymerization was completed in approximately 15 mins, after which water was evaporated from the sample in an oven at  $130\text{ }^{\circ}\text{C}$ . ErNa composed of 80 wt% of erythritol, 21.9 wt% of sodium polyacrylate, 2 wt% of ethylene dimethacrylate and 0.1 wt% of potassium persulfate. Three samples of  $15.00 \pm 0.05\text{ mg}$  were extracted from the melt and placed between two glass slides, in a way that the sample thickness was approximately  $200\text{ }\mu\text{m}$ . The thickness of the bottom glass was 1 mm and the top glass 0.16 mm to minimize the thermal resistance between the sample and the ambient.

### 2.1. Measurement method and analysis

Crystal growth velocity of ErNa was measured using a setup illustrated in Figure 1A. First, the sample was melted in an oven at  $125\text{ }^{\circ}\text{C}$  and cooled in a refrigerator for 60 mins to reach  $5 \pm 1\text{ }^{\circ}\text{C}$ . After the cooling, the sample was quickly placed in a thermal chamber at a constant temperature,  $T_{cc}$ , as shown in Figure 1A. The chamber (working space of 35 l) maintained a constant temperature by circulating chamber air with a flow rate of approximately 24 l/s. After the sample was placed in the slide holder, thermal chamber was closed, and digital camera begun to image the sample at a predetermined constant time interval.

The crystal growth analysis was conducted using ImageJ software. The crystal radius was determined from each image of the sample by measuring the length of a straight line with a fixed angle from a fixed point at the centre of the crystal. The centre point was determined from the first three images of the crystal by fitting a circle on the perimeter of the crystal. The length of the radius was determined using two different angles perpendicular to each other. The estimated accuracy of the length was  $\pm 0.05\text{ mm}$ . Thus, the radial growth velocity at time  $t$ ,  $v_t$  (mm/h) was determined as the change in the radius length,  $r$  (mm) during the time step of the images,  $\Delta t$  as

$$v_t = (r_t - r_{t-1})/\Delta t \quad (1)$$

## 3. Results

Images of the cold crystallization process of ErNa are shown in Figure 1B-C. Usually, one crystal formed in a sample, but sometimes only one of the three samples crystallized. Therefore, the used imaging method ensures adequate sample size ( $> 45\text{ mg}$ ) to capture cold crystallization ErNa. Increasing the sample size increases the probability of crystallization, which is evidenced in Figure 1D, where 100-g sample of ErNa forms numerous crystals at room temperature.

The image analysis yielded the radius of ErNa crystals as a function of time, as shown in Figure 2A. The length of the radius increased linearly in time which was evidenced by the high  $R^2$  values above 0.999 for all the measurements. These linear fits were obtained with a least square method. In other words, the growth velocity remained constant. Therefore, the average radial growth velocity ( $v_{avg}$ ) and standard deviation were determined for each cold crystallization temperature.

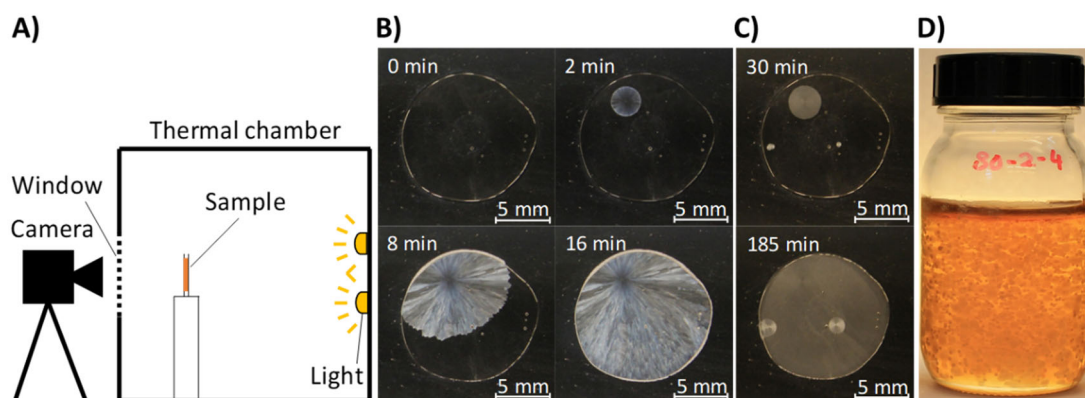


Figure 1. A) The setup for imaging cold crystallization of ErNa samples. B) Progress of the cold crystallization of ErNa in a thermal chamber at 100 °C. C) Metastable polymorph (small white circles) formed simultaneously with the stable polymorph (greyer white) when ErNa was cold crystallized in a thermal chamber at 55 °C. The elapsed time is indicated at the top left corner of each image. D) Crystallization of 100-g sample of ErNa at ~20 °C after it was cooled to 5 °C.

The samples reached  $T_{cc}$  (oven temperature) in a few minutes. This is exemplified in Figure 2A, where  $v_t$  increased in the beginning of the measurement and then decreased to a constant level. This occurred because  $v_{avg}$  peaked at approximately 85 °C, hence the growth velocity increased until the sample reached 85 °C and decreased as the sample temperature reached the oven temperature. Therefore, the first few minutes of the imaging were excluded from the analysis. Sometimes, the radius length jumped, because of the imperfectness of the spherical growth, as illustrated at 14 min in Figure 2A. These jumps were excluded from the analysis.

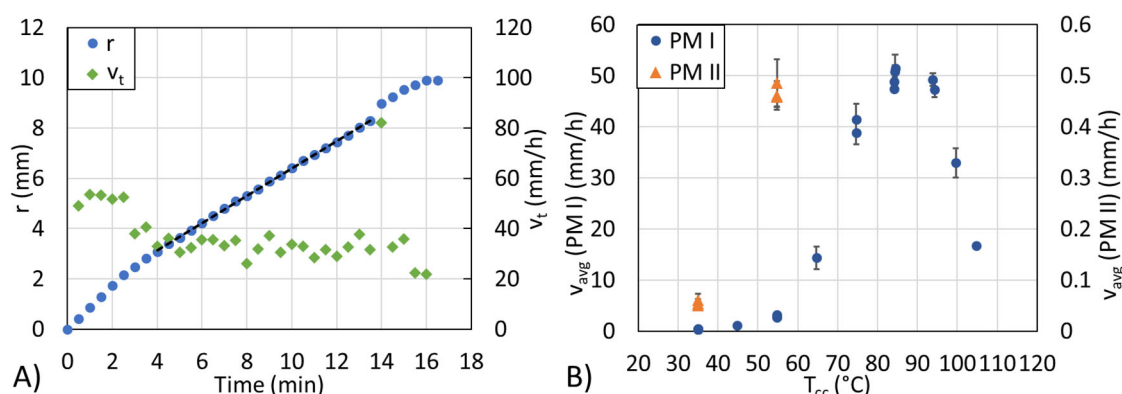


Figure 2. A) Crystal radius and crystal growth velocity of ErNa in a thermal chamber at 100 °C. The dashed line indicates a linear fit. B) The average crystal growth velocity of ErNa at different temperatures. PM I and PM II refer to stable and metastable polymorph, respectively. Error bars indicate the standard deviation.

Sometimes whiter crystal appeared during the crystallization, as shown in Figure 1C. These crystals formed at  $T_{cc}$  of 35 °C and 55 °C. Furthermore, their growth velocity was approximately six times slower than the usually formed crystals' (greyer colour). The different appearance and slower growth rate indicate formation of a metastable polymorph. Metastable polymorph of ErNa was identified in DSC under similar thermal history and it had the overall crystallization time approximately four times slower than the stable polymorph [4]. Even though this work measured growth velocity and DSC the heat flow, i.e., the overall crystallization rate (nucleation and growth), the slower crystallization rate of the metastable polymorph is evident in both analyses. This corroborates that the whiter crystals were indeed metastable polymorph of ErNa.

In general, the crystal growth velocity of ErNa was slow ( $< 50$  mm/h), but because numerous nuclei form in bulk crystallization (Figure 1D), the overall crystallization rate of ErNa suffices for applications [3]. As shown in Figure 2B, the growth velocity increases, peaks, and decreases as  $T_{cc}$  increases. The velocity nullifies at the melting temperature, which is  $108 \pm 1$  °C for ErNa [2]. This bell-shaped curve is typical and expected for the growth velocity: The increased thermodynamic driving force (Gibbs free



energy between stable and metastable state) accelerates the growth rate when supercooling degree ( $T_m - T$ ) increases, but the significantly increased viscosity will eventually slow down the molecular movement and crystal growth rate [6].

#### 4. Conclusions

This work determined the crystal growth velocity of erythritol in sodium polyacrylate network (ErNa) when it was cold crystallized at different constant temperatures. The 15-mg samples were cold crystallized in a temperature-controlled oven while digital camera imaged the crystallization process. The growth velocity exhibited an expected bell-shaped curve as a function of crystallization temperature. This enables prediction and modelling of the crystal growth velocity more accurately which is beneficial in the design process of thermal energy storage applications that use ErNa. The analysis also revealed that ErNa crystallized to metastable polymorph, which showed six times slower crystal growth velocity than the stable polymorph. The future research should determine the nucleation rate of ErNa and the influence of thermal history on the crystallization kinetics to provide deeper understanding of the crystallization behaviour.

#### Acknowledgements

This research was funded by KAUTE foundation (20220292) and Technology Industries of Finland Centennial Foundation and Jane and Aatos Erkkö Foundation (Future Makers 2019 Program). The author wish to acknowledge D.Sc Ari Seppälä for his valuable comments.

#### References

- [1] H. Mahon, D. O'Connor, D. Friedrich, and B. Hughes, "A review of thermal energy storage technologies for seasonal loops," *Energy*, vol. 239, p. 122207, 2022, doi: 10.1016/j.energy.2021.122207.
- [2] K. Turunen, M. R. Yazdani, S. Puupponen, A. Santasalo-Aarnio, and A. Seppälä, "Cold-crystallizing erythritol-polyelectrolyte: scaling up reliable long-term heat storage material," *Appl. Energy*, vol. 266, p. 114890, 2020, doi: 10.1016/j.apenergy.2020.114890.
- [3] K. Turunen, V. Mikkola, T. Laukkanen, and A. Seppälä, "Long-term thermal energy storage prototype of cold-crystallizing erythritol-polyelectrolyte," *Appl. Energy*, vol. 332, no. December 2022, 2023, doi: 10.1016/j.apenergy.2022.120530.
- [4] K. Turunen, M. R. Yazdani, A. Santasalo-aarnio, and A. Seppälä, "Exceptional cold-crystallization kinetics of erythritol-polyelectrolyte enables long-term thermal energy storage," *Sol. Energy Mater. Sol. Cells*, vol. 230, no. June, pp. 0–11, 2021, doi: 10.1016/j.solmat.2021.111273.
- [5] S. Puupponen and A. Seppälä, "Cold-crystallization of polyelectrolyte absorbed polyol for long-term thermal energy storage," *Sol. Energy Mater. Sol. Cells*, vol. 180, pp. 59–66, 2018, doi: 10.1016/j.solmat.2018.02.013.
- [6] P. G. Debenedetti, *Metastable liquids - concepts and principles*. New Jersey, USA: Princeton University Press, 1996.

EUROTHERM2023-U172

## **Solar salt and ceramic particles compatibility test and evaluation.**

Marc Majó, Alejandro Calderón, Adela Svobodova-Sedlackova, Camila Barreneche, Inés Fernández

University of Barcelona, Martí i Franquès, 1, Barcelona, Spain, Phone: +34 934 03 72 44, e-mail: marc.majo@ub.edu

### **Abstract**

Energy storage strategies are needed today more than ever. Improving these technologies and implementing new, will help us to make a better use of the renewable energies. Thermal storage using ceramic solids and molten salts as heat transfer fluid, is a strategy under study for the new generation solar power plants. This study is based on the analysis of the compatibility between molten salts and ceramic solids to determine their chemical stability over time.

**Keywords:** TES, CSP, thermal energy storage, molten salts, compatibility, solid particles

### **1. Introduction**

A concentration solar power (CSP) plant with a tower configuration and molten salts as thermal energy storage (TES) is a type of solar power generation system that uses mirrors to concentrate the sun's energy to heat a fluid, which is then used to generate electricity. The heat is stored in molten salts, which allows the plant to continue generating electricity even when the sun is not shining. The use of TES can help to store excess energy generated during periods of low demand, such as during the day when solar power is abundant, and then release it during periods of high demand, such as at night or during cloudy weather. TES can be achieved through a variety of methods, including using water, molten salt, or phase change materials [1].

The molten salt used in CSP plants is usually a mixture of sodium nitrate and potassium nitrate (60:40  $\text{NaNO}_3:\text{KNO}_3$ ), which have a high heat capacity and can be heated to temperatures over 400 °C. The salt is stored in a large insulated tank and can be used to generate electricity for several hours after the sun goes down. This allows the plant to continue generating electricity during periods of low sunlight, such as at night or on cloudy days. This plant configuration is considered to be one of the most advanced and mature technologies for utility-scale solar power generation. However, while molten salts have several advantages as thermal energy storage medium, there are also some drawbacks and limitations to consider such as: corrosiveness to certain metals and alloys, cost and degradation temperature of the compound above 550 °C [2]. In spite of these, molten salts are already in use today, also other TES technologies, such as solid-state thermal storage using concrete or solid particles, are being trialed. As the raw material in this example is inexpensive, it could reduce the capital cost of CSP applications [3].

The use of alternative materials, such as wastes or by-products, for thermal energy storage is an important aspect of the circular economy concept and a fundamental strategy for future energy systems [4]. This concept aims to keep resources in use for as long as possible, extracting the maximum value from them. In this sense, using alternative materials for thermal energy storage is a way of repurposing these materials and giving them a new life, rather than disposing as waste.

This study, is focused on the evaluation of the compatibility between solar salt and various particulate solids at high temperature. The different solids, natural materials and wastes, will be heated together with the solar salt at 400 °C for 500 h in an air atmosphere. After 500 h of contact at 400 °C, the solid particle material and the solar salt were separated, and evaluated independently. Then, a chemical and thermal evaluation of solar salt has been done.

## 2. Materials and method

The solid particle materials in this study are comprised by natural materials, silica sand and wastes from mining industry, flotation. Solar salt mixture consists of sodium nitrate and potassium nitrate (60:40 wt.% respectively). Both compounds were obtained from the company Merck ACS reagent grade with a purity > 99.5%. The solar salt mixtures were obtained with the preparation of 60:40 weight percentage of sodium nitrate and potassium nitrate respectively.

The compatibility test of solar salt and the different particulate materials were carried out under air atmosphere with an alumina crucible in a standard furnace. The test conditions were an isotherm of 400 °C for 500 h and the mixture of the materials were done near 300 °C to avoid bubbling and some solids decomposition.

Chemical analysis and thermal characterization were carried out with all samples in order to evaluate the change of thermal properties and the chemical stability of the solar salt. Specifically, a UV-Vis spectrophotometer equipment was used to determine the evolution of solar salt degradation after the thermal exposure for 500 h.

## 3. Results and discussion

### 3.1. Chemical analysis

XRD comparison of molten salts samples in contact with different materials are reported in Figure 1. It reveals a diffraction peak in solar salt / flotation sterile sample that matches with  $\text{Ca}(\text{OH})_2$  presence at 18° and 34°, which according to peak list of  $\text{Ca}(\text{OH})_2$ , higher intensity is detected at 34° and 18°. This could probably be due to the solar salt / solid separation and is not relevant to solar salt degradation.

The indirect method used to quantify the nitrite concentration was already used by Svobodova-Sedlackova, et al. [5] for the determination of  $\text{NO}_2^-$  in a  $\text{NaNO}_3$  mixture with nanoparticles. A nitrite quantification will help to determine the stability of the salt and its degradation process. Figure 2 shows the UV-Vis spectra of 0.3 M solution of all solar salt in contact with each material during thermal treatment. Also, in Table 1 it is represented the calculation of nitrite percentage in each solar salt following the linear fit equation  $y = 0.0722x - 0.0024$ . The calculations of  $[\text{NO}_2^-]$  presence, show a slight increase in the presence of nitrite in solar salt samples in contact with flotation sterile waste. The nitrite concentration is around 0.6 times more that compared to the other samples.

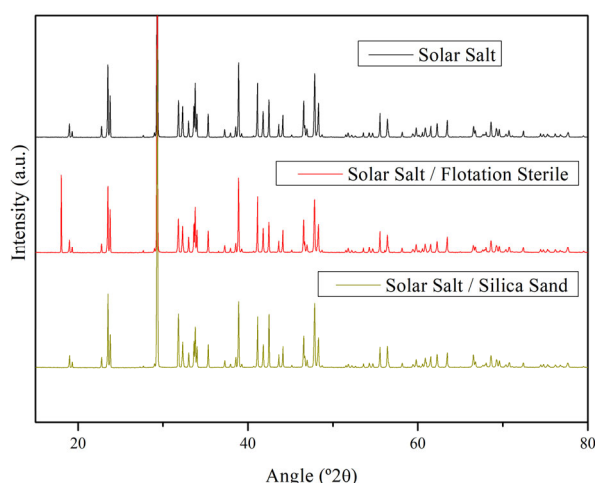


Figure 1. XRD comparison of molten salts in contact with the solids after the treatment.

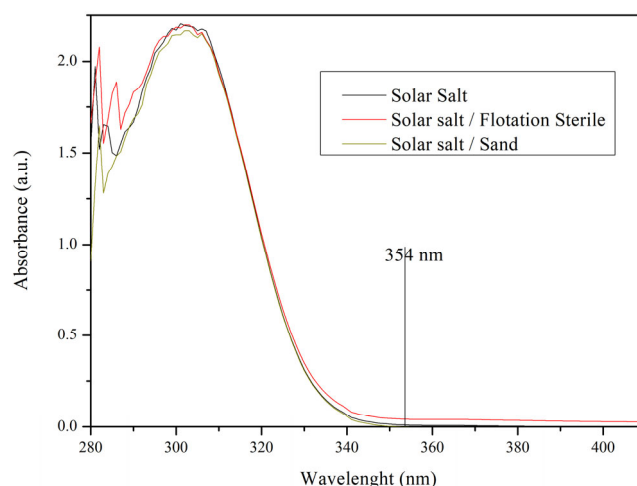


Figure 2. UV-Vis spectra of 0.3 M solution for all solar salt in contact with solid particle materials

Table 1. UV- Vis spectra calculation result of  $[\text{NO}_2^-]$  presence in solar salt samples.

Solar salt + materials	Abs. Peak at 354 nm (a.u.)	Calculation of $[\text{NO}_2^-]$ presence in the sample (wt.%)
Solar Salt	0.0103	0.17
Solar salt / Flotation Sterile	0.0420	0.61
Solar salt / Sand	-0.0015	0.01

### 3.2. Thermal evaluation

Specific heat measurements were done at 400 °C and the variation of heat capacity regarding the initial value of solar salt are reported at Table 2.

Table 2. Heat capacity at 400 °C of solar salt in contact with the samples.

Solar salt + materials	As received (kJ/kg·K)	After thermal exposure (kJ/kg·K)
Solar Salt	1.56 ± 0.01	1.56 ± 0.01
Flotation sterile	-	1.48 ± 0.01
Sand	-	1.60 ± 0.01

## 4. Conclusions

A thermal compatibility test was carried out for solar salt and several solids. Chemical and thermal evaluation of solar salt stability was evaluated. XRD does not show a pattern that fits with  $\text{NaNO}_2$  presence in any sample. This was confirmed and quantified with UV-Vis test, where following a linear calibration, a calculation of  $[\text{NO}_2^-]$  presence could be done. Near 0,6 wt.% of  $[\text{NO}_2^-]$  was present in solar salt / flotation sterile sample, whereas the other samples expressed a value around 0 wt.%. This led us to think in a possible early degradation of solar salt with depending on the kind of particles. This behaviour of some materials as a degradation catalyst could affect power plant lifespan.

On the other hand, heat capacity values of molten salts in contact with the solids experienced a slight variation, probably due to some compound that remained in the salt after the separation. The highest variation was a drop around 5% on its heat capacity in solar salt / flotation sterile sample.

## Acknowledgements

This work is part of PCI2020-120695-2 and PCI2020-120682-2 projects funded by Ministerio de Ciencia e Innovación - Agencia Estatal de Investigación (MCIN/AEI/10.13039/501100011033) and by the European Union “NextGenerationEU”/PRTR”, Development and evaluation of novel concepts for

LHTES funded by CSO - Israeli Ministry of Energy, 120N663 project funded by TÜBITAK— Scientific and Technological Research Council of Turkey, and 121N737 project funded by TÜBITAK.

## References

- [1] A. Calderón, C. Barreneche, C. Prieto, M. Segarra, A.I. Fernández, Concentrating Solar Power Technologies : A Bibliometric Study of Past , Present and Future Trends in Concentrating Solar Power Research, 7 (2021) 1–22. <https://doi.org/10.3389/fmech.2021.682592>.
- [2] T. Delise, A.C. Tizzoni, M. Ferrara, N. Corsaro, C. D'Ottavi, S. Sau, S. Licoccia, Thermophysical, environmental, and compatibility properties of nitrate and nitrite containing molten salts for medium temperature CSP applications: A critical review, J. Eur. Ceram. Soc. 39 (2019) 92–99. <https://doi.org/10.1016/j.jeurceramsoc.2018.07.057>.
- [3] IRENA, Innovation Outlook: Thermal Energy Storage, 2020. <https://www.irena.org/publications/2020/Nov/Innovation-outlook-Thermal-energy-storage>.
- [4] E.M.R. Society, Materials Innovation for the Global Circular Economy and Sustainable Society, VI World Mater. Summit. (2017). [https://www.esf.org/fileadmin/user\\_upload/esf/2018\\_WMS\\_online.pdf](https://www.esf.org/fileadmin/user_upload/esf/2018_WMS_online.pdf).
- [5] A. Svobodova-Sedlackova, S. Huete-Hernández, A. Calderón, C. Barreneche, P. Gamallo, A.I. Fernandez, Effect of Nanoparticles on the Thermal Stability and Reaction Kinetics in Ionic Nanofluids, Nanomaterials. 12 (2022). <https://doi.org/10.3390/nano12101777>.

EUROTHERM2023-R173

## Tool for restoring street life through the design of thermal conditioning strategies

M. Paz Montero Gutiérrez, Teresa Palomo Amores, Rafael Monge Palma,  
M. Carmen Guerrero Delgado, José Sánchez Ramos, Servando Álvarez Domínguez

Grupo Termotecnia, Energy Engineering Department, Universidad de Sevilla, Camino de los Descubrimientos,  
41092 Sevilla, Spain, Phone: 630125814, e-mail: mmontero1@us.es

### Abstract

The importance of comfort in urban spaces has been reinforced by the concept of the Heat Island in large cities. The aim is to restore the livability, fighting against climate change and its adverse effects. Likewise, qualified technical personnel need a platform to help in the decision making to establish conditioning strategies in outdoor spaces. To this end, within the framework of the CONSTANCY and NATURBEAM projects a catalog in the form of a database is developed. It can store technical information on items existing in urban areas. The tool can also analyse any area of interest through its direct connection with Google Maps, including different calculation engines to generate a file of results for the user's interpretation. The file shows the comfort index through an intuitive and versatile spatio-temporal representation, recommending technologies and urban elements to solve the detected problems.

**Keywords:** Design tool, thermal comfort, urban spaces, urban heat island.

### 1. Introduction

The use of urban space is reduced due to frequent heat waves caused by the Heat Island phenomenon [1]. Leisure activities are not an option on hot days in southern European cities. It is essential to redesign and sustainably fit out open spaces using innovative solutions and natural techniques [2]. These techniques help to achieve comfort conditions that create pleasant, attractive, and liveable spaces [3].

To this end, urban planners, architects, and engineers need computer software that allows them to make decisions on strategies to mitigate high temperatures in urban space. Analysing urban elements and their characteristics is essential to ensure comfort in outdoor spaces [4]. To this end, an intuitive tool capable of proposing a solution to the problem is designed making use of the Cartuja QANAT project's component catalogue (UIA03-301). Different calculation modules are designed for the control of solar radiation by means of shading elements that do not overheat, as well as the reduction of air temperature and surface elements.

### 2. Materials and method

#### 2.1. Tool modules and functionality

This software makes it possible to analyse the elements that make up an urban space and propose improvements to make them more liveable, helping to mitigate heat by planning actions. Figure 1 shows the task bar of the programme, where it can be seen a module for calculating the comfort index of people outdoors, a database with geometric and radiant properties of urban elements and a platform to implement technologies that help mitigate the heat island.

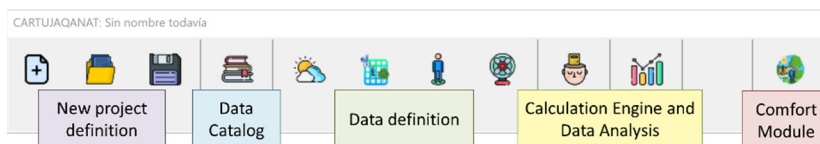


Figure 69. Programme task bar

Figure 2 shows the catalogue in the form of a database, storing technical information on existing elements in urban spaces: vegetation, natural techniques, vertical screens (façades or vegetation screens) and horizontal urban screens (covers). The tool currently consists of a module for the analysis of any area of interest through its direct connection to Google Maps. The maps allow the design of a complete study area. The extracted document locates pavements, trees, and covers, as well as their main radiant properties and geometric characteristics.

Besides, the programme includes different calculation engines to generate a results file for quick interpretation by the user. These results show the comfort indices and radiant properties by means of an intuitive and versatile spatio-temporal representation. In the same output file, help is offered on those technologies or elements to be considered in the urban space to solve the problems detected.

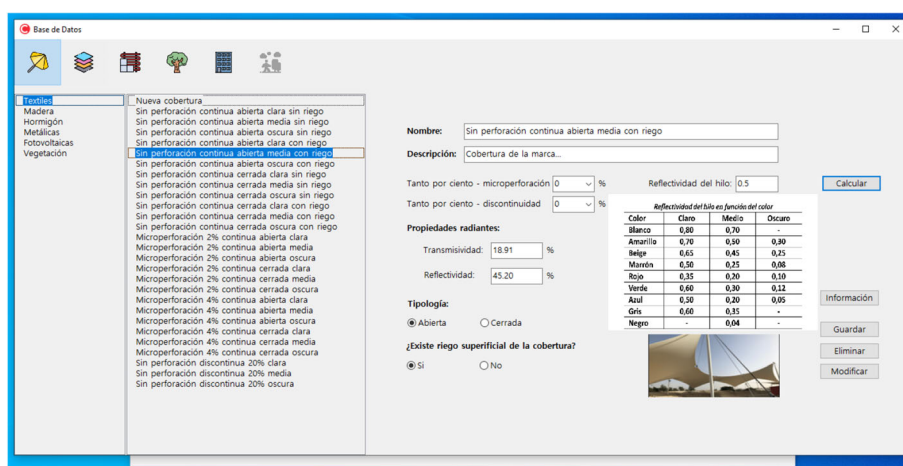


Figure 70. Catalogue of urban element components

## 2.2. Case of study

The case studies defined have made it possible to design the pilot of the LIFE WATERCOOL project (LIFE18 CCA/ES/001122): *Water efficient systemic concept for climate change adaptation in urban areas*. One of the main objectives of the project is to renovate the square located in the Avenida de la Cruz Roja in Seville. It is planned to plant a larger number of trees to create a green and liveable space during summer periods. Likewise, a set of hexagonal parasols has been designed to ensure shade in the square until the trees have reached the adult stage, as shown in Figure 3. This hexagonal cover is made up of equilateral triangles that can be easily disassembled and reused according to the need for shade in the space.

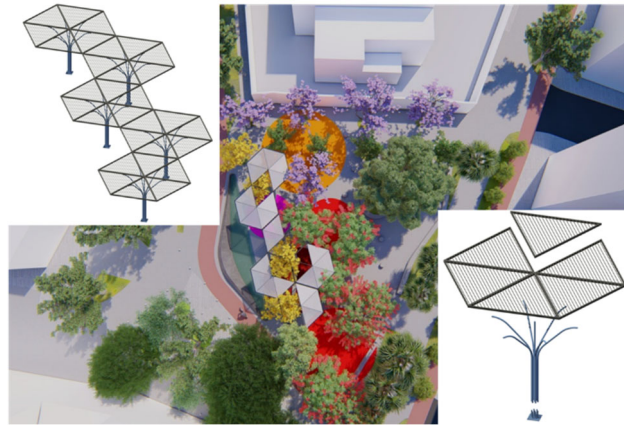


Figure 71. Hexagonal sunshades of the case study

### 3. Results and discussion

In the different cases defined, the same living area formed by the same number of cells is studied (Figure 4). It is a rectangular area with cells of 3 meters on each side, occupying the space in which a hexagonal roof structure is located. It is desired to analyze how the PET comfort index (°C) changes in these zones as the complexity of the case studied increases.

- Case 1: Actual state of the square.
- Case 2: Effect caused by hedges.
- Case 3: Effect caused by hedges and introduction of preconditioned air.
- Case 4: Effect caused by tree planting.
- Case 5: Effect caused by tree planting and introduction of preconditioned air.



Figure 72. Case study 5 in the tool

Figure 5 shows the different results that have been obtained by studying the cases presented. As mitigation techniques are implemented in the urban space analysed, the comfort index improves by up to 30%. The analysis of the proposed case study has made it possible to validate the use of the tool.

Case 1		Case 2		Case 3		Case 4		Case 5	
Hour	PET (°C)	Hour	PET (°C)	Hour	PET (°C)	Hour	PET (°C)	Hour	PET (°C)
12:00	44,40	12:00	41,40	12:00	31,70	12:00	28,58	12:00	25,56
14:00	49,20	14:00	46,90	14:00	34,90	14:00	35,35	14:00	29,94
16:00	50,40	16:00	48,60	16:00	38,40	16:00	42,35	16:00	35,97
18:00	48,90	18:00	47,00	18:00	37,40	18:00	44,64	18:00	37,89
20:00	37,80	20:00	35,20	20:00	28,20	20:00	32,98	20:00	28,63
Mean value: 35,27°C		Mean value: 31,00°C		Mean value: 27,20°C		Mean value: 28,51°C		Mean value: 24,95°C	

Figure 73. PET comfort index results obtained with the tool



#### 4. Conclusions

Thanks to the tool, the user can optimize the environmental design of a specific space using an intuitive and simple conceptual guide. It also makes it possible to dimension and quantify economically all the urban elements that integrate the solution.

- The number of hours in discomfort is reduced by 23% when the adaptive solar shading is incorporated and by 30% when fully grown trees are considered.
- Introducing pre-conditioned air greatly enhances the comfort of the living area. Case 3 and case 5 provide a 12% improvement over case 2 and case 4, respectively.
- Thanks to the adaptive solar solution, it is possible to reduce the number of hours of discomfort during the central hours of the day.

Bringing life back to the streets in cities with predominantly warm climates is possible. Combining vegetation, adaptative sunshades and preconditioning air strategies make the urban area more liveable.

#### Acknowledgments

This study has been funded by the projects "CONSTANCY - Resilient urbanisation methodologies and natural conditioning using imaginative nature-based solutions and cultural heritage to recover the street life" (Grant Agreement PID2020-118972RB-I00) and the project "NATURBEAM - Lighting the way to a greener future to restore urban habitability through nature-based solutions" (Grant Agreement TED2021-130416B-I00) by the Science and Innovation Ministry of Spain. Also, this study has been co-financed by the European Regional Development Funds (ERDF).

#### References

- [1] F. Marando et al., "Urban heat island mitigation by green infrastructure in European Functional Urban Areas," *Sustain Cities Soc*, vol. 77, p. 103564, Feb. 2022, doi: 10.1016/j.scs.2021.103564.
- [2] Y. Dzyuban et al., "Outdoor thermal comfort research in transient conditions: A narrative literature review," *Landsc Urban Plan*, vol. 226, p. 104496, Oct. 2022, doi: 10.1016/j.landurbplan.2022.104496.
- [3] S. Coccolo, J. Kämpf, J.-L. Scartezzini, and D. Pearlmutter, "Outdoor human comfort and thermal stress: A comprehensive review on models and standards," *Urban Clim*, vol. 18, pp. 33–57, Dec. 2016, doi: 10.1016/j.uclim.2016.08.004.
- [4] C.-H. Huang, H.-H. Tsai, and H. Chen, "Influence of Weather Factors on Thermal Comfort in Subtropical Urban Environments," *Sustainability*, vol. 12, no. 5, p. 2001, Mar. 2020, doi: 10.3390/su12052001.

EUROTHERM2023-E174

## **Radiant solution for thermal conditioning of short-term urban spaces**

M. Paz Montero Gutiérrez, Teresa Palomo Amores, Rafael Monge Palma,  
M. Carmen Guerrero Delgado, José Sánchez Ramos, Servando Álvarez Domínguez

Grupo Termotecnia, Energy Engineering Department, Universidad de Sevilla, Camino de los Descubrimientos,  
41092 Sevilla, Spain, Phone: 630125814, e-mail: mmontero1@us.es

### **Abstract**

Urban space is a hostile place for the citizens of large cities in southern Europe during the summer. Besides, the use of public transport is reduced because of the urban heat island. For this reason, the creation of climate shelters is essential to improve the thermal comfort of their occupants. This study proposes the design of a self-sufficient bus stop to be installed in the city of Seville. To this end, a bus stop is designed through the integration of Falling-Film technology and the incorporation of radiant cooling modules. Based on a prototype assembly, its behavior is evaluated in a fully sensorised climate chamber to study the efficiency of the systems. The results obtained in the experiment focus on the analysis of convective and radiant heat flux under different thermal conditions, ensuring that 60% of the total heat flow is due to radiation. Thermographic images also show that the prototype helps to reach comfort in 20 minutes.

**Keywords:** Public transport infrastructure, short-term stay, urban shelter, urban heat island, thermal comfort.

### **1. Introduction**

Society has experienced an exceptional situation with the SARS-COV-2 virus [1]. Society spends most of its time indoors. It is demonstrated that prolonged stay indoors can become a potential health risk in the absence of air quality assessment [2]. This is why scientists recommend making use of outdoor spaces to mitigate risks [3]. Despite this recommendation, extreme heat events, such as heat waves, are becoming more frequent [4]. Climate change is real, and citizens are suffering from one of its main adverse effects: the urban heat island. Temperatures in cities are higher than in rural areas due to unsustainable and resilient urban patterns [5].

For this reason, big city administrations are creating climate shelters to help mitigate the effects of climate change [6]. The focus of attention is on bus stops [7]. In the summer season their use is reduced due to high urban temperatures. In addition, leisure time in the middle of the day in large cities is affected. This is why climate shelters become a pioneering solution to help citizens cope with these harsh weather conditions. These areas are usually parks or shady places that have been renovated and are open to the public free of charge. They aim to provide thermal comfort, safety, acoustic comfort, and wind protection in urban spaces.

### **2. Materials and method**

A new concept of air-conditioned bus stop is designed using natural techniques for urban transport in the city of Seville. It is prototyped following the geometry and dimensions of the existing bus shelters in this city. Water is the main fluid used to cool and achieve comfort levels inside the semi-open area. Two circuits with radiant technology are used to reduce the temperature of the fluid and the studied area. The main objective of the concept is to achieve total self-sufficiency of the infrastructure. This is possible thanks to the implementation of the radiant Falling-Film technique [8], [9]. These are solar

collectors that generate energy easily during the day and use the sky as a heat sink at night. Meanwhile, the study area of the bus stop is cooled by radiant surface cooling modules.

The climate chamber is fully sensorised and equipped. The air inside is controlled by an air-to-air heat pump that allows the temperature to be regulated. Similarly, the presence of underfloor heating simulates the thermal radiation emitted by the urban pavement. Figure 74 shows the prototype installed in a climate chamber at the School of Engineering of the University of Seville. The cooling modules are tested thanks to the installation of a chiller that provides water at different setpoint temperatures. This technology provides the same performance as the Falling-Film technique, allowing different experiments to be carried out.

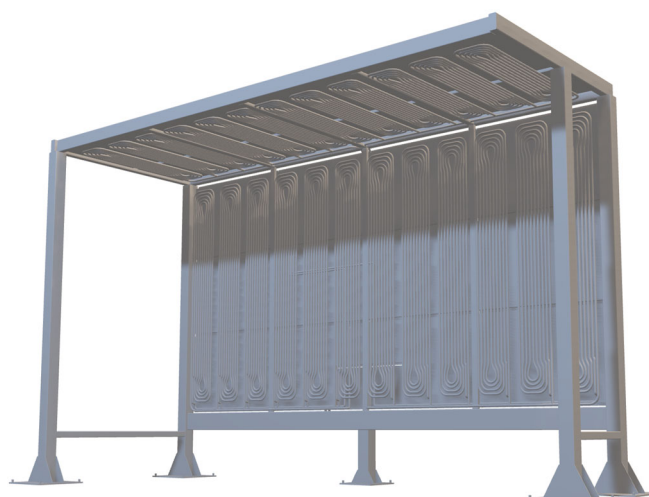


Figure 74. Prototype bus stop installed inside the climate chamber.

The radiant modules are protected at the rear by thin insulation. This ensures that all heat flow is transferred to the study area. At the front, the modules are protected by a perforated metal sheet. Figure 75 shows different parts of the bus stop inside the climate chamber. First, a detail of the perforated metal sheet and the insulation is shown. Secondly, the water pump that drives the cooled water to the radiant modules of the bus stop and the pump for the correct operation of the underfloor heating are shown. Thirdly, the collector on the prototype is shown. This allows the water to be distributed to the radiant cooling modules located on the ceiling and the front of the prototype. Finally, the chiller is shown, which allows the set-point temperatures of the water to be established. The water is stored in a 500-litre tank.

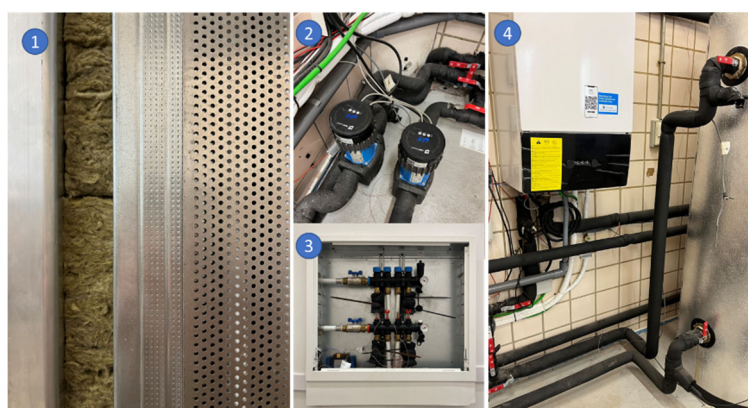


Figure 75. Technologies installed in the climate chamber

Three types of experiments are carried out depending on the flow rate provided to the modules: Low (125L/h), medium (442 L/h) and high (742 L/h) flow rates. The air inside the climatic chamber is at

30°C thanks to the air-to-air heat pump. The set temperature of the chiller varies between 18, 20 and 22°C.

### 3. Results and discussion

Figure 3 shows the results obtained in the characterisation of the convective and radiant heat flow of the cooling modules. In both graphs the convective heat flux (W/m<sup>2</sup>) is plotted against the convective LMTD, for the ceiling and the front, respectively. The higher the flow rate of the water pump, the higher the convective heat flow. From these graphs it can be deduced that 60% of the heat flow emitted by the prototype is radiant.

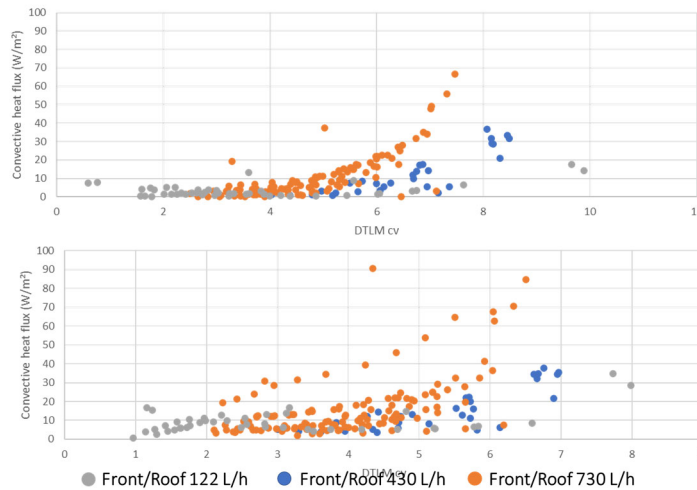


Figure 76. Characterisation of the convective and radiant heat flow

Thermographic images ensure the correct operation of the bus stop. Figure 4 shows four snapshots taken from a video. The temperature of the roof and the front of the bus stop reaches 19°C in only 20 minutes. The cooling heat flow is uniform.

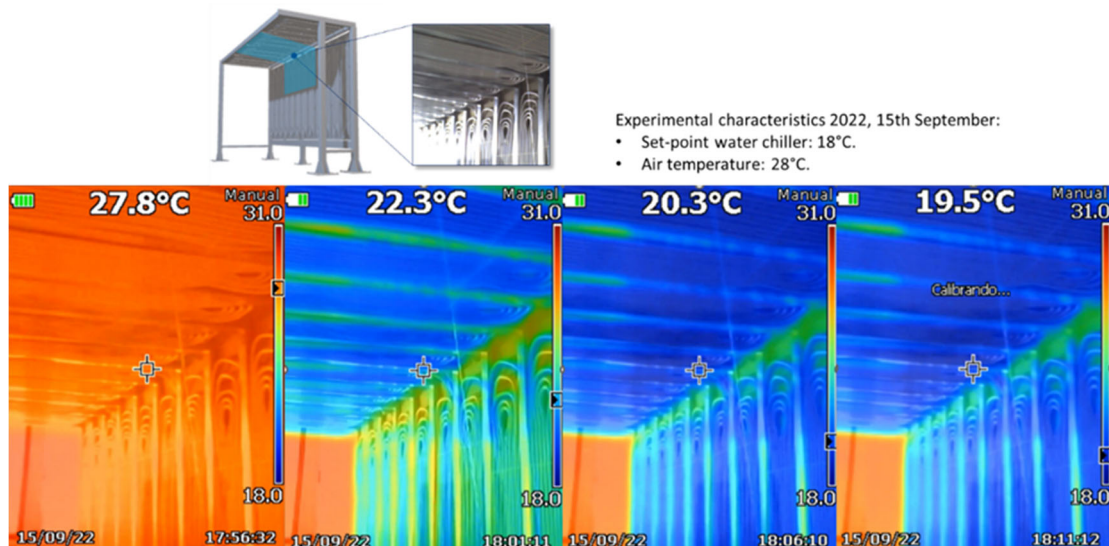


Figure 77. Thermographic images of the ceiling and front of the bus stop

## 4. Conclusions

A short-term stay solution for bus stops has been developed. It is shown that 60% of the heat flux emitted by refrigerating modules is by radiation. The results of the experiments carried out prove the radiant cooling possibilities of the system. This new technology can be applied to winter heating periods.

In addition, the research carried out allows obtaining a characterization model, which could be used for the design and sizing of new urban facilities. The technological solution is efficient and cost-effective, so it would be easily replicable throughout the city.

## Acknowledgments

This study has been funded by the projects "CONSTANCY - Resilient urbanisation methodologies and natural conditioning using imaginative nature-based solutions and cultural heritage to recover the street life" (Grant Agreement PID2020-118972RB-I00) and the project "NATURBEAM - Lighting the way to a greener future to restore urban habitability through nature-based solutions" (Grant Agreement TED2021-130416B-I00) by the Science and Innovation Ministry of Spain. Also, this study has been co-financed by the European Regional Development Funds (ERDF).

## References

- [1] World Health Organization, "Modes of transmission of virus causing COVID-19: implications for IPC precaution recommendations.," Mar. 29, 2020.
- [2] T. Greenhalgh, J. L. Jimenez, K. A. Prather, Z. Tufekci, D. Fisman, and R. Schooley, "Ten scientific reasons in support of airborne transmission of SARS-CoV-2," *The Lancet*, vol. 397, no. 10285, pp. 1603–1605, May 2021, doi: 10.1016/S0140-6736(21)00869-2.
- [3] J. W. Tang et al., "Dismantling myths on the airborne transmission of severe acute respiratory syndrome coronavirus-2 (SARS-CoV-2)," *Journal of Hospital Infection*, vol. 110, pp. 89–96, Apr. 2021, doi: 10.1016/j.jhin.2020.12.022.
- [4] F. Marando et al., "Urban heat island mitigation by green infrastructure in European Functional Urban Areas," *Sustain Cities Soc*, vol. 77, p. 103564, Feb. 2022, doi: 10.1016/j.scs.2021.103564.
- [5] P. K. Cheung and C. Y. Jim, "Comparing the cooling effects of a tree and a concrete shelter using PET and UTCI," *Build Environ*, vol. 130, pp. 49–61, Feb. 2018, doi: 10.1016/j.buildenv.2017.12.013.
- [6] Ayuntamiento de Cataluña, "Red de refugios climáticos. Barcelona por el Clima: Ecología, Urbanismo, Infraestructuras y Movilidad," 2022.
- [7] R. Mokhtari, G. Ulpiani, and R. Ghasempour, "The Cooling Station: Combining hydronic radiant cooling and daytime radiative cooling for urban shelters," *Appl Therm Eng*, vol. 211, Jul. 2022, doi: 10.1016/j.applthermaleng.2022.118493.
- [8] Mc. Guerrero Delgado, J. Sánchez Ramos, Mc. Pavón Moreno, J. A. Tenorio Ríos, and S. Álvarez Domínguez, "Experimental analysis of atmospheric heat sinks as heat dissipators," *Energy Convers Manag*, vol. 207, p. 112550, Mar. 2020, doi: 10.1016/j.enconman.2020.112550.
- [9] Mc. Guerrero Delgado, J. Sánchez Ramos, and S. Álvarez Domínguez, "Using the sky as heat sink: Climatic applicability of night-sky based natural cooling techniques in Europe," *Energy Convers Manag*, vol. 225, p. 113424, Dec. 2020, doi: 10.1016/j.enconman.2020.113424.

## Development of PCM-based Heat Exchangers

Dan Gotesman<sup>1</sup>, Tomer Shockner<sup>1</sup>, Dmitry Portnikov<sup>1</sup>, Elad Shoham<sup>1</sup>,  
Michael Koenig<sup>2</sup>, Gennady Ziskind<sup>1</sup>

<sup>1</sup>Ben-Gurion University of the Negev, Beer-Sheva 84105, Israel, e-mail: [gziskind@bgu.ac.il](mailto:gziskind@bgu.ac.il)

<sup>2</sup>Rafael Ltd. Haifa 31021, Israel

### Abstract

This paper discusses the challenge of transient thermal behavior with periodic characteristics in various applications. The high heat flux from temporary power spikes can cause severe temperature fluctuations. A solution for this challenge is the design of a thermally capacitive heat exchanger (TCHX), using phase change materials (PCMs), as they have large heat storage capacity due to their latent heat of solid-liquid phase change. The current work focuses on developing a modeling strategy for designing PCM-based TCHX devices, using commercial and in-house codes. It is envisioned that the computational model will be validated with experimental results.

**Keywords:** Thermal energy storage, Phase change materials, Heat exchanger

### 1. Introduction

Various studies have been conducted in the field of thermal energy storage (TES) on geometries that are inspired by heat exchangers, including in our group. For instance, Ezra et al. [1] implemented a tube bank configuration for cross-flow tubular PCM-air heat exchanger, as the tubes contained PCM. When we investigate on how to incorporate PCM into heat exchangers, while simultaneously charging and discharging heat from the PCM, we can look at works that use similar ideas. For example, Kozak et al. [2] presented a work that deals with a combined device in which the heat may be both absorbed by a PCM and dissipated to the ambient air. The heat is generated at the heat sink base, and then is transferred by conduction through PCM using partitions that connect the sink base with a standard air heat sink, cooled by an attached fan.

Heat exchanger with incorporated PCM may serve as a possible solution for an effective thermally capacitive heat exchanger (TCHX), used to accumulate the generated heat from a device load and mitigating temperature rise or fluctuations by absorbing and releasing thermal energy. The current work focuses on developing a modeling strategy for designing of TCHX devices, inspired by the knowledge gained from latent heat thermal energy storage (LHTES) field in order to design PCM-based TCHX systems. This work is an initial effort of developing a computational model that include both simplified and sophisticated modeling approaches, using commercial and fully developed in-house codes being developed by the first author as part of his ongoing M.Sc. research.

### 2. Configuration and results

Based on the literature survey, a concept of TCHX is presented. It is desirable to have a way for quick estimates of a potential engineering system in order to find, even approximately, the preferable case, which may be fine-tuned at the next step. Here, too, it is important to have a modular model, based on the understanding of the processes in elementary units of which the full system consists. Elementary unit is identified such that two aims are addressed simultaneously: (1) it reflects as close as possible the processes in the entire exchanger; (2) its size and structure allow a complete and detailed numerical simulation. It is important to mention that the geometry is modeled in 3D. It is thus obvious that a

modular system, built of several units, is desirable. It is suggested to identify a basic unit that could be modeled in the most detailed fashion. The results will serve as building blocks for modeling of the entire TCHX.

The concept studied in this work is a shell-and-tube concept. One tube, which is a part of a tube bank heat exchanger, is chosen as a model of elementary unit. This geometry consists of a tube and shell with inner and outer longitudinal fins, where PCM is embedded in the shell. Fig. 1 shows the models that are being tested. We analyze both configurations where fins are attached to both tubes and where fins are embedded into the PCM without connecting the tubes. In this configuration, a full symmetry is assumed (i.e., when the axis of the unit is vertical), in order to significantly reduce the computation time.

The unit shown in Fig. 1 is a 1/24 slice of the elementary unit (shell and tube unit). Based on the results for this unit, assuming full symmetry, results for the full elementary unit can be deduced. It should be noted that in the literature, the analysis of a single-tube unit is usually done. For a longitudinal flow either inside or outside the tube, this approach can be quite reliable, since a practically important multi-tube unit may be considered as comprised of several single-tube units which do not affect one another while contributing to the total performance. This also depends on the flow path and connectivity of different units. For a series connection of tubes (multiple passes), this assumption would not hold. Also, analyzing a single tube in a cross-flow tube bank as elementary unit will clearly result in unidentical conditions for each row, because there each row will depend on the effect of the preceding row.

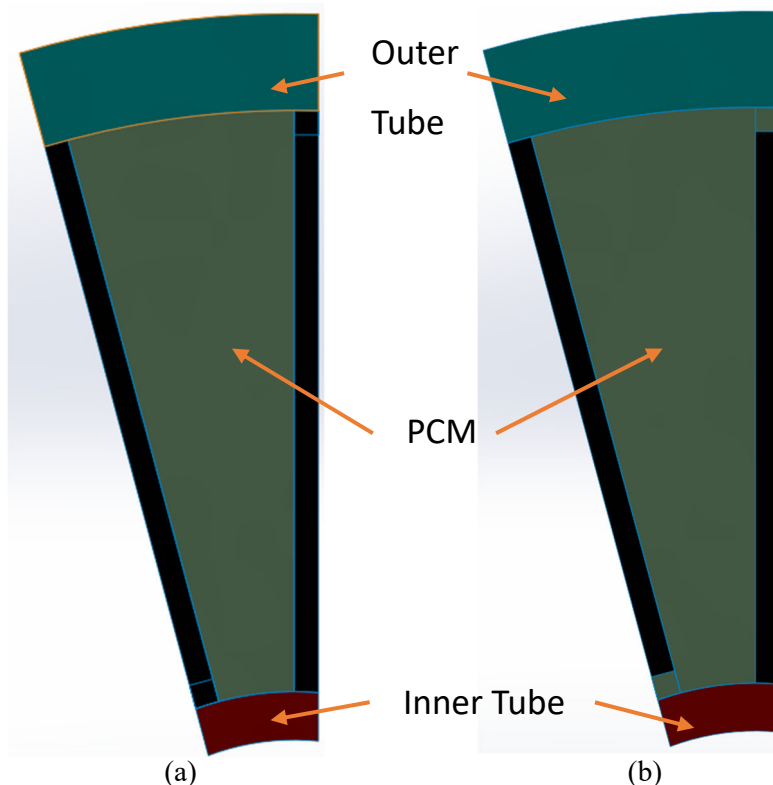


Figure 1. Cross section of a shell and tube unit with longitudinal fins (a), and shell and tube unit with longitudinal fins embedded into the PCM (b).

The numerical solutions that are presented here are obtained using in-house coding with MATLAB software. The model geometry dimensions are: inner tube radius of 5 mm and thickness of 1 mm, outer tube radius of 18 mm and thickness of 2 mm, fins length of 12 mm and thickness of 1 mm (0.5 mm is modeled due to symmetry) and tube length of 500 mm. This geometry dimensions were chosen as a starting point from previous studies on a similar finned tube geometry. While it was proven as a reliable and practical device.

In the simulations, the unit is tested under boundary conditions of constant heat transfer coefficient with temperatures of 30 °C and 0 °C at its hot (inner) and cold (outer) tube, respectively. The temperatures are set with consideration of n-Tetradecane melting temperature of 6 °C. Liquid (melt) fraction is monitored throughout the calculation process, in addition to the temperatures in the unit.

Fig. 2 shows results for the 3D "slice" of Fig. 1, 100 seconds after the start of the simulation. when the boundary conditions are set as mentioned above. The presented figures show both configurations and will provide us with the necessary information for further investigating and optimizing the given model.

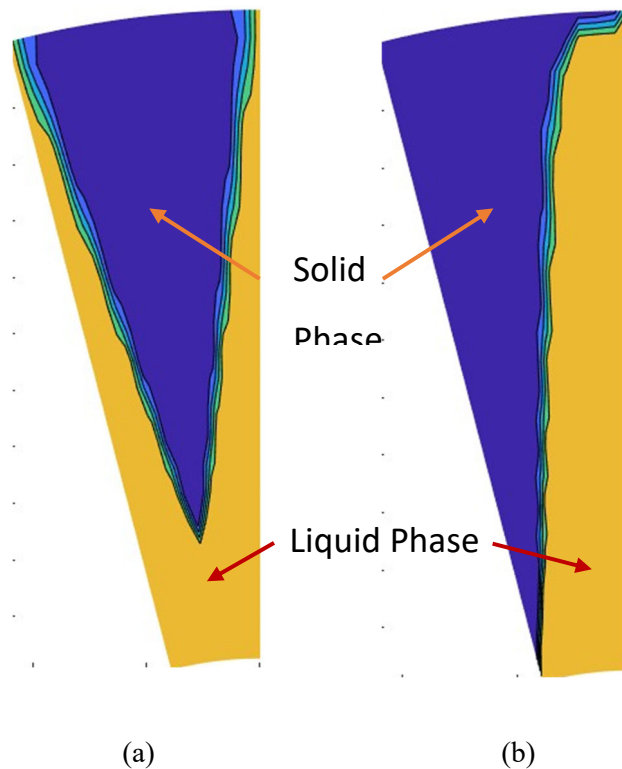


Figure 2. Melt fraction results for the model presented in Fig. 2a (a), and Melt fraction results for the model presented in Fig. 2b (b).

### 3. Closure

The present work is aimed at incorporating PCM into a heat exchanger, as a part of development of an effective thermally capacitive heat exchanger (TCHX). An example of simulation using an in-house code is presented with promising results. Still, there is a need for more thorough optimization on the specific geometry and the entire system. This work is an initial effort for developing a computational model and design strategy for TCHX devices that incorporate PCMs. It is envisioned that experiments will be conducted to validate the numerical modelling.

### References

- [1] M. Ezra, Y. Kozak, V. Dubovsky, G. Ziskind, Analysis and optimization of melting temperature span for multiple-PCM latent heat thermal energy storage unit, *Applied Thermal Engineering* 93 (2016) 315-329.
- [2] Y. Kozak, B. Abramzon, G. Ziskind, Experimental and numerical investigation of a hybrid PCM-air heat sink, *Applied Thermal Engineering* 59 (2013) 142-152.



EUROTHERM2023-Y177

## Innovative solutions using thermal energy storage in buildings

Teresa Palomo Amores, M<sup>a</sup> Carmen Guerrero Delgado, Rafael Monge Palma, M<sup>a</sup> Paz Montero Gutierrez, José Sánchez Ramos, Servando Álvarez Domínguez

Grupo termotecnia, University of Seville, Avenue Camino de los Descubrimientos S/N 41092 Seville  
Email: tpalomo@us.es

### Abstract

The social housing districts in energy poverty in southern Spain present a serious problem of overheating in cooling regime. In these cases, conventional measures to improve the performance of the building envelope are not enough. In this work, an innovative roof solution is designed and integrated into a promotion of social housing in block located in Camas, Seville. This solution consists of an active roof that allows the exploitation of thermal inertia and the integration of environmental sinks.

**Keywords:** buildings, innovative solutions, natural sinks, thermal mass

### 1. Introduction

The high energy consumption of the construction sector, climate change and energy poverty are some of the serious problems that appear in cities [1]. Cities have become one of the cornerstones in the fight against climate change due to their growing energy demand. Faced with the objective of combating climate change, there is also the phenomenon of Urban Heat Island (UHI), which is an increasingly important global problem [2]. The problem of overheating faced by urban centres has led to a rapid increase in hot days and extreme weather, extremely increasing the demand for cooling in buildings [3]. Increased demand for cooling leads to increased energy consumption, leading to increased greenhouse gas emissions. According to the IEA [4] cooling needs have tripled in buildings since 1990, with refrigeration responsible for 10% of total electricity consumption in 2019 worldwide.

In this line, the roof of buildings is a critical element of the envelope in the demand for cooling due to high solar gains [5]. Different authors have studied how to optimize the performance of the roof of buildings, however, the literature does not solve the scientific and technological development that requires the practical implementation in a real building of air chambers on ventilated roofs. Likewise, the integration of this type of elements in decision-making procedures for the optimal definition of energy rehabilitation interventions on existing buildings is not resolved.

The main objective of the work is to integrate a roof element on a proposal for the integral rehabilitation of a residential building. This integration involves solving the design and evaluation of a roof element that allows the integration of natural cooling techniques in the envelope of the building itself for the use of thermal inertia. All with a hybrid solution day-night mode, with a totally affordable extra cost and high profitability improving the performance of the envelope in heating and cooling mode.

### 2. Materials and method

The active roof is a concept developed within the framework of a research project of the Ministry of Development and Housing of the Junta de Andalucía through the Public Works Agency of Andalusia. The title of the project was: "Analysis of the energy behavior of concrete enclosures based on the maximization of the advantages derived from their thermal inertia", the main researcher was Servando Álvarez from the University of Seville and was developed in the period 2014 to 2016.

The active ventilated cover is formed by two layers or main sheets between which there is a space or air chamber through which forced ventilation can be established by a fan system. The operation of the ventilation is automated in such a way that ventilation is carried out only when it is convenient from the energy point of view. The main purpose of the roof is to reduce solar gains and cool the spaces under cover. To do this, it presents three fundamental modes of operation:

- Mode 1. During the day when there is solar radiation and outside temperatures are high, air circulation is stopped (fan off and closed gates). The outer sheet when insulated rejects most of the heat, simultaneously preventing the cold stored overnight in the inner leaf from escaping to the outside. The consequence is that the cold enters the interior of the building.
- Mode 2. During the night, when the outside temperature is low enough, the air circulation is activated (fan on and doors open) and dissipates heat from the inner sheet of the cover that consequently cools.
- Mode 3. In case the minimum nighttime temperatures do not drop enough to trigger heat from the deck, the cold loading mode described in 2 is ineffective. For this circumstance, an evaporative cooling system is included to achieve an additional reduction in air temperature.

The designed solution consists of an air chamber between the existing roof and the outer wall, in such a way that it resembles a conventional ventilated façade. The outer wall is insulated in the form of an EPS "sandwich", providing a great insulation capacity while lightness and thus helping to reduce the temperature transfer achieved in the chamber to the outside. Finally, the air distribution channels are generated from the integration of a deck sheet to the existing roof in order to facilitate its construction. Below is the constructive detail of the air chamber of the active roof designed for the rehabilitation project of the 36 public housing units in Guadalquivir and Geranio de Camas streets.

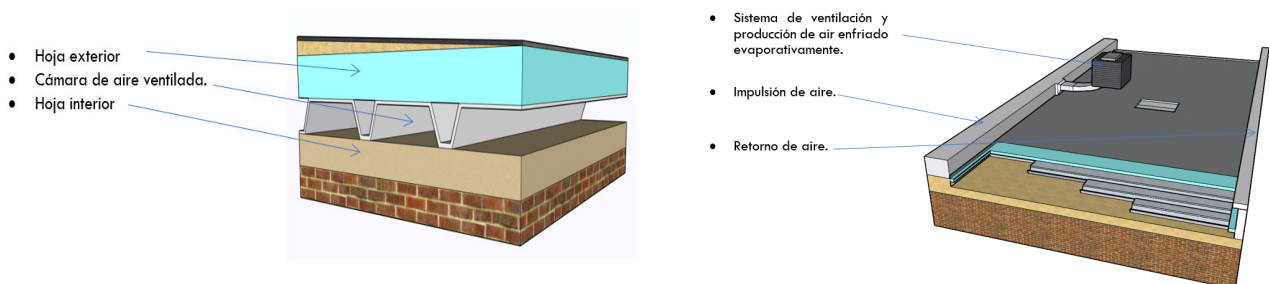


Figure 1. Construction details of the innovative roof

### 3. Results and discussion

Below are the results of the energy impact assessment of the integration of this active roof solution in the housing district located in Camas. The following table shows the results corresponding to the entire plant under cover of a block for the energy simulation of the system in the typical year.

Table 1. Cooling demands before and after the activation of the cover.

	Cooling needs (KWh/m <sup>2</sup> ) Active Roof OFF	Q active roof (kWh/m <sup>2</sup> )	Cooling needs (KWh/m <sup>2</sup> ) Active Roof ON	Used Q active roof (kWh/m <sup>2</sup> )	Utilisation factor
June	1.58	4.04	0.20	1.37	0.34
July	4.65	4.53	2.70	1.94	0.43
August	4.83	4.35	3.27	1.55	0.36
September	2.36	3.92	0.85	1.50	0.38
Summer	13.37		7.00		

The first column shows the monthly and seasonal demands of the plant under cover when the innovative roof is not activated (fan off). The second column shows the raw heat dissipated by the active cover each month following the operating scheme that was used during the experimental campaign of the system. The third column shows the monthly and seasonal demands of the plant under cover when the innovative roof is activated. As can be seen, the demand goes from 13.37 kWh/m<sup>2</sup> to 7.00 kWh/m<sup>2</sup>, that is, a reduction of the order of 50%. Column 4 includes the net heat dissipated by the active cover, i.e. the heat that has been used to remove cooling load according to the operational conditions of the HULC calculation standard. Since this standard only provides for conditioning for 8 hours a day, any improvement in conditions outside those 8 hours has not been taken into account. Finally, the fifth column presents the ratio of net dissipated heat to gross dissipated heat, i.e. the 1-time ratio of the total heat dissipated used to combat cooling load. In the most favorable month, 43% of the heat dissipated by the roof is used, which is remarkable since the production of cold occurs during the night, while the demand for cooling is requested from 4 pm the next day. In terms of the energy rating relative to the cooling demand, the innovative roof implemented allows to improve two classes of efficiency (C to A) the energy rating of the house under cover, compared to the rehabilitation with conventional roof. The final impact in terms of the rating scale of the complete block is not relevant due to the dampening effect of the heating regime, DHW and the remaining dwellings

In terms of thermal comfort, Table 2 shows the comparison of thermal comfort indicators with and without the integration of the active roof solution developed.

Table 2. Comfort indicators without (left) and with (right) activation of the innovative cover.

CONFORT	CON CUBIERTA ACTIVA OFF			CONFORT	CON CUBIERTA ACTIVA ON		
	NH	GH	GHpp		NH	GH	GHpp
Junio	355	407	84	Junio	46	22	2
Julio	665	2208	1582	Julio	437	856	401
Agosto	717	2765	2157	Agosto	522	1042	417
Septiembre	555	952	298	Septiembre	186	139	13
Verano	2292	6332	4121	Verano	1191	2059	833

As can be seen, the innovative roof implemented allows to reduce by 80% the discomfort (in terms of weighted degree-hours) of the house under cover, compared to the rehabilitation with conventional roof.

#### 4. Conclusions

Housing under cover is the weak point of multi-family housing. The significant increase in the level of insulation in summer climates is unfavorable for the cooling regime in homes without air conditioning equipment except active roofs or other systems that cool the building naturally. In the work described, the design and integration of an innovative roof solution that allows the integration of two environmental heat sinks has been carried out: cold night air and evaporative cooling. The designed roof solution is a hybrid day-night solution, with a totally affordable and highly profitable extra cost. The assessment of the impact of this innovative solution was analyzed in the pre-design phase, obtaining favorable results and therefore motivating the integration of the solution in a social housing development in Camas. The innovative roof implemented allows to improve two classes of efficiency (C to A) the energy rating of the houses under cover, reduce thermal discomfort by 80% and allows practically placing the building in a passive building situation, thereby reducing energy poverty.

#### Acknowledgements

This study has been funded by the projects "CONSTANCY - Resilient urbanisation methodologies and natural conditioning using imaginative nature-based solutions and cultural heritage to recover the street life" (Grant Agreement PID2020-118972RB-I00) and the project "NATURBEAM - Lighting the way to a greener future to restore urban habitability through nature-based solutions" (Grant Agreement TED2021-130416B-I00) by the Science and Innovation Ministry of Spain. Also, this study has been co-financed by the European Regional Development Funds (ERDF).

#### References

- [1] Santamouris M. Innovating to zero the building sector in Europe: Minimising the energy consumption, eradication of the energy poverty and mitigating the local climate change. *Sol Energy* 2016;128:61–94. <https://doi.org/10.1016/j.solener.2016.01.021>.
- [2] Nastran M, Kobal M, Eler K. Urban heat islands in relation to green land use in European cities. *Urban For Urban Green* 2019;37:33–41. <https://doi.org/10.1016/j.ufug.2018.01.008>.
- [3] Yang X, Peng LLH, Jiang Z, Chen Y, Yao L, He Y, et al. Impact of urban heat island on energy demand in buildings: Local climate zones in Nanjing. *Appl Energy* 2020;260:114279. <https://doi.org/10.1016/j.apenergy.2019.114279>.
- [4] Cooling – Tracking Buildings 2020 – Analysis - IEA n.d.
- [5] Guerrero Delgado McC, Sánchez Ramos J, Palomo Amores TR, Castro Medina D, Álvarez Domínguez S. Improving habitability in social housing through passive cooling: a case study in Mengíbar (Jaén, Spain). *Sustain Cities Soc* 2022;78. <https://doi.org/10.1016/j.scs.2021.103642>.

EUROTHERM2023-R178

## Natural conditioning of open spaces through natural techniques, its night storage and daytime use. Cartuja Qanat Project.

Teresa Palomo Amores, M<sup>a</sup> Carmen Guerrero Delgado, M<sup>a</sup> Paz Montero Gutierrez, Rafael Monge Palma, José Sánchez Ramos, Servando Álvarez Domínguez

Grupo Termotecnia, University of Seville, Avenue Camino de los Descubrimientos S/N 41092 Seville  
e-mail: tpalomo@us.es

### Abstract

The open spaces of cities have become hostile to citizens due to high temperatures. It is necessary to combat these phenomena to bring life back to the streets in cities with predominantly warm climates. The objective will be to mitigate the high temperatures reached in open spaces in a city like Seville, in southern Spain by using night storage for later use during the day. To this end, microclimate control is proposed based on natural cooling techniques associated with environmental sinks. This work addresses a real degraded and disused space as a case study to demonstrate the feasibility of the methodology used.

**Keywords:** Bioclimatic techniques, urban space, thermal comfort, natural solutions, climate adaptation.

### 1. Introduction

From the initial conception of EXPO '92 [1], it was intended that open spaces were the component that gave unitary meaning to the enclosure. The function of the public space was therefore not limited to allowing the transition between the different pavilions, but they were spaces with their own personality that favored their use. The aim of climate control work [2] of open spaces is simply to allow people to stay outside and carry out the planned activities in a sufficiently comfortable manner.

Actions that included confinement, solar control, surface cooling and air cooling were progressively used in many different ways, including those later popularized by micronization systems.

For this reason, it is proposed to reactivate the bioclimatic design that Expo 92 implemented on the Isla de la Cartuja. The fundamental piece of the project is social dynamization: people who want to be on the street in the warm months and need the street to be revitalized. The CartujaQanat project proposes to use groundwater in order to generate new urban microclimates that help combat the consequences of climate change.

The project is building a new urban space on Thomas Alba Edison Avenue to host the public life of workers and visitors to the Cartuja Science and Technology Park. This new space will be the scene of the actions aimed at revitalizing street life by offering comfort conditions in open spaces during the hottest seasons of Seville. The philosophy of the project is the use of natural conditioning techniques and obtaining a self-sufficient installation.

### 2. Materials and method

It is an innovative urban design experience that aims to improve environmental comfort through natural techniques through the control of air quality and thermal comfort. The design principles of the integrated system encompassing radiation reduction can be described in Table 1.

Table 1. Principles of design

Criterion	Generic actions	Specific techniques
Reduction of solar radiation	Obstruction of direct, diffuse and reflected radiation	-Coverage -Confinement -Treatment of adjacent surfaces
Reduction of long-wavelength radiation	Reduction of surrounding surface temperatures	-Floors: Cold pavements, water laminates. -Coverages: Irrigation, water sheets. -Vertical surfaces: Waterfall, water curtain.
Convective exchange reduction	Reduction of air temperature and movement of cooled air	-Confinement -Sensitive cooling and latente -Water jets

The pilot consists of the rehabilitation of an existing amphitheater from the EXPO 92 era, the construction of a new space, the souk, and the set of connection elements between them.

The climate control strategies used in the souk and amphitheater can be grouped according to three criteria and different technologies. Criterion 1 is reduction of solar radiation. Criterion 2 is the reduction of the surface temperature, reducing the long-wavelength radiant exchange. Finally, criterion 3 is the reduction of air temperature through confinement techniques and production of cold air.

To alleviate the high temperatures and improve thermal comfort, water will be used as a heat transfer fluid accompanied by bioclimatic techniques that allow a pleasant thermal sensation to be achieved. The water used as a heat transfer fluid is cooled by a dual day-night technique, which consists of launching and creating a falling-film [3] on photovoltaic panels during the night, obtaining surprising results of natural cooling of the water by means of a radiant exchange with the temperature. from the sky. On the other hand, during the day, these panels are responsible for producing the energy necessary for the installation to comply with the zero energy balance. The system can be seen in Figure 1.



Figure 2. Falling-film system

On the other hand, the objective is to maximize the nocturnal use of environmental sinks to cool the water[4]. For this reason, the water is stored in a Qanat, a ditch built below the surface for this project. There, it mixes with the air to reduce its temperature. Later, with the rising of the sun and the arrival of the most intense hours of heat, this air will return to the surface to soften the temperature of the environment enabled in the street [5].

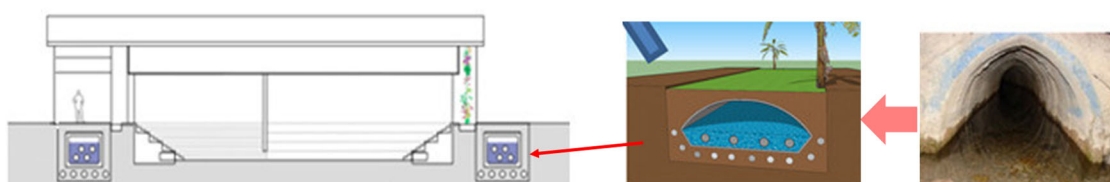


Figure 3. Buried and submerged pipeline system- Qanats

Specifically, the Anfiteatro (Figure 3) is a space used during the EXPO'92 period as a show kiosk. It has a capacity for 200 people. It includes actions such as confinement, contemplated by a diametrical wall

that closes the stage and the cypresses that surround the area of the stands, as well as the impulsion of cooled air with natural techniques mentioned above.

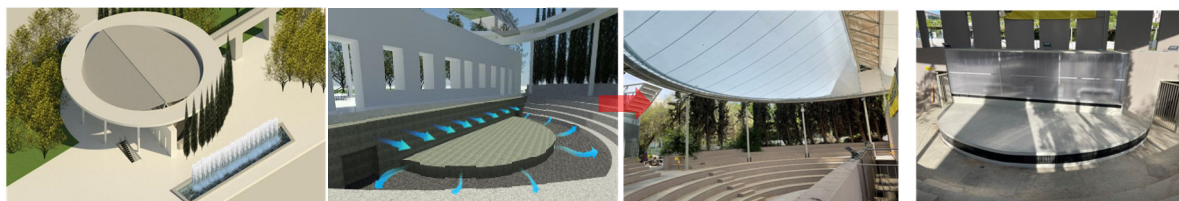


Figure 4. Design and current situation of the Anfiteatro

The Zoco (Figure 4) is a newly created space with a rectangular shape of 750 m<sup>2</sup>. It is located 2 m in depression with respect to the level of the avenue to minimize the entry of outside air. It combines a wide catalog of climate control techniques.



Figure 5. Design and current situation of the Zoco

### 3. Results and discussion

For the correct evaluation of the bioclimatic techniques, the results obtained for the different solutions will be shown, finally showing the level of thermal satisfaction of the occupants, the final objective of the action. Below are the temperature results achieved in the Zoco with the joint operation of evaporative barriers and buried conduits, for a typical day in Seville.

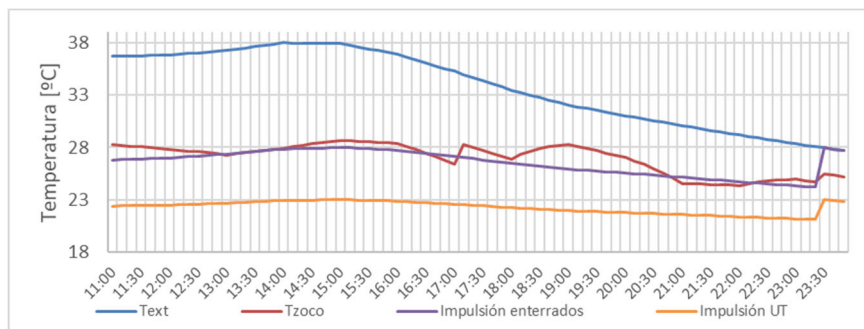


Figure 6. The Zoco temperature on a typical day

It can be seen that the temperature of the souk is below the 28°C established in summer compared to the 38°C outside air temperature, achieving a notable reduction in the temperature inside.

On the other hand, the system's production data, together with the proposed consumption and the resulting surpluses, verify the self-consumption in the project with an annual production of 75MWh and a consumption of 25 MWh. This means that 33% of the production is self-consumed and the other 67% is transferred to the network.

Finally, a survey campaign is carried out in different points of the rooms with the aim of knowing the perception of the occupant, the final objective of the action.



Figure 7. survey campaign

With an outside temperature above 30°C, 84% of the occupants of the different rooms conditioned using bioclimatic techniques, consider that their thermal perception and therefore their level of thermal comfort can be defined as "Thermal Comfort-Well".

#### 4. Conclusions

The continued rise in global temperatures and the increase in energy consumption make it necessary to look for innovative natural techniques that help to condition outdoor spaces. In the present work we have sought to reactivate the bioclimatic design that Expo 92 implanted in the Isla de la Cartuja. The CartujaQanat project has built a new urban space on Avenida Thomas Alba Edison based on the use of natural conditioning techniques with the aim of revitalizing street life by offering comfortable conditions in open spaces during the hottest seasons in Seville. Thanks to the combination of bioclimatic techniques, the use of night lighting and environmental drains, it is possible to reduce the outside temperature by 10°C. Comfort conditions are obtained in the conditioned rooms, prevailing the well-being of the visitors to the Isla de la Cartuja.

#### Acknowledgements

This study has been funded by the projects "CONSTANCY - Resilient urbanisation methodologies and natural conditioning using imaginative nature-based solutions and cultural heritage to recover the street life" (Grant Agreement PID2020-118972RB-I00) and the project "NATURBEAM - Lighting the way to a greener future to restore urban habitability through nature-based solutions" (Grant Agreement TED2021-130416B-I00) by the Science and Innovation Ministry of Spain. Also, this study has been co-financed by the European Regional Development Funds (ERDF).

#### References

- [1] J. Guerra Macho, J.M. Cejudo López, J.L. Molina Félix, S. Álvarez Domínguez, R. Velázquez Vila, Control climático en espacios abiertos: Evaluación del proyecto EXPO'92, Sevilla, Sevilla, Spain, 1994.
- [2] R. Velazquez, S. Alvarez, J. [Seville U. (Spain)] Guerra, Climatic control of outdoor spaces in EXPO 92, (1992).
- [3] Mc.C. Guerrero Delgado, J. Sánchez Ramos, J. Tenorio Rios, S. Álvarez Domínguez, Falling-film as natural cooling technique: Modelling and energy impact assessment, *Energy Convers. Manag.* 225 (2020). <https://doi.org/10.1016/j.enconman.2020.113424>.
- [4] S. Alvarez, I.R. Maestre, R. Velazquez, Design methodology and cooling potential of the environmental heat sinks, *Int. J. Sol. Energy.* 19 (1997) 179–197. <https://doi.org/10.1080/01425919708914336>.
- [5] Mc.C. Guerrero Delgado, J. Sánchez Ramos, Mc.C. Pavón Moreno, J.A. Tenorio Ríos, S. Álvarez Domínguez, Experimental analysis of atmospheric heat sinks as heat dissipators, *Energy Convers. Manag.* 207 (2020) 112550. <https://doi.org/10.1016/j.enconman.2020.112550>.



EUROTHERM2023-V179

## Chemically enhanced phase separation in Direct Contact Thermal Energy Storage

Halvard Thon<sup>1</sup>, Galina Simonsen<sup>2</sup>, Paul Roger Leinan<sup>3</sup>

<sup>1</sup>SINTEF Multiphase Flow Research Group, Trondheim, Norway, Phone: +47 92621328, e-mail: halvard.thon@sintef.no

<sup>2</sup> SINTEF Multiphase Flow Research Group, Trondheim, Norway, Phone: +47 41018485, e-mail: galina.simonsen@sintef.no

<sup>3</sup> SINTEF Multiphase Flow Research Group, Trondheim, Norway, Phone: +47 48181457, e-mail: paul.roger.leinan@sintef.no

### Abstract

In situ testing of the destabilizing performance of surfactants on emulsions formed in a direct contact thermal energy storage (DCTS) were performed in this study. An experimental DCTS pilot was developed for latent heat storage using a bio-based phase change material (PCM) and a heat transfer fluid (HTF). Surfactants were selected based on a bottle shaking test screening procedure and their solubility. Performance of the surfactants in the experimental DCTS was compared to results from the shaking tests. Our results show that surfactants provide an effective method of suppressing the emulsion build-up in DCTS, and surfactant performance can be predicted based on shaking tests.

**Keywords:** Thermal energy storage, direct contact, latent heat, PCM, phase separation, surfactants

### 1. Introduction

Thermal energy storage (TES) has the potential to play a key role in decarbonizing energy consumption by enabling a larger share of renewable but unreliable energy sources, for instance solar and wind, which are expected to increase (IEA, 2021). Latent heat storage using a phase change material (PCM) is a promising method of TES as it offers high storage capacities at constant temperatures (Belén Zalba, 2003). However, traditional latent heat storages, in which PCM and a heat transfer fluid (HTF) are physically separated in a structural heat exchanger, do suffer from diminishing power outputs due to thermal resistance at heat transfer surfaces. As crystallized PCM builds up at surfaces, heat transfer changes from convective to conductive. This greatly reduces the power output from the storage as most PCMs have low thermal conductivity (0.1 ~0.5 W/m·K) (Ioan Sarbu, 2019).

To address this issue, the concept of direct contact thermal storage (DCTS) has been proposed (DD Edie, 1980). By removing the heat exchanger separating the PCM and HTF, thermal resistance is effectively eliminated. HTF flows through the PCM in form of droplets, exchanging heat, and is extracted at the storage outlet. This requires immiscibility and a difference in specific gravity between the respective fluids. This concept is shown to have high and persistent power output (Takahiro Nomura, 2013).

An important issue with DCTS is the risk of PCM carry-over (Lukas Hegner, 2021). This occurs by extensive emulsification of the PCM and HTF in the storage and may lead to clogging of the system if the emulsified layer is allowed to reach the storage outlet. It is therefore desirable to increase the droplet coalescence rate in the storage unit. Surfactants are widely used to break emulsions (Ana M Sousa, 2021). Considering surfactants do not require additional energy to operate, they pose a promising method of addressing the emulsification issue in a DCTS.

The main purpose of this study is to investigate the use of surfactants to increase the coalescence rate and improve phase separation in a DCTS. Secondly, we explore a simple and time-efficient screening procedure on how to select appropriate surfactants.

## 2. Materials and method

>97% pure methyl palmitate (MP), a fatty acid methyl ester with a phase change temperature of ~30°C was purchased from Sigma Aldrich and used as PCM. De-ionized water was used as HTF. MP is insoluble in water and has a high heat of fusion, which makes it an attractive material for latent heat storage in a DCTS. A range of surfactants with demulsifying functions were obtained from CRODA and Clariant.

An experimental DCTS was developed at the SINTEF Multiphase Flow laboratory in Trondheim, Norway. The setup is designed to resemble a latent heat storage coupled with a thermal reservoir. A gear pump was used to circulate HTF through a plate heat exchanger before entering the storage vessel containing the PCM. A simplified schematic representation of the DCTS with its main components is given in Figure 2-1.

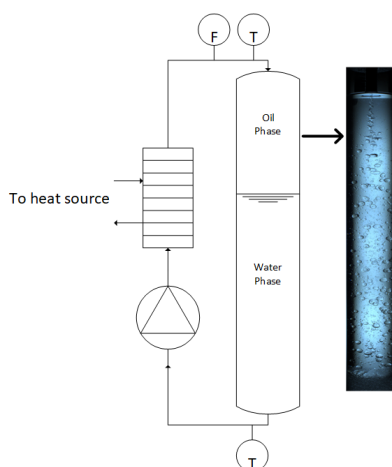


Figure 2-1. Schematic representation of the DCTS

Both the flowrate and temperature of the water were kept constant during the emulsion build-up tests. To best reflect conditions of a real DCTS, inlet temperature of the water should be slightly above the melting point of the MP. Hence, a water temperature of 38°C was selected. To get an indication of the temperature effect on emulsion development, a second series of tests were run with an inlet temperature of 50°C. In both series, the flowrate of the water was constant at 300 ml/min.

30 mL samples of water and MP with surfactants were prepared and shook by hand to form emulsions. Emulsions were then kept at rest while a camera recorded the phase separation. By comparing the separation time  $t_S$  of an emulsion treated with a surfactant to the separation time of a pure system  $t_R$ , we define a separation efficiency parameter according to eq. (1):

$$\varepsilon = 1 - \frac{t_S}{t_R} \quad (1)$$

A total of 8 surfactants (denoted S1 – S8) were selected based on the shaking tests and tested in the rig, in addition to a reference sample with pure MP and DI-water. Before each test, the residual emulsion in the storage vessel was allowed to collapse by opening a bypass valve for the water. Once all the residual emulsion had collapsed, water was diverted to the storage vessel and the emulsion development was monitored. Tests continued until the emulsion layer reached a cut-off height in the tube, at which point the test was terminated to avoid carry-over of the PCM. All tests were done in triplicate.

By comparing the time required for the emulsion layer to reach the cut-off height, a quantitative measure of the surfactant performance in enhancing coalescence is obtained. An emulsion suppression factor was defined according to eq. (2):

$$\eta = \frac{t_{C,S}}{t_{C,R}} - 1 \quad (2)$$

In eq. (2),  $t_{C,S}$  is the time required for the surfactant laden emulsion layer to reach the cut-off height, while  $t_{C,R}$  is the corresponding time required for the reference system. In our setup, the cut-off height was set at 780 mm.

### 3. Results and discussion

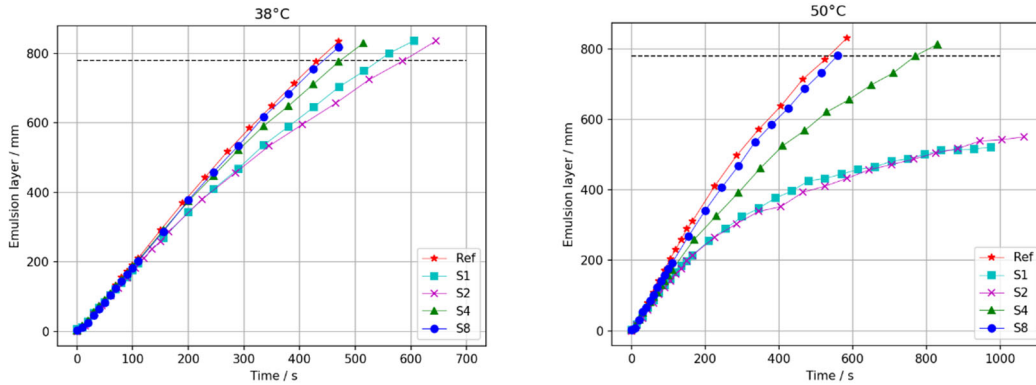


Figure 3-1. Emulsion development for a selection of surfactants and a reference at 38°C (left) and 50°C (right). Dashed lines indicate the cut-off height.

Results from emulsion tests at both 38 and 50°C are shown in Figure 3-1. Initially, the rate at which the emulsion builds up in the DCTS depends only on the water flow rate. This is seen from the near constant slope of the curves initially, for both temperatures. Freshly formed water droplets accumulate in a layer at the water / MP interface with practically no coalescence. After some time, the curves diverge, indicating coalescence is starting to become significant. At 38°C, coalescence is moderate, and the emulsion layer reached the cut-off height within 400 – 600 seconds for all samples. At 50°C, on the other hand, a greater variation in build-up rates is seen. In fact, for emulsions treated with S1 & S2, the emulsion layer assumed a near-constant height below the cut-off, meaning the coalescence rate approached the water flowrate. An increase in coalescence with temperature is mainly explained by the reduced viscosity of the continuous phase between droplets.

In Figure 3-2, surfactant performance at 38°C is shown in terms of the emulsion suppression factor (eq. (2)). Efficiency of surfactant performance varied greatly between the systems. While some surfactants barely increased the run-time of the system before carry-over occurred, others could allow the system to run at this flow rate almost 30% longer than the reference system.

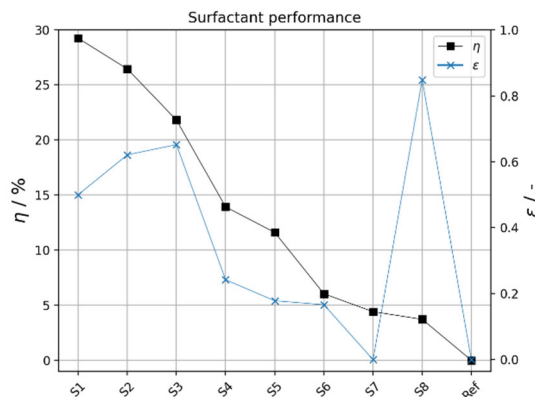


Figure 3-2. Surfactant performance at 38°C. Squares represent emulsion suppression in the DCTS, while x's denote the corresponding surfactant efficiency in the shake-tests.

When compared to the separation efficiency parameter (eq. (1)), results from the shake-tests display the same trends seen in the DCTS. In other words, the small-scale samples used in shaking tests replicates quite accurately the conditions in the DCTS in terms of emulsion behaviour.

#### 4. Conclusions

In this investigation we have demonstrated the applicability of using surfactants to address the issue of emulsification in a DCTS. We are also proposing the use of shaking tests as a reasonably accurate and time-efficient screening method for surfactant selection. By the correct choice of surfactant, it is possible to significantly suppress the emulsion build-up in the storage vessel.

#### Acknowledgements

This work was funded by the Norwegian Research Council.

#### References

- Ana M Sousa, M. J. (2021). Oil-in-water and water-in-oil emulsions formation and demulsification. *Journal of Petroleum Science and Engineering*.
- Belén Zalba, J. M. (2003). Review on thermal energy storage with phase change: materials, heat transfer analysis and applications. *Applied Thermal Engineering*, 251-283.
- DD Edie, S. M. (1980). Immiscible fluid - heat of fusion heat storage system. *Thermal Energy storage: Forth annual review meeting*, 391.
- IEA. (2021). *World Energy Outlook 2021*. Paris: IEA.
- Ioan Sarbu, A. D. (2019). Review on heat transfer analysis in thermal energy storage using latent heat storage systems and phase change materials. *International journal of energy research*, 29-64.
- Lukas Hegner, S. K. (2021). Experimental Feasibility Study of a Direct Contact Latent Heat Storage Using an Ester as a Bio-Based Storage Material. *Energies*.
- Takahiro Nomura, M. T. (2013). Performance analysis of heat storage of direct-contact heat exchanger with phase change material. *Applied Thermal Engineering*, 108 - 113.

EUROTHERM2023-X181

## Thermosyphon assisted Latent and Sensible Heat Thermal Battery

Julio Bravo<sup>a</sup>, Ahmed Abdulridha<sup>b</sup>, Shuoyu Wang<sup>b</sup>, Dominic Matrone<sup>a</sup>, Zheng Yao<sup>a</sup>, , Clay Naito<sup>b</sup>, Spencer Quiel<sup>b</sup>, Muhannad Suleiman<sup>b</sup>, Carlos Romero<sup>a</sup>, Sudhakar Neti<sup>a,\*</sup>

<sup>a</sup> Energy Research Center, <sup>b</sup> ATLSS Engineering Research Center,  
Lehigh University, 117 ATLSS Drive, Bethlehem, PA 18015, USA

\* Corresponding author. Tel.: +1(610) 597-6885. Email address: sn01@lehigh.edu

### Abstract

One cost competitive energy storage option to meet the climate goals is based on storing sensible heat in concrete along with latent heat energy storage in phase change materials. This paper reports research and development of a thermal battery capable of storing energy with temperatures up to 450°C. The novel concept consists of a concrete matrix, and an array of thermosyphon elements, engineered for dual action, and designed and fabricated into a single thermal battery. The current work describes the inclusion of latent heat storage into such a thermal battery with the use of encapsulated phase change materials included inside the concrete. Such a battery can economically deliver energy quickly (kW) with fast power change rates (kW/s). An overall energy into and out of the storage media of 95% along with an end-to-end thermal battery round trip efficiency of >70% was demonstrated with several tests of the of the battery.

**Keywords:** Energy storage, sensible, latent, thermosyphons, thermal energy, thermal battery

### 1. Introduction

Thermal energy storage (TES) will play a crucial role in many aspects of our lives as we increase the use of renewable energies and since such source do not always match the energy demand-supply patterns. While electrical power is essential, there are numerous opportunities to use TES and thermal energy directly in many commercial and industrial applications. A versatile, economical, scalable thermal battery (Lehigh Thermal Battery - LTB) that can be used to improve the performance of industrial processes as well as for power generation is described here. The thermal battery (TB) was demonstrated using air flow for the energy into and out of the TB and engineered cementitious media for sensible heat storage of energy. Use of encapsulated phase change materials (PCM) enhancing the performance of the TB is also described.

Concrete with improved thermo-mechanical properties has been proposed for thermal energy storage with a modular design [1] and work at DLR [2] and elsewhere has promoted the use of concrete for energy storage. We build upon their experiences and make TES in concrete better with the use of thermosyphons.

### 2. Materials and methods

Since most materials used for TES are poor thermal conductors, the LTB incorporates an innovative use of thermosyphons, that are essentially super-thermal-conductors, to mitigate the thermal conductivity issue. The LTB is very flexible in its design for the choice of temperatures at which it can be used, the total quantities of energies stored (capacity in kWh, MJ) thanks to its scalability, and the power levels of operation (kW). It is also capable of quick changes in thermal power delivery (kW/s). The current

version of the TB is shown schematically in Figure 1. It consists of a concrete cylinder (0.76 m  $\phi$  x 2.13 m h) with 22 thermosyphons with finned ends that are housed in ducting to manage the charging and discharging flow streams. The concrete used has been engineered for thermal and structural stability as well as stress containment over many heating and cooling cycles for performance up to 450°C. The LTB was insulated with a 0.15 m mineral wool layer with a reflective radiative layer to achieve an outside temperature around 40°C.

Electrically heated compressed air was used for both charging and discharging the LTB in laboratory experiments, depicting the separation of energy input (battery charge) and output (discharge) streams.

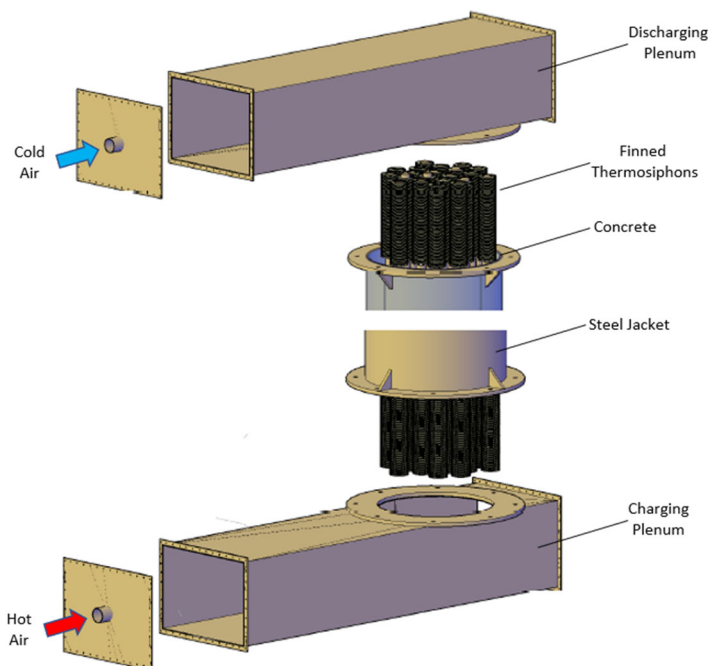


Figure 1. A Schematic of the Lehigh Thermal Battery (TB)

number of thermocouples, flow sensors, and power meters. Figure 2 shows a cross-sectional view of the LTB illustrating one possible set of TS locations. An extensive transient 3-D numerical analysis determined the ideal locations of the TS to achieve near uniform radial temperature distribution in the concrete – with axial isothermality assured. In the case of the LTB fitted with phase change materials (PCM) to enhance thermal performance, the PCM can be included in encapsulations (illustrated by darker rings in Figure 2) as indicated between the TS banks. In this TS arrangement, the larger ring has an 0.635 m OD and 0.533 m ID, and a height of 0.2 m. The aspect ratio of the encapsulation  $[h/(OD-ID)]$  is an important parameter to ensure good performance and the proper melting and freezing of the PCM. Any captive part of the PCM that cannot have freedom to expand cannot be allowed to melt first since the volumetric expansion of PCM will generate undue stresses. The axial isothermal nature of LTB helps with the near uniform melting of PCM in the encapsulations, axially. The LTB illustrated in Figure 1 was shown to store up to 150 kWh<sub>th</sub> and operate at temperatures up to 425°C.

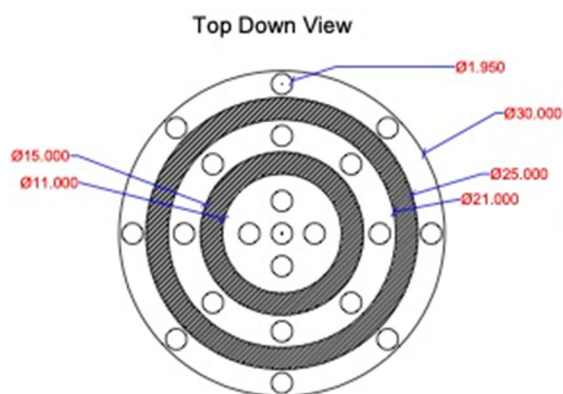


Figure 2. Cross-sectional view of the LTB. The darker rings include NaNO<sub>3</sub> PCM

### 3. Results and discussion

Numerous tests were conducted to charge and discharge the LTB. Energy input to the TB consisted of exposing the thermosyphon fins in the manifolds to target air flow rates and temperatures. The inlet to outlet temperature difference of the air in the flow plenum is a measure of the efficacy of heat transfer between the air and the TS fins. This also corresponds to the energy transferred from the fluid flow stream through the TS fins to the TS and in turn to the storage medium – concrete. In the current tests an air flow of 0.14 kg/s at 460°C was used to charge the TB using the bottom (charge) plenum. The charging process was deemed complete when the volume averaged concrete temperature reaches 400°C with peak values of about 425°C. Tests with several air mass flow rates proved the ability to charge the TB with volume averaged temperatures ranging between 300°C and 400°C, resulting in an energy density as high as 143.5 kWh/m<sup>3</sup>. During the discharging process, air at 185°C was flown through the top (discharge) plenum at a mass flow rate of 0.26 kg/s. During this process, the TS temperature dropped from 416°C to 330°C in 1.5 hours. By the end of the discharging, in 6.2 hours, the TS temperature was as low as 252°C. The energy transferred to/from concrete from/to air for the charging and discharge processes and the energy stored during the cycle was about 139 kWh<sub>th</sub>.

The efficacy of the TES process is described in terms of two Round-Trip-Efficiencies, RTE1 and RTE2. RTE1 is defined as the ratio between the energy discharged from the TB media and the energy stored in the TB. The RTE1 of the TB was estimated to be around 95%. This result can be interpreted as the effectiveness of the TB to store energy and discharge thermal energy. The second, RTE2 is defined as the ratio between the energy needed from the air to achieve the desired energy stored in the TB and the energy transferred to the air from the TB during the discharge process. RTE2 is thus a measure of air-to-air RTE, and it includes fin efficiency, heat losses, etc. For this design identical TS arrangements were used for the top and bottom plenums. The RTE2 of the LTB was estimated to be around 70% leaving some room for finned TS end improvement.

Inclusion of PCMs, like NaNO<sub>3</sub>, could improve the performance of TB systems. The impact of including encapsulated PCM (as in Figure 2) with sixteen, 0.2 m high rings amounting to a total of about 423 kg of NaNO<sub>3</sub>, compared to the approximately 2,500 kg of concrete used for storage, is described here. NaNO<sub>3</sub> melts around 304°C with a latent heat of about 173 kJ/kg. With specific heat, Cp, of concrete of 1.29 kJ/kg-K and 1.67 for NaNO<sub>3</sub> kJ/kg-K, and with the 423 kg of NaNO<sub>3</sub> included in the TB, Figure 3 shows temporal temperature variations during a charging process for the modified LTB. With PCM, the energy stored will be 150.4 kWh<sub>th</sub>. The energy stored is calculated as the sum of all the energies corresponding to the TB media (concrete, steel, NaNO<sub>3</sub>). In Figure 3, for a certain input power, different media have different responses (dT/dt) due to their different properties. NaNO<sub>3</sub> shows isothermality at 304°C from 1.5 h to 2.9 h and then it displays increasing temperature based on its Cp. The energy stored is 101 kWh<sub>th</sub> stored in concrete and 49.2 kWh<sub>th</sub> in the PCM adding up to 150.4 kWh<sub>th</sub>. Even with just ~14% PCM, the PCM makes a significant (~32%) difference.

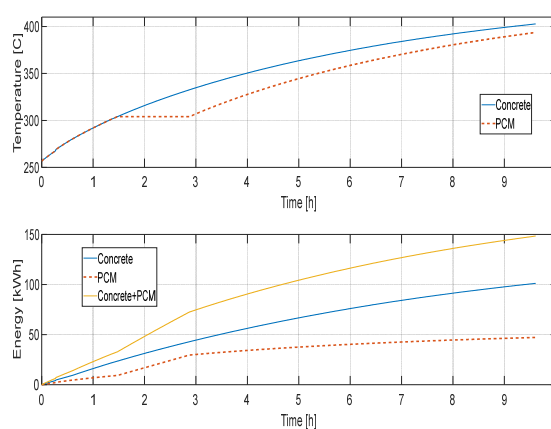


Figure 3. Temperature variation and energy stored in LTB with NaNO<sub>3</sub> PCM

Energy storage and discharge results of the cyclic performance of the LTB are shown in Figure 4. The purpose of cycling at different temperatures was to optimize the operating conditions for charging and discharging, and to demonstrate the repeatability of the system as would be expected in any application. The TB temperatures for five consecutive cycles varied from 261°C to 403°C while keeping the charging air mass flow rate at 0.14 kg/s with a temperature of 460°C resulting in energy stored of 139 kWh<sub>th</sub>. The TB is discharged using air flowrate of 0.26 kg/s and a temperature of 185°C discharging the TB back to 261°C. Inclusion of NaNO<sub>3</sub> could achieve 49.2 kWh<sub>th</sub> in the PCM with 21 kWh<sub>th</sub> as latent heat and the total energy stored for the concrete and PCM would be 150.4 kWh<sub>th</sub>.

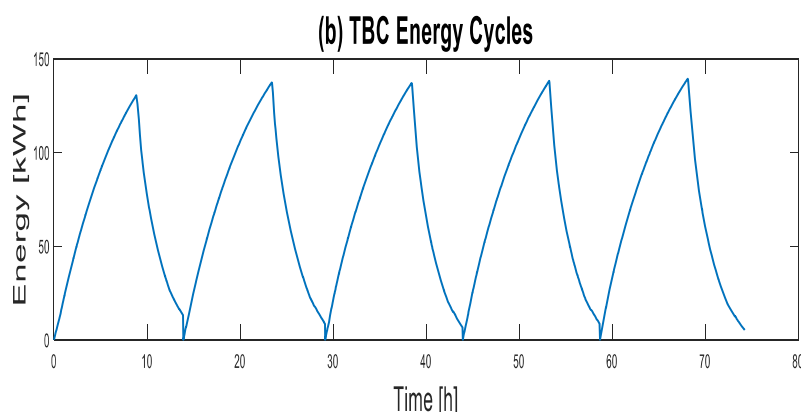


Figure 4. Charge – discharge cyclic performance of the TB domain, potentially resulting in much larger energy storage densities.

The PCM provides for significant increase in the energy stored even with small amounts. Nominally very simplistic ways of including the PCM in the system can have good benefits. There are indeed much better ways of including the PCM into the storage media, say as 30 mm encapsulated PCM balls distributed through the sensible heat storage

## 4. Conclusions

The Lehigh Thermal Battery uses concrete for sensible heat storage with thermosyphons to mitigate the poor thermal conductivity of the storage medium, and to allow a fast, efficient transfer of thermal energy. Addition of  $\text{NaNO}_3$  for latent heat storage is also described. A single set of dual action thermosyphons have been engineered to be effective for charging (energy in) as well as discharging (energy out) of the thermal battery; thus, minimizing equipment cost. Even with a poor heat transfer medium such as air flow used for the transfer of energy, good heat transfer rate (kW) response to/from the storage media was demonstrated. Temperature measurements in the concrete showed that radial temperature variation can be minimized with a judicious distribution of thermosyphons in the concrete and the thermosyphons ensure isothermal axial distribution of energy. The inlet to outlet temperature difference of air in the flow plenums indicates that the heat transfer between the air and the fins in the plenums is very good. Tests at several air mass flow rates proved the ability to charge and discharge the thermal battery with  $139 \text{ kWh}_{\text{th}}$  of energy in the concrete with volume averaged temperatures ranging between  $300^\circ\text{C}$  and  $403^\circ\text{C}$ . Storage with a small amount of latent heat storage media in place can push this to  $151 \text{ kWh}_{\text{th}}$ . The Lehigh Thermal Battery is capable of energy-to-energy Round-Trip-Efficiency of 95% and an air energy-to-air energy RTE  $> 70\%$ . The operational temperature range as well as the overall energy storage capacity of the LTB can be engineered to meet larger and a broad set of applications; for example, operation at temperatures in the  $750^\circ\text{C}$  range, expected for future  $\text{s-CO}_2$  cycles. The Lehigh Thermal Battery is currently at a Technology Readiness Level of 7 and it is ready for demonstration in different challenging industrial applications.

## Acknowledgements

"This material is based upon work supported by the Department of Energy Award Number DE-FE0031755". The information presented here is not endorsed by the U.S. DOE.

## References

- [1] N. Hoivik *et al.*, "Long-term performance results of concrete-based modular thermal energy storage system," *J. Energy Storage*, vol. 24, no. April, p. 100735, 2019, doi: 10.1016/j.est.2019.04.009.
- [2] D. Laing, D. Lehmann, M. Fi, and C. Bahl, "Test results of concrete thermal energy storage for parabolic trough power plants," *J. Sol. Energy Eng. Trans. ASME*, vol. 131, no. 4, pp. 0410071–0410076, 2009, doi: 10.1115/1.3197844.
- [3] J. Bravo, *et al.*, Design and Experimental Testing of a 150 kWh Thermal Battery Using Thermosiphons Embedded in a Concrete Matrix for Power Plant Flexible Operation, submitted to **Energy**.



EUROTHERM2023-G182

## Thermodynamic performance assessment of an innovative layered radial-flow high-temperature packed bed thermal energy storage

Silvia Trevisan<sup>1</sup>, Rafael Guedez<sup>1</sup>

<sup>1</sup>Department of Energy Technology, KTH Royal Institute of Technology, Brinellvägen 68, 100 44 Stockholm, Sweden, e-mail: trevisan@kth.se

### Abstract

This work introduces an innovative layered radial flow packed-bed TES concept able to reduce the pressure drop while improving the thermal performance of the TES. The thermodynamic performance of the proposed TES concept has been analysed via a preliminary numerical investigation. The influence of the relative thickness of two layers, different particle sizes, and aspect ratio have been investigated. Pressure drop, useful charge and discharge operation and thermocline thickness have been considered as the main performance indicators. The results show that a set of optimally equivalent TES designs can be identified. The relative thickness of the layers has a major influence directly affecting both the pressure drop and the useful operation time. This work is a steppingstone toward a future comprehensive TES design, optimization, prototyping and validation work.

**Keywords:** Thermal energy storage, packed bed, radial flow, high temperature

### 1. Introduction

Thermal energy storage (TES) will play a crucial role in the future energy sector. TES can provide high renewable penetration (such as in concentrating solar power (CSP) plant), ensuring dispatchable green power, as well as flexibility on the demand side with a smart management of the demand and enabling possibilities for waste heat recovery. Commercial large-scale TES units, developed for CSP applications, exploit solar salts and are limited to maximum temperatures lower than 580°C, due to thermal decomposition of the salt mixture. Solid based sensible TES can offer a technically viable and cost-effective alternative which could boost the exploitation of TES at higher temperatures, particularly when operated via a gaseous heat transfer fluid (HTF) [1]. Packed bed sensible TES (PBTES) systems store thermal energy by heating and cooling solid particles by means of a HTF that flows through the bed [2]. Different PBTES designs, among which the most promising ones, have been previously proposed and experimentally validated. The traditional cylindrical tank with axial HTF flow has been deeply investigated [3], at various working temperatures and using different solid materials [4]. The main drawbacks of this design, which have been limiting its large-scale exploitation, are the high sensitivity to thermal ratcheting and thermomechanical stresses on the tank, elevated thermal losses, and high pressure drop for the HTF during operation. The buried truncated conical TES with axial HTF flow permits limiting the thermal ratcheting; however, the thermal losses from the top surface are increased

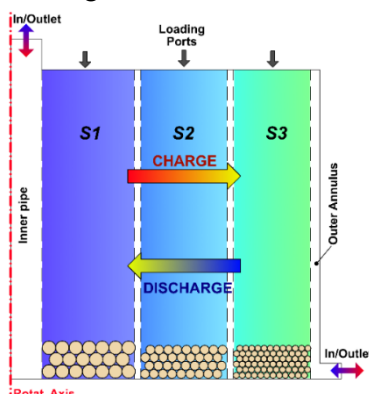


Figure 81. Proposed radial-flow packed bed TES geometry sketch

[2]. The unconstrained self-insulated concept [5] minimize the cost, but is likely to lead to thermocline instabilities, linked to the unpredictability of the flow passage through the bed [6]. The radial-flow packed bed TES design ensures limited pressure drops and thermal losses during dwell; however, the temperature degradation and thermocline spread are identified as key drawbacks [7]. To boost the exploitation of high temperature PBTES, advances are needed and thermodynamic and structural challenges should be addressed simultaneously. The present work introduces an innovative layered radial flow packed-bed TES concept, leveraging from the previous authors' experience [7], able to maximize the pressure drop while reduction improving local heat transfer.

## 2. Materials and methods

A conceptual 2D axis-symmetric design of the innovative layered radial flow packed bed TES is shown in Figure 1. The TES is comprised of multiple annular coaxial packed bed segments (shown as S1, S2, and S3). During charge, air enters from the inner central pipe, flows radially outwards, is collected in the outer annulus, and exits from the lower outlet port. During discharge, the flow direction is reversed. Each layer has dedicated loading ports to facilitate the filling procedure. If required by the specific application, different materials could be used in the different segments. In homogeneous single material radial flow packed bed TES, the HTF speed is higher in the inner region of the TES due to smaller cross-sectional area. Different HTF flow speed along the radial direction leads to an uneven development of the pressure drops and thermocline. The majority of the pressure losses occurs in the inner section, where higher flow speed are registered. Contrarily, the thermocline is affected by the effectiveness of the heat transfer between HTF and solids. Thus, the thermocline degrades more rapidly in the outer section of the TES. From a TES design perspective, pressure drops and thermocline degradation limitations typically requires contrasting approaches leading to critical trade-offs. The proposed PBTES design targets both performance metrics. In S1 a good heat transfer between HTF and solid is guaranteed by the high flow speed. Thus, larger particles can be introduced limiting the pressure drop without compromising the effectiveness TES. Contrarily, S3 is filled with smaller particles which increase the heat transfer area between filler and HTF improving the convective heat transfer while hindering the effective thermal conductivity limiting the thermocline degradation. Thanks to the low flow speed in S3, smaller particles will not cause drastic increments of the pressure drop.

The thermodynamic behavior of the PBTES has been described by adapting the Schumann model [8] to the radial geometry. Specifically, the 1D two phases model can be summarized by Eqs. (1) and (2). The pressure drop has been calculated via the Ergun equation, [9].

$$\frac{\partial T_F}{\partial t} + \frac{G}{\varepsilon \rho_F} \frac{\partial T_F}{\partial r} = \frac{k_{F,eff}}{\varepsilon \rho_F c_{p,F}} \left( \frac{1}{r} \frac{\partial}{\partial r} \left( r \frac{\partial T_F}{\partial r} \right) \right) + \frac{h a_s (T_s - T_F)}{\varepsilon \rho_F c_{p,F}} + \frac{U_w (T_\infty - T_F)}{H \varepsilon \rho_F c_{p,F}} \quad (1)$$

$$\frac{\partial T_s}{\partial t} = \frac{k_{s,eff}}{(1-\varepsilon) \rho_s c_{p,s}} \left( \frac{1}{r} \frac{\partial}{\partial r} \left( r \frac{\partial T_s}{\partial r} \right) \right) + \frac{h a_s}{(1-\varepsilon) \rho_s c_{p,s}} (T_F - T_s) \quad (2)$$

The investigated PBTES consists of only two radial layers and a small lab scale unit (50kWh). Four main design variables have been considered: the layer ratio (defined as the ratio  $(R^* - R_{in}) / (R_{out} - R_{in})$ , where  $R^*$ ,  $R_{in}$  and  $R_{out}$  are the radius of the layers separation, inner radius and outer radius, respectively) in the range 0.1 – 0.9, the inner particle diameter in the range 5 – 21 mm, the outer particle diameter in the range 2 – 8 mm, and the aspect ratio, defined as  $\alpha = (R_{out} - R_{in}) / H$ , in the range 0.64 – 1.44. The pressure drop and the useful duration of charge and discharge, defined as the time at which the outlet fluid temperature reaches the cut-off value ( $T_{min} - 100^\circ\text{C}$  in charge or  $T_{max} - 100^\circ\text{C}$  in discharge), and the maximum thermocline thickness have been considered as the main KPIs describing the TES thermodynamic performance. Additionally, to evaluate the influence of each decision variable over the KPIs the different correlation coefficients, between each independent variable and the KPIs, have been calculated.

### 3. Results and discussion

Figure 2 summarizes the main results of the preliminary PBTES design optimization, describing its behavior and main thermodynamic KPIs during both charge (left) and discharge (right). The expected trade-off between pressure drop and useful operation time is highlighted. PBTES designs ensuring minimal pressure drops would lead to limited useful operation, characterized by both short operation time and widespread thermocline. Confirming what observed during experimental validation of radial flow PBTES, the charge useful operation is longer than in discharge mode. This phenomenon could be caused by the HTF entering the TES at lower speed during discharge and causing a poorer heat transfer. Additionally, the thermocline spread has different behaviors in charge and discharge operation. In charge operation, longer useful operation coincides with thinner thermocline spread. Contrarily, in discharge operation, long useful operation are obtained even at high (>70%) thermocline spread. This trend is caused by the fact that during discharge the temperature profiles along the PBTES radius are flatter. In configurations with low thermocline spread the thermocline starts to be discharged very early during operation causing an early decrease of the outlet temperature and short useful discharge. Longest useful discharge periods are ensured by configurations in which the thermocline spreads inside the bed but the heat transfer between HTF and solid is good enough to delay the outlet temperature drop. By comparing the different Pareto curves obtained at different aspect ratios, it can be seen that higher aspect ratio (larger and shorter tanks) leads to longer useful operation time during both charge and discharge. Specifically, for the same pressure drop (i.e. 50 Pa) an  $\alpha$  of about 1.5 leads to an increment of the useful operation of about 5 % with respect to  $\alpha$  lower than 1. With respect to axial flow packed bed where higher aspect ratios leads to very relevant increment of the pressure drop, the proposed radial flow and layered structure contributes in limiting them. It can be observed that for scaled up radial flow PBTES, higher aspect ratios would lead to larger land footprint. Thus, vertical stacking of parallel units could be considered.

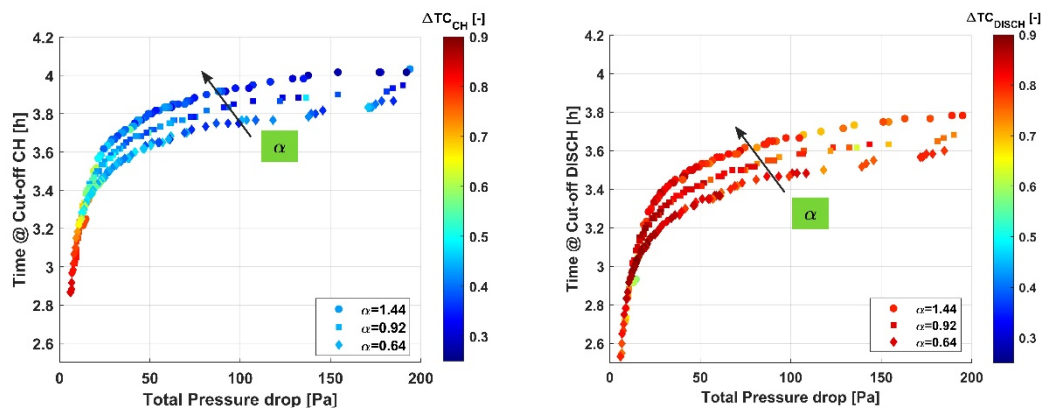


Figure 82. Pareto front for TES design optimization during charge (left) and discharge (right) operation

**Error! No s'ha trobat l'origen de la referència.** summarizes the regression coefficient of each decision variable on the different KPIs. LR has the highest impact on all KPIs, except on the thermocline thickness during charge. In particular, low LR (meaning a PBTES where the largest part of the TES is filled by smaller particles) causes higher pressure drop but better thermal performance with both reduction of the thermocline and extension of the useful operation. The aspect ratio affects the influence of LR on the thermocline degradation observed during discharge. In particular, at smaller  $\alpha$  an increase of LR leads to a more rapid increase of the thermocline thickness. The suggested LR is in the range 0.4 – 0.6. **Error! No s'ha trobat l'origen de la referència.** shows also that the inner particle diameter has a higher relevance than the outer one. An increase of the inner particle size would cause a reduction of the pressure drops, shorter useful operation, wider thermocline spread in charge phase and lower thermocline spread in discharge operation.

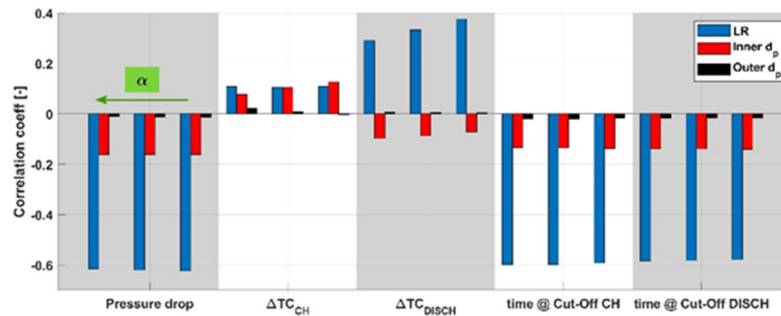


Figure 1: Correlation coefficients between each independent variable and the KPIs at various aspect ratios

## 4. Conclusions

This work introduces an innovative layered radial flow packed-bed TES concept able to reduce the pressure drop while improving the thermal performance of the TES. From the presented results the follow main conclusion can be drawn:

1. Sets of equally optimal PBTES designs can be identified which minimize the pressure drop while maximizing the useful charge and discharge operation.
2. In the proposed PBTES design LR has the major influence over the performance
3. The inner particle has a higher influence than the outer one. Thus, the first should be selected more carefully, whilst simplicity and costs could drive the selection of the latter.

Future works will be focused on the detailed TES design optimizations aimed at prototyping, testing and validating the proposed innovative PBTES unit.

## Acknowledgements

This project has received funding from the European Union's Horizon Europe research and innovation programme under grant agreement No 101083899.

## References

- [1] Trevisan S, Guédez R, Laumert B. Thermo-economic optimization of an air driven supercritical CO<sub>2</sub> Brayton power cycle for concentrating solar power plant with packed bed thermal energy storage. *Sol Energy* 2020;211:1373–91. <https://doi.org/10.1016/j.solener.2020.10.069>.
- [2] Zanganeh G, Pedretti A, Zavattoni S, Barbato M, Steinfeld A. Packed-bed thermal storage for concentrated solar power - Pilot-scale demonstration and industrial-scale design. *Sol Energy* 2012;86:3084–98. <https://doi.org/10.1016/j.solener.2012.07.019>.
- [3] Marti J, Geissbühler L, Becattini V, Haselbacher A, Steinfeld A. Constrained multi-objective optimization of thermocline packed-bed thermal-energy storage. *Appl Energy* 2018;216:694–708. <https://doi.org/10.1016/j.apenergy.2017.12.072>.
- [4] Klein P, Roos TH, Sheer TJ. Experimental investigation into a packed bed thermal storage solution for solar gas turbine systems. *Proc. SolarPACES 2013 Int. Conf.*, 2014, p. 840–9. <https://doi.org/10.1016/j.egypro.2014.03.091>.
- [5] Gauché P. South African provisional patent application. 2014/03555, 2014.
- [6] Laubscher HF, Von Backström TW, Dinter F. Developing a cost effective rock bed thermal energy storage system: Design and modelling. *AIP Conf. Proc.*, 2017. <https://doi.org/10.1063/1.4984436>.
- [7] Trevisan S, Wang W, Guedez R, Laumert B. Experimental Evaluation of an Innovative Radial-Flow High-Temperature Packed Bed Thermal Energy Storage. *Appl Energy* 2022;311. <https://doi.org/10.1016/j.apenergy.2022.118672>.
- [8] Schumann TEW. Heat transfer: A liquid flowing through a porous prism. *J Franklin Inst* 1929. [https://doi.org/10.1016/S0016-0032\(29\)91186-8](https://doi.org/10.1016/S0016-0032(29)91186-8).
- [9] Ergun S, Orning AA. Fluid Flow through Randomly Packed Columns and Fluidized Beds. *Ind Eng Chem* 1949;41:1179–84. <https://doi.org/10.1021/ie50474a011>.

EUROTHERM2023-F183

## Hybrid solar driven modular Heatcube™ for industrial process heat and power

Silvia Trevisan<sup>1</sup>, Bjarke Buchbjerg<sup>2</sup>, Rafael Guedez<sup>1</sup>

<sup>1</sup>Department of Energy Technology, KTH Royal Institute of Technology, Brinellvägen 68, 100 44 Stockholm, Sweden, e-mail: [trevisan@kth.se](mailto:trevisan@kth.se)

<sup>2</sup>KYOTO Group AS, 1366 Lysaker, Norway

### Abstract

Solutions aimed at decarbonizing the industrial sector are highly deemed in order to achieve worldwide sustainable development goals. Hybridized solar technologies together with power-to-heat system including storage could be a game changer in the sector. This work presents the innovative KYOTO Heatcube™, a low melting point molten salts based modular, customizable and flexible power-to-heat system including a thermal energy storage aimed at providing decarbonized heat to the industrial sector. The techno-economic performance of a Heatcube™ unit integrating solar technologies and batteries. The results show that the proposed hybrid integration of solar thermal, PV, and power to heat systems including TES can provide cost-competitive solution for the decarbonisation of the industrial sector.

**Keywords:** Thermal energy storage, Power to heat, Hybrid solar, Molten salts, Industrial decarbonization

### 1. Introduction

Nowadays, the industrial sector, emitting large share of greenhouse gases [1], represents a major challenge towards an effective sustainability development [2]. This sector demands about 22 % of the overall energy demand as heat and emits about 30% of the whole global carbon emissions [3]. About 16 % of the overall energy is required as heat at temperatures higher than 150 °C [4]. Industrial sectors such as metallic industries, chemical and petrochemical, construction and cement, pulp and paper are among the main heat consumers. To decarbonize the industrial sector different alternatives have been proposed [5,6]. Electrification of the heat demand is recognized as a key pathway. However, a major enabler of such a transition is the integration of thermal energy storage (TES). Specifically, storage solutions embedded in power-to-heat systems can maximize the sector coupling, minimize the strain on the power grid while maximizing the system flexibility and facilitating the penetration of renewables, finally enhancing the economic profitability of the power-to-heat solutions. For power-to-heat system to become cost-competitive solutions against commercial alternatives such as NG fuelled or electric boiler, low operational costs (OPEX) are required. Indeed, the levelized cost to heat (LCoH) attainable by typical industrial power-to-heat system is largely dominated by the OPEX, which could account for more than 80% of the LCoH. Thus, grid-based systems need for low average electricity prices and high price fluctuations [7]. Alternatively, further OPEX reduction could be attained by means of on-site renewable energy sources exploitation. For example, based on 2021 spot market prices, Spain and Italy would have a limited economic attractiveness for power-to-heat solutions solely based on grid connection. However, southern European countries have good solar irradiance (typical GHI between 1400 kWh/m<sup>2</sup> and 1900 kWh/m<sup>2</sup>). This offer the potential for solar based integration in power-to-heat systems with TES. The benefits of both solar thermal, such as parabolic trough thermal collectors (STC), and PV could be exploited and maximized in hybrid system. STC can be easily modularized, sized, and customized to the specific thermal load needs of the industrial site, achieving process thermal energy in the temperature range between 100 and 250 °C. PV could produce cheap electricity during the day complementing the grid connection. For industrial users requiring not only heat but also power, the PV

could be exploited, also in connection with battery energy storage systems (BESS), to fulfil the power demand. Such system integration is also based on fully commercial, off-the-shelf available components, meaning that rapid adoption of the technology could be performed.

The aim of this paper is twofold: 1) to present the innovative KYOTO Heatcube™, a low melting point molten salts based modular, customizable and flexible power-to-heat system including TES; 2) to assess the techno-economic of the system once hybridized with STC, PV, and BESS as a fully renewable based solution for industrial decarbonisation.

## 2. Materials and methods

The schematic layout of the hybrid system investigated in this work is shown in Figure 1. The central unit of the system is a Heatcube™, a molten salts (MS) based modular TES system, which can be delivered on-site as a prefabricated solution, ready to be integrated in the industrial production facility. KYOTO's Heatcube™ enables load shifting by exploiting energy from renewable sources when it is abundant and cheap, and storing it for later use. KYOTO Heatcube™ is a cost-effective solution with limited CAPEX and ensuring reduced OPEX over a long lifespan of 20 to 30 years. Specifically, a STC field is used to preheat the MS, via an indirect connection with dedicated heat exchanger. Such specific arrangement causes lower heat recovery efficiency but represent the most mature alternative fully based on off-the-shelf components. If needed the STC can also direct provide the required thermal energy for the industrial process during the day; also a secondary electric heater is integrated to boost the temperature of the flow coming from the STC field when if directly exploited for process heat production at higher temperatures. The Heatcube™ is then further charged by means of a dedicated electric heater, which can exploit power produced by the PV or from the grid during cheap power price periods. The PV installation is used not only to provide green electricity for charging the TES unit but also to cover the industrial power demand. BESS are integrated to ensure the required flexibility on the power side and potentially to offer a fully stand-alone installation.

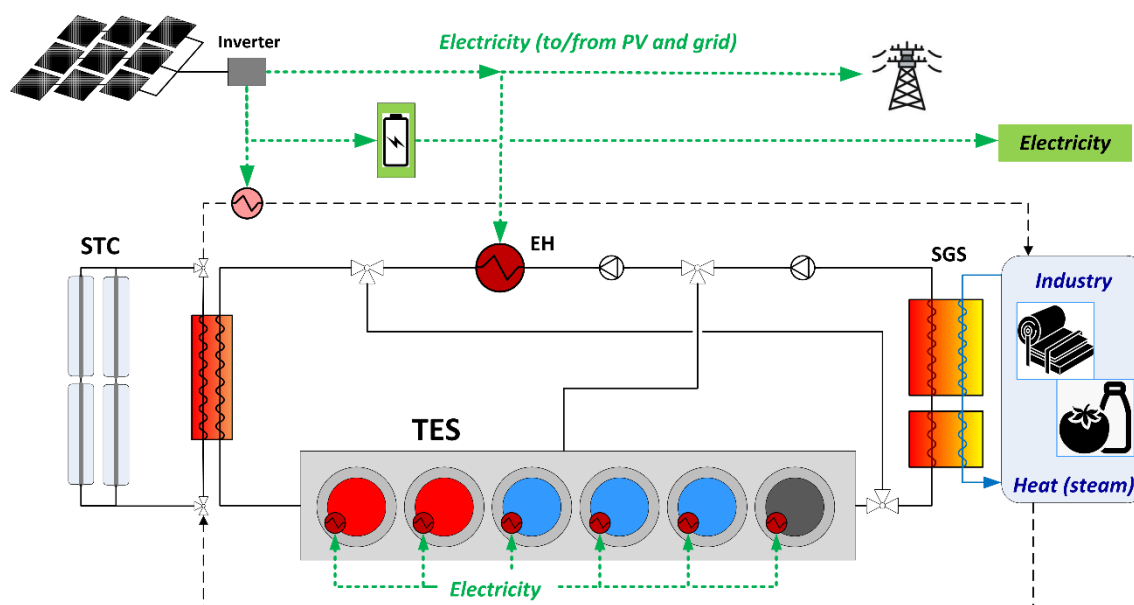


Figure 83. Proposed system integration layout

To investigate the thermo-economic performance of the proposed solar based hybrid system, a quasi-steady state model including a dispatch optimization algorithm has been built. The model includes all the key technical and operational inputs such as the specifications of the TES units, STC, PV, and EH, as well as the time series describing the electricity prices and solar resources availability. The dispatch algorithm, based on mixed integer linear programming, optimizes the operation of the integrated system aiming at ensuring the thermal and power load whilst minimizing the operational cost (OPEX) and maximizing the exploitation of renewables. More details on the techno-economic model and dispatch algorithm have been described by the authors in [7]. The considered reference case is based on a

cardboard production facility with a two shift operation schedule with constant thermal and power requirement during the day (specifically, constant  $3\text{MW}_{\text{th}}$  and  $0.75\text{MW}_{\text{e}}$  between 06.00 and 22.00 every day) [8]. The hybrid installation is located in Sevilla ( $37.39^{\circ}\text{N}$ ,  $5.99^{\circ}\text{W}$ ,  $\text{DNI} = 2090\text{ kWh/m}^2$ ,  $\text{GHI} = 1845\text{ kWh/m}^2$ ) and the Spanish electric market spot price during 2021 has been considered. The performance of the proposed system is assessed against solely grid based Heatcube<sup>TM</sup> systems as well as against traditional industrial heat production exploiting NG and electric boilers. KPIs such as the OPEX savings, Levelized Cost of Heat (LCoH), and CO<sub>2</sub> emission savings have been considered. Optimal sizing of the key components (STC and PV field, TES and BESS capacity) are also optimized aiming at attaining minimal LCoH.

### 3. Results and discussion

The main preliminary results are summarized in Figure 2. Specifically, focusing on the heat production, main demand of the considered case, Figure 2 (left) shows the attainable LCoH and OPEX savings by the proposed hybrid solar based system with respect to a NG fuelled boiler. A reference target range for industrial LCoH, as gathered from [9], is also shown as a grey area.

The preliminary results reports the values attainable by only PV or only STC based systems. The STC introduction is more beneficial than the integration of PV, particularly when high share of thermal load is required and in location with high DNI. Additionally, STC providing high solar share can contribute in limiting the OPEX of the system attaining more cost-effective solutions. Power to heat systems including TES but without solar integration recorded an OPEX saving of about  $0.5\text{ M€}/\text{y}$  with respect to a traditional NG fuelled boiler. The hybridization with solar technologies permits to lower the electricity consumption from the grid, leading to lower OPEX and higher achievable OPEX savings. For example, an STC installation of  $6\text{ MW}$  would ensure an annual OPEX savings of more than  $1.5\text{ M€}/\text{y}$ . Additional OPEX savings could be also provided by the PV installation which can lower the amount of energy bought from the grid. Notwithstanding the positive influence on a LCoH and OPEX perspective, it should be highlighted that the proposed system has a higher land footprint than solely grid based alternative power to heat solutions. Specifically, the combined installation of STC and PV might require more than 5 hectares, which might represent a limitation for industrial applications characterized by limited land availability or high land prices. To account for this a base land cost of  $50\text{ €/m}^2$  has been considered. Figure 2 (right) shows the influence of the assumed land cost over the attainable LCoH, specifically the base case considering a land cost of  $50\text{ €/m}^2$  is compared against a case with free unconstrained available land ( $0\text{ €/m}^2$ ). Considering free land substantial LCoH reductions of up to 18% can be achieved. The assumed land cost has a large influence over the techno-economic performance associated with the PV installation, which has a higher footprint that comparable STC.

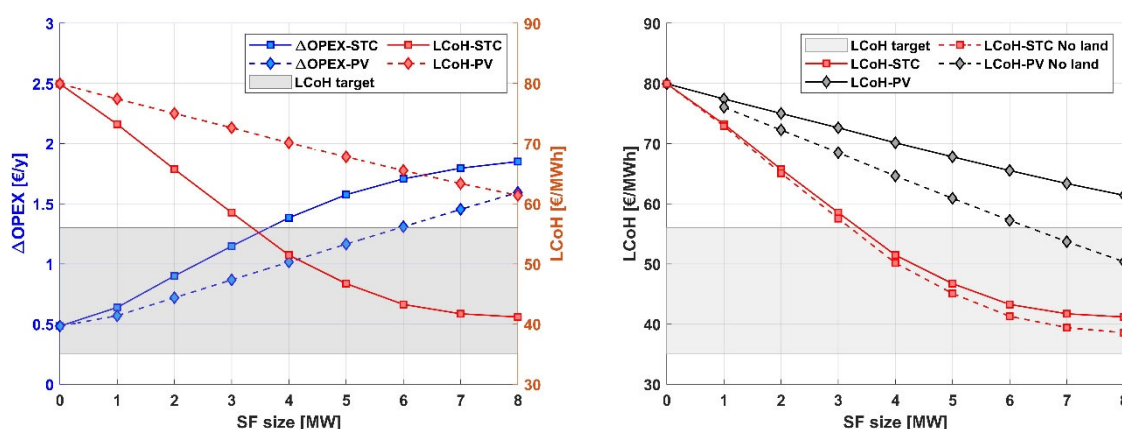


Figure 84. (left) OPEX savings against a NG fuelled boiler and LCoH for different solar field nominal sizes, (right) LCoH attainable assuming different land prices.

## 4. Conclusions

The present work introduced a hybrid solar driven system based on the innovative KYOTO Heatcube™, a low melting point molten salts based modular, customizable and flexible power-to-heat system including a thermal energy storage (TES) aimed at providing decarbonized heat and power to the industrial sector. The proposed system is based on fully commercial off-the-shelf components ensuring a potential rapid and reliable uptake by the industrial end-users. The techno-economic performance of the proposed system and his optimization have also been investigated. From the presented results the following key conclusions can be drawn:

1. The integration of solar driven and power to heat systems including TES can lead to cost-competitive solutions for the decarbonisation of the hard-to-abate industrial sector
2. Levelized cost of heat lower than 60 €/MWh, and relevant OPEX savings compared to state of the art solutions can be achieved
3. The elevated land use of solar technologies, and the need for collocated systems for solar thermal installations, might hinder the applicability of the solution particularly in highly urbanized contexts.
4. Hybrid STC and PV system can provide enhanced techno-economic performance whilst combining the specific benefits of both technologies.

Future works will be focused on further evaluating the potential of solar assisted power to heat systems for different industrial applications, including more efficient and innovative components.

## Acknowledgements

This research has been funded by Kyoto Group AS through the research project “Renewable Industrial Heat On-Demand” (RIHOND).

## References

- [1] Ritchie H, Roser M, Rosado P. CO<sub>2</sub> and Greenhouse Gas Emissions. Publ Online OurWorldInDataOrg 2020. <https://ourworldindata.org/co2-and-other-greenhouse-gas-emissions>.
- [2] United Nations. Transforming our world: the 2030 Agenda for Sustainable Development. 2015. <https://doi.org/10.1163/15718093-12341375>.
- [3] IRENA. Global Energy Transformation: A Roadmap to 2050. Abu Dhabi: 2019.
- [4] Naegler T, Simon S, Klein M, Gils HC. Quantification of the European industrial heat demand by branch and temperature level. *Int J Energy Res* 2015;39:2019–30. <https://doi.org/10.1002/er.3436>.
- [5] Cresko J. Industrial Decarbonization and Thermal Processes. 2021.
- [6] Sandalow D, Friedmann J, Aines R, McCormick C, McCoy S, Stolaroff J. ICEF Industrial Heat Decarbonization Roadmap. 2019.
- [7] Trevisan S, Buchbjerg B, Guedez R. Power-to-heat for the industrial sector : Techno-economic assessment of a molten salt-based solution. *Energy Convers Manag* 2022;272. <https://doi.org/10.1016/j.enconman.2022.116362>.
- [8] Pag F, Jesper M, Jordan U. Reference applications for renewable heat. 2021. <https://doi.org/10.17170/kobra-202104263730>.
- [9] LDES Council, McKinsey & Company. Net-zero heat. 2022.



EUROTHERM2023-B184

## Evaluation of thermochemical materials for thermal energy storage applications using TGA-DSC and existing material databases

Daniel Lager<sup>1</sup>, Jovana Kovacevic<sup>1</sup>

<sup>1</sup>AIT Austrian Institute of Technology GmbH, Center for Energy, Giefinggasse 2, 1210 Vienna, Austria, e-mail: daniel.lager@ait.ac.at

### Abstract

Research and development of thermochemical materials (TCM) for thermal energy storage (TES) need an accurate determination of the actual reachable energy density of the material based on experiments. This work shows an accurate approach to determine the actual water uptake and corresponding enthalpy of potential TCMs based on Thermogravimetric Analysis (TGA) and Differential Scanning Calorimetry (DSC) followed by an automatic comparison to existing literature based on a free sorption database “NIST NIST/ARPA-E Database of Novel and Emerging Adsorbent Materials”.

**Keywords:** Thermogravimetric Analysis, Differential Scanning Calorimetry, Thermochemical energy storage, Adsorbent Materials Database

### 1. Introduction

Thermochemical materials (TCM) for thermal energy storage (TES) must fulfill several requirements to compete with existing materials. In addition to economic efficiency and mechanical robustness, high energy density or, in the case of sorption materials, a high adsorbate loading, and associated sorption enthalpy are of particular importance. In this work we show a methodological approach how to determine the actual water uptake and sorption enthalpy based on (TGA) and Differential Scanning Calorimetry (DSC) and how the measured data can be evaluated and compared to existing literature data of a large sorption database provided by the National Institute of Standards and Technology (NIST).

### 2. Materials and Methods

#### 2.1. Investigated thermochemical heat storage material candidates

The experiences and evaluations shown in this work come from several different TCM with different partial pressure water vapor in the surrounding atmosphere which are analyzed via TGA-DSC. These include among several zeolite materials like natural clinoptilolite or synthetic zeolite 4A also composites with impregnated inorganic salts like  $\text{CaCl}_2$ ,  $\text{SrBr}_2$ ,  $\text{MgCl}_2$ ,  $\text{MgSO}_4$  or  $\text{LiCl}$  [1,2]. The developed approach will be applied on a new class of materials with promising sorption behavior due to their structure and polarity and are currently analyzed in the research project ENEPHOS.

## 2.2. Measurement Setup

For sorption isotherm and isobar measurements a TGA-DSC (NETZSCH STA 449F1) and a connected humidity generator (ProUmid MHG32) were used. The STA 449 F1 system is equipped with a special water vapor furnace which has an additional connection for the humidity generator. This setup provides the generated water vapor at the sample position and avoids condensation from the humidity generator outlet to the gas outlet of the TGA-DSC by a controlled heated path. The DSC Sensor in the system is a heat flow disc type S sensor (Pt/Rh) and the thermocouple wires are protected with  $\text{Al}_2\text{O}_3$  sleeves. Pure TGA measurements (without DSC signal) were done on  $\text{Al}_2\text{O}_3$  plates while TGA-DSC measurements were conducted in Pt/Rh crucibles with pierced lids.

## 2.3. Calibration

The mass calibration of the TGA system is done with accredited reference weights and verified by the dehydration of  $\text{CaC}_2\text{O}_4 \cdot \text{H}_2\text{O}$  [3]. The applied temperature calibration and the heat flow calibration of the DSC sensor to evaluate the characteristic temperatures as well as the enthalpy of sorption, hydration or solution effects, is based on the phase transition temperatures and enthalpy of fusion of pure reference substances as described in [4]. Finally, two additional approaches were conducted: Empty measurements to analyze the sorption behavior of the TGA/DSC sensor and its materials itself and the actual humidity at sample position based on pure reference salts and their humidity fixed points based on the binary saturated aqueous solutions of NaCl, MgCl and  $\text{K}_2\text{CO}_3$  [5].

## 2.4. TGA-DSC water vapor experiment

For the TCM measurement of the current load and the resulting exo- and endothermic effects, following protocol was chosen: As first step the material was filled as delivered into the Pt/Rh crucible (TG-DSC) or on the  $\text{Al}_2\text{O}_3$  plate (TGA) and the current mass of the sample was weight inside the STA. Then, the furnace temperature was heated to the defined desorption temperature and kept until the mass stayed constant. After this preconditioning of the sample, the STA was cooled down to room temperature and the initial dry mass of the sample was defined. Subsequently, the sorption experiment started according to a defined temperature and water vapor program

## 2.5 Evaluation method

Finally, the experiment data can be used to identify the actual uptake and the corresponding heat consumption or release. To find out whether the actual uptake is comparable and therefore competitive with existing materials, the NIST/ARPA-E Database of Novel and Emerging Adsorbent Materials (<https://adsorption.nist.gov/>) and a specially developed query code in Python are used. This database is a free catalog of adsorbent materials and measured adsorption properties of numerous materials obtained from article entries from the scientific literature.

## 3. Results and Discussion

### 3.1 Humidity accuracy and sample carrier sorption behavior

In Figure 7 the results for the equilibrium relative humidity generated over the saturated solutions of NaCl, MgCl and  $\text{K}_2\text{CO}_3$  are shown. The results show the deviation of the set value at the humidity generator and the actual value on the sample position of approx. 5%.

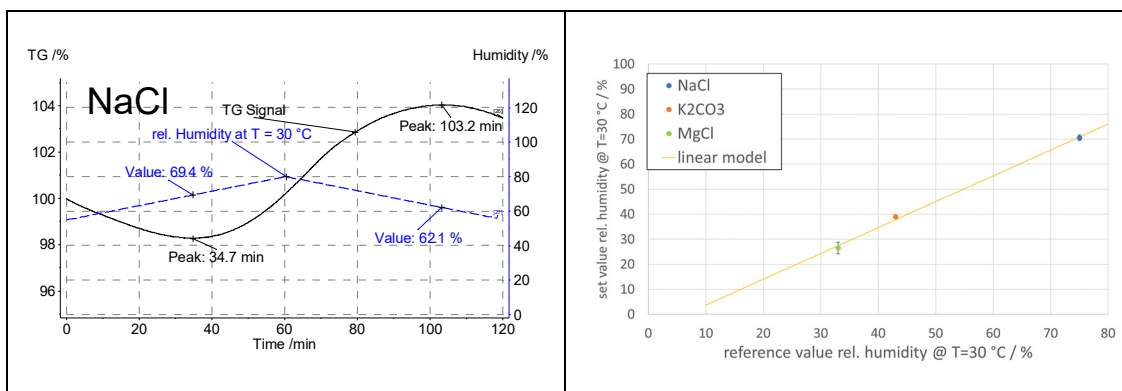


Figure 7. left: TGA results of the equilibrium values of the NaCl saturated solution; right: measured calibration points with NaCl, K<sub>2</sub>CO<sub>3</sub> and MgCl

Due to this result, the corrected value can be used as set point at the humidity generator for more accurate humidity conditions at the sample position. Additional measurements of the deviation of the mass at  $T = 30\text{ }^{\circ}\text{C}$  and a rel. humidity of 60 % showed deviations below  $\Delta m < 0,1\text{ mg}$ .

### 3.2 Sorption isotherm and enthalpy results on a zeolite

As shown in Figure 8 left, in case of the zeolite 4A measurement, a maximum temperature of  $T_{max} = 230\text{ }^{\circ}\text{C}$  and three adsorption steps with  $T = 35\text{ }^{\circ}\text{C}$ ,  $55\text{ }^{\circ}\text{C}$  and  $80\text{ }^{\circ}\text{C}$  at three different water vapor partial pressures  $p_{H_2O} = 6\text{ mbar}$ ,  $12\text{ mbar}$  and  $24\text{ mbar}$  are applied. The sample was placed into a Pt/Rh crucible without lid and being weighted inside the TGA. No separate preconditioning is conducted because the desorption of the zeolite took place before and after an adsorption step during one measurement run.

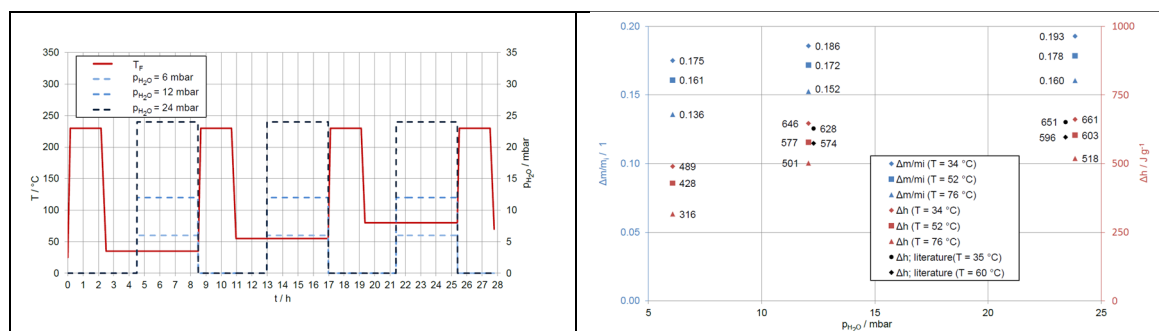


Figure 8. left: Furnace temperature program and water vapor pressure during the zeolite 4A TGA-DSC measurements right: Zeolite 4A water uptake  $\Delta m/m$ ; and enthalpy change  $\Delta h$  results from the TGA-DSC measurements

### 3.3 Evaluation of the material to already existing data sources

Based on the TGA-DSC results (Figure 8 right) the data can be directly compared to the literature data available for this specific adsorbate (water vapor) and the adsorbent (zeolite 4A) in the given temperature range. The developed software selects according to the given adsorbent ( $> 8000$ ), adsorbate ( $> 400$ ) and temperature the correct adsorption isotherms and displays them in comparison to the own data. Figure 9 represent the result of the automatic database search for zeolite 4A and delivers adsorption isotherms at  $T = 24,85\text{ }^{\circ}\text{C}$  from [6] in comparison to the experimental derived data with the TGA-DSC system.

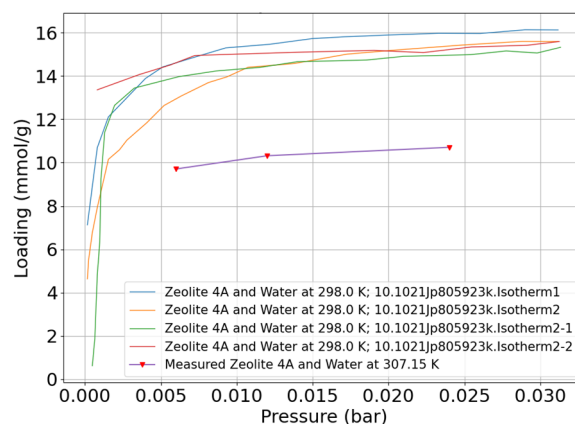


Figure 9. Result of the evaluation for the measured zeolite 4A in comparison to the available literature data from [6]

## 4. Conclusion

We conclude that TGA-DSC measurements can deliver high accurate measurements for sorption loading as well as sorption enthalpy with water vapor according to the presented protocol. Mass, temperature, heat flow and humidity calibration are mandatory to reduce the uncertainty in the uptake and enthalpy results. The developed software with the automatic comparison of the measurement data with the available literature data allows a fast and uncomplicated comparison with already existing adsorbate/adsorbent pair uptake data to recognize the competitiveness on an early stage of material development. The shown approach will be applied on the current research project ENEPHOS where the applicability and competitiveness of a new class of materials as adsorbents for TES is tested.

## Acknowledgements

The research leading to these results has received funding from the climate and energy fund (Klima- und Energiefonds) energy research program (Energieforschung – 8. Ausschreibung, Project Number: FO999896624) of the Republic of Austria.

## References

- [1] Gerald Englmaier, Bernhard Zettl, Daniel Lager. Characterisation of a Rotating Adsorber Designed for Thermochemical Heat Storage Processes. In: Frank E, Papillion P, editors. Conference proceedings / EuroSun 2014, International Conference on Solar Energy and Buildings, Aix-les-Bains, France, 16 - 19 September. Freiburg: International Solar Energy Society; 2015.
- [2] Reichl C, Lager D, Englmaier G, Zettl B, Popovac M. Fluid dynamics simulations for an open-sorption heat storage drum reactor based on thermophysical kinetics and experimental observations. *Applied Thermal Engineering* 2016;107:994–1007.
- [3] Chang H, Huang PJ. Thermal Decomposition of  $\text{CaC}_2\text{O}_4 \cdot \text{H}_2\text{O}$  Studied by Thermo-Raman Spectroscopy with TGA/DTA. *Anal. Chem.* 1997;69(8):1485–91.
- [4] Höhne G, Hemminger W, Flammersheim H-J. *Differential scanning calorimetry: With 19 tables.* 2nd ed. Berlin, Heidelberg, New York, Hong Kong, London, Milan, Paris, Tokyo: Springer; 2003.
- [5] Greenspan L. Humidity fixed points of binary saturated aqueous solutions. *J. RES. NATL. BUR. STAN. SECT. A.* 1977;81A(1):89.
- [6] Wu JY, Liu QL, Xiong Y, Zhu AM, Chen Y. Molecular simulation of water/alcohol mixtures' adsorption and diffusion in zeolite 4A membranes. *The journal of physical chemistry. B* 2009;113(13):4267–74.

EUROTHERM2023-Y185

## Optimal control of sorption storage in the context of enhancing seasonable performance of low-temperature district heating

Mustapha Habib<sup>1</sup>, Qian Wang<sup>1,2</sup>

<sup>1</sup>Division of Building Technology and Design, KTH Royal Institute of Technology, Department of Civil and Architectural Engineering, 11428 Stockholm, Sweden  
mushab@kth.se

<sup>2</sup>Uponor AB, Hackstavägen 1, 721 32, Västerås, Sweden  
qianwang@kth.se

### Abstract

District heating and cooling (DHC) networks are becoming, recently, promising solutions for the decarbonization of heating and cooling systems. The low supply temperature of 4<sup>th</sup> and 5<sup>th</sup> generation DHC make it possible lowering the heat losses in the pipes and integrating renewable energy sources (RES)-based heat generators. DHC network owners aim, continually, to keep large enough the temperature difference between supply and return in their plant generators in order to make heat transfer to the end-user more efficient. However, in summer scenario, this task is not trivial due to the low heat demand, and in summer, it can be even more challenging. This article is addressing and validating a potential solution based on the use of sorption energy thermal system (SETS) to enhance the seasonable DHC network performance, such as return temperature and heat pump setpoints. With an optimal real-time operation, SETS can fulfil the cooling demand in summer and help in lowering the DHC return temperature to a tolerable range.

**Keywords:** district heating and cooling; sorption energy thermal system; optimal control.

### 1. Introduction

Return temperature of DHC networks has been recently a crucial matter for network owners due to its impact on the energy production efficiency. This fact becomes inevitable in summer, when generally many DHC systems operate only to meet the domestic hot water (DHW) demand [1]. Current efforts on accelerating the transformation of conventional DHC network to the 4th and 5th generation DHC networks, focuses on integrating different renewable solutions in the network with significant low operating temperatures, e.g., 30-45 degrees as supply [2]. However, how to operate such renewables is heavily relying on storage solutions [3].

Thermochemical heat-storage technology, which has the advantages of high energy density and long-term operation, is recognized as a promising thermal energy storage (TES) technology [3]. In this regard, sorption energy thermal storage (SETS) has shown encouraging solutions for long-term storage, particularly for the integration with solar thermal systems [4]. e.g.,  $\text{MgCl}_2\text{-NH}_3$  can provide up to 2000 KJ/Kg [5]. However, taking advantage of the high specific storage energy of SETS for enhancing the DHC local operation in summer has not been treated yet.

This article addresses a potential solution for lowering the DHC return temperature in summer using SETS, in which, the end-user is the key play-actor. This technique consists on performing continuous charging process during summer using a heat pump (HP), which boosts the DHC temperature. This may have two main advantages: ensuring lower DHC return temperature over the year, and satisfying cooling demand in summer. In this work, the DHC temperature return

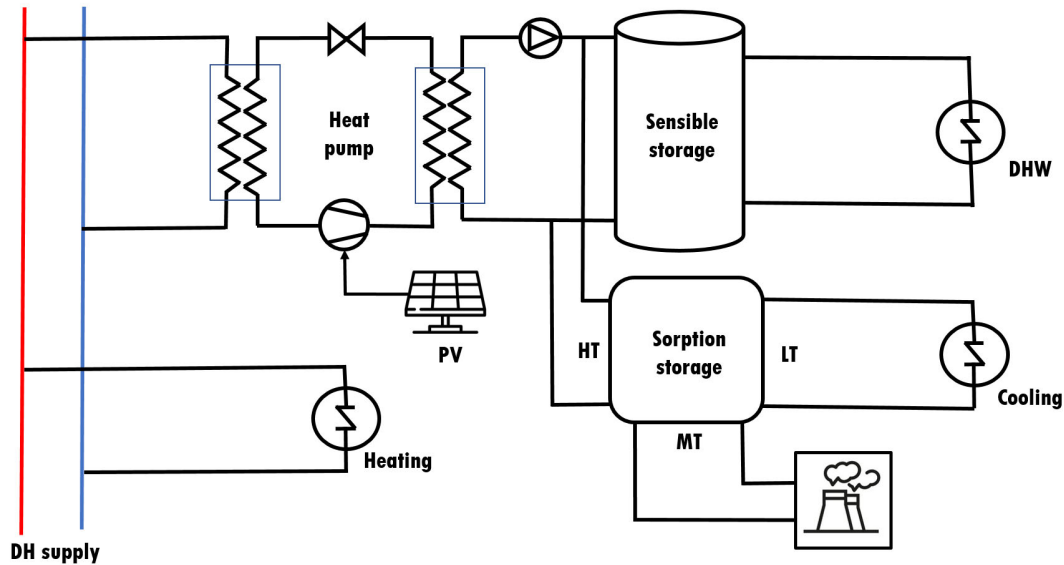


Figure 1. Proposed substation connection topology

limit is formulated as a constraint within an energy optimization problem, in which, the final objective is to maximize the photovoltaic (PV) power share in local energy community (LEC). Additional constraints should be also added as sensible storage tank state of charge (SOC) limits.

## 2. Materials and method

The solution addressed in this article is to be formulated as an optimization problem, in which, the PV energy self-sharing is targeted. For this reason, a specific connection topology for the sensible and latent storage technologies is suggested as shown in Fig.1.

### 2.1. System presentation

The system adopted in this article is integrating both sensible and latent TES solutions: a storage tank is added to upgrade the DHC temperature, via a booster HP, to desired values needed for DHW (~65°C); and SETS for seasonable storage purposes. Thanks to the low-temperature supply, DHC can satisfy the energy demand related to the space heating without any additional heat sources. To deal with the low DHC operation rate in summer, SETS is included as a seasonal storage system, it stores energy from DHC, via booster HP during summer, and discharges it in winter to assist the heating demand.

### 2.2. Method

This article aim to evaluate and validate the real-time optimal control of the booster HP, in the system presented earlier. The final optimization target is to maximize the use of PV power in feeding HP compressor, while respecting the storage tank SOC and DHC return temperature limits. For validation, real data for heat demand of a building district, located in Turin, Italy, is chosen. One year data, with hourly resolution, is selected as a long-term assessment of the DHC operation under the proposed control technique. The flowchart for the optimization method is illustrated in Fig. 2. In the proposed topology, HP has simultaneous impact on both thermal energy flow (from DHC to the storage tank and SETS) and electric energy flow (from PV/grid utility to the refrigerant compressor).

Due to the high computing effort, characterizing the optimization problem over one year hourly data, a performance map model for SETS is preferred instead of a physical model. Using the

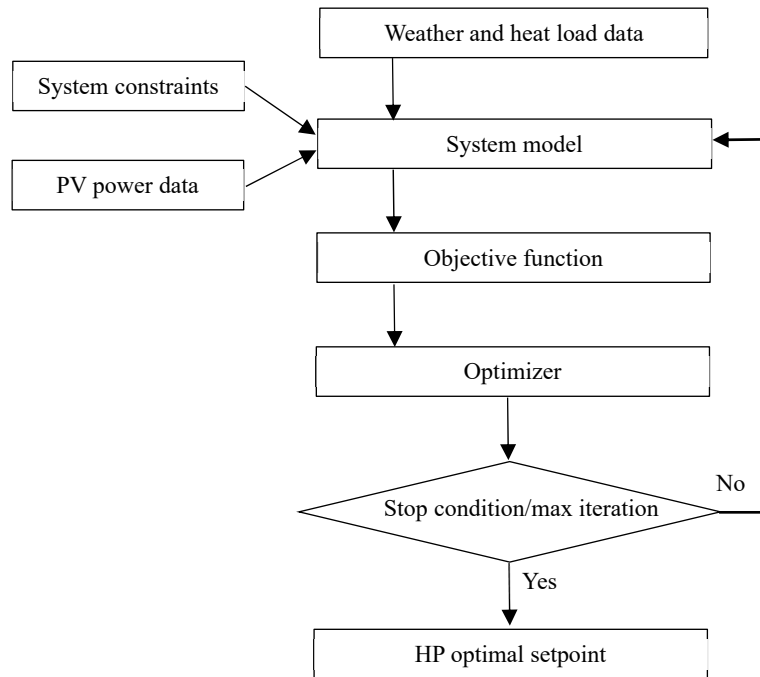


Figure 2. Flowchart of the proposed optimization problem

performance map approach, the model maps the input variables to the output instantaneously, with which, no calculations are needed. The desorption heat power was obtained based on the SETS condenser inlet temperature – ambient temperature – and the desorber inlet temperature. In the same way, the adsorption heat power was obtained based on the evaporator inlet temperature and the adsorber inlet temperature.

### 3. Results and discussion

Below, simulation results are displayed concerning the optimized management of heat energy for DHW and space heating taking the heat energy demand scenario of 2019 (Fig. 3). The chosen optimizer is “Interior Point” method [6]. In Fig. 4, the HP setpoint, sent by the optimizer in hourly basis, is displayed along with the corresponding supplied heat power. In Fig. 5, we see clearly that during the energy optimization process, the DHC return temperature is kept below a predefined threshold (here is 35°C).

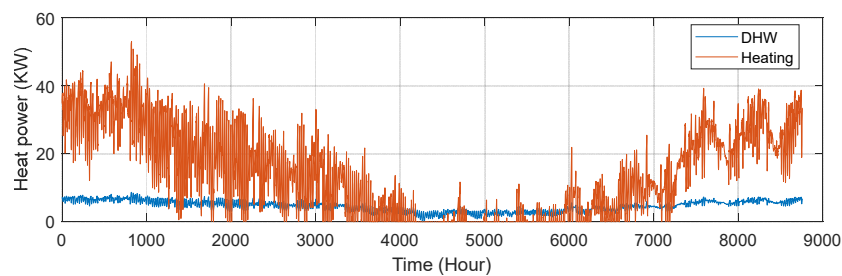


Figure 3. DHW and heating data

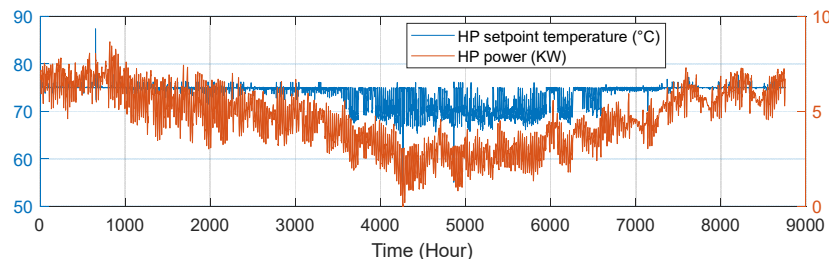


Figure 4. Optimal HP setpoint

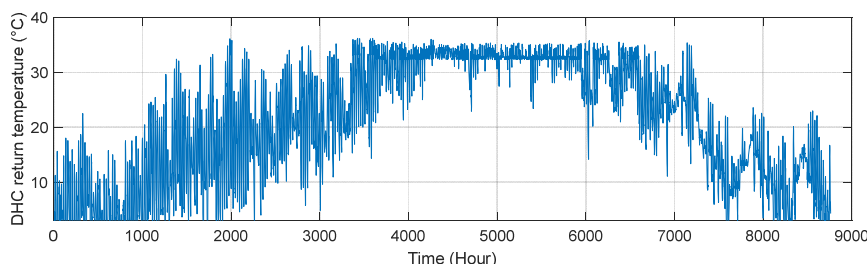


Figure 5. DHC return temperature data

## 4. Conclusions

This article addresses a solution for optimizing the DHC energy use in a buildings district in the framework of a general energy optimization problem. By taking advantage of potential long-term thermal storage solution, such as SETS, it is possible to drive optimally the booster HP to control the heat energy extracted from DHC, along with the electric energy consumed by the HP refrigerant compressor. For this regard, HP changes, in real-time, its operation temperature to control the energy stored in SETS.

## Acknowledgements

This study is funded by the Swedish Energy Agency (grant number 51544-1), and the European Commission (grant agreement number 101036656). Special thanks go to the project partner Environment Park in the Science and Technology Park (EnviPark) for providing data and case information.

## References

- [1] Simone Buffa, Marco Cozzini, Matteo D'Antoni, Marco Baratieri, Roberto Fedrizzi. 5th generation district heating and cooling systems: A review of existing cases in Europe. *Renewable and Sustainable Energy Reviews* 104 (2019) 504–522.
- [2] Kristian Gjoka, Behzad Rismanchi, Robert H. Crawford. Fifth-generation district heating and cooling systems: A review of recent advancements and implementation barriers. *Renewable and Sustainable Energy Reviews* 171 (2023) 112997.
- [3] M. Hlimi, B.E. Lebrouhi, A. Belcaid, B. Lamrani L. Balli, M.C. Ndukwu, T. El Rhafiki, T. Kousksou. A numerical assessment of a latent heat storage system for district heating substations. *Journal of Energy Storage* 57 (2023) 106210.
- [4] Alicia Crespo, Cèsar Fernández, Alvaro de Gracia and Andrea Frazzica. Solar-Driven Sorption System for Seasonal Heat Storage under Optimal Control: Study for Different Climatic Zones. *Energies* 2022, 15, 5604. <https://doi.org/10.3390/en15155604>.
- [5] Alicia Crespo, Cèsar Fernández, David Vérez, Joan Tarragona, Emiliano Borri, Andrea Frazzica, Luisa F. Cabeza, Alvaro de Gracia. Thermal performance assessment and control optimization of a solar-driven seasonal sorption storage system for residential application. *Energy* 263 (2023) 125382.
- [6] Li TX, Wang RZ, Yan T, Ishugah TF. Integrated energy storage and energy upgrade, combined cooling and heating supply, and waste heat recovery with solid–gas thermochemical sorption heat transformer. *Int J Heat Mass Transf* 2014;76: 237–46.
- [7] Arkadi S. Nemirovski. Interior-point methods for optimization. *Acta Numerica* (2008), pp. 191–234 doi: 10.1017/S0962492906370018.



EUROTHERM2023-G186

## Characterizing melting in rectangular latent thermal energy storage heat exchangers using the melting time liquid fraction method

Robin Tassenoy<sup>1</sup>, Wim Beyne<sup>1</sup>, Wout De Keyser<sup>1</sup>, Xander van Heule<sup>1</sup>, Michel De Paepe<sup>1,2</sup>

<sup>1</sup>Ghent University, Sint-Pietersnieuwstraat 41, Ghent, Belgium, e-mail: robin.tassenoy@ugent.be

<sup>2</sup>FlandersMake@UGent – Core lab EEDT-MP, Gaston Geenslaan 8, Heverlee, Belgium

### Abstract

This extended abstract proposes the melting time liquid fraction method to characterize constant wall temperature melting experiments in rectangular latent thermal energy storage heat exchangers. This method distinguishes itself from classical methods as the fitting coefficients are a discrete function of the liquid fraction, which implies a relation between liquid fraction and time. The method was validated experimentally for constant wall temperature melting experiments in a rectangular enclosure and compared to the classic characterization method. The melting time method systematically showed a lower root mean square deviation (RMSD) during the whole melting process, with a maximum RMSD below 6%. This improved prediction follows mainly from the varying fitting constants, which capture the different heat transfer mechanisms during different melting stages more effectively than constant fitting parameters.

**Keywords:** melting time liquid fraction method, constant wall temperature melting, PCM, rectangular enclosure, LTES

### 1. Introduction

Heat is the world's most used energy form, accounting for almost half of the global final energy use in 2021 [1]. This large energy demand fluctuates on daily, weekly and seasonal basis. Thermal energy storage systems (TES) can buffer these variations and are thus an essential part of the energy system [2].

This work focusses on latent heat TES (LTES), which stores heat by phase change of the storage medium. The solid-liquid phase change is mostly used because of the high storage capacity and limited volume change [3]. Despite their advantages, the uptake of LTES is currently limited as no effective characterization and design method is available [4]. Development of such a method requires a profound understanding of the melting and solidification behaviour. It has been shown that this behaviour depends on both the enclosure shape of the LTES and the direction of the phase transition [5]. Therefore, this work will focus on the characterization of the constant wall temperature (CWT) melting process in rectangular enclosures.

Shokouhmand and Kamkari [6] identified four main stages during the melting process in CWT experiments in rectangular enclosures: conduction, transition, strong convection and vanishing convection. Conduction from the wall to the PCM is the dominant mode of heat transfer during the early stage of melting. This stage is followed by a brief transition regime where the dominant heat transfer mode changes from conduction to convection. Convection is dominant during the remainder of the melting process. The final stage, the vanishing convection, starts when the melting front touches the opposite wall of the enclosure. The strength of the convective currents diminishes and a stratified temperature field develops at the upper part of the enclosure. The authors indicate that the heat transfer strongly depends on the melting stage.

The instantaneous liquid fraction is one of the main parameters to characterize the melting process. In literature, several liquid fraction correlations have been proposed, but none of them explicitly captures

the different melting stages due to the assumption of constant fitting coefficients for the whole melting process. This work proposes a novel method for liquid fraction prediction in melting problems: the melting time liquid fraction method (MTLFM). This method is based on the charging time energy fraction method introduced by Beyne et al. [4] and expanded by Couvreur et al. [7]. The original method for LTES heat exchangers is adapted for melting in a rectangular enclosure under a CWT boundary condition. Applied to this case, the method allows to predict the liquid fraction of the storage system as function of time and the applied wall temperature.

## 2. Method and experimental apparatus

The goal of the melting time liquid fraction method is to characterize the phase change behaviour by adequately predicting the liquid fraction as function of time, initial conditions of the storage and input parameters. The liquid fraction is defined as Equation 1.

$$\lambda(t) = \frac{m_{liquid}(t)}{m_{PCM}} \quad (1)$$

Beyne et al. [4] defined two issues that should be addressed to reach this goal. Firstly, a parametrized function for  $\lambda(t)$  as function of the initial conditions and input parameters should be defined. Secondly, the parameters of this function should be fitted to the measured liquid fraction according to a suitable objective function.

Beyne et al. proposed a method to decompose the fitting problem in a series of fitting problems by fitting the charging time as function of the liquid fraction instead of the liquid fraction as function of time. This means a limited series of  $\lambda_i$  are chosen between 0 and 1. A charging time measurement  $t_c(\lambda_i)$  corresponds with each  $\lambda_i$ . The problem of fitting the liquid fraction function  $\lambda(t)$  is consequently split in finding a correlation for the charging time for each liquid fraction level  $t_c(\lambda_i)$ . Equation 2 shows the adaptation of the correlation proposed by Beyne et al. to be suitable for characterization of CWT melting experiments in rectangular enclosures. This correlation predicts the time it takes to charge the system given the applied hot wall temperature. The predicted charging times are noted as  $\hat{t}_c$ , the predefined liquid fractions as  $\lambda_i$  and the fitting constants as A and B. The temperature difference between the hot wall temperature  $T_w$  and the PCM melting temperature  $T_m$  is selected as driving temperature difference.

$$\hat{t}_c(\lambda_i) = A(\lambda_i) \cdot \left( \frac{1}{T_m - T_w} \right)^{B(\lambda_i)} \quad (2)$$

The fitting constants  $A(\lambda_i)$  and  $B(\lambda_i)$  can be determined by minimizing the root mean square error between the measured charging time  $t_c(\lambda_i)$  and the predicted charging time  $\hat{t}_c(\lambda_i)$ .

The classic correlation method is also investigated as an alternative to the novel melting time method proposed. In this case the liquid fraction as a function of time is fitted by Eq. 3 where the fitting coefficients a, b and c are fixed coefficients.

$$\hat{\lambda}(t) = a \cdot t^c \cdot (T_m - T_w)^b \quad (3)$$

A major difference between the classic method and the melting time method is in the fitting constants. In the melting time correlation (Eq. 2), the fitting coefficients are fitted for each of the selected liquid fractions. As a result, the fitting coefficients are a discrete function of the liquid fraction which implies the relation between liquid fraction and time. In contrast, the fitting coefficients in the classic method are constants. Therefore, the relation between time and liquid fraction has to be posed explicitly.

An experimental setup was designed to test the phase change characterization method. The PCM RT26 is melt in a rectangular enclosure of 100 mm x 100 mm x 100 mm. This enclosure has a transparent front plate which allows visual tracking of the melting front with a camera, after which the liquid fraction as function of time is determined using image processing. One wall is kept at a constant temperature by circulating water-glycol mixture. The temperature of this wall and the PCM are measured with

thermocouples. The wall temperature cannot be controlled directly. Instead, the outlet temperature of the glycol heater was kept constant and the corresponding wall temperature was noted. This wall temperature was the average temperature of the aluminium plate during the constant phase of the experiment. The transient heating at the start of the experiment was thus excluded. The reported initial PCM temperature is the average of all thermocouples in the enclosure. An overview of the experiments is given in Table 11.

Table 11. Initial wall temperatures and PCM temperatures for the different melting experiments.

$T_{heater}$ (°C)	$T_w$ (°C)	$T_{PCM,initial}$ (°C)
80	$52.6 \pm 3.1$	$19.5 \pm 2.7$
70	$47.8 \pm 3.1$	$20.8 \pm 0.1$
60	$44.3 \pm 2.7$	$20.3 \pm 2.4$
52.5	$40.8 \pm 1.7$	$19.8 \pm 2.6$
45	$36.5 \pm 1.2$	$21.1 \pm 2.0$

### 3. Results

Figure 10 (a) shows the fitting results for the melting time method and the classic correlation. It is clear that the melting time method predicts the liquid fraction more accurately. Remark that the melting time method is a discrete method, predicting the melting time at predefined liquid fractions in contrast to the classical methods that make a continuous prediction.

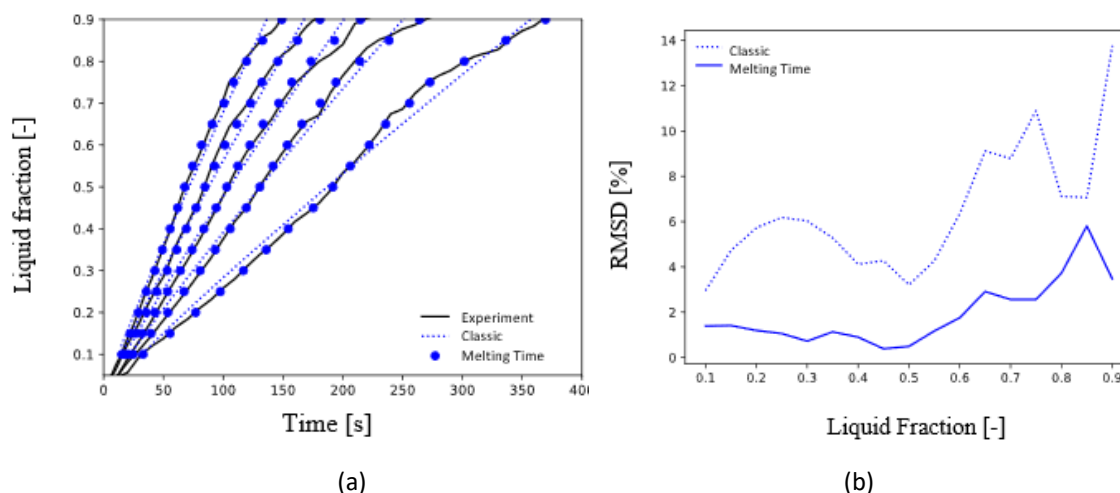


Figure 10. Liquid fraction for the five experiments with the prediction using the classic method and the melting time method (a) prediction (b) RMSD.

Figure 10 (b) quantifies the predictive accuracy of both methods by calculating the root mean square deviation between prediction and experiment for the classic and melting time correlation. The novel correlation method significantly reduces the error. Moreover, it can be seen that the error of the melting time method is significantly less fluctuating during the experiment as the different melting stages are taken into account. The classic method clearly performs best at a liquid fraction of 0.5 and the error systematically increased at both sides of this optimum. For the melting time method the error remains flat during the initial stages and increases slightly towards the end of the experiment. Nevertheless, the melting time method is a better prediction during the whole experiment with a maximum RSMD below 6%, while the error of the classic model increases significantly towards the end of the experiment to

more than 13%. Closer examination of the fitting constants shows that the exponent of the temperature difference variable in the MTLFM is not constant, but varies according to the dominant heat transfer mechanism. Taking this variation into account during the prediction thus significantly improves the accuracy over the course of the whole experiment.

#### 4. Conclusions

In this extended abstract, the melting time liquid fraction model for characterization of constant wall temperature melting experiments in rectangular enclosures has been proposed. This method distinguishes itself from classical methods as the fitting coefficients are a discrete function of the liquid fraction, which implies a relation between liquid fraction and time. The method has been demonstrated for CWT melting experiments in rectangular enclosures and compared to the classic method. The melting time method consequently showed a lower RMSD during the whole course of the melting process, with a maximum deviation below 6%. It has been shown that this improvement follows mainly from the varying fitting constants as the different heat transfer mechanisms are captured more effectively.

#### Acknowledgements

The authors declare the following financial relationships: Xander van Heule reports financial support provided by Research Foundation Flanders grant 1SD9721N.

#### References

1. Agency, I.E. Heating, 2021 [cited 2022 25/10/2022]; Available from: <https://www.iea.org/fuels-and-technologies/heating>.
2. Dincer, I.R., Marc, Thermal Energy Storage: Systems and Applications, Second Edition. 2011: John Wiley & Sons, Ltd.
3. Chandel, S.S. and T. Agarwal, Review of current state of research on energy storage, toxicity, health hazards and commercialization of phase changing materials. *Renewable and Sustainable Energy Reviews*, 2017. 67: p. 581-596.
4. Beyne, W., et al., A charging time energy fraction method for evaluating the performance of a latent thermal energy storage heat exchanger. *Applied Thermal Engineering*, 2021. 195.
5. Dhaidan, N.S. and J.M. Khodadadi, Melting and convection of phase change materials in different shape containers: A review. *Renewable and Sustainable Energy Reviews*, 2015. 43: p. 449-477.
6. Shokouhmand, H. and B. Kamkari, Experimental investigation on melting heat transfer characteristics of lauric acid in a rectangular thermal storage unit. *Experimental Thermal and Fluid Science*, 2013. 50: p. 201-212.
7. Couvreur, K., et al., Characterization of a latent thermal energy storage heat exchanger using a charging time energy fraction method with a heat loss model. *Applied Thermal Engineering*, 2023. 219.

EUROTHERM2023-W187

## Impact of the combined addition of textile-reinforced mortar and phase change material on the thermal behavior of buildings

Rabeb Ayed<sup>1</sup>, Salwa Bouadila<sup>1</sup>, Emiliano Borri<sup>2</sup>, Luisa F. Cabeza<sup>2</sup>, and Mariem Lazaar<sup>1</sup><sup>1</sup> Centre de Recherches et des Technologies de l'Energie, Technopole de Borj-Cédria, BP: 95, Hamam Lif, Ben Arous, Tunisia.<sup>2</sup>GREiA Research Group, Universitat de Lleida, Pere de Cabrera s/n, 25001 Lleida, Spain.

### Abstract

Combining thermal insulation and phase change materials (PCM) into building construction seems to be a promising opportunity to enhance the thermal efficiency of buildings. Accordingly, this study aims to investigate the impact of textile-reinforced mortar and phase change materials on the thermal performance of building roofs under a Mediterranean climate. Various configurations were investigated numerically, varying between combining the use of a PCM panel with regular cementitious mortar or mortar reinforced with textile for the construction of building roofs. The results show that the addition of the PCM panel caused a temperature drop of 3% compared to the reference case. However, combining the incorporation of the PCM and the thermal insulation caused a drop of 5% in temperature.

**Keywords:** Thermal insulation, Phase change material, Textile wastes, Cement mortar, Buildings, Heat transfer analysis.

### 1. Introduction

According to the International Energy Agency, buildings are the largest contributor to energy use, accounting for 36% of global consumption [1]. This high proportion is attributed to the building envelope as a major source of energy loss, especially in poorly insulated buildings. Therefore, improving the thermal performance of building envelopes is an absolute necessity [2]. Recently, there has been renewed interest in phase change materials as a viable and effective approach in the construction sector due to their major role in regulating the thermal performance of a building envelope during the phase change phenomenon [3–5]. Although several researchers have highlighted the potential of PCM to save energy and improve the thermal efficiency of building envelopes [6], they still have some serious limitations related to their incomplete solidification/freezing in passive applications, their stability over time [7], and other integration concerns. From another perspective, it was recognized that near-zero-energy buildings cannot be achieved without thermal insulation [8]. Accordingly, a number of studies have examined the possibility of combining the addition of thermal insulation and phase change materials in building materials. Jia et al. [9], for example, conducted a numerical investigation on seven brick walls that were aggregated with various thermal insulation materials (TIM) and PCM. The results showed that the combination of TIM and PCM affects the thermal behavior of the bricks differently. The integration of TIM increases the thermal resistance of the bricks, while, the PCM improved their thermal inertia. In fact, the incorporation of PCM into the bricks decreased the decrement factor from 12.3%-17.0% to 1.7%-2.2%, increased the time delay from 1.5-2 hours to 6.2-6.5 hours, and decreased the peak heat flux from 35.2-38.7 W/m<sup>2</sup> to 19.2-26.1 W/m<sup>2</sup>. Kalbasi and Afrand [10] conducted a study to ascertain the highly efficient choice for reducing the annual energy use of walls with integrated insulation, PCM, or a combination of both. The results showed that PCM integrated into walls performs better in summer, while the insulation is more effective in winter. The combination of PCM and insulation has been found to reduce overall energy requirements more than using either alone. Meshgin et al. [11] studied the effect of adding PCM and rubber particles to cement mortar for use as insulating mortar. The thermal conductivity results show that as the size of the rubber particles decreases, the conductivity of the rubberized mortar decreases. The incorporation of PCM results in a peak in the

thermal conductivity curve at the melting point of the PCM. In terms of thermal properties, the rubber particles can significantly reduce the thermal conductivity of the mortar, while the PCM can increase its heat capacity.

In an attempt to further enhance the thermal efficiency of buildings, this study aims to investigate the potential of combining the addition of textile-reinforced mortar (TRM) with a PCM panel into the roof under summer conditions. Textile-reinforced mortar is a composite material made of textile fiber wastes and cementitious matrix, which have been shown to improve the thermal properties of building elements [12]. The most suitable composition of the building roof was determined by evaluating the air temperature change in a room. It is anticipated that the results of this work will help address the problem of energy consumption in buildings by helping to understand the potential of combining PCM and textile fibers in building materials.

## 2. Materials and method

This study aims to numerically model the effect of textile-reinforced mortar and PCM on the thermal performance of a building roof under summer conditions using the COMSOL Multiphysics software. This numerical study was following an experimental study performed on a stand-alone cubicle room with a volume of 1 m<sup>3</sup>, built on the Mediterranean coast of northern Tunisia, precisely at the Research and Technology Center of Energy in Borj Cedria (latitude 36.69 and longitude 10.38). Figure 1(a) shows the experimental chamber, which consists mainly of brick walls coated on both sides with a 2 cm thick layer of cement mortar. Concerning the roof, it consists of a 10 cm thick layer of concrete. The methodology followed in this work consists of changing the configuration of the roof each time with one of the configurations mentioned below:

- **Case 1:** A reference room that is an exact replica of the experimental room used for validating the model.
- **Case 2:** A room in which a 3 cm thick PCM panel was incorporated into the 10 cm thick concrete roof.
- **Case 3:** A room where a 3 cm thick PCM panel has been incorporated in the roof between a 5 cm thick layer of concrete and a 2 cm thick layer of cement mortar.
- **Case 4:** A room where a 3 cm thick PCM panel has been incorporated in the roof between a 5 cm thick layer of concrete and a 2 cm thick layer of cement mortar reinforced with 40% by volume of textile fibers.

To assess the thermal environment of the mentioned room, a 3D geometry was developed and a time-dependent study was chosen to take into account the transient nature of the problem. The conjugate heat transfer component, phase change material feature, and the laminar flow module were used to study transient temperature transfer in the 3D geometry. The impact of solar radiation on temperature changes was taken into account through the use of the surface-to-surface radiation feature. The impact of changing the room configuration was studied based on the air temperature change in three different positions of the room (Figure 1(b)).

Table 1. Thermal properties of the used materials.

Material	PCM DS5001 X	Cement mortar	Textile reinforced mortar	Concrete
Solid thermal conductivity [W/m·K]	0.2	1.45	0.91	1.8
Liquid thermal conductivity [W/m·K]	0.13	-	-	-
Solid heat capacity [J/kg·K]	1700	631	1815	880
Liquid heat capacity [J/kg·K]	2153	-	-	-
Latent heat [kJ/kg]	130	-	-	-
Density [kg/m <sup>3</sup> ]	995	1840	1690	2300

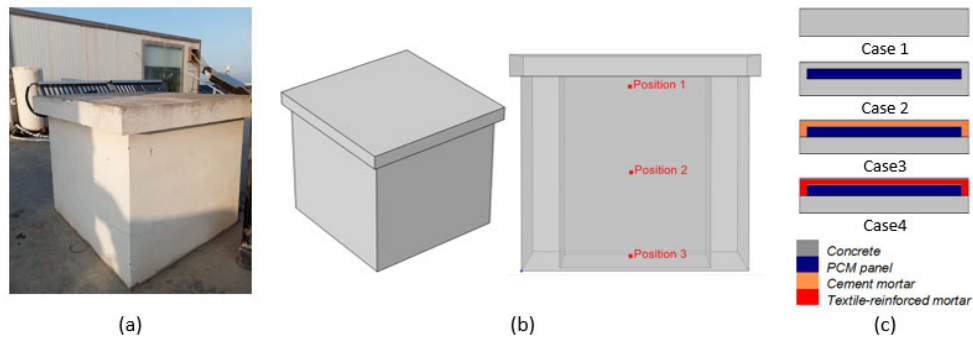


Figure 1. (a) Experimental room, (b) 3D geometry designed with COMSOL, and (c) studied configurations of the roof.

### 3. Results and discussion

To validate the numerical model, the air temperature change measured at the center of the room was compared to the predicted temperature of Case 1 (Figure 2(a)). The graph illustrates a comparable trend between the numerical and experimental values, with a root mean square error of 0.48. This similarity in the results corroborates the credibility of the developed model in anticipating heat transfer in the chosen room. The comparison between the air temperature changes in the four cases is depicted in Figure 2(b). As shown in the graph, the room shows a temperature stratification, which is highlighted at position 1 of the measurement. The addition of the PCM in the concrete layer caused a temperature drop of 3% compared to case 1. Concerning Case 3, the air temperature in the position 1 shows a maximum of around 42 °C, measuring a difference of 4.5% compared to case 1. However, by adding 2 cm thick layer of textile-reinforced mortar as a thermally enhanced material on the PCM panel, the air temperature shows the lowest values, showing a decrease in the maximum temperature of 5% compared to case 1.

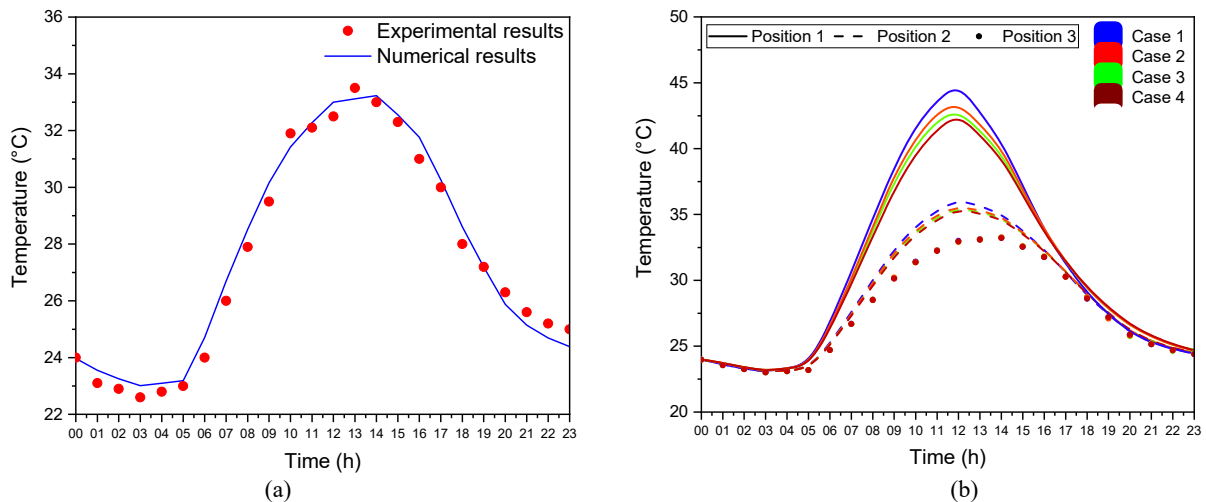


Figure 2. (a) Model validation (b) Comparison of temperature change in the four cases.

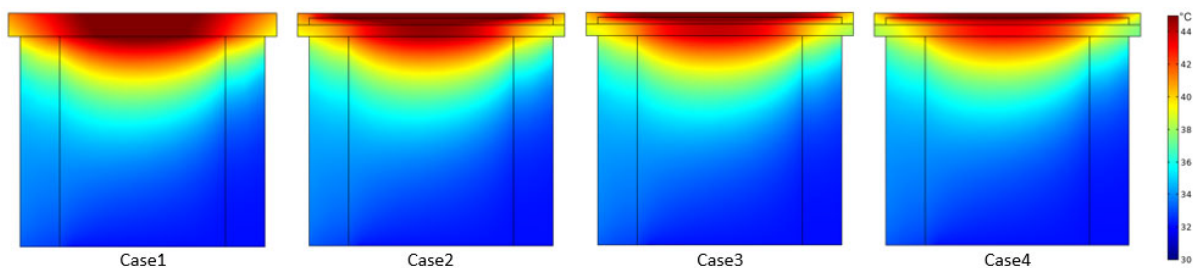


Figure 3. Air temperature profile in the four configurations studied.

Figure 3 shows the temperature contour in each case at 12 am. Areas of warm and hot temperatures are depicted in orange and red, while cold areas are shown in blue. As can be seen, the results confirmed what was reached previously, as the combination of using thermal insulation and phase change materials in the roof construction causes the greatest reduction in the temperature profile.

## 4. Conclusions

In this study, the combination of TRM and PCM was suggested as a potential solution to improve the energy efficiency of buildings. The evaluation of the thermal behavior of a room under summer conditions after the combined addition of TRM and PCM in the roof revealed a decrease in temperature peak of 5% compared to the reference case.

## Acknowledgments

This study was supported by the Thermal Processes Laboratory of the Research and Technology Center of Energy (CRTE<sub>n</sub>) in Tunisia. This study was partially funded by the Ministerio de Ciencia e Innovación - Agencia Estatal de Investigación (AEI) (PID2021-123511OB-C31 - MCIN/AEI/10.13039/501100011033/FEDER, UE). The authors from University of Lleida would like to thank the Catalan Government for the quality accreditation given to their research group (2021 SGR 01615). GREiA is certified agent TECNIO in the category of technology developers from the Government of Catalonia. This work is partially supported by ICREA under the ICREA Academia programme.

## References

- [1] International Energy Agency. Net Zero by 2050: A Roadmap for the Global Energy Sector. Int Energy Agency 2021:224.
- [2] Paraschiv S, Paraschiv LS, Serban A. Increasing the energy efficiency of a building by thermal insulation to reduce the thermal load of the micro-combined cooling, heating and power system. Energy Reports 2021;7:286–98. <https://doi.org/10.1016/J.EGYR.2021.07.122>.
- [3] Kharbouch Y. Effectiveness of phase change material in improving the summer thermal performance of an office building under future climate conditions: An investigation study for the Moroccan Mediterranean climate zone. J Energy Storage 2022;54:105253. <https://doi.org/10.1016/J.EST.2022.105253>.
- [4] Li H, Li Y, Wang Z, Shao S, Deng G, Xue H, et al. Integrated building envelope performance evaluation method towards nearly zero energy buildings based on operation data. Energy Build 2022;268:112219. <https://doi.org/10.1016/J.ENBUILD.2022.112219>.
- [5] Dellagi A, Ayed R, Bouadila S, Guizani A. Study of the thermal behavior of a heated brick containing a phase change material. 2022 13th Int. Renew. Energy Congr. IREC 2022, vol. 1, IEEE; 2022. <https://doi.org/10.1109/IREC56325.2022.10002002>.
- [6] Stropnik R, Koželj R, Završ E, Stritih U. Improved thermal energy storage for nearly zero energy buildings with PCM integration. Sol Energy 2019;190:420–6. <https://doi.org/10.1016/J.SOLENER.2019.08.041>.
- [7] Devanuri JK, Gaddala UM, Kumar V. Investigation on compatibility and thermal reliability of phase change materials for low-temperature thermal energy storage. Mater Renew Sustain Energy 2020;9:1–16. <https://doi.org/10.1007/s40243-020-00184-4>.
- [8] Amani N, Kiaee E. Developing a two-criteria framework to rank thermal insulation materials in nearly zero energy buildings using multi-objective optimization approach. J Clean Prod 2020;276:122592. <https://doi.org/10.1016/J.JCLEPRO.2020.122592>.
- [9] Jia C, Geng X, Liu F, Gao Y. Thermal behavior improvement of hollow sintered bricks integrated with both thermal insulation material (TIM) and Phase-Change Material (PCM). Case Stud Therm Eng 2021;25:100938. <https://doi.org/10.1016/j.csite.2021.100938>.
- [10] Kalbasi R, Afrand M. Which one is more effective to add to building envelope: Phase change material, thermal insulation, or their combination to meet zero-carbon-ready buildings? J Clean Prod 2022;367:133032. <https://doi.org/10.1016/J.JCLEPRO.2022.133032>.
- [11] Meshgin P, Xi Y, Li Y. Utilization of phase change materials and rubber particles to improve thermal and mechanical properties of mortar. Constr Build Mater 2012;28:713–21. <https://doi.org/10.1016/J.CONBUILDMAT.2011.10.039>.
- [12] Ayed R, Bouadila S, Skouri S, Boquera L, Cabeza luisa F. Recycling Textile Waste to Enhance Building Thermal Insulation and Reduce Carbon Emissions : Experimentation and Model-Based Dynamic Assessment 2023.



EUROTHERM2023-G188

## Thermal performance analysis of multi-pass macro encapsulated phase change material/expanded graphite compressed discs thermal energy storage unit

Ajay Muraleedharan Nair<sup>1, \*</sup>, Christopher Wilson<sup>1</sup>, Ming Jun Huang<sup>1</sup>, Philip Griffiths<sup>1</sup>,  
Simon Hodge<sup>2</sup>, Neil Hewitt<sup>1</sup>

<sup>1</sup> Centre for Sustainable Technologies, Belfast School of Architecture and Built Environment, Ulster University, BT15 1ED, UK, a.nair@ulster.ac.uk

<sup>2</sup> Engineering Composites Research Centre, School of Engineering, Ulster University, BT15 1ED, UK

### Abstract

An efficient, stable, and cost-effective Phase change material (PCM)-Thermal energy Storage (TES) system combined with heat pumps solar panels is an excellent way to store off-peak renewable energy and provide demand side management to decarbonise the heating sector. This paper presents a detailed discussion of the development of a novel multi-pass organic PCM/Expanded graphite (EG) TES unit and the experimental data analysis, and the results obtained from the thermal performance studies. The analysis of charging period showed a uniform temperature rise of the PCM throughout the process. The highly conductive heat transfer network provided by the combination of EG, circular aluminium fins and the multi-pass tube arrangement resulted in high heat transfer rate during charging process with an average charging power of 1.32kW. The total energy content of the system after 160 minutes of charging was around 4kWh.

**Keywords:** Thermal energy storage, Phase change materials, expanded graphite, heat transfer enhancement, hot water application

### 1. Introduction

Thermal Energy Storage (TES) utilising phase change materials (PCM) has the ability to harvest, store, and conserve thermal energy for short or extended periods of time. PCM TES system integrated solar panels or heat pump (HP) units are effective for demand-side management to reduce the carbon emission associated with domestic hot water applications (Griffiths and Eames, 2007; Navarro *et al.*, 2016). However, the low heat transfer kinetics of the PCM TES systems must be resolved for the successful commercialisation of PCM based thermal energy storage systems. This can be achieved either by the design modification of the heat exchanger system by using various fin configurations, encapsulation of the PCM or by impregnating PCM into highly porous materials like expanded graphite (EG) (Nair *et al.*, 2022). Shell and tube heat exchangers (Agyenim and Hewitt, 2010) and concentric tube heat exchangers (Fuxin *et al.*, 2013) are the two most commonly studied heat exchangers in both organic and inorganic PCM based TES systems. Fin and tube and plate fins configurations were used to achieve high heat transfer rate without compromising the thermal energy storage capacity of the system (Li *et al.*, 2019). Researchers have investigated the feasibility of using PCM storage units for residential heating applications both numerically and experimentally under various operating conditions and optimised the system performances (Huang, Eames and Hewitt, 2006). Also, expanded graphite has been widely investigated as a heat transfer enhancer due to its high thermal conductive network structure, thermal reliability, and chemical inertness (Galazutdinova *et al.*, 2018). The thermophysical properties of PCM/EG composite and its cyclability studies were conducted over last two decades to optimise the wt% of the EG. TES unit fabricated with compressed PCM/EG composite blocks with

various configurations of the heat exchanger systems design has been studied for domestic and industrial TES applications (Merlin *et al.*, 2016).

This paper experimentally investigates the feasibility of a multi tube macro encapsulated Crodatherm60/EG compressed modules TES system for the DHW application. The proposed system presents the combined advantages of shell and tube heat exchanger, EG and fins for the heat transfer enhancement. Besides it focusses on the effectiveness of macro encapsulated PCM/EG modules in reducing the possible segregation liquid PCM from EG.

## 2. Materials and methods

A commercially available bio derived organic PCM having phase change temperature of 60°C, thermal conductivity of  $0.28 \text{ W m}^{-1} \text{ K}^{-1}$  and latent heat of  $217 \text{ kJ kg}^{-1}$  was used for the study. The PCM/25wt%EG mixture is prepared by melt blending. Then the composite material prepared was compressed into a disc of 280mm diameter and 20mm thickness to a density of  $1050 \text{ kg.m}^{-3}$ . Twelve 12mm holes were drilled on the disc to pass a 12mm copper pipe for HTF as represented in Fig. 11(a). To reduce the segregation of EG and PCM and to prevent the leakage of liquid PCM from the EG, the compressed Croda60/EG discs were macro encapsulated with an aluminium container of 280mm internal diameter and 40mm height and two 1mm thick radial fins at both the sides of the container. Each macro module contains two such Croda60/EG discs. Sixteen such modules were joined vertically one above another to fabricate the TES unit of 3.5kWh capacity as shown in Fig. 11(b). Sixteen thermocouples were inserted into the storage unit to evaluate the temperature profile of the system during both charging and discharging cycle processes. The thermal performance of the system during the charging period was evaluated at heat transfer fluid (HTF) inlet temperature of 80°C and  $7.5 \text{ l.min}^{-1}$  volume flow rates.



Fig. 11. Image of (a) the Croda60/EG disc and (b) PCM/EG TES unit

## 3. Result and discussions

The temperature evolution of the PCM storage unit during the charging process with HTF at 80°C inlet temperature and  $7.5 \text{ l.min}^{-1}$  volume flow rate is represented in Fig. 12. All the thermocouples showed a uniform rate of temperature rise during the charging process. The PCM exhibited only minimal thermal stratification due to the uniform conductive network provided by the EG/Al fin combination. This asserts that conduction was the major mode of heat transfer. The temperature difference between the inlet and outlet of HTF was high at the initial period of charging and as the PCM temperature increased, this difference diminished and approached nearly zero. Fig. 13. illustrates the thermal energy accumulated during the charging process and corresponding average PCM temperature of the TES unit. A clear phase transition period extending over 60 minutes is visible from the average PCM temperature curve. As can be seen, in 150 minutes of charging, nearly 4kWh thermal energy was transferred into the system from the HTF. Average charging power of the multi pass PCM/EG configuration over every five minutes of charging is represented in Fig. 14. The average heat transfer rate followed the same trend as the

difference between the inlet and outlet of the HTF temperature with an average heat transfer rate of 1.32kW over the charging period. The system exhibited four times more heat transfer rate than the average heat transfer of the system during the first five minutes of charging. This is due to the higher temperature gradient between the HTF and the PCM. As the PCM temperature increased, there is a corresponding and expected drop in the heat transfer rate.

Fig. 12. Dynamic temperature variation of the TES unit during charging period analysis at 80°C and 7.5 l.min<sup>-1</sup>.

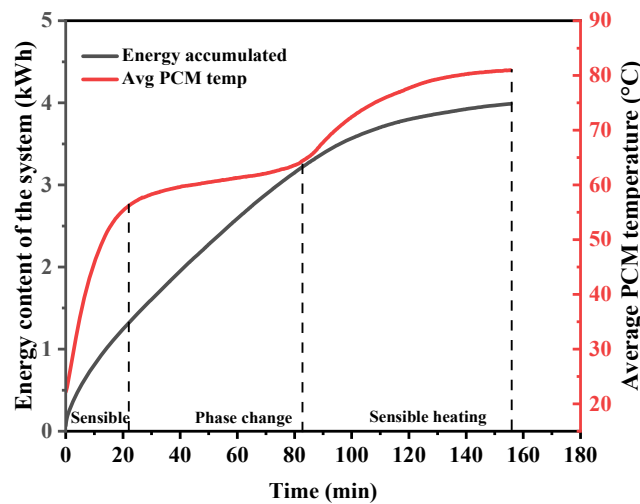


Fig. 13. Energy accumulated in the PCM TES unit and the variation of average PCM temperature over the charging period.

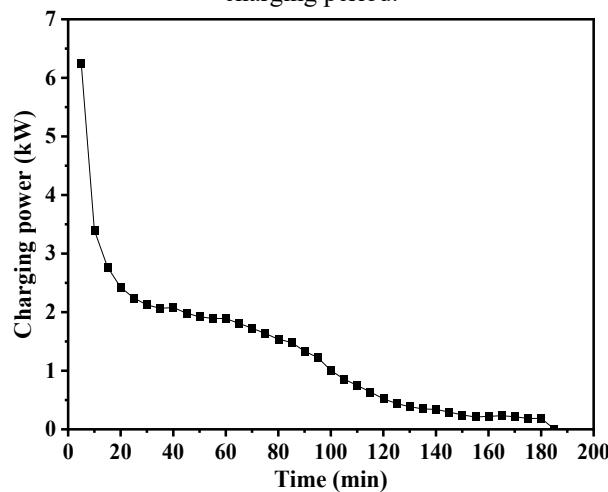


Fig. 14. Average charging power of the PCM TES unit in every five minutes of charging with 80°C and 7.5 l.min<sup>-1</sup>HTF

## 4. Conclusions

This study aimed to develop a TES unit with CrodaTherm60 PCM for the domestic hot water production application. A novel TES unit was designed with macro encapsulated organic PCM/EG discs and a multi-pass tube arrangement to enhance the heat transfer rate during charging and discharging. The uniform temperature rise of the PCM during the charging cycle is attributed to the highly conductive heat transfer network provided by the combination of EG, circular aluminium fins and the multi-pass tube arrangement. The possible segregation of liquid PCM was successfully contained by the macro encapsulation of PCM/EG modules. 4kWh of thermal energy was transferred to the system in 160 minutes of heating at an average heat transfer rate of 1.32kW.

## Acknowledgement

This study is a part of the SPIRE-2 project and EPSRC funded HP-FITS project (Grant Number: EP/T025581/1). The authors acknowledge the financial support from the European Union's INTERREG VA Programme (Grant Number IVA5038). The authors are grateful to all the partner institutes and industries of the project. The research was also undertaken as part of the inpath-tes.eu thermal energy storage research network. The authors would like to extend their gratitude to Roy Brestford and Simon Hodge for their selfless support during the fabrication process of the TES system.

## References

- Agyenim, F. and Hewitt, N. (2010) 'The development of a finned phase change material (PCM) storage system to take advantage of off-peak electricity tariff for improvement in cost of heat pump operation', *Energy and Buildings*, 42(9), pp. 1552–1560. doi:10.1016/j.enbuild.2010.03.027.
- Fuxin, N., Long, N., Minglu, Q., Yang, Y. and Shiming, D. (2013) 'A novel triple-sleeve energy storage exchanger and its application in an environmental control system', *Applied Thermal Engineering*, 54(1), pp. 1–6. doi:10.1016/j.applthermaleng.2012.11.022.
- Galazutdinova, Y., Vega, M., Grágeda, M., Cabeza, L.F. and Ushak, S. (2018) 'Preparation and characterization of an inorganic magnesium chloride/nitrate/graphite composite for low temperature energy storage', *Solar Energy Materials and Solar Cells*, 175(June 2017), pp. 60–70. doi:10.1016/j.solmat.2017.09.046.
- Griffiths, P.W. and Eames, P.C. (2007) 'Performance of chilled ceiling panels using phase change material slurries as the heat transport medium', *Applied Thermal Engineering*, 27(10), pp. 1756–1760. doi:10.1016/j.applthermaleng.2006.07.009.
- Huang, M.J., Eames, P.C. and Hewitt, N.J. (2006) 'The application of a validated numerical model to predict the energy conservation potential of using phase change materials in the fabric of a building', *Solar Energy Materials and Solar Cells*, 90(13), pp. 1951–1960. doi:10.1016/j.solmat.2006.02.002.
- Li, T.X., Xu, J.X., Wu, D.L., He, F. and Wang, R.Z. (2019) 'High energy-density and power-density thermal storage prototype with hydrated salt for hot water and space heating', *Applied Energy*, 248(April), pp. 406–414. doi:10.1016/j.apenergy.2019.04.114.
- Merlin, K., Soto, J., Delaunay, D. and Traonvouez, L. (2016) 'Industrial waste heat recovery using an enhanced conductivity latent heat thermal energy storage', *Applied Energy*, 183, pp. 491–503. doi:10.1016/j.apenergy.2016.09.007.
- Nair, A.M., Wilson, C., Huang, M.J., Griffiths, P. and Hewitt, N. (2022) 'Phase change materials in building integrated space heating and domestic hot water applications : A review', 54(March).
- Navarro, L., de Gracia, A., Colclough, S., Browne, M., McCormack, S.J., Griffiths, P. and Cabeza, L.F. (2016) 'Thermal energy storage in building integrated thermal systems: A review. Part 1. active storage systems', *Renewable Energy*, 88, pp. 526–547. doi:10.1016/j.renene.2015.11.040.

EUROTHERM2023-M189

## Techno economic comparison of a commercial phase change material heat battery with a hot water tank operated with a high temperature air source heat pump

Ajay Muraleedharan Nair, Christopher Wilson, Ming Jun Huang, Philip Griffiths, Neil Hewitt

Centre for Sustainable Technologies, Belfast School of Architecture and Built Environment, Ulster University,  
BT15 1ED, UK, a.nair@ulster.ac.uk

### Abstract

Phase change material (PCM) thermal energy storage (TES) systems are potential alternatives to large hot water tanks (HWT), requiring less space, can be retrofitted easily and ideal for demand-side management when operating with a heat pump (HP). A techno-economic comparison of a commercial PCM thermal battery with a HWT was conducted when operated with a high temperature air source heat pump (ASHP) based on the normalised electricity consumption to deliver same amount of useful thermal energy. Based on the difference in electricity consumption, annual running cost savings and greenhouse gas (GHG) emission reductions were calculated for various countries of Europe. The HWT consumed 2.65kWh of more electricity than the PCM battery to produce same amount of useful energy and this can lead to a significant annual running cost saving (£50-388) and considerable reduction in CO<sub>2e</sub> emission (50-700 kg) in different countries in Europe.

**Key words:** Thermal energy storage, phase change materials, domestic heating, heat pump, hot water tank, greenhouse gas emission

### 1. Introduction

In Europe, households account for 24.7% of the total energy consumption. Sanitary hot water and space heating represents more than 75% of total domestic energy consumption and a major share of this is covered by heaters operated either by gas, oil, or electricity, (Tsemekidi Tzeiranaki *et al.*, 2018; Eurostat Energy data 2020, 2020; Nair *et al.*, 2022). To decarbonise the domestic sector, renewable energy penetration of the electricity grid using heat pumps (HP) is an option. HP with an efficient thermal energy storage device can effectively solve the mismatch between supply and demand of energy and provides significant economic benefits (Shah *et al.*, 2018) and reduced associated CO<sub>2</sub> emissions (Arteconi, Hewitt and Polonara, 2012; da Cunha and Eames, 2018). Sanitary hot water is essential for daily life domestic applications. Domestic hot water (DHW) tanks are simple to manufacture, easy to install, and affordable. However, it can occupy a large space, uses more energy to maintain a set point, and possesses relatively high standing energy losses as it requires high storage temperatures (Cabeza *et al.*, 2002). PCM thermal stores are promising alternatives to HWT, possessing high storage densities, save space, have a better utilization efficiency, and lower energy losses. Research activities aiming to develop an efficient thermal store have increased substantially, and industries are investing in the energy storage sector by collaborating with universities worldwide (Seddegh *et al.*, 2015). Low temperature thermal energy storage (LHTES) units can be integrated with solar collectors or with an HP for effective demand-side management (Griffiths, Huang and Smyth, 2007).

A techno economic evaluation was undertaken of a commercial PCM battery operated with a HP and compared with a large hot water tank (HWT) with the normalised volume for the equal amount of thermal energy discharged, useful energy efficiency, the useful energy per unit volume normalised

thermal energy transferred into the thermal stores and normalised electrical consumption examined. From this the annual economic benefit and carbon emission reduction when using the PCM battery compared to the HWT in different regions of Europe was calculated based on the 2021 emission factors and the winter 2022 domestic electricity price per kWh.

## 2. Materials and methods

Two commercial thermal batteries received as part of the SPIRE-2 project were tested with a high temperature air source heat pump (ASHP) to examine its feasibility in domestic hot water application. The results were compared with that of a 600L HWT. A test facility was developed which consisted of a Daikin cascaded high temperature ASHP, two PCM thermal batteries connected in series and the HWT. The operating temperature of the HP was set to the required value and the charging continued until the temperature of the heat transfer fluid (HTF) at the outlet of the thermal store reached the setpoint temperature. The discharging cycles were initiated immediately after the complete charging of the thermal stores with mains water at  $8.5 \text{ l}\cdot\text{min}^{-1}$ . A mixing valve was used in the discharging loop to maintain the temperature of the discharged water in the useful range of  $38\text{-}40^\circ\text{C}$  (B S I Standards, 2015). Two Pt100 temperature sensors and a flow meter were installed in the charging loop to measure the inlet and outlet temperature of the HTF and the mass flow rate during charging process. In addition, three pt100 and a pulse flow meter were used to measure the temperature of the HTF at the inlet and outlet of the discharging loop, temperature at the mixing valve and the discharging flow rates respectively.



Fig. 15. Cascaded heat pump indoor unit with the commercial heat battery and the HWT thermal store test rig

## 3. Result and discussion

The key technical parameters evaluated based on the energy analysis of the thermal stores during the charging and discharging cycle analysis are listed in Table 1. At  $8.5 \text{ l}\cdot\text{min}^{-1}$  discharge flow rates at the mixing valve, nearly 75% of the total thermal energy stored was discharged within the useful temperature range from the PCM battery whereas it was only 57% for the HWT. To discharge the same amount of useful energy, nearly 24% more thermal energy would need to be added to the HWT compared to the PCM battery and associated electricity consumption would be 2.65kWh more than that for the PCM battery. The HWT should be 46.58% larger than the PCM thermal battery to deliver the same amount of thermal energy in the useful temperature range.

Table 12. Key performance parameters of the energy analysis of HWT and PCM thermal battery at 8.5l.min<sup>-1</sup> discharge flow rates.

Parameter	Unit	HWT	PCM battery
Energy transferred in	kWh	30.2445	17.886
Electricity consumption	kWh	13.332	7.724
>38°C water availability period	min	66	43
Volume of >38°C water	L	561	365.5
Useful energy available	kWh	17.237	13.407
Volume of thermal store	m <sup>3</sup>	0.734	0.305
Useful energy/unit volume	kWh/m <sup>3</sup>	23.484	43.957
Useful energy efficiency	%	56.99	74.96
Normalised electricity consumption	kWh	10.37	7.72
Normalised volume of thermal store	m <sup>3</sup>	0.571	0.305
Average COP of HP		2.272	2.273

Fig.2. represent the annual running cost savings and the annual reduction in CO<sub>2e</sub> emission of the PCM thermal battery compared to the HWT in different regions of the Europe. There is a significant running cost savings variation from £50 to £388 across Europe. Based on the current electricity price, the payback period of the thermal battery is less than 6 years in most of the countries. With the thermal battery, the annual GHG emission can be reduced by 50-700 kg/household across Europe. I.e., by replacing domestic HWT with the PCM thermal batteries, almost all the countries in Europe can reduce more than 200kg of CO<sub>2e</sub>/household with less than 11 years of payback period.

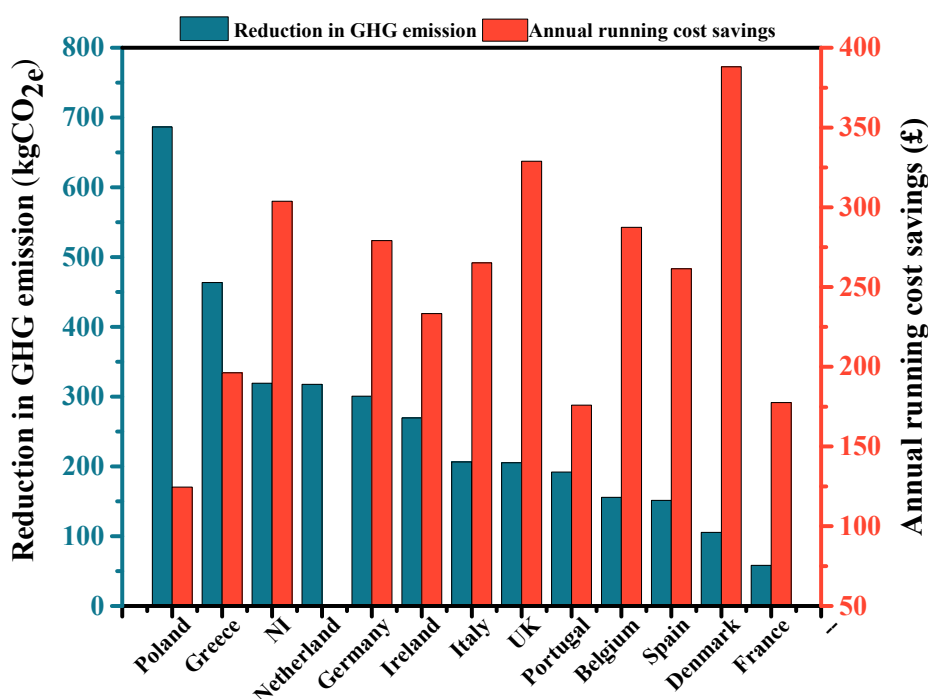


Fig. 16. Annual running cost savings and reduction in CO<sub>2e</sub> emission of PCM battery compared to the HWT operated with a high temperature ASHP in different regions of Europe.

#### 4. Conclusions

The research demonstrates that PCM thermal batteries have advantages such as annual running cost savings, reduced annual GHG emissions and installation space savings compared to HWT. The decarbonisation of heat through electrification can be successfully augmented with thermal stores, and their payback is within acceptable limits. The current global political and economic situation (Spring 2022) is seeing energy prices rise significantly and this, if sustained, will further enhance the economic advantages of thermal stores. Large thermal stores may be a simple technology which is readily understood, but the use of PCM battery stores can significantly reduce the space required, making them easier to retrofit into existing buildings.

#### Acknowledgements

This study is a part of the SPIRE-2 project and the authors acknowledge the financial support from the European Union's INTERREG VA Programme (Grant Number IVA5038). The authors are grateful to all the partner institutes and industries of the project. The research was also undertaken as part of the inpath-tes.eu thermal energy storage research network.

#### References

- Arteconi, A., Hewitt, N.J. and Polonara, F. (2012) 'State of the art of thermal storage for demand-side management', *Applied Energy*, 93, pp. 371–389. doi:10.1016/j.apenergy.2011.12.045.
- BSI Standards (2015) *BSI Standards Publication Guide to the design, installation, testing and maintenance of services supplying water for domestic use within buildings and their curtilages – Complementary guidance to BS EN 806, BS EN 806*.
- Cabeza, L.F., Mehling, H., Hiebler, S. and Ziegler, F. (2002) 'Heat transfer enhancement in water when used as PCM in thermal energy storage', *Applied Thermal Engineering*, 22(10), pp. 1141–1151. doi:10.1016/S1359-4311(02)00035-2.
- da Cunha, J.P. and Eames, P. (2018) 'Compact latent heat storage decarbonisation potential for domestic hot water and space heating applications in the UK', *Applied Thermal Engineering*, 134(February), pp. 396–406. doi:10.1016/j.applthermaleng.2018.01.120.
- Eurostat Energy data 2020 (2020) *Energy data 2020 edition*. Available at: <https://ec.europa.eu/eurostat/web/products-statistical-books/-/KS-HB-20-001?inheritRedirect=true&redirect=%2Fenergy%2Fpublications>.
- Griffiths, P.W., Huang, M.J. and Smyth, M. (2007) 'Improving the heat retention of integrated collector/storage solar water heaters using Phase Change Materials Slurries', *International Journal of Ambient Energy*, 28(2), pp. 89–98. doi:10.1080/01430750.2007.9675029.
- Nair, A.M., Wilson, C., Huang, M.J., Griffiths, P. and Hewitt, N. (2022) 'Phase change materials in building integrated space heating and domestic hot water applications: A review', 54(March).
- Seddegh, S., Wang, X., Henderson, A.D. and Xing, Z. (2015) 'Solar domestic hot water systems using latent heat energy storage medium: A review', *Renewable and Sustainable Energy Reviews*, 49, pp. 517–533. doi:10.1016/j.rser.2015.04.147.
- Shah, N.N., Wilson, C., Huang, M.J. and Hewitt, N.J. (2018) 'Analysis on field trial of high temperature heat pump integrated with thermal energy storage in domestic retrofit installation', *Applied Thermal Engineering*, 143(June), pp. 650–659. doi:10.1016/j.applthermaleng.2018.07.135.
- Tsemekidi Tzeiranaki, S., Bertoldi, P., Labanca, N., Castellazzi, L., Ribeiro Serrenho, T., Economidou, M. and Zangheri, P. (2018) *Energy consumption and energy efficiency trends in the EU-28 for the period 2000-2016*, Publications Office of the European Union. doi:10.2760/6684.



EUROTHERM2023-G190

## Visual tracking of the phase change front in a tube in tube phase change material heat exchanger

Maité Goderis<sup>1,2\*</sup>, Kenny Couvreur<sup>1,2</sup>, Wim Beyne<sup>1,2</sup>, Michel De Paepe<sup>1,2</sup>

<sup>1</sup> Department of Electromechanical, Systems and Metal Engineering – UGent, Ghent, Belgium,  
Maite.Goderis@UGent.be

<sup>2</sup> FlandersMake@UGent – Core lab EEDT-MP, Leuven, Belgium, www.flandersmake.be

### Abstract

Renewables will take up a larger part of our energy mix in the near future, because of the ambitious goals set by the European Union. Thermal energy storage systems using the latent heat of phase change materials, will play an important role. To design such systems, conventional heat exchanger design methods cannot be used, due to the transient operation of these storage systems. LTES systems can be characterized by the overall liquid fraction of the heat exchanger as a function of time. The overall liquid fraction can be determined by integrating the local liquid fraction as a function of time, which is linked to the position of the phase change front as a function of time. In this paper, solidification and melting experiments on a tube in tube heat exchanger are performed while the phase change front is visually tracked. The front moves linearly in time, especially during solidification. During melting experiments different melting regimes can be recognized, because of the influence of natural convection in the liquid material.

**Keywords:** Latent thermal energy storage, Phase change material, Tube in tube heat exchanger, Phase change front movement, Experimental

### 1. Introduction

The European Union (EU) has set ambitious goals for reducing greenhouse gas emissions and increasing the use of renewable energy sources [1]. Thermal energy storage plays a crucial role in this energy transition, as about 50% of our energy use is thermal [2]. There are three types of thermal energy storage: sensible, latent and thermochemical energy storage [3]. Latent thermal energy storage (LTES) systems have a large potential for various applications such as domestic hot water production, building heating and cooling, cold chain transport and grid-level power storage [3]. However, there are still challenges in sizing and designing LTES systems.

Conventional analytical models for heat exchangers such as the logarithmic mean temperature difference and the effectiveness number of transfer units method are not applicable to LTES systems due to their transient nature. Alternatives are Computational Fluid Dynamics calculations and experimental testing but these are time-consuming and expensive. Several methods have been proposed to provide an alternative, for example, the average effectiveness method by Tay et al. [4], [5], or prediction of the total phase change time by Raud et al. [6]. However, these methods only predict one aspect of the outlet state.

Recently, Beyne et al. [7] developed an expression for the one-dimensional movement of the phase change front in a cross-section of a simple planar geometry, based on the solution of the Stefan problem. Computation of the phase change front location over time allows deducing the phase change fraction as a function of time, which relates to the PCM internal energy per unit of heat transfer surface. This solution is integrated to determine the overall phase change fraction of the complete LTES heat exchanger, which had good agreement with the numerical validation model.

Based on the movement of the phase change front, one can thus predict the performance of an LTES heat exchanger. In the present study, the phase change front movement of a tube in tube PCM heat exchanger is visually tracked over time, both during solidification and melting.

## 2. Setup description

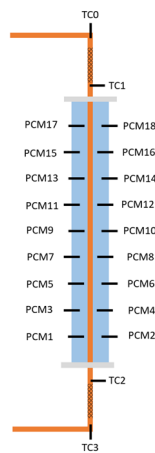
A 1m long, vertically placed tube in tube heat exchanger was tested. The inner tube contains the heat transfer fluid (HTF), and the shell region houses the phase change material (PCM). The direction of HTF flow can be reversed by two three-way valves, flowing from top to bottom during melting and bottom to top during solidification. The HTF flows through a 15mm diameter copper tube with a 2mm wall thickness, placed inside a 60mm diameter polycarbonate tube containing the PCM. A total of 1.772 kg of PCM (RT54HC, see Table 1) was used in the experiments, corresponding with a latent heat capacity of 420 kJ. The polycarbonate tube was insulated with 3 cm of Rockwool, with the ability to visually follow the phase change front at the outer diameter of the tube, by partly removing the insulation.

Table 13. RT54HC properties [8].

Melting / congealing area	53-54 / 54-53	°C
Specific heat capacity	2	kJ/kgK
Density solid (at 25°C) / liquid (at 60°C)	0.85 / 0.8	kg/l
Heat conductivity	0.2	W/mK



(a)



(b)

Table 14. Overview of discussed experiments.

<i>Exp</i>	$\dot{m}$	$\Delta T_0$	$\Delta T_{init}$	<i>Re</i>
S1	21.9	17.1	10.7	208.0
S2	20.9	9.4	5.7	229.3
S3	24.9	25.4	13.2	200.7
M1	24.2	26.6	11.6	444.2
M2	19.6	12.2	19.6	299.5

Figure 17. (a) picture of tube in tube heat exchanger and (b) schematic of temperature measurements.

Figure 1 displays the thermocouples used to monitor the temperatures of the PCM and HTF. 18 1mm K-type thermocouples with an uncertainty of  $\pm 0.15^\circ\text{C}$  are placed 10cm apart along the axial direction inside the PCM to measure its temperature. They are connected to a Keithley 2700 multiplexer and sampled at a rate of 2.5s. The HTF inlet and outlet temperatures are monitored with four 1.5mm K-type thermocouples, calibrated with a similar uncertainty of  $\pm 0.15^\circ\text{C}$  and sampled at a rate of 0.5s. Mixers are placed at the in- and outlets to ensure the bulk HTF temperature is measured. During melting, TC1 and TC3 are used as inlet and outlet, while TC2 and TC0 during solidification as the flow direction changes.

In Table 14, an overview is given of the solidification and melting experiments, denoted by the letters S and M respectively, which will be analyzed in the next sections. For each experiment, the HTF mass flow rate and two temperature differences are given.  $\Delta T_0$  quantifies the difference between the HTF inlet temperature and the phase change temperature ( $54^\circ\text{C}$ ).  $\Delta T_{init}$  is the difference between the phase change

temperature and the initial temperature of the PCM. To define the initial PCM temperature, the mean of the PCM temperature measurements is used. The last column of the table gives the Reynolds number linked to the HTF.

### 3. Results and discussion

The position of the phase change front is visually tracked as a function of time at the outside of the heat exchanger. The position of the front is normalized to the total height of the PCM  $L_{PCM}$  (Equation 1). As the tube is not completely filled with PCM, to account for the volume expansion during phase change,  $L_{PCM}$  (0.93m) is a bit smaller than  $L_{tube}$  (1m).

$$\xi = \frac{x}{L_{PCM}} \quad (1)$$

Figure 2 shows the phase change front measurements for the solidification and melting experiments. It can be seen that the front moves quite linearly as a function of time. The  $r^2$ -values of the considered data sets are respectively: 0.980, 0.984, 0.943, 0.982, 0.989. All values are close to one, meaning an accurate linear relation can be fitted through the points. In Figure 2 the dotted lines show this linear fitting.

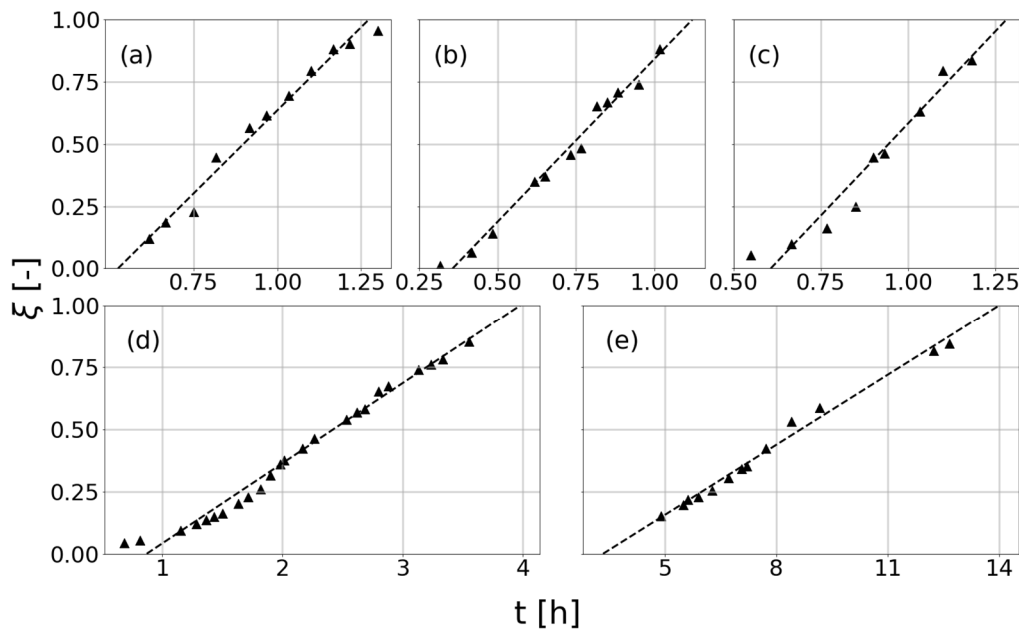


Figure 18. Visual phase change front measurements for experiments (a) S1, (b) S2, (c) S3, (d) M1, and (e) M2.

For the melting experiments (Figure 2 (d,e)) more of an S-shape can be recognized in the data set, compared to the data for the solidification experiments. The melting process can be subdivided into multiple melting regimes [9]. Initially during regime I, pure conduction is present as dominant heat transfer mode. When more PCM has melted, natural convection becomes more and more important and the melting rate will speed up (regime II). In the plots, this can be recognized by the locally steeper front-curve. In regime III convection is the dominant heat transfer mode and there is quasi-steady heat transfer. The front now moves linearly in time. Eventually, when almost all PCM is liquid, the process enters the shrinking solid regime (regime IV) and the heat transfer rate lowers again, resulting in a flattening of the front movement-curve.

During solidification (Figure 2 (a,b,c)), conduction is dominant through the complete experiment as convection plays less of a role [10]. When assuming pure conduction, the phase change front will move radially from the center to the outer edge of the tube. This explains the significantly shorter time the melt front needs to move over the whole length of the heat exchanger, compared to melting.

Important to note is that, during solidification, it is more difficult to determine the exact location of the phase change front, as was also experienced by Longeon et al. [11]. This implies larger errors in the visual measurements for solidification compared to melting.

#### 4. Conclusions

The movement of the phase change front is tracked during solidification and melting experiments in a tube in tube PCM heat exchanger. The front moves linearly over time, especially during solidification. During melting experiments, more of an S-shape is seen when the front location is plotted as a function of time, due to the different melting regimes throughout an experiment.

Additional experiments are required to further investigate and quantify this linear behaviour in the movement of the phase change front.

#### Acknowledgements

The authors would like to express their gratitude and appreciation to the technical staff of Ghent University, especially Frederik Martens, Bart Van Daele, and Thomas Blancke for building and maintaining the setup used to obtain the discussed experimental data.

#### References

- [1] “European Commission, official website.” [https://ec.europa.eu/info/index\\_en](https://ec.europa.eu/info/index_en) (accessed Sep. 16, 2022).
- [2] “Heating - Fuels & Technologies - IEA.” <https://www.iea.org/fuels-and-technologies/heating> (accessed Feb. 24, 2023).
- [3] A. Castell and C. Solé, “Design of latent heat storage systems using phase change materials (PCMs),” *Advances in Thermal Energy Storage Systems: Methods and Applications*, pp. 285–305, Jan. 2015, doi: 10.1533/9781782420965.2.285.
- [4] N. H. S. Tay, M. Belusko, and F. Bruno, “An effectiveness-NTU technique for characterising tube-in-tank phase change thermal energy storage systems,” *Appl Energy*, vol. 91, no. 1, pp. 309–319, Mar. 2012, doi: 10.1016/J.APENERGY.2011.09.039.
- [5] N. H. S. Tay, F. Bruno, and M. Belusko, “Experimental validation of a CFD and an  $\epsilon$ -NTU model for a large tube-in-tank PCM system,” *Int J Heat Mass Transf*, vol. 55, no. 21–22, pp. 5931–5940, Oct. 2012, doi: 10.1016/J.IJHEATMASSTRANSFER.2012.06.004.
- [6] R. Raud, M. E. Cholette, S. Riahi, F. Bruno, and W. Saman, “Design optimization method for tube and fin latent heat thermal energy storage systems,” *Energy*, vol. 134, pp. 585–594, 2017, doi: 10.1016/j.energy.2017.06.013.
- [7] W. Beyne, R. Tassenoy, and M. de Paepe, “An approximate analytical solution for the movement of the phase change front in latent thermal energy storage heat exchangers,” *J Energy Storage*, vol. 57, p. 106132, Jan. 2023, doi: 10.1016/j.est.2022.106132.
- [8] “Rubitherm GmbH.” <https://www.rubitherm.eu/en/productcategory/organische-pcm-rt> (accessed Sep. 16, 2022).
- [9] P. Jany and A. Bejan, “Scaling theory of melting with natural convection in an enclosure,” 1988.
- [10] M. Medrano, M. O. Yilmaz, M. Nogués, I. Martorell, J. Roca, and L. F. Cabeza, “Experimental evaluation of commercial heat exchangers for use as PCM thermal storage systems,” *Appl Energy*, vol. 86, no. 10, pp. 2047–2055, 2009, doi: 10.1016/j.apenergy.2009.01.014.
- [11] M. Longeon, A. Soupart, J. F. Fourmigué, A. Bruch, and P. Marty, “Experimental and numerical study of annular PCM storage in the presence of natural convection,” *Appl Energy*, vol. 112, pp. 175–184, 2013, doi: 10.1016/J.APENERGY.2013.06.007.

EUROTHERM2023-1191

## Adaptive envelopes using PCMs: numerical analysis of the effect of external environment and internal conditions in the thermal inertia

Matias Alvarez-Rodriguez<sup>1</sup>, Mar Alonso-Martinez<sup>2</sup>, Inés Suárez-Ramón<sup>3</sup>

<sup>1</sup> University of Oviedo, GICONSIME Research Group, Gijón, Asturias, Spain, Phone: 985 18 23 53, e-mail: alvarezrmatias@uniovi.es

<sup>2</sup> University of Oviedo, GICONSIME Research Group, Gijón, Asturias, Spain, Phone: 985 18 23 53, e-mail: alonsomar@uniovi.es

<sup>3</sup> University of Oviedo, GICONSIME Research Group, Gijón, Asturias, Spain, Phone: 985 18 23 65, e-mail: ines@uniovi.es

### Abstract

Incorporation of PCMs in envelopes confers buildings the ability of responding to variations of the exterior or interior conditions. The dynamic modification of properties of envelopes makes them adaptive solutions. The selection of specific PCMs is crucial for an adequate adaptive performance. In this work, it was assessed the effect of the position of the PCM and the interior conditions on the thermal inertia of an adaptive envelope. A numerical model was developed using the finite difference method. It was found that, for an adaptive envelope design, where the thickness of the PCM layer reduces the insulation layer, thermal inertia is increased only if a suitable PCM is selected and placed in the right position. Considering the climate conditions in the PCM selection and location may reduce thermal inertia about 80%.

**Keywords:** Phase change materials (PCMs), thermal inertia, finite difference method, adaptive envelope, energy efficiency.

### 1. Introduction

Phase change materials (PCMs) accumulate or release latent energy when they undergo a phase change process. Adaptive envelopes incorporating PCMs take advantage of the accumulation of thermal energy: when the phase change happens, large amounts of thermal energy are exchanged between the PCM and its surroundings, modifying the thermal response of the envelope. Since the phase change process is almost isothermal, building indoor temperature is stabilized and heating and cooling energy consumption is reduced while thermal comfort is enhanced [1]. Furthermore, PCMs exhibit greater energy storage density than materials used for sensible heat storage (conventional high thermal mass materials). As such, adaptive envelopes with PCMs require much less volume and weight for increasing thermal inertia [2]. However, special care should be taken when choosing the specific PCM. Properties of PCMs are of course relevant (mainly their phase change temperature), but *in situ* conditions (climate, envelope composition, PCM incorporation method and thickness) determine the efficiency of the PCM in the envelope [3]. Interior temperature conditions will also affect. That is why in this work the effect of the PCM position and interior thermal conditions on the thermal behavior of an adaptive envelope with PCM are studied.

### 2. Materials and methods

A traditional standard building envelope system is studied without PCM (as a reference) and with a layer of PCM in two different positions, to assess the relevance of the position of the PCM in its behavior. Composition and geometry of each studied solution are shown in Figure 19. Note that the total thickness of the envelopes is the same, as the insulation thickness is reduced in order to allow the PCM layer to fit in.

The selected PCM for the application is Q23 BioPCM, by Phase Change Solutions. This is a macroencapsulated PCM in the shape of blankets, whose phase change temperature is around 23°C. Each blanket consists of several individual pouches containing the PCM [4]. The studied PCM changes from solid into gel phase.

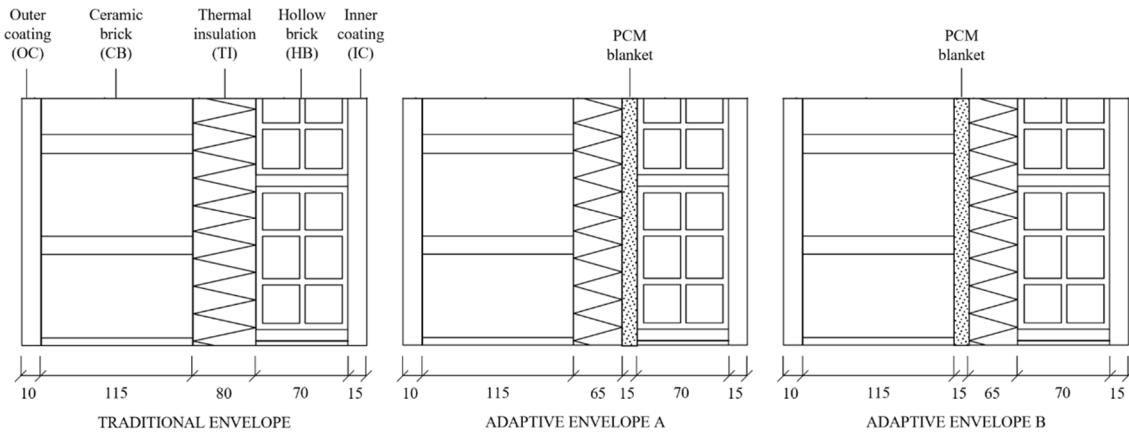


Figure 19. Geometry of the three studied envelopes, with thickness of each layer in mm

Finite difference method was used for developing a numerical model of the transient heat transfer across studied envelopes. This method consists of dividing the simulation domain in discrete elements or cells and solving the heat diffusion equation in each of them. Top and bottom surfaces were modelled as adiabatic. A convection boundary condition was established in the surface of the inner coating and a heat flux boundary condition was imposed in the surface of the outer coating for modelling the climate conditions. This heat flux combines convection with surrounding air, global solar irradiation and radiation losses into the sky. Climate conditions of Gijón (coastal city in northwestern Spanish region of Asturias) for a typical meteorological day of February were used. February was chosen as it is the coldest time of the year for the studied location. As per interior conditions, the effect of varying the temperature between 21°C and 26°C was assessed.

Phase change of the PCM was modelled through the effective heat capacity method, using a symmetric Gaussian function for the effective specific heat as a function of temperature  $C_{p,eff}(T)$  [5]. Based on the technical specifications,  $C_{p,eff}(T)$  is expressed according to Eq. (1) for temperature of the PCM in [°C]. Thermophysical properties of all other materials, as well as density ( $\rho$ ) and conductivity ( $k$ ) of both phases of the PCM are constant and shown in Table 15.

$$C_{p,eff}(T) = 2000 + 85484.04 \cdot \exp\left(\frac{(T-23)^2}{-1.6}\right) \quad (1)$$

Table 15. Thermophysical properties of the building materials and PCM

	OC	CB	TI	HB	IC	PCM
$\rho$ [kg/m <sup>3</sup> ]	1900	2170	55	930	1300	820
$C_p$ [J/kg·K]	1000	1000	1200	1000	1000	Eq. (1)
$k$ [W/m·K]	1.3	0.96	0.034	0.44	0.57	0.1

As top and bottom surfaces were set as adiabatic and the PCM oscillates between solid and gel phases, heat transfer only occurs in the horizontal direction and the problem is one-dimensional.

Cell size was set to 5 mm and timestep size to 600 s after performing a grid size and timestep size independence study. A fully-implicit scheme was used for the temporal discretization and central difference scheme was set for spatial discretization. For each envelope, five consecutive days were simulated to ensure that thermal stabilization was reached. Only the results of the last simulated day were used for comparison.

### 3. Results and discussion

This section assesses the performance of the two studied adaptive envelopes. Figure 20 presents the temperature of the inner surface of the envelope,  $T_{w,i}$ , throughout a whole day, for the different studied values of interior temperature,  $T_{int}$ . As it is shown, traditional envelopes do not change their performance for any exterior or interior conditions. However, adaptive designs do modify their thermal response to varying exterior and interior conditions. Furthermore, the position of the PCM greatly affects the outcome. Regardless of the interior temperature, adaptive envelope B does not contribute to thermal inertia augmentation of the envelope. In fact, it worsens its behavior: inner surface temperature in adaptive envelope B is lower than in the traditional one, and the temperature oscillation remains the same. However, for adaptive envelope A, thermal behavior depends on the interior temperature. For interior temperatures lower than 23°C, a slight dampening of the temperature fluctuation occurs. For interior temperatures of 23°C or greater, thermal inertia is clearly increased, as the temperature on the inner surface highly reduces its oscillation and it remains quasi-constant.

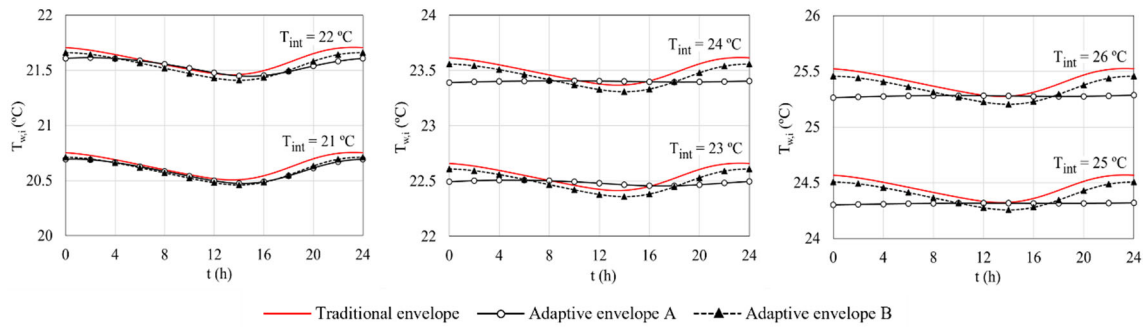


Figure 20. Temperature on the inner surface of the studied envelopes depending on the interior temperature

The effect of the position of the PCM layer and of the interior conditions on the reduction of the thermal oscillation is shown in Figure 21 (a). It is observed that, for adaptive envelope A, thermal oscillation is reduced more than 80% for interior temperatures higher than 22°C. Thermal oscillation and its reduction have been determined according to Eq. (2).

$$Red\ TO = \frac{TO_{trad} - TO_{adaptive}}{TO_{trad}} \cdot 100 = \frac{(T_{w,i\ max} - T_{w,i\ min})_{trad} - (T_{w,i\ max} - T_{w,i\ min})_{adaptive}}{(T_{w,i\ max} - T_{w,i\ min})_{trad}} \cdot 100 \quad (2)$$

To explain this behavior, the average effective heat capacity of the PCM layer has been determined. Figure 21 (b) shows the quotient of the average effective heat capacity and its maximum value, for all the cases. This represents how much of the latent energy of the PCM is exchanged. The higher the ratio, the more latent energy is accumulated and released, meaning the thermal inertia of the adaptive envelope is increased. Thus, it is observed that this ratio is far greater in adaptive envelope A than in adaptive envelope B, which is in accordance with results of reduction of the thermal inertia. On top of that, in adaptive envelope B, it takes a constant value close to zero, indicating that none or negligible latent energy is exchanged. Contrarily, in adaptive envelope A, this quotient reaches values as high as 95% for interior temperature of 25°C.

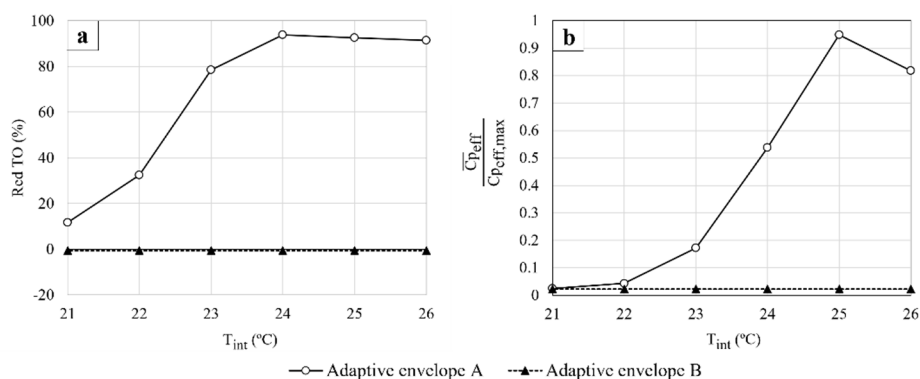


Figure 21. Reduction of the thermal oscillation on the inner surface of adaptive envelopes (a) and average effective heat capacity of the PCM over its maximum capacity (b), depending on the interior temperature

## 4. Conclusions

It has been demonstrated that to reduce thermal oscillation in the inner surface of the envelope, and increase thermal inertia, latent energy must be exchanged. Thermal behavior of the envelope worsens if the PCM layer does not reach the phase change temperature, since its thermal conductivity is higher than that of the insulation that it partially replaces.

As a result, this work highlights the necessity of developing a methodology to identify the appropriate PCM (in terms of phase change temperature) for specific exterior conditions which mainly depend on the climate. Besides, the methodology must take into account to a great extent interior environment, as well as the typology of envelope and the position of the PCM in the envelope, to ensure that the latent heat of the phase change is harnessed.

## Acknowledgements

This work was partially financed by Fundación para el Fomento en Asturias de la Investigación Científica Aplicada y la Tecnología (FICYT) through the project SV-PA-21-AYUD/2021/51328, by Ministerio de Ciencia e Innovación through the project PID2021-128056OA-I00 and by the Ministerio de Universidades through the FPU program (FPU21/05062).

## References

- [1] K. Faraj, M. Khaled, J. Faraj, F. Hachem, and C. Castelain, "A review on phase change materials for thermal energy storage in buildings: Heating and hybrid applications," *J Energy Storage*, vol. 33, p. 101913, Jan. 2021, doi: 10.1016/J.EST.2020.101913.
- [2] R. Andrade Santos, I. Flores-Colen, N. Simões, and J. D. Silvestre, "Auto-responsive technologies for thermal renovation of opaque facades," *Energy Build*, vol. 217, p. 109968, 2020, doi: 10.1016/j.enbuild.2020.109968.
- [3] P. Arumugam, V. Ramalingam, and P. Vellaichamy, "Effective PCM, insulation, natural and/or night ventilation techniques to enhance the thermal performance of buildings located in various climates – A review," *Energy Build*, vol. 258, p. 111840, Mar. 2022, doi: 10.1016/J.ENBUILD.2022.111840.
- [4] Phase Change Solutions, "ENRG Blanket," Jul. 18, 2016. <https://phasechange.com/enrgblanket/> (accessed Feb. 15, 2023).
- [5] M. Zálešák, P. Charvát, and L. Klimeš, "Identification of the effective heat capacity–temperature relationship and the phase change hysteresis in PCMs by means of an inverse heat transfer problem solved with metaheuristic methods," *Appl Therm Eng*, vol. 197, p. 117392, Oct. 2021, doi: 10.1016/J.APPLTHERMALENG.2021.117392.



EUROTHERM2023-R192

## Experimental investigation of phase change material integrated in a gasketed-plate heat exchanger

Jorge Salgado-Beceiro, Alexis Sevault

SINTEF Energy Research, Postboks 4761 Torgarden, 7465 Trondheim, Norway, e-mail:  
jorge.beceiro@sintef.no, alexis.sevault@sintef.no

### Abstract

Latent heat storage (LHS), based on phase change materials (PCM), plays an increasingly role in decarbonized energy processes by providing flexibility. The potential of the technology is well demonstrated and the integration in industry is in full development. One main challenge with PCMs is their limited thermal conductivity, which can be compensated by the selection and design of the adequate heat exchanger configuration where the PCM is implemented. In this work, we present the experimental results from a symmetric-gasketed-plate heat exchanger tested for thermal energy storage applications using a commercial PCM. First, a 10-plates configuration was tested, followed by a second test with 100 plates. The results show that the most profitable use of the latent heat provided by the PCM could be made by increasing the number of plates and reconsidering the plate design.

**Keywords:** Thermal Energy Storage; Latent Heat Storage; Phase Change Materials; Gasketed Plate; Heat Exchanger

### 1. Introduction

In the path to decarbonization of energy use/supply processes, thermal energy storage (TES) enables a better time-match between supply and demand with the potential of representing a meaningful impact reducing global greenhouse gas emissions.<sup>1,2</sup> TES is in full development, and even though there are some commercial options, research focuses on short- to long-term storage alternatives for a wide range of operational temperatures with the maximum energy storage capacity and compactness at the lowest price.<sup>3-5</sup> For TES becoming the consolidated enabler of the scale-back from fossil fuels and scale-up of renewable sources of energy, specific solutions are necessary for each activity, adapting the storage capacity, time of charge/discharge, etc. to each application.

For cases with fluctuating heat sources (such as excess heat or renewable sources), TES can contribute to a more constant heat production by thermal buffering (charge when heat is available and discharge when the demand is higher than the availability).<sup>4</sup> TES based on phase change materials (PCM) is a demonstrated TES technology in this respect.<sup>6,7</sup> However, implementation has some associated challenges, including achieving high heat transfer rates.<sup>8</sup> To ensure an effective heat transfer, the design and configuration of a heat exchanger that can fit the properties of the PCM in use (operational temperatures, thermal conductivity, mechanical properties, etc.) is critical.<sup>9</sup> There are many examples of heat exchanger configurations tested with PCM: cylindrical<sup>10</sup>, rectangular<sup>11</sup> or plates<sup>12</sup>. For processes where a quick heat supply is needed in case of a sudden variation in the inlet temperature, the heat exchanger must allow a fast charge/discharge of the PCM, and plate-type heat exchangers have shown the best results in these cases.<sup>13</sup> Pillow-plate heat exchangers, which are commonly used as condensers and reboilers/evaporators in distillation columns for process industry, have been studied recently as medium for heat transfer using PCM, showing great performance.<sup>14,15</sup> There is another type of plate heat exchangers, gasketed plates (widely used in petrochemical, food, and textile industries), which offer smaller configurations than the pillow-plates type.<sup>16</sup> Even though the gasketed-plate configuration has been considered as a promising alternative for PCM use in a simulation study<sup>17</sup>, there are only few experimental studies on this heat-exchanger type using PCM.<sup>18,19</sup>

In this work, a gasketed-plate heat exchanger was tested using PCM to study the potential of this configuration with this TES technology.

## 2. Materials and methods

The selected PCM for this work is the CrodaTherm™ 9.5, whose properties are summarized in Table 1.<sup>20</sup> This PCM is a 100% bio-based material with long-term stability and high latent heat.

Table 1. Properties of the PCM CrodaTherm™ 9.5.<sup>20</sup>

PCM melting/solidification temperature [°C]	9.7 / 6
PCM latent heat of fusion/crystallisation [kJ/kg]	186
PCM density (liquid) [kg/m <sup>3</sup> ]	858 (liquid), 963 (solid)
PCM thermal conductivity [W/(m.K)]	0.15 (liquid), 0.24 (solid)
PCM specific heat capacity [kJ/(kg.K)]	2.1 (liquid), 2.2 (solid)
PCM degradation temperature [°C]	195
Total heat capacity of fusion/crystallization (latent + sensible heat) [kJ/kg]	220 / 216

The heat exchanger configuration (see Figure 22) consists of a series of an even number of symmetric corrugated stainless-steel plates assembled between a frame made of two pressure plates (blue plates in figure). The corrugated plates have a large contact surface area to assure the highest possible heat transfer rates. Located between the plates, the gaskets seal the surrounding space between each channel. There are two different channels that are intercalated with each other along the heat exchanger. The first channel has water flow, which acts as heat transfer fluid (HTF) with a controlled inlet temperature and flow rate. The second channel is sealed and filled with PCM in liquid state at room temperature.

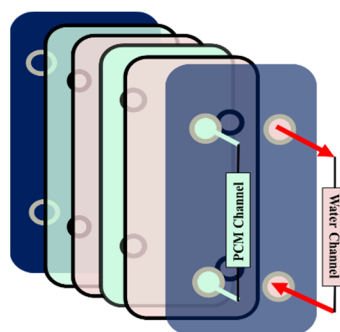


Figure 22. Gasketed-plate configuration with PCM and water independent channels.

To analyse the TES performance of the system, 4 thermocouples were set up, 2 in the water channel (inlet and outlet) and 2 in the PCM channel. The tests consisted in a cooling (discharge) and heating (charge) cycles between 22 °C and 3.5 °C. Two tests were carried out with 10 and 100 plates. The tests were run without thermal insulation.

## 3. Results and discussion

The results of the temperature profile of the water input and output for the 10-plates configuration are shown in Figure 23 (left). The temperature difference between the input and output in most of the period with low-temperature profile reflects the heat loss of the system to the surrounding.

The energy output of the system ( $Q$ ), shown in Figure 23 (right) was calculated by:  $Q = m \cdot C_p \cdot \Delta T$ . Here,  $m$  is the mass flow rate of water,  $C_p$  is the heat capacity of water and  $\Delta T$  is the temperature difference between the water input and output.

Looking at the solidification and melting, the full discharge and charge occur in an interval of approximately 2 hours each. This is a fast process comparing to other latent heat storage units with other plate heat exchangers, where the interval can be up to 10 hours.<sup>21</sup> By integrating the heat output, the energy stored and released by the system was calculated. The maximum heat stored is 0.250 kWh. Considering the heat loss (~8%), the net heat stored is 0.230 kWh. Of this value, only 0.018 kWh correspond to the PCM, given that most of the thermal mass of the system is taken by the two large pressure plates. Though far from constant, the average heat transfer rate is 0.5 kW during the discharge and charge processes (which take around 2 hours according to Figure 2) and is a magnitude order higher

than the predicted by Gürel<sup>17</sup> for a similar gasketed-plate configuration. By dividing the heat transfer by the maximum heat storage capacity, the system has 2.17 kW/kWh. To investigate a higher relative importance of the PCM in the system, the next test was carried out using 100 plates. The results are shown in Table 2.

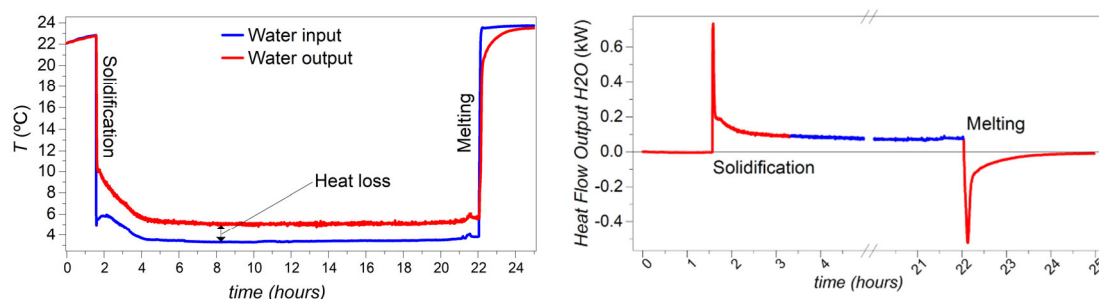


Figure 23. Temperature of water input and output (left) and heat flow output (right) as function of time for the 10-plates configuration. The blue colour (right) represents the region where the heat loss can be seen.

For the 100-plate test, the maximum heat stored by the system increases up to 0.460 kWh, with 0.155 kWh provided by the PCM (10 times more than in the 10-plate configuration). The heat loss remains the same (8%). The heat transfer rate is similar, but the charge/discharge times are considerable higher. The heat transfer divided by the maximum heat stored is 0.98 kW/kWh for the 100-plates configuration, approximately half of the value for the 10-plates configuration, which means that the system was underperforming. This is certainly due to the lack of thermal insulation and the difficulties in holding the HTF inlet temperature sufficiently low. Thus, the temperature difference between inlet and PCM was never too far apart, limiting the full performance characterization of these experiments. Given a lower and more stable inlet temperature, a relatively higher volume of PCM compared to the volume of circulating water in the heat exchanger could be of interest for further experiments.

Table 2. Properties of the 10-plates and 100-plate configurations

	<b>10 Plates</b>	<b>100 Plates</b>
<b>PCM mass</b>	340 g	3 kg
<b>Water flow</b>	10 mL/s	24 mL/s
<b>Charge/Discharge time</b>	2 hours / 2 hours	10 hours / 8 hours
<b>Heat loss</b>	8%	8%
<b>Maximum heat stored (after loss)</b>	0.230 kWh	0.460 kWh
<b>Heat transfer rate during charge and discharge (average)</b>	0.50 kW	0.45 kW
<b>Heat stored by PCM (sensible and latent)</b>	0.018 kWh	0.155 kWh

## 4. Conclusions

A gasketed-plated heat exchanger with 10- and 100-plate configurations was studied using PCM for TES applications. The results show that by using 2 symmetric channels filled with PCM and water as heat transfer fluid in the stainless-steel heat exchanger, most of the heat storage capacity is given by the stainless-steel frame and plates, while the PCM contributes up to only ~33% (in the case of the 100-plate configuration). It was observed that by having more PCM when increasing the number of plates, the TES capacity is improved, and so is the percentage of energy stored by the PCM (which means more compactness). However, the observed charge/discharge intervals were larger, which could be given by having the same volume of PCM and HTF and not sufficient control of the  $\Delta T$  with the HTF temperature controller. These results lead to think that a higher  $\Delta T$  (10 °C or more) and a higher volume of PCM, and comparatively lower volume of HTF, could lead to a more efficient, quicker, and more compact system. Thus, the next step on this research will be to study asymmetric plates with more volume in the PCM channel than on the heat transfer fluid side.

## Acknowledgements

This study was carried out through the research project KSP PCM-STORE (308847) supported by the Research Council of Norway and industry partners.

## References

1. Cabeza, L. F., Martorell, I., Miró, L., Fernández, A. I., & Barreneche, C. (2015). Introduction to thermal energy storage (TES) systems. In *Advances in thermal energy storage systems* (pp. 1-28). Woodhead Publishing.
2. Henry, A., Prasher, R., & Majumdar, A. (2020). Five thermal energy grand challenges for decarbonization. *Nature Energy*, 5(9), 635-637.
3. De Gracia, A., & Cabeza, L. F. (2015). Phase change materials and thermal energy storage for buildings. *Energy and Buildings*, 103, 414-419.
4. Kauko, H., Sevault, A., Beck, A., Drexler-Schmid, G. et. al. (2022). [Industrial Thermal Energy Storage Supporting the transition to decarbonise industry](#) White paper.
5. Cabeza, L. F., de Gracia, A., Zsembinszki, G., & Borri, E. (2021). Perspectives on thermal energy storage research. *Energy*, 231, 120943.
6. Selvnes, H., Allouche, Y., Manescu, R. I., & Hafner, A. (2021). Review on cold thermal energy storage applied to refrigeration systems using phase change materials. *Thermal Science and Engineering Progress*, 22, 100807.
7. da Cunha, S. R. L., & de Aguiar, J. L. B. (2020). Phase change materials and energy efficiency of buildings: A review of knowledge. *Journal of Energy Storage*, 27, 101083.
8. Zayed, M. E., Zhao, J., Li, W., Elsheikh, A. H., Elbanna, A. M., Jing, L., & Geweda, A. E. (2020). Recent progress in phase change materials storage containers: Geometries, design considerations and heat transfer improvement methods. *Journal of Energy Storage*, 30, 101341.
9. Kalapala, L., & Devanuri, J. K. (2018). Influence of operational and design parameters on the performance of a PCM based heat exchanger for thermal energy storage—A review. *Journal of Energy Storage*, 20, 497-519.
10. Gasia, J., Tay, N. S., Belusko, M., Cabeza, L. F., & Bruno, F. (2017). Experimental investigation of the effect of dynamic melting in a cylindrical shell-and-tube heat exchanger using water as PCM. *Applied energy*, 185, 136-145.
11. Pakalka, S., Valančius, K., & Streckienė, G. (2020). Experimental comparison of the operation of PCM-based copper heat exchangers with different configurations. *Applied Thermal Engineering*, 172, 115138.
12. Hu, Y., Heiselberg, P. K., Johra, H., & Guo, R. (2020). Experimental and numerical study of a PCM solar air heat exchanger and its ventilation preheating effectiveness. *Renewable Energy*, 145, 106-115.
13. Gürel, B. (2020). A numerical investigation of the melting heat transfer characteristics of phase change materials in different plate heat exchanger (latent heat thermal energy storage) systems. *International Journal of Heat and Mass Transfer*, 148, 119117.
14. Joybari, M. M., Selvnes, H., Sevault, A., & Hafner, A. (2022). Potentials and challenges for pillow-plate heat exchangers: State-of-the-art review. *Applied Thermal Engineering*, 118739.
15. Selvnes, H., Allouche, Y., Hafner, A., Schlemminger, C., & Tolstorebrov, I. (2022). Cold thermal energy storage for industrial CO<sub>2</sub> refrigeration systems using phase change material: An experimental study. *Applied Thermal Engineering*, 212, 118543.
16. Martins, G. S. M., Santiago, R. S., Beckedorff, L. E., Possamai, T. S., Oba, R., Oliveira, J. L. G., ... & Paiva, K. V. (2022). Structural analysis of gasketed plate heat exchangers. *International Journal of Pressure Vessels and Piping*, 197, 104634.
17. Gürel, B. (2020). Thermal performance evaluation for solidification process of latent heat thermal energy storage in a corrugated plate heat exchanger. *Applied Thermal Engineering*, 174, 115312.
18. Medrano, M., Yilmaz, M. O., Nogués, M., Martorell, I., Roca, J., & Cabeza, L. F. (2009). Experimental evaluation of commercial heat exchangers for use as PCM thermal storage systems. *Applied energy*, 86(10), 2047-2055.
19. Elsharafi, M., Elmozughi, A., Vidal, K., Thomas, R., Almutairi, S., Senevirathne, T., & Lambright, J. (2020, November). Energy Recovery Unit Using Phase Change Materials. In *ASME International Mechanical Engineering Congress and Exposition* (Vol. 84560, p. V008T08A065). American Society of Mechanical Engineers.
20. [Phase Change Material 9.5 | Energy Technologies \(crodaenergytechnologies.com\)](#) 17.02.2023.
21. Sevault, A., Böhmer, F., Næss, E., & Wang, L. (2019, October). Latent heat storage for centralized heating system in a ZEB living laboratory: integration and design. In *IOP Conference Series: Earth and Environmental Science* (Vol. 352, No. 1, p. 012042). IOP Publishing.

EUROTHERM2023-1193

## Bio-Based Latent Thermal Energy Storage for Air Conditioning

Giulia Righetti<sup>1</sup>, Claudio Zilio<sup>1</sup>, Dario Guarda<sup>1</sup>, Domenico Feo<sup>2</sup>, Marco Auerbach<sup>3</sup>, Martin Butters<sup>3</sup>, Simone Mancin<sup>1</sup>

<sup>1</sup>Department of Management and Engineering  
Vicenza, Italy - University of Padova

e-mail: giulia.righetti@unipd.it, claudio.zilio@unipd.it, dario.guarda@phd.unipd.it, simone.mancin@unipd.it

<sup>2</sup>Sunservice srl, Altivole, Italia  
email: domenico.feo@thermalink.it

<sup>3</sup>Croda International Plc, Goole, East Yorkshire, UK  
email: Marco.Auerbach@croda.com, Martin.Butters@croda.com,

### Abstract

Future smart and efficient energy management systems for space cooling and heating in building applications call for novel solutions to store heat in order to decouple the energy demand and the availability of renewable energy sources. Latent thermal energy storages represent one of the most promising solutions; however, their cost-effective implementation in terms of energy and cost savings, payback time needs to be verified case-by-case. This work is meant to present the experimental behavior of a novel 18 kWh latent thermal energy storage which uses the roll-bond technology to efficiently store and release cold energy exploiting the solid/liquid phase change process of 300 kg of a bio-based phase change material having a melting temperature of 9 °C. The effects of inlet water temperature and flow rate are studied to understand how the performance varies and to identify possible control strategies.

**Keywords:** PCM, Latent Thermal Energy Storage, Air Conditioning, Roll-Bond Technology, Modelling

### 1. Introduction

According to IEA report [1], about 37 Gton CO<sub>2</sub> were estimated having been released in the atmosphere during 2019. A similar value was obtained for 2020. It is absolutely essential to reduce this figure, calling the researchers to focus on finding and developing innovative solutions. A huge amount of the energy is used for space heating and cooling and, in the last decades, energy management and indoor thermal comfort have become challenging issues. Gagliano et al. [2] reported that in the European Countries the total cooled floor area is destined to grow up to 2 billion m<sup>2</sup> in 2020 (it was 1000 million m<sup>2</sup> in 2012). Therefore, more than 100 TWh year<sup>-1</sup> will be required for building cooling only.

In a recent critical review work, Cabeza and Chafer [3] reported the passive and active strategies needed to achieve zero energy buildings. Among other solutions, the presence of energy storages has been recommended. Thermal Energy Storage (TES) can be considered an enabling technology to promote a great, more efficient adoption of renewable sources which are one of the solutions to reduce the GHG emissions. The TES technologies can be classified into four types: sensible, latent, thermochemical, and mechanical-thermal. Compared to other types of TES, Latent Thermal Energy Storages (LTESs) equipped with Phase Change Materials (PCMs) exhibit many advantages. In fact, as described by Colla et al. [4], by virtue of the latent heat of fusion, the LTESs energy storage density capability is remarkably higher as compared to sensible-only TES systems. Considering the same temperature range, when using LTESs, from 5 to 14 times the energy of a sensible thermal energy storage system can be stored in the same volume; in addition, the phase change process can be considered almost isothermal [4]. These characteristics permit to maximize both the storing capabilities and the heat transfer process. It is also important to note that the use of PCMs allows for the decoupling between energy demand and

availability; this point is of fundamental interest for the effective integration of renewable sources, that are intermittent by definition.

One of the most interesting applications of this technology is in the air conditioning (i.e. space cooling) field, in which the possibility of a direct integration of the LTES with an air/water or water/water heat pump powered by photovoltaics (PVs) can lead to huge energy savings by matching the energy source availability with the cooling demand, which are commonly mismatched. This is particularly true especially in hot and humid climates. In general, there is the lack of understanding if the data collected in small scale prototypes can be used to anticipate the performance of the systems at larger scale; moreover, it is also not clear so far if the models developed and validated on the basis of these results are representative to simulate the behavior of LTES at system or building level.

Only few papers deal with large amount of PCM. Among those, Atalay and Cankurtaran [6] experimentally tested an industrial solar dryer for strawberries coupled to a latent energy storage made by 300 kg of paraffin wax which allowed the drying process to continue during the absence of sunshine. Wu et al. [7] studied a 96 kWh storage tank made of 2442 encapsulated ice/water nodules to be coupled with a heat pump while Liu et al. [8] tested the thermal behavior of a refrigerated truck when a LTES was added to maintain the refrigerated truck at a temperature of  $-18\text{ }^{\circ}\text{C}$ . In this application, 136.8 kg PCM having a melting temperature of  $-26.7\text{ }^{\circ}\text{C}$  were subdivided in 19 parallel flat slabs to store cold energy generated by a refrigeration unit located off the vehicle when stationary.

This work aims at presenting a novel 18 kWh LTES especially designed for space cooling, which uses the roll-bond technology to efficiently store and release the energy exploiting the solid/liquid phase change process of a commercially available bio-based PCM, CRODATHERM9.5. This PCM, it is a water insoluble organic PCM derived from plant-based feedstocks and has the form of a crystalline wax or oily liquid (depending on temperature). This material is completely bio-compatible and biodegradable. Besides, the roll-bond heat exchanger is a simple, almost inexpensive cold (hot) plate, which can be easily used in any type of LTES due to its versatility. It can be produced in different sizes and it allows for a direct scalability of both capacity and heat transfer capabilities of the LTESs. The LTES is fully experimentally characterized as a function of the main operating conditions, trying to identify the optimum set of parameters which maximizes the performance of the LTES.

## 2. Experimental setup

A specific setup was built to run the experimental characterization of the LTES under study. Figure 1 shows a schematic of the experimental apparatus. It consists of an off-the-shelf storage tank with internal dimensions of 1400 mm x 710 mm x 650 mm. The wall contains 50 mm of insulation to limit heat losses to the surroundings, covered with an aluminum sheet.

The tank is filled with 300 kg of a commercially available bio-based PCM, named CRODATHERM9.5 supplied by CRODA. Its main thermophysical properties are listed in Table 1. The phase change temperature peak is at around  $9\text{ }^{\circ}\text{C}$  and the latent heat is 220 kJ/kg.

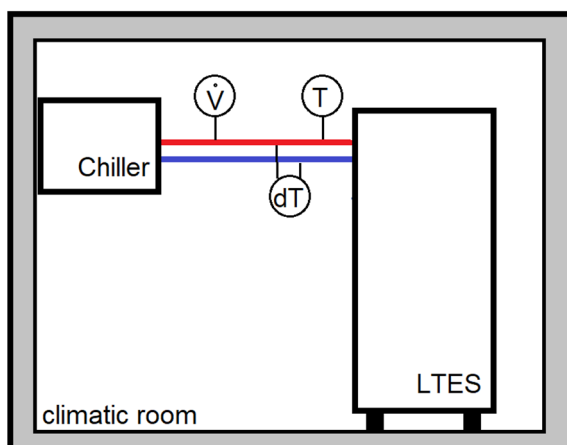


Figure 1. Experimental set up scheme.

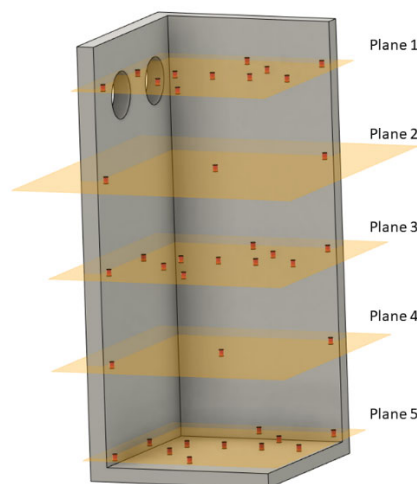


Figure 2. Thermocouples positioning inside the tank

Inside the tank there are 16 roll-bond heat exchangers made of aluminum having dimensions 1170 mm x 570 mm x 1.5 mm. The heat exchanger pitch is 31 mm and it is filled by PCM. The roll-bonds allow the passage of hot and cold water and, thanks to the presence of their continuous aluminum plate, they promote the heat transfer within the PCM that has a relatively low thermal conductivity, similarly to the large majority of PCMs. The roll-bond heat exchangers are fed in pairs in parallel by two manifolds located on the top of the tank. The water flowing inside the inlet manifold is supplied by an external thermostatic bath that can independently regulate the flow rate and the inlet temperature. The volumetric flow rate is measured by an Endress + Houser Promag H electromagnetic flow meter with an accuracy of  $\pm 0.5\%$  of the full scale (full scale  $40 \text{ l min}^{-1}$ ). The inlet water temperature is measured with a calibrated T-type thermocouple (copper-constantan) with uncertainty (coverage factor  $k=2$ ) equal to  $\pm 0.1 \text{ K}$  since it is connected to a Kaye K170 Ice Point Reference with stability of  $\pm 0.005 \text{ }^\circ\text{C}$  and accuracy of  $\pm 0.005 \text{ }^\circ\text{C}$ . A thermopile with uncertainty (coverage factor  $k=2$ ) of  $\pm 0.05 \text{ K}$  measures the temperature difference between water inlet and outlet. In addition, 39 calibrated T-type thermocouples (uncertainty  $\pm 0.1 \text{ K}$ ) were immersed inside the PCM. They were located using 11 stainless steel rods at 5 different heights as depicted in Figure 2. In this way it was possible to analyze the temperature field during the experimental tests. All data were acquired by means of a Keysight 34970A acquisition system with a sampling rate of 1 Hz. The data are then processed using LabView software. The tank was placed inside a climatic room whose temperature was maintained during all the tests at  $9.0 \pm 0.2 \text{ }^\circ\text{C}$  to avoid heat losses from the tank to the environment.

### 3. Results

The (cold) energy charging test started when the LTES had an average temperature of  $14^\circ\text{C}$ . Cold water flowed through the roll-bond heat exchangers at an inlet temperature of  $2^\circ\text{C}$  and a flow rate of  $17 \text{ l min}^{-1}$ , which are the reference rating conditions. The test ended when all the thermocouples inside the PCM recorded a temperature of  $7^\circ\text{C}$ , i.e. 2 K lower than the PCM phase change temperature. The (cold) energy discharging test began immediately thereafter; the average temperature of the PCM under these conditions was  $6^\circ\text{C}$ . An equal water flow rate ( $17 \text{ l min}^{-1}$ ) at a temperature of  $16^\circ\text{C}$  flowed inside the heat exchangers until the PCM reached an average temperature of  $14^\circ\text{C}$ , 2 K lower than the water temperature. During this test the climatic chamber was set at  $9^\circ\text{C}$  to limit as much as possible the heat loss to the surroundings. Figure 3 reports the complete charging and discharging cycle collected at constant water flow rate of  $17 \text{ l min}^{-1}$  and inlet water temperature equal to  $2^\circ\text{C}$  and  $14^\circ\text{C}$  during the charging and discharging phases, respectively.

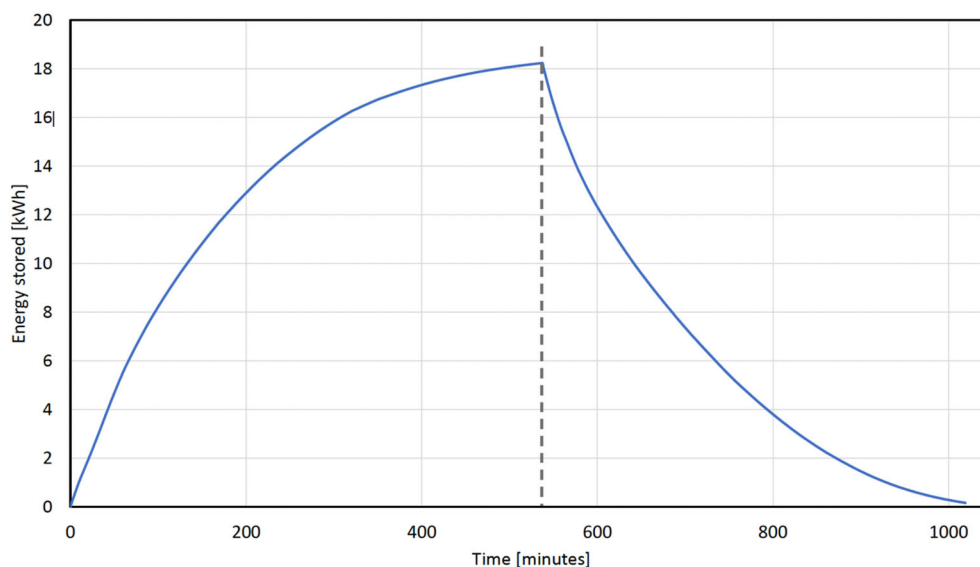


Figure 3. Cold energy stored and released during gone complete cycle as a function of the time at constant water flow rate of  $17 \text{ l min}^{-1}$ . Inlet water temperature equal to  $2^{\circ}\text{C}$  and  $14^{\circ}\text{C}$  during the charging and discharging phases, respectively.

#### 4. Conclusions

This work presents an experimental assessment of a novel 18 kWh LTES based on roll-bond technology, which uses a bio-based PCM CRODATHERM9.5 specifically developed for air conditioning applications. The results showed that this technological solution permitted to store cold energy and then release it when needed; in this way, it is possible to efficiently decouple the renewable energy source availability with the cooling demand. The collected experimental measurements can be considered one of the first databases that collects temperature distributions during the phase change process, and energy stored profiles of a real-scale LTES for air-conditioning, allowing for the development and validation of both local numerical simulations of the LTES when integrated in a complex heating/cooling energy system equipped with heat pump and solar PV/T array for household applications.

#### Acknowledgements

This research work was funded by the PRIN 2017 FlexHeat 2017KAAECT project.

#### References

- [1] International Energy Agency IEA, [www.iea.org](http://www.iea.org)
- [2] Gagliano, A., F. Patania, F. Nocera, A. Ferlito and A. Galesi, 2012. Thermal performance of ventilated roofs during summer period, *Energy and Buildings* 49:611-618.
- [3] Cabeza, L. F. and M. Chafer, 2020. Technological options and strategies towards zero energy buildings contributing to climate change mitigation: A systematic review. *Energy and Buildings* 219:110009.
- [4] Colla, L., Ercole, D., Fedele, L., Mancin, S., Manca, O., Bobbo, S. , 2017, Nano-phase change materials for electronics cooling applications, *J. Heat Transfer*. 139, 1–9.
- [5] Atalay, H., Cankurtaran E., 2021, Energy, exergy, exergo-economic and exergo-environmental analyses of a large scale solar dryer with PCM energy storage medium, *Energy*, 216, 119221.
- [6] Wu, J., Tremeac, B., Terrier, M. F., Charni, M., Gagniere, E., Couenne, F., Hamroun, B., Jallut, C., 2016, Experimental investigation of the dynamic behavior of a large-scale refrigeration e PCM energy storage system. Validation of a complete model, *Energy* ,116, 32-42.
- [7] Liu, M., Saman, W., Bruno, F., 2012, Development of a novel refrigeration system for refrigerated trucks incorporating phase change material. *Applied Energy*, 92, 336–342.



## Design of ternary Al-alloy phase change material

Yuto Shimizu<sup>1</sup>, Takahiro Nomura<sup>2</sup>

<sup>1</sup>Graduate School of Engineering, Hokkaido University, Japan, Phone: 81-11-7066842,  
e-mail: y.shimizu2241@eng.hokudai.ac.jp

<sup>2</sup>Faculty of Engineering, Hokkaido University, Japan., Phone: 81-11-7066842,  
e-mail: nms-tropy@eng.hokudai.ac.jp

### Abstract

A type of power-to-heat-to-power type system that uses thermal energy storage (TES), the Carnot Battery, has been attracting attention as a way to make renewable energy the main source of electricity. As a promising TES method, high-temperature latent heat TES (LHTES) using alloy-based phase change materials (PCMs) is being considered. In this study, ternary Al-Si-Fe alloy which melts at approximately 580-620°C was found as a suitable PCM for Carnot Battery, by thermodynamic calculation.

**Keywords:** Thermal energy storage, Latent heat storage, Phase change material (PCM), Aluminum alloy, Carnot Battery.

### 1. Introduction

Carnot batteries, a type of power to heat to power type system that uses TES, are attracting attention as a way to achieve a decarbonized society [1]. One of the main objectives of the Carnot battery is to reuse the conventional coal-fired power generation plants that use an ultra-supercritical steam turbine. This concept is an environmentally friendly and economical way to achieve decarbonization.

The development of high-temperature TES suitable for conventional steam turbine applications is important for the advancement of the Carnot battery. The input steam temperature for conventional ultra-supercritical steam turbine power generation is limited by the heat resistance temperature of the structural materials, which is often approximately 600-620°C [2].

Therefore, the purpose of this study is to design a 600°C-class PCM by thermodynamic equilibrium calculation using FactSage.

### 2. Method

A phase diagram of an alloy was created using the "Phase Diagram" module of FactSage 8.1 software and the "SGTE 2020 alloy" database. The relationship between accumulated heat storage capacity and temperature was also calculated using the "Epuilib" module of the FactSage 8.1 software for the selected alloy compositions as 600°C-class PCM found in the phase diagram.

### 3. Results

Fig. 1 shows a phase diagram of  $\text{Al}_{0.992}\text{Fe}_{0.008}\text{-Si}$  on  $\text{Al}_{0.992}\text{Fe}_{0.008}$  rich-side for an Al-Si-Fe alloy created from thermodynamic equilibrium calculation using FactSage. The phase diagram shows that the Al-5.9%Si-1.6%Fe [mass%] alloy melts at 576-619°C and has potential as a 600°C-class PCM. In addition, the calculation of the relationship between accumulated heat storage capacity and temperature shows that the Al-5.9%Si-1.6%Fe alloy have a latent heat capacity of  $173 \text{ J g}^{-1}$  at a constant temperature of 576°C and  $263 \text{ J g}^{-1}$  due to the continuous phase change from 576 to 619°C. In other words, Al-5.9%Si-1.6%Fe was expected to have a total latent heat capacity of  $436 \text{ J g}^{-1}$  from 576 to 619°C. Thus, the Al-

5.9%Si-1.6%Fe alloy that phase change at temperatures up to approximately 620°C are excellent 600-class PCM.

Al-Si-Fe PCM is not only promising as a 600°C-class PCM, but also has many cost and environmental advantages. In terms of cost, Al, Al-Si alloys, and Fe are the most popularly used metallic materials and are therefore inexpensive. Another challenge is that even though Fe is a major impurity in Al-based products, it negatively affects the castability and mechanical strength of Al alloys<sup>[3,4]</sup>. However, if Al alloys that contain Fe as an impurity can be used as TES materials, they can demonstrate their value without the effort of recycling. Therefore, we considered Al-Si-Fe PCM to be an excellent TES material not only in cost but also in environmental aspects, because of its low original material cost and the possibility of using it as a receptacle for Al scrap, which is difficult to recycle.

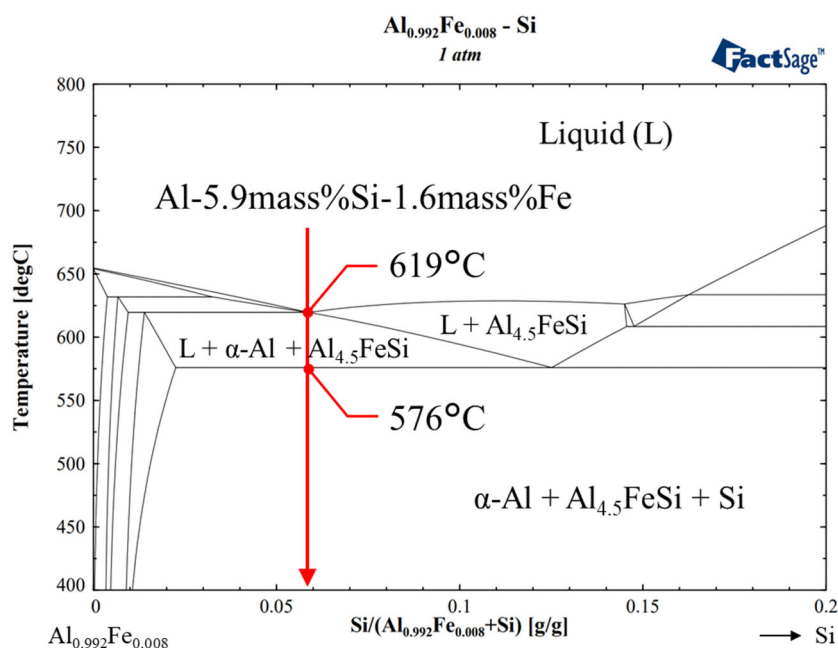


Figure 1. Phase diagram of  $\text{Al}_{0.992}\text{Fe}_{0.008}\text{-Si}$  on  $\text{Al}_{0.992}\text{Fe}_{0.008}$  rich-side.

#### 4. Conclusions

The investigation of 600°C-class PCMs using FactSage software revealed that Al-Si-Fe alloy is promising. Al-5.9%Si-1.6%Fe alloy undergoes a solid-liquid phase change from 576 to 619°C, and the total latent heat capacity was calculated to be  $436 \text{ J g}^{-1}$ . The calculated total latent heat capacity ( $436 \text{ J g}^{-1}$ ) consists of latent heat capacities of  $173 \text{ J g}^{-1}$  at 576°C constant temperature and  $263 \text{ J g}^{-1}$  from 576 to 619°C.

#### Acknowledgement

A part of this work was conducted at Hokkaido University, supported by the "Nanotechnology Platform" Program of the Ministry of Education, Culture, Sports, Science and Technology (MEXT), Japan. This article is based on results obtained from a project (No. JPNP16002) subsidized by the New Energy and Industrial Technology Development Organization (NEDO).

#### References

- [1] O. Dumont et al., *Journal of Energy Storage*, **32**, (2020), p. 101756.
- [2] N. Rogalev et al., *Contemporary Engineering Sciences*, **7**, (2014), No.34, pp. 1807–1825.
- [3] E. Taghaddos et al., *Journal of Alloys and Compounds*, **468**, (2009), pp. 539–545.
- [4] J. A. Taylor et al., *Procedia Materials Science*, **1**, (2012), pp. 19–33.

## Copper base organometallic solid-solid phase change materials

Rebeca Salgado-Pizarro, Camila Barreneche and A. Inés Fernandez

Departament de Ciència de Materials i Química Física, Secció de Ciència de Materials, Facultat de Química,  
Universitat de Barcelona, C/ Martí i Franquès 1-11, 08028, Barcelona, Spain, e-mail:  
ana\_inesfernandez@ub.edu

### Abstract

This work focuses on the investigation of organometallic solid-solid phase change materials, which can store energy due to polymorphism transitions and are thus suitable candidates for cooling electronics. Three different compounds were synthesized,  $(C_{12}H_{28}N)_2CuCl_4$ ,  $(C_{14}H_{32}N)_2CuCl_4$  and  $(C_{16}H_{36}N)_2CuCl_4$ . The crystal and molecular structure were assessed as well as their thermal stability at temperatures between 25 °C and 90 °C at 0, 50, and 100 thermal cycles. Before and after thermal cycling, we characterized and compared the thermal degradation, and thermophysical properties. A maximum enthalpy of 98.1 Jg<sup>-1</sup> was obtained for  $(C_{16}H_{36}N)_2CuCl_4$ . Moreover, all the components were thermally stable up to 100 thermal cycles, with non-evidence of structural degradation or reduction in their thermal properties. Thus, these organometallic solid-solid phase change materials present good potential as cooling electronic materials.

**Keywords:** Solid-Solid Phase Change Materials (ss-PCM), Organometallic materials, Cooling electronics, Thermal Energy Storage (TES).

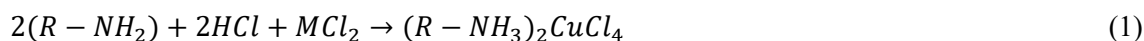
### 1. Introduction

A crucial component of portable electronic device design is effective to heat management, which directly affects the gadget's functionality [1]. Internal overheating is the cause of failure or damage in 55% of electrical devices [2,3]. Due to their great energy storage capacity, latent heat TES (LHTES) technology would be an ideal option for temperature control in an electronic device. Nevertheless, the most utilised LHTES are those involving solid-liquid phase transitions, which have significant limitations when employed in electronics due to corrosion, leakage, or limited heat transmission. Solid-solid transition LHTES materials (solid-solid phase change materials, ss-PCM) would be ideal for the electrical device due to their small volume change during the phase transition, higher thermal conductivity than conventional paraffin, and no leakage issues [4]. Organometallic ss-PCM, are ideal candidates for this kind of application since the polymorphic transitions occur between 32 to 160 °C and the enthalpies are between 62 and 154 Jg<sup>-1</sup> [5].

The performance of three distinct organometallic ss-PCM will be evaluated in this study. CuC12, CuC14, and CuC16 will be synthesised, and their crystal and molecular structures, as well as their thermal performances, will be investigated. Nevertheless, these attributes will be assessed at 0, 50, and 100 cycles.

### 2. Materials and methods

The synthesis of the organometallic ss-PCM was carried out according to the following reaction and stoichiometry of Eq.1, where R represents the organic components with the desired, in an anhydrous methanol medium. The reactants n-dodecylammonium 98%, n-tetradecylammonium 98% and n-hexadecylammonium 90% were acquired from Acros Organics, copper (II) chloride dehydrated from VWR international, hydrochloric acid 37% from Labbox and anhydrous methanol (max 0.003% H<sub>2</sub>O) from Merk Group.



The procedure followed to do the synthesis was established in previous studies. Consisting of reacting the stoichiometry amount of each reactant in a round-bottomed flask with 50 mL of anhydrous methanol and the obtained solution is refluxed at 64 °C for 4 hours under constant stirring. The solution was then poured into a petri dish and dried for 7 days in a desiccator.

The nomenclature used to identify each component was CuCX, where X represents the length of the alkylamine used.

## 2.1 Characterisation

The crystalline structure was determined by X-ray powder diffraction (XRD) conducted in a PANalytical X'Pert PRO MPD  $\theta/\theta$  powder diffractometer of 240 mm of radius. The molecular structure was studied by a Fourier-transformed infrared spectrometer coupled with Attenuated Total Reflectance (FTIR-ATR) conducted in a Spectrum Two form Perkin Elmer. The thermal characterization was done with a differential scanning calorimeter (DSC) from Mettler Toledo. A heating ramp from 300 K to 370 K at 1 K·min<sup>-1</sup> was set to determine the polymorphic transitions. Moreover, the thermal stability of the samples was evaluated with a thermal cycler Q T-18 from Bioer Gene at 0, 50 and 100 cycles from room temperature to 353 K.

## 3. Results and discussions

### 3.1. Crystal and molecular structure

The XRD spectra of synthesised ss-PCM are presented in Figure 1. Due to the detection of diffraction peaks at angles 6°, 9°, 12°, etc., which correspond to the (00l) plane perpendicular to the c-axis, a layered structure is evident in all cases [6–9]. The increase in amine length also results in a shift to lower angles.

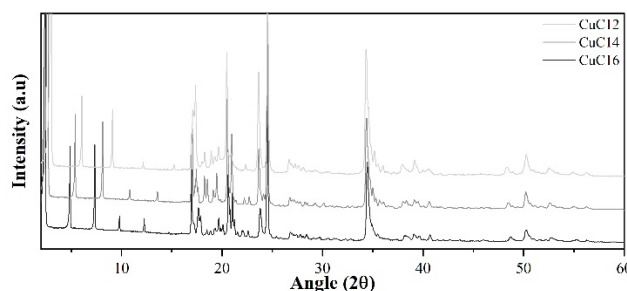


Figure 1. XRD spectra of the synthesised ss-PCM.

Figure 2 depicts the FT-IR spectra of different CuCX ss-PCM. The FT-IR spectra of all samples are comparable. The main bands of each part of the ss-PM are detected. The bands assigned to the primary amine are: 3400-3250 cm<sup>-1</sup> stretching vibration of N-H, 1581 cm<sup>-1</sup> asymmetric deformation of R-NH<sub>3</sub><sup>+</sup>, 1491 and 1480 cm<sup>-1</sup> symmetric deformation of R-NH<sub>3</sub><sup>+</sup>, 1215 cm<sup>-1</sup> stretching of C-N and 769 cm<sup>-1</sup> wagging of R-NH<sub>3</sub><sup>+</sup> [6,10]. The bands associated with the alkane are: 2955, 2871, 2917 and 2849 cm<sup>-1</sup> asymmetric and symmetric stretching of R-CH<sub>3</sub> and R-CH<sub>2</sub>-R, respectively [6], 1472 and 1463 cm<sup>-1</sup> bending of R-CH<sub>2</sub>-R, 1377 cm<sup>-1</sup> symmetric bending of R-CH<sub>3</sub>, 728 and 720 cm<sup>-1</sup> rocking of R-CH<sub>2</sub>-R and 891 cm<sup>-1</sup> stretching of C-C [6,10–12].

Until 100 cycles, no substantial changes are detected in any of the cases. Moreover, no degradation of the alkane is detected since the C=O band is not detected.

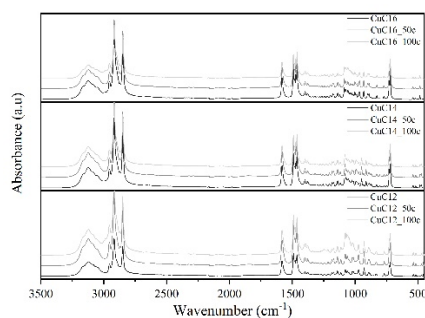
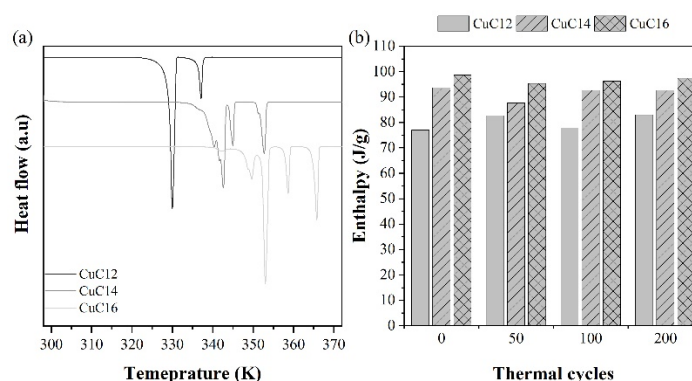


Figure 2. FTIR spectra of the ss-PCM thermal cycled.

### 3.2. Calorimetry study

Figure 3 (a) shows the heat flow curves extracted from the DSC. There are distinct differences between each component. The SS-PCMs exhibit two, three, and four transitions, with the number of transitions increasing as the amine length increases. CuC12 has a total enthalpy of  $74.5 \text{ Jg}^{-1}$ , CuC14 of  $87.1 \text{ Jg}^{-1}$ , and CuC16 of  $98.1 \text{ Jg}^{-1}$ . The results are consistent with previously published data [10,13–16]. In general, SS-PCM with a shorter amine length has lower peak temperature and enthalpy values. This phenomenon could be attributed to the energy generated during the restructuring of the carbon chain. The longer the amine chain, the more energy is required for its restructuring. Figure 3 (b) shows an evaluation of the stability of energy storage under heat cycles for all of the samples under consideration. Slight variations in enthalpy are detected, which might be attributed to crystallinity loss or carbon chain restructuring.



## 4. Conclusions

Three different organometallic ss-PCM were successfully synthesised. The XRD spectra reveal the layered structure and the increase of the molecular size as it was expected. The thermal and chemical stability were analysed at 0, 50 and 100 thermal cycles. The chemical stability was demonstrated by FTIR and DSC. Further research is required in terms of conductivity and a higher number of cycles to assess their applicability in cooling electronics.

## References

- [1] P.K. Schelling, L. Shi, K.E. Goodson, Managing heat for electronics, *Materials Today*. 8 (2005) 30–35. [https://doi.org/10.1016/S1369-7021\(05\)70935-4](https://doi.org/10.1016/S1369-7021(05)70935-4).
- [2] M. Ikhlaiq, M. Yasir, M. Demiroglu, M. Arik, Synthetic Jet Cooling Technology for Electronics Thermal Management - A Critical Review, *IEEE Trans Compon Packaging Manuf Technol*. 11 (2021) 1156–1170. <https://doi.org/10.1109/TCPMT.2021.3087829>.
- [3] L.T. Yeh, Review of Heat Transfer Technologies in Electronic Equipment, *J Electron Packag*. 117 (1995) 333–339. <https://doi.org/10.1115/1.2792113>.

- [4] V. Busico, P. Corradini, M. Vacatello, F. Fittipaldi, L. Nicolais, Solid-Solid Phase Transitions for Thermal Energy Storage, in: C. den Duden (Ed.), *Thermal Storage of Solar Energy*, Springer Netherlands, Dordrecht, 1981: pp. 309–324. [https://doi.org/10.1007/978-94-009-8302-1\\_30](https://doi.org/10.1007/978-94-009-8302-1_30).
- [5] A. Fallahi, G. Guldentops, M. Tao, S. Granados-Focil, S. Van Dessel, Review on solid-solid phase change materials for thermal energy storage: Molecular structure and thermal properties, *Appl Therm Eng.* 127 (2017) 1427–1441. <https://doi.org/10.1016/j.applthermaleng.2017.08.161>.
- [6] M. Bochalya, P.K. Kanaujia, G. Vijaya Prakash, S. Kumar, Structural and optical diversity in copper halide-based ferromagnetic inorganic-organic layered hybrids, *J Solid State Chem.* 273 (2019) 219–225. <https://doi.org/10.1016/j.jssc.2019.03.012>.
- [7] D. He, Y. Di, Y. Yao, Y. Liu, W. Dan, Crystal Structure, Low-Temperature Heat Capacities, and Thermodynamic Properties of Bis(dodecylammonium) Tetrachlorocuprate ( $C_{12}H_{28}N$ )<sub>2</sub>CuCl<sub>4</sub> (s), *J Chem Eng Data.* 55 (2010) 5739–5744. <https://doi.org/10.1021/jc100699g>.
- [8] M. Bochalya, G.V. Prakash, S. Kumar, Magnetism and phase segregation in two-dimensional inorganic-organic ( $C_{12}H_{25}NH_3$ )<sub>2</sub>Cu<sub>1-y</sub>Mn<sub>y</sub>Cl<sub>4</sub> hybrids, *J Solid State Chem.* 273 (2019) 32–36. <https://doi.org/10.1016/j.jssc.2019.02.025>.
- [9] M. Bochalya, P.K. Kanaujia, G.V. Prakash, S. Kumar, Structural phase transitions and thermal stability in Cu-based 2D inorganic-organic hybrid perovskite systems, in: *AIP Conf Proc*, American Institute of Physics Inc., 2019: p. 030001. <https://doi.org/10.1063/1.5122329>.
- [10] J.-K. Kang, J.-H. Choy, M. Rey-Lafon, Phase transition behavior in the perovskite-type layer compound ( $n$ - $C_{12}H_{25}NH_3$ )<sub>2</sub>CuCl<sub>4</sub>, *Journal of Physics and Chemistry of Solids.* 54 (1993) 1567–1577. [https://doi.org/10.1016/0022-3697\(93\)90351-Q](https://doi.org/10.1016/0022-3697(93)90351-Q).
- [11] L. Ricard, M. Rey-Lafon, C. Biran, Vibrational study of the dynamics of  $n$ -decylammonium chains in the perovskite-type layer compound decylammonium tetrachlorocadmate (( $C_{10}H_{21}NH_3$ )<sub>2</sub>CdCl<sub>4</sub>), *J Phys Chem.* 88 (1984) 5614–5620. <https://doi.org/10.1021/j150667a031>.
- [12] R.G. Snyder, Vibrational spectra of crystalline  $n$ -paraffins, *J Mol Spectrosc.* 7 (1961) 116–144. [https://doi.org/10.1016/0022-2852\(61\)90347-2](https://doi.org/10.1016/0022-2852(61)90347-2).
- [13] V. Busico, C. Carfagna, V. Salerno, M. Vacatello, F. Fittipaldi, The layer perovskites as thermal energy storage systems, *Solar Energy.* 24 (1980) 575–579. [https://doi.org/10.1016/0038-092X\(80\)90356-4](https://doi.org/10.1016/0038-092X(80)90356-4).
- [14] G.F. Needham, R.D. Willett, H.F. Franzen, Phase transitions in crystalline models of bilayers. 1. Differential scanning calorimetric and x-ray studies of ( $C_{12}H_{25}NH_3$ )<sub>2</sub>MCl<sub>4</sub> and ( $C_{14}H_{29}NH_3$ )<sub>2</sub>MCl<sub>4</sub> salts (M = Mn<sup>2+</sup>, Cd<sup>2+</sup>, Cu<sup>2+</sup>), *J Phys Chem.* 88 (1984) 674–680. <https://doi.org/10.1021/j150648a012>.
- [15] E. Landi, M. Vacatello, Metal-dependent thermal behaviour in ( $n$ - $C_nH_{2n+1}NH_3$ )<sub>2</sub>MCl<sub>4</sub>, *Thermochim Acta.* 13 (1975) 441–447. [https://doi.org/10.1016/0040-6031\(75\)85084-2](https://doi.org/10.1016/0040-6031(75)85084-2).
- [16] W. Li, D. Zhang, T. Zhang, T. Wang, D. Ruan, D. Xing, H. Li, Study of solid–solid phase change of ( $n$ - $C_nH_{2n+1}NH_3$ )<sub>2</sub>MCl<sub>4</sub> for thermal energy storage, *Thermochim Acta.* 326 (1999) 183–186. [https://doi.org/10.1016/S0040-6031\(98\)00497-3](https://doi.org/10.1016/S0040-6031(98)00497-3).

EUROTHERM2023-N196

## Alternative methods for the in-situ encapsulation of PCMs into polymeric fibres

Mikel Duran<sup>1,2</sup>, Angel Serrano<sup>1</sup>, Artem Nikulin<sup>1</sup>, Jean Luc Dauvergne<sup>1</sup>, Jalel Labidi<sup>2</sup>, Elena Palomo del Barrio<sup>1,3</sup>

<sup>1</sup> Centre for Cooperative Research on Alternative Energies (CIC energiGUNE), Basque Research and Technology Alliance (BRTA), Alava Technology Park, Albert Einstein 48, 01510 Vitoria-Gasteiz, Spain, e-mail: mduran@cicenergigune.com; epalomo@cicenergigune.com

<sup>2</sup> University of the Basque Country (UPV/EHU), Plaza Europa, 1, 20018 Donostia-San Sebastián, Gipuzkoa, Spain

<sup>3</sup> Ikerbasque, Basque Foundation for Science, 48013 Bilbao, Spain

### Abstract

The production of polymeric fibres with encapsulated PCMs presents a great potential to produce textiles and garments with thermal management properties. The most popular techniques to encapsulate PCMs into fibres are complex and low productive. Looking for an alternative, this work presents a method based on solvent extraction and emulsion injection to produce this kind of material. Fibres with encapsulated PCM were produced with low and high polymer concentrations and their latent heat, PCM content and PCM distribution were analyzed. The fibres produced with low and high polymer concentration presented average PCM contents of 33% and 63% respectively, with dispersity of 13% and 6%. The use of high polymer concentration promoted a higher control of the PCM droplet distribution inside the fibres, allowing to obtain higher PCM contents reaching up to 127 J/g with a lower dispersity. Moreover, the produced fibres are easily adaptable to other geometries like rolls and pellets.

**Keywords:** Phase change materials, Thermal management, Fibres, Microfluidics

### 1. Introduction

The encapsulation of PCMs into polymeric fibres is of high interest for several applications in thermal management and thermal responsive textile production, among other applications. Up to now, the main used methods to produce these fibres are based on electrospinning techniques or the use of prefabricated microencapsulated PCMs during fibre production (1,2). The electrospinning techniques obtain as a product a mat of nanofibers that cannot be handled as a single fibre and their production rate is low, not overpassing the feed flowrates of 3 mL/h (3,4). This work presents a simple method for the in-situ production of polymeric fibres with encapsulated PCMs, avoids the use of high voltage and allows to use feed flowrates up to 30 mL/h to produce single fibres in a simpler way for their potential use in thermal management and thermal energy storage applications.

### 2. Materials and methods

The fibres were produced using solvent extraction mechanism. In the proposed system (Fig. 1), a precursor formed by a PCM emulsion into a polymer solution was injected into water through a capillary. When the precursor contacts with water, the solvent extraction process starts, promoting the solidification of the polymer into a fibre shape and trapping the PCM emulsion, giving place to its encapsulation. Two kind of fibres were produced by using high and low polymer concentrations in the precursors. The following techniques have been used to study these materials: Scanning electron microscopy (SEM) and Differential scanning calorimetry (DSC).

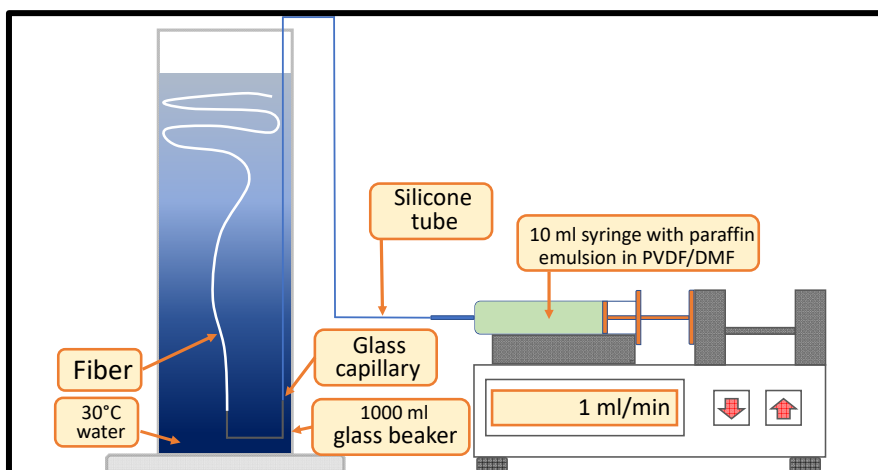


Figure 24. Schemes of the emulsion injection device.

### 3. Results and discussion

#### 3.1. Morphology

The produced fibres present a core-shell structure where a polymer matrix is full of cavities where the PCM can be distributed. It must be noted that the fibres produced with high polymer concentration (Fig. 2 Right) present a denser structure with a more homogeneous distribution of cavities than the fibres produced with low polymer concentration (Fig. 2 left) that present bigger cavities.

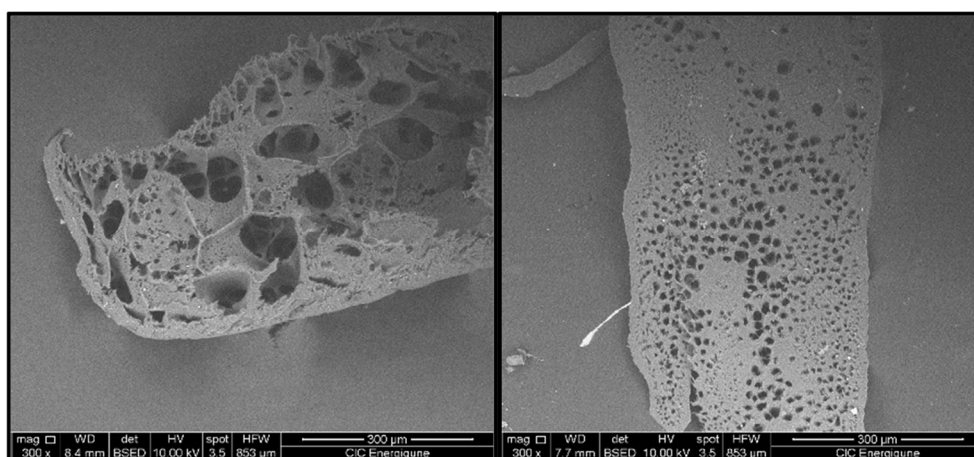


Figure 25. Internal structure of fibres produced with low (Left) and high (Right) polymer concentrations.

Moreover, as can be seen in Figure 3. The produced fibres present a robust shape that is easy to handle and can be adapted to different geometries like rolls of pellets.



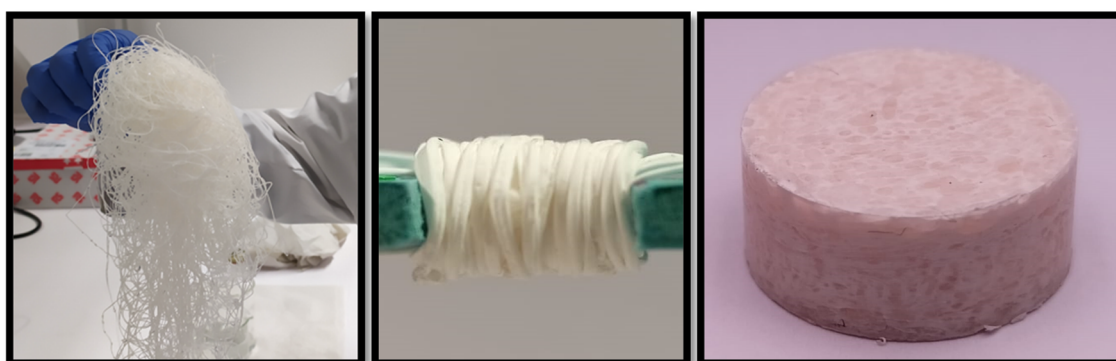


Figure 26. Shape adaptability of the produced fibres as produced (left), rolled (middle) and as a pellet (right)

### 3.2. PCM content and dispersity

The results obtained by DSC analysis of the fibres (Fig.3) indicate that the latent heat of the fibre produced low polymer concentration ranges between 73 and 98 J/g, while the values for the fibre produced with high polymer concentration goes from 108 to 137 J/g.

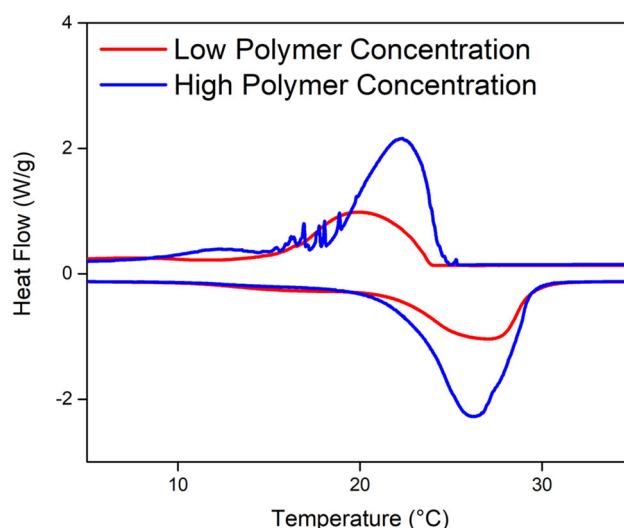


Figure 27. DSC thermograms of random samples from fibres produced with low and high polymer concentrations.

From these results, the average enthalpy, average PCM content and PCM dispersity are calculated (Table 1). The average PCM content for the low polymer concentration fibres is 33% with a dispersity of 13%. On the other side, the fibres produced with high polymer concentration have an average PCM content of 63% and a dispersity of 6%. Therefore, the higher viscosity of the precursor with a higher polymer concentration enhances the homogeneous distribution of the PCM inside the fibre, what could be deductible from the internal morphology seen in the SEM images.

Table 1. Average enthalpy, average PCM content and PCM dispersity values of the produced fibres.

Method	Avg. $\Delta H$ (J/g)	Avg. PCM (%)	Dispersity (%)
Low polymer concentration	82	33	13
High polymer concentration	127	63	6

Moreover, it must be noted that the use of higher polymer concentrations also allows to obtain higher PCM contents and therefore to increase the potential thermal management capability of the fibres.

#### 4. Conclusions

This work has presented a simple method for the simultaneous production of shape adaptable polymeric fibres and encapsulation of PCMs into them. The fibres obtained with different polymer concentrations presented PCM contents above 30%. Moreover, using the adequate polymer concentration, the PCM content on the fibres can be increased up to 63% with a PCM dispersion of only 6%. Therefore, the proposed method can be considered as a potential alternative for the current polymer/PCM fibre production techniques, as well as a useful tool for thermal energy storage and thermal management material production.

#### Acknowledgements

Mikel Duran Lopez would like to thank the Department of Education, Linguistic Politics and Culture of the Basque Country government for the granted pre-doctoral contract (PRE\_2019\_1\_0154).

#### References

1. Iqbal K, Sun D. Development of thermo-regulating polypropylene fibre containing microencapsulated phase change materials. *Renew Energy* [Internet]. 2014;71:473–9. Available from: <http://dx.doi.org/10.1016/j.renene.2014.05.063>
2. Ahn Y ho, Dewitt SJA, McGuire S, Lively RP. Incorporation of Phase Change Materials into Fibers for Sustainable Thermal Energy Storage. 2021;
3. Golestaneh SI, Mosallanejad A, Karimi G, Khorram M, Khashi M. Fabrication and characterization of phase change material composite fibers with wide phase-transition temperature range by co-electrospinning method. *Appl Energy*. 2016 Nov 15;182:409–17.
4. Haghghat F, Abdolkarim S, Ravandi H, Esfahany MN. Polymers A comprehensive study on optimizing and thermoregulating properties of core – shell fibrous structures through coaxial electrospinning. *J Mater Sci* [Internet]. 2017; Available from: <https://doi.org/10.1007/s10853-017-1856-1>

EUROTHERM2023-S197

## Improving the thermal conductivity of sand pack-bed for Electro-thermal energy storage system (ETES)

Sampson Tetteh, Mika Järvinen, Annukka Santasalo-Aarnio

Research Group of Energy Conversion & Systems, Department of Mechanical Engineering, School of Engineering, Aalto University, PO Box 14400, FI-00076 AALTO, Finland  
\*Phone: +358504776797, e-mail: sampson.tetteh@aalto.fi

### Abstract

Decarbonising the energy sector has caused the demand for energy storage systems to bridge the intermittency of renewable energy production. As a result, several new energy storage systems have been proposed, including Electro-Thermal Energy Storage (ETES) system. ETES converts electrical energy into heat that is stored and can be converted back to electricity by Sterling engines. This technology offers a low-cost option for future electricity storage as it has high energy density, compatibility with existing power systems, and flexibility to utilise a larger variety of abundant thermal energy storage (TES) materials. Among the TES materials, such as molten salts and thermal oils, sand was considered the most suitable TES material due to its high thermal tolerance capacity, abundant availability, and low cost. However, low thermal conductivity is a drawback of sand, and in this work, we aim to improve it by mixing aluminium chips with sand. The experiment carried out in this work also investigated two mixing techniques.

**Keywords:** Electro-Thermal Energy Storage, Thermal Conductivity, Thermal Energy Storage Material, Sand-bed, Electric heating, cost-effective.

### 1. Introduction

The growth in renewable energy sources has created a large need for energy storage systems. One low-cost energy storage solution is the Electro-Thermal Energy Storage (ETES) system[1], which stores electricity as thermal energy in a thermal energy storage (TES) material. The stored thermal energy can then be converted back into electricity using the Stirling Engine. ETES offers many benefits, including low-cost, high-energy density, flexibility in using different thermal energy storage materials, and compatibility with existing power systems. These advantages make it a promising technology for future energy storage[2]. This system can contribute to the success of 100% renewable energy in fighting climate change.

Several alternative energy storage solutions have been proposed to cater to grid utilities running on renewable energy. For instance, a 1 MWh packed-bed thermal energy storage system[3], a large-scale thermal energy storage plant with a long duration[4], a storage system called TES POD that stores electricity in molten aluminium alloy[5], and a system that stores electricity in insulated underground sand[6]. Among the existing energy storage systems, thermal energy storage systems pose a higher potential for renewable energy storage for their appealing low cost compared to electrochemical energy storage[7].

In previous studies, we proposed the ETES[1] system to store electricity in variable thermal energy storage materials like thermal oil, molten salts, sands, or minerals with high thermal properties. The ETES discharges electricity to the grid through Stirling Engines embedded in the thermal storage tank. Sands have numerous benefits when used in Thermal Energy Storage systems. These include high tolerance to heat, high specific heat capacity, low cost of energy storage, and non-toxicity. Additionally, sand is a readily available material. However, sands have low thermal conductivity, which can reduce the performance and efficiency of the TES system. This work studies the improvement of the thermal

conductivity in sand beds by testing different mixing techniques with waste aluminium chips from machine shops.

## 2. Methods and materials

The study aimed to find temperature distribution in a 380mm x 230mm x 380mm sand bed using 2 kW electric heating elements at its centre (Figure 28). These heating elements are composed of Kanthal, a resistive coiled wire alloy, and are encased within an Inconel metal tube filled with electric insulation powder (MgO) commonly found in sauna heaters. The sand used in this study was brown silica dry sand, with an average particle size ranging between 100 to 400  $\mu\text{m}$  (Figure 29A). The sand bed was assumed to be homogeneous and isotropic, with an initial conductivity of 0.3 W/m.K. The edges of the bed were in contact with 11°C ambient conditions, and no insulation was used. Heating elements (298mm x 309mm x 50mm) were 95mm apart with the labels T1 and T2. The temperature sensor between the heaters is T3, and the sensor 30mm from the heater is T4, as shown in Figure 28.

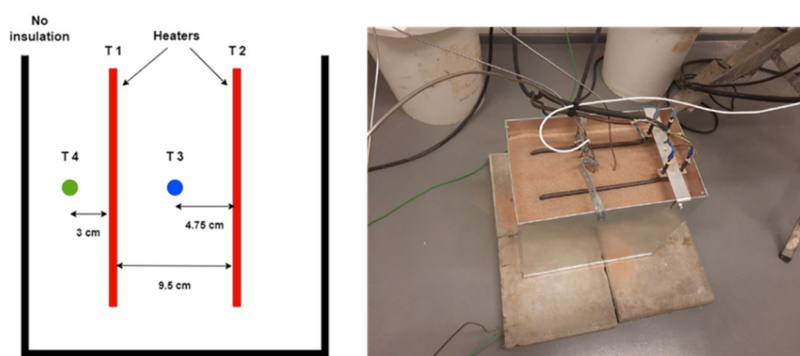


Figure 28. Section view schematic (left) and the experimental setup of sand bed with two heating elements (right).

The aluminium chips used are waste materials from a machine shop with an average length between 10mm to 15mm and a thickness of 0.5mm (Figure 29B). Two mixing methods were assessed. One is a homogeneous mixture, and the other is a sandwich mixture where the aluminium chips have 100mm layers of thickness, and the sand has 600mm layers of thickness (Figure 29C). The ratio of aluminium chips to the sand mixture is 7:26 in volume neglecting the porosity. The sand, aluminium chips and the sandwich-type mix are shown in Figure 29A, B and C, respectively.

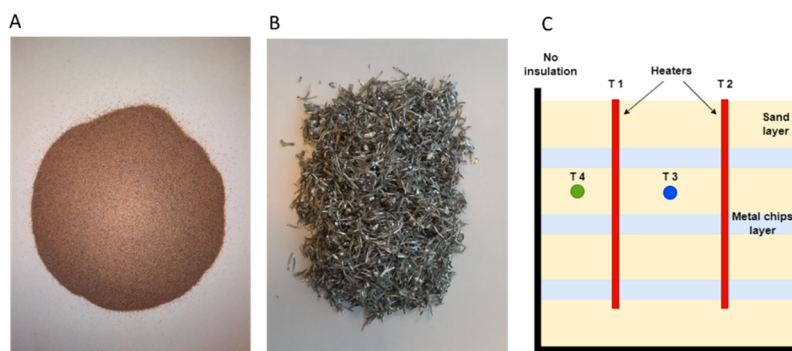


Figure 29. Materials used in the study (A) sand, (B) aluminium chips, and (C) a sandwich-like mix method with the high and placement of each layer.

In order to study the heat conduction properties of different mixtures, the study included three different experimental procedures: pure sand, sand with aluminium chips in a sandwich-like structure and a homogeneous mixture of sand and aluminium chips. The experiments were initiated by weighing the storage components and their placement for the contained. Then, the control box for the heaters was turned on to 500 °C, and temperature data were recorded.

### 3. Results and discussion

To examine the heat transfer in the sand bed, the recordings of the different heat sensors (T1, T3, and T4) in the pure sand bed are presented in Figure 30. The blue curve (T1 in Figure 30) represents the temperature recorded on the electric heating elements spaced 95mm apart. The black curve (T3) represents the temperature recorded between the electric heating elements. In contrast, the red curve (T4) represents the temperature recorded at a distance of 30 mm away from the electric heating elements.

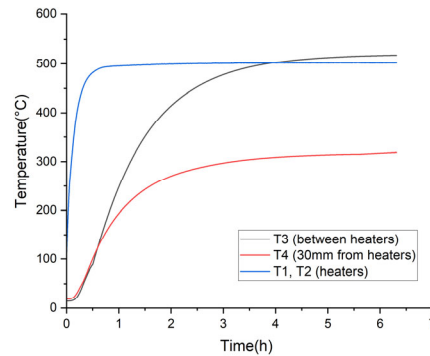


Figure 30. Temperature at different heating sensors: at heating element surface T1,T2, between heating elements T3 and 30mm away from heating elements T4

As can be observed in Figure 30, the heating elements, which are the heating source of the packed bed, quickly heat up to the set temperature of 500 °C. Since there was no insulation around the packed bed, the temperature did not reach the surface temperature of the heating elements due to the heat loss to the environment. However, the space between the two heaters slightly exceeded the surface temperature of the heating elements by 30 °C over time. This gives us the insight to design the heating system of the ETES effectively, where a particle TES material like sand can be heated homogeneously. Moreover, the overshoot temperature of T3 might be because the space between the heating elements is quite a short distance, and more investigation is required.

Heat source arrangements can achieve a uniform temperature in a sand bed. Still, the low thermal conductivity of sand can negatively impact the performance of the ETES system due to the slow heat transfer rate from sand to the Stirling engines. Two methods of mixing sand with aluminium chips were utilised to enhance the heat transfer through the sand bed, and the results are displayed in

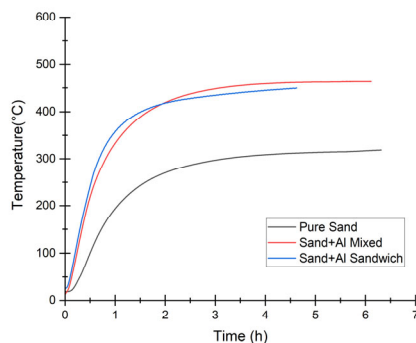


Figure 31.

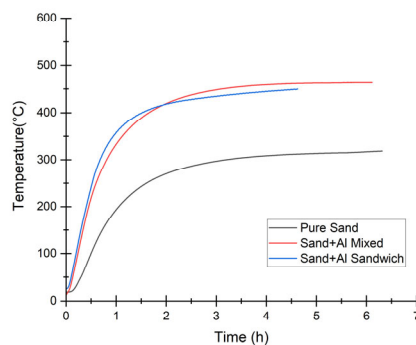
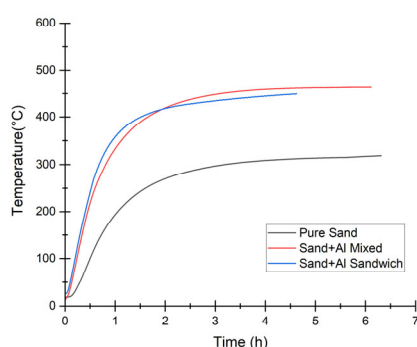


Figure 31. Results showing temperature distribution in pure sand and different mix methods with aluminium at 30 mm away from heat sensors positions.



In

Figure 31, we can see that the mixture has a significant increase in temperature with a faster time than pure sand. This also means that, by increasing the thermal conductivity of the sand, the thermal storage capacity also increases. After 4 hours, the temperature of the pure sand was observed to be 308 °C, while the sand-aluminium homogeneous mixture reached a temperature of 458 °C, and the sand-aluminium sandwich mixture reached a temperature of 444 °C. These observations were made for a sand-to-aluminium volume ratio of 26:7. It can be concluded that the thermal conductivity of the sand-aluminium sandwich mixture increased by 44%. In comparison, the sand-aluminium homogeneous mixture showed an increase of 48% in temperature. Furthermore, the sandwich mixture method heated up slightly faster than the uniform mixture; however, the homogeneous mixture shows a higher thermal capacity. Although the presented results suggest a promising solution for using sand in the ETES system, further studies are necessary to determine the ultimate ratio of the sand-to-aluminium chips mixture.

#### 4. Conclusion

In conclusion, the studies aimed to improve the thermal conductivity of sand bed energy storage by mixing sand with waste aluminium chips while enhancing the charge and discharge rate of ETES. The experiment shows that the thermal conductivity of the sand bed can be improved by mixing other materials with higher thermal conductivity, such as aluminium chips. A sand to aluminium chips ratio of 27:7 increased the thermal conductivity by 44% to 48%. The results indicate that the homogeneous mixture of a packed bed has better thermal conductivity. Since the aluminium chips were a waste product, they would be available at a low cost. Finally, a uniform temperature profile can be archived in a packed bed by carefully designing the heat source arrangements.

#### Acknowledgements

We want to thank Suomen Kulttuurirahasto (The Finnish Cultural Foundation) for funding.

## References

- [1] S. Tetteh, M. R. Yazdani, and A. Santasalo-Aarnio, ‘Cost-effective Electro-Thermal Energy Storage to balance small scale renewable energy systems’, doi: 10.1016/j.est.2021.102829.
- [2] ‘100% Renewable Energy’, *One Earth*. <https://www.oneearth.org/100-renewable-energy/>
- [3] K. Knobloch, T. Ulrich, C. Bahl, and K. Engelbrecht, ‘Degradation of a rock bed thermal energy storage system’, doi: 10.1016/j.applthermaleng.2022.118823.
- [4] J. R. Eggers, M. von der Heyde, S. H. Thaele, H. Niemeyer, and T. Borowitz, ‘Design and performance of a long duration electric thermal energy storage demonstration plant at megawatt-scale’, doi: 10.1016/j.est.2022.105780.
- [5] ‘Start page’, *Azelio*. <https://www.azelio.com/>
- [6] ‘Climate change: “Sand battery” could solve green energy’s big problem’, *BBC News*, Jul. 05, 2022. [Online]. Available: <https://www.bbc.com/news/science-environment-61996520>
- [7] H. Abdi, B. Mohammadi-ivatloo, S. Javadi, A. R. Khodaei, and E. Dehnavi, ‘Chapter 7 - Energy Storage Systems’, in *Distributed Generation Systems*, G. B. Gharehpetian and S. M. Mousavi Agah, doi: 10.1016/B978-0-12-804208-3.00007-8.

EUROTHERM2023-J198

## Revisiting the effect of nanoparticle concentration on melting of phase change material for latent heat energy storage systems

Deepti Sachan, Jishnu Bhattacharya

Indian Institute of Technology, Kanpur, Uttar Pradesh, India, e-mail: [deeptim@iitk.ac.in](mailto:deeptim@iitk.ac.in)

### Abstract

This study investigates the effect of nanoparticles on the melting behaviour of phase change materials (PCMs) used in energy storage systems. PCMs are widely used for thermal energy storage due to their high latent heat of fusion, which enables them to store large amounts of energy in a small volume. However, their low thermal conductivity limits their rate of charging and discharging, which can be improved by adding nanoparticles to the PCM. This study explores the effect of various concentrations of nanoparticles on the melting behaviour of PCMs. The results show that the addition of nanoparticles can significantly enhance the melting rate of PCMs, thereby improving their overall performance as energy storage materials.

**Keywords:** Heat Transfer, Nanoparticles, Phase Change Materials, Energy Storage Systems, Melting

### 1. Introduction

The incorporation of phase change materials (PCMs) into thermal energy storage systems has gained significant attention due to their ability to store and release thermal energy in a controlled manner. However, the low thermal conductivity of PCMs has hindered their widespread application in energy storage systems. To address this issue, nanoparticles have been introduced into PCMs to enhance their thermal conductivity and improve their energy storage performance. In this study an overview of the effect of nanoparticles on the melting behaviour of PCMs for energy storage systems. Nanoparticles can be incorporated into PCMs through various methods such as direct mixing, encapsulation, and in-situ synthesis. The type, size, and concentration of nanoparticles can significantly affect the properties of the PCM-nanoparticle composite.

E. Oró (2012) reviewed phase change materials for cold storage systems. The review covers the types of PCMs available, their properties, and their applications in cold thermal energy storage systems. Most organic PCM are non-corrosive and chemically stable, however they have lower thermal conductivity, lower latent heat, larger volume change between solid and liquid phase and they are relatively expensive was one of the conclusions of their study. Wang et al. (2016) explores a novel approach to enhance the thermal conductivity of paraffin-based phase change materials by using copper foam as a filler. The study investigates the effect of copper foam content on the thermal properties and performance of the composite material. The results show that the addition of copper foam significantly enhances the thermal conductivity of the composite material, with the thermal conductivity increasing by up to 4.4 times with the addition of 30% copper foam.

This study presents numerical modelling of effect of nanoparticles concentration on phase change materials. Nano-enhanced phase change material is considered as single phase material for numerical modelling. Comparison of melt fraction for different case has been presented.



## 2. Mathematical model

### 2.1. System, geometry and material

In this study, the experimental setup shown in Fig. 1 was used, which is based on the design of a solar photovoltaic collector [5]. The PCM was contained within a box that had a height of  $H = 0.132$  m and a width of  $L = 0.02$  m, and the top and bottom of the box were thermally insulated. To ensure rapid heat transfer to the PCM, sheets of aluminium with a thickness of  $l = 0.004$  m were placed on both sides of the PCM, which mimicked the setup of a PV system. The initial conditions of the experiment involved the entire PCM being in a solid state at room temperature, which was set to  $T_o = 293$  K. At  $t = 0$ , a heat flux of  $q'' = 1000$  W/m<sup>2</sup>, representing the absorbed solar radiation, was applied to the left outside wall of the box. Additionally, forced convection was present on both outside walls, with convection coefficients of 10 W/m<sup>2</sup>K and 5 W/m<sup>2</sup>K on the left and right walls, respectively, and a constant temperature of  $T_\infty = T_o$ . The RT25 commercial PCM from Rubitherm GmbH was selected for this study, and its thermophysical properties, as presented in Table 1, were manually input into the COMSOL Multiphysics simulation software.

Table 1. Thermophysical Properties of RT25, Aluminium and Copper

	Solid RT25	Liquid RT 25	Aluminium	Copper
Specific Heat at constant Pressure(J/kg.K)	1800	2400	903	383
Thermal Conductivity(W/m.K)	0.19	0.18	211	389
Density(kg/m <sup>3</sup> )	785	749	2675	8000
Melting Temperature(K)	299.75	-	-	-
Latent Heat(J/kg)	232000	-	-	-
Viscosity(kg/m.s)	-	1.798e-3	-	-

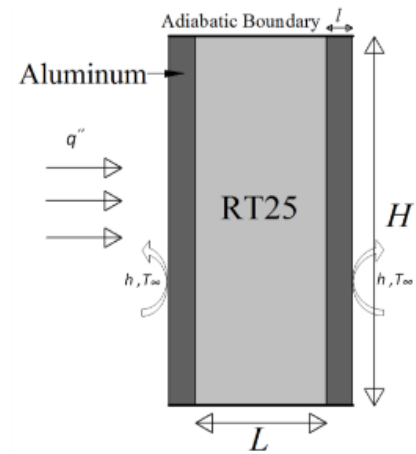


Fig 1. Schematic Diagram [5].

### 2.2. Governing equations

Enthalpy Porosity Technique has been used to model phase change heat transfer in the system. Assumptions are as follows:

- The Nano enhanced phase change material is homogeneous and isotropic.
- The phase change process in the phase change material is isothermal
- Radiation heat transfer is negligible.
- Thermophysical properties of the phase change material are different for the solid and liquid phases.
- The phase change material behaves ideally (i.e. property degradation and subcooling are not accounted for)

$$\text{Continuity Eq: } \nabla \cdot \vec{u} = 0 \quad (1)$$

$$\text{Momentum Eq: } \frac{\partial}{\partial t}(\rho \vec{u}) + \nabla \cdot (\rho V \vec{u}) = \nabla \cdot \mu [\nabla \vec{u} + (\nabla \vec{u})^T] - \frac{\partial p}{\partial x} + S_x + \rho \vec{g} \quad (2)$$

$$S_x = \frac{C(1 - f_l)^2}{f_l^3 + \varepsilon} \vec{u}$$

$$\text{Energy Eq: } \frac{\partial}{\partial t}(\rho c_{eff} T) + \nabla \cdot (\rho c_{eff} \vec{u} T) = \nabla \cdot \vec{q}_{cond} + S_{energy} \quad (3)$$

$$S_{energy} = - \left[ \frac{\partial}{\partial t} (\rho f_t \Delta H) + \nabla \cdot (\rho \vec{u} \Delta H) \right] \quad \begin{cases} \Delta H = f_t L & T \geq T_{melt} \\ 0 & T < T_{melt} \end{cases}$$

The following models are employed to estimate the effective thermophysical properties of the NePCM, namely thermal expansion, heat capacity, density, thermal conductivity and viscosity [4]:

Thermal Conductivity: 
$$k_{nf} = \frac{k_p + 2k_f - 2(k_f - k_p)\phi}{k_p + 2k_f + (k_f - k_p)\phi} k_f \quad (4)$$

Coefficient of thermal expansion: 
$$(\rho\beta)_{nf} = (1 - \phi)(\rho\beta)_f + \phi(\rho\beta)_p \quad (5)$$

Heat capacity: 
$$(\rho c_p)_{nf} = (1 - \phi)(\rho c_p)_f + \phi(\rho c_p)_p \quad (6)$$

Density: 
$$\rho_{nf} = (1 - \phi)\rho_f + \phi\rho_p \quad (7)$$

Viscosity: 
$$\mu_{nf} = \frac{\mu_f}{(1 - \phi)^{2.5}} \quad (8)$$

Fig 2. Shows the coupling between two Multiphysics in COMSOL to model above Equations.

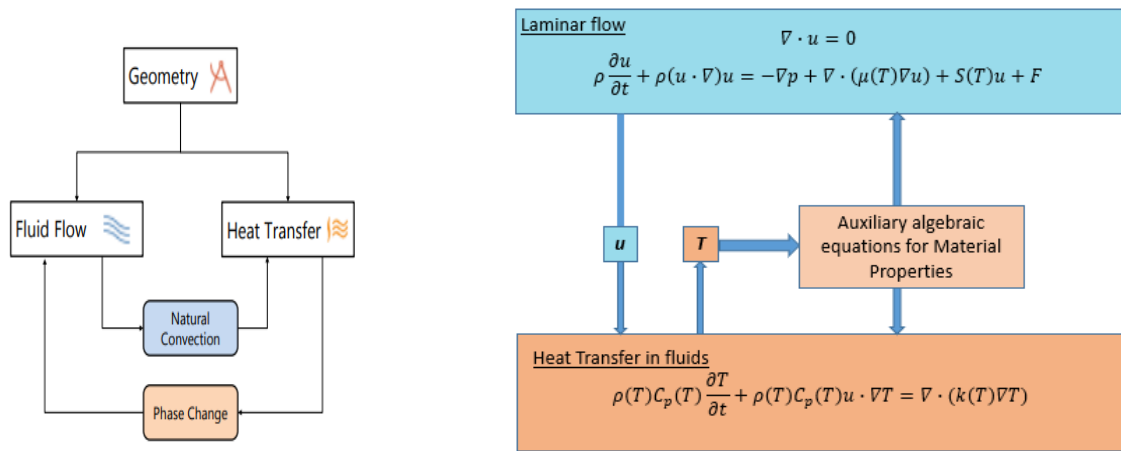


Fig 2. Flow chart of Model Implementation in COMSOL Multiphysics.

### 3. Results and discussion

The results of simulations compared in lights of the obtained melting fraction of the PCM as a function of time and the progression of the melting interface as a function of time. In fig. 3 melt fraction contours at different concentraion have been shown at 4000s. It clearly shows that the melting is faster with higher concentration of nanoparticles in the PCM. In the right side of fig.3 liquid fraction vs time graph shows the time it takes to melt fully.

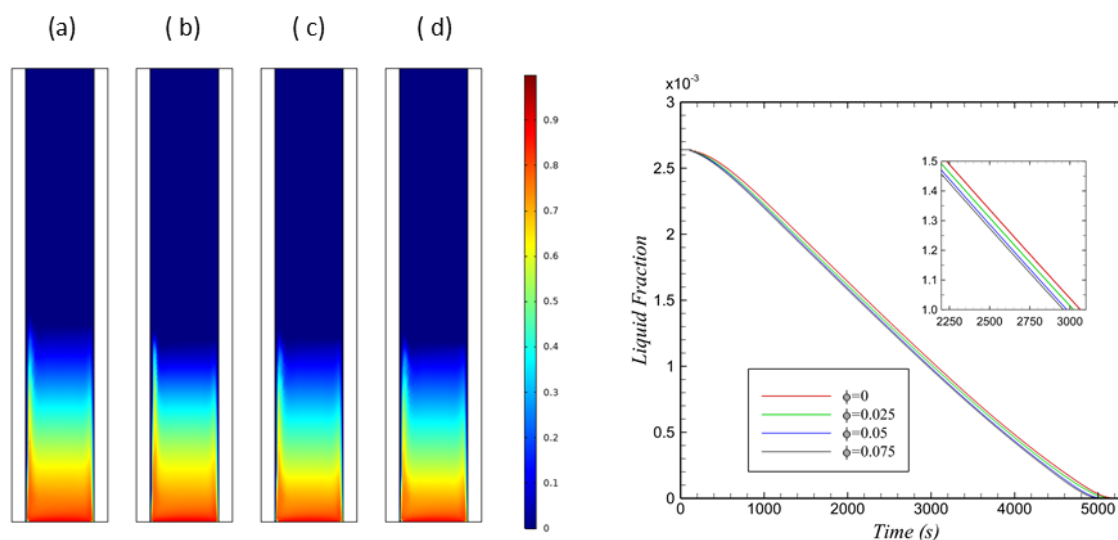


Fig 3. Left Side: Melt fraction contours for (a)  $\phi=0.00$ , (b)  $\phi=0.025$ , (c)  $\phi=0.050$ , (d)  $\phi=0.075$ , Right side: Liquid fraction vs time plot.

## 4. Conclusions

In summary, the addition of nanoparticles into PCMs has been shown to significantly enhance melting performance and hence improve their energy storage capacity. Nanoparticles can affect the melting behavior of PCMs in various ways, including altering the nucleation and growth of crystals, changing the heat transfer mechanisms, and affecting the morphology and structure of the PCM crystals. Future research could focus on optimizing the type, size, and concentration of nanoparticles in PCM-nanoparticle composites for specific energy storage applications. The long-term stability and durability of PCM-nanoparticle composites should also be investigated to ensure their practical applicability in energy storage systems.

## References

1. E. Oró, A. de Gracia, A. Castell, M.M. Farid, L.F. Cabeza. (2012). Review on phase change materials (PCMs) for cold thermal energy storage applications. *Applied Energy*, 99, 513 – 533.
2. Wang, C., Lin, T., Li, N., & Zheng, H. (2016). Heat transfer enhancement of phase change composite material: Copper foam/paraffin. *Renewable Energy*, 96, 960–965.
3. Abdelghani Laouer et. al. (2021). Effect of Magnetic Field and Nanoparticle Concentration on Melting of Cu-Ice in a Rectangular Cavity under Fluctuating Temperatures. *Journal of Energy Storage*, 36, 102421
4. Farid Samara, Dominic Groulx, Pascal H. Biwole (2012). Natural Convection Driven Melting of Phase Change Material: Comparison of Two Methods. COMSOL Conference Boston.

EUROTHERM2023-M199

## Long-term Power-to-Heat Storage based on $\text{Ca}(\text{OH})_2$ – Experimental Development of Pilot Plant

Venizelos E. Sourmelis T.<sup>1</sup>, Viktor Kühl<sup>1</sup>, Marc Linder<sup>2</sup>, Matthias Schmidt<sup>1</sup><sup>2</sup>German Aerospace Center (DLR), Institute of Engineering Thermodynamics, Pfaffenwaldring 38-40, 70569 Stuttgart, Germany, Phone: +49 711 6862-8034, e-mail: marc.linder@dlr.de<sup>1</sup>German Aerospace Center (DLR), Institute of Engineering Thermodynamics, Linder Hoehe, 51147 Cologne, Germany, Phone: +49 2203 601-4091, e-mail: matthias.schmidt@dlr.de

### Abstract

Natural limestone is an abundant and inexpensive material in Europe. Therefore, using the reversible thermochemical reaction of  $\text{Ca}(\text{OH})_2$  (calcium hydroxide), which is obtained from limestone, to  $\text{CaO}$  (calcium oxide) and water vapor for energy storage is a promising approach. After the energy charging process,  $\text{CaO}$  can be stored in solid form at ambient temperature for an indefinite amount of time free of thermal energy losses. Hence, such a storage principle has a particular advantage compared to latent or sensible storage methods, in case a longer storage duration (several weeks to months) is required. Consequently, an application that is of particular interest is, charging  $\text{Ca}(\text{OH})_2$  during summer using excess renewable electricity, storing the  $\text{CaO}$  for several months and discharging it during winter supplying heat for the building sector. Based on this concept, a storage system including a novel reactor has been developed at the DLR. This publication presents its experimental data during operation including its performance and the challenges for the application of the storage system.

**Keywords:** thermochemical energy storage, seasonal energy storage, calcium hydroxide, calcium oxide, power-to-heat, reactor development

### 1. Introduction

The reversible reaction of  $\text{Ca}(\text{OH})_2$  for thermochemical energy storage has been investigated for many years now. Important aspects such as the characterization of the material's properties, the reaction kinetics and the validation of models have been clarified in several works [Schaube et al., 2013; Afflerbach et al., 2017; Funayama et al., 2022]. Additionally, successful demonstrations with lab-scale reactors have been reported [Risthaus et al., 2022]. However, reactor concepts that enable the separation of power and storage capacity and are cost-efficiently scalable are still missing. The cohesive bulk properties and the low thermal conductivity of the material complicate an adequate reactor design. For example, the application of known fluidized bed reactor concepts is hindered by the poor fluidization properties of the material in powder form. The low thermal conductivity limits the power density and scalability of fixed bed reactors. The tendency to agglomerate hinders the free flow of the material through simple reactor geometries and thus impedes the application of gravity-assisted moving bed reactor concepts.

In order to address this challenge, a novel reactor concept has been developed at the DLR, capable of overcoming the drawbacks related to the poor properties of the material in powder form. The reactor concept is based on a rotating mixing device inside the reaction chamber. The rotation induces mechanical fluidization of the powder inside the chamber. The continuous agitation of the powder prevents agglomeration and enhances the heat transfer between the surrounding surface and the powder drastically. Along with the reactor, a complete storage system has been developed and includes ways to transport and store the powder as well as the handling of the reaction's gas (water vapor). This publication outlines the system's development including its latest operation data and discusses its general technological and economical aspects and its challenges.

## 2. Materials and Method

Figure 32 shows the newly developed reactor with  $\text{Ca(OH)}_2$ -powder inside. The rotating shovels are also visible inside of it, which are responsible for the mechanical fluidization of the bed. A coil of electrical heating wires surrounds the reactor, in order to heat it up during the charging cycles. For the discharging of  $\text{CaO}$ , liquid water can be added into the reaction chamber. The heat generated during the discharging can be transferred to a separate stream of water that flows through the double wall of the reactor's casing.

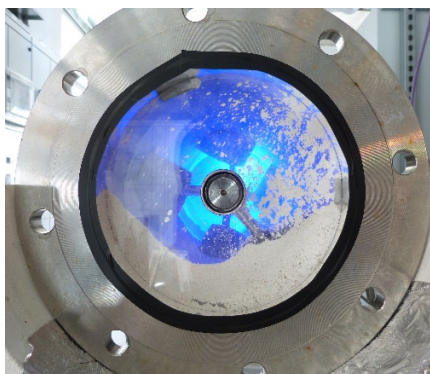


Figure 32. Novel reactor

Figure 33 shows the whole storage system. It consists of two silos capable of storing 250 kg of  $\text{Ca(OH)}_2$  corresponding to an energy amount of 100 kWh. The reactor can be seen at the center of the figure and has a maximum thermal power of 8 kW. Furthermore, an automatic conveying system is installed to transport the material between the silos and the reactor. The system also includes a condenser for condensing the water vapor generated during the material's charging. The experimental setup is equipped with temperature, pressure and mass flow sensors in order to thermodynamically analyze the system's operation fully. The electrical energy input, the thermal energy output and the recovered heat energy of condensation can be determined, thus, the efficiency and limitations of the current reactor design can be specified.



Figure 33. Storage system

## 3. Results and Discussion

Figure 34 shows a thermal charging procedure in the reactor. The temperature values in the reaction bed increase rapidly and homogeneously up to app. 470 °C. At 470 °C a temperature plateau can be observed (top graph). Simultaneously, water vapor release is present and measured at the condenser. A temperature increase in the heat transfer fluid of the condenser indicates the recovery of the heat of condensation. The charging procedure is finished when no more water vapor release is observed in the condenser. After the charging procedure, TGA measurements confirmed a conversion of  $\text{Ca(OH)}_2$  to  $\text{CaO}$  of 79 %. The

signal in the lower graph shows the input of electrical charging energy. Based on the measurements, a charging power of 1,9 kW, corresponding to a specific power density of 8,0 kW/m<sup>2</sup> and an efficiency of 45 % were reached.

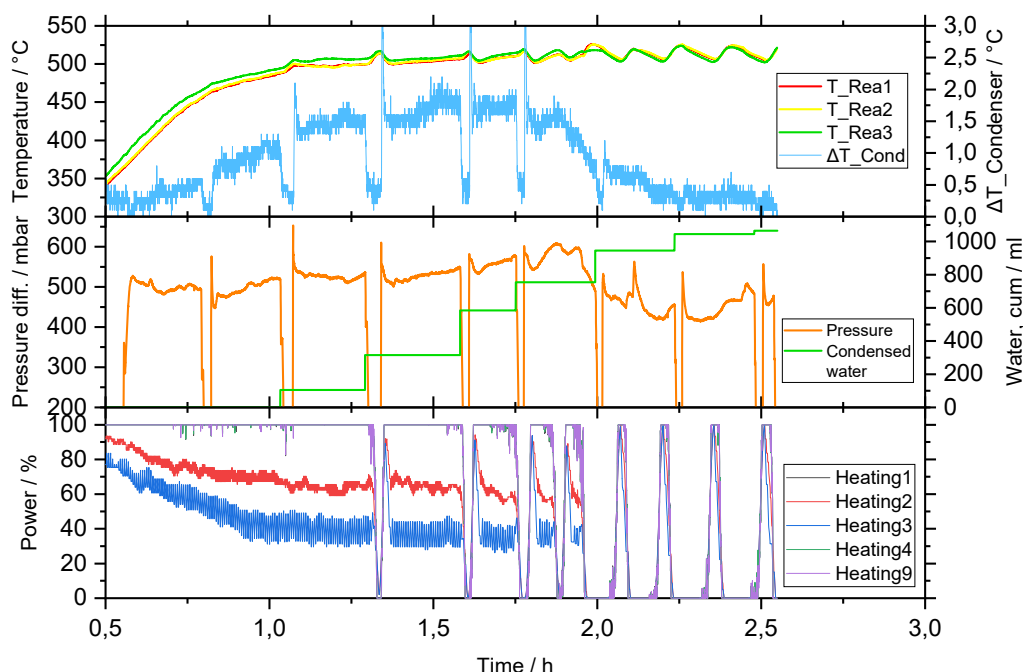


Figure 34. Experimental results from a thermal charging

Further analysis of the reactor revealed that a layer of powder covers the filter in the reactor during operation. The powder layer compresses and it seems that it causes a significant pressure drop of the water vapor transferred out of the reactor (middle graph). The reaction is therefore limited by the gas transport. The negative influence of the “filter cake” on the reaction is currently being investigated and the aim is to minimize its thickness.

Figure 35 shows a thermal discharging with water. By adding water in the reaction chamber, the CaO reacts with it, converting into Ca(OH)<sub>2</sub> and generates heat. The material reaches and sustains a temperature of app. 80 °C for 40 min. Consequently, the outlet temperature of the water reaches 40 °C ( $\Delta T = 30$  K) and sustains it for 45 min, corresponding to a constant thermal power of 1 kW for 45 min.

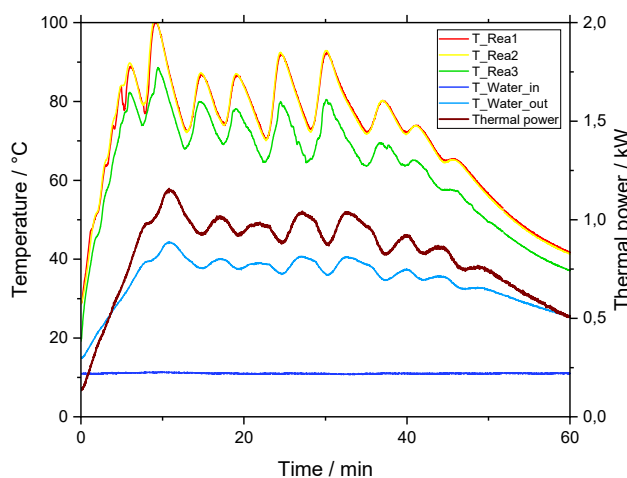


Figure 35. Experimental results from a thermal discharging

Analyzing the graph, the reaction temperature is sufficiently high to reach an even higher water outlet temperature. Main limitations are the agglomeration of already-reacted material on the inner walls of the reactor, worsening the transfer of thermal energy as well as heat losses from the reactor to the environment, both of which are currently being tackled.

#### 4. Conclusions

Overall, this storage system, which includes an innovative reactor concept, has been developed and is successfully in operation in the laboratory. Its function principle has been demonstrated, as shown here. The operation of the system and further optimization of the components based on an upgraded reactor concept is currently ongoing with the aim of demonstrating it in a field environment in summer 2023. The main drawbacks that are currently being tackled are heat losses of the reacted material and the reactor to the environment and the pressure drop through the filter due to powder agglomeration.

#### Acknowledgements

The work has been partially funded by the Helmholtz-Validierungsfonds - Project-ID HVF-0092 and the Deutsche Forschungsgemeinschaft (DFG, German Research Foundation) - Project-ID 279064222 - SFB 1244.

#### References

- Schaube, F., Utz, I., Wörner, A., Müller-Steinhagen, H., 2013. De- and rehydration of  $\text{Ca}(\text{OH})_2$  in a reactor with direct heat transfer for thermo-chemical heat storage. Part B: Validation of model. *Chemical Engineering Research and Design*. 91(5), 865-873.
- Afflerbach, S., Kappes, M., Gipperich, A., Trettin, R., Krummb, W., 2017. Semipermeable encapsulation of calcium hydroxide for thermochemical heat storage solutions. *Solar Energy*. 148, 1-11.
- Funayama, S., Schmidt, M., Mochizuki, K., Linder, M. Takasu, H., Kato, Y., 2022, Calcium hydroxide and porous silicon-impregnated silicon carbide-based composites for thermochemical energy storage, *Applied Thermal Engineering*, 220(2):119675
- Risthaus, K., Linder, M., Schmidt, M., 2022. Experimental investigation of a novel mechanically fluidized bed reactor for thermochemical energy storage with calcium hydroxide/calcium oxide. *Applied Energy*, 315(6):118976

EUROTHERM2023-M200

## Generation of packed bed structures and assessment of shape effects of various particle geometries

William Delgado-Diaz<sup>1,2,\*</sup>, Adina Hochuli<sup>1</sup>, Anastasia Stamatou<sup>1</sup>,  
Sophia Haussener<sup>2</sup>, Jörg Worlitschek<sup>1</sup>

<sup>1</sup>Competence Center Thermal Energy Storage, Lucerne University of Applied Sciences and Arts,  
Technikumstrasse 21, Horw, Switzerland

\*e-mail: williamorlando.delgadodiaz@hslu.ch

<sup>2</sup>Laboratory for Renewable Energy Science and Engineering, EPFL, Rte Cantonale,  
Lausanne, Switzerland.

### Abstract

Macro-encapsulated latent heat energy storage systems stand out due to their compactness and flexibility for customization and modularity. They contain capsules filled with phase change material (PCM), which are arranged as a packed bed heat exchanger structure. The interaction between the flowing heat transfer fluid and the capsules has a major influence on the performance of the TES and, thus, the geometry of the individual PCM capsules plays an important role. This study aimed to identify correlations between the characteristics of a single capsule's geometry and the characteristics of a packed bed by means of a dimensionless analysis. Therefore, experimental data for different particle shapes in different containers was generated using computed tomography in parallel to simulations using a numerical rigid body dynamics routine. The data was then compared and evaluated to create a data set for a regression analysis based on dimensionless quantities.

**Keywords:** Macro-encapsulation, Packed bed, packing density, Computed tomography.

### 1. Introduction

Thermal energy storage (TES) technologies are of great importance to compensate the fluctuating nature of solar energy. Among various TES systems, the principle of latent heat energy storage (LHES) is particularly promising for applications that require high energy density. Solutions with macro-encapsulation (ME) are of specific interest due to their compactness and flexibility.

In an ME-LHES system, capsules filled with phase change material are arranged as a packed bed heat exchanger structure to enhance the heat storage capacity. The interaction between the flowing heat transfer fluid and the packed bed structure has a major influence on the performance of the TES and, thus, the geometry of the capsules plays an important role.

The characteristics of a packed bed, e.g. the packing density, depend on the geometry of the individual particles. This study aims to identify correlations between a single particle's geometry characteristics, e.g. sphericity, flatness and aspect ratio, and the characteristics of the resulting packed bed.

The generation and characteristics of packed bed structures with various shapes both numerically with different simulation methods and using image-based methods in combination with experimental methods has been investigated in studies focus on discreet shapes such as spheres, cuboids, cylinders and ellipsoids[1-14].

However, to the authors knowledge no analysis has been conducted considering a broad range of geometries and a generalized approach to condense a particle's shape to its dimensionless characteristics and to extrapolate from these the behavior of a randomly packed bed in terms of packing density and surface characteristics.



## 2. Methodology

To identify such correlations, experimental data of packed beds has been generated using computed tomography obtained through the digitalization of physical particle sets of several shapes, shown in Figure 2. Additionally, simulated data of analog particle sets was obtained and characterized using a numerical rigid body dynamics routine. The data was then compared to validate the numerical packed bed generation routine and further evaluated to create a data set for a regression analysis, based on dimensionless numbers representing shape characteristics such as aspect ratio, sphericity, flatness, and relative diameter as predictors and packing density and surface ratio as response variables. Figure 36, shows an overall schematic of the methodology used:

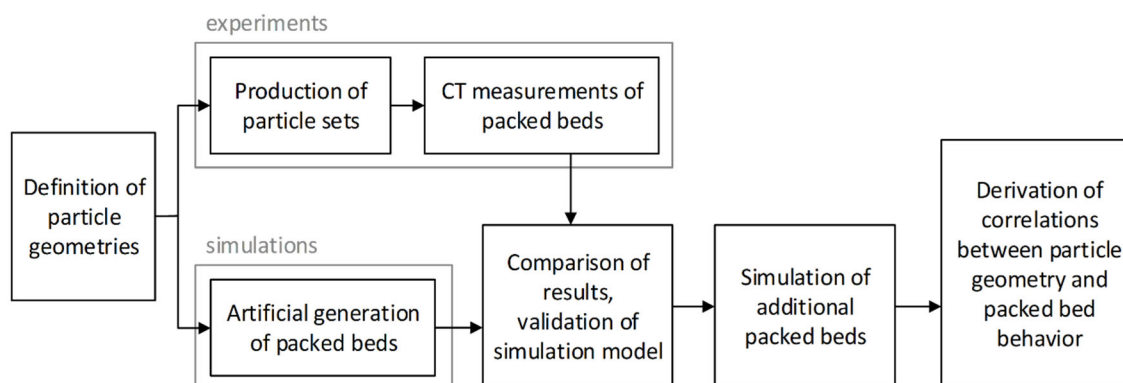


Figure 36. Overview of the methodology employed.

Figure 37. shows the investigated shapes produced using 3D printing and laser cutter techniques (except for spheres). Sets of around 1200 particles were produced and scanned using computed tomography to produce the experimental data to be compared with the simulations.



Figure 37. Overview of the produced particles, from top left to bottom right: Sphere, Cub\_AR10, Cyl\_AR10, SE01, Ell\_AR25, Cub\_AR25, Cyl\_AR25, SE02, Ell\_AR05, Cub\_AR05, Cyl\_AR05.

## 3. Results and conclusions

Figure 38. shows a sample comparison between a physical model of the packed bed, the reconstructed surface using computed tomography scans of the physical model, and the simulated packed bed structure using the numerical rigid body routine.

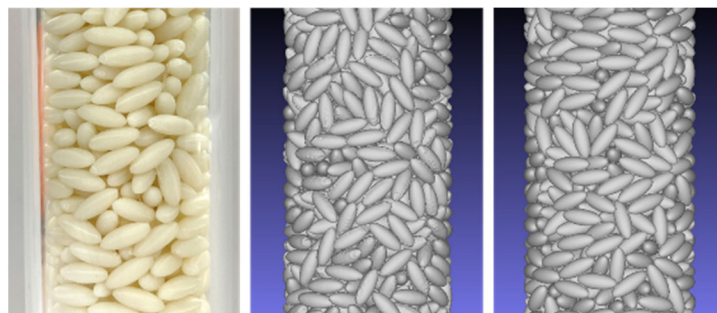


Figure 38. Experimental (left), CT scanned (middle) and simulated packed beds of ellipsoids with an aspect ratio 2.5.

The experimental results showed that the characteristics of the geometry lead to differently structured arrangements in the packed beds. For example, particles with flat faces tend to arrange in packs of similarly oriented particles. Also, the dimensions of the container influence the packing density, due to its wall effects. In a container with a small diameter, the radial wall effects are predominant, whereas for the same particle set, but in a container with a large diameter, the axial wall effects prevail. Figure 39. summarizes the experimental results regarding the packing density of the packed beds.

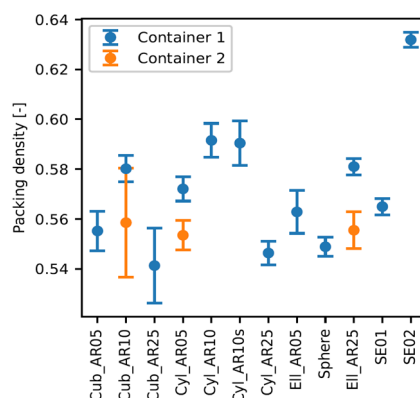


Figure 39. Packing density of packed beds, poured with different particle shapes. Error bars represent the standard deviation based on three measurements.

The validation of the simulation routine showed that the results of the packing density meet the expected accuracy, whereas the resulting surface ratios are not completely satisfying. Regarding the relationship between the particles' metrics, and the packed beds' metrics, which function as response variables, no simple relation between one predictor and one response variable can be identified. However, the multiple linear regression shows that the interaction of the particles' metrics can lead to a regression function that can predict the packed beds' response variables. The regression analysis based on linear and polynomial relations between predictors and response yielded that the predictor flatness can be omitted due to multicollinearity with sphericity. Further on, additional options should be investigated to depict the non-linear relation between the predictors and the response quantities.

#### 4. Conclusions

The evaluation of the experimental data showed that, depending on the shape and aspect ratio of the particles, the packed beds present distinct structured arrangements. Particles with flat faces tend to arrange in packs of similarly oriented particles, whereas particles with curved surfaces are arranged more randomly. The curvature of the surface also leads to a higher surface ratio of the packed bed because no face-face contacts occur. The packed bed or rather the packing density is influenced by the axial and radial wall effects of the container. Depending on the container's diameter, either the axial or the radial wall effects are more pronounced. The evaluation of several models reveals that neither for the experimental data as basis nor for the simulation data as basis, a linear relationship between the

predictors and the response variables is accurate. However, a polynomial relationship leads to an increased fit of the regression function to the data points.

## References

- [1] T. Aste, M. Saadatfar, A. Sakellariou, and T. J. Senden, “Investigating the geometrical structure of disordered sphere packings,” *Phys. A Stat. Mech. its Appl.*, vol. 339, no. 1–2, pp. 16–23, 2004.
- [2] R. Caulkin *et al.*, “Simulations of structures in packed columns and validation by x-ray tomography,” *Ind. Eng. Chem. Res.*, vol. 48, no. 1, pp. 202–213, 2009.
- [3] S. J. Rodrigues, N. Vorhauer-Huget, and E. Tsotsas, “Effective thermal conductivity of packed beds made of cubical particles,” *Int. J. Heat Mass Transf.*, vol. 194, p. 122994, 2022.
- [4] B. Li, H. Zhang, K. Saranteas, and M. A. Henson, “A rigid body dynamics model to predict the combined effects of particle size and shape on pressure filtration,” *Sep. Purif. Technol.*, vol. 278, no. December 2020, p. 119462, 2022.
- [5] S. Flaischlen and G. D. Wehinger, “Synthetic Packed-Bed Generation for CFD Simulations: Blender vs. STAR-CCM+,” *ChemEngineering*, vol. 3, no. 2, p. 52, 2019.
- [6] J. Gan and A. Yu, “DEM simulation of the packing of cylindrical particles,” *Granul. Matter*, vol. 22, no. 1, pp. 1–19, 2020.
- [7] R. Hesse, F. Krull, and S. Antonyuk, “Prediction of random packing density and flowability for non-spherical particles by deep convolutional neural networks and Discrete Element Method simulations,” *Powder Technol.*, vol. 393, pp. 559–581, 2021.
- [8] L. Liu and S. Li, “Uniform shape elongation effects on the random packings of uniaxially variable superellipsoids,” *Powder Technol.*, vol. 376, pp. 60–71, 2020.
- [9] L. Liu and S. Li, “Shape effects on packing properties of bi-axial superellipsoids,” *Powder Technol.*, vol. 364, pp. 49–59, 2020.
- [10] E. M. Moghaddam, E. A. Foumeny, A. I. Stankiewicz, and J. T. Padding, “Heat transfer from wall to dense packing structures of spheres, cylinders and Raschig rings,” *Chem. Eng. J.*, vol. 407, no. December 2020, p. 127994, 2021.
- [11] L. J. H. Seelen, J. T. Padding, and J. A. M. Kuipers, “A granular Discrete Element Method for arbitrary convex particle shapes: Method and packing generation,” *Chem. Eng. Sci.*, vol. 189, pp. 84–101, 2018.
- [12] S. Wang, D. Marmysh, and S. Ji, “Construction of irregular particles with superquadric equation in DEM,” *Theor. Appl. Mech. Lett.*, vol. 10, no. 2, pp. 68–73, 2020.
- [13] Y. Wu, X. An, and A. B. Yu, “DEM simulation of cubical particle packing under mechanical vibration,” *Powder Technol.*, vol. 314, pp. 89–101, 2017.
- [14] B. Zhao, X. An, Y. Wang, Q. Qian, X. Yang, and X. Sun, “DEM dynamic simulation of tetrahedral particle packing under 3D mechanical vibration,” *Powder Technol.*, vol. 317, pp. 171–180, 2017.

EUROTHERM2023-B201

## The multi-objective optimization of a stand-alone liquid air energy storage

Ting Liang<sup>1</sup>, Xiaohui She<sup>2</sup>, Yongliang Li<sup>1</sup>, Tongtong Zhang<sup>1</sup>, Yulong Ding<sup>1\*</sup>

<sup>1</sup> Birmingham Centre for Energy Storage, School of Chemical Engineering, University of Birmingham, Birmingham B15 2TT, UK, email: [txl880@student.bham.ac.uk](mailto:txl880@student.bham.ac.uk)

<sup>2</sup> School of Mechanical Engineering, Shijiazhuang Tiedao University, Shijiazhuang 050043, China, e-mail: [y.ding@bham.ac.uk](mailto:y.ding@bham.ac.uk) (Corresponding Authors)

### Abstract

This work is to conduct the multi-objective optimization of LAES by using Genetic algorithm, taking the round trip efficiency (RTE) and economic indicators as the optimization objectives. After the optimization, the optimal design and operational parameters of LAES under different configurations and scenarios can be determined, including the optimal charging and discharging pressure, heat transfer areas, and mass flow rates of hot and cold storage media, etc. The increase of energy efficiency by 9%~14% and the decrease of exergy destruction by 16% were seen. The Pareto Front of capital expenditure, energy efficiency and occupied space energy density of a LAES system provides system operators good investment advice. Specifically, when the RTE of the LAES increases by 1%, the optimized capital cost increases by 0.5-1%. Overall, the optimization framework developed by this work can for the first time determine the optimal design and operational parameters, the design guidelines and provide investment guidance for LAES systems under different conditions.

**Keywords:** Liquid air energy storage, multi-objective optimization, Pareto Front, Surrogate model, Genetic algorithm, Aspen HYSYS

### 1. Introduction

To keep the global warming well below 2 °C, and continue to reduce emissions to net zero by 2050, large amounts of renewable penetration would increase power system fluctuations and weaken the system reliability due to the intermittency and variation of renewables. It is acknowledged that storage technologies would play crucial roles in tackling these problems [1]. Liquid air energy storage (LAES) has the advantages including its low costs, ease of deployment and scalability without geographical constraints, which can provide alternatives to Pumped hydro energy storage (PHES) and compressed air energy storage (CAES).

In terms of the studies about LAES systems, most researchers have revealed the crucial effects of the charging and discharging pressures, and cold energy recovery. So far, few researchers have worked on the multi-objective optimization of whole LAES system. Only Li et al. [2] investigated a combined system with solar thermal heat and LAES, the system has been optimized by using a sequential quadratic programming method. The results indicated that the optimal system presents 30% of higher power output and 15.3% of higher exergy efficiency. Liu et al. [3] applied GA to optimize LAES system. The results revealed the optimal RTE (as high as 63.1%) and the optimal system configuration with two compression stages and three expansion stages. But the author only take the RTE as the optimization objective. J. Pimm et al. [4] developed an optimization algorithm and control strategy to determine the optimal operation of a hybrid storage system (CAES and LAES). The results suggested that the ROI can be maximized if the charging time of the hybrid system is higher than 36 h, and 80% of total storage capacity is in liquid air form (charge time /discharge time is 2.5:1). Above all, fewer work has covered the thermo-economic optimization of whole LAES system by using artificial intelligence (AI) algorithms, like GA, NSGA-II and Particle Swarm Optimization (PSO) etc. Thus, this study aims to achieve the thermo-economic multi-objective optimization of a stand-alone LAES by using GA.

## 2. System description

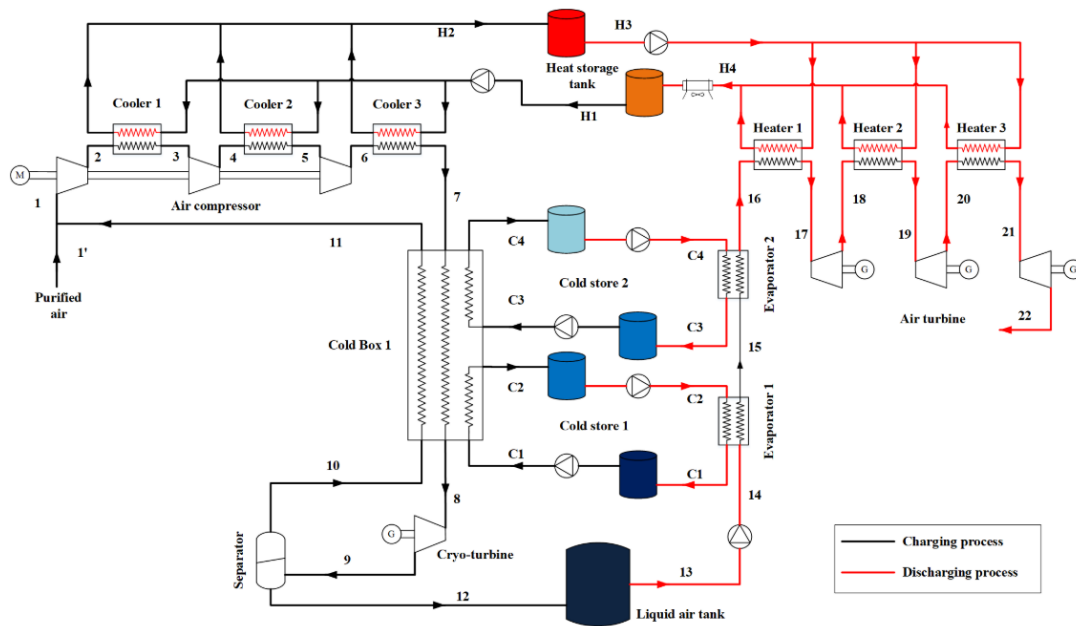


Fig. 1. LAES thermodynamic layout [5]

The thermodynamic diagram of a stand-alone of LAES is shown in Fig. 1, which consists of a liquefaction unit, a storage unit and a power recovery unit. The system consists of a three-stage compression, three coolers, a cold box, a cryo-turbine, a liquid air tank, a cryogenic pump, two cold-recovery evaporators, three re-heaters and three-stage expansion.

### 2.1. Optimization modelling

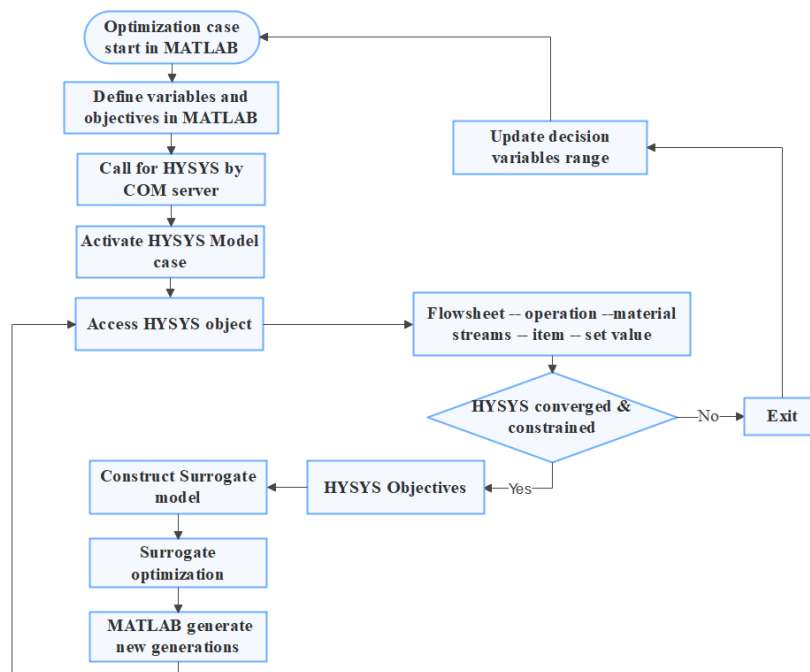


Fig. 2. The system optimization framework

The thermodynamic simulation of LAES in this study was conducted in Aspen HYSYS. The model has been validated by She's work [6]. At nominal conditions, the obtained system RTE is 52.6%, which is 4.5% higher than that of She's work (50.3%), which is considered within 5% of range [7].

For the optimization model, it consists of the optimization variables, constraints and objectives, as well as the algorithms. The selected design and operational variables are the charging pressure, discharging pressure, the inlet and outlet temperature of air-propane cold box. The optimization objectives include round-trip efficiency (RTE), the net present value (NPV), the total capital expenditure (CAPEX) and the occupied space energy density (OSDE) of a LAES plant. In order to reduce the computation time, the GA-based optimization based on the surrogate model was adopted. MATLAB has been configured to control the custom interface server of Aspen HYSYS by creating a COM object through the command (actxserver) [24]. Data exchange between MATLAB and HYSYS has been implemented by the commands structured according to the procedures shown in Fig. 2.

### 3. Results and discussion

#### 3.1 One-objective optimization – energy analysis

For the LAES system with the configuration shown in Fig. 1, the single-objective optimization of the system on RTE was first conducted. It starts from three different initial points and runs for 100 generations, the optimization curves are shown in Fig. 3. It can be seen that the optimal RTEs from three different initial points all have been optimized by 9.5% ~ 14.4%, reaching around 61% under the nominal conditions. The corresponding optimal charging and discharging pressures are ~15 MPa and 11.2~11.8 MPa respectively. The optimal inlet and outlet air temperature of air-propane cold box are ~218 K and ~105 K. These parameters further indicates the optimal sizes of air-propane and air-methanol cold boxes and evaporators, as well as the optimal mass flow rates of propane and methanol for recovering cold energy. The heat transfer areas of cold boxes and evaporators, as well as the mass flow rates of cold media all increase remarkably, leading to higher liquefaction rate and hence more turbine power output.

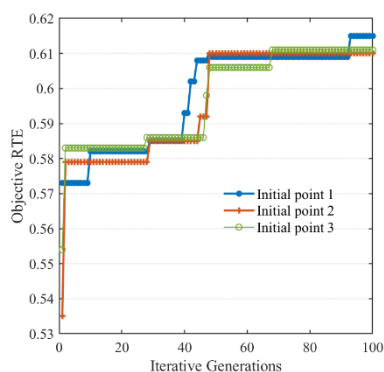


Fig. 3. Single-objective optimization of LAES from different initial points

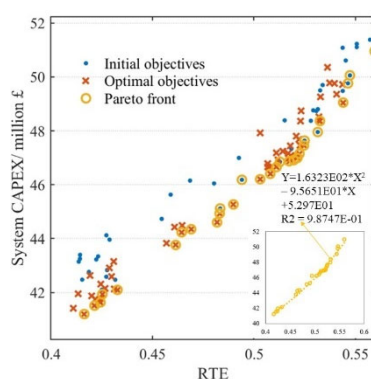


Fig. 4. The optimal Pareto front of RTE and CAPEX

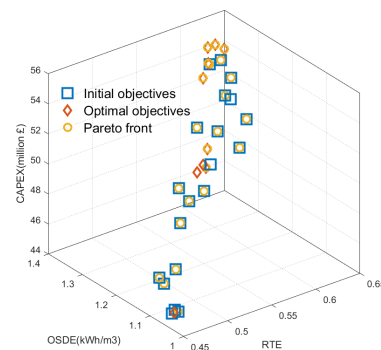


Fig. 5. The optimal Pareto front of three-objective optimization

#### 3.2 Two-objective optimization – energy analysis

For the two-objective optimization of the LAES system shown in Fig. 1, the RTE and CAPEX were chose as two objectives, the optimal Pareto front is shown in Fig. 4. It can be seen that higher RTEs are at the cost of higher capital investments, but also resulting in higher NPV. Specifically, when the RTE increases by 1%, the optimized CAPEX increases by 0.5-1% (the regression equation is shown in Fig. 4). After the two-objective optimization, it is observed that the inlet and outlet temperatures of air-propane cold box decrease remarkably, accordingly, the heat transfer areas of HEXs are enhanced significantly, but the increases in their CAPEXs are limited, as the HEX costs only account for 3%-5% of total CAPEX of LAES.

### 3.3 Three-objective optimization – energy analysis

Take the LAES configuration with three-stage compressor and four-stage turbine as an example, three-objective optimization was conducted, to optimize the RTE, CAPEX and OSDE simultaneously, the optimal design and operational parameters were obtained and the optimal Pareto front is shown as in Fig. 5. It shows the more investment is made, the higher the RTE and OSDE are obtained. Though the higher RTE means more liquid air is produced, accordingly triggering larger volumes of liquid air tank and cold storage tank. But the enhancement in power output is more than the total increase in tank volume, producing higher OSDE.

## 4. Conclusions

This paper works on the parametric study and multi-objective optimization of a stand-alone LAES system, the major contributions and conclusions are drawn as followings: 1) Through the single-objective optimization of a three-stage LAES system, the optimal design and operational variables were derived. The RTE can be optimized by 7%~14% to be ~61%. 2) From the two-objective and three-objective optimization of the LAES, the Pareto Fronts of RTE, CAPEX and OSDE were presented. It indicated that more capital investment can lead to higher RTE, NPV and OSDE. Different LAES systems and configurations should be tailored depending on different investment budgets.

## Acknowledgements

Ting Liang acknowledges the partial support from Priestley Joint Ph.D. Scholarship from the University of Birmingham (UK) and University of Melbourne (Australia);

## References

- [1] Strbac G, Aunedi M, Pudjianto D. Strategic Assessment of the Role and Value of Energy Storage Systems in the UK Low Carbon Energy Future Improving Offline Security Rules for Dynamic Security Assessment View project Smarter Network Storage View project 2012. <https://doi.org/10.13140/RG.2.1.1418.5684>.
- [2] Li Y, Wang X, Jin Y, Ding Y. An integrated solar-cryogen hybrid power system. *Renew Energy* 2012;37:76–81. <https://doi.org/10.1016/j.renene.2011.05.038>.
- [3] Liu Z, Yu H, Gundersen T. Optimization of Liquid Air Energy Storage (LAES) using a Genetic Algorithm (GA). vol. 48. Elsevier Masson SAS; 2020. <https://doi.org/10.1016/B978-0-12-823377-1.50162-2>.
- [4] Pimm AJ, Garvey SD, Kantharaj B. Economic analysis of a hybrid energy storage system based on liquid air and compressed air. *J Energy Storage* 2015;4:24–35. <https://doi.org/10.1016/j.est.2015.09.002>.
- [5] Liang T, Zhang T, Li Y, Tong L, Wang L, Ding Y, et al. Thermodynamic Analysis of Liquid Air Energy Storage (LAES) System. *Encycl. Energy Storage*, vol. 2020, 2023.
- [6] She X, Peng X, Nie B, Leng G, Zhang X, Weng L, et al. Enhancement of round trip efficiency of liquid air energy storage through effective utilization of heat of compression. *Appl Energy* n.d.;206:1632–42. <https://doi.org/10.1016/j.apenergy.2017.09.102>.
- [7] Wang C, Akkurt N, Zhang X, Luo Y, She X. Techno-economic analyses of multi-functional liquid air energy storage for power generation, oxygen production and heating. *Appl Energy* 2020;275. <https://doi.org/10.1016/j.apenergy.2020.115392>.

EUROTHERM2023-F202

## Experimental characterization of a PCM-heat exchanger: Impact of PCM properties on comparison metrics

Ryan L. Callaghan, Dominic Groulx

Dalhousie University, Halifax, Nova Scotia, Canada, Phone: +1 902 494-8835  
e-mail: dominic.groulx@dal.ca

### Abstract

This paper presents a research plan related to an on-going research project in the authors' lab looking at the characterization of Phase Change Material (PCM)-based Thermal Energy Storage (TES) systems towards an effort to create comparison metrics, and performance indicators, which isolate the system characteristics related to PCM behaviour and properties. This paper identifies a gap in research related to the impact of PCM properties on the operation of a given system and aims to isolate this impact experimentally to define the role of PCM properties on the possible system's comparative metrics. The overarching goal of this line of research is to create design rules for PCM TES systems and help facilitate their acceptance and usage in consumer markets. The paper outlines a research plan to perform a comparative analysis of a TES system behaviour using two different PCMs and the experimental setup for the study. The parameters affecting system's performance will be kept constant to isolate the PCM characteristics that impact the design characteristics of the PCM TES system.

**Keywords:** Phase Change Materials (PCMs), PCM-Based Thermal Storage, Heat exchanger, Comparative Experimental Characterization, Comparison Metrics

### 1. Introduction

Phase Change Material (PCM)-based Thermal Energy Storage (TES) is a subject of rapidly evolving research. This research has branched off into many directions including studying the effects of nano-enhanced PCM [1, 2], container geometry for heat exchangers [3], as well as analysis of tubes and fins in heat exchangers [4, 5]. All of these studies are centered by the underlying understanding that PCM offers increased storage capability for TES applications which can yield energy savings using load management and peak shaving techniques [3, 6]. While recent research directions point towards optimized heating systems integrated with PCM TES systems. Future trends of PCM-based research are pointing towards potential application development like refrigeration applications or the use of PCM in evaporators [7]. A gap in the literature, which has not made it to lists of future research [7] yet is the impact of the PCM and its physical properties on the operation of a given TES system, with respect to the optimization of the PCM-TES device itself, and their impact on the determination of comparison metrics, performance indicators and design rules.

With a PCM-heat exchanger, the choice of PCM can sometimes be as important as the choice of geometry in the pursuit of optimizing the heat transfer characteristics. Also, in defining a PCM-TES system, PCM properties can be used to help define design parameters for the system. In 2014 Barreneche *et al.* [8] attempted to build a database of PCM characteristics, most of which were taken from the IEA's summary on PCM [9]. Apart from this, there is very little research into the comparative metrics of different PCM properties and their effects on the power and energy storage (the significant design characteristics) of PCM-TES systems.

Using the geometry and size of the system as constants, this research isolates the PCM specifically in order to define comparative metrics based solely on the impact of different PCMs so that performance indicators for PCM-TES systems can be developed relating specifically to the PCM selection alone.



This extended abstract will present the research plan and methodology for such a research project that is currently underway. Preliminary research results will be presented at the conference.

## 2. Material Selection

A comparative analysis will be performed using a PCM-TES system. The heat exchanger geometry will remain constant for the duration of the experiments, while the type of PCM used will be varied in order to obtain experimental results for multiple PCMs. The first PCM selected for this comparative analysis is dodecanoic acid. Its properties can be seen in Table 1. The second PCM selected is currently being determined. In order to clearly identify any trends that may be observed from this experimental study, the properties of this second PCM should be as different as possible from the dodecanoic acid properties while having a melting point between 25-65°C which can be accommodated by the experimental setup. Keeping PCMs with properties that are too similar will wash out any possible differences in the results.

Table 1. Thermophysical properties of dodecanoic acid

Properties	Dodecanoic Acid
Density (solid)	930 ± 20 kg/m <sup>3</sup>
Density (liquid)	885 ± 20 kg m <sup>3</sup>
Heat capacity (solid)	2.4 ± 0.2 kJ/kg·K
Heat capacity (liquid)	1.95 ± 0.03 kJ/kg·K
Thermal conductivity (solid)	0.150 ± 0.004 W/m·K
Heat of fusion	184 ± 9 kJ/ kg
Melting temperature	43.0 ± 1.5 °C

## 3. Experimental methodology

A diagram of the experimental setup can be seen in Fig. 1. This figure shows a water bath which is both the heater and chiller for the heat transfer fluid (HTF). The bath also contains a pump which pumps HTF into the heat exchanger through *Hot Side* tubing (in red on the figure). Temperature measurements of the HTF are made at the inlet and outlet of the PCM-TES system and a  $\Delta T$  is obtained from this for the HTF. The water then exits the heat exchanger containing the PCM via the *Cold Side* tubing (in blue) and is returned to the bath for reheating/cooling.

Data will be gathered based on the experimental results will be used to calculate the power exchanged from the HTF to and from the system:

$$\dot{Q} = \dot{m}c_p\Delta T \quad (1)$$

And total energy stored or recovered will be calculated by numerically integrating power over time.

In order to allow for the study of comparison of PCM metrics and the development of performance indicators focusing on the impact of the PCM and its properties, all variables which affect the system's performance, such as geometry, flow rate, insulation and heat loss, are kept constant or accounted for through assumptions. This allows for the isolation of the PCM characteristics which impact the design characteristics of the PCM-TES system.

Figure 2 shows two different types of charging and discharging experiments based on defined temperatures (initial and final/HTF temperatures) which are the only significant design variables changed for the entirety of the experiments (beyond performing tests with two different PCMs). The flowrate will be kept constant, and the geometry of the heat exchanger also will remain the same for both sets of experiments.

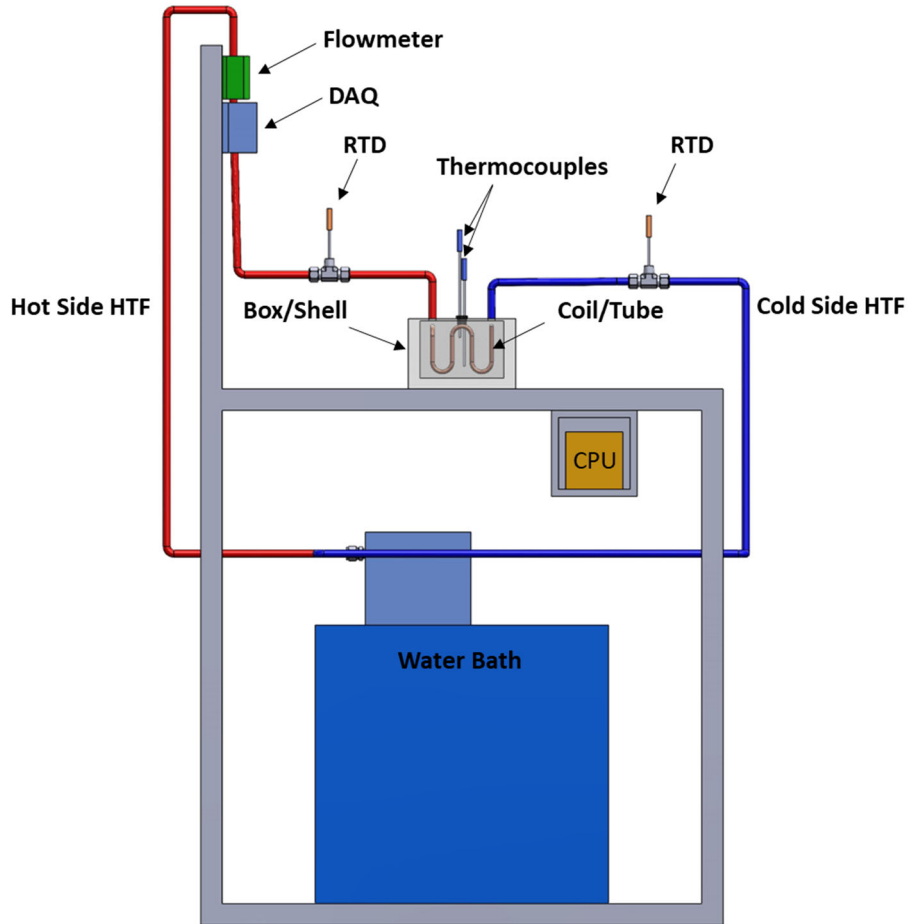


Fig. 1. Schematic representation of the experimental setup.

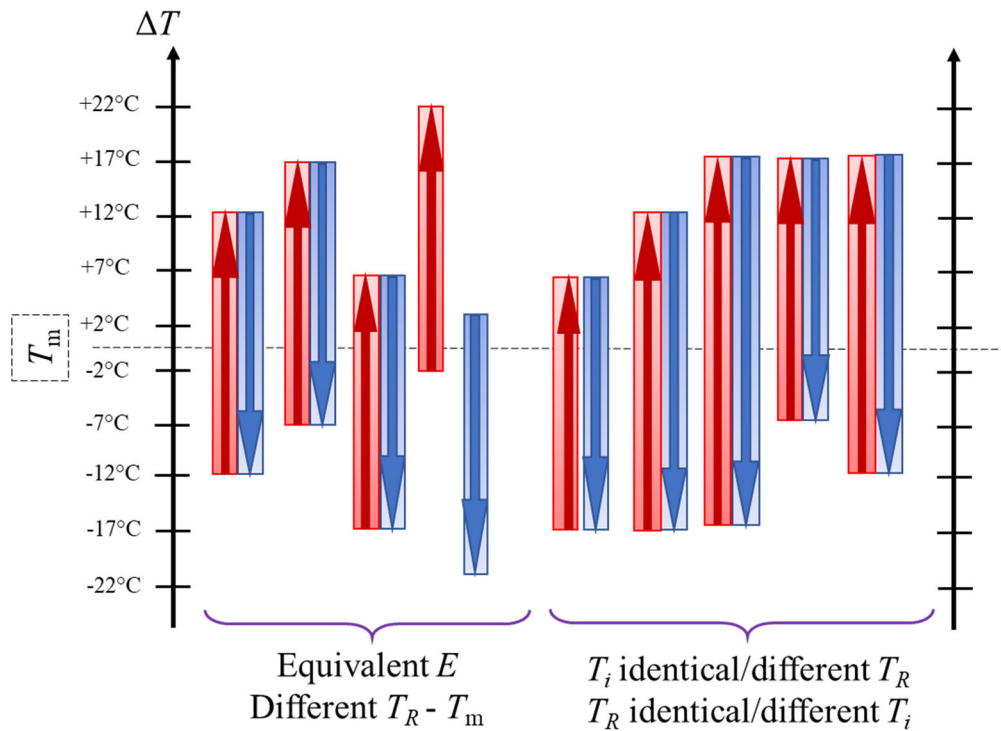


Fig. 2. Temperatures for charging and discharging experimental trials in relation to the PCM melting temperature.

The first type of trials is to be done with a constant temperature change between initial PCM temperature and final HTF temperature. So, each trials have equivalent energy stored by the PCM (both from latent and sensible sources). The second set of experiments consist of trials with equal initial temperatures (for both charging and discharging) but different final HTF temperature. The choice of using predefined initial and final temperatures is made to characterize the system based on these parameters.

Since both PCMs will more than likely have different melting temperatures, the initial and final temperatures for each characterization experiment, as defined through Fig. 2, is determined as a temperature differential to the melting point for each given PCM.

The experimental procedure for each individual trial should be to first, initialize the PCM temperature by turning on the water bath to the correct initial temperature and pumping HTF through the heat exchanger until it is reached. Once the PCM is at the initial temperature (verified using the thermocouples embedded in the PCM) the water bath will be changed over from the main loop to the heat exchanger to the bypass loop using valves. The water bath will be then set to the final temperature, allowing all of the HTF to reach the final temperature within the bypass loop. Once the HTF has reached the final temperature, the valves are changed back to the main loop and simultaneously the LabVIEW program is started, recording the data. Once it is ensured that the PCM has reached the final temperature (by measuring the PCM temperature using the thermocouples) and verifying the system is now at steady state (through a constant power exchange over time), the trial being complete, the system is prepared for the next experimental run, essentially starting back at the top of this list.

Results from this work will be used to continue the development of comparison metrics, with an eye towards design rules, as previously done in the author's lab [10, 11].

## References

- [1] Kalbande, V.P., Fating, G., Mohan, M., Rambhad, K., Sinha, A.K., "Experimental and theoretical study for suitability of hybrid nano enhanced phase change material for thermal energy storage applications," *Journal of Energy Storage*, 51, 104431, (2022).
- [2] Khedher, N.B., Bantan, R.A., Kolsi, L., Omri, M., "Performance investigation of a vertically configured LHTES via the combination of nano-enhanced PCM and fins: Experimental and numerical approaches," *International Communications in Heat and Mass Transfer*, 137, 106246, (2022).
- [3] Punniakodi, B.M.S., Senthil, R., "A review on container geometry and orientations of phase change materials for solar thermal systems," *Journal of Energy Storage*, 36, 102452, (2021).
- [4] Patel, S., Tasnim, S.H., Mahmud, S., "Phase Change Process inside Toroidal Tube Heat Exchanger with Internal Fins," *Journal of Energy Storage*, 48, 103695, (2022).
- [5] Rahimi, M., Ranjbar, A., Ganji, D., Sedighi, K., Hosseini, M., Bahrapoury, R., "Analysis of geometrical and operational parameters of PCM in a fin and tube heat exchanger," *International Communications in Heat and Mass Transfer*, 53, pp. 109-115, (2014).
- [6] Xu, T., Humire, E.N., Chiu, J.N., Sawalha, S., "Latent heat storage integration into heat pump based heating systems for energy-efficient load shifting," *Energy Conversion and Management*, 236, 114042, (2021).
- [7] Mselle, B.D., Zsembinszki, G., Borri, E., Vérez, D., Cabeza, L.F., "Trends and future perspectives on the integration of phase change materials in heat exchangers," *Journal of Energy Storage*, 38, 102544, (2021).
- [8] Barreneche, C., Navarro, H., Serrano, S., Cabeza, L.F., Fernández, A.I., "New database on phase change materials for thermal energy storage in buildings to help PCM selection," *Energy Procedia*, 57, pp. 2408-2415, (2014).
- [9] International Energy Agency, *Task 42/Annex 24 Subtask 2 PCM: On development and characterization of improved Materials*.
- [10] Herbinger, F., Groulx, D., "Experimental comparative analysis of finned-tube PCM-heat exchangers' performance," *Applied Thermal Engineering*, 211, 118532 (2022).
- [11] Callaghan, R.L., D'Oliveira, E.J., Groulx, D., Costa Pereira, S.C., "Characterization of a small-scale PCM-heat exchanger: impact of PCM selection," IHTC-17, Cape Town (South Africa), 10 p. (2023)

EUROTHERM2023-K204

## Nucleation studies of a THF-hydrate phase-change material

Hannah T. Logan<sup>1</sup>, David E. Oliver<sup>2</sup> and Colin R. Pulham<sup>1</sup>

<sup>1</sup>School of Chemistry, University of Edinburgh, UK, email: Hannah.logan@ed.ac.uk, C.R.Pulham@ed.ac.uk

<sup>2</sup>Sunamp Ltd., Macmerry, UK, email: David.Oliver@sunamp.com

### Abstract

Attractive low temperature phase change materials (PCMs) are clathrate systems, specifically THF-hydrate<sup>1</sup>. However, this system suffers from subcooling<sup>2</sup>, making integration into heat-storage systems challenging. In this work, we have explored ways of preventing the subcooling of THF-hydrate using heterogeneous nucleators. A new formulation of the 1:17 molar<sup>3</sup> THF hydrate system was developed including an aluminosilicate additive that increases the nucleation temperature from -15 °C to 2 °C. Scanning electron microscopy and thermal-cycling studies were used to ascertain the nucleation mechanism of these materials. It was found that the role of a binding agent was crucial to the material's ability to nucleate the THF-hydrate PCM. The THF hydrate system has therefore been improved to a stage where it can be implemented into heat batteries, however the mechanism of nucleation in this system is yet to be confirmed.

**Keywords:** Phase change material; THF-hydrate clathrate; nucleation; aluminosilicate.

### 1. Introduction

PCMs for refrigeration and air-conditioning applications have been of particular interest for domestic and industrial settings, requiring transition temperatures -60 °C - 20 °C<sup>4</sup>. THF-hydrate is a clathrate-hydrate that has been of interest as a PCM due to its attractive melting point of 4.4 °C and a latent heat comparable to ice of 260 kJ kg<sup>-1</sup><sup>5</sup>. The THF-hydrate clathrate is formed of THF molecules trapped in hydrogen bonded water cages. The polyhedral cages that form the structure are shown in Figure 1.

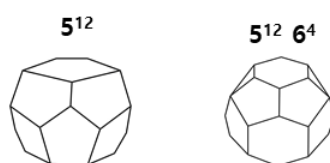


Figure 40. Cage structures present in THF clathrate; the larger 5<sup>12</sup> 6<sup>4</sup> cage contains the THF molecule.

The homogeneous freezing point of THF-hydrate was determined by Zhang *et al* as -32 °C, using DSC, sub-cooling 36.4°C below its melting point<sup>6</sup>. This is an issue for implementation of THF-hydrate as a PCM as this requires a more powerful chiller to freeze the THF-hydrate. Hence, there will be a higher energy cost to operate a chiller, lowering the efficiency of the system. Hence the aim of this research is to increase the nucleation temperature of the THF-hydrate system by investigating the use of a heterogeneous nucleator.

### 2. Materials and methods

The THF-hydrate system forms in a ratio of 1:17 moles of THF to water. The main method used to study the system is thermal cycling at a 15 ml vial scale using a Cambridge Reactor Design Polar Bear Plus.

Thermal cycling at this scale allows larger scale analysis compared to differential scanning calorimetry (DSC). This is beneficial when studying nucleation as it can mitigate poor nucleation, which is often observed at the 5 mg scale.

The THF-hydrate was doped with 1wt.% of various additives. The system was then thermally cycled between -20 °C and 15 °C to observe nucleation behavior.

The new formulation of the THF-hydrate system was also further studied using 3-layer calorimetry (3LC), DSC and powder X-ray diffraction to also understand the nucleation behavior and energy density of the optimized system.

### 3. Results and discussion

The THF-hydrate system was thermally cycled with silica (Figure 2). Sub-cooling of ~19.5 °C below the freezing point (4.4 °C) is observed for the silica and un-doped samples, thus indicating that the silica behaves no differently to the un-doped sample and is therefore not a nucleator for the THF-hydrate system.

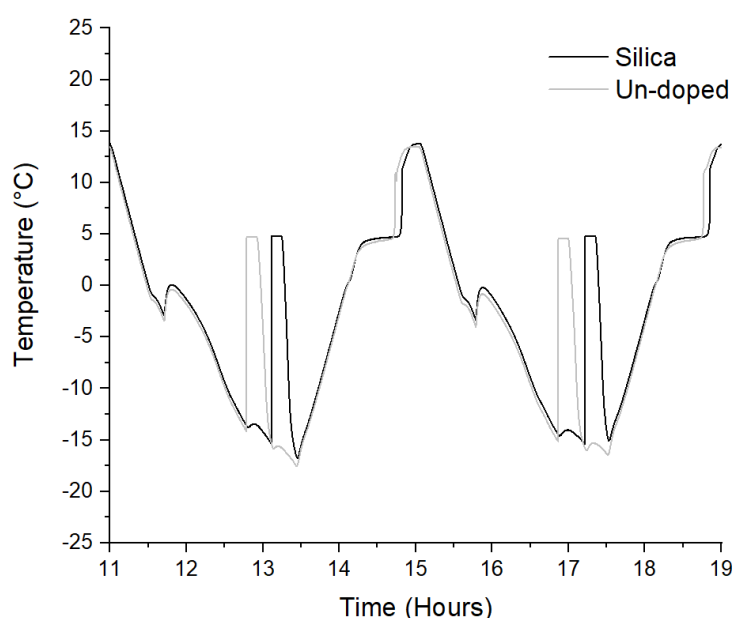


Figure 41. Thermal cycling of THF-hydrate with a silica additive between 15 °C and -20 °C.

The thermal cycling experiment was also carried out for a processed aluminosilicate pellet (Figure 3). The aluminosilicate shows sub-cooling of ~3 °C, demonstrating a significant reduction of sub-cooling with the use of this additive. Crucially, the nucleation of the THF-hydrate was raised to above 0 °C, making the material compatible with lower grade chillers. These results were repeated for other processed aluminosilicate pellets.

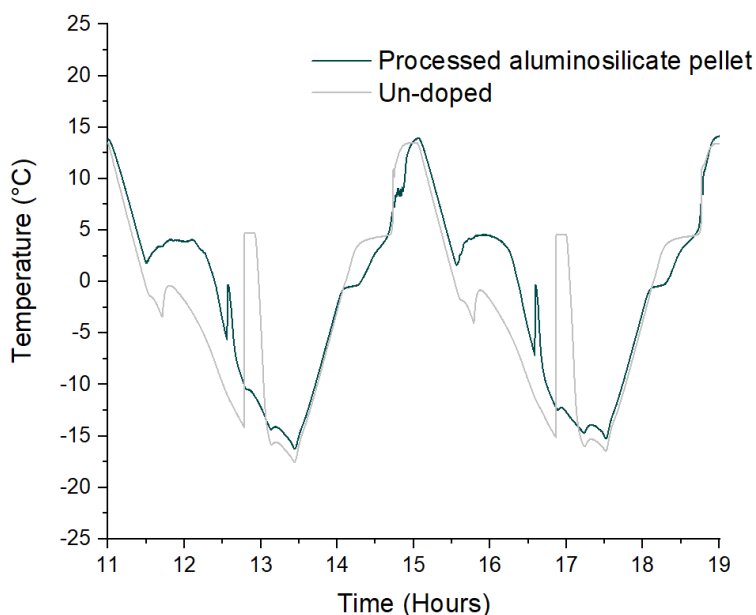


Figure 42. Thermal cycling of THF-hydrate with a processed aluminosilicate additive between 15 °C and -20 °C.

Further experiments were carried out to determine the nucleator mechanism, including degassing and surface modification of the aluminosilicate material. It was determined that the likely mechanism for nucleation is the similarity of crystal structure of the THF-hydrate and the aluminosilicate.

#### 4. Conclusions

A new series of nucleators has been discovered for the THF-hydrate system. The use of these aluminosilicate compounds as nucleators for the system allows the implementation of THF-hydrate as a PCM in refrigeration and air-conditioning applications. Attempts were made to understand the nucleation mechanism of the system. Surface modification and degassing experiments let to the conclusion that the helped determine that the mechanism for nucleation is the similarity of crystal structure. However, future work will aim to ascertain this fully.

#### References

1. E. Oró *et al*, *Applied Energy*, 2012, **99**, 513-533.
2. G. Lorsch *et al*, *Energy Conversion*, 1975, **15**, 1-8.
3. S. R. Grough and D. W. Davidson, *Can. J. Chem.*, 1971, **49**, 2691-2699
4. H. Selvnes, Y. Allouche, R. I. Manescu and A. Hafner, *Thermal Science and Engineering Progress*, 2021, **22**, 100807.
5. D. G. Leaist, J. J. Murray, M. L. Post and D. W. Davidson, *J. Phys. Chem.*, 1982, **86**, 4175–4178.
6. Y. Zhang, P. G. Debenedetti, R. K. Prud'homme and B. A. Pethica, *J. Phys. Chem. B*, 2004, **108**, 16717–16722

EUROTHERM2023-L205

## The IEA energy storage TCP Task 36 – Carnot Batteries: Three years later, where do we stand now?

Andrea Gutierrez\*, Annelies Vandersickel

German Aerospace Center, Pfaffenwaldring 38 – 40, 70569 Stuttgart Germany

\*Corresponding e-mail: Andrea.GutierrezRojas@dlr.de

### Abstract

Carnot batteries are an emerging technology for inexpensive, site-independent storage of medium- to large-scale electrical energy. During the last years the interest in such technologies increased significantly, this can be reflected on the number of publications on this topic. To discuss the potential of these technologies in the global storage scenario and push their development closer to the market, the working group Task 36 in the frame of the IEA energy storage Collaboration Program (TCP) was created. This Task was carried out for three years, from January 2020 to December 2022, and managed by the German Aerospace Center. This work presents the main themes discussed during this period of time and the results generated within this working group.

**Keywords:** Carnot Batteries; Electricity storage; Thermal energy Storage; International Network

### 1. Introduction

Carnot Batteries are an emerging technology for low-cost, location-independent electrical energy storage. They are also known as “Pumped Thermal Electricity Storage” (PTES) or as “Pumped heat storage” (PHS). A Carnot Battery transforms electricity into thermal energy, stores the thermal energy in inexpensive storage media like water or molten salt and transforms the thermal energy back to electricity when required. A simplified scheme of a generic Carnot Battery is shown in Figure 43.

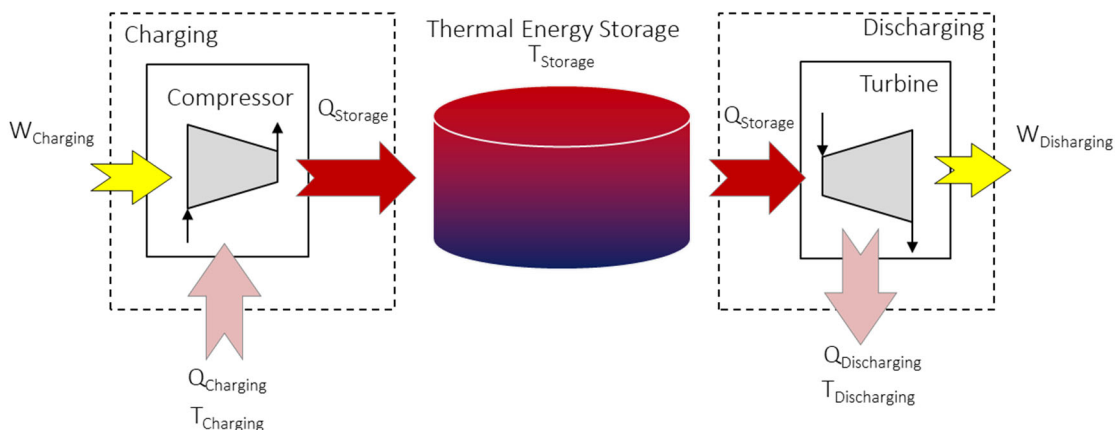


Figure 43. Schematical description of the basic principle of Carnot Battery

The charging process can be carried out by a heat pump through different thermodynamic cycles, Rankine, Brayton or others to charge the thermal energy storage system. In this case, low temperature heat e.g. waste heat, can be used to increase the efficiency of the heat pump. As an alternative, an electrical resistance can be used to charge the thermal energy storage system. The discharging process, hence, the thermal conversion to electricity can proceed through different thermodynamic cycles.

In the case of the Rankine based discharging cycles, Steam Rankine cycles, Organic Rankine Cycles and trans-critical CO<sub>2</sub> cycles can be used.

The main characteristic of the Rankine-cycle based systems is the phase transition of their storage medium or refrigerant. Thus, the latent heat thermal energy storage system fits ideally to this type of Carnot batteries.

In the case of the Brayton-cycles based systems, where a one-phase medium is used as a heat transfer fluid or refrigerant, the best fitting thermal energy storage system would be a sensible heat energy storage system.

Given that these technologies don't use any critical materials and are site independent, Carnot Batteries have the potential to solve the global storage problem of renewable electricity in an economic and environmentally friendly way.

To discuss the potential of these technologies and push their development closer to the market, the working group Task 36 in the frame of the IEA energy storage Collaboration Program (TCP) was created. This Task was carried out for three years, from January 2020 to December 2022, and managed by the German Aerospace Center.

The present communication will provide an overview of the Task 36 along with the outcomes generated during the period of execution of this working group. In addition, an overview of the technical concepts behind Carnot batteries will be presented, specially the technical aspects focused on the thermal energy storage systems will be highlighted.

## 2. Objectives and scope

The main objective of this Task was to create an international platform bringing together experts from industry and academia to systematically explore, evaluate and understand the potential role of Carnot batteries in future energy systems and to give them international visibility, which would significantly strengthen the community.

The key objectives of Task 36 were then to collect and provide information to all stakeholders. Thus, its work plan included mapping the main Carnot battery technologies, developing key performance indicators, and critically assessing technology competitiveness and R&D needs. The working group aimed to help the technology define the paths to reach maturity and to delimit its scope in the market by identifying the services that Carnot batteries should or can provide, informing policy makers and providing a basis for appropriate regulation. International dissemination of the technologies through workshops, white papers, open source datasets and scientific papers was also an important part of the work plan.

The scope of the Task was restricted to the conversion and storage of electricity in the form of thermal (sensible, latent and thermochemical) energy. Other technologies such as electrochemical and mechanical storage technologies were excluded.

## 3. Task 36 Structure and subtask descriptions

The work and discussions of the Task 36 carried out by the experts were divided into five different Subtasks, as shown in Figure 44. Subtask 0 was responsible of deliberate on the definitions of the Carnot batteries, their configurations and what requirements have to be meet to define a concept as a Carnot Battery. Subtask A, B and C had a scientific oriented perspective and were responsible of collecting the information available on existing Carnot Batteries in the respective categories, as well as components that fit to the respective concepts. Finally, the Participants in these three subtasks were also focused on collecting the modelling and simulation tools to analyze the components and systems in each of the categories. Finally, the Subtask D, was responsible of analyzing the current scenario for such technologies and generate recommendation in the policy and market area to help pushing these technologies to a further degree of development.



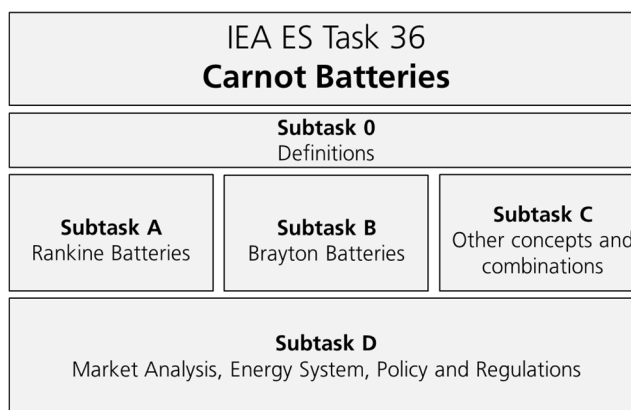


Figure 44. Structure of the Task 36 - Carnot Batteries

#### 4. Status of participation

The subtask began with a pre-definition phase consisting of two meetings in 2019. During these two meetings the goals, scope, structure and expected outcomes were defined. After this phase the proposal was submitted to the ES TCP Executive Committee and the Task was officially approved to begin in January 2020. The number of institutions and countries that participated in the Task 36 during the whole period, pre-definition phase and official phase, increased over the years. Growing 28 institutions from 9 Country members that attended the first definition meeting to about 50 institutions from 16 country members (out of 19), which attended the 6<sup>th</sup> expert workshop in September 2022 in Stuttgart, Germany (see Figure 45).

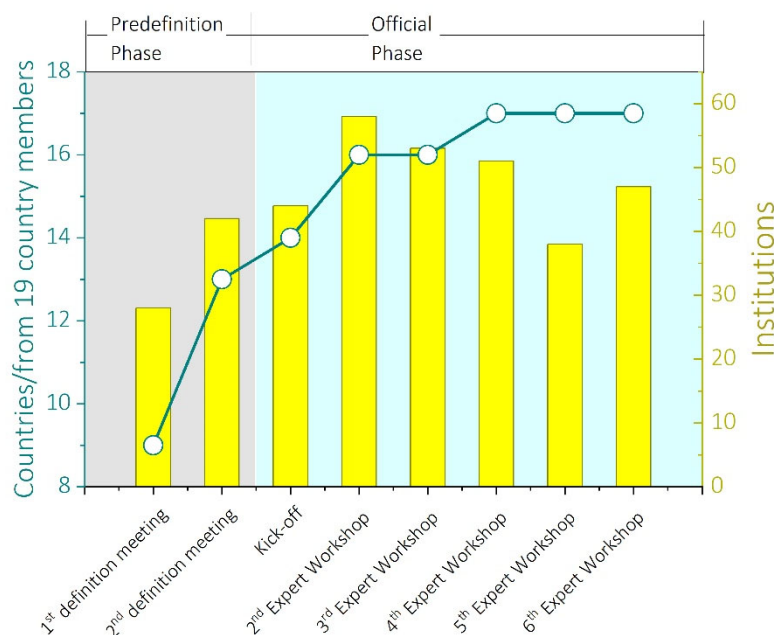


Figure 45. Attendance to the Task 36 during the pre-definition phase and official phase, categorized as countries and institutions

By the end of the Task 36, 61 Institutions from 16 country members officialized their participation in the Task 36. This generated a platform with more than 100 contacts across the world, coming from universities, private companies and governmental agencies.

## 5. Main outcomes and results

The Task 36 working group was very active and generated several outcomes, such as white papers and fact sheets on the existing Carnot Batteries and their components, among others. The Outcomes were classified by Subtasks and are summarized in the Table 16.

Table 16. List of outcomes generated within the Task 36

<b>Main Outcome: Final Report of the Task 36 on Carnot Batteries</b>	
Subtask	Specific outcomes
0	<ul style="list-style-type: none"> <li>• Key performance indicator of:               <ul style="list-style-type: none"> <li>○ Carnot Batteries</li> <li>○ Components</li> <li>○ Materials</li> </ul> </li> <li>• White Paper on State of the Art of Carnot Batteries</li> <li>• White paper on available Thermal energy storage Technologies for Carnot Batteries</li> <li>• Wikipedia page on Carnot Batteries (available in 9 languages)</li> </ul>
A/B/C	<ul style="list-style-type: none"> <li>• In depth analysis of Carnot batteries:               <ul style="list-style-type: none"> <li>○ Technical description of each type of carnot battery</li> <li>○ Summary of available Carnot Batteries to date, commercial and at pilot plant scale</li> <li>○ Simulation and modelling tools for Carnot batteries and they components</li> <li>○ TRL assessment of available Carnot Batteries</li> <li>○ R&amp;D need report</li> </ul> </li> </ul>
D	<ul style="list-style-type: none"> <li>• Report on Market Analysis, Energy System, Policy and Regulations               <ul style="list-style-type: none"> <li>○ Assessment of barriers to deployment</li> <li>○ Policy recommendations</li> </ul> </li> </ul>

EUROTHERM2023-D206

## Development of protective coatings for lithium/sodium sulfate salts intended for high-temperature thermal energy storage

Angel Serrano<sup>1</sup>, Ricardo M. Silva<sup>2</sup>, María Taeño<sup>1</sup>, Luis González<sup>1</sup>, Rui F. Silva<sup>2</sup>, Elena Palomo del Barrio<sup>1,3</sup>

<sup>1</sup> Centre for Cooperative Research on Alternative Energies (CIC energiGUNE), Basque Research and Technology Alliance (BRTA), Alava Technology Park, Albert Einstein 48, 01510 Vitoria-Gasteiz, Spain, e-mail: aserrano@cicenergigune.com

<sup>2</sup> CICECO - Aveiro Institute of Materials and DEMaC - Department of Materials and Ceramic Engineering, University of Aveiro, 3810-193 Aveiro, Portugal  
e-mail: rmsilva@ua.pt and rsilva@ua.pt

<sup>3</sup> Ikerbasque, Basque Foundation for Science, 48013 Bilbao, Spain  
Email: epalomo@cicenergigune.com

### Abstract

Lithium/sodium sulfate system is a promising material intended for high-temperature thermal energy storage based on solid-state reactions. Despite their great advantages, their application in the field of thermal storage is very recent, so crucial aspects that would allow their jump to the energy market have not yet been solved. Due to the novelty of these materials, their compatibility with the main heat transfer fluid (nitrate-based molten salts such as Hitec XL) has not been addressed to date. The present work tackles this problem through the in-situ formation of protective carbonate coatings. The coating formation process relies on an initial carbon film deposition via thermal chemical vapor deposition (T-CVD) catalyzed by nickel (Ni). In the second stage, the carbonate coating is in-situ created by direct contact with the molten salt.

**Keywords:** Lithium/sodium sulfate, solid-state, molten salt, Hitec XL, coatings.

### 1. Introduction

Among the various thermal storage options, the novel development of solid-state reactions for high-temperature storage presents potential advantages over current systems [1]. This concept allows the design of compact and low-cost systems consisting of a single tank without using a costly heat exchanger.  $\text{Li}_2\text{SO}_4\text{-Na}_2\text{SO}_4$  is a promising system for solid-state thermal energy storage (TES) in the 400-600°C temperature range [2]. This system shows an unusual phase transition enthalpy (up to  $\approx 320$  J/g) and high specific heat (1.6-2.2 J/g·K) and thermal conductivity (2.3 W/m·K). They have also been subjected to various durability tests (e.g. prolonged thermal cycling) which they have successfully passed, even in contact with air.

One of the main advantages of solid-state systems is the possibility of using them in direct contact with the heat transfer fluid. In their working temperature range (400-600°C), the main heat transfer fluids are molten salts, mainly nitrates such as Hitec XL (42wt%  $\text{Ca}(\text{NO}_3)_2$ -15wt%  $\text{NaNO}_3$ -43wt%  $\text{KNO}_3$ ) and HITEC (53wt%  $\text{KNO}_3$ -40wt%  $\text{NaNO}_2$ -7wt%  $\text{NaNO}_3$ ) salts. These salts are nitrate-based, and therefore, compatibility with sulfate-based storage systems through direct contact is still a challenge to be solved.

Thus, to implement these novel materials in the high-temperature energy storage market, this work addresses the development of protective coatings for lithium/sodium sulfate salts against nitrate-based molten salts. Previous works focused on anticorrosion methods for steel showed that, in direct contact with molten nitrate salt, the presence of graphite forms a carbonate phase that reduces the corrosion rate [3]. Therefore, the present work explores the viability of this concept, taking advantage of this reaction between carbon and nitrates to achieve the in-situ formation of the protective carbonate layer. The

coating formation process consists of an initial deposition of carbon on the sulfate surface using thermal chemical vapor deposition (T-CVD). In the second stage, the carbonate coating is created by direct contact with the molten salt.

## 2. Materials and methods

The proof of concept is conducted on the stoichiometric LiNaSO<sub>4</sub> system, for which the casting and cold sintering processing techniques are initially compared. For this purpose, the microstructure (SEM), thermal properties (DSC), and mechanical strength of LiNaSO<sub>4</sub> pellets processed with these techniques are evaluated.

*Carbon deposition by T-CVD:* Successful deposition requires temperatures below the sulfate transition temperature. This has been possible by performing a first physical nickel deposition (PVD), which acts in a second stage as a catalyst for the carbon from acetylene, thus being possible to process a homogeneous carbon layer by T-CVD at 480°C for 12 minutes. The layer thus formed has been characterized by Raman spectroscopy and high-resolution SEM.

*Hitec XL-carbon reaction in an inert atmosphere:* To evaluate the behavior of the carbon layer in the presence of Hitec XL, a molten salt drop was placed on the surface of the carbon-coated sulfate pellet. To better monitor the process, parallel experiments were carried out with control samples without carbon layer. The materials were subjected to 310°C in an inert atmosphere (Argon). After the reaction period, the results were evaluated by Raman, Infrared (FITR), X-ray diffraction (XRD), SEM of the surface and cross-section, and energy dispersive spectroscopy (EDS).

*Immersion test:* to determine the protective action of the created coating, the coated samples were immersed in Hitec XL at 550°C for 100 h.



Figure 46. PVD (left) and CVD (right) devices (DEMaC facilities) and comparison of LiNaSO<sub>4</sub> pellets before and after the deposition process [4].

## 3. Results and discussion

### 3.1. LiNaSO<sub>4</sub> processing and carbon deposition

The specimens obtained exhibited a reaction enthalpy of 160 J/g with an initial transition temperature of 520°C and no subcooling. Between these two processes, cold sintering is of greater interest, since its production involves lower energy consumption (200°C vs. 650°C), in addition to obtaining pieces with a higher density and superior mechanical properties than the casting process.

In relation to the initial formation of a carbon layer, the deposition of carbon nanotubes on the surface of LiNaSO<sub>4</sub> via T-CVD has been successfully accomplished. This carbon deposition has been achieved at 480°C for 12 min, supported by catalysis from nickel particles. As can be seen in Figure 2, the film created is homogeneous, about 2-3 microns thick, covering the entire surface roughness of the substrate.

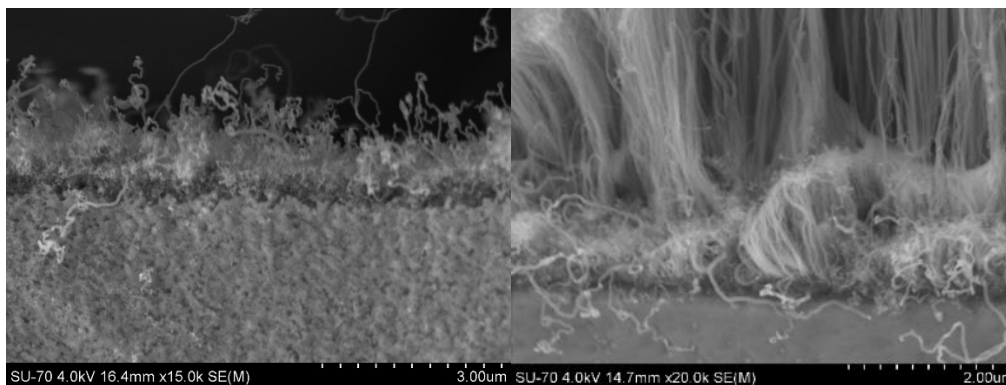


Figure 47. Cross-section of LiNaSO<sub>4</sub> pellet coated by carbon nanotubes.

### 3.2. In-situ formation of carbonate

To initially verify the reaction between carbon and nitrates, the carbon deposition was performed on silicon as a substrate. This test allowed the carbonate formation process to be monitored, isolating the effect of the molten salt and carbon from the presence of sulfates. The results (Figure 3) confirm the replacement of the initial carbon layer by a homogeneously deposited carbonate-based layer.

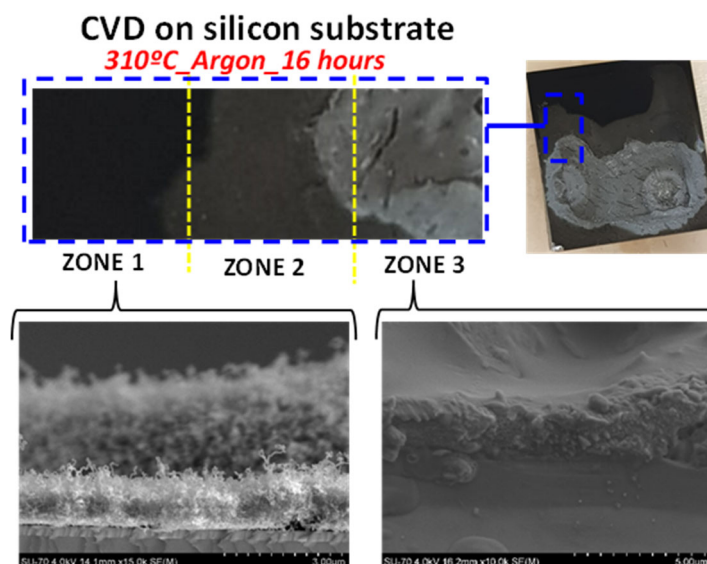


Figure 48. Hitec XL-carbon layer interaction (310°C, 16 hours in Argon).

In a next step, the formation of carbonates has been tested directly on carbon-coated LiNaSO<sub>4</sub> tablets under the previously defined conditions (310°C, 16 h in Argon). FTIR, XRD and Raman of the samples demonstrated that this reaction consumes carbon nanotubes to form some kind of carbonate or mixture of carbonates (CaCO<sub>3</sub>, K<sub>2</sub>CO<sub>3</sub>, K<sub>2</sub>Ca(CO<sub>3</sub>)<sub>2</sub>) with the potential capacity to protect sulfates against molten salts.

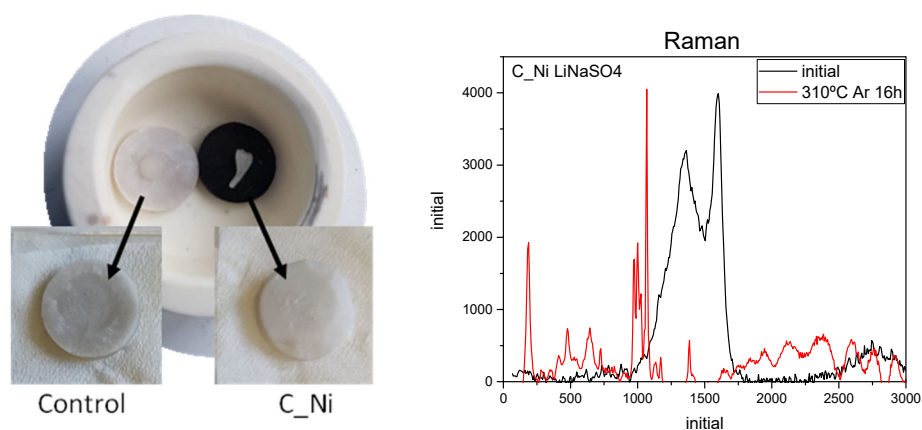


Figure 49. Images of LiNaSO<sub>4</sub> pellets (control and coated sample) before and after the test with molten salt (left). Raman spectra of the coated sample (right).

The immersion tests carried out for 100 hours confirm the formation of carbonates, however, although promising, the results indicate that the homogeneity and stability of the protective layer formed under immersion conditions need to be improved to obtain full protection of the system.

### 3. Conclusions

The use of carbon coatings on sulfates as promoters of in-situ protective layer in contact with molten salts has been demonstrated. Further efforts are required to improve the homogeneity, densification, and stability of the carbonate coating.

The achievement of this protection would allow the use of these materials in the demanding working conditions of final applications, representing a disruptive leap in the field of thermal energy storage at high temperatures (450-600°C).

### Acknowledgements

Ángel Serrano acknowledges the financial support of the Ministry of Universities of the Spanish Government through the mobility grant “José Castillejo” (CAS21/00079).

### References

- [1] S. Doppiu, J.L. Dauvergne, E.P. Del Barrio, Solid-state reactions for the storage of thermal energy, *Nanomaterials*. 9 (2019). <https://doi.org/10.3390/nano9020226>.
- [2] S. Doppiu, J.-L. Dauvergne, A. Serrano, E. Palomo del Barrio, The Li<sub>2</sub>SO<sub>4</sub>–Na<sub>2</sub>SO<sub>4</sub> System for Thermal Energy Storage, *Materials (Basel)*. 12 (2019) 3658. <https://doi.org/10.3390/ma12223658>.
- [3] Y. Grosu, U. Nithiyantham, A. Zaki, A. Faik, A simple method for the inhibition of the corrosion of carbon steel by molten nitrate salt for thermal storage in concentrating solar power applications, *Npj Mater. Degrad.* 2 (2018). <https://doi.org/10.1038/s41529-018-0055-0>.
- [4] I.E. Oliveira, R.M. Silva, A. V. Girão, J.L. Faria, C.G. Silva, R.F. Silva, Facile Preparation of ZnO/CNTs Nanocomposites via ALD for Photocatalysis Applications, *Eur. J. Inorg. Chem.* 2020 (2020) 1743–1750. <https://doi.org/10.1002/ejic.202000032>.

EUROTHERM2023-J208

## Proof of concept of a bio-inspired heat exchanger for heat transfer enhancement in thermal energy storage systems

Emiliano Borri, Gabriel Zsembinszki, Sara Risco, Edgar F. Rojas Cala, Nadiya Mehraj, Carles Mateu, Ramon Bejar, David Vérez, Luisa F. Cabeza

GREiA Research Group, University of Lleida, Pere de Cabrera s/n, 25001-Lleida, Spain, Phone: +34 973 003576, e-mail: luisaf.cabeza@udl.cat

### Abstract

The increase of heat transfer between the storage medium and the working fluid is one of the key challenges in the design of thermal energy storage systems, especially when using phase change materials, which are characterized by low thermal conductivity. The use of optimized fins represents a well-established technique already extensively investigated in the literature. Recent trends are focused on the use of innovative approaches, including bio-inspired geometries, which have the potential to further increase the heat transfer. This study shows a preliminary proof of concept of a bio-inspired heat exchanger that implements the hierarchical structure present in circulatory systems of living beings in the design and distribution of the pipes. Future work will focus on strengthening the proof of concept with preliminary numerical analysis and the manufacturing and testing of a lab-scale prototype.

**Keywords:** thermal energy storage; heat transfer enhancement; bio-inspired solutions; phase change materials; genetic algorithms.

### 1. Introduction

The use of thermal energy storage (TES) in energy systems was proven to be an effective way to integrate the use of renewables, increase the system generation capacity, and decrease the operation cost. Nevertheless, the design of efficient thermal energy storage components able to maximize the process of charging, discharging, and storing thermal energy is the key challenge which has stimulated in recent years researchers and industry to develop innovative TES solutions. Indeed, some of the TES materials, especially those involving phase changes (i.e. phase change materials - PCM) suffer from low thermal conductivity, which limits the charging and discharging power of the storage devices, thus being inefficient in terms of heat transfer between the storage material and the heat transfer fluid (HTF). In the literature, different techniques were proposed to enhance the heat transfer in TES technology. When shell and tube configurations are adopted, the most common technique is to increase the heat transfer surface area by the use of fins [1–3]. Different studies available in the literature propose to optimize the shape and distribution of fins inside the TES. In this direction, one recent trend in the design of heat exchangers is to implement bio-inspired geometries in order to increase the heat transfer. In this case, fins and components are designed inspired by nature that define functional behaviors of animals and plants. Bio-inspired heat exchangers for energy systems were already proposed by different authors. Yu et al. [4] numerically investigated the performance of a latent heat TES with tree-like fins. Sheikholeslami et al. [5] numerically investigated a novel fin configuration based on snowflake crystal structure applied to a TES with phase change materials. The concept proposed in this paper presents a heat exchanger with a bio-inspired pipes design to be used as a TES.

## 2. Thermal energy storage concept

The heat exchanger concept proposed in this study is inspired by the hierarchical structure present in the circulatory system of living beings in the design and distribution of the pipes. In nature, hierarchical bifurcating flow passages, such as tree-like and leaf-like networks, are able to both reduce pressure drops and increase the heat transfer surface area compared to traditional parallel flow heat exchangers [6,7]. The use of branching networks and fractal-like geometries inspired by nature already attracted interest in the field of electronics, including micro-channels cooling techniques and heat sinks [8,9]. In this case, the concept is applied to a thermal energy storage (TES) system using phase change materials to overcome the drawback of low thermal conductivity that these materials present (Figure 1).

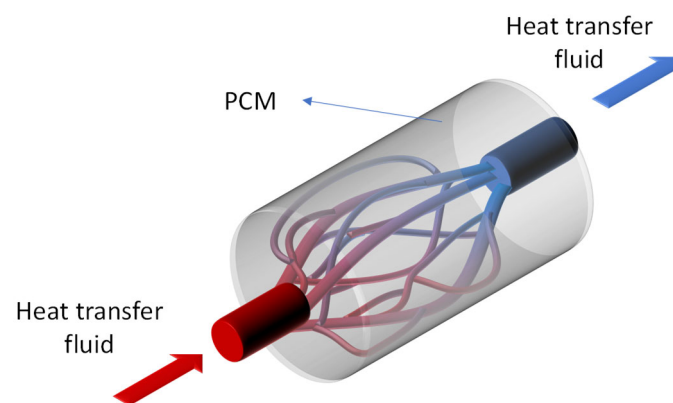


Figure 8. Concept of TES based on bio-mimetic geometry

The heat transfer fluid enters a main tube connected to the heat (or cold) source. The tube is then divided into smaller tubes following a hierarchical structure. The minimum diameter of tubes should guarantee minimum pressure losses to limit the pumping work of the heat transfer fluid. In this concept, phase change materials can be included in the shell. The optimized fractal distribution of the tubes will be designed to maximize the heat transfer area between the storage medium and the heat transfer fluid.

## 3. Future work

Future work will focus on strengthening the proof of concept with preliminary numerical analysis and the realization and testing of a lab-scale prototype. The distribution and geometry of the pipes will be optimized with the use of numerical tools and optimization algorithms, which will represent the next step.

## Acknowledgments

This work was partially funded by the Ministerio de Ciencia e Innovación - Agencia Estatal de Investigación (AEI) (PID2021-123511OB-C31 - MCIN/AEI/10.13039/501100011033/FEDER, UE), and Ministerio de Ciencia e Innovación - Agencia Estatal de Investigación (AEI) - NextGeneration EU (TED2021-129462B-I00 - MCIN/AEI/10.13039/501100011033/ NextGenerationEU/PRTR). This work is partially supported by ICREA under the ICREA Academia programme. The authors would like to thank the Departament de Recerca i Universitats of the Catalan Government for the quality accreditation given to their research group (2021 SGR 01615). GREiA is certified agent TECNIO in the category of technology developers from the Government of Catalonia.



## References

- [1] Gasia J, Maldonado JM, Galati F, de Simone M, Cabeza LF. Experimental evaluation of the use of fins and metal wool as heat transfer enhancement techniques in a latent heat thermal energy storage system. *Energy Convers Manag* 2019;184:530–8.  
<https://doi.org/10.1016/j.enconman.2019.01.085>.
- [2] Gharebaghi M, Sezai I. Enhancement of Heat Transfer in Latent Heat Storage Modules with Internal Fins. *Numerical Heat Transfer* 2008;53:749–65.  
<https://doi.org/10.1080/10407780701715786>.
- [3] Sciacovelli A, Gagliardi F, Verda V. Maximization of performance of a PCM latent heat storage system with innovative fins. *Appl Energy* 2015;137:707–15.  
<https://doi.org/10.1016/j.apenergy.2014.07.015>.
- [4] Yu C, Wu S, Huang Y, Yao F, Liu X. Charging performance optimization of a latent heat storage unit with fractal tree-like fins. *J Energy Storage* 2020;30:101498.  
<https://doi.org/10.1016/j.est.2020.101498>.
- [5] Sheikholeslami M, Lohrasbi S, Ganji DD. Numerical analysis of discharging process acceleration in LHTESS by immersing innovative fin configuration using finite element method. *Appl Therm Eng* 2016;107:154–66.  
<https://doi.org/10.1016/j.applthermaleng.2016.06.158>.
- [6] Calamas D, Baker J. Performance of a biologically inspired heat exchanger with hierarchical bifurcating flow passages. *J Thermophys Heat Trans* 2013;27:80–90.  
<https://doi.org/10.2514/1.T3950>.
- [7] Wang XQ, Xu P, Mujumdar AS, Yap C. Flow and thermal characteristics of offset branching network. *International Journal of Thermal Sciences* 2010;49:272–80.  
<https://doi.org/10.1016/j.ijthermalsci.2009.07.019>.
- [8] Huang Z, Hwang Y, Radermacher R. Review of nature-inspired heat exchanger technology. *International Journal of Refrigeration* 2017;78:1–17.  
<https://doi.org/10.1016/j.ijrefrig.2017.03.006>.
- [9] Werner DH, Ganguly S. An overview of fractal antenna engineering research. *IEEE Antennas Propag Mag* 2003;45:38–57.

EUROTHERM2023-N209

## Design of an experimental set-up for testing a new high temperature thermal energy storage unit using concrete

Gabriel Zsembinszki, J. Ramon Castro, Alba Bravo, David Vérez, Luisa F. Cabeza

GREiA Research Group, University of Lleida, Pere de Cabrera s/n, 25001-Lleida, Spain, Phone: +34 973 003576, e-mail: luisaf.cabeza@udl.cat

### Abstract

The use of concrete as thermal energy storage (TES) material for concentrating solar power (CSP) plants presents a great potential because of its versatility, relatively low cost, and the possibility to reach high operating temperatures, which allows increasing the plant efficiency. However, current configurations based on concrete have several drawbacks, such as issues during the manufacturing on-site, different thermal expansion coefficients between concrete and pipes, and poor thermal conductivity of concrete. In order to address such challenges, this study investigates a new thermal energy storage concept using concrete as storage material, which relies on three main pillars: modularity, improved concrete formulation, and the lack of pipes inside the concrete. Moreover, an experimental set-up was designed to perform thermal cycling tests with the concrete formulation to be used in the new storage concept.

**Keywords:** Thermal energy storage, sensible TES, concrete, CSP, modular concept, thermal cycling

### 1. Introduction

Solar energy is today the main renewable energy source for both thermal and electric power generation. One of the main large-scale technologies to convert solar energy into electricity is represented by concentrating solar power (CSP) plants. According to REN21, the total capacity installed in 2020 worldwide was 6.2 GWe [1]. To deal with the intermittency of solar radiation availability, thermal energy storage (TES) is an essential component. Current CSP technologies mainly rely on the use of molten salts as TES material, which has some drawbacks such as corrosion issues and limited maximum operating temperature (up to 560 °C). This has a negative effect on both the global performance and cost of the CSP plants. The use of concrete as TES material is a viable option due to its versatility, relatively low cost, and the possibility to reach a higher operating temperature compared to molten salts. One of the first storage concepts using concrete was developed by DLR and tested in Plataforma Solar de Almeria. Blast furnace cement was used with iron oxides, flue ash, and auxiliary materials. The system used thermal oil as heat transfer fluid (HTF) flowing through an array of pipes (tube register) embedded in the storage material [2]. Another concept, EnergyNest, developed and tested a 2-modules TES of 500 kW<sub>th</sub> storage capacity, based on a modular design and using concrete as a storage material, able to resist to temperatures up to 400 °C [3]. Although concrete has a high potential for TES storage, there are still some challenges related to this technology that need to be addressed. This study investigates a novel concept of TES unit using concrete in a modular design proposed to improve the currently available configurations.

### 2. Challenges of current concrete tank concepts

Nowadays, TES tanks using concrete show different drawbacks that need to be overcome to ensure concrete TES deployment. Such drawbacks are:

- (i) Difficulties in the on-site production of concrete tanks, which is influenced by weather conditions (such as humidity).

- (ii) Different values of the thermal expansion coefficients of concrete and metal pipes where the HTF flows.
- (iii) In the first charging process, the water contained in the concrete evaporates, which can cause cracks that can induce immediate or long-term breakage.
- (iv) Poor thermal conductivity of concrete.
- (v) Limited maximum operation temperature of the HTF (e.g., thermal oil, molten salts).
- (vi) If no pipes are used for the HTF flowing in the concrete tank, migration of the HTF into the concrete can occur, which can induce breaking of the concrete tank (i.e., solidification of molten salts) or contamination of the HTF by concrete.

### 3. New concept proposal

To address the challenges presented in the previous section, a new concrete TES design was developed. In the new concept, air is used as HTF, and the design of the TES unit is modular, containing hexagonal concrete blocks of 460 mm diameter and 2000 mm height (Figure 35) with simple direct-fit male-female connections (Figure 36).

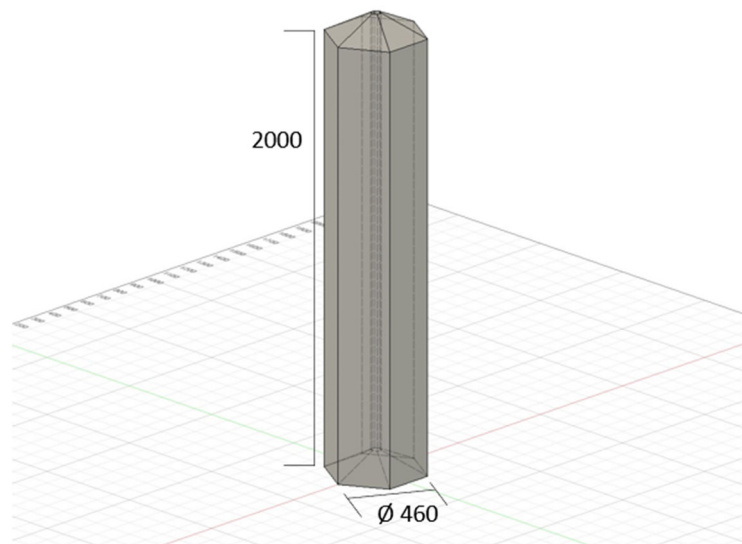
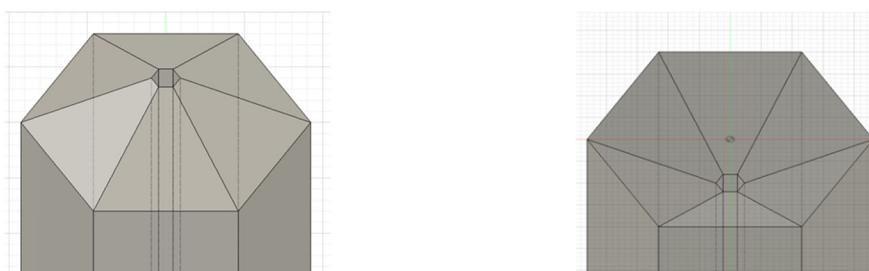


Figure 50. Concept of concrete block and block dimensions [mm]

The blocks were designed to be stacked and nested to suit the thermal needs of the installation and the space available. To meet challenge (i), the design is based on a modular concept with blocks of relatively small dimensions that allow them to be manufactured in a controlled industrial environment and transported to the installation site. In addition, no pipes are used in the concrete, which avoids the problems related to challenge (ii). Related to challenges (iii) and (iv), an improved concrete formulation will be used with respect to the one reported in a previous study [5], which should have a higher thermal conductivity and a better response to temperature variations. Finally, challenges (v) and (vi) are solved by using air as HTF and no pipes inside the concrete modules.



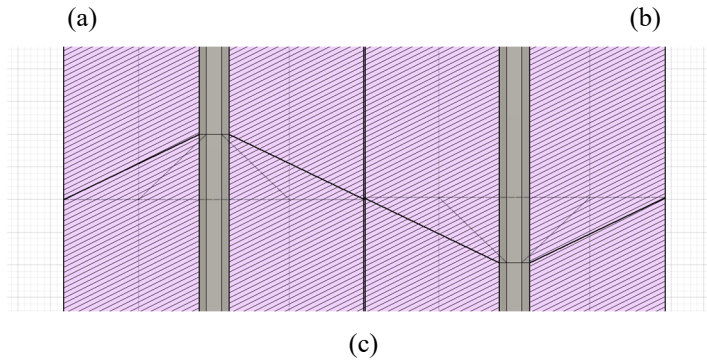


Figure 51. Concrete concept: (a) fitting connections, (b) stacked distribution example, and (c) connection points

#### 4. Set-up design for thermal cycling

To test the suitability of the improved concrete formulation, thermal cycling tests with small concrete samples must be carried out. For that, an experimental set-up (Figure 52) was designed for its implementation at the laboratory of the GREiA research group of the University of Lleida. The set-up consists of two furnaces; one at the top, which allows heating the sample up to 1000 °C, and another one below, which is used to cool down the sample below 400 °C. In this way, the sample can be subjected to thermal cycling by moving the sample up and down between the two furnaces through a mechanic actuator.

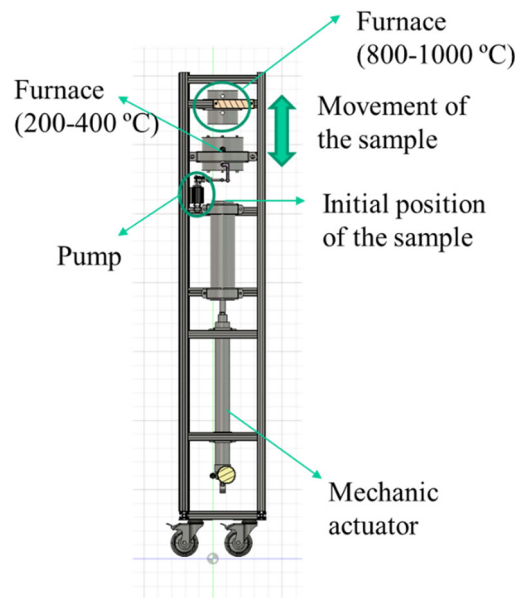


Figure 52. Schematic of the set-up for thermal cycling

#### 5. Conclusions

The use of concrete as TES material in CSP plants is a viable option due to its versatility, relatively low cost, and the possibility of reaching operating temperature above 565 °C. However, to become technologically and economically feasible, concrete storage systems must overcome a number of challenges. To deal with all challenges identified, a novel design of a high temperature TES system using concrete was proposed. The new design is composed of modular concrete blocks with direct-fit male-female connections and hexagonal design. These were designed to be stacked and interlocked in a honeycomb shape, thus enabling quick and easy customized sizing according to energy needs. Moreover, air is used as HTF with no pipes in the TES unit. The thermal conductivity of the concrete is expected to be enhanced by using an improved formulation. To experimentally test the improved concrete formulation, a new set-up was designed to carry out thermal cycling tests.

## Acknowledgements

This work was partially funded by the Ministerio de Ciencia e Innovación - Agencia Estatal de Investigación (AEI) - NextGeneration EU (PCI2020-120695-2 - MCIN/AEI/10.13039/501100011033/NextGenerationEU/PRTR) and by the Ministerio de Ciencia e Innovación - Agencia Estatal de Investigación (AEI) (PID2021-123511OB-C31 - MCIN/AEI/10.13039/501100011033/FEDER, UE). The authors would like to thank the Catalan Government for the quality accreditation given to their research group GREiA (2021 SGR 01615). GREiA is a certified agent TECNIO in the category of technology developers from the Government of Catalonia. This work is partially supported by ICREA under the ICREA Academia programme.

## References

- [1] REN21, Renewables 2020 Global Status Report, 2020.
- [2] D. Laing, D. Lehmann, M. Fi, C. Bahl, Test results of concrete thermal energy storage for parabolic trough power plants, *Journal of Solar Energy Engineering, Transactions of the ASME*. 131 (2009) 0410071–0410076. <https://doi.org/10.1115/1.3197844>.
- [3] N. Hoivik, C. Greiner, J. Barragan, A.C. Iniesta, G. Skeie, P. Bergan, P. Blanco-Rodriguez, N. Calvet, Long-term performance results of concrete-based modular thermal energy storage system, *Journal of Energy Storage*. 24 (2019) 100735.
- [4] Autodesk, Autodesk Fusion 360, (2022). <https://www.autodesk.es/products/fusion-360/overview> (accessed September 7, 2022).
- [5] L. Boquera, J.R. Castro, A.L. Pisello, C. Fabiani, A. D’Alessandro, F. Ubertini, L.F. Cabeza, Thermo-mechanical stability of supplementary cementitious materials in cement paste to be incorporated in concrete as thermal energy storage material at high temperatures, *J Energy Storage*. 54 (2022) 105370. <https://doi.org/10.1016/j.est.2022.105370>.

EUROTHERM2023-P210

## Experimental system for testing adsorption heat storage materials

Urška Mlakar<sup>1</sup>, Alenka Ristić<sup>2</sup>, Uroš Stritih<sup>1</sup>

<sup>1</sup> University of Ljubljana, Faculty of Mechanical Engineering, Aškerčeva cesta 6, 1000 Ljubljana, Slovenia,  
Phone: +386 1 4771 421, +386 1 4771 408, e-mail: urska.mlakar@fs.uni-lj.si

<sup>2</sup> Laboratory for adsorbents, National Institute of Chemistry, Hajdrihova ulica 19, 1000 Ljubljana, Slovenia,  
Phone: +386 1 4760 215, e-mail: alenka.ristic@ki.si

### Abstract

The efficient use of energy and the balancing of the gap between the availability of a given energy source and the energy demand are one of the key areas to which we must devote more time in order to be able to achieve the set goals of energy use and the use of renewable energy sources in the coming years. An experimental system for testing TCM adsorbents has been developed for short-term and seasonal heat storage. Experiments have been conducted for zeolite 13X with granulation from 1,6-2,5 mm. The charging phase for air flow of 2 l/s and temperature at the inlet of industrial drier around 215 °C lasted 33 minutes, after that the industrial drier was turned off. The maximum temperature that we reached before the entrance of the bulk material was 78 °C and at the exit of the bulk material 60 °C. After 54 minutes temperature reached 26 °C.

**Keywords:** Experimental system, TCM testing, adsorption, heat storage

### 1. Introduction

If we want to improve the efficiency of systems in the building sector in future generations, the application of storage technologies will be necessary. Storage technologies allow energy to be stored during times of excess energy and the use of stored energy to be used when demand is greater. Energy can be stored by various storage technologies, such as sensible, latent, and thermochemical (reversible reaction/sorption) storage technologies, as presented by Wu et al. [1] In this work, we would like to present our experimental system, which we will use to test different materials for thermal energy storage, including some new ones that we will acquire in the framework of the collaboration with the National Institute of Chemistry in Ljubljana.

Currently, we are building such an experimental system and trying out different solutions to the problems or obstacles we have discovered so far. All experiments so far have been performed with zeolite 13X, as this material is the most researched [2], [3]. For example, Tatsidjodoung et al [4] investigated an open system using 13X zeolite and water, which was intended for use in buildings and obtained energy for storage from solar energy. Koll et al [5] designed and tested a demonstration system for domestic hot water and space heating in a single-family house. Once the experimental system is in its final version and good results have been obtained, we will proceed with testing other materials.

### 2. Materials and method

Figure 1 shows the experimental system for testing adsorbents. At the entrance of the pipe, we have a fan that ensures the desired air flow through the measuring system. This is followed by the supply of hot air with an industrial dryer, which allows the air to be heated during the filling or drying phase of the material being tested. The used industrial hair dryer is manufactured by Black&Decker and fits nicely on the hot air supply due to the groove that the mouth of the industrial hair dryer has.

This is followed by a double mesh coupling to ensure a steady flow of air behind the heated air intake using an industrial dryer. Next comes the supply pipe for supplying moist air during the discharge phase.

The air humidifier, manufactured by Gorenje, is connected with the experimental line via an inlet pipe, which is currently not fixed to the main structure of the track due to the search for the most suitable inlet solution, as it must be appropriately adjusted according to the different phases (Moist air inlet – the pipe is in use; We do not supply moist air – the humidifier is removed and the inlet is sealed). This is followed by a second coupler with a double mesh, to ensure a steady flow of air behind the humid air supply.

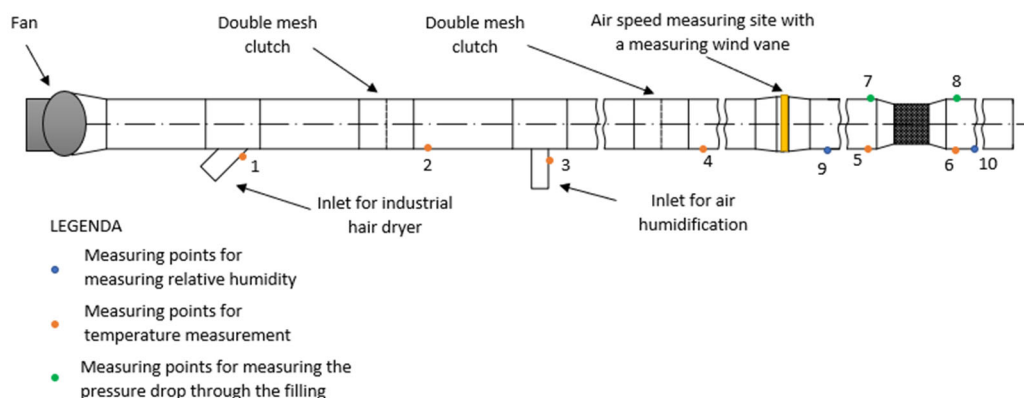


Figure 53. Experimental line for testing adsorption materials

The next elements of the experimental line are two diameter adjustment channels for the flow meter. The channel in front of the meter increases the diameter from 100 to 110 mm, while the channel behind the meter reduces the diameter back to 100 mm. At the end of the experimental line, there is a key part where we can insert the tested material.

The material testing part consists of a channel to reduce the diameter from 100 mm to 80 mm and a channel to re-increase the diameter to 100 mm. Behind the part of the experimental line, where we test the material, we have a 700 mm long outlet channel.

The numbers in the picture indicate the individual measuring points, where they are:

(1) Inlet temperature of the industrial hair dryer (charging phase); (2) Temperature before air humidification; (3) Humid air inlet temperature (discharge phase); (4) Temperature in front of the measuring vane; (5) Temperature before entering the bulk material; (6) Temperature at the exit from the material dump; (7) Pressure before entering the bulk material; (8) Pressure at the exit from the material dump; (9) Relative humidity at the entrance to the bulk material and (10) Relative humidity at the exit from the bulk material.

The air speed is measured approximately 400 mm before the work by pouring the material to be tested. To measure air speed, we use a Testo measuring wind vane.

The temperature of air is measured at six places in the experimental line. T-type thermocouples are used for the temperature measurements, apart from the heated air supply thermocouple in the charging phase, where a K-type thermocouple is used, which has a wider temperature sensing range than T-type.

The air humidity between the entrance and the filling of the material is measured with a high-temperature air humidity sensor. To measure the humidity of the air after pouring the material is measured with a hot-wire temperature and humidity meter from Testo.

Materials that will be tested will be composites, zeolites and aluminophosphates with different size of granules.

### 3. Results and discussion

We measured few sets to see how the experimental system works in different parameters of air flow, temperatures and rate of air humidification conditions. Example of the results can be seen in figure 2. For the set of results in figure 2, we tested 100 g of granulated Zeolite 13X with size between 1, 6 and 2, 5 mm and had air flow of 2 l/s and temperature at the inlet of industrial drier around 195 °C.

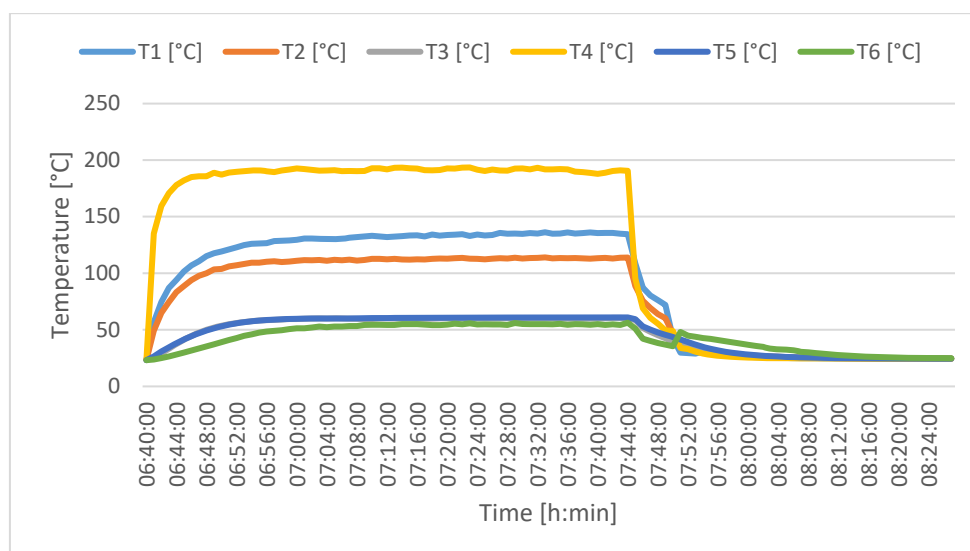


Figure 54. Measurement results for temperatures at inlet temperature of industrial drier at 195 °C

Temperatures that we were measuring at different sections of the experimental system mean:

- 1 – Temperature before air humidification
- 2 – Humid air inlet temperature (discharge phase)
- 3 – Temperature in front of the measuring vane,
- 4 – Inlet temperature of the industrial hair dryer (charging phase),
- 5 – Temperature before entering the bulk material,
- 6 – Temperature at the exit of the material filling,

The charging phase lasted 64 minutes, after that the industrial drier was turned off. The maximum temperature that we reached before the entrance of the bulk material was 61 °C and at the exit of the bulk material 56 °C. After 36 minutes temperature reached 25 °C.

The charging phase for conditions: air flow of 2 l/s and temperature at the inlet of industrial drier around 215 °C lasted 33 minutes, after that the industrial drier was turned off. The maximum temperature that we reached before the entrance of the bulk material was 78 °C and at the exit of the bulk material 60 °C. After 54 minutes temperature reached 26 °C.

With these two examples we can see the improvement – we have higher temperature difference between the entrance and exit of the bulk material, we store more energy.

After few sets of measurements while raising the temperature on the inlet of the industrial drier, it was decided that experimental system needs to be completely insulated to gain more useful experimental results. Next steps have been partly realized, but the measurements will be carried out in the following months after few other improvements of the system and measuring equipment.

#### 4. Conclusions

An experimental system has been designed to test sorption heat storage materials. Here, we present the part of work dedicated to the measuring points of the experimental line and the measuring equipment used. It was mentioned in the results that the system should be further improved, so some weaknesses of the system and possible solutions are highlighted below:

- 1) To ensure the quality of the results, it would be good to perform a leak test of the system. The experimental system is three and a half meters long and consists of several separate pipe sections. It would be necessary to ensure that no leakage occurs between the individual pipe connections, which can be guaranteed by a suitable sealing procedure.



- 2) During the design of the experiment, its set-up and the execution of the measurements, it was also found that at the temperatures we have during the charging phase (drying of the material), the problem arises that we do not have suitable measuring devices for certain measured quantities, that can be exposed to such high temperatures (above 100 °C and higher) during the charging phase. We are in the process of acquiring new equipment that could solve some of the problems.
- 3) When measuring the temperature difference before and after adding the material, it would be reasonable to change the measuring devices for temperature measurement from thermocouples T to measuring sensors for temperature Pt 100, as they provide higher measurement accuracy and thus lower measurement uncertainty. In case of small temperature differences before and after adding the material, a large measurement uncertainty may occur.
- 4) Additional protection of the part of the experimental track where we test the material for storage would also be necessary, possibly with a rubber cover - it is desirable that the final solution allows easy replacement of the samples of the materials under test.

## References

- [1] W. Wu, 'Low-temperature compression-assisted absorption thermal energy storage using ionic liquids', *Energy Built Environ.*, vol. 1, no. 2, pp. 139–148, 2020, doi: 10.1016/j.enbenv.2019.11.001.
- [2] B. de Gennaro *et al.*, 'Use of Zeolites in the Capture and Storage of Thermal Energy by Water Desorption—Adsorption Cycles', *Materials (Basel)*, vol. 15, no. 16, 2022, doi: 10.3390/ma15165574.
- [3] Y. C. Lin, Y. B. Fan, S. Chen, X. J. Zhang, A. Frazzica, and L. Jiang, 'Wave analysis method for air humidity assisted sorption thermal battery: A new perspective', *Energy Convers. Manag.*, vol. 277, no. January, p. 116638, 2023, doi: 10.1016/j.enconman.2022.116638.
- [4] P. Tatsidjodoung, N. Le Pierrès, J. Heintz, D. Lagre, L. Luo, and F. Durier, 'Experimental and numerical investigations of a zeolite 13X/water reactor for solar heat storage in buildings', *Energy Convers. Manag.*, vol. 108, pp. 488–500, Jan. 2016, doi: 10.1016/J.ENCONMAN.2015.11.011.
- [5] R. Köll *et al.*, 'An experimental investigation of a realistic-scale seasonal solar adsorption storage system for buildings', *Sol. Energy*, vol. 155, pp. 388–397, 2017, doi: 10.1016/j.solener.2017.06.043.

EUROTHERM2023-B211

## Development of an experimentally validated model of a PCM tank for cold storage applications in combination with heat pumps

Omais Abdur Rehman<sup>1</sup>, Valeria Palomba<sup>1</sup>, Andrea Frazzica<sup>1</sup>, Vincenza Brancato<sup>1</sup>, David Verez<sup>2</sup>, Emiliano Borri<sup>2</sup>, Luisa F. Cabeza<sup>2,\*</sup>

<sup>1</sup>National Research Council of Italy – Institute for Advanced Energy Technologies (CNR-ITAE), Salita S.Lucia sopra Contesse 5, 98126 Messina, Italy. E-mail: [omais.rehman@itae.cnr.it](mailto:omais.rehman@itae.cnr.it)

<sup>2</sup>GREiA Research Group, Universitat de Lleida, Pere de Cabrera s/n, 25001 Lleida, Spain  
e-mail: [luisaf.cabeza@udl.cat](mailto:luisaf.cabeza@udl.cat)

### Abstract

The design of phase change materials' encapsulation is one of the key parameters which affects the heat transfer rate along with charging and discharging times. This paper presents a numerical model for the design and integration of a latent thermal energy storage tank. The model is developed in Modelica language within Dymola environment, and it is calibrated using the experimental testing carried out on a PCM tank which employs commercial macro-encapsulated PCMs with 17°C nominal melting point temperature. Results will be helpful in evaluating the integration of the storage with other components of a building energy system, such as heat pumps and cold distribution system.

**Keywords:** Phase change material, Modelica, latent storage, macro-encapsulation

### 1. Introduction

One of the enabling technologies for the decarbonization of the heating and cooling industry, which in turn represents the focal point of programs like the "Green Deal" and the "Renovation Wave" in light of the widespread deployment and integration of renewables in the energy system, is thermal energy storage. Latent thermal energy storage with the use of phase change materials (PCM) is one of the thermal energy storage (TES) technologies used at the residential level that is not only moving towards commercial maturity [1], but is also the most active segment with TES systems at the research level, as shown by one of the bibliometric analyses performed in [2].

This field still needs to adequately solve the present difficulties preventing its widespread application in huge building structures and HVAC systems. Application-oriented research should concentrate on improving heat transmission, lowering the cost of materials, and developing management and control systems, as mentioned in [3].

One of the limitations of PCM lies in low thermal conductivity which can be addressed through addition of some particles (such as carbon elements, nano particles, and metallic particles) and increase in heat transfer area using fins and micro and macro-encapsulation. Micro-encapsulation involves complex and expensive process which include spray drying or interfacial polymerization while macro-encapsulation requires simple processes which result in less production time and lower costs. Macro capsules come in different sizes and shapes such as rectangular slabs or tubular capsules. The macro-encapsulation employed in this study is a commercial product and is called FlatICE from PCM Products Ltd [4]. The objective of this study is to develop and validate the model of a thermal energy storage tank which contains phase change material in FlatICE macro-encapsulation. The nominal melting temperature of the employed PCM is 17°C. The developed model will be later integrated in an existing model including a reversible HP for design purposes and to further evaluate possible advanced control logics, such as dynamic pricing.

## 2. Materials and method

### Thermal energy storage description

The PCM tank studied consists of an open container with dimensions of 1700 mm x 560 mm x 510 mm, filled with FlatICE macroencapsulation. The PCM selected is a commercial S17, a salt hydrate with nominal melting temperature of 17°C. The slabs were placed horizontally inside the storage, using spacers between them to allow for HTF passage. Different number of rows and columns of slabs were selected in order to test different arrangements and packing factors. A picture of the storage is shown in Figure 1.

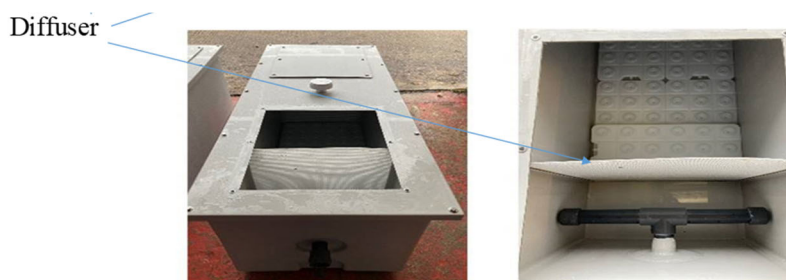


Figure 1. The PCM tank tested and modelled.

### Model assumption

The model is developed using Modelica language and TIL library components in Dymola environment [5][6]. Following assumptions are made:

- The thermophysical characteristics of the PCM are not temperature-dependent; nevertheless, the solid-phase characteristics differ from those of the liquid-phase characteristics.
- Radiative heat transfer is not taken into account.
- The heat loss to the environment is negligible.
- HTF is incompressible.
- The temperature of the, HTF, and metal walls varies only in the flow direction (x-direction) along their lengths, which are divided into n nodes.
- Natural convection in the liquid PCM is ignored because this effect is minimal due to the low thickness of macro-encapsulation [7][8].
- The phase change phenomena is modelled using the solid-liquid equilibrium application available in the TIL media libraries which makes use of enthalpy method [7][9].
- The pressure drop in the HTF cells is considered constant.

### Model description

Using Modelica language, momentum and energy balance equations are solved for each cell of HTF. For PCM, energy balance is calculated using energy equation involving mass, specific heat capacity, temperature, and latent heat of fusion. A term is added to this equation which represents sum of all the heat flows for the cell resulting from heat transfer within PCM layer itself as well as with the HTF and plastic encapsulation.

The developed lumped model contains a channel of heat transfer fluid (HTF) followed by a wall (plastic encapsulation), solid liquid equilibrium material (SLE) which refers to PCM, wall (plastic encapsulation again) and HTF channel, following the approach developed in [10]. Therefore, the storage is schematically divided as an array of sub-units with the HTF, SLE and wall cells in two directions. Each

sub-unit corresponds to the macro-capsule with the surrounding HTF channels. A schematic representation is shown in Figure 2.

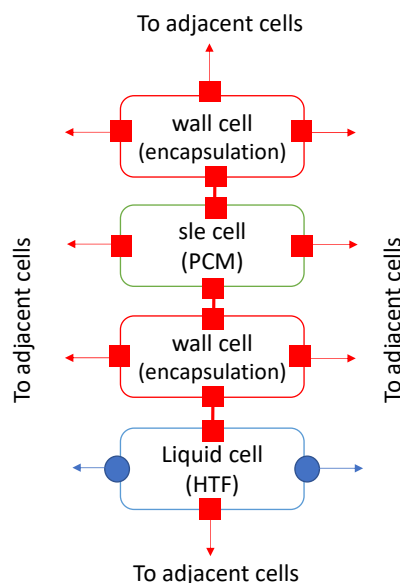


Figure 2. Schematic of the sub-units for the developed model.

Boundary conditions are used to provide inlet temperature, pressure and mass flow rate of the tank. Inlet temperature is set at 27 °C while mass flow rate of 0.07 kg/s is provided. The tank operates at atmospheric pressure. There are thirteen PCM capsules in the tank vertically which means the same amount of channels for HTF flow. So, the mass flow rate is further divided in to these HTF channels. For discharging process, inlet temperature is set at 7 °C while mass flow rate is similar as charging process.

Moreover, model required thermal properties of PCM. These properties include heat of fusion, specific heat capacity in liquid and solid phase, thermal conductivity and melting range of the material. Furthermore, dimensions of TES tank are needed to define the geometry. It is also required to provide the number of cells in the direction of flow in the tank and across the flow.

### 3. Experimental setup and methodology

The experimental results are obtained from a setup designed to test latent thermal energy storage systems in laboratory of GREiA research group at University of Lleida, Spain. The experimental setup has a 25 dm<sup>3</sup> inertial water tank which is used to charge or discharge the TES tank. The temperature of this inertial tank is controlled by a vapor compression unit of 5 kW cooling power and two immersion thermostats of 6 kW each. Thermocouples are attached to the surface of encapsulation to get temperature of PCM at top, middle and bottom of tank. These sensors are of Pt-100 class B, IEC 60751 standard type with an accuracy of (0.3+0.005\*T). The sensors used at the inlet and outlet of storage tank to measure HTF temperature are of Pt-100 class A, IEC, 60751 standard type with and accuracy of (0.15+0.002\*T).

An inlet temperature of 27 °C is supplied at the TES tank while PCM inside the tank is at 7 °C. The mass flowrate is set at 0.07 kg/s. The temperature sensors are placed on the surface of PCM encapsulation and in HTF channels. Three repetitions of charging and discharging experiments have been made. For discharging, inlet temperature of tank is set at 7 °C while PCM inside the tank is at 27 °C.

### 4. On-going activity and future perspectives

The model calibration is currently on-going. Once completed, the fully validated model will be integrated with an already developed model of reversible HP in Dymola, to be simulated in different

climates, to assess how the presence of latent TES affects the performance of an energy system. Moreover, it will also make it easier to understand how TES will help in peak-shaving in different European climates. Furthermore, the analysis will also include how TES will help in coping the heat load variations and increasing the flexibility of system. Lastly, an economic analysis will be made to identify the payback time period of energy system.

## Acknowledgements

This project has received funding from the European Union's Horizon 2020 research and innovation programme under the Marie Skłodowska-Curie grant agreement No 101007976. The authors from GREiA research group from University of Lleida would like to thank the Catalan Government for the quality accreditation given to their research group (2021 SGR 01615). GREiA is certified agent TECNIO in the category of technology developers from the Government of Catalonia. This work is partially supported by ICREA under the ICREA Academia programme.

## References

- [1] "Phase Change Material Market, Global Industry Size Forecast." .
- [2] A. Calderón, C. Barreneche, K. Hernández-Valle, E. Galindo, M. Segarra, and A. I. Fernández, "Where is Thermal Energy Storage (TES) research going? – A bibliometric analysis," *Sol. Energy*, vol. 200, pp. 37–50, Apr. 2020, doi: 10.1016/J.SOLENER.2019.01.050.
- [3] A. Sevault, F. Vullum-Bruer, and O. L. Tranås, "Active PCM-Based Thermal Energy Storage in Buildings," *Encyclopedia of Energy Storage*. Elsevier, 01-Jan-2020, doi: 10.1016/B978-0-12-819723-3.00008-1.
- [4] PCMproducts, "PCM products webpage." .
- [5] "TIL Suite." .
- [6] "Dymola - Dassault Systèmes®." .
- [7] H. Neumann *et al.*, "A simplified approach for modelling latent heat storages: application and validation on two different fin-and-tubes heat exchangers," *Appl. Therm. Eng.*, 2017, doi: 10.1016/j.applthermaleng.2017.06.142.
- [8] V. Palomba, E. Varvagiannis, S. Karellas, and A. Frazzica, "Hybrid Adsorption-Compression Systems for Air Conditioning in Efficient Buildings: Design through Validated Dynamic Models," *Energies*, vol. 12, no. 6, p. 1161, Mar. 2019, doi: 10.3390/en12061161.
- [9] V. Palomba *et al.*, "Latent Thermal Storage for Solar Cooling Applications: Materials Characterization and Numerical Optimization of Finned Storage Configurations," <https://doi.org/10.1080/01457632.2018.1451236>, vol. 40, no. 12, pp. 1033–1048, Jul. 2018, doi: 10.1080/01457632.2018.1451236.
- [10] V. Palomba and A. Frazzica, "A Fast-Reduced Model for an Innovative Latent Thermal Energy Storage for Direct Integration in Heat Pumps," *Appl. Sci. 2021, Vol. 11, Page 8972*, vol. 11, no. 19, p. 8972, Sep. 2021, doi: 10.3390/APP11198972.

EUROTHERM2023-C212

## Potential for high temperature waste material as thermal energy storage media for industrial heat decarbonization

Vasilis Gkoutzamanis<sup>1</sup>, Anestis Kalfas<sup>1</sup>, Stefano Barberis<sup>2</sup>, Tommaso Reboli<sup>2</sup>,  
Silvia Trevisan<sup>3</sup>, Rafael Guédez<sup>3</sup>

<sup>1</sup>Dept. of Mechanical Engineering, Aristotle University of Thessaloniki, Thessaloniki, Greece  
Phone: +302310996033, e-mail: vgkoutzam@meng.auth.gr

<sup>2</sup>Dept. of Mechanical Engineering, University of Genoa, Genoa, Italy  
Phone: +39 010 353 2463 e-mail: stefano.barberis@unige.it

<sup>3</sup>Dept. of Energy Technology, KTH Royal Institute of Technology, Stockholm, Sweden  
e-mail: trevisan@kth.se

### Abstract

In the framework of their international cooperation activities, three European universities are developing a promising concept of high-temperature thermal energy storage (HT-TES). It is based on the up-cycling of metal slags from the energy-intensive metal industries such as Steel, Copper and Aluminium, to integrate the HT-TES directly in the production processes. Hence, technical solutions for solid media embedded in TES are sought. The goal of the R&D activities is firstly to characterize and evaluate the metal slags' thermal and mechanical performance in high-temperature processes between 250°C up to 900°C. Such slags could be then integrated into the TES systems and tested with various heat transfer fluids such as air, molten salts and diathermic oil, depending on the industrial process needs. As part of a system design optimization study, the most promising component solutions in terms of overall efficiency and cost can then be derived. Prior to detailing these activities, the purpose of this first work is to conduct a preliminary techno-economic analysis and quantify the overall concept performance, to holistically evaluate how the proposed TES can practically enable material circularity and industrial symbiosis.

**Keywords:** metal by-products, materials recycling, industrial symbiosis, circular economy, waste heat recovery, metal slags.

### 1. Introduction

Climate-neutrality by 2050 is unequivocally a goal of utmost importance, to ensure a cleaner and safer planet for the present and future generations. About 48% of today's overall energy demand is in the form of heat while almost half of it is requested as medium to high temperature heat by the industry. It is thus evident that the need for cost-effective solutions capable to provide this heat reliably and at low or zero CO<sub>2</sub>, is an urgency. Reducing emissions and encouraging the circularity of the hard-to-abate and energy intensive metallurgic industry is crucial, also contributing to its further decarbonization while exploring new possible revenue streams. The industrial heat demand in Europe is diversified in multiple heat requirements depending on the type of industry. Approximately one third requires heat above 1000°C, another from 500 to 1000°C and the remaining industry needs heat below 500°C, out of which more than half concentrates in the range 100-500°C. It is seen that the main industries requiring heat above 1000°C are related to the metal and mining sectors, whereas the food, paper and chemical industries dominate the rest of the heat demand spectrum [1].

From a technological and material standpoint, it can be challenging to satisfy the high temperature heat requirements of the energy intensive metallurgic and mining industries, in a cost-effective way. However, the fact that these operate at such high temperatures means they have an increased potential to enhance and fully realize the concept of industrial symbiosis and overall circularity [2]. This can be

attained through two routes: (i) waste heat recovery (WHR) and (ii), waste material re-utilization and up-cycling. Even though WHR techniques are already robustly in place in these processes, a large amount of heat remains underutilized despite the possibility to be exploited by the same industry or another (boosting symbiosis). The reasons for this typically relate to techno-economic hurdles to employ conventional WHR methods, temporary or geographical mismatch between the energy release and its heat demand [3], as well as the cost and inefficiencies linked to heat transportation. In addition, significant amounts of waste materials and by-products such as metal slags and sludge are produced daily, also remaining underutilized [4] and typically sent to landfills. It is estimated that global metallurgical waste accounts to approximately 400 million tons per year [5].

The WH from the metal and mining sectors can potentially be used by the remaining two thirds of the industry to satisfy their needs, and the referred waste media from such metal and mining sectors could also be exploited as a viable means to solve the problem of decoupling heat release from the demand. The latter can be achieved by valorising the waste materials as TES and insulating media, for which a thorough understanding of the material properties and pre-treatment requirements is needed. Such TES media could be enhanced and innovative containment components (including novel means of insulation) and heat exchangers (HEXs) can be developed to optimize heat transfer and the system performance, depending on the final industrial application. The food and beverage, pulp and paper and chemical sectors can be clear beneficiaries of such technologies, particularly when the TES concept not only valorises waste heat, but also exploits RES for charging. These new TES-RES integrated systems built upon waste media and could also directly serve as a technology that can significantly reduce the heat demand and CO<sub>2</sub> footprint of the metal sector when used for pre-heating.

TES systems can thus offer a realistic solution for the combined and sophisticated exploitation of WHR, fluctuating RES and waste material by-products. The integration of TES in the industrial sector is paramount to boost the sector's efficiency, limit operational costs and financial risks and reduce GHG emissions. Particularly in EU, steel and metallurgy are key industrial sectors, affected by relevant energy consumptions, which can benefit from the possibility of exploiting their by-products as TES materials to reduce their energy bill. Despite their high temperature levels (Figure 1), some of metallurgic industry processes could be optimized using TES in a temperature range 200 – 600 °C where metal slags could be used as solid media at this purpose and where up to now, some kinds of TES media were applied or tested, like molten salts, ceramic, concrete etc. [7]. The proposed concept is presented in Figure 2.

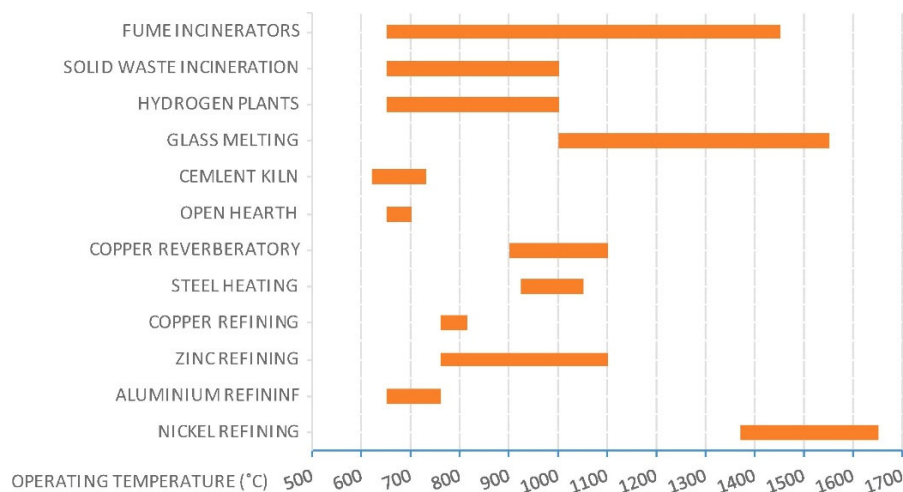


Figure 55. Typical operating temperature range of different energy-intensive industry processes [6].

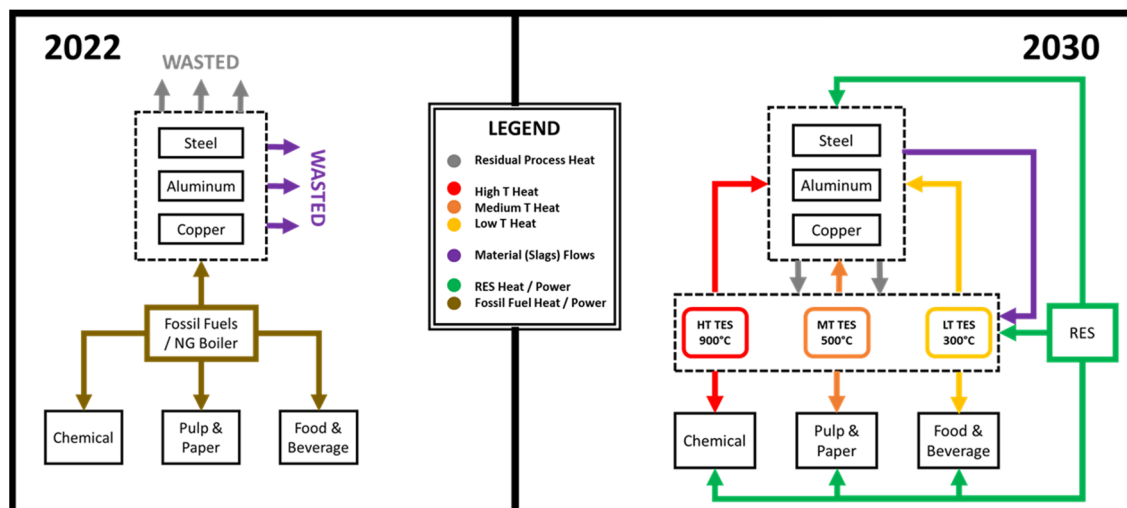


Figure 56. Main concept of the presented metal slag-based HT-TES concept.

## 2. Materials and methods

In order to achieve its ambition, the proposed HT-TES concept has to undergo through the following critical steps, to gain a better awareness of its residing challenges and benefits:

- Material characterization and development: This part includes the thermo-mechanical and physical properties' identification, of the produced by-products.
- TES design, optimization, prototyping and validation: This step aims to develop optimized, system level solutions and cover most of the industrial heat demand in a temperature range of 200°C up to 900°C.

### 2.1. Environmental and economic performance quantification

Prior to performing detailed characterization and component design optimization activities, a preliminary techno-economic assessment is performed herein, to identify the potential impact of HT-TES integration in the industrial sector within the EU. This will in essence show whether an actual potential exists to justify further research and the actual potential for high temperature waste material as TES media for industrial heat decarbonization.

The considered key performance indicators (KPIs) are the nominal levelized cost of heat (LCoH) and the operational expenditure (OPEX) [8]. The potential applicability of the proposed concept in EU markets is evaluated, according to local energy contexts and industrial sector energy requirements. The introduction of TES units is modelled assuming relevant heat demand profiles gathered from the clustering analysis of IEA's Solar Heating and Cooling programme (SHC) and SolarPACES research [9]. Additionally, optimal dispatch strategies and TES sizing aimed at ensuring minimal LCoH and OPEX while maximizing the attainable savings with respect to traditional solutions (NG, diesel burners and electric boilers, heat pumps – only included for the lowest temperature range up to 250°C considering recent developments and ongoing R&D) are considered. Fuel and electricity costs for 2021 are assumed as the reference case, as more representative of potential longer term price patterns.

## 3. Preliminary techno-economic assessment and discussion

In Figure 3 (left), the share of heat demand in different temperature ranges for the German industrial sector [1] is shown. Germany is the largest consumer of heat in the EU, with a total annual demand of more than 530 TWh. Italy, France, UK, and Spain are the other main EU indus-



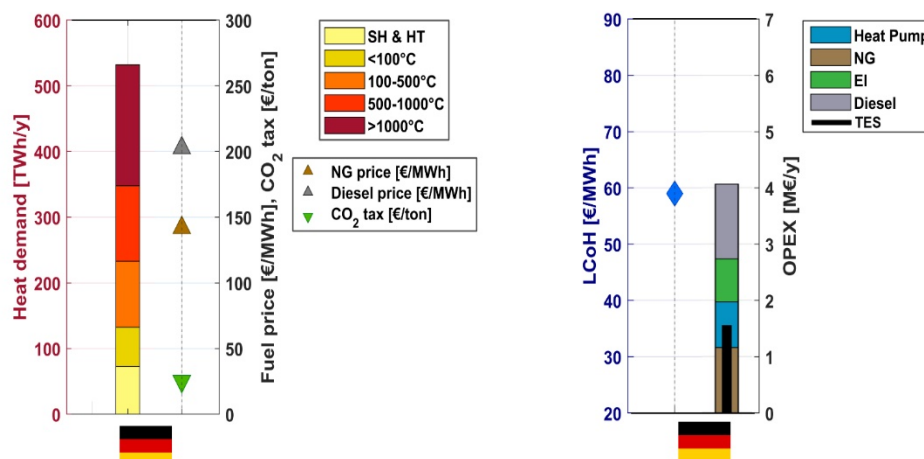


Figure 3. (left) Heat demand by temperature range, average fuel prices and CO<sub>2</sub> taxes; (right) LCoH and OPEX for the proposed system in comparison with different Business-As-Usual (BAU)

trial countries, and, together with Germany they represent about 60 % of the EU-28 industrial thermal energy consumption. Figure 3 (right) shows the main KPIs attainable by the TES introduction and the OPEX savings provided by the proposed system against different BAU alternatives. The base case considers a thermal load of 3MW peak and about 50 MWh/day and 25% of potential energy from WHR and direct electrification for the remaining load. The proposed system can attain LCoH around 60 €/MWh and is the most cost-effective alternative among non-fossil fuel based alternatives. The flexibility provided by the TES permits large OPEX reduction in comparison with directly electrified systems. It should be also highlighted that the most recent increase in carbon taxes would likely make the proposed solution cost competitive also against NG based alternatives, further boosting the potential industrial uptake of solid media sensible heat based TES for WHR and reuse.

## References

- [1] Naegler T, et al., ‘Quantification of the European industrial heat demand by branch and temperature level’, *Int J Energy Res* 2015, doi: 10.1002/er.3436.
- [2] Oughton C., et al., ‘Industrial symbiosis to circular economy: What does the literature reveal for a successful complex industrial area?’, *Circular Economy and Sustainability*, doi: 10.1007/s43615-022-00153-1.
- [3] Miró L., Gasia J., Cabeza L., ‘Thermal energy storage (TES) for industrial waste heat (IWH) recovery: A review’, *Applied Energy*, Vol. 179, 2016, doi: 10.1016/j.apenergy.2016.06.147.
- [4] Das B., et al., ‘An overview of utilization of slag and sludge from steel industries’, *Resources, Conservation and Recycling*, Vol. 50 (1), 2007, doi: 10.1016/j.resconrec.2006.05.008.
- [5] Ilutiu-Varvara D-A. and Aciu C., ‘Metallurgical wastes as resources for sustainability of the steel industry’, *Sustainability*, 2022, 14(9), 5488; doi: 10.3390/su14095488.
- [6] Royo P., Acevedo L., et al., ‘High-temperature PCM-based thermal energy storage for industrial furnaces installed in energy-intensive industries’, *Energy*, Volume 173, 2019, Pages 1030-1040, ISSN 0360-5442, <https://doi.org/10.1016/j.energy.2019.02.118>
- [7] Manente G., Ding Y., Sciacovelli A., ‘A structured procedure for the selection of thermal energy storage options for utilization and conversion of industrial waste heat’, *Journal of Energy Storage*, Volume 51, 2022, 104411, ISSN 2352-152X, <https://doi.org/10.1016/j.est.2022.104411>.
- [8] Trevisan S, Buchbjerg B, Guedez R. Power-to-heat for the industrial sector : Techno-economic assessment of a molten salt-based solution. *Energy Convers Manag* 2022;272. <https://doi.org/10.1016/j.enconman.2022.116362>.
- [9] Pag F., Jesper M., Jordan U., ‘Reference applications for renewable heat’ D.A1, doi: 10.17170/kobra-202104263730.

EUROTHERM2023-P213

## Utilisation of composite phase change materials in a novel mobile thermal energy storage (M-TES) system

Benjamin Grégoire, Mengqi Bai, Song Yang, Tongtong Zhang, Anabel Palacios, Hongkun Ma, Yulong Ding

Birmingham Centre for Energy Storage (BCES), School of Chemical Engineering, University of Birmingham, Birmingham B15 2TT, United Kingdom, Phone: +44 (0) 121 414 5279, e-mail: y.ding@bham.ac.uk

### Abstract

This paper concerns with Mobile Thermal Energy Storage (M-TES) using high energy-density TES materials aimed for reducing greenhouse gases emission and increasing energy efficiency. The focus is on the development and thermal characterisation of a novel medium-temperature Composite Phase Change Material (CPCM) with high energy density, cost-effectiveness and easy scalability for manufacturing large CPCM modules ( $\approx 8.6$ - $8.7$  kg). The novel CPCM contains a salt-based PCM for latent and sensible heat storage, a ceramic matrix material for shape-stabilisation and a thermal conductivity enhancer material (TCEM) for improved heat transfer kinetics. Up to 60 CPCM modules were successfully manufactured at the University of Birmingham and were then loaded into a novel M-TES device to efficiently recover industrial waste heat, store and subsequently utilise this recovered heat for end users. Most recent findings will be presented at the seminar.

**Keywords:** Mobile heat, Composite phase change material, Latent heat, Energy density, Decarbonisation

### 1. Introduction

Shape-stabilised composite phase change materials (CPCMs) have attracted wide attention for thermal energy storage (TES) applications [1] and could accelerate the deployment of TES solutions for the decarbonisation of heat. An ideal shape-stabilised CPCM should meet the following requirements: (i) suitable melting point for working conditions, (ii) high specific heat capacity and phase change enthalpy to deliver high energy density and compact TES system, (iii) reproducible and consistent phase change temperature, (iv) good thermal/chemical stability and long cycle life, (v) good thermal conductivity, which can meet the requirements in terms of charging/discharging time of the heat storage system.

Shape-stabilised CPCMs usually contain (i) a PCM for latent heat storage, (ii) a three-dimensional structural material or ‘skeleton material’ to confine the PCM and (iii) a thermal conductivity enhancer material (TCEM) dispersed within the PCM for increased heat transfer capacity. CPCMs can store energy as TES coming from renewables by storing directly heat from concentrated solar power (CSP) plants or, for instance, by using the electricity from wind farms to produce the heat that will be stored. This technology, due to its PCM component, can store heat at a given temperature coming from a waste heat constant temperature and lately deliver that heat at a given temperature. These characteristics make CPCMs suitable for industrial application and, in particular, for waste heat recovery and mobile energy stored as heat [2]. While research on CPCMs is quickly growing, there are still some fundamental and technical challenges to overcome before successful integration for large scale applications. With a very high potential to decarbonising heating and electricity generation, this motivates the development of CPCMs with a careful screening and selection of its constituents as well as an optimisation of the manufacturing process [3]. There is also a drive to design, model and build innovative storage concepts utilising TES materials such as shape-stabilised CPCMs.

In this work, a novel CPCM based on  $\text{NaNO}_2$ - $\text{NaNO}_3$  eutectic mixture was developed for efficient heat recovery and transport with a working temperature range of 80-350 °C. The study focused on (i) the

thermal characterisation of the novel CPCM to calculate its energy storage density within the operating temperature range, (ii) the stability of the CPCM and (iii) the manufacture of large CPCM modules for integration into an advanced M-TES device. After optimisation of the CPCM formulation, 60 CPCM modules ( $\approx 8.6$ - $8.7$  kg) were successfully produced at the University of Birmingham and integrated into the novel M-TES device. This device is expected to efficiently recover industrial waste heat, store and subsequently utilise this recovered heat for end users (e.g. domestic heating applications).

## 2. Materials and method

Sodium nitrate ( $\text{NaNO}_3$ ), sodium nitrite ( $\text{NaNO}_2$ ) and magnesium oxide ( $\text{MgO}$ ) were purchased from Plater Group, UK. All three materials had purity levels between 96-98% (technical grade), which make them more cost-effective for large-scale application compared to lab-grade materials usually employed for formulation studies in the literature. Expanded graphite was purchased from Graphit Kropfmühl GmbH, Germany. To determine the thermal properties of the new CPCM formulation, CPCM samples were prepared and analysed by DSC (Mettler Toledo DSC3+) in aluminium crucibles to obtain the heat flow curves upon heating/cooling between 35 and 400 °C at a heating rate of 10 °C/min and cooling rate of 5 °C/min. Specific heat measurements were obtained following the sapphire method and using small CPCM tablets (5 mm diameter). The experimental data was then used to calculate the energy density of the novel CPCM within its operating temperature range (80-350 °C).

The manufacturing process of CPCM modules follows three main steps (Figure 57), (i) milling of the salts, (ii) mixing of the raw materials and (iii) compacting into a tablet by uniaxial compression. Milling of the salts was performed with a Retsch rotor beater mill SR 200. After milling, sodium nitrate and sodium nitrite were mixed with a Cyclomix® to the desired eutectic composition (55 $\text{NaNO}_2$ -45 $\text{NaNO}_3$ , wt.%). The PCM salt mixture, magnesium oxide and expanded graphite were then mixed again with a Cyclomix® to obtain a homogeneous CPCM powder mixture. Compacting of the CPCM powder mixture was carried out with a LLOYD LS100 tensile/compression machine at a pressure of between 5-50 MPa into  $\approx 50$  g cylindrical tablets ( $\approx 50$  mm and  $\approx 15.7$  mm thickness). The thermal stability of the CPCM was investigated by thermal cycling tests in an electric furnace at a maximum temperature of 350 °C (Figure 57). Heating ramps were fixed at 5 °C/min. After cycling tests, leakage was examined to reveal the cycling stability of the CPCM modules. Based on these results, the maximum PCM loading for the newly-developed CPCM module to maintain stable shape without any salt leakage was selected.

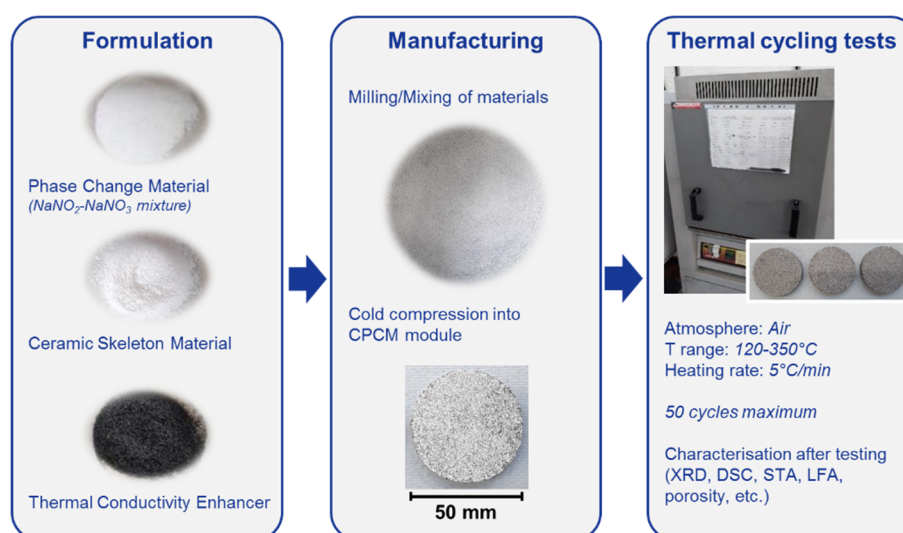


Figure 57. Manufacturing process of composite phase change materials into cylindrical modules and thermal cycling test conditions.

### 3. Results and discussion

#### 3.1. Thermal characterisation of CPCM

The DSC curves for the first and second melting/solidification cycles of the optimised CPCM formulation are given in Figure 58a and b, respectively. Three sample repetitions were performed for each cycle and the thermodynamic data extracted from the curves is presented on the graphs (average values with standard deviation). The DSC results indicate that while the new CPCM formulation developed in this study has a decent latent heat value ( $\approx 65$  J/g for the solid-liquid transition at about 223 °C), its energy density is further increased by the occurrence of a solid-solid transition in the temperature range 175-189 °C upon heating and 124-161 °C upon cooling. The novel CPCM formulation shows overall a high latent heat of about 120 J/g. Heat capacity measurements of small CPCM tablets were also conducted and gave a specific heat capacity of  $1.30 \pm 0.04$  J.g<sup>-1</sup>.K<sup>-1</sup> and  $1.55 \pm 0.09$  J.g<sup>-1</sup>.K<sup>-1</sup> in solid and liquid states, respectively. The calculated energy density of the novel CPCM between 80-350 °C was, therefore, 502 J/g. In addition, the thermal analyses of the CPCM after cycling tests confirmed that the formulation is thermally stable up to 350 °C and shows high potential for the manufacturing of CPCM modules with high energy density.

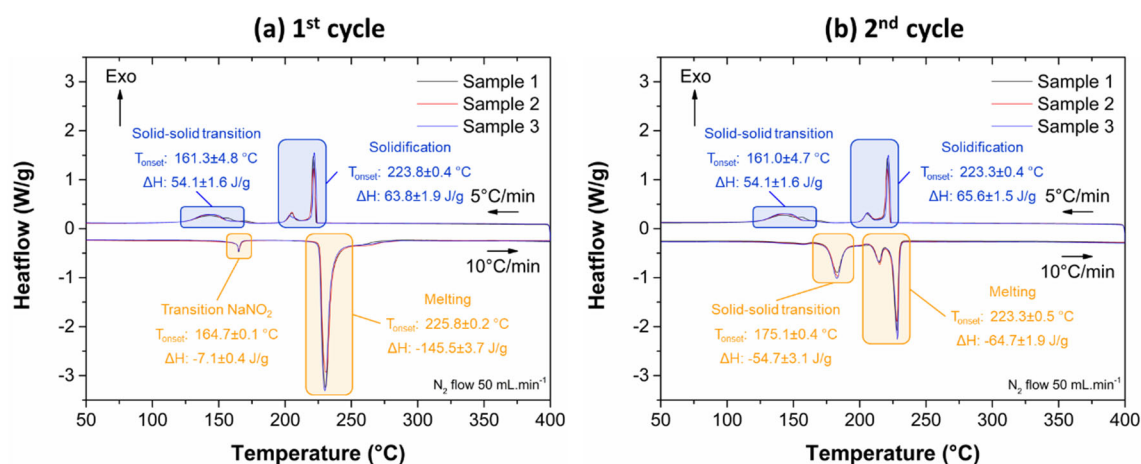


Figure 58. DSC curves of the CPCM powder mixture based on NaNO<sub>2</sub>-NaNO<sub>3</sub>. Three samples were tested and two cycles were performed for each sample for repeatability.

#### 3.2. Thermal cycling results of CPCM modules

Figure 59 presents the thermal cycling results of cylindrical CPCM modules and the corresponding evolution of their bulk density. No leakage and minor shape change was observed.

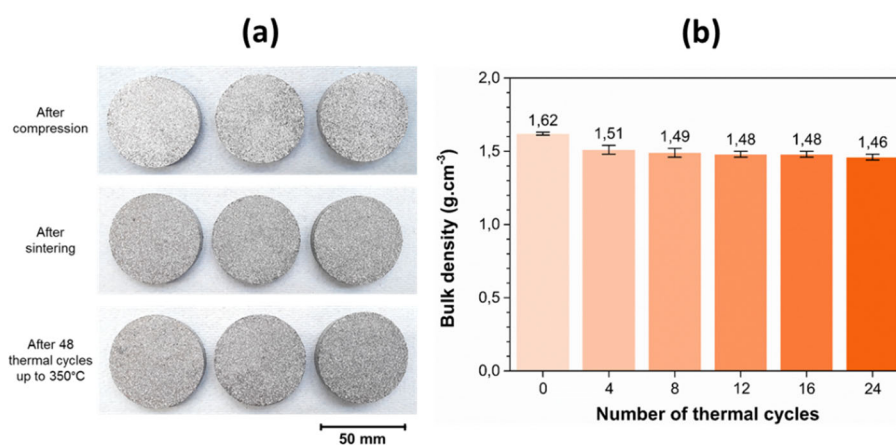


Figure 59. (a) Macrographs of cylindrical CPCM modules and (b) evolution of bulk density with thermal cycling.

### 3.3. Manufacture of large CPCM modules for integration into the novel M-TES system

Large CPCM modules (285 x 285 x 70 mm) of about 8.6-8.7 kg were manufactured at the University of Birmingham for integration into the novel M-TES system. Up to 60 CPCM modules were then loaded into individual stainless steel drawers and fitted into the M-TES system as shown in Figure 60. The total energy storage capacity of the 60 CPCM modules is about 250 MJ between 80-350 °C while the overall storage capacity of the M-TES system is further increased due to sensible heat contribution from the stainless steel container and drawers. A 20 kW electric heater (emulating industrial waste heat) is used to charge the system and test its performance. The M-TES system is currently being assembled and the first experimental results are expected to be presented at the seminar.

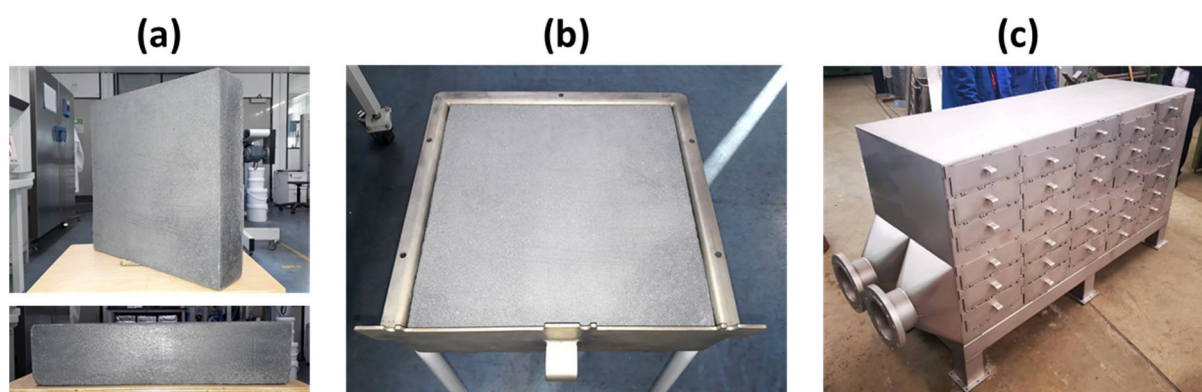


Figure 60. Pictures of (a) a manufactured CPCM module in side view and cross-section view, (b) a stainless steel drawer loaded with a CPCM module and (c) the novel M-TES container (patented).

## 4. Conclusions

A novel medium-temperature CPCM formulation was developed with a high latent heat value (about 120 J/g) associated with a solid-liquid transition at about 223 °C and a solid-solid transition in the temperature range 175-189 °C (heating) and 124-161 °C (cooling). The optimised CPCM formulation was used to manufacture large CPCM modules that were loaded into a novel M-TES container. This device is aimed to recover industrial waste heat, store this heat and later distribute the heat to end users. The development and operation of this innovative concept is an important milestone for the deployment of advanced TES solutions.

## Acknowledgements

This work is supported and funded by the Engineering and Physical Sciences Research Council under Grant EP/V027050/1 (Industrial Decarbonisation Research and Innovation Centre) in the United Kingdom.

## References

- [1] Z. Jiang, A. Palacios, B. Zou, Y. Zhao, W. Deng, X. Zhang, Y. Ding, A review on the fabrication methods for structurally stabilised composite phase change materials and their impacts on the properties of materials, *Renewable and Sustainable Energy Reviews* 159 (2022) 112134.
- [2] K. Du, J. Calautit, P. Eames, Y. Wu. A state-of-the-art review of the application of phase change materials (PCM) in Mobilized-Thermal Energy Storage (M-TES) for recovering low-temperature industrial waste heat (IWH) for distributed heat supply. *Renewable Energy* 168 (2021) 1040-1057.
- [3] M.E. Navarro, A. Palacios Trujillo, Z. Jiang, Y. Jin, Y. Zhang, Y. Ding, Chapter 7 – Manufacture of Thermal Energy Storage Materials, in *Thermal Energy Storage: Materials, Devices, Systems and Applications*, 2021. Ed. Yulong Ding. Royal Society of Chemistry.



**Eurotherm Seminar #116**  
Innovative solutions for thermal energy storage deployment



EUROTHERM2023-F214

## Effect of the pressurization program on the thermal properties and stability of *Pinus radiata* wood impregnated with octadecane

Ignacio Urzúa Parra<sup>1</sup>, Jonathan Cofré-Toledo<sup>1</sup>, Diego A. Vasco<sup>1</sup>, Assed Haddad<sup>2</sup>

<sup>1</sup>Departamento de Ingeniería Mecánica, Universidad de Santiago de Chile, Av. Lib. Bdo O'Higgins 3363, Santiago, Chile, Phone: 56-2-2-7183120, e-mail: [diego.vascoc@usach.cl](mailto:diego.vascoc@usach.cl)

<sup>2</sup>Departamento de Construção Civil, Escola Politécnica da Universidade Federal do Rio de Janeiro, Av. Athos da Silveira Ramos 149, Rio de Janeiro, Brasil, e-mail: [assed@poli.ufrj.br](mailto:assed@poli.ufrj.br)

### Abstract

Wood has become an attractive material to encapsulate phase change materials (PCMs) forming a wood-based shape stabilized PCMs (WSSPCMs) to be used in the thermal envelope of buildings. PCMs are incorporated into the wood porous structure by using impregnation, obtaining WSSPCMs with higher energy density, and thermal conductivity and mechanical properties similar to wood. Nevertheless, the stability of WSSPCMs is an issue since the PCM leaks during melting. The hypothesis of this work is that the pressurization stage during impregnation has an important influence on the stability and the PCM load inside the wood porous structure. The present work shows the effect of three pressurization programs on the stability, PCM load, and thermal properties of prepared WSSPCMs by using octadecane as PCM.

**Keywords:** Shape stabilized PCM, Wood, Impregnation, Stability, Thermal properties

### 1. Introduction

There are some studies regarding impregnation of PCMs using wood as a substrate. Li et al. [1] impregnated green fir wood with an aqueous solution of PEG at atmospheric pressure. They obtained a composite with a melting and freezing point of 26.74 °C and 36.14 °C, respectively and a latent heat of 73.59 J/g. They applied a surface coating to avoid leakage of the PCM and conducted leaching and thermal stability tests. Barreneche et al. [2] impregnated black alder wood with paranic PCMs RT-21 and RT-27 from Rubitherm by applying vacuum. The authors measured a range of latent heat of 2.41 J/g to 20.62 J/g for a weight proportion of PCM of 10.5% to 29.9%, respectively. The authors applied a polystyrene solution to prevent the composite from any leakage when the PCM was in the liquid state. Vasco et al. [3] studied the kinetics of the impregnation process of *Pinus radiata* wood with reactive grade octadecane at four manometric pressures (0 to 3 bar) and a constant temperature of 50 °C. Nevertheless, they found that leakage of octadecane is an issue during its melting. Mathis et al. [4] impregnated two species of hardwood with a microencapsulated PCM to improve the thermal inertia of wood boards for flooring manufacturing. The authors report heat storage improvements of 77.0% and 7.1% for red oak and sugar maple, respectively. Temiz et al. [5] impregnated Scots pine sapwood with a eutectic mixture of capric and stearic acid. They found values of enthalpy and phase change temperature of 94 J/g and 82 J/g, and 22.97 °C and 22.05 °C. Ma et al. [6] delignified and then vacuumed impregnated cedar wood with a eutectic capric-palmitic acid mixture. They found that the impregnation ratio of the eutectic PCM mixture in the delignified wood reached 61.2% without leakage. Also, the melting temperature of the composite was 23.4 °C, and the melting latent heat was 94.4 J/g. Moreover, the thermal conductivity improved significantly by 133.3%. Fuentes-Sepúlveda et al. [7] thermally

characterized *Pinus radiata* wood, impregnated with octadecane. They found that the composite could reach values of melting enthalpies in 36 to 122 J/g, depending on the PCM load. Montanari et al. [8] prepared a SSPCM with polyethylene glycol/polymethyl methacrylate (PEG/PMMA) and delignified wood as a substrate. The delignified wood showed excellent capacity to absorb the PEG/PMMA polymer blend, and the novel material exhibits a melting and solidification latent heat of 76 and 74 J/g, respectively. By pressure impregnation, Hartig et al. [9] impregnated spruce, beech, and poplar wood with a paraffin PCM. The largest levels of PCM per 1 m<sup>3</sup> of wood found by the authors were 250 kg for beech, 230 kg for poplar, and 150 kg for spruce. Moreover, PCM-impregnated beech has a melting and solidification latent heat of 23 J/g and 22 J/g, respectively.

## 2. Materials and method

The used wood of *Pinus radiata* for impregnation is commercially available. The wood samples are rectangular prism-shaped whose dimensions are shown in Table 1. The moisture content of the wood specimens is approximately 12%, and the PCM used for wood impregnation is technical grade 90% octadecane (Gute Chemie).

Table 1. Dimensions of wood samples:

Dimensions	Sample 1	Sample 2	Sample 3	Sample 4	Sample 5	Sample 6
Length (mm)	295.0	300.0	300.0	300.0	300.0	295.0
Width (mm)	59.5	59.5	60.0	59.5	59.5	59.0
Height (mm)	19.0	19.0	19.0	19.0	19.5	19.5

The wood samples were immersed inside a container filled with liquid octadecane inside a vacuum oven (Memmert VO29). The pressurization program consists of three protocols where the vacuum is released at different steps (Figure 1). The sample is submerged in a container with liquid PCM for 45 min. In the first protocol, the vacuum is released instantaneously (Figure 1a). In the second protocol, the vacuum is released in a controlled manner using a ramp of 15 minutes (Figure 1b). Finally, in the third protocol, the vacuum is released in a controlled manner using a ramp of 30 minutes (Figure 1c). The entire impregnation process takes 90 minutes for each impregnated specimen. Once each impregnation process is completed, the specimens were removed from the container and dried with absorbent paper and kept at a temperature lower than the melting point to calculate the load of PCM in the samples for each protocol.

## 3. Results and discussion

Regarding the stability results of the impregnated samples in the different protocols, Figure 2 shows that protocol (c) gives place to the more stable samples, losing between 0.7% to 1.0% of the total mass of PCM. The impregnation protocol (a) shows a major quantity of mass gain, and it shows losses due to the PCM leakage close to 1.1%. Table 2 presents the mass variation of each sample during the wood impregnation process. The variation of the thermal conductivity before and after impregnation (Table 3) ranges between 60% and 90%. It is evident that the highest thermal conductivity value corresponds to the wood with a higher mass of PCM after the impregnation process.



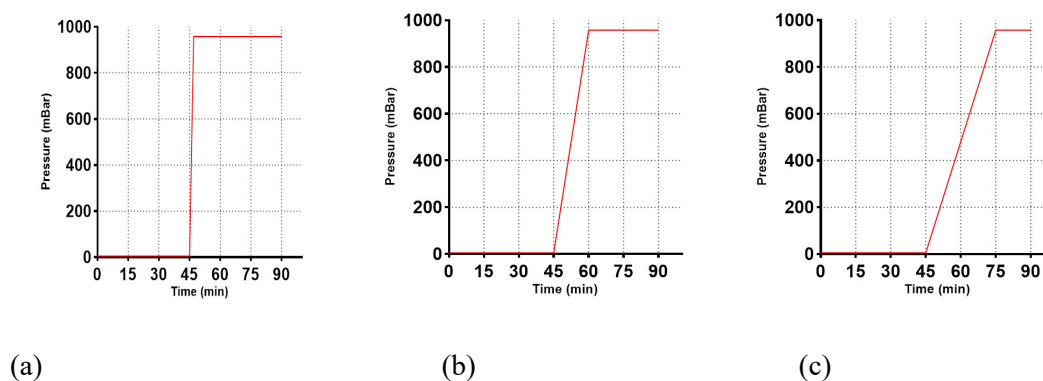


Figure 1. Stages of impregnation process.

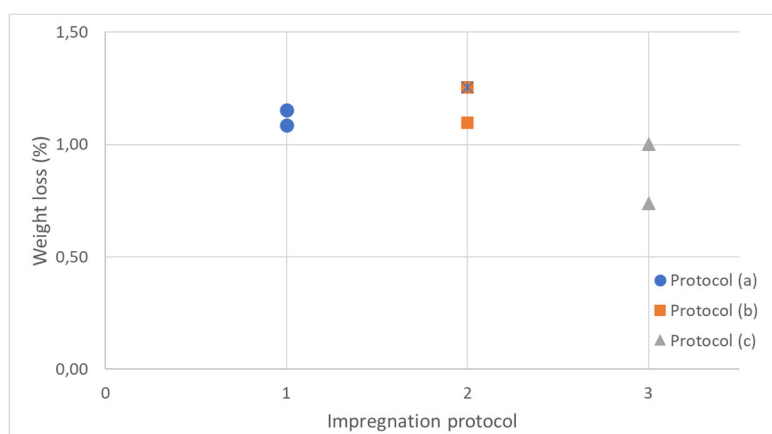


Figure 2. Weight loss graph in the impregnation protocol.

#### 4. Conclusions

The impregnation protocol (a) has a greater homogeneity between the percentage of mass losses among the specimens. Due to wood anisotropy, it is necessary to extend this test to a larger number of samples. The variation of thermal conductivity of the impregnated samples is proportional to the volume of impregnated PCM. It is important to comment that this study will be complemented with visual studies of the distribution of the PCM within the wood structure, as well as studies with DSC and TGA at different positions of wood specimens.

Table 2. Impregnated wood mass through each protocol:

Sample	Impregnation Method	Drywood mass (mm)	Impregnation mass (mm)	Final mass (mm)	Weight loss (%)
1	a	168.27	303.65	300.35	1.09
2	b	166.92	256.44	253.23	1.25
3	c	140.56	315.04	312.71	0.74
4	a	172.70	294.51	291.11	1.15
5	b	157.83	261.35	258.48	1.10
6	c	167.89	274.47	271.73	1.00

Table 3. Thermal conductivity of drywood and impregnated wood at 28°C:

Sample	Protocol	k (W/m K) Drywood	k (W/m K) impregnated wood	%
1	a	0.116	0.212	82.23
2	b	0.125	0.201	61.50
3	c	0.116	0.224	91.55
4	a	0.129	0.217	68.39
5	b	0.114	0.192	68.42
6	c	0.128	0.210	63.38

### Acknowledgements

ANID-Chile, grant number Fondecyt 1201520 funded this research.

### References

- [1] Y. Li, X. Li, Dandan Liu, X. Cheng, X. He, Y. Wu, X. Li, and Q. Huang. Fabrication and properties of polyethylene glycol-modified wood composite for energy storage and conversion. *BioResources*, 11(3):7790-7802, 2016.
- [2] C Barreneche, J Vestaudza, D Bajare, and A.I. Fernandez. PCM/wood composite to store thermal energy in passive building envelopes. *IOP Conference Series: Materials Science and Engineering*, 251:012111, 2017.
- [3] D. Vasco, C. Salinas-Lira, I. Barra-Reyes, and D. M. Elustondo. Kinematic characterization of the pressure-dependent pcm impregnation process for radiata pine wood samples. *European Journal of Wood and Wood Products*, 76(5):1461-1469, 2018.
- [4] D. Mathis, P. Blanchet, V. Landry, and P. Lagire. Impregnation of wood with microencapsulated bio-based phase change materials for high thermal mass engineered wood flooring. *Applied Sciences*, 8(12): 2696, 2018.
- [5] A. Temiz, G. Hekimoğlu, G. Köse Demirel, A. Sarı, and M. H. Mohamad-Amini. Phase change material impregnated wood for passive thermal management of timber buildings. *International Journal of Energy Research*, 44(13): 10495–10505, 2020.
- [6] L. Ma, Q. Wang, and L. Li. Delignified wood/capric acid-palmitic acid mixture stable-form phase change material for thermal storage. *Solar Energy Materials and Solar Cells*, 194: 215–221, 2019.
- [7] R. Fuentes-Sepúlveda, C. García-Herrera, D. A. Vasco, C. Salinas-Lira, and R. A. Ananías. Thermal Characterization of Pinus radiata Wood Vacuum-Impregnated with Octadecane, *Energies*, 13(4): 942, 2020.
- [8] C. Montanari, Y. Li, H. Chen, M. Yan, and L. A. Berglund. Transparent Wood for Thermal Energy Storage and Reversible Optical Transmittance. *ACS Applied Materials and Interfaces*, 11 (22): 20465–20472, 2019.
- [9] J. U. Hartig, F. Hilkert, J. Wehsener, and P. Haller. Impregnation of wood with a paraffinic phase change material for increasing heat capacity. *Wood Material Science and Engineering*, 18(1): 19-28, 2023.

EUROTHERM2023-N215

## Thermal investigation on different shell and tube thermal energy storage systems with inclined flat or wavy internal tubes and filled by PCM and metal foam

Bernardo Buonomo<sup>1</sup>, Oronzio Manca<sup>1</sup>, Sergio Nardini<sup>1</sup>, Renato Elpidio Plomitallo<sup>1</sup>

<sup>1</sup>Dipartimento di Ingegneria, Università degli Studi della Campania “Luigi Vanvitelli”  
via Roma 29, 81031 Aversa (Italy), Phone: +39-081-5010217, Fax: +39-081-5010283, e-mail:  
oronzio.manca@unicampania.it

### Abstract

In the present study, a numerical comparison is conducted between two configurations of latent heat thermal energy storage (LHTES). The two LHTES configurations are shell-and-tube systems with different internal vertical tubes. One tube is inclined flat, i.e. convergent or divergent, while the other one is wavy. The hollow cylinder is filled with a composite phase change material (PCM) composed of pure paraffin wax and aluminum foam. The comparison is based on the liquid fraction and average temperature profiles. The melting time for the converging case, with an inclination angle of 10°, is the lowest among the configurations studied. However, it is comparable to the wavy configurations with the highest amplitude value considered in this study.

**Keywords:** thermal energy storage, phase change material, metal foam, shell and tube system, inclined flat and wavy

### 1. Introduction

The increase in the use of renewable energy sources can result in a mismatch between energy demand and delivery, which highlights the need for improved Thermal Energy Storage (TES) systems. TESs can generally be classified into three categories based on their energy storage mechanisms: sensible heat storage (SHS), latent heat energy storage (LHTES), and thermochemical storage (TCS). SHS stores thermal energy by changing the temperature of the material without any phase transformation. LHTES, on the other hand, stores energy during phase transformation of the material, while TCS requires a reversible physio-chemical condition upon heating to store thermal energy [1]. Among the three types, LHTES shows the most promise as a TES technique due to its high energy storage density and isothermal phase transitions [2].

The performance of Phase Change Materials (PCMs) in Latent Heat Thermal Energy Storage Systems (LHTESS) is hindered by their low thermal conductivities and poor heat transfer capabilities. However, the incorporation of composite PCMs with metal foams has been shown to effectively address these limitations, resulting in improved thermal conductivity and the full utilization of their high energy density [3]. In fact, the use of metal foams as matrices for enhancing the thermal conductivity of thermal energy storage systems and incorporating PCMs within them can significantly improve their thermal conductivity. This allows for the creation of a thermal storage system with a fast-absorbing energy zone characterized by low thermal resistance, even though the heat storage capacity of the composite MF-PCMs may be slightly reduced. It is interesting also to compare some possible solutions related to the shell and tube system with PCM and metal foam with different internal tube geometries such as inclined flat tube and wavy tube [4,5].

In the present work, a comparison between two latent heat thermal energy storage (LHTES) configurations is numerically investigated. The two LHTES configurations are shell and tube systems with different internal vertical tube, one tube is inclined flat, i.d., the tube is convergent or divergent and the other one is wavy. In the investigation the hollow cylinder is filled by composite PCM which is

made up of a pure paraffin wax and aluminum foam. The comparison is given in terms of liquid fraction and average temperature profiles.

## 2. Materials and method

The two geometries, in Figure 1, related to the considered thermal energy storage under investigation are both a vertical shell and tube unit with a corrugated internal cross section, in Figure 1a, and an inclined flat tube either convergent or divergent, respectively in Figure 1b and 1c. The main geometric parameters of these configuration are listed below:  $L$  is the cylinder height, equal to 100 mm,  $r_i$  is the internal radius, and  $r_e$  is the external radius equal to 50 mm. The average internal radius for the wavy is equal to 6 mm and the minimum internal radius is for the convergent and divergent tube equal to 6 mm.

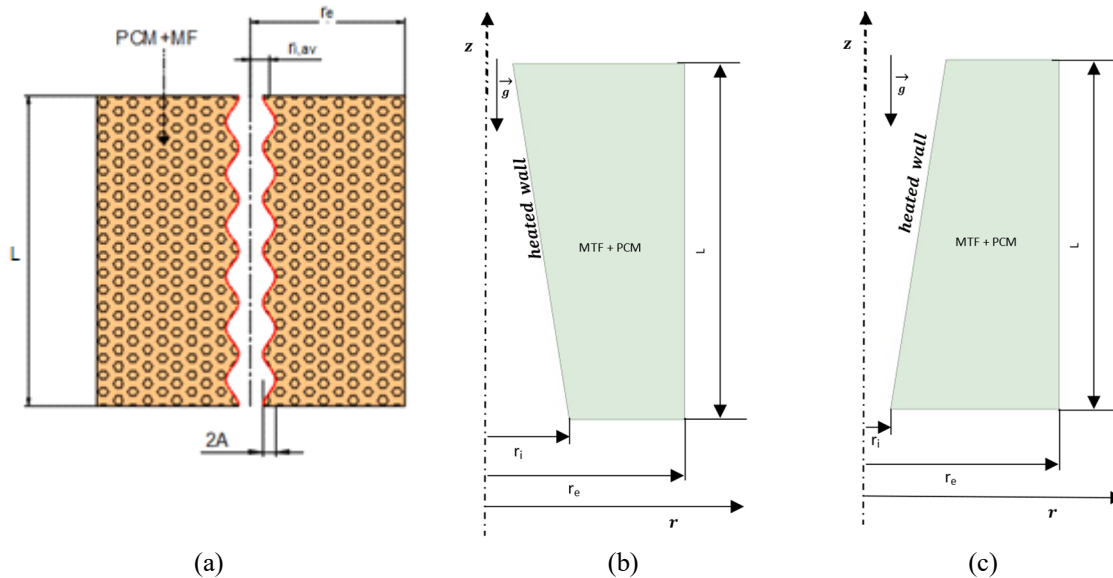


Figure 1. Sketch of the two thermal energy storage considered: a) wavy internal tube, b) convergent internal tube, c) divergent internal tube.

The aluminum foam has porosity equal to  $\epsilon = 0.9546$  and a pore density of 20 PPI. The enthalpy-porosity method is employed to analyze the melting process of PCM. Furthermore, the Forchheimer-extended Darcy model under the local thermal non equilibrium (LTNE) hypothesis is adopted to model the heat transfer between the phase change material and the metal foam. The PCM is considered the fluid part of the porous media and the metal foam is considered the solid one. All the assumptions are described in [4]. The governing equations are given in [4,5]. Moreover, the external surface is assumed adiabatic, the internal tube is considered at assigned uniform temperature equal to 350 K and the initial temperature is uniform and equal to 293 K. In Table 1 are reported the thermophysical properties.

The governing equations are numerically solved by means Ansys-Fluent. The finite volume method (FVM) is employed in Ansys-Fluent code to discretize and solve the problem. Using the SIMPLeC and PRESTO algorithms the pressure-velocity coupling and the pressure calculation are solved, respectively. The chosen time step to perform the transient analysis is equal to 0.2 s. The convergence errors are assumed equal to  $10^{-5}$  for continuity and momentum equations, and  $10^{-8}$  for energy equations. More details are given in [4,5].

Table 1. Thermophysical properties.

Properties	RT 50	Aluminum
$\rho$ [kg/m <sup>3</sup> ]	820	2719
$c_p$ [J/kg K]	2000	871
$k$ [W/m K]	0.2	202.4
$\mu$ [kg/ms]	0.0038	-
$\gamma$ [W/m K]	0.0006	-
$H_L$ [J/kg]	168000	-
$T_s$ [K]	318	-
$T_L$ [K]	324	-

### 3. Results

Figures 2 and 3 show the liquid fractions and average temperatures for the wavy (Figure 2) and inclined flat tube (Figure 3), respectively. Among the three cases examined, the one with an amplitude  $A=4$  exhibits a shorter melting time and reaches its final equilibrium temperature faster. It should be noted that increasing the amplitude  $A$  also increases the surface area of the internal tube, which in turn improves heat transfer. In Figure 3, the same variables are given for the cases related to the inclined internal tube. The lowest melting time is obtained for the converging case with an inclination angle equal to  $10^\circ$ . The case with higher melting time is the vertical tube without inclination. The increase of melting for the inclined tubes is due to the increase in the heat transfer surface between the internal tube and composite PCM. Moreover, the converging cases for the same inclination angle present a lower melting time than the diverging cases due to the presence of a more intense natural convection effect.

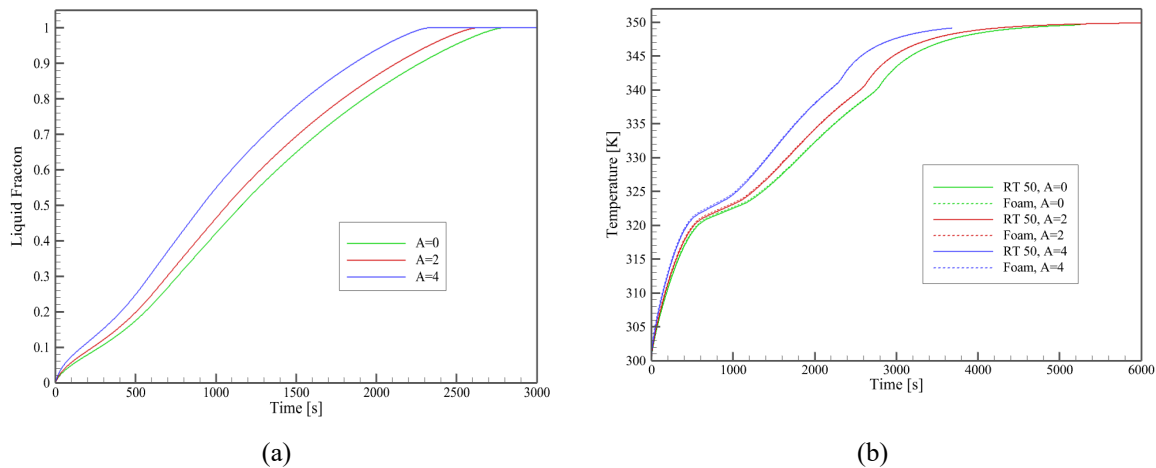


Figure 2. Results for wavy internal tube: a) liquid fraction, b) average temperature in the TES.

### 4. Conclusions

The results shown that by increasing the waves amplitude and reducing the wavelength, the phase change process is enhanced and, consequently, the same does the storage rate. Moreover, it is shown that the converging system reaches the melting and the maximum energy storable faster than the diverging one. The melting time for the converging case with an inclination angle equal to  $10^\circ$  presents the lowest melting time but is comparable to the wavy configurations with the highest amplitude value here considered.

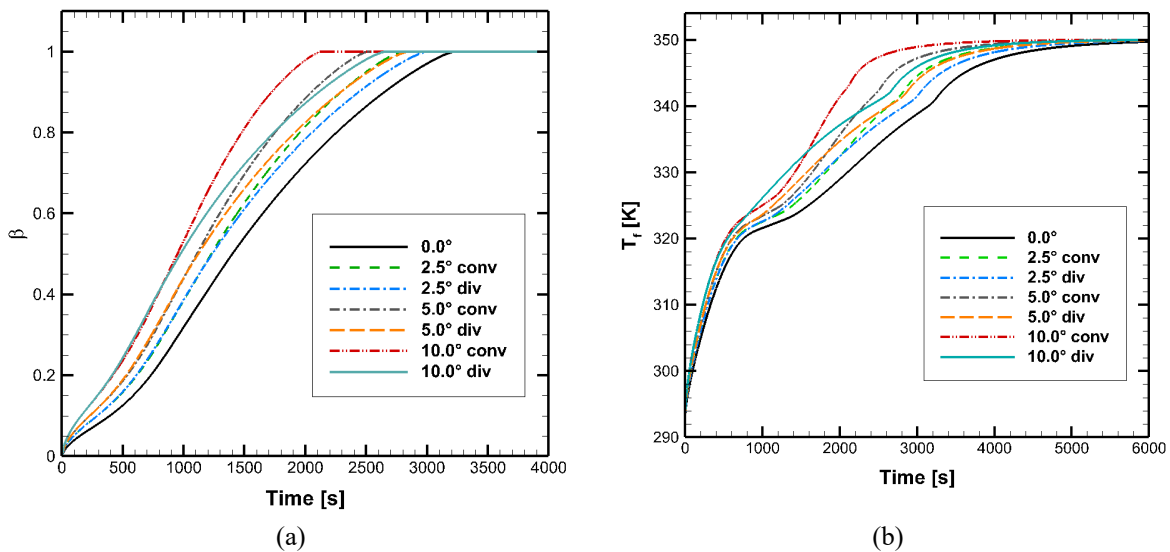


Figure 3. Results for inclined internal tube: a) liquid fraction, b) average temperature in the TES.

## Acknowledgements

This research was partially funded by MIUR (Ministero dell'Istruzione, dell'Università e della Ricerca), grant number PRIN-2017F7KZWS.

## References

- [1] Dincer, I., and Rosen, M. A., 2010, Thermal Energy Storage: System and Application, John Wiley & Sons, New York.
- [2] Jaisatia Varthani, A., Shasthri, S., Baljit, S., and Kausalyah, V., 2022, A Systematic Review of Metal Foam and Heat Pipe Enhancement in Latent Heat Thermal Energy Storage System, J Energy Storage, 56, p. 105888.
- [3] Gasia, J., Miró, L., de Gracia, A., Cabeza, L.F., 2022, Heat transfer enhancement for latent heat storage components, Advances in Energy Storage: Latest Developments from R&D to the Market, pp. 675-693
- [4] Buonomo, B., di Somma, F., Manca, O., Nardini, S., and Plomitallo, R. E., 2021, "Numerical Investigation on Latent Thermal Energy Storage in Shell and Corrugated Internal Tube with PCM and Metal Foam," E3S Web of Conferences, 312, p. 03003.
- [5] B. Buonomo, M. R. Golia, O. Manca, S. Nardini, R. E. Plomitallo, Composite phase change material with metal foam in shell and convergent tube thermal energy storage systems, paper submitted to ASME-SHTC 2023 Summer Heat Transfer Conference, Washington DC, USA July 10–12, 2023.

EUROTHERM2023-U216

## Development of innovative sorption-based technology for cooling and desalination of water on board of vessels

Y. Zhang<sup>1</sup>, V. Brancato<sup>1</sup>, D. Palamara<sup>2</sup>, L. Calabrese<sup>1,2</sup>, V. Palomba<sup>1</sup>, F. Costa<sup>1</sup>, D. La Rosa<sup>1</sup>, G. Penello<sup>3</sup>, W. Mittelbach<sup>3</sup>, A. Frazzica<sup>1,\*</sup>

<sup>1</sup>National Research Council of Italy – Institute for Advanced Energy Technologies (CNR-ITAE), Salita S.Lucia sopra Contesse 5, 98126 Messina, Italy. e-mail:valeria.palomba@itaecnr.it

<sup>2</sup>Department of Engineering, University of Messina, Contrada di Dio Sant'Agata, 98166, Messina, Italy

<sup>3</sup>Sorption Technologies GmbH, Christaweg 52, 79114 Freiburg im Breisgau, Germany

### Abstract

This study focuses on the comparative testing of lab-scale adsorbers developed for adsorption cooling and desalination applications. The target is to design a technology able to co-generate both fresh water and cooling on board of vessels by exploiting low temperature waste heat. Two different materials were comparatively tested, namely, micro-porous silica gel and a composite sorbent employing Silica gel with 30% LiCl embedded inside the pores. Adsorbers were realized by embedding the adsorbent materials inside aluminum heat exchangers, testing them in a lab-scale testing rig, applying the T-LTJ (thermal-large temperature jump) method. This method allows to evaluate the adsorption/desorption kinetic of the process. Different boundaries were tested to evaluate their influence on the main performance indicators, namely, specific daily water production (SDWP) and specific cooling production (SCP). A numerical model will be implemented, based on the obtained results, to optimize the architecture of the adsorption cooling and desalination technology.

**Keywords:** sorption, cooling, desalination, vessels, waste heat

### 1. Introduction

Adsorption desalination (AD) integrated with cooling represents an innovative technology that can help in increasing overall energy efficiency in several fields (e.g. industrial, residential, shipping sectors). It can supply high-quality freshwater and cooling at the same time or autonomously. Sorption materials are the core components, they extract the water vapour from the fed brine inside the evaporator during the adsorption process, and release the adsorbed water in the form of water vapour which is then condensed in the condenser to get the portable water during the desorption process. Composite adsorbents are promising candidates for high water uptake and tunable working operating temperature and pressure ranges. However, only a few composite sorbents have been developed and tested in adsorption desalination (AD) systems [1].

In this study, an innovative composite based on, silica gel embedded with 30% LiCl was developed and tested against the purely micro-porous silica gel, commonly employed in adsorption chillers. Their ad/desorption dynamics were tested and analyzed in a thermal-large temperature jump (T-LTJ) apparatus. Based on the results, a numerical model will be developed and calibrated to evaluate the achievable performance of an optimized architecture.

### 2. Material selection and preparation

Silica gel-30% LiCl composite was synthesized through the dry impregnation method. The sorption isobars and sorption kinetics under the selected typical operating conditions were measured by the dynamic vapor sorption (DVS) instrument. Sorption isobars show that the composite experiences three adsorption stages: physisorption, hydration reaction + deliquescence and solution absorption. It

possesses good mass transfer efficiency, with a water equilibrium extremely high compared to micro-porous silica gel. The calculation of the theoretical SDWP indicated that silica gel-30% LiCl can contribute to high water production ranging from 43 to 60 m<sup>3</sup>/tonne/day for the selected typical conditions.

### 3. Experimental testing of the lab-scale adsorber and modelling

#### 3.1. Experimental testing

The thermal large temperature jump (T-LTJ) apparatus (see Figure 1) consists of a vacuum chamber, an evaporator/condenser, four thermostats and a vacuum pump. A finned flat-tubes aluminum heat exchanger serves as the ad/desorber, and it was filled with the sorbent particles, packed between the fins. Fast temperature jumps/drops are operated by quickly switching the valves after reaching desorption/adsorption equilibrium, aiming to simulate practical adsorption and desorption process. The differential temperature of the inlet and outlet heat transfer fluid (HTF) contributes to calculating the adsorption/desorption characteristic time by:

$$\Delta T_{ad/de}(t) = \Delta T_{\infty} + \Delta T_0 \cdot \exp\left(-\frac{t}{\tau_{ad/de}}\right) \quad (1)$$

where  $\Delta T_{\infty}$  and  $\Delta T_0$  are fitting parameters.  $\tau_{ad/de}$  refers to the characteristic time, reflecting the ad/desorption rates. The analyzed results under various conditions ( $T_{eva/cond}=5, 10, 15, 20, 25$  °C,  $T_{de}=60, 70, 80, 85$  °C) revealed that the  $\tau_{ad/de}$  of silica gel-30% composite increases with the raised  $T_{eva/cond}$  and decreased  $T_{de}$ . Furthermore, the obtained  $\tau_{ad/de}$  and adsorption equilibrium were used to calculate the maximum SDWP for different system designs (2-bed, 3-bed and 4-bed). It shows that the SDWP can reach 69 m<sup>3</sup>/tonne/day when  $T_{eva/cond}=20$  °C and  $T_{de}=80$  °C by adopting the 3-beds-configuration.

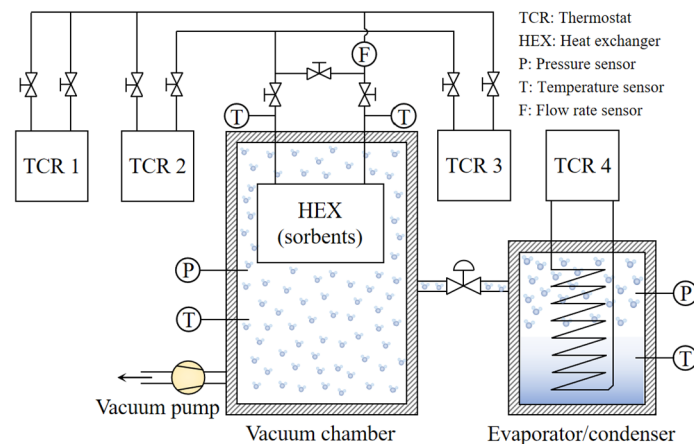


Figure 61. Schematic representation of the T-LTJ apparatus employed for the kinetic characterization

#### 3.2. Mathematical modelling

A numerical model is planned to be developed from the SorpLib, which is a library of components modelled using Modelica language and realised by the Institute of Technical Thermodynamics at RWTH Aachen university [2]. Its validation will be verified by the lab-scale testing results, and then further estimations on the influencing factors on performance will be conducted.

### 4. Conclusions

In summary, silica gel-30% LiCl looks as a promising candidate for adsorption desalination and cooling applications. It has good mass transfer efficiency and can reach high SDWP. Its practical ad/desorption dynamic in reactors was measured by a lab-scale adsorption desalination device. Results reveal that the ad/desorption rates are more sensitive to evaporation/condensation temperature than the desorption





temperature. Both material characterizations and system performance indicate that silica gel-30% LiCl is an excellent material to build high-efficiency adsorption desalination systems. A numerical model will be implemented to further support the future design activities.

### **Acknowledgements**

This project has received funding from the European Union's Horizon Europe research and innovation programme under grant agreement No 101056801 (ZHENIT).

### **References**

- [1] Zhang, Y., Palomba, V., Frazzica, A.. Understanding the effect of materials , design criteria and operational parameters on the adsorption desalination performance – A review., Energy Conversion and Management, 2022.
- [2] Gibelhaus, A., Tangkrachang, T., Bau, U., Seiler, J., Bardow, A.. Integrated design and control of full sorption chiller systems. Energy, 2019.

EUROTHERM2023-B217

## Numerical investigation on a solar chimney integrated with a thermal energy storage system using PCM

Bernardo Buonomo, Maria Rita Golia, Oronzio Manca, Sergio Nardini

<sup>1</sup>Dipartimento di Ingegneria, Università degli Studi della Campania “Luigi Vanvitelli”  
via Roma 29, 81031 Aversa (Italy), Phone: +39-081-5010217, Fax: +39-081-5010283, e-mail:  
oronzio.manca@unicampania.it

### Abstract

This paper presents the findings of a two-dimensional numerical investigation of a solar chimney that has been combined with an absorptive capacity wall on the south façade of a building. The solar chimney includes a glass panel that is inclined at an angle of  $2^\circ$ , as well as a converging duct that features a vertical absorptive wall. The dimensions of the chimney are as follows: 5.0 m total height, 4.0 m channel height, and 0.34 m and 0.20 m for inlet and outlet channel width, respectively. A thermal energy storage system is used in the study, which can be of length  $L/2$  or  $L$  and thickness  $s$  or  $s/2$ . To determine the optimal configuration of the hybrid system in terms of thermal performance, four potential positions are examined. The analysis is carried out on June 21 and December 21 between sunrise and sunset, at Aversa (Italy). The aim of evaluating the thermal and fluid dynamics behaviors is to provide suggestions for improving the energy conversion system.

**Keywords:** Solar energy system, Solar chimney, Renewable energy, Thermal energy storage

### 1. Introduction

The solar chimney is a relatively new solution in the field of renewable energy that can passively heat and cool buildings. Solar radiation heats the air inside the chimney barrel, and due to the buoyancy phenomenon, the heated air moves through the chimney system. Although there are not many real-world applications in buildings, the solar chimney seems to be a promising technology both for the benefits it can bring to space heating and cooling and from an aesthetic point of view. In addition, there are numerous studies related to solar chimney improvement. One of the possible ways to improve the performance of the chimney is the addition of a phase change material (PCM) layer, which together with a careful choice of size, geometry, placement angle, and absorbing materials leads to the achievement of a more efficient system. In fact, the addition of PCM increases thermal comfort and extends ventilation duration, and electrical generation period when combined with power plants. [1,2] The combination of PCM and solar chimney gives to the system a latent heat capacity. The presence of PCM creates thermal energy storage that ensures to the chimney a better performance during summertime and wintertime. During the wintertime, the solar chimney heats the indoor environments pushing hot air inside and during the summertime it cools the indoor environments pushing out the hot air and increasing the air mass flow rate [3].

Kotani et al. [4] and Kaneko et al. [5] developed a novel design for the solar chimney using sodium sulphate decahydrate as the PCM for latent heat storage, and they verified the numerical findings using results from experiments. They analysed the case when the PCM melted entirely and when it did not, and they found that when the PCM melted totally during the day, the ventilation period is lengthened during the nighttime. Nateghi and Jahangir [6] highlight that solar chimney changes the air inside the room constantly with fresh air and which reduce the infection spreading and provide more thermal comfort. They analysed the PVM thermal index of the solar chimney in three different climate conditions to understand where it provides comfort and quantify it.

This paper presents a two-dimensional numerical investigation of a solar chimney combined with an absorptive capacity wall on the south façade of a building. The study examines four potential positions for the solar chimney.

## 2. Materials and method

The solar chimney, depicted in Figure 1, consists of a vertical channel with an absorbing wall of height  $L$  and a thermal energy storage unit placed behind it. The height of the thermal energy storage unit is  $L/2$  for configurations A, B, and C, and  $L$  for configuration D. The system also features a low emissivity glazed wall inclined at two degrees. To simulate the effects of solar radiation during the months of June and December, a homogeneous heat source equal to the solar radiation was imposed on the chimney. The solar radiation data was obtained from the PVGIS website. Table 1 lists the thickness of the thermal energy storage unit (indicated by "s") and the inlet and outlet portions of the airflow (indicated by " $b_{max}$ " and " $b_{min}$ ," respectively).

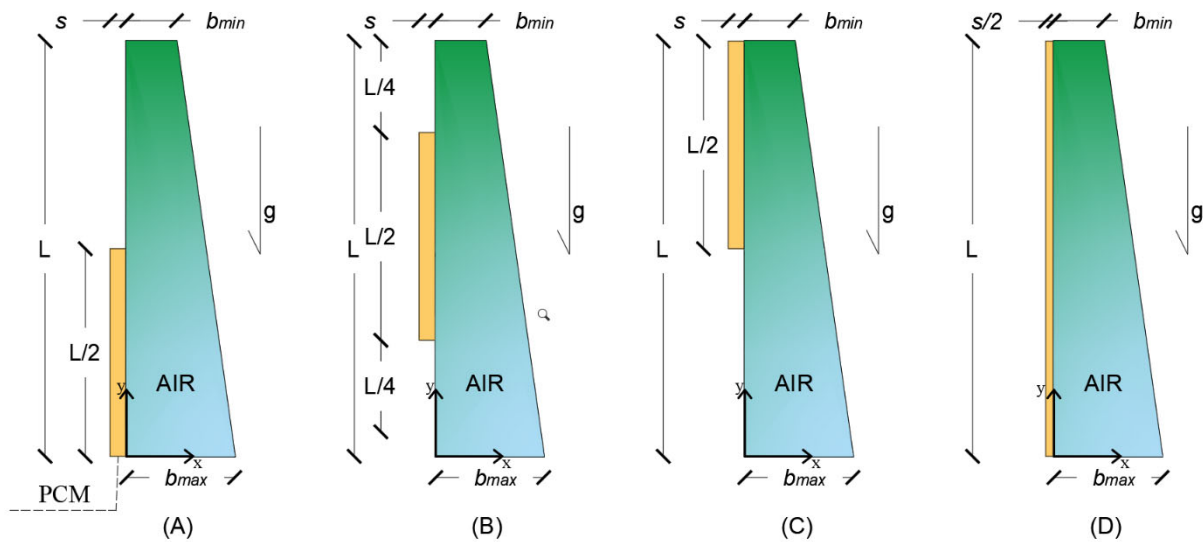


Figure 2. Solar chimney sketch

Table 1. Solar chimney dimensions

$L$	$L/2$	$s$	$s/2$	$b_{max}$	$b_{min}$
<b>4.00 m</b>	2.00 m	0.01 m and 0.03 m	0.005 m and 0.015 m	0.34 m	0.20 m

The PCM, chosen for this simulation is paraffin wax RT42, and its thermal characteristics are shown in Table 2 [7].

Table 2. Properties of the paraffin wax RT42[15]

$C_p$ [J kg <sup>-1</sup> K <sup>-1</sup> ]	$\gamma$ [K <sup>-1</sup> ]	$\lambda$ [W m <sup>-1</sup> K <sup>-1</sup> ]	$\mu$ [kg m <sup>-1</sup> s <sup>-1</sup> ]	$\rho$ [kg m <sup>-3</sup> ]	$H_L$ [kJ/kg]	$T_{sol}$ [K]	$T_{liq}$ [K]
<b>2100</b>	0.004	0.21	0.0055	829	228	314.15	316.15

## 3. Results

The results of simulations on the solar chimney combined with a phase change material thermal storage system are shown in terms of liquid fraction.

Fig. 2 shows the liquid fraction in June and December for thicknesses  $s=1$  cm (Fig. 2.a and Fig. 2.c) and  $s=3$  cm (Fig. 2.b and Fig. 2.d). As can be seen in Figure 4.b the PCM is unable to achieve complete melting, despite the high irradiance and high temperature in the summer month, the PCM thickness is

too high, and the complete melting does not happen. Configuration D (Fig. 2.b) has a thickness of  $s/2=1.5$  cm, with the same volume of configurations A, B and C, its trend makes clear that the melting and solidification time depends on the thickness of the PCM layer and not only on the amount of volume, since otherwise the configuration D would also have had a trend similar to the other three configurations. The difference in PCM layer thicknesses affects both the melting and solidification phases, since the conductivity of PCM alone is very low, both the melting and solidification phases for thicknesses greater than 1 cm turn out to be longer. Another

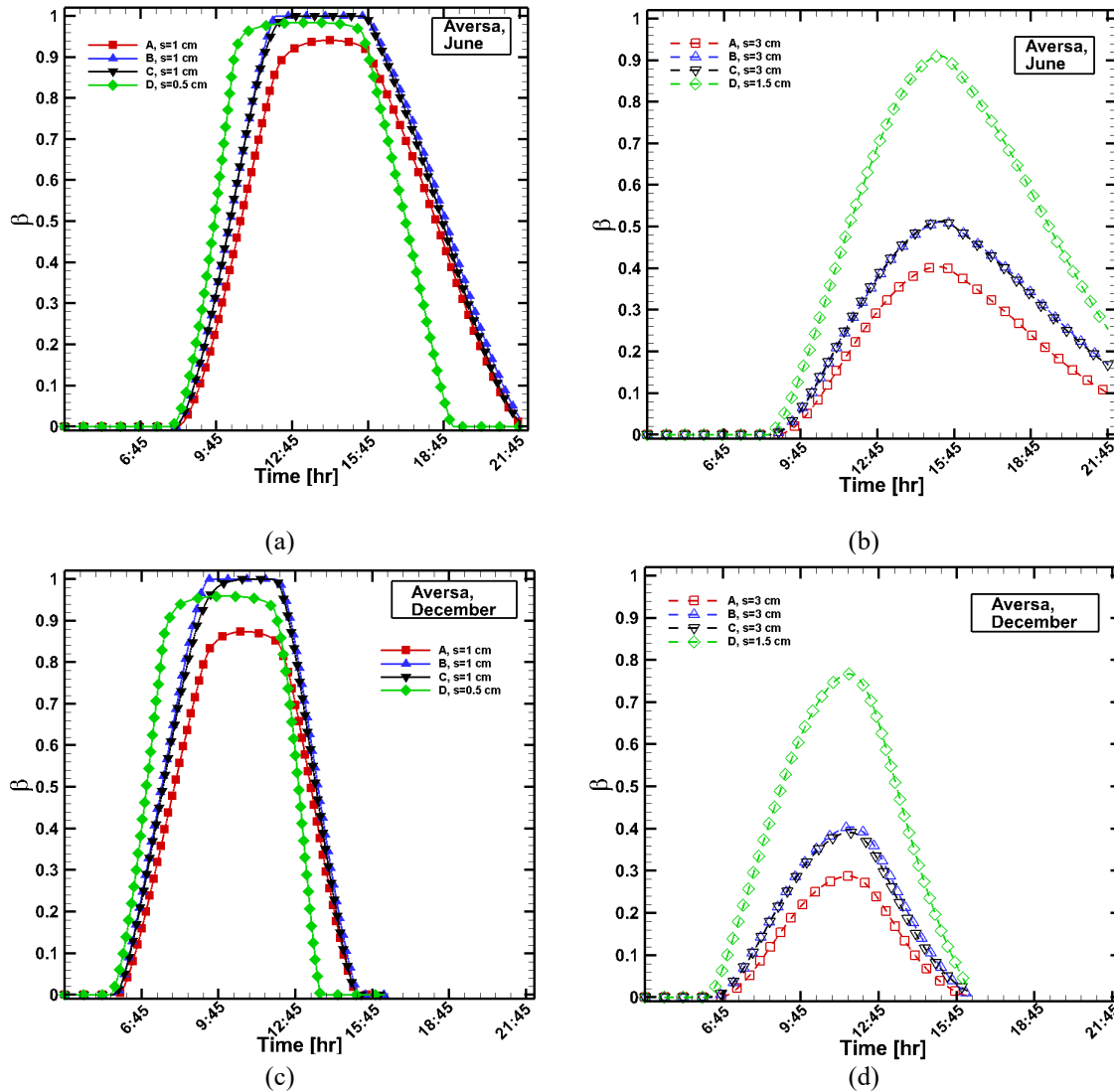


Figure 3. Liquid fraction as a function of time in June,  $s=1$  cm (a) and  $s=3$  cm (b) and December,  $s=1$  cm (c) and  $s=3$  cm (d).

parameter that influences the trend of stored energy, liquid fraction and mass flow rate is the position of the PCM box along the wall. In fact, configuration A, both in the case of  $s=1$  cm and  $s=3$  cm, has the least melting being the PCM box placed downward. This can be attributed to the chimney configuration itself and the effect of hot air rising upward.

#### 4. Conclusions

The study analysed the behavior of a solar chimney integrated with thermal storage, in four different configurations with different thicknesses of the PCM layer, during the summer and winter periods, in the city of Aversa (IT). The solar chimney represents one of the most interesting passive heating and cooling methods that can be integrated in different building types. The study aims to identify the trend of the liquid fraction, mass flow rate and stored energy in different configurations to understand which

thicknesses and positions are most appropriate depending on the outdoor environment. It was noted how placing the PCM box at the bottom of the solar chimney does not allow full melting of the PCM and it is correlated with lower stored energy. It is also pointed out how the behavior of the PCM box in the D configuration varies greatly depending on the thickness, where at the maximum point it almost triples going from  $s=0.5$  cm to  $s=1.5$  cm. Finally, the authors believe it is necessary for more simulations to be carried out with different types of PCMs and different thicknesses.

## Acknowledgements

This research was partially funded by MIUR (Ministero dell'Istruzione, dell'Università e della Ricerca), grant number PRIN-2017F7KZWS.

## References

- [1] Kassaei, F.; Ghodsi, A.; Jadidi, A. M. and Valipour, M. S., "Experimental studies on solar chimneys for natural ventilation in domestic applications: a comprehensive review". *Environmental Science and Pollution Research*, 29, pp. 73842–73855, <http://doi:10.1007/s11356-022-22956-3>, (2022).
- [2] Omara, A. A. M.; Mohammed, H. A.; al Rikabi, I. J.; Abuelnuor, M. A. and Abuelnuor, A. A., "Performance improvement of solar chimneys using phase change materials: A review". 228, pp. 68–88, *Solar Energy* (2021).
- [3] Cabeza, L. F.: *Advances in Thermal Energy Storage Systems: Methods and Applications*; Elsevier; ISBN 9780128198858.
- [4] Kotani, H.; Sharma, S. D.; Kaneko, Y.; Yamanaka, T. and Sagara, K., "Development of Solar Chimney with Built-In Latent Heat Storage Material for Natural Ventilation" (2005).
- [5] Kaneko, Y.; Sagara, K.; Yamanaka, T. and Kotani, H., "Ventilation Performance of Solar Chimney with Build-in Latent Heat Storage", <https://www.researchgate.net/publication/265989559>, (2006).
- [6] Nateghi, S. and Jahangir, M. H., "Performance evaluation of solar chimneys in providing the thermal comfort range of the building using phase change materials". *Cleaner Materials*, 5, 100120, <http://doi:10.1016/j.clema.2022.100120>, (2022).
- [7] Xamán, J.; Vargas-López, R.; Gijón-Rivera, M.; Zavala-Guillén, I.; Jiménez, M. J. and Arce, J., "Transient thermal analysis of a solar chimney for buildings with three different types of absorbing materials: Copper plate/PCM/concrete wall". *Renewable Energy*, 136, pp. 139–158; <http://doi:10.1016/j.renene.2018.12.106>; (2019).

EUROTHERM2023-E220

## Stability Investigation of PCM-Emulsions

Stefan Gschwander

Fraunhofer Institute for Solar Energysystems, Freiburg, Germany, Phone: +49-761-45885494,  
e-mail: [stefan.gschwander@ise.fraunhofer.de](mailto:stefan.gschwander@ise.fraunhofer.de)

### Abstract

Phase Change Slurries (PCS) are one option to use phase change materials (PCM) in thermal systems. By dispersion of a PCM in a carrier fluid it is possible to increase the heat capacity of water in the temperature range of the PCM's phase transition. In PCM-emulsion (PCME) the hydrophobic PCM is directly dispersed in the carrier fluid, mostly water, and stabilized by emulsifiers. Like every emulsion PCME are metastable systems tending to separate in two phases (water and PCM). Compared to usual emulsions PCME must withstand on one hand side the PCM's repeated phase transition and on the other side the high shear rates applied in pumps and other hydraulic components. This is a challenge in the stabilization of this innovative heat transfer fluids. This contribution presents results of two steps in the stability investigation on small-scale applied in a rheometer and on application scale showing different aging characteristics.

**Keywords:** Phase Change Slurry, PCM-Emulsion, Stability, Supercooling, Heat Transfer Fluid

### 1. Introduction

Already in the 1990s there was a lot of research on PCM slurries in Japan. The first huge PCS storage application was also installed in Japan at Narita airport (Tokyo) using microencapsulated PCM in a 900 m<sup>3</sup> storage tank to store cold for peak shaving in an air conditioning system [1]. Unfortunately, there is no information available about the stability of the PCS during operation.

In 2002 at Fraunhofer ISE work on PCS was started using microencapsulated paraffin as PCM to disperse it into water. The shell of these microcapsules was made of PMMA showing a high stability, but due to the density difference between the microcapsules and water the system tends to separate quickly making it difficult to convey the PCS through a hydraulic piping system after keeping the system for some hours without fluid circulation. But nevertheless, at the end of the development it was possible to build a first 5 m<sup>3</sup> demonstration system having twice as much storage capacity than a pure water storage of the same size [2].

In the next development phase, the focus was turned on PCME with the goal to overcome the separation issues of microencapsulated PCS. Additionally, PCME should be more cost efficient due to the abandonment of the shell synthesis process in the production. The PCME investigated here are produced using paraffin as PCM, nonionic emulsifiers for the stabilization and since supercooling is triggered by the emulsification [3], crystallization seeds are used to suppress it.

In principle all emulsions are metastable systems tending to separate the oil from the water phase. Especially PCME require high stability since the oil, PCM in this case, change its phase between solid and liquid frequently and facing a high shear stress additionally due to the flow regime and especially when passing centrifugal pumps conveying it through the hydraulic network. So, experimentation on cycle stability of PCME is important to qualify these materials for a wider range of applications. Therefore different cycle tests are applied to gain information about its stability [4].

## 2. Material and methods

The production of PCME is done in a 5 kg scale which is enough material to fill a test facility. The test facility shown in Figure 62 includes two heat exchangers, a centrifugal pump, valves, expansion vessel and measurement sensors to monitor temperature, volume flow and pressure drop. In the first step stability is tested by applying the emulsion to a rotational rheometer (Anton Paar MCR 502) using a concentric cylinder geometry (cc 27). This set up allows to apply repeated temperature cycles and a defined shear stress at the same time. During the measurement heating and cooling ramps with a rate of 2 K/min and 10 min isothermal phases in between are applied. The shear rate applied during the temperature cycles is  $100 \text{ s}^{-1}$ . Enthalpy determination is made by using a DSC Q2500 from TA-Instruments and particle size is measured by using the light scattering system LS13320 from Beckman Coulter.

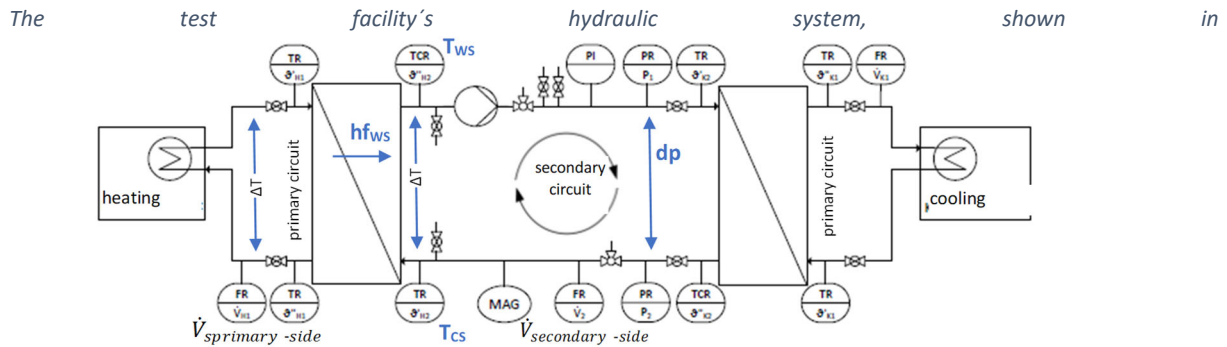


Figure 62, has a fill volume for PCME of four liters. In the experiments the volume flow is controlled to 150 l/h, so every hour 37.5 cycles are done summarizing in a day to 900 [5]. In the hydraulic circuit two flat plate type heat exchangers are integrated, the first one is used to heat up the PCME above the melting temperature and the second is cooling it down again to a temperature below the crystallization temperature. Temperatures are measured by using Pt100 sensors, which are calibrated to an uncertainty of  $\pm 0.05 \text{ K}$ , the volume flows are measured by using a magnetic inductive volume flow meter (Krone Optiflux 5000). Pressure drop is measured on the PCME side (secondary side) of the heat exchanger cooling the PCME, because in case of degradation or breakage of the emulsion the PCM will crystallize on the heat exchanger plates which led to an increase of the pressure drop. Energy flows are monitored by heat flow determination using temperature difference and volume flow of the primary sides of the heat exchanger heating the PCME as well as the specific heat capacity of water which in this circuit. The temperatures of the primary warm sides are controlled by a heater Weinreich WTD ) and the cold side is controlled by a thermostat (Huber unistat 510). All data is acquired with a Keysight 34970A data acquisition system equipped with two 20 channel multiplexer modules 34901A for temperature, volume flow and pressure measurement and a multifunction module 34907A for controlling the pump, the heater and the thermostat.

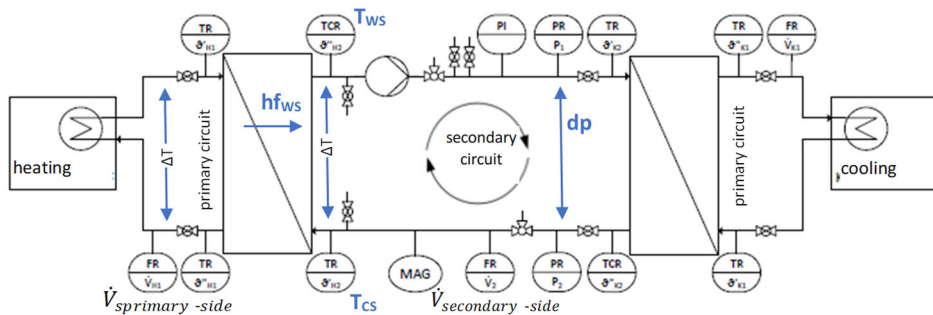


Figure 62. Schematic of the test facility for cycling PCM, heat Flow warm side  $hf_{ws}$ , temperature PCME warm side  $T_{ws}$ , temperature PCME cold side  $T_{cs}$ , volume flow  $\dot{V}$ , difference pressure over heat exchanger  $dp$

Additional to the analyses of enthalpies and particle size the water-equivalent factor is determined by using the DSC results (mass-related) like published in [6] and volume-related according to the following equation on the basis of the measurements gained with the test facility:

$$water-eq = \frac{\dot{V}_{primary-side} \cdot \Delta T_{primary-side}}{\dot{V}_{secondary-side} \cdot \Delta T_{secondary-side}}$$

The water-equivalent factors determined over the DSC measurements are presented as bar diagram and the values determined over the measurement in the test facility are presented as heat map diagram.

### 3. Results

Figure 63 shows the results from the rheometer cycling. Its visible that during the cycling (a) the viscosity is rising which is caused by water evaporation from the sample during the experiment. The water evaporation can be also seen in the enthalpy curve (c); after the cycling the enthalpy is slightly higher which result in higher water-equivalent factors (d). The differences in particle size are within the measurement uncertainties, so that in total it can be stated, that there is no degradation within this test.

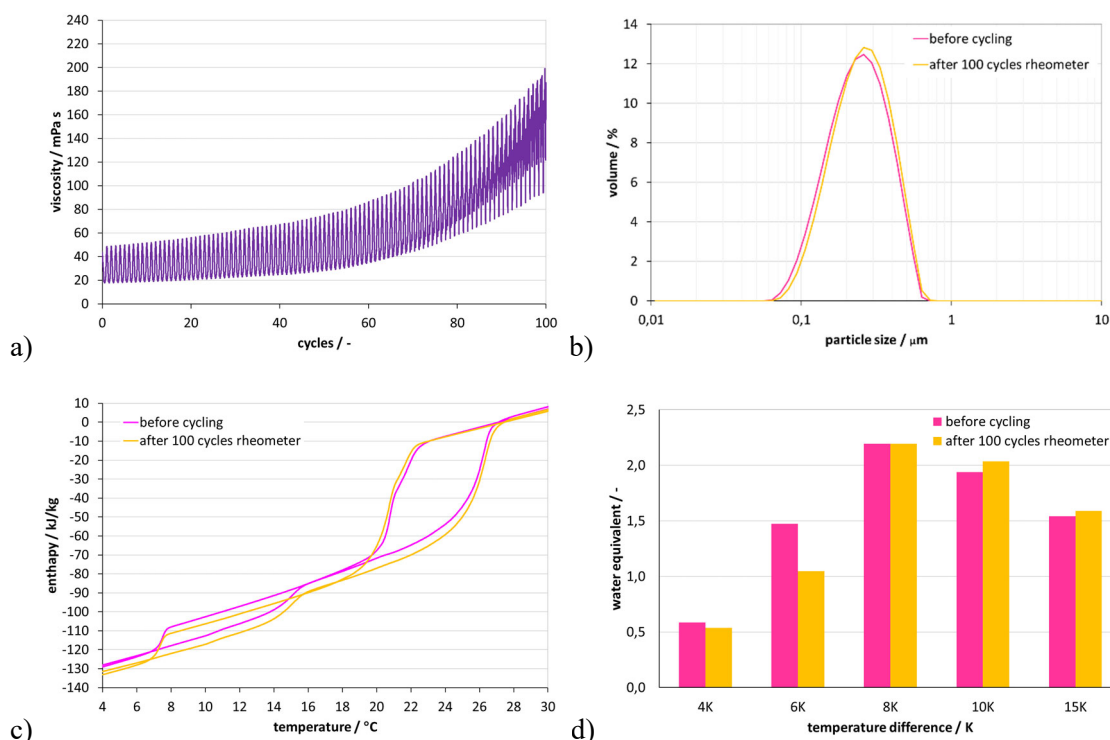


Figure 63. Results of cycling results in the rheometer: a) viscosity development over 100 cycles, b) particle size and c) enthalpy before and after the cycling, d) water-equivalent factor before and after cycling

Figure 65 displays the results from the test facility. The samples was cycled for 14 days summarizing to 12600 cycles in total. During the measurement shown in (a) the temperature  $T_{ws}$  and  $T_{cs}$  were varied to determine the water-equivalent factor in dependency on temperatures shown in (Figure 65b). Samples taken during the experiment showing a change in particle size, the size distributions getting broader (Figure 142b). The enthalpy curves indicating a change for the first sample taken after one day but then again, the same behavior as the uncycled sample (Figure 65a).



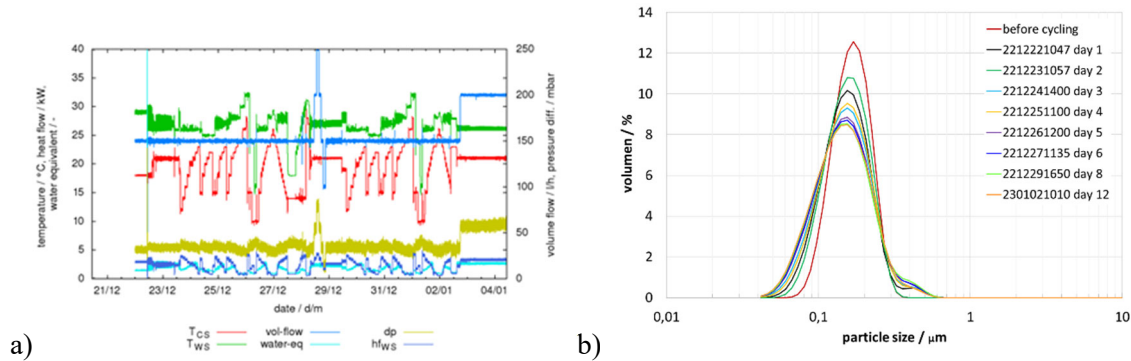


Figure 142. Results from the test facility: a) parameters measured and determined during the experiment, b) particle size distributions taken at different days

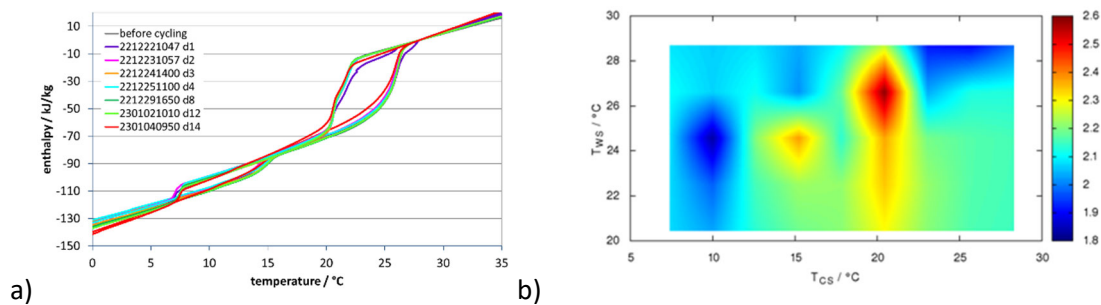


Figure 65. Results from the test facility: a) corresponding enthalpies and b) water equivalent factor determined using the measurement data

## 4. Conclusions

The results presented here showing that degradation experiments on a small scale (in the rheometer) can be a good indication of the stability of PCME but they cannot replace further degradation investigation in a more application related experiment. In the example presented there is almost no degradation visible in the rheometer experiment but there is degradation visible in the test facility experiment, which is indicated by the particle size measurement of samples taking during the experiment. In the given example enthalpy determination via DSC is not enough to qualify the PCME as stable for an application. The water-equivalent factor is an indicator for the benefit of PCM-system on a water system operated within the same temperature ranges. The example shows that the values determined by using the enthalpy curves might be different to those determined in an application. In the given case it was higher in the test facility (especially taking considering the lower density of PCME compared to water) which might be explained by less supercooling of the PCME due to the fluid flow in the hydraulic system.

## Acknowledgements

We are grateful to the Federal Ministry of Economics and Climate Protection for funding this work within the Optimus research project (Fkz 03EN6001A) and to PtJ for administrative support.

## References

- [1] H. Inaba, The current trends in research and development on phase change material slurry, Yverdon-les-Bains, Switzerland, 2003.
- [2] L. Vorbeck, S. Gschwander, P. Thiel, B. Lüdemann, P. Schossig, Pilot application of phase change slurry in a 5 m<sup>3</sup> storage, *Applied Energy* 109 (2013) 538–543. <https://doi.org/10.1016/j.apenergy.2012.11.019>.
- [3] E. Günther, T. Schmid, H. Mehling, S. Hiebler, L. Huang, Subcooling in hexadecane emulsions, *International Journal of Refrigeration* 33 (2010) 1605–1611. <https://doi.org/10.1016/j.ijrefrig.2010.07.022>.



- [4] S. Niedermaier, M. Biedenbach, S. Gschwander, Characterisation and Enhancement of Phase Change Slurries, *Energy Procedia* 99 (2016) 64–71. <https://doi.org/10.1016/j.egypro.2016.10.098>.
- [5] C. Rathgeber, S. Hiebler, R. Bayón, L.F. Cabeza, G. Zsembinszki, G. Englmair, M. Dannemand, G. Diarce, O. Fellmann, R. Ravotti, D. Groulx, A.C. Kheirabadi, S. Gschwander, S. Höhlelein, A. König-Haagen, N. Beaupere, L. Zalewski, Experimental Devices to Investigate the Long-Term Stability of Phase Change Materials under Application Conditions, *Applied Sciences* 10 (2020) 7968. <https://doi.org/10.3390/app10227968>.
- [6] S. Gschwander, S. Niedermaier, S. Gamisch, M. Kick, F. Klünder, T. Haussmann, Storage Capacity in Dependency of Supercooling and Cycle Stability of Different PCM Emulsions, *Applied Sciences* 11 (2021) 3612. <https://doi.org/10.3390/app11083612>.

EUROTHERM2023-M221

## Testing a new design of a thermal energy storage prototype based on selective water sorbents (SWS)

Andrea Frazzica<sup>1</sup>, Alicia Crespo<sup>2</sup>, Valeria Palomba<sup>1</sup>, Vincenza Brancato<sup>1</sup>, Makram Mikhaeil<sup>3</sup>, Belal Dawoud<sup>3</sup>, Ralph Herrmann<sup>4</sup>, Emiliano Borri<sup>2</sup>, Luisa F. Cabeza<sup>2</sup>, Sven Pesson<sup>5</sup>

<sup>1</sup>Istituto di Tecnologie Avanzate per l'Energia "Nicola Giordano", CNR-ITAE, Messina, Italy, e-mail: andrea.frazzica@itaecnr.it

<sup>2</sup>GREiA Research Group, University of Lleida, Pere de Cabrera s/n, 25001 Lleida, Spain

<sup>3</sup> East Bavarian Technical University of Applied Sciences (OTH-Regensburg), Regensburg, Germany

<sup>4</sup>Fahrenheit GmbH, Siegfriedstr. 19, 80803 Munich, Germany

<sup>5</sup>InnoHeat Sweden AB, Hanögatan 5, SE-211 24, Malmö, Sweden

### Abstract

Sorption thermal energy storage is a promising technology for long-term heat storage since it presents low thermal losses at long-term. Selective water materials (SWS) consist of a salt embedded in a porous matrix and they present several advantages compared to other sorbent materials, such as better kinetics characteristics. However, their mature level is low, and few prototypes have been analyzed for now. One of these few studies was reported by the authors of this work. The authors performed preliminary experiments of a sorption TES prototype filled by a mixture of LiCl/silica gel. The results indicated low mass transport of vapour in the adsorbent domain. In this study, to enhance the performance of the original sorption TES prototype, a new design filled by 8.5 kg of a mixture of LiCl/silica gel and microporous silica gel is studied. The experiments are being carried out at the moment and full results will be reported.

**Keywords:** sorption storage, thermal energy storage, sorption composite, LiCl/SilicaGel

### 1. Introduction

Sorption thermal energy storage (TES) technology is gaining attention in the last years for its potential application as long-term TES due its low thermal losses during the idle period and its high potential energy storage density. Sorption TES is very suitable for residential applications since the adsorbent materials can be charged at regeneration temperatures below 100 °C, which allows the use of non-concentrating solar thermal collectors (cheaper and lighter). Furthermore, their discharging temperatures match with the end user temperature of space heating systems (traditional system or underfloor heating system).

Sorption technology has been already studied in the literature for different applications (e.g., chillers, heat pumps, TES), mainly focused on material and on small-scale adsorbent reactors. Nevertheless, in spite of its potential, they have some intrinsic limitations that do not allow to reach the theoretical energy density values under real operating conditions [1]. Selective water sorbents (SWS), such as LiCl-silica gel, present several advantages over traditional adsorbents. SWS consist of salt embedded in a porous matrix, which helps to limit agglomeration and improves the kinetics during the adsorption process. However, their development is in an initial stage. Among the few publications on this topic, Frazzica et al. [1] studied SWS at material level for the application in seasonal TES in Central and Northern Europe TES obtaining successful results. Crespo et al. [2] went one step further and performed preliminary experiments of a sorption thermal energy storage prototype at ITAE laboratories. The adsorption heat exchanger of that prototype was filled in with 8.9 kg of an SWS material manufactured by impregnating mesoporous silica gel with 30wt.% of LiCl. The results indicated that the process was affected by the

low mass transport characteristics through the adsorbent domain of the applied adsorber heat exchanger, which slowed down the adsorption process. In this paper, with the purpose of enhancing the mass transport, new experiments of the sorption storage system will be performed using a mixture of the composite material studied by Crespo et al. [2] (LiCl/Silicagel) and microporous silica gel. Moreover, the orientation of the adsorbent domains was changed to avoid the particle densification around the sieves during transportation of the module. This work was done in the framework of the European Project SWS-Heating.

## 2. Materials and methods

The sorption TES comprised an adsorber/desorber heat exchanger, and an evaporator/condenser heat exchanger as shown in Figure 144. An asymmetric plate heat exchanger with 120 plates each was applied for both components. The adsorber was filled in with loose grains of a mixture of 30% LiCl embedded in silica gel [1] and microporous silica gel. The thermochemical stability of this mixture was previously studied at material level in the laboratory.

The orientation of the sorption prototype was changed to avoid the particle densification around the sieves during transportation of the module. Therefore, in the new design, the adsorber was set in vertical orientation as Figure 144 shows.

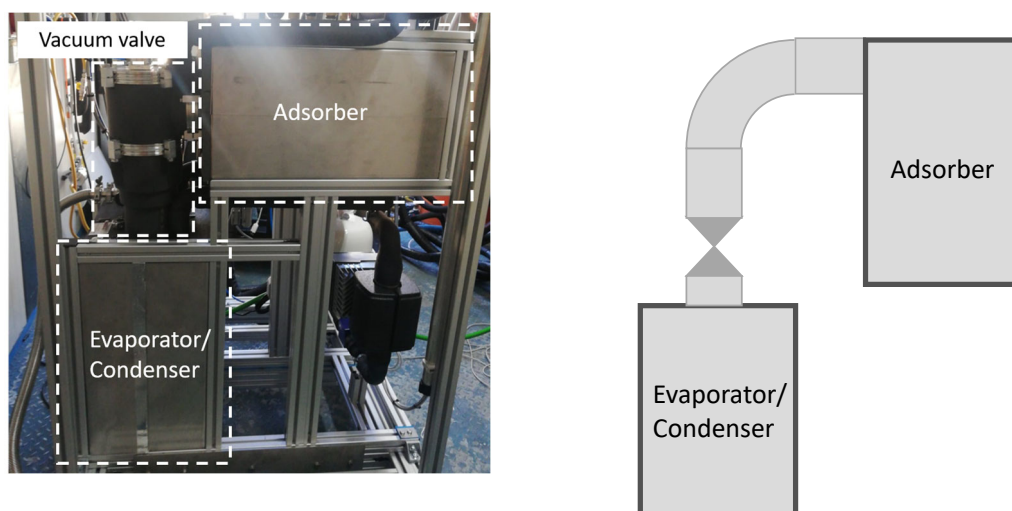


Figure 144. Layout of the different components of the sorption prototype at CNR ITAE. (a) Original design [2], (b) Enhanced designed.

The sorption TES system final goal is delivering space heating to a building. Hence, the nominal regeneration temperature of the composite is 90 °C and the adsorption temperature is 35 °C, matching with the equilibrium curves of the material and the application (radiant floor space heating).

## 3. Results

Figure shows the accumulated energy measured during one charge and one discharge of the original sorption module using LiCl/silicagel. The results show that during the charging process 3.73 liters of water were exchanged. In contrast, during the discharging process, just 1.7 liters were exchanged. This fact suggested that there was a mass transfer resistance for water vapor through the adsorbent domain.

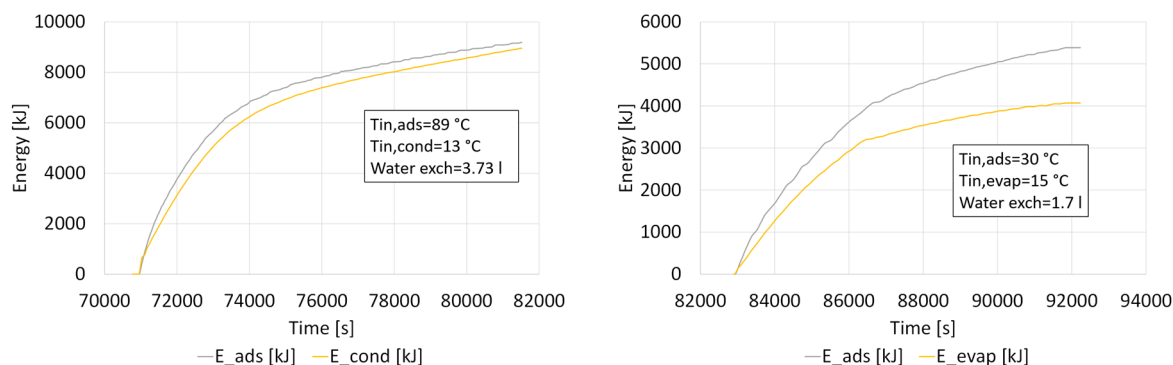


Figure 145. Energy of adsorber and evaporator/condenser during one charge (left) and one discharge (right).

To enhance the performance of the sorption TES system using SWS, new experiments of the sorption storage system will be performed using a mixture of the composite material LiCl/Silicagel and microporous silica gel. In this way, it is expected that the mass transfer of the sorbent material will increase. Moreover, the orientation of the adsorbent domains was changed to avoid the particle densification around the sieves during transportation of the module which was the main cause of mass transfer limitation. These experiments are being carried out at the moment and the new investigation results will be obtain soon.

#### 4. Conclusions

Experimental results of the sorption TES filled with LiCl/Silicagel indicated that the process was affected by the low mass transport vapour through the adsorbent domain of the adsorber heat exchanger. To enhance the adsorption module performance a design review has been carried out to allow for a uniform vapour gap in each adsorbent domain. The orientation of the adsorber was changed from horizontal to vertical to avoid the particle densification around the sieves during transportation of the module. Based on these considerations, a new system designed using an 8.5 kg of a mixture of LiCl-Silica gel and microporous silica gel was manufactured. Further experiments are being performed now to complete the characterization of the sorption TES prototype and they will be presented in the full-length paper.

#### Acknowledgements

Alicia Crespo would like to acknowledge the financial support of the FI-SDUR grant from the AGAUR of the Generalitat de Catalunya and Secretaria d'Universitats i Recerca del Departament d'Empresa i Coneixement de la Generalitat de Catalunya. This project was funded by the European Union's Horizon 2020 Research and Innovation Programme under grant agreement No. 764025 (SWS-HEATING). The authors would like to thank the Catalan Government for the quality accreditation given to their research group GREiA (2021 SGR 01615). GREiA is a certified agent TECNIO in the category of technology developers from the Government of Catalonia.

#### References

1. Frazzica, A.; Brancato, V.; Capri, A.; Cannilla, C.; Gordeeva, L.G.; Aristov, Y.I. Development of "salt in porous matrix" composites based on LiCl for sorption thermal energy storage. *Energy* **2020**, *208*, 118338, doi:10.1016/j.energy.2020.118338.
2. Crespo, A.; Palomba, V.; Mikhaeil, M.; Dawoud, B.; de Gracia, A.; F. Cabeza, L.; Frazzica, A. Experimental study of a LiCl/Silicagel sorption thermal energy storage prototype. *Proc. B. - XII Natl. III Int. Conf. Eng. Thermodyn.* **2022**, 1325.

EUROTHERM2023-V222

## Using in-situ X-ray computed tomography to study the crystallization of salt hydrates

Anastasia Stamatiou<sup>1</sup>, Jorge Martinez-Garcia<sup>1</sup>, Rebecca Ravotti<sup>1</sup>, Poppy O'Neill<sup>1</sup>, Benjamin Fenk<sup>1</sup>, Dario Guarda<sup>2</sup>, Simone Mancin<sup>2</sup>, Damian Gwerder<sup>1</sup>, Ludger J. Fischer<sup>1</sup>, Jörg Worlitschek<sup>1</sup>, Philipp Schuetz<sup>1</sup>

<sup>1</sup> Lucerne University of applied sciences and arts, Competence centre for thermal energy storage, Horw, Switzerland

<sup>2</sup> Department of Management and Engineering, University of Padova, Italy

### Abstract

Salt hydrates are considered as very promising phase change materials (PCMs) for latent thermal energy storage due to their low cost and high volumetric energy densities. However, their applicability in commercial latent heat storage units is limited so far, mainly due to the formation of different hydrate phases with varying densities during solidification. This can lead to segregation of the various hydrated salts, and inhomogeneities in the PCM that have a detrimental effect on their energy density. Segregation is promoted or prevented by a series of interconnected mechanisms which are influenced by a series of thermodynamic, kinetic and thermophysical properties and are not fully understood. This work proposes the use new characterization method based on in-situ X-ray computed tomography to study phase formation in salt-hydrate-based PCMs and eventually promote the understanding of the segregation mechanisms.

**Keywords:** Phase change materials, Salt-hydrates, segregation, X-ray computed tomography, crystallization

### 1. Introduction

Salt hydrates are considered as very promising phase change materials for latent thermal energy storage. Despite their high storage capacity and low material cost, the applicability of salt hydrates is limited so far due to their bias towards segregation, large supercooling and low thermal conductivity [1]. Segregation is a particularly difficult challenge to understand and to tackle, as it depends on a combination of thermodynamic, kinetical and thermophysical factors[2]. The state of the art to hinder segregation issues is to by utilizing thickeners and gelling agents. These methods are based on trial-and-error approaches and have only been proven to guarantee the stable long-term performance of the salt hydrate in very few cases. Emerging measurement techniques combined with the advances in crystallization modelling, can open new paths in understanding the mechanisms of segregation, elucidating the key influencing factors and ultimately engineering of novel methodologies for the prevention of segregation.

In this work a novel measurement methodology based on in-situ X-ray computed tomography (XCT) and a series of analytical methodologies is proposed to study phase formation and segregation during solidification of salt hydrates in a non-destructive manner. The XCT measurements and the information gathered through the complementary analysis methods are combined to extract distribution, morphology and composition of the salt hydrates along time. XCT facilitates the analysis of the morphological properties of solid and liquid phase in the full volume and allows to gain information about the distribution of the individual phases. XCT has already been used for the volumetric quantification of solidification and melting of both organic[3] and inorganic PCMs[4], [5]. Key asset of this imaging technique is that it requires no interaction with the sample itself and therefore enables a direct reuse of the sample for further experiments. In consequence, the evolution of the segregation processes in time

may be directly observed and quantified. The goal is to promote a profound understanding of the interaction of segregation, occurrence of different solid phases, crystallization mechanisms and mass transport will be established. In this presentation we will present the first results of applying this methodology in sodium acetate and calcium chloride-based materials.

## 2. Materials and methods

The main analysis technique applied is X-ray computed tomography (XCT). Additional techniques include differential scanning calorimetry (DSC), moisture analysis and hot stage microscopy.

The materials used in this work are different mixtures of sodium acetate (SA) and water at different concentrations and calcium chloride ( $\text{CaCl}_2$ )/water mixtures at different concentrations.

The SA based samples were produced by heating water at  $90^\circ\text{C}$  and subsequently adding the required amount of SA to achieve the desired concentration and stirring until the salt was diluted. In this presentation results with stoichiometric sodium acetate trihydrate (SAT) will be presented as well as with SAT that is mildly water rich or SA rich. The ( $\text{CaCl}_2$ )/water mixtures were prepared by melting  $\text{CaCl}_2 \cdot 6\text{H}_2\text{O}$  at  $50^\circ\text{C}$  and adding either water or  $\text{CaCl}_2$  to achieve mildly water rich or salt rich samples.

## 3. Results and discussion

Figure 146 (left) shows a photograph of a test tube containing supercooled SAT sample at room temperature (melting point SAT:  $58^\circ\text{C}$ ). On the bottom of the sample SA crystals can be observed that have formed and precipitated out of the bulk volume of the liquid. The liquid that can be observed on the top part of the sample is the remaining diluted SAT. Figure 146 (right) shows a high-resolution CT scan of the bottom of the test tube. Close observation reveals that both needle-like crystals and bulkier crystals have been formed and are dispersed in the bulk phase. The dark circles distributed in the sample are assumed to be air bubbles.

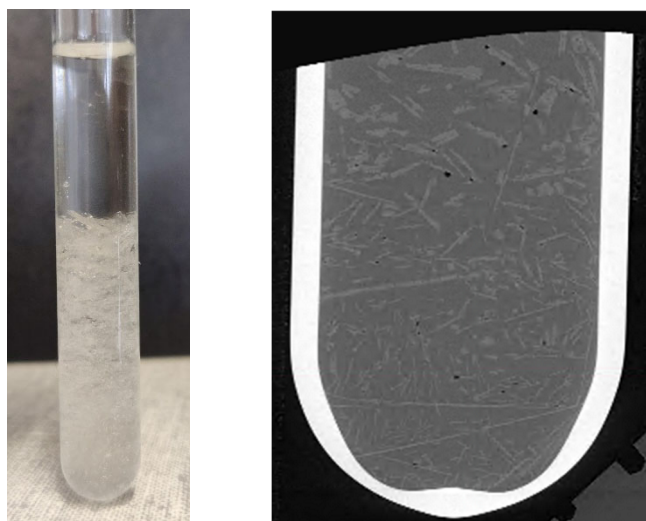


Figure 146. Photograph of a supercooled sample of sodium acetate trihydrate (left) and close up of a CT scan demonstrating the crystal distribution in the sample.

Figure 147 shows a CT-scan of a  $\text{CaCl}_2 \cdot 6\text{H}_2\text{O}$  that was crystallized at room temperature (melting point  $\text{CaCl}_2 \cdot 6\text{H}_2\text{O}$ :  $29^\circ\text{C}$ ). The formation of crater-like cavities can be observed on the top part of the sample due to the contraction of the material during solidification. Despite the sample having the  $\text{CaCl}_2$  concentration that should correspond to the formation of pure solid hexahydrate at room temperature, the darker grey areas indicate the presence of a liquid phase in the sample. The liquid sample was collected and a DSC measurement revealed that it was diluted  $\text{CaCl}_2 \cdot 6\text{H}_2\text{O}$ .

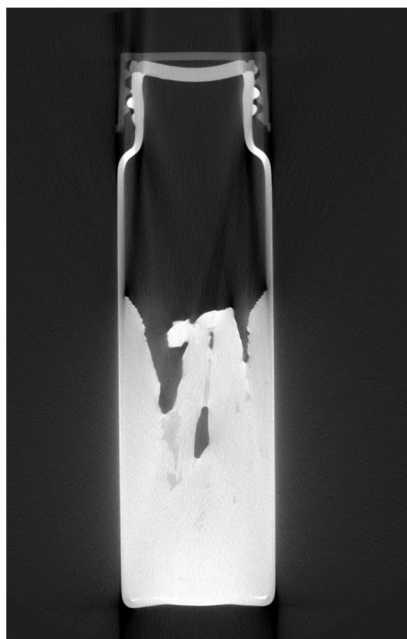


Figure 147. CT image of solidified calcium chloride hexahydrate sample

It should be noted that the CT-scans presented here are a selection from hundreds of acquired CT scans of the two samples which allow for observation of the crystal structures and different phases within the entire volume of the samples.

#### 4. Conclusions

In this work, a novel methodology based on a combination of XCT and analytical techniques is proposed for the identification of the formation of different phases during the solidification of salt hydrates. Preliminary results with SAT and  $\text{CaCl}_2 \cdot 6\text{H}_2\text{O}$  show that the technique is able to provide useful information concerning crystal structure as well as formation of cavities and liquid/air inclusions in the volume of the sample. The next steps will focus on targeted efforts to distinguish solid crystal phases from each other (e.g. SA vs. SAT and  $\text{CaCl}_2 \cdot 4\text{H}_2\text{O}$  vs.  $\text{CaCl}_2 \cdot 6\text{H}_2\text{O}$ ). If this is achieved, it would open new horizons in the non-destructive analysis of salt hydrates samples. Thus it would enable trouble shooting of defective latent heat storage units but could also be used as a tool to enhance the understanding of the fundamental processes that guide salt hydrate segregation.

#### Acknowledgements

The authors would like to thank to the Swiss National Science Foundation, Switzerland for the support of the acquisition of the LuCi instrument (Grant 206021-189608) and the support of the research projects CutAWAY, Switzerland (Grant 200021E-183684) and Investigation of Salt Hydrates Segregation with XCT, Switzerland (Grant 200021-201088)

#### References

- [1] N. Kumar, J. Hirsche, T. J. LaClair, K. R. Gluesenkamp, and S. Graham, “Review of stability and thermal conductivity enhancements for salt hydrates,” *J. Energy Storage*, vol. 24, no. May, p. 100794, 2019, doi: 10.1016/j.est.2019.100794.
- [2] A. Stamatiou, S. Maranda, L. J. Fischer, and J. Worlitschek, “Solid–Liquid Phase Change Materials for Energy Storage Opportunities and Challenges,” in *Solid–Liquid Thermal Energy Storage*, 2022, p. 22.
- [3] D. Guarda *et al.*, “New liquid fraction measurement methodology for Phase Change Material analysis based on X-ray Computed Tomography,” *submitted*, 2022.
- [4] J. Martinez-Garcia *et al.*, “Volumetric tracking of melting and solidification of phase change materials by in-situ X-ray computed tomography,” *J. Energy Storage*, vol. 61, no. October





- 2022, p. 106726, 2022, doi: 10.1016/j.est.2023.106726.
- [5] D. Guarda *et al.*, “Phase Change Material numerical simulation: enthalpy-porosity model validation against liquid fraction data from an X-ray computed tomography measurement/system,” *Nondestruct. Test. Eval.*, vol. 37, no. 5, pp. 508–518, 2022, doi: 10.1080/10589759.2022.2070164.

EUROTHERM2023-B223

## Leakage-free phase change insulation material for thermal management

Maryam Roza Yazdani\* and Sampson Tetteh

Department of Mechanical Engineering, School of Engineering, Aalto University, P.O. Box 14400, 00076 Aalto,

Finland, email: roza.yazdani@aalto.fi

### Abstract

Highly porous phase change aerogels (PCA) were developed via hybridization of polyethylene glycol (PEG) with cellulosic scaffolds. PCA was tested as lightweight bio-based thermoregulating materials for passive energy storage and insulation purposes. The PCA displayed a high latent energy storage up to 160 J/g and mechanical resistance. The PCA systems effectively regulated the air temperature inside a model wooden box exposed to temperature variation induced by irradiation. This is a promising alternative material for insulation and passive energy storage usable in smart building, electronics, and packaging.

**Keywords:** Insulation; Latent heat; Energy storage; Phase change materials

### 1. Introduction

Insulation and heat transfer are important for thermal management in powerful electronic devices, aerospace apparatuses, products handling, indoor thermal comfort, and buildings [1]. Density and porosity influence the insulation properties of insulation materials. Aerogels are used for thermal insulation purposes due to their highly porous structure, low density, and low thermal conductivity [2]. Heat transfer can be adjusted by porosity content and dimension. Nanostructured materials have the advantage of forming smaller pores [2].

Although light weight facilitates the handling, installation, and transportation of aerogels, it can result in low thermal inertia of the insulation and poor dissipation of thermal energy during hot seasons [3]. This challenges their use for example in building applications, which can be solved by incorporating phase change materials (PCMs) to increase the thermal inertia and protection against thermal shocks of the aerogel compositions. As such, this work introduces highly porous phase change aerogels (PCA) composed of nanocellulose and PCM. PCA can undergo a leakage-proof reversible phase transition with high fusion enthalpy while maintaining the porous structure during the transition. The lightweight PCA provides high porosity, low thermal conductivity as well as high fusion enthalpy suitable for high thermal inertia insulation materials.

### 2. Materials and methods

PCA compositions were prepared by mixing nanocellulose (NC) water suspension with polyethylene glycol (PEG, Sigma- Aldrich, Mw 4000) under mechanical stirring, resulting in sample concentrations that contained 80% and 75% PEG by dry weight. The suspensions were first pre-frozen and then freeze dried. Table 1 compiles the developed compositions.

The dynamic mechanical analysis was performed on a DMA Q800, TA Instruments. Differential scanning calorimetry (DSC) was done on a NETZSH DSC204F1 Phoenix device. Scanning electron microscopy (SEM) was conducted using a Zeiss Sigma VP.

### 3. Results and discussion

Figure 1 shows an image of PCA. The composition indicated appropriate mechanical resistance. Under a 16N compressive force, it indicated a 69 % overall strain; while after 1 min of relaxation, it showed 43.8% height recovery. SEM provided insight on porosity revealing pore interconnectivity, open or closed cell configuration. Phase segregation or leakage was not observed for any of the samples. This highly porous structure of PCA differ from that of previously reported PCM composites [4], which plays a significant role in insulation properties [5]. The compositions showed relatively high heat storage capability as written in Table 1. PEG is capable of latent heat storage up to 180 J/g. The DSC heating and cooling was repeated for 100 consecutive cycles, which demonstrated excellent cycling abilities (Figure 1c).

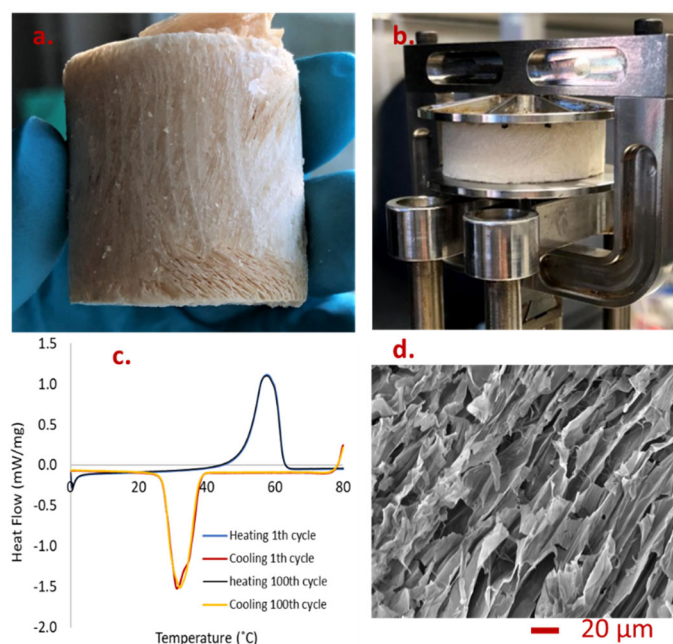


Figure 1. a) Image of PCA; b) mechanical resistance of PCA; c) DSC heating and cooling under 100 consecutive cycles; d) SEM image of PCA.

Table 1. Thermal properties of the phase change aerogels

Name	Composition PEG%	T <sub>m</sub> ( °C)	ΔH <sub>m</sub> (J g <sup>-1</sup> )	ΔH <sub>c</sub> (J g <sup>-1</sup> )
PCA-1	80%	57	160	-153
PCA-2	75%	58	152	-148

PCA was used to insulate a wooden box (Figure 2a). The temperature inside the box was measured during a radiation heating and consecutive cooling with radiation-off period (Figure 2b). The maximum temperature for bare wooden box and a commercial insulated were around 10 °C higher than that of the PCA model indicating its better insulating ability. The thermal conductivity of PCA was 0.04 W m<sup>-1</sup> K<sup>-1</sup>.

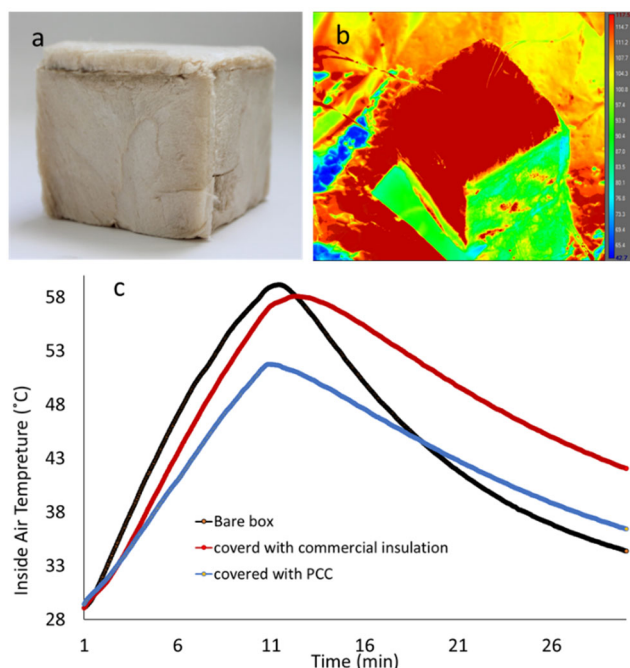


Figure 2. a) image of PCA covering a model box; b) thermal image of PCA covering a model box; c) inside temperature variation.

#### 4. Conclusions

This work aimed at preparing porous phase change aerogels (PCA) composed of polyethylene glycol (PEG) and nanocellulose. The PCA samples exhibited 160 J/g latent heat of melting and good mechanical flexibility. The PCA systems effectively regulated the air temperature inside a model wooden box exposed to irradiation heating. This is a promising alternative material for insulation applications thanks to its lightweight, latent heat storage ability and low thermal conductivity ( $0.04 \text{ m}^{-1} \text{ K}^{-1}$ ).

#### Acknowledgements

This work was funded by the Academy of Finland (343192) and Business Finland (7428/31/2022, PCMI project). The author thanks Wendy Lee for data acquisition.

#### References

1. V. Apostolopoulou-Kalkavoura, P. Munier, L. Bergström, Thermally Insulating Nanocellulose-Based Materials, *Advanced Materials*. (2020) 2001839.
2. N. Lavoine, L. Bergström, Nanocellulose-based foams and aerogels: processing, properties, and applications, *Journal of Materials Chemistry A*. 5 (2017) 16105–16117.
3. Y. Konuklu, M. Ostry, H.O. Paksoy, P. Charvat, Review on using microencapsulated phase change materials (PCM) in building applications, *Energy and Buildings*. 106 (2015) 134–155.
4. Yazdani, M. R. Ajdary, R., Kankkunen, A., Rojas, O. J., Seppälä, A. (2021). Cellulose Nanofibrils Endow Phase-Change Polyethylene Glycol with Form Control and Solid-to-gel Transition for Thermal Energy Storage, *ACS Appl. Mater. Interfaces* 2021 13 (5), 6188-6200.
5. H. Baniasadi, J. Seppälä, A. Kankkunen, A. Seppälä, M. R. Yazdani, Water-resistant gum-based phase change composite for thermo-regulating insulation packaging, *J. Energy Storage* 61, 2023, 106725.

EUROTHERM2023-F229

## Determination of effective thermal conductivity of host matrices used for thermochemical energy storage material

Natalia Mikos-Nuszkiewicz, Piotr Łapka, Piotr Furmański

Faculty of Power and Aeronautical Engineering, Warsaw University of Technology,  
Nowowiejska 21/25, 00-665 Warsaw, Poland, e-mail: natalia.mikos.dokt@pw.edu.pl

### Abstract

The objective of the work was to develop a method for determining the effective thermal conductivity of a host matrix, making the porous bed of the thermochemical energy storage reactor. It has been achieved using a microscale transport model and volume averaging techniques. The developed tools were applied to the morphology of the expanded clay capsule making up the bed obtained from X-ray micro-computed tomography scans.

**Keywords:** effective thermal conductivity, thermochemical energy storage, numerical modelling, thermochemical material, microscale modelling

### 1. Introduction

The principle of thermochemical energy storage (TChES) technology is based on reversible chemical reactions, which are accompanied by the release or absorption of heat. The reaction during which the heat is absorbed is called an endothermic reaction, and the reaction which results in heat release is called an exothermic reaction [1]. The TChES process consists of three main steps, i.e., the heat storage step, where thermochemical materials absorb heat and decompose into two types of substances; the storage step, during which both substances are stored separately and the exothermic step, in which the two substances react under the right conditions, releasing stored heat.

The selection of the best material for TChES is not an easy task. Many selection criteria are inconsistent; thus, giving obvious and clear criteria is problematic. Many reviews show salt hydrates are promising energy storage materials with suitable exothermic temperatures, low costs, nontoxicity, etc. [2]. Due to their favourable properties, salt hydrates have become the preferred materials for low-temperature energy storage systems in building applications [3].

Researchers found through many experiments that pure salt hydrate has many drawbacks, such as easy deliquescence caking, low thermal conductivity, and poor heat and moisture transfer conditions. To some extent, the listed problems can be eliminated by impregnating salt hydrate into a porous matrix (e.g., expanded clay, expanded graphite, zeolite, silica gel, activated carbon, etc.). Porous substrates support salt hydrate particles, thus ensuring an even distribution of salt hydrate particles in the matrix and increasing the contact area, heat transfer intensity, and mass transfer paths for water vapour in the material [4]. Such structure is called thermochemical composite material (TCM).

The thermodynamic parameters of pure salt hydrates are more accessible than those of TCMs. Applying TCMs instead of pure salt hydrates as the reaction bed creates additional difficulties in modelling the TChES systems and predicting their behaviour [5]. Under these circumstances, some TCM parameters and properties can be determined using numerical modelling. Thus, in this paper, the method for the determination of the effective thermal conductivity of TCM, which is one of the most important parameters describing the thermochemical reaction bed, is presented.

The effective bed properties were determined using the microscopic model that combines the lattice Boltzmann method (LBM) and an iterative approach. The LBM was used for the computations related

to heat conduction through the material at the microscale level and the determination of temperature distributions throughout the geometry. The iterative approach was used for the calculation of the effective thermal conductivity. The effective bed properties calculated by the proposed microscopic approach can then be transferred to the macroscopic model to determine temperatures in an entire storage unit, vapour concentration, amount of heat stored, etc.

## 2. Materials and method

### Generation of computational geometry

The material used as a host matrix was expanded clay. A 2D micro-computed tomography ( $\mu$ CT) scan of the expanded clay granule (Fig. 1) was generated to perform computations. The scan was then transformed into a binary image (Fig. 2), further used as a computational geometry.

The LBM was used for the computations related to heat conduction through the material and for determining temperature distributions throughout the geometry. The results of computations done using LBM were then applied to calculate the effective thermal conductivity of the host matrix used in our numerical experiments. This paper only discusses the iterative method of calculating effective thermal conductivity. The method is described in the next section.

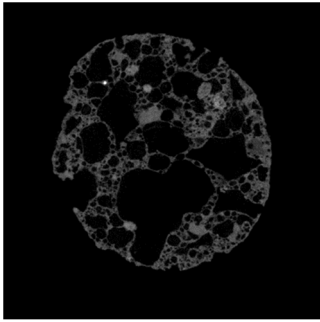


Fig. 1. 2D  $\mu$ CT scan of the expanded clay granule

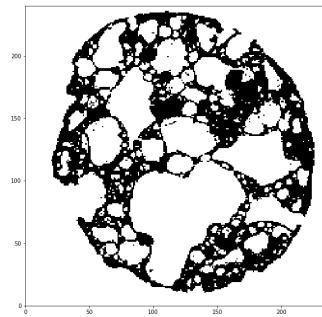


Fig. 2. Binary image obtained from Fig. 1 defining computational domain (white – air, black – clay)

### Method of effective thermal conductivity calculation

The heat transfer in TCM is described by the following equation and boundary condition:

$$\nabla \cdot [k(\mathbf{r})\nabla T] = 0 \quad \text{in the volume } V \quad (1)$$

$$-k(\mathbf{r})\nabla T \cdot \mathbf{n} = \{\mathbf{q}\} \cdot \mathbf{n} \quad \text{on the external surface of the volume } A \quad (2)$$

where:  $k$  – thermal conductivity,  $\mathbf{n}$  – unit vector external to the surface  $A$ ,  $\mathbf{q}$  – heat flux vector,  $\mathbf{r}$  – vector of the location of a point in volume  $V$ ,  $T$  – temperature,  $\{\_ \}$  – ensemble average (statistical mean value).

If different configurations of the constituents in volume  $V$  are assumed to be obtained by translation, then due to the so-called ergodic hypothesis, the ensemble average (mean value) of the heat flux vector can be found from the volume averaging [6]:

$$\{\mathbf{q}\} = -\{k(\mathbf{r})\nabla T\} = \langle \mathbf{q} \rangle = -\langle k(\mathbf{r})\nabla T \rangle \quad (3)$$

where:  $\langle \_ \rangle$  – volume averaging.

The iterative process of calculating the effective thermal conductivity starts by obtaining the first approximation of temperature in the computational domain and the mean heat flux density (unknown) by solving eq. (1) initially with a boundary condition presented in the following equation:

$$T(\mathbf{r}) = \{T\} + \nabla\{T\} \cdot \mathbf{r}_A \quad \text{on the external surface of the volume } A \quad (4)$$

where it is assumed that  $\{T\} = \text{const}$  and  $\nabla\{T\} = \nabla\langle T \rangle = \text{const}$ , while  $\mathbf{r}_A$  is the location vector of a point on the external surface  $A$ .

Knowing the first approximation of temperature distribution within a volume  $V$ , the mean heat flux can be calculated from eq. (3). Subsequently, knowing the right-hand side of eq. (2) and solving eq. (1) with the boundary condition given by eq. (2) the next approximation of temperature and the new

approximation of mean heat flux  $\langle \mathbf{q} \rangle$  can be found according to eq. (3). The iteration process should be continued until the desired accuracy is attained, i.e., the required difference between temperature and the mean heat flux in the subsequent and previous iteration is obtained. Then, effective thermal conductivity can be obtained from the following equation:

$$\langle \mathbf{q} \rangle = -\mathbf{k}_{ef} \cdot \nabla \{T\} \quad (5)$$

where  $\mathbf{k}_{ef}$  is generally the second-order tensor of the form:

$$\mathbf{k}_{ef} = \begin{bmatrix} k_{xx} & k_{xy} & k_{xz} \\ k_{yx} & k_{yy} & k_{yz} \\ k_{zx} & k_{zy} & k_{zz} \end{bmatrix} \quad (6)$$

where should be  $k_{ij} = k_{ji}$  (therefore, six coefficients should be calculated) and thus eq. (5) can be written as:

$$\begin{bmatrix} \langle q_x \rangle \\ \langle q_y \rangle \\ \langle q_z \rangle \end{bmatrix} = - \begin{bmatrix} k_{xx} & k_{xy} & k_{xz} \\ k_{yx} & k_{yy} & k_{yz} \\ k_{zx} & k_{zy} & k_{zz} \end{bmatrix} \begin{bmatrix} \nabla_x \langle T \rangle \\ \nabla_y \langle T \rangle \\ \nabla_z \langle T \rangle \end{bmatrix} \quad (7)$$

The matrix above considers 3D space, but in this paper, a simpler, 2D example is developed, consequently:

$$\mathbf{k}_{ef} = \begin{bmatrix} k_{xx} & k_{xy} \\ k_{yx} & k_{yy} \end{bmatrix} \quad (8)$$

$$\begin{bmatrix} \langle q_x \rangle \\ \langle q_y \rangle \end{bmatrix} = - \begin{bmatrix} k_{xx} & k_{xy} \\ k_{yx} & k_{yy} \end{bmatrix} \begin{bmatrix} \nabla_x \langle T \rangle \\ \nabla_y \langle T \rangle \end{bmatrix} \quad (10)$$

In the first case, denoted by (1),  $\nabla \{T\}$  vector is parallel to the  $x$ -axis direction. In the second case, denoted by (2),  $\nabla \{T\}$  vector is parallel to the  $y$ -axis direction. Due to that, we can create the following matrix and find elements of  $\mathbf{k}_{ef}$  tensor:

$$\begin{bmatrix} \langle q_{x1} \rangle \\ \langle q_{y1} \rangle \\ \langle q_{x2} \rangle \\ \langle q_{y2} \rangle \end{bmatrix} = - \begin{bmatrix} \nabla_x \langle T_1 \rangle & \nabla_y \langle T_1 \rangle & 0 & 0 \\ 0 & 0 & \nabla_x \langle T_1 \rangle & \nabla_y \langle T_1 \rangle \\ \nabla_x \langle T_2 \rangle & \nabla_y \langle T_2 \rangle & 0 & 0 \\ 0 & 0 & \nabla_x \langle T_2 \rangle & \nabla_y \langle T_2 \rangle \end{bmatrix} \begin{bmatrix} k_{xx} \\ k_{xy} \\ k_{yx} \\ k_{yy} \end{bmatrix} \quad (9)$$

### 3. Results and discussion

The developed tools were initially applied to very simple, artificially generated geometry and compared to the analytical result to check the method's accuracy, which highly depends on the contrast between selected thermal conductivity values of matrix and intrusion and on volume fraction. The method agreed with the analytical solutions with a 1% error for 0.68 volume fraction and contrast ratio 10. Then the actual morphology of the expanded clay capsule making up the bed was used. Figure 3 shows the temperature distribution in selected geometry in a quasi-steady state obtained using LBM. Based on the iterative method presented in the previous section, the effective values of the thermal conductivity for expanded clay were computed. The results, i.e., effective thermal conductivity tensor components, are presented in Table 1.

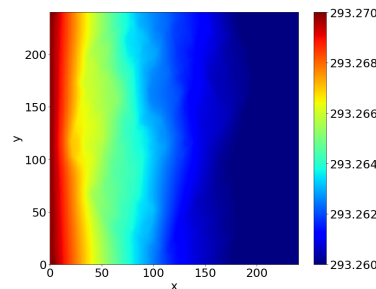


Fig. 3. Temperature field in the computational domain in the quasi-steady state

Table 1. Thermal conductivity of materials and effective values of the thermal conductivity tensor

	Air	Expanded clay	Effective $k_{xx}$	Effective $k_{xy}$	Effective $k_{yy}$	Effective $k_{yx}$
Thermal conductivity (W/m/K)	0.025	0.15	0.038912	0.001513	0.041738	0.000642

#### 4. Conclusions

The averaging technique was used to determine the effective thermal conductivity of the heterogeneous material by solving the microscale transport equations. The microscopic model was implemented for the 2D capsule of the host matrix, making the porous bed of the TChES system using the in-house computational code. The computations enabled to find the components of the effective thermal conductivity tensor. The microscopic model will be used in future works to develop a 3D micro-macroscopic model of transport phenomena in the packed bed thermochemical reactor.

#### Acknowledgements

This work was financially supported by the National Science Centre (Poland) within project no. 2020/37/B/ST8/04021.

#### References

- [1] R. A. Huggins, *Energy storage*. Springer US, 2010. doi: 10.1007/978-1-4419-1024-0.
- [2] A. Gutierrez *et al.*, “Characterization of wastes based on inorganic double salt hydrates as potential thermal energy storage materials,” *Sol. Energy Mater. Sol. Cells*, vol. 170, pp. 149–159, Oct. 2017, doi: 10.1016/j.solmat.2017.05.036.
- [3] L. Scapino, H. A. Zondag, J. Van Bael, J. Diriken, and C. C. M. Rindt, “Sorption heat storage for long-term low-temperature applications: A review on the advancements at material and prototype scale,” *Appl. Energy*, vol. 190, pp. 920–948, Mar. 2017,
- [4] W. Hua, H. Yan, X. Zhang, X. Xu, L. Zhang, and Y. Shi, “Review of salt hydrates-based thermochemical adsorption thermal storage technologies,” *Journal of Energy Storage*, vol. 56. Elsevier Ltd, p. 106158, Dec. 15, 2022. doi: 10.1016/j.est.2022.106158.
- [5] A. Fopah Lele, K. E. N’Tsoukpoe, T. Osterland, F. Kuznik, and W. K. L. Ruck, “Thermal conductivity measurement of thermochemical storage materials,” *Appl. Therm. Eng.*, vol. 89, pp. 916–926, Oct. 2015, doi: 10.1016/j.applthermaleng.2015.06.077.
- [6] P. Furmafiski, “Heat conduction in composites: Homogenization and macroscopic behavior,” *Appl. Mech. Rev.*, vol. 50, no. 6, pp. 327–356, Jun. 1997



EUROTHERM2023-Y233

## Experimental and numerical estimation of thermal conductivity of bio-based building material with an enhanced thermal capacity

Piotr Łapka<sup>1</sup>, Michał Kubiś<sup>1</sup>, Fabian Dietrich<sup>1</sup>, Maris Sinka<sup>2</sup> and Diana Bajare<sup>2</sup><sup>1</sup>Faculty of Power and Aeronautical Engineering, Warsaw University of Technology,  
Nowowiejska 21/25, 00-665 Warsaw, Poland, e-mail: piotr.lapka@pw.edu.pl<sup>2</sup>Institute of Materials and Structures, Faculty of Civil Engineering, Riga Technical University,  
Kalku 1, LV-1658 Riga, Latvia.

### Abstract

The paper presents an experimental and numerical estimation of the thermal conductivity of the bio-based building material with enhanced thermal mass. The bio-filler considered was hemp shives which were mixed with the magnesium binder, and additionally, the composite contained 0, 5, 10, and 20% wt. of microencapsulated phase change material (PCM). Thermal conductivity was measured by the guarded hot plate (GHP) method. It varied in the 0.12-0.27 W/m/K range depending on the moisture and PCM contents and the average temperature during the measurements. Numerical calculations of dry composites' thermal conductivities were based on using the real composite microstructure obtained from micro-computed tomography ( $\mu$ CT) and the volume averaging theory. Good matching of the measured and predicted results was obtained.

**Keywords:** bio-based composite, thermal conductivity, PCM, measurements, modeling

### 1. Introduction

The building sector is one of the biggest CO<sub>2</sub> emitters and energy consumers. Reducing its harmful effect on the environment and society is necessary, but the problem is very complex [1]. Recently, building materials with bio-additives gained attention because they may help make the building sector more sustainable. Such materials are usually produced using, e.g., agricultural or industrial waste or by-products that are locally available and have a low price. Bio-based materials have a minor or even negative CO<sub>2</sub> footprint, as CO<sub>2</sub> is consumed during the growth of bio components and, in some composites (e.g., based on lime binder) absorbed throughout the whole lifecycle [2]. Accordingly, applying bio-based materials may promote the circular economy and eco-design principles in the building sector [1].

Plenty of different bio-based construction materials have been proposed, with different bio-fillers in the form of husks, shives, and fibers [3, 4, 5, 6, and 7]. Among them, hemp shives [6, 7] are very popular as their application significantly improves the building materials' thermal insulating and moisture buffering properties. But traditional hemp concrete based on lime binder is very fragile. Therefore, many mixture modifications or applications of alternative binders have been proposed to improve hemp concrete mechanical properties. Although hemp-based materials have excellent insulation properties (low thermal conductivity typically in the 0.08-0.2 W/m/K range), their thermal masses are very low. Considering these problems, the paper considers hemp shives-based composite with magnesium binder, stronger than the lime one, and with microencapsulated phase change material (PCM) to improve its thermal capacity. The proposed building composite's thermal conductivity is experimentally investigated and numerically predicted.

### 2. Composite development and sample preparation

The considered composite was made of the following constituents. Commercially available hemp shives were used as bio-based fillers and reinforced. As a binder, caustic magnesia RKMH-F industrially

calcined at a temperature close to 750°C was used. This magnesia contained 73% pure MgO, 4% CaO, 4 % SiO<sub>2</sub>, 3% Fe<sub>2</sub>O<sub>3</sub>, and 1% Al<sub>2</sub>O<sub>3</sub>. As a PCM, the paraffin wax enclosed in polyurethane capsules (MikroCapsPCM25-S50) was used. Its melting temperature and dried microcapsules' heat storage capacity ranges were 23-27°C and 140-175 J/g, respectively.

Samples were prepared in the following steps. The hemp shives were preliminarily moistened at a ratio of 2:1 (hemp:water by mass) during initial mixing in a laboratory pan mixer. Then, dry MgO powder was added, allowing it to stick to the wet hemp shives. Afterward, MgCl<sub>2</sub> hexahydrate solution (ratio 1:1 with water) was added. The last added constituent was the microencapsulated PCM in the amount of 5, 10, and 20% wt. After mixing, the mixture was filled in oiled plywood formworks, and a load of 2 kN/m<sup>2</sup> was applied. After 24 h, the samples were demolded and cured in laboratory conditions, i.e., at a temperature of 20±2°C and a relative humidity (RH) of 50±10%. The samples for thermal conductivity tests of dimensions 50×250×250 mm (see Fig. 1) were cut from the produced bigger plates. Four composite types (with two samples per each type) were investigated, i.e., without the PCM and with 5, 10, and 20% wt. of the PCM. Their densities were accordingly equal to 498, 521, 514, and 537 kg/m<sup>3</sup>.



Fig. 1. The composite sample (left) and the prepared sample before the measurement (right).

### 3. Method and protocol of thermal conductivity measurements

The thermal conductivity was measured with a guarded hot plate (GHP) apparatus, whose working principle is based on a 1D steady-state heat conduction regime. The GHP method requires larger samples to ensure the correct representation of the tested material. So it is well suited for heterogeneous hemp shive-reinforced composites.

The building composites' samples were tested in four states, i.e., dry and conditioned in RH of 50, 75, and 90%. Moreover, the thermal conductivity was measured in three average temperatures selected with respect to PCM melting temperature, i.e.,  $T_1 = 18^\circ\text{C}$  (below the PCM melting point),  $T_2 = 25^\circ\text{C}$  (in the melting range), and  $T_3 = 32^\circ\text{C}$  (above the melting point). These temperatures corresponded to the following temperature set at the cold and hot plates in the GHP apparatus: 13°C and 23°C, 15°C and 35°C, and 27°C and 37°C. The effect of absorbed moisture on thermal conductivity was obtained by conditioning samples at different RH levels and subsequent thermal conductivity tests when samples achieved an equilibrium state with the surroundings, i.e., had steady masses. Firstly, the samples were dried in the oven at a temperature of 50-60°C until a steady dry state was reached. Next, dry samples' thermal conductivities were measured. Then samples were conditioned in the climatic chamber (Pol-Eko KKS 240) at RH of 50, 75, and 90% and a constant temperature of 23°C. For each RH set point, when the samples achieved steady mass, the thermal conductivity was tested. Before the measurement, each sample was warped tightly in three layers of PE stretch foil and sealed with duct tape to prevent moisture loss during the test (see Fig. 1). The top and bottom surface temperatures were measured by a pair of thermocouples stuck to the samples before wrapping them with foil (see Fig. 1).

### 4. Results of measurements

The measurements are shown in Fig. 2. Strong dependence of the composite thermal conductivity on the RH is observed for all measurement temperatures. Building materials containing bio-based additives absorb large amounts of moisture from the surroundings, resulting in a significant rise in their thermal conductivity. The higher the surroundings RH, the higher moisture amounts absorbed in the equilibrium state by the composite and higher thermal conductivity. Moreover, this dependence is stronger for

composites without and with 5% PCM and decreases with the rise in the PCM content. Microcapsules with PCM have very small dimensions (diameters of 1-15 $\mu\text{m}$ ), and for the higher fraction of the PCM in composite, fill the pores and decrease the material porosity, restraining moisture absorption from the surroundings. Therefore, for 10 and 20% PCM, the rise in thermal conductivity with RH is lower than for composite with no and 5% PCM. The composite thermal conductivity also depends on the PCM amount. It rises for the 5% PCM addition due to an increase in the composite density and a decrease in the porosity. But for 10 and 20% PCM, the composite thermal conductivity decreases as a result of the lower value of the thermal conductivity of PCM material than the binder. There is also a rise in thermal conductivity with the rise in the average sample temperature during measurements. This effect is probably due to more uniform moisture distribution in the composite in the higher measurements temperature than in the lower ones and also could be related to the state of the PCM materials.

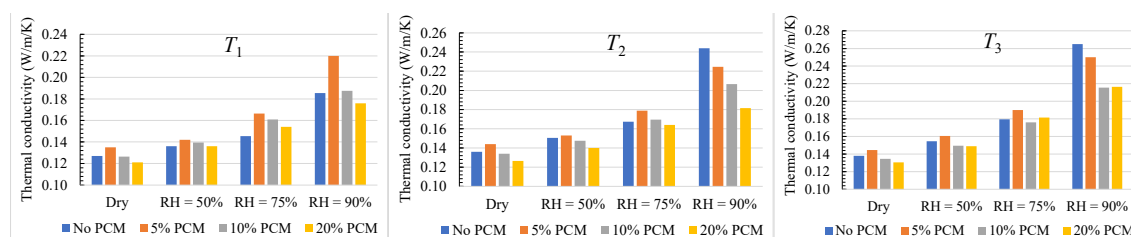


Fig. 2. Measured thermal conductivity (average of two samples) for different moisture and PCM contents and average temperatures.

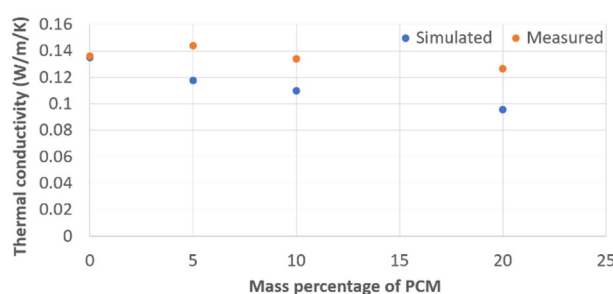
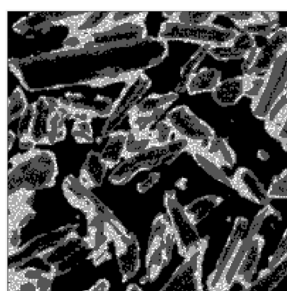


Fig. 3. The cross-section of micro-scale computational domains with artificially distributed microcapsules with PCM in the amount of 10% wt. (color scale from black to white: air, hemp shives, binder, PCM), and calculated and experimental values of thermal conductivity for dry composite.

## 5. Numerical modeling of thermal conductivity of the composite

A method of calculating the thermal conductivity of bio-based building composites enhanced with microencapsulated PCM to improve their thermal masses was developed [8, 9]. It used the real sample morphology for which the unsteady heat conductivity equation was solved, and a local (micro-scale) transient temperature field was obtained. The 3D composite sample microstructure was obtained by applying micro-computed tomography ( $\mu\text{CT}$ ) scanning. Then, by assuming a certain weight fraction, the microencapsulated PCM was randomly distributed in the space of the computational domain occupied by the binder substituting for it. In this way, the artificial bio-composite with PCM microcapsules was generated based on the real distributions of pores, hemp shives, and binder. Fig. 3 presents the microstructure of the composite of density 489  $\text{kg}/\text{m}^3$  applied in the simulations with 10% wt. of PCM. The average effective thermal conductivity of the composite was calculated by applying the volume averaging technique. The simulations were performed for dry composites only, as the model does not consider moisture transfer. First, the model was tuned by selecting a representative elementary volume (REV) to be 200 $\times$ 200 $\times$ 200 of grid elements and adjusting the thermal conductivity of hemp shives to be 0.105  $\text{W}/\text{m}/\text{K}$ . Then, the method was applied to predict the thermal conductivities of composites without PCM and with 5, 10, and 20 % wt. of microencapsulated PCM – see Fig. 3. The simulations were also compared with measurements for dry composites. The prediction error was lower than 1% for the composite without PCM. However, the model underestimated thermal conductivity for the modified composites with an average error of 20%. The most likely cause lies in the preparation process of the artificial domains. Since the PCM addition is realized by direct substitution of binder,

sample density dropped, while real samples show that the density rose with increasing PCM content, i.e., the amount of binder in real samples was more or less the same for all PCM shares. Modification of PCM addition algorithm to mitigate density change, i.e., by maintaining a constant amount of binder in the sample, should alleviate this issue. Nevertheless, the predicted thermal conductivities for samples with PCM follow the trends observed experimentally.

## 6. Conclusions

The thermal conductivities of bio-based composites made of hemp shives filler, magnesium binder, and 0, 5, 10, and 20% wt. of microencapsulated PCM were measured. Dry and conditioned in RH of 50, 75, and 90% samples were tested. Thermal conductivity was measured by the GHP method. It varied in the 0.12-0.27 W/m/K range. Higher thermal conductivities were observed for samples that absorbed more moisture. The addition of 5% of PCM increased the thermal conductivity, while 10 and 20% decreased it, which could be connected to hindering moisture absorption by PCM microcapsules that occupied the pores in the composite. Also, the average measurement temperature and resulting different PCM states affected the thermal conductivities. The numerical approach based on micro-scale modeling and volume averaging predicted general trends of thermal conductivity changes of dry composites with varying PCM amounts well.

## Acknowledgments

The work was supported by NCBiR (Poland) under grant no. M-ERA.NET2/2019/4/2020.

## References

- [1] Munaro MR, Tavares SF, Bragança L: Towards circular and more sustainable buildings: A systematic literature review on the circular economy in the built environment, *J Clean Prod* 260 (2020) 121134.
- [2] Jami T, Karade SR, Singh LP: A review of the properties of hemp concrete for green building applications, *J Clean Prod* 239 (2019) 117852.
- [3] Zhang K, Zheng S, Liu Y, Lin J: Isolation of hierarchical cellulose building blocks from natural flax fibers as a separation membrane barrier, *Int J Biol Macromol* 155 (2020) 666-673.
- [4] Carcassi OB, Minotti P, Habert G, Paoletti I, Claude S, Pittau F: Carbon footprint assessment of a novel bio-based composite for building insulation, *Sustainability* 14 (2022) 1384.
- [5] Bertoft E, Laohaphatanalert K, Piyachomkwan K, Sriroth K: The fine structure of cassava starch amylopectin. Part 2: Building block structure of clusters, *Int J Biol Macromol* 47 (2010) 325-335.
- [6] Brzyski P, Gładecki M, Rumińska M, Pietrak K, Kubiś M, Łapka P: Influence of hemp shives size on hygro-thermal and mechanical properties of a hemp-lime composite, *Materials* 13 (2020) 5383.
- [7] Łapka P, Brzyski P, Pietrak K, Cieślikiewicz Ł, Suchorab Z: Hygro-thermal characterization of the hemp concrete modified with the gum Arabic admixture, *Constr Build Mater*, 368C (2023) 130392.
- [8] Dietrich F, Łapka P, Cieślikiewicz Ł, Furmański P, Sinka M, Vitola L, Bajare D: Micro-scale modeling-based approach for calculation of thermal conductivity of bio-based building composite, *AIP Conf Proc* 2429 (2021) 020023.
- [9] Dietrich F, Łapka P, Furmański P, Sinka M, Bajare D: Modeling of thermal conductivity of bio-based building composites, *ICHMT DIGITAL LIBRARY ONLINE, Proc of CONV-22: Int Symp on Conv Heat Mass Transf*, June 5-10 2022, Izmir, Turkey, pp. 289-296, DOI: 10.1615/ICHMT.2022.CONV22.310.

EUROTHERM2023-Q243

## Latent energy storage integration in industry processes: planning of three on-site demonstrations

Alexis Sevault<sup>1</sup>, Håkon Selvnes<sup>1</sup>

<sup>1</sup> SINTEF Energy Research, Postboks 4761 Torgarden, 7465 Trondheim, Norway; Alexis.Sevault@sintef.no, Håkon.Selvnes@sintef.no

### Abstract

To unlock the full benefits of using thermal energy storage (TES) in the industry, there is an urgent demand for research and demonstration projects showcasing the benefits of TES for both the industry, energy companies and the policy makers. The research project KSP PCM-STORE, led by SINTEF Energy Research, identified industrial opportunities to demonstrate latent heat storage technologies at end-user facilities. The type of PCM-TES technology and the methods used for process integration are explained, followed by the description of three industry cases with a focus on the best integration path for the given PCM-TES technology.

**Keywords:** Phase change materials, latent heat storage, flexible energy systems, peak shaving, load shifting

### 1. Introduction

Electrification of industry and transport, in addition to the simultaneous increase in intermittent renewable energy sources in the electricity production sector, puts an enormous pressure on the power grid. Globally, the total energy storage capacity needs to increase by up to six times within 2050 compared to the 2021 capacity, depending on the region [1]. About 25 % of this required flexibility will be covered by demand-side response where TES is seen as one of the main pillars [1].

While the energy debate is mostly focused on electricity and electric energy storage such as batteries, possibilities and advantages with TES are largely overlooked. Efficient and flexible interaction between electric and thermal energy systems can contribute significantly to a sustainable and robust energy system. Industrial TES is a key technology in such interaction, by enabling a decoupling of industrial energy supply and demand, catalyzing an increase in the proportion of renewable energy supply, and facilitating surplus heat recovery. Furthermore, up to 80% of the energy demand in the European process industry is required in the form of heating and cooling, proving that TES will be important for realizing the flexibility in this sector [2]. It also provides a means to store cheap, off-peak electricity as thermal energy, and use the stored thermal energy for peak shaving and backup. To unlock the full benefits of using TES in the industrial sector, there is an urgent demand for research and demonstration projects showcasing the benefits of TES for both the industry, energy companies and the policy makers [2].

The research project KSP PCM-STORE, led by SINTEF Energy Research, gathers technology suppliers, end-users and energy companies in a competence-building research consortium that has worked in close cooperation since 2020 on identifying industrial opportunities to demonstrate latent heat storage technologies at end-user facilities. The next paragraphs will introduce the core TES technology investigated in the project, followed by the presentation of three industrial case studies.

## 2. Materials and methods

### 2.1. Latent heat storage technology

SINTEF Energy Research and NTNU have jointly developed and demonstrated one latent heat storage technology using pillow-plate heat exchangers [3] [4]. Within the timeline of the PCM-STORE project, the technology has been successfully demonstrated in the laboratory for refrigeration systems. Furthermore, a demonstration unit integrated into the heating system of an office building on NTNU campus has been installed and operated successfully since 2020. TES units applying the pillow-plate heat exchanger design are very flexible in terms of storage capacity and operating temperature range. Virtually any type of phase change material (PCM) and heat transfer fluid can be used with this technology. This technology is meant to be commercialized by a SINTEF spin-off company to be established prior to install the demonstration units.

### 2.2 Process integration methods and dimensioning

The process integration method is usually based on process diagrams from the end-user industrial partners, together with information from live-data streams from energy meters and other forms of process data. The collective information processed from each industrial site gives the basis for the first estimates of the required storage capacity, suitable temperature range and the heat flow requirement from the TES unit. This information is then translated into dynamic system models representing the thermal system at the industrial site using the Dymola/Modelica simulation environment. In addition, the project PCM-STORE has developed a lab-validated Modelica library representing the pillow-plate PCM-TES system [5]. Using this Modelica component enables to tune the dimensioning of the PCM-TES unit as well as evaluate the thermodynamic performance of the integrated systems. Finally, a techno-economic analysis is performed to connect the more precise dimensioning to actual costs and possible savings in energy costs at the factories, providing indicative payback times. Several iterations may be performed between dimensioning in the system model and techno-economic to fall within an acceptable payback time for the end-user industries.

## 3. Results and discussion

### 3.1 Dairy

Thermal energy meters were strategically installed in a dairy in Norway map the thermal energy demand of the various heat and cold consumers in the dairy energy system. CO<sub>2</sub> refrigeration units with heat recovery provides the cooling and simultaneously produces hot water for the warm side of the dairy process [6]. The energy data is used to identify the potential for reducing energy use and quantify the benefits of a potential PCM-TES integration. The hot/warm side of the dairy thermal energy system dominates the total energy use for thermal processes, especially the electric boiler (36%) that provides the final heating for pasteurization and cleaning-in-place processes. A heat storage of minimum 1 MWh energy storage capacity at 95 °C would enable significant peak shaving during the 8-hour peak period by load shifting and allow for potential increase in production capacity with the same boiler.

Compared to the warm side of the dairy energy system, the magnitude of the cooling demands is relatively limited, with the process-water cooling circuit as the main driver of the cooling demands at the plant. One solution to achieve peak shaving and load shifting of the refrigeration demand at this temperature level is to implement a PCM-TES unit using ice as the storage medium, as recently demonstrated using CO<sub>2</sub> as the refrigerant [3]. The implementation at the dairy would use the existing capacity of the CO<sub>2</sub> refrigeration systems to charge the PCM-TES unit during off-peak periods (nights and weekends) and then supply cooling to the return stream of process water during the peak hours (temperature in the range of 3-5 °C during operation). Considering the daily cooling demand during working days, a PCM-TES unit of minimum storage capacity 880 kWh with a maintained output of 170 kW would be a suitable solution.

### 3.2. Poultry processing facilities

The refrigeration load in industrial food processing plants can be subject to significant variations during the day due to production scheduling and batch processes. The temperature requirement of the various processes can span a substantial range, including thermal demands such as steam for cooking, hot water for cleaning and sanitation, cooling for dehumidification and air-conditioning, and refrigeration for chilling and freezing processes. A fully integrated energy system in such plants will minimize the primary energy input by utilizing and upgrading the excess heat from the low-temperature processes. After the production, the equipment needs to be cleaned and sanitized, followed by dehumidification of the production facilities to avoid bacterial growth by circulating and cooling the air in the air handling units (AHU). This process is energy intensive and requires a substantial amount of refrigeration capacity over a short period from the refrigeration plant.

The potential for using a PCM-TES unit integrated into an R717/R744 cascade refrigeration plant has been investigated at a poultry processing facility in Norway to achieve peak shaving of the refrigeration load for the dehumidification process. The PCM-TES unit uses water/ice as the storage medium, and the charging is achieved by evaporating CO<sub>2</sub> from the bottom circuit of the cascade refrigeration plant. The CTES unit then supplies cooling to the AHU during the discharging process. Process data from the food processing plant is used to calculate the reduction in peak power consumption using CTES technology compared to the conventional solution. While the order of magnitude of storage capacity needed is in the range of 5-10 MWh, fine dimensioning is on-going based on process data from the processing factory.

### 4. Conclusions

The progress within the research project KSP PCM-STORE is described with explanation of the developed PCM-TES technology, integration strategy and ongoing demonstration projects. Three industry cases are described with focus on the best integration path for a demonstrated PCM-TES technology using a pillow-plate heat exchanger. Two cases are planned using water as the PCM, which provides the best cost-benefit ratio for the end-users. The third case concludes on a PCM-TES unit using a PCM with melting temperature in the range of 95 °C. All three cases are in the MWh-capacity range, to be used on a day-cycle basis, with commissioning planned within 2024-2025. Further work will include detailed dimensioning of the PCM-TES unit (especially in terms of thermal input & output) and a detailed techno-economic assessment to evaluate the actual benefits for the end-users. Additional demonstration cases of the PCM-TES technology are planned for industrial processes and buildings and not presented in this extended abstract due to space restrictions.

### Acknowledgements

This study was carried out through the research project KSP PCM-STORE (308847) supported by the Research Council of Norway and industry partners. PCM-STORE aims at building knowledge on novel PCM technologies for low- and medium temperature thermal energy storage systems.

### References

- [1] « World Energy Outlook 2022,» IEA (International Energy Agency), 2022.
- [2] H. Kauko, A. Sevault, A. Beck, H. Zondag et al., «Industrial Thermal Energy Storage Supporting the transition to decarbonise industry,» EERA White Paper, 2022.
- [3] H. Selvnes, A. Hafner et al., «Experimental characterisation of a cold TES unit with a pillow-plate heat exchanger design,» *Appl. Thermal Eng.*, vol. 199, p. 117507, 2021.
- [4] A. Sevault, F. Bohmer & E. Næss, «Latent heat storage for centralized heating system in a ZEB living laboratory: integration and design,» *IOP Conference Series: Earth and Environmental Science*, vol. 352, n° 1, p. 012042, 2019.



- [5] S. Försterling, H. Selvnes & A. Sevault, «Validation of a Modelica numerical model for pillow plate heat exchangers using PCM,» *Gustav Lorentzen 2022 Proceedings, Norway, 2022.*
- [6] H. Selvnes, S. Jenssen, A. Sevault, K. N. Widell, M. U. Ahrens, S. Ren & A. Hafner, «Integrated CO<sub>2</sub> refrigeration and heat pump systems for dairies,» de *15th IIR-Gustav Lorentzen Conference on Natural Refrigerants (GL2022). Proceedings. Trondheim, Norway, June 13-15th 2022, 2022.*



EUROTHERM2023-X244

## Melting Front Evolution of a Phase Change Material Inside a Metal Foam at Different Wall Temperatures

Leonardo Bernardini, Alekos Ioannis Garivalis, Mauro Mameli\*, Sauro Filippeschi,  
Paolo Di Marco

University of Pisa, Department of Energy, Systems, Territory and Construction Engineering (DESTEC), Pisa,  
Italy, \*mauro.mameli@unipi.it

### Abstract

Among the methods studied in the literature to enhance the Phase Change Materials (PCM) thermal response, the coupling of open cell metallic foams is one of the most promising. In the literature, experiments on melting fronts are mainly conducted by imposing a constant heat flux. The novelty of this work is to perform experiments at constant wall temperatures to detect the melting front propagation at fixed Rayleigh numbers. During the tests an ohmic heater provides the heat load on one side of the test cell, while a PID controller keeps the wall temperature constant. A Zinc-Selenide window, transparent to the Long Wave Infra-Red (LWIR) spectrum, allows acquiring the evolution of the foam/PCM temperature distribution with an IR camera. An in-house MATLAB<sup>®</sup> algorithm analyses the IR images and quantifies the role of the natural convection at different Rayleigh numbers.

**Keywords:** PCM, Foam, Convection, InfraRed, Melting front evolution, Scale analysis.

### 1. Introduction

The development of efficient thermal and electrical storage systems is a fundamental step towards the effective penetration of renewable energy sources. Thermal storage systems can foster the spread of technologies such as concentrator solar power plants, solar heating, solar cooking, solar greenhouses, thermal control in buildings, off-peak electricity storage, and waste heat recovery [1]. Thermal storage technologies can be classified into sensible, latent, and thermochemical [2]. Latent heat thermal energy storages can store and release high amounts of energy in relation to their volume by taking advantage of Phase Change Materials (PCM). The low thermal conductivity of organic PCMs limits the power transferred during the phase change process, increasing the charge and discharge times [3]. Various enhancement techniques have been investigated to compensate for PCM low conductivity and it is well-established in the literature that coupling PCM with metallic foam significantly increases the heat transfer rate [4]. The PCM melting process inside the metal foam can occur in different ways: conductive, mixed conductive-convective, purely convective regime [5]. The aim of this work is to identify, using an infrared camera and a transparent infrared window, the evolution of the melting front at different Rayleigh numbers. The novelty of this paper lies in conducting the experiments at imposed wall temperature, while, generally, these experiments were carried out at imposed heat flux [6,7]. Working with imposed wall temperature makes it possible to effectively control the Rayleigh number so that it is kept constant during the experiment.

### 2. Materials and methods

The Test Cell shown in Figure 1 consists of the electric heater (Minco<sup>®</sup>, max heat flux 17 W/cm<sup>2</sup>), the composite material, the polycarbonate box, and the Zinc-Selenide (ZnSe) window (transparent to the LWIR spectrum), the composite material, alias an aluminum open cell foam (ERG<sup>®</sup>, 50x50x50 ± 0.5 mm, porosity  $\varepsilon = 92\%$ , 10 PPI), filled with commercial paraffin wax (Ph EUR, BP, NF CAS 8002-74-2) with a

solidification point between 56 and 58°C. Three K-type thermocouples are located respectively in the center of the aluminum plate at the interface between the aluminum and the composite material (TC1); in the middle (TC2) and at the end (TC3) of the composite matrices.

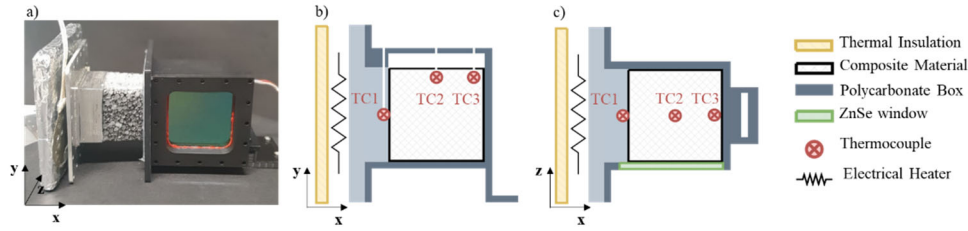


Figure 1. Test Cell: a) exploded view; b) components scheme side section view; c) top section view.

A LWIR camera (FLIR®, A655sc) and the test cell are located inside a black cavity to prevent external disturbances. A programmable power supply (ELC®, ALR3260T) is connected to the electrical heater, provides current measurement (accuracy ±10 mA), and communicates via USB with the Control Unit (CU), i.e. a PC equipped with LabVIEW®, also connected to the LWIR, and the Data Acquisition system (DAQ LabJack®, T7-Pro). The DAQ records temperatures (accuracy ± 0.5 K) and the heater voltage (accuracy ±14 mV). The IR camera is calibrated using a pre-calibrated thermocouple spanning from 25 °C to 90 °C. Lastly, an in-house PID controller manages the current keeping constant the temperature at the interface between the aluminum and the composite material.

The main interest of the present study is identifying the conditions where the PCM melting regime changes from pure conduction to convection inside the porous matrices heated from the side. Thus, we performed tests at constant wall temperature, to detect the melting front propagation by tracking the PCM surface temperature distribution temporal evolution at fixed Rayleigh numbers. Concerning convection in porous media, it is helpful to introduce the definition of Rayleigh number for Darcy flow [8]:

$$Ra_D = Ra \cdot Da = \frac{\beta g (T_w - T_m) H^3}{\alpha \nu} \cdot \frac{K}{H^2} = \frac{\beta g (T_w - T_m) K H}{\alpha \nu} \quad (1)$$

where  $H = 0.05$  m is the characteristic length of the porous medium in the gravity vector direction,  $g$  is the gravity acceleration,  $\beta = 0.000778 \text{ K}^{-1}$  is the PCM volumetric thermal expansion coefficient,  $\nu = 6.51 \times 10^{-6} \text{ m}^2/\text{s}$  is the PCM kinematic viscosity,  $K = 3.21 \times 10^{-7} \text{ m}^2$  is the permeability of the porous medium calculated according to [9],  $T_m = 57 \text{ °C}$  is the phase change temperature of the PCM. Finally,  $T_w$  is the heated surface temperature, namely the temperature measured by TC1. The composite material thermal diffusivity is  $\alpha = \lambda/\rho c = 8.28 \times 10^{-6} \text{ m}^2/\text{s}$ , where the thermal conductivity  $\lambda$  is calculated according to [7] and the volumic heat capacity is evaluated as a volume weighted average,  $\rho c = (\rho c)_{\text{PCM}} \varepsilon + (\rho c)_{\text{foam}} (1 - \varepsilon)$ . First, the composite material is heated up to 40°C, then the PID comes into play by maintaining the set point temperatures (60, 70, 80 °C, corresponding to  $Ra_D = 7, 30$  and 52, respectively) until the PCM melts completely. Throughout the experiment, the CU records the voltage, the current, and the temperatures with a sample rate of 1 Hz and the IR images at 2 Hz.

### 3. Results and discussion

Jany and Bejan [5] were the first to define the different regimes during the melting process of a PCM inside a porous medium, followed by other authors. The melting process of a PCM within a side-heated porous medium may exhibit four distinct regime: i) the conductive regime, where the melting front is vertical, and conduction dominates; ii) mixed conductive-convective regime, in which heat transfer occurs by both conduction and convection; this regime ends when the convection-dominated zone fills the entire height of the composite material; iii) the convective regime, in which the melting front takes the typical inflected form; iv) shrinking solid, when the melting front first reaches the wall opposite the heated one. An in-house MATLAB® algorithm analyzed the IR images and traced the evolution of the melting front position. When the temperature measurement is in the PCM melting range, a "mushy" zone is identified in all the IR images. The melting front comes from a smoothing spline interpolation of the mushy zone. Figure 2

shows the shape and position of the melting front over time at different wall temperature, and thus, different  $Ra_D$ , for the present case. When  $T_w = 60^\circ\text{C}$ , the PCM did not begin to melt even for long times (46 min). On the other hand, when the wall temperatures are  $70^\circ\text{C}$  and  $80^\circ\text{C}$  conduction in the liquid, convection, and shrinking solid regimes can be recognized. In particular, when  $T_w = 80^\circ\text{C}$  the PCM takes significantly less time to melt completely. A comparison in terms of dimensionless parameters between the test performed at  $T_w = 80^\circ\text{C}$  and the test at  $T_w = 70^\circ\text{C}$  is proposed here below.

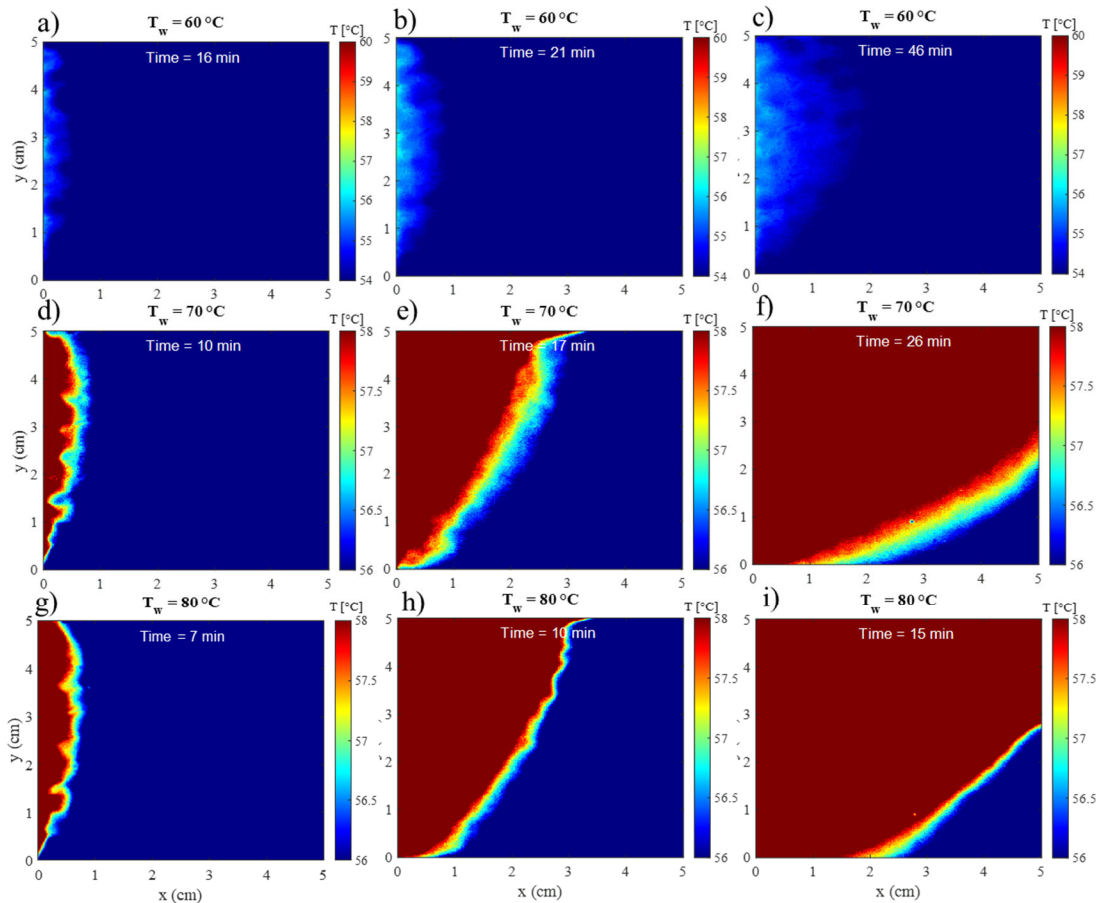


Figure 2. IR images, melting front evolution for different wall temperatures and times.

To compare the cases, the non-dimensional analysis proposed by Jany and Bejan [5] is followed. The product between the Stefan number and the Fourier number,  $SteFo$ , represents a dimensionless time:

$$SteFo = \frac{c(T_w - T_m)}{h_{sl}} \cdot \frac{at}{H^2} \quad (2)$$

In this definition,  $t$  is the time,  $c$  is the specific heat capacity of the composite material and  $h_{sl}$  the latent heat of fusion of the PCM. In addition, the vertical and horizontal coordinates, are plotted in their dimensionless form  $X = x/H$  and  $Y = y/H$  as shown in the dimensionless maps (Figure 3).

Let's assume a fixed Rayleigh number and analyze the effect of the  $SteFo$  number on the melting front evolution: in the case of small  $SteFo$  numbers, the interface moves relatively slowly. Therefore, it is reasonable to assume that the liquid flow is not disturbed by the interface motions. As the  $SteFo$  number increases, the influence of natural convection on the melting front shape and velocity is more relevant. The deviation from the pure heat conduction is more and more relevant as the  $SteFo$  number increases. In Figures 3a and 3b, it is possible to distinguish all the phases of the melting process clearly, and it seems that with these  $Ra_D$  numbers, the transition from pure conduction to convection happens without the mixed conductive-convective regime. Furthermore, Figure 3c shows how the evolution of the melting front in terms of dimensionless time  $SteFo$  is almost identical in both cases.

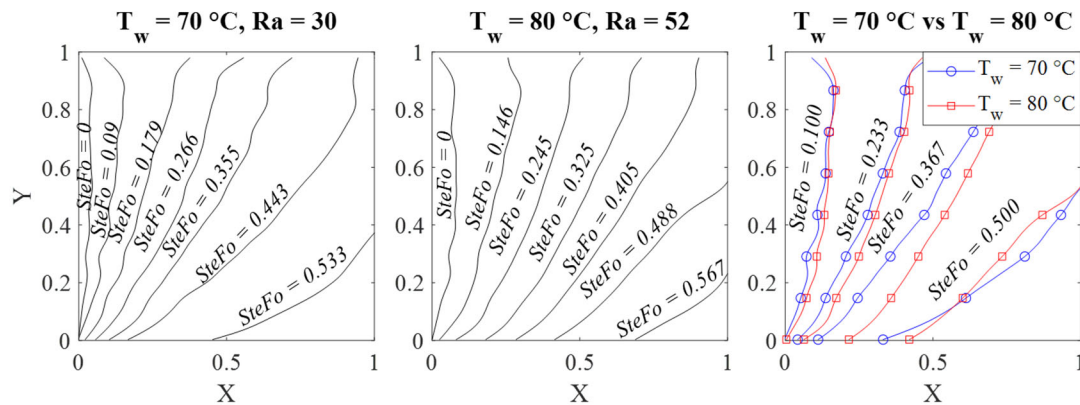


Figure 3. Melting front position as a function of  $SteFo$ : a)  $T_w = 70\text{ °C}$ ; b)  $T_w = 80\text{ °C}$ ; c) Comparison between  $T_w = 70\text{ °C}$  and  $T_w = 80\text{ °C}$ .

## 4. Conclusions

The melting of a PCM inside an aluminum foam is experimentally investigated at a constant wall temperature of  $60\text{ °C}$ ,  $70\text{ °C}$ , and  $80\text{ °C}$ , corresponding to constant  $Ra_D$  numbers of 7, 30 and 52, respectively. The LWIR camera records the evolution of the melting front over time, and an in-house code analyzes the IR images and traces the development of the melting front position. IR images show that with a wall temperature of  $60\text{ °C}$ , the melting of the PCM after 46 minutes is yet to begin. Instead, for  $T_w = 70\text{ °C}$  and  $80\text{ °C}$ , the melting of the PCM starts after a few minutes. The dimensionless analysis reveals that: i) for  $Ra_D$  numbers 30 and 52, the transition from the pure conductive regime to the convective one seems to happen without the mixed conductive-convective regime; ii) the dimensionless position of the melting front over  $SteFo$  is similar for both Rayleigh numbers, despite the actual time needed to melt the entire material is about half for  $80\text{ °C}$  with respect to  $70\text{ °C}$ .

## Acknowledgements

The PhD grant of Mr. Bernardini is sponsored by DRINKSTATION inc., Los Angeles, USA.

## References

- [1] Koohi-Fayegh, S., & Rosen, M. A. (2020). A review of energy storage types, applications and recent developments. *Journal of Energy Storage*, 27, 101047.
- [2] Cabeza, L. F., Martorell, I., Miró, L., Fernández, A. I., & Barreneche, C. (2021). Introduction to thermal energy storage systems. In *Advances in Thermal Energy Storage Systems* (pp. 1-33). Woodhead Publishing.
- [3] Farid, M. M., Khudhair, A. M., Razack, S. A. K., & Al-Hallaj, S. (2004). A review on phase change energy storage: materials and applications. *Energy conversion and management*, 45(9-10), 1597-1615.
- [4] Ali, H. M., Janjua, M. M., Sajjad, U., & Yan, W. M. (2019). A critical review on heat transfer augmentation of phase change materials embedded with porous materials/foams. *International Journal of Heat and Mass Transfer*, 135, 649-673.
- [5] Jany, P., & Bejan, A. (1988). Scaling theory of melting with natural convection in an enclosure. *International Journal of Heat and Mass Transfer*, 31(6), 1221-1235.
- [6] Iasiello, M., Mameli, M., Filippeschi, S., & Bianco, N. (2021). Metal foam/PCM melting evolution analysis: Orientation and morphology effects. *Applied Thermal Engineering*, 187, 116572.
- [7] Wang, Z., Zhang, Z., Jia, L., & Yang, L. (2015). Paraffin and paraffin/aluminum foam composite phase change material heat storage experimental study based on thermal management of Li-ion battery. *Applied Thermal Engineering*, 78, 428-436.
- [8] Nield, D. A., & Bejan, A. (2006). *Convection in porous media* (Vol. 3). New York: Springer.
- [9] Fourie, J. G., & Du Plessis, J. P. (2002). Pressure drop modelling in cellular metallic foams. *Chemical Engineering Science*, 57(14), 2781-2789.

EUROTHERM2023-Z245

## A study of graphene nanoplatelets-based phase change material for low-temperature thermal energy storage applications

Muhammad Aamer Hayat\* &amp; Yong Kang Chen\*\*

School of Physics, Engineering and Computer Science, University of Hertfordshire, Hatfield, AL10 9AB, United Kingdom, email \*: [m.hayat2@herts.ac.uk](mailto:m.hayat2@herts.ac.uk); \*\*: [y.k.chen@herts.ac.uk](mailto:y.k.chen@herts.ac.uk)

### Abstract

This experimental study focuses on the preparation and evaluation of the thermal properties of nano-phase change materials (nano-PCMs) based on RT-18HC as a phase change material (PCM) and graphene nanoplatelets (GNP) as a thermal conductivity enhancer. The GNP concentration was varied between 0 to 1.0 wt.% in RT-18HC and the thermal properties of the prepared nano-PCMs were measured using differential scanning calorimetry (DSC), and a hot disk thermal conductivity equipment. The results revealed that incorporating GNP significantly enhanced the thermal conductivity of the nano-PCMs, with a maximum increase of 80.9% at 1.0 wt.% of GNP. However, the addition of GNP particles results in a small reduction of latent heat, with a maximum decline of -2.67% at 1.0 wt.% of GNP. The results suggest that the developed nano-PCMs have the potential as an effective solution for low-temperature thermal energy storage applications.

**Keywords:** Phase change material, graphene nanoplatelets, thermal energy storage, thermal conductivity, latent heat.

### 1. Introduction

The detrimental effects of CO<sub>2</sub> emissions on climate change have reached a critical point and sustainable energy sources are needed to cut the arising need for fossil fuels to reduce CO<sub>2</sub> emissions [1,2]. The CO<sub>2</sub> emissions could be reduced by storing excess energy with thermal energy storage (TES) materials, which store and preserve thermal energy for later use rather than releasing it into the atmosphere [3]. These TES materials are identified as phase change materials (PCMs), and they can store a significant amount of heat due to their high energy storage density during heating and cooling cycles. One of PCM key problems is that they possess low thermal conductivity (TC) which affects their overall thermal performance [4]. The various methods including fins, metallic foams, heat pipes, and nanoparticles[5] were used by the researchers to augment PCM's TC. Among all these methods, nanoparticles have captured the attention of researchers and innovators in recent years because of their exceptional properties, such as low density, greater surface area, and good compatibility with PCM molecules [6].

Nanoparticles, especially carbon-based nano additives (i.e., carbon nanotubes, diamond, graphene), have the advantage of high TC values, and their greater surface areas provide good intermolecular interactions with PCM matrices [7]. For instance, Choi et al. [8] examined different carbon-based nanofillers (i.e., multi-walled carbon nanotubes (MWCNTs), graphene, and graphite) with stearic acid as PCM. They found that the maximum TC value of PCM was improved by 21.5% with 0.1 vol.% of graphene particles. Similarly, Arshad et al. [6] investigated the effect of carbon and metal oxide-based nanofillers on the thermal properties of paraffin. Their results showed that compared to the metal oxide particles the carbon-based particles depicted a greater increase in the TC value (i.e., 71.4%) and a decrease in the melting and crystallization enthalpies of the paraffin. Li et al. [9] incorporated expanded graphite (EG) into the salt hydrate PCM to examine the thermophysical properties of the composite material. The results revealed that with the addition of 7 wt.% of EG, the heating and cooling enthalpies resulted in 114 J/g and 105.5 J/g, correspondingly. Moreover, a maximum TC value of 1.96W/m.K was noticed.

However, the incorporation of carbon-based nanofillers increases the TC values of the pristine PCMs, but decreases the latent heat (LH) of these materials considerably [3]. In this paper, different concentrations of GNP were impregnated into the low-temperature PCM (RT-18HC) to determine an ideal concentration with the least effect on the LH and the greatest increase in the TC values.

## 2. Materials and Methodology

RT-18HC was selected as a PCM with a melting temperature range of 17-19 °C supplied by Rubitherm GmbH, Germany. Graphene nanoplatelets with a surface area of 750 m<sup>2</sup>/g, and a surfactant, sodium dodecylbenzene sulfonate (SDBS), obtained from Sigma-Aldrich, UK, were employed directly without any chemical treatment.

A two-step process was used to prepare nano-PCMs. GNP was impregnated into the base PCM at four different concentrations (0.3, 0.5, 0.7, and 1.0 wt.%). Figure 1 depicts a schematic of the two-step process employed for a sample preparation. Moreover, ¼ of SDBS as a surfactant was added to each concentration of GNP. More details of the two-step process were reported in our recent paper [5].

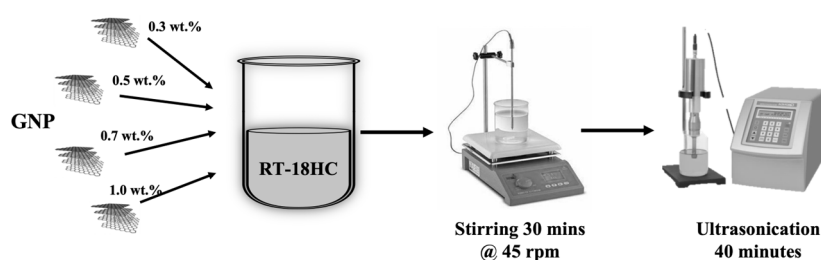


Figure 148. Schematic of the two-step method.

Differential scanning calorimetry (DSC) from TA Instrument, UK and a hot disk thermal conductivity instrument (TPS-2500S) were employed for a thermal analysis of the pristine RT-18HC and the RT-18HC incorporated with GNP particles. Both instruments were calibrated before experiments.

## 3. Results and discussion

### 3.1 DSC analysis

Both melting and crystallisation temperatures and enthalpies of the pristine PCM and nano-PCMs were examined at the temperature ranging from 5 °C to 30 °C in an N<sub>2</sub> atmosphere at a heating and cooling rate of 1 °C.min<sup>-1</sup>. The endothermic and exothermic peaks for all the samples are shown in Figure 2. The single endothermic peak of RT-18HC and its composites confirms the isomorphous crystallisation structure of the samples, and the two exothermic peaks refer to the bimodal crystallisation phenomenon. It can be seen that the inclusion of GNP particles had a very small effect on the melting and crystallisation temperatures of the nano-PCMs. The melting enthalpies of RT-18HC and RT-18HC/GNP (0.3%), RT-18HC/GNP (0.5%), RT-18HC/GNP (0.7%), and RT-18HC/GNP (1%) were 239.6 J/g, 238.2 J/g, 237.4 J/g, 235.8 J/g, and 233.2 J/g, respectively, and solidification enthalpies were 241.6 J/g, 240.1 J/g, 239.5 J/g, 236.5 J/g, and 234.7 J/g, respectively. The slight decrease in the heating and cooling enthalpies with the addition of GNP is because of the non-melting enthalpies of the GNP [10]. Furthermore, the addition of GNP particles reduced the degree of supercooling of nano-PCMs. This DSC analysis suggests that the developed nanocomposites have the potential to be employed in TES applications.

### 3.2 An analysis of thermal conductivity

A hot disk instrument was used to measure the TC values of the samples. At a constant temperature of 15 °C, the TC values were measured for RT-18HC, and RT18-HC mixed with GNP at four different concentrations (0.3, 0.5, 0.7 and 1.0 wt.%). As shown in Figure 3, the TC values increased as the concentration of GNP was increased. It can be seen that the TC values obtained for RT-18HC and RT-18HC at 0.3, 0.5, 0.7, and 1.0 wt.% concentration were 0.199 W/m.k, 0.289W/m.k, 0.31 W/m.k,

0.33W/m.k, and 0.36W/m.k, respectively. The maximum increase of 80.9% was observed at 1.0 wt. % of GNP in RT-18HC.

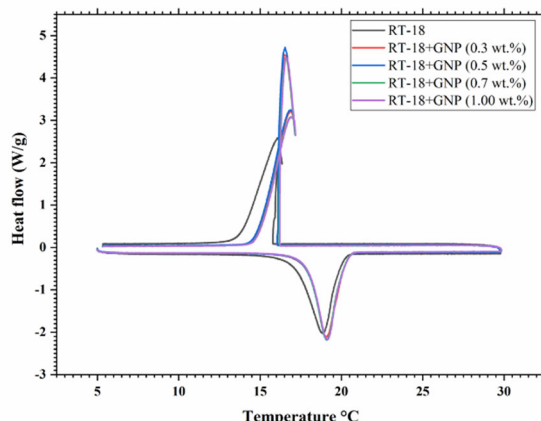


Figure 149. DSC peaks of pure PCM and nano-PCMs

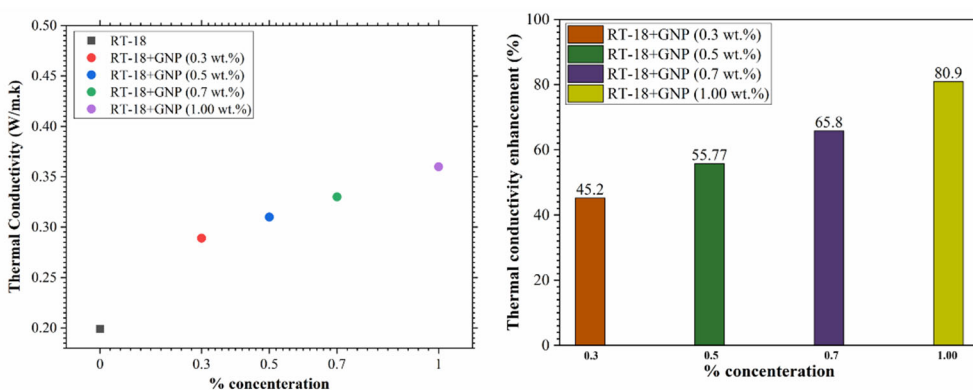


Figure 150. Thermal conductivity of pure and nanocomposite samples.

### 3.3 Optimisation analysis

An analysis of variance (ANOVA) was used to identify the suitable concentration at which LH reduction is minimum and TC value is maximum. Two responses were analysed in this model; thermal conductivity and latent heat. In the analysis, TC and LH responses were given the same importance. Figure 4 (a, b) depicts a 3D plot of particle concentration and temperature as a function of LH and TC. The optimal concentration of GNP for achieving the highest overall TC value was found to be 0.464 wt.%, which corresponded to a minor decrease of -1.0% in LH.

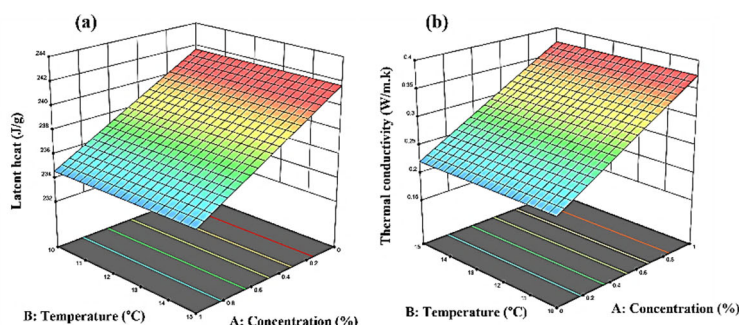


Figure 151. 3D Plot of particle concentration and temperature as a function of (a) LH, (b) TC.

## 4. Conclusions

Key findings from the current studies are summarised as follows.

- DSC results have shown that incorporating GNP into the PCM did not have a major effect on the peak heating and cooling temperatures. Furthermore, LH decreases as a GNP concentration increases, with a maximum decrement of -2.67% and -2 % noted at 1.0 wt.% of GNP for LH of heating and cooling, respectively.
- The TC results revealed an increasing trend in TC values as GNP concentration increased. The TC enhancement for 0.3, 0.5, 0.7, and 1.0 wt.% of GNP-based PCM was 45.2%, 55.77%, 65.8%, and 80.9%, respectively.
- Finally, a statistical analysis using ANOVA was performed to determine the optimum concentration, and 0.464 wt.% of GNP particles was discovered to be the optimal value.

In future work, it would be interesting to investigate the long-term stability and durability of the GNP/RT-18HC nano-PCMs for TES applications.

## Acknowledgements

The authors would like to acknowledge the European Union's Horizon 2020 research and innovation programme, particularly the Marie Skłodowska-Curie grant agreement No 801604.

## References

- [1] Y. Li, Z. Ding, M. Shakerin, N. Zhang, A multi-objective optimal design method for thermal energy storage systems with PCM: A case study for outdoor swimming pool heating application, *J Energy Storage*. 29 (2020) 101371.
- [2] O. Akashi, T. Hanaoka, T. Masui, M. Kainuma, Halving global GHG emissions by 2050 without depending on nuclear and CCS, *Clim Change*. 123 (2014) 611–622.
- [3] M.A. Hayat, Y. Chen, M. Bevilacqua, L. Li, Y. Yang, Characteristics and potential applications of nano-enhanced phase change materials: A critical review on recent developments, *Sustainable Energy Technologies and Assessments*. 50 (2022) 101799.
- [4] M.A. Hayat, H.M. Ali, M.M. Janjua, W. Pao, C. Li, M. Alizadeh, Phase change material/heat pipe and Copper foam-based heat sinks for thermal management of electronic systems, *J Energy Storage*. 32 (2020) 101971.
- [5] M.A. Hayat, Y. Yang, L. Li, M. Bevilacqua, Y.K. Chen, Preparation and thermophysical characterisation analysis of potential nano-phase transition materials for thermal energy storage applications, *J Mol Liq.* (2023) 121464.
- [6] A. Arshad, M. Jabbal, Y. Yan, Preparation and characteristics evaluation of mono and hybrid nano-enhanced phase change materials (NePCMs) for thermal management of microelectronics, *Energy Convers Manag.* 205 (2020) 112444.
- [7] A. Arshad, M. Jabbal, L. Shi, Y. Yan, Thermophysical characteristics and enhancement analysis of carbon-additives phase change mono and hybrid materials for thermal management of electronic devices, *J Energy Storage*. 34 (2021) 102231. <https://doi.org/10.1016/j.est.2020.102231>.
- [8] D.H. Choi, J. Lee, H. Hong, Y.T. Kang, Thermal conductivity and heat transfer performance enhancement of phase change materials (PCM) containing carbon additives for heat storage application, *International Journal of Refrigeration*. 42 (2014) 112–120.
- [9] C. Li, B. Zhang, B. Xie, X. Zhao, J. Chen, Tailored phase change behavior of Na<sub>2</sub>SO<sub>4</sub>·10H<sub>2</sub>O/expanded graphite composite for thermal energy storage, *Energy Convers Manag.* 208 (2020) 112586.
- [10] A.M. Taggart, F. Voogt, G. Clydesdale, K.J. Roberts, An examination of the nucleation kinetics of n-alkanes in the homologous series C<sub>13</sub>H<sub>28</sub> to C<sub>32</sub>H<sub>66</sub>, and their relationship to structural type, associated with crystallization from stagnant melts, *Langmuir*. 12 (1996) 5722–5728.



EUROTHERM2023-V246

## Performance Evaluation of a Thermal Energy Storage System based on Waste Foundry Sand Composite Phase Change Materials

A. Anagnostopoulos<sup>1,2,\*</sup>, A. Ahmad<sup>1</sup>, M. H. Navarro<sup>1</sup>, Y. Maksum<sup>1</sup>, S. Sharma<sup>1</sup>, P. Seferlis<sup>2</sup>, Y. Ding<sup>2,\*</sup>

<sup>1</sup> Birmingham Centre for Energy Storage & School of Chemical Engineering, University of Birmingham, Birmingham B15 2TT, United Kingdom., e-mail: [y.ding@bham.ac.uk](mailto:y.ding@bham.ac.uk)

<sup>2</sup> Department of Mechanical Engineering, Aristotle University of Thessaloniki, PO Box 454, 54124, Thessaloniki, Greece, e-mail: [argyana@meng.auth.gr](mailto:argyana@meng.auth.gr)

### Abstract

This study demonstrates the technical and economic viability of utilising waste foundry sand (WFS) as a thermal energy storage (TES) material for medium-high temperature waste heat recovery applications. A waste heat storage and reuse unit was developed, operated, and monitored using TES materials containing WFS. The composite material comprised 40% PCM, 20% WFS, and 20% MgO. To enhance the system's efficiency by maximising latent heat, two PCMs were selected: NaNO<sub>3</sub> and a 60-40 NaNO<sub>3</sub>-KNO<sub>3</sub> mixture, with melting points of 309°C and 218°C, respectively. The materials had a density of 1.65 g/cm<sup>3</sup> and 1.93 g/cm<sup>3</sup>, with an average specific heat capacity of 1.23 J/gK and 1.22 J/gK, and an average thermal conductivity of 1.63 W/mK and 1.48 W/mK for NaNO<sub>3</sub> and SS CPCMs, respectively. The TES device was charged using a high-temperature fan with an average mass flow rate of 0.028 kg/s and an inlet temperature of 400 °C, the maximum achievable temperature at the full capacity of the 10 kW heater. The total charging time was 10 hours. The system's charging efficiency was found to be 82%.

**Keywords:** thermal energy storage, waste heat recovery, foundry sand, composite, phase change

### 1. Introduction

Effective energy storage is essential for optimising resource usage, especially in thermally driven renewable energy and large-scale industrial processes that require significant amounts of heat. Thermal energy storage (TES) systems efficiently decouple non-continuous thermal sources from heat-demanding applications, such as batch industrial processes and solar radiation(1). TES systems are cost-effective and have a proven track record compared to other energy storage options. A promising sector for TES implementation is industrial waste heat recovery. 20-50% of energy input in heavy industrial processes is lost as waste heat(1). Recovering and storing this heat could reduce primary energy supply and associated emissions, decoupling heat production in batch processes with heat-demanding applications and providing valuable energy dispatch ability.

TES technology can be categorised into three types: sensible heat TES, latent heat TES, and thermochemical TES(2). Sensible heat TES is widely used because of its low cost and wide range of raw materials. Latent heat TES (LTES) has a higher heat storage density and stable phase transition temperature, and combining ceramic materials with phase change materials can enhance charging/discharging. Thermochemical TES has high heat storage density and long heat storage time but is still in the laboratory research stage(2). Phase change materials (PCMs) have become popular because of their high heat storage density, wide availability, and affordability(2). They are categorised into organic, inorganic, and liquid metals, with inorganic salts being the most commonly used in LTES systems. However, inorganic salts have disadvantages, such as low thermal conductivity, strong corrosiveness, and high reactivity at high temperatures. Encapsulation of PCM is an effective method to improve charging and discharging performance, expand the heat transfer area, and prevent PCM leakage(2).

Waste foundry sand (WFS) is a surplus material from metal casting processes in ferrous and non-ferrous metal casting industries. Sand is used to make molds for casting, and after solidification, the sand is reused until it no longer meets quality standards (3). The surplus sand cannot be accommodated in foundry warehouses and is disposed of in landfills, which is expensive due to transportation and landfill taxes. WFS accounts for 4% of the annual turnover of an average sand foundry, with China, India, and the USA being the largest producers (4). Only a small fraction of WFS is used in concrete production, low-strength controlled materials, and road pavement materials, and its utilisation rate is still low (5). However, the chemical composition, density, particle size, and specific surface area of WFS make it a good candidate as a supporting material for a CPCMs.

This work focuses on showcasing a packed-bed latent heat storage system (PBLHS) system based on a novel CPCMs suited for medium-to-high-temperature range ( $>200\text{ }^{\circ}\text{C}$ ) based on WFS. The PBLHS has emerged as a promising solution due to its low investment cost, high overall efficiency, and good application prospects. However, few experimental studies have been conducted on the thermal performance of the PBLHS system under medium and high-temperature conditions(6). Most studies focus on low-temperature conditions. However, streams at these temperatures are commonly present in foundation industries (7). Overall, this work provides a novel utilisation pathway for recycling the WFS as a key material for CPCMs for capturing, storing, and reusing waste heat.

## 2. Materials

To fabricate the CPCMs, sand, MgO, and salt grains are mixed in a mass ratio of 0.4-0.2-0.4 and milled in a ceramic mortar following a previously reported process(8). Mantec Technical Ceramics Ltd. (MTC), the company assigned with fabricating the bricks for lower production volumes (i.e. few thousand), only cylindrical pellets with a diameter of 50 mm and a height of 60 mm were available. As such, the CPCMs were fabricated accordingly.

A cascade system containing two PCMs with different melting points was used to maximise the storage capacity of the TES system. One PCM is  $\text{NaNO}_3$  with a melting point of  $308^{\circ}\text{C}$ , and the other uses Solar Salt (SS), a mixture of  $\text{NaNO}_3$  and  $\text{KNO}_3$  at a 0.6-0.4 mass ratio. The fabricated CPCMs were stable after 25 cycles, consisting of heating up to  $400^{\circ}\text{C}$ , an isothermal step at  $400^{\circ}\text{C}$  for 12 hours, and a cooling step to ambient temperature followed by an isothermal step for 2 hours.

After cycling, the two materials had identical mass compositions but varied substantially in density and porosity. The SS-based CPCMs had a density (measured through mass and volume) of  $1.94 \pm 0.03\text{ g/cm}^3$  and a porosity of  $27 \pm 0.01\%$ , while  $\text{NaNO}_3$ -based CPCMs had a density of  $1.61 \pm 0.01\text{ g/cm}^3$  and a porosity of  $39 \pm 0.01\%$ . The specific heat capacity was calculated using simple mixture theory and was found to be  $1.28\text{ J/gK}$  and  $1.23\text{ J/gK}$  for  $\text{NaNO}_3$  and SS CPCMs, respectively. The higher specific heat capacity of  $\text{NaNO}_3$ -based CPCMs is due to their better thermal properties compared to SS. Using the specific heat capacity and density values the energy storage density of the  $\text{NaNO}_3$  and SS based CPCMs was found to be 571 and 610 kJ/kg, respectively.

## 3. Experimental setup

To simulate the waste heat source, typical of a casting foundry melting pot, an open cross-shaped spiral was selected as the heating element, which maximizes heat transfer and is ideal for delivering heat at high temperatures. The spiral, with a length of 390mm, was fitted in a 590mm tube with the same diameter as that of the tank inlet (10cm). The tube was mounted on top of the tank and connected to a VOK series fan from MMotors SA. After setting up the heating system, the material's mechanical stability was evaluated before loading it into the tank. Unfortunately, when heated to  $400^{\circ}\text{C}$ , the load flattened the pellets. To overcome this issue, a series of metallic sieve trays and a 12" metallic rod were procured. A total of 26 trays were stacked and fastened on the metallic rod, and a total of 75 pellets were placed on each tray with a small gap left between them to account for thermal expansion (Fig. 1). This resulted in a total of 1950 pellets (48 % porosity) in a tank with a height of 2.08m and a diameter of 0.628m.



Figure 1. Right: 1: Stack of trays loaded in the tank; 2: Stack of trays inside a cylindrical aluminium sieve; 3: top of tank after loading the tray; 4: First pellets loaded on the bottom tray.; Left: Thermocouple positions in the tank.

After loading the material, the tank was sealed with a flange and covered with insulation. The chosen insulation material was a flexible microporous panel called Siltherm Quilt, which has low thermal conductivity ( $0.024 \text{ W/mK}$ ) and a nominal density of  $220 \text{ kg/m}^3$ . A 40mm and 10mm thickness was sufficient for the tank insulation and pipe, respectively. Increasing the thickness did not significantly reduce heat loss and was not cost-effective. Apart from this, a series of 16 thermocouples were also purchased and installed on the rig (Fig. 1, right).

Tank charging occurred at an average mass flow rate of  $0.028 \text{ kg/s}$  (depending on inlet temperature). The heating element was set at  $410^\circ\text{C}$ . The entire charging process lasted 9 hours. After the first 6 hours, the temperature at the top of the tank stabilised around  $335^\circ\text{C}$ , exceeding the melting point of  $\text{NaNO}_3$  (Fig. 2). A thermal gradient was observed throughout the tank, with a  $200^\circ\text{C}$  temperature difference between the bottom and top layers. Initially, the air was directed through the center of the tank, as evidenced by T2L being higher than T2S and T2M. However, at T5 and T8, the larger portion of air was directed to the tanks' side, as T5S was higher than T5M and T5L. The temperature differences were significant at the start of the charging process but became almost identical, particularly for T2 thermocouples, indicating that the bottom layers of the tank were thermally equilibrated and fully charged, given the charging capacity. Phase change points were visible, especially near the melting point of SS ( $218^\circ\text{C}$ ), with T3 showing the most pronounced effect and T4 and T5L showing less. The temperature trend showed a small plateau around 5 and 6.5 hours, respectively, followed by a change in trend, even when the inlet temperature (T1) remained stable. The displacement of the plateau on the right for thermocouples positioned at the lower parts of the tank indicates a step-wise charging process. It is worth noting that the thermocouples were not placed inside the pellets and reflected the air temperature at certain positions in the tank. The charging efficiency was calculated to be 82%, which falls within the range typically reported in the literature.

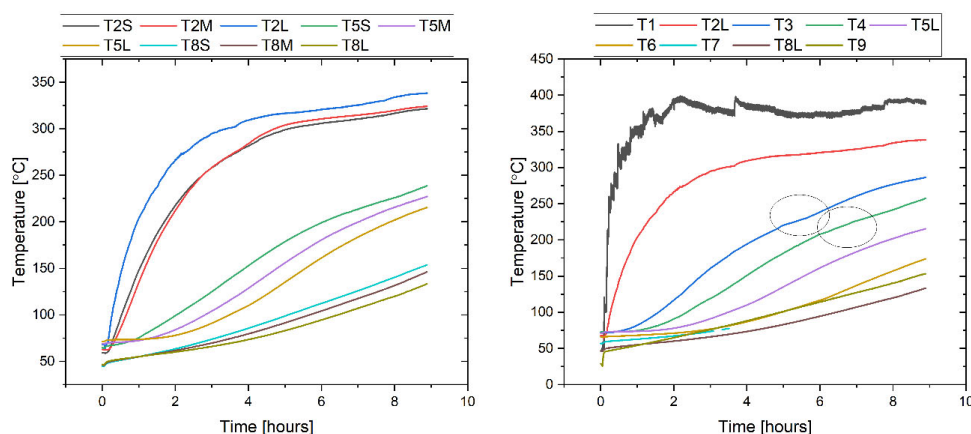


Figure 2. Thermocouple readings at various positions of the tank. Left: Multiple series, positioned at the center of the tank, the edge and in between. Right: Single series, positioned only at the middle of the tank.

## 4. Conclusions

In this work, a novel medium–high temperature packed-bed latent heat storage (PBLHS) experimental system is designed and constructed based on WFS CPCMs. The following main outcomes are derived:

- CPCMs consisting of WFS-MgO and NaNO<sub>3</sub>/ SS where fabricated at a 0.4-0.2-0.4 mass ratio and found to be stable after 25 cycles with an energy storage density of 571 and 610 kJ/kg, respectively.
- The pellets were found to be mechanically unstable under load when heated to 400°C and were therefore positioned on metallic sieve trays.
- A thermal gradient was observed throughout the tank during tank charging, with a 200°C temperature difference between the bottom and top layers. The temperature trend showed a small plateau around 5 and 6.5 hours, respectively, followed by a change in trend, even when the inlet temperature remained stable. The charging efficiency was calculated to be 82.
- A displacement of phase change plateau on the right for thermocouples positioned at the lower parts of the tank indicated a step-wise charging process.

Conclusively, this work demonstrates a novel utilisation pathway for WFS, both on the material and device level, as a thermal energy storage material.

## References

1. A. I. Fernández, C. Barreneche, L. Miró, S. Brückner, L. F. Cabeza, *Adv. Therm. Energy Storage Syst. Methods Appl.*, 479–492 (2015) doi: 10.1533/9781782420965.4.479.
2. F. Jiang *et al.*, *Renew. Sustain. Energy Rev.* **119**, 109539 (2020). Doi: 10.1016/j.rser.2019.109539
3. R. Siddique *et al.*, *Resour. Conserv. Recycl.* **53** (2008). doi:10.1016/j.resconrec.2008.09.007
4. M. R. Sabour *et al.* *Environ. Sci. Pollut. Res.* **28**, 37312–37321 (2021). Doi: 10.1007/S11356-021-13251-8/FIGURES/7.
5. R. Siddique, G. Singh, Utilization of waste foundry sand (WFS) in concrete manufacturing. *Resour. Conserv. Recycl.* **55** (2011)doi:10.1016/j.resconrec.2011.05.001.
6. W. Wang *et al.*, *Appl. Energy.* **309** (2022), doi:10.1016/j.apenergy.2021.118433.
7. B. Peris *et al.*, *Energy* (2015), doi:10.1016/j.energy.2015.03.065.
8. A. Anagnostopoulos *et al.* *J. Hazard. Mater.* **413** (2021). doi:10.1016/j.jhazmat.2021.125407.

EUROTHERM2023-Y247

## Contribution of thermal energy storage (TES) in the decarbonisation of our world

Luisa F. Cabeza<sup>1</sup>, Emiliano Borri<sup>1</sup>, Gabriel Zsembiszki<sup>1</sup>, Dieter Boer<sup>2</sup>, A. Inés Fernández<sup>3</sup>, Manel Valles<sup>2</sup>, Camila Barreneche<sup>3</sup>, Carles Mateu<sup>1,2</sup>

<sup>1</sup>GREiA Research Group, University of Lleida, Pere de Cabrera s/n, 25001-Lleida, Spain, Phone: 34-973-003576, e-mail: luisaf.cabeza@udl.cat, emiliano.borri@udl.cat, gabriel.zsembiszki@udl.cat, carles.mateu@udl.cat

<sup>2</sup>Departament d'Enginyeria Mecànica, Universitat Rovira i Virgili, Av. Paisos Catalans 26, 43007 Tarragona, Spain, Phone 34-977-559631, e-mail: dieter.boer@urv.cat, manel.valles@urv.cat

<sup>3</sup>Department of Materials Science & Physical Chemistry, Universitat de Barcelona, c/ Martí I Franqués 1, 08028 Barcelona, Phone: 34-934021317, e-mail: ana\_inesfernandez@ub.edu, c.barreneche@ub.edu

### Abstract

Achieving the goal of climate neutrality by 2050 without negatively affecting economic growth is one of the biggest challenges facing humanity today. Climate neutral economy and Europe decarbonisation means addressing several challenges in different sectors of human activities. Thermal energy storage was identified as a key ingredient of most of the solutions that have been proposed to pave the way towards decarbonisation. The aim of this contribution is to identify the performance indicators that are commonly used in the assessment of the impact of implementing thermal energy storage in energy systems, which can also potentially contribute to the decarbonisation goals.

**Keywords:** thermal energy storage (TES), decarbonisation, performance indicator (PI)

### 1. Introduction

The European Union (EU) aims to be climate neutral by 2050; an economy with net-zero greenhouse gas (GHG) emissions. This objective is at the heart of the European Green Deal [1] and in line with the EU commitment to global climate action under the Paris Agreement [2]. All parts of society and economic sectors (from the power sector to industry, mobility, buildings, agriculture, and forestry) will play a role in the needed transition that we need to undertake.

While the European Union has led the fight against climate change, it has also successfully decoupled GHG emissions, with a decrease of 22% in the period 1990-2017, from economic growth, with an EU gross domestic product (GDP) increase of 58% in the same period [3]. Moreover, 93% of Europeans believe that climate change is caused by human activity and 85% agree that fighting climate change and using energy more efficiently can create economic growth and jobs in Europe.

On the other hand, Cabeza and Palomba [4] showed that thermal energy storage (TES), directly or by direct conversion of electricity, can be installed in any part of the energy system (Figure 152). It can be installed in the generation, in the transmission, and in the demand side parts. TES is included in the generation to increase the penetration of renewable energy sources, to reduce the levelized cost of electricity (LCoE), for peak shifting or increased flexibility. On the demand side, TES is implemented to contribute to the SER framework (sufficiency-efficiency-renewables) [5] contributing to decrease of energy demand, increase of energy efficiency, and increased self-consumption and energy balance at district/micro-grid level.

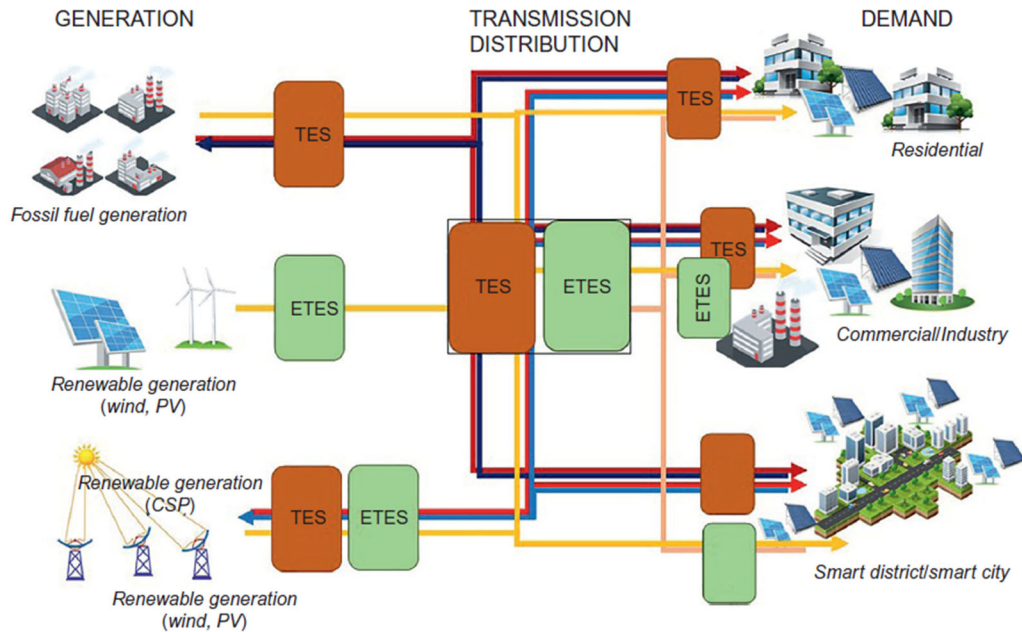


Figure 152. Potential interaction of thermal energy storage (TES) and electrical thermal energy storage (ETES) in the energy system [4]

## 2. Decarbonisation challenges

The EU targets for 2030 are achieving 32.5% energy efficiency, 32% electricity will be coming from renewable energy sources, and 55% less GHG emissions.

Achieving a climate neutral economy and Europe decarbonisation means addressing several challenges [6]:

- i. Decarbonisation of the energy supply, including deployment of renewable energy sources.
- ii. Decarbonisation of mobility, using alternative means of transport and rolling-up electric vehicles.
- iii. Decarbonisation of industry, developing new carbon neutral and circular economy-compatible technologies and systems.
- iv. Decarbonisation of the building sector, reducing energy demand, improving energy efficiency, and using more renewable energy sources.

## 3. Contribution of TES to the decarbonisation challenges

The benefits of TES in the energy system, including demand side, listed above are very aligned with the challenges of decarbonisation. Therefore, the aim of this contribution is to identify the performance indicators used in TES implementation and evaluation that will also contribute to the decarbonisation goals. The identified relations between TES-related performance indicators and the different challenges of decarbonisation are shown in Table 17.

Table 17. Contribution of TES to the decarbonisation challenges

Challenge / Performance indicator	Reduction of energy demand	Improvement of energy efficiency	Deployment of renewable energy sources	Improvement of circularity	References
<b>Technical performance indicators at TES system level</b>					
Storage capacity	✓				[7]
Storage time		✓	✓		[7]
Total solar efficiency			✓		[8]
Operating temperature	✓	✓			[9]
Full-discharge efficiency		✓			[7]
Efficiency			✓		[10]
Primary energy consumption	✓		✓		[11]
Response time	✓	✓	✓		[10]
Depth of discharge				✓	[12]
Durability				✓	[12]
<b>Technical performance indicators at TES material level</b>					
Energy density	✓	✓	✓	✓	[13]
Operating temperature	✓	✓			[13]
Degradation				✓	[14]
Availability				✓	[15]
Recyclability				✓	[16]
<b>Economic performance indicators</b>					
OPEX	✓	✓	✓		[9]
CAPEX	✓	✓	✓		[9]
LCoE			✓		[17]
LCoH	✓	✓			[18]
<b>Environmental performance indicators</b>					
CO <sub>2</sub> emissions savings				✓	[8]
GHG emissions savings				✓	[8]

## Acknowledgements

This work was partially funded by the Ministerio de Ciencia e Innovación - Agencia Estatal de Investigación (PID2021-123511OB-C31 / PID2021-123511OB-C32 / PID2021-123511OB-C33 - MCIN/AEI/10.13039/501100011033/FEDER, EU, and RED2022-134219-T). The authors thank the Generalitat de Catalunya for the quality accreditation granted to their research groups (GREiA 2021 SGR 01615, SUSCAPE2021 SGR 00738, DIOPMA 2021 SGR 00708). GREiA and DIOPMA are TECNIO-certified agents in the category of technological development of the Government of Catalonia. This work is partially supported by ICREA under the ICREA Academia programme.

## References

- [1] European Commission. EU Green Deal 2020. [https://ec.europa.eu/info/strategy/priorities-2019-2024/european-green-deal\\_en](https://ec.europa.eu/info/strategy/priorities-2019-2024/european-green-deal_en).
- [2] United nations framework convention on climate change. Paris Agreement. Sustainable Innovation Forum 2015 2015.

- [3] European Commission. An EU Strategy on Heating and Cooling. 2016.
- [4] Cabeza LF, Palomba V. The Role of Thermal Energy Storage in the Energy System. Reference Module in Earth Systems and Environmental Sciences, Elsevier; 2020. <https://doi.org/10.1016/B978-0-12-819723-3.00017-2>.
- [5] Cabeza LF, Bai Q, Bertoldi P, Kihila JM, Lucena AFP, Mata É, et al. Buildings. In: Shukla PR, Skea J, Slade R, Khourdajie A Al, Diemen R van, McCollum D, et al., editors. IPCC, 2022: Climate Change 2022: Mitigation of Climate Change. Contribution of Working Group III to the Sixth Assessment Report of the Intergovernmental Panel on Climate Change, CAMBRIDGE UNIV PRESS; 2022. <https://doi.org/10.1017/9781009157926.011>.
- [6] European Commission D-G for CA. Going climate-neutral by 2050 : a strategic long-term vision for a prosperous, modern, competitive and climate-neutral EU economy. Luxembourg: 2019. <https://doi.org/https://data.europa.eu/doi/10.2834/02074>.
- [7] AENOR. UNE 206009:2013 Centrales termosolares. Terminología. 2013.
- [8] Key Performance Indicators. Deliverable 2.5 of the SWS-Heating project funded under the European Union's Horizon 2020 research and innovation programme GA No: 764025. 2019.
- [9] Palomba V, Frazzica A. Comparative analysis of thermal energy storage technologies through the definition of suitable key performance indicators. Energy Build 2019;185:88–102. <https://doi.org/10.1016/j.enbuild.2018.12.019>.
- [10] Cabeza LF, Galindo E, Prieto C, Barreneche C, Inés Fernández A. Key performance indicators in thermal energy storage: Survey and assessment. Renew Energy 2015;83:820–7. <https://doi.org/10.1016/j.renene.2015.05.019>.
- [11] Malenković I. Definition of performance figures for solar and heat pump systems. Vienna, Austria 2012.
- [12] Del Pero C, Aste N, Paksoy H, Haghghat F, Grillo S, Leonforte F. Energy storage key performance indicators for building application. Sustain Cities Soc 2018;40:54–65. <https://doi.org/10.1016/j.scs.2018.01.052>.
- [13] Romani J, Gasia J, Solé A, Takasu H, Kato Y, Cabeza LF. Evaluation of energy density as performance indicator for thermal energy storage at material and system levels. Appl Energy 2019;235:954–62.
- [14] Hoivik N, Greiner C, Barragan J, Iniesta AC, Skeie G, Bergan P, et al. Long-term performance results of concrete-based modular thermal energy storage system. J Energy Storage 2019;24:100735. <https://doi.org/10.1016/j.est.2019.04.009>.
- [15] Fernandez AI, Martínez M, Segarra M, Martorell I, Cabeza LF. Selection of materials with potential in sensible thermal energy storage. Solar Energy Materials and Solar Cells 2010;94:1723–9. <https://doi.org/10.1016/j.solmat.2010.05.035>.
- [16] Tatsidjodoung P, Le Pierrès N, Luo L. A review of potential materials for thermal energy storage in building applications. Renewable and Sustainable Energy Reviews 2013;18:327–49.
- [17] Gibb D, Seitz A, Johnson M, Romani J, Gasia J, Gabeza LF, et al. Applications of thermal energy storage in the energy transition-Benchmarks and developments. IEA Technology Collaboration Programme on Energy Conservation through Energy Storage (IEA-ECES); 2018.
- [18] Abokersh MH, Saikia K, Cabeza LF, Boer D, Vallès M. Flexible heat pump integration to improve sustainable transition toward 4th generation district heating. Energy Convers Manag 2020;225:113379.



## EU-funded project workshop

During the conference, a workshop was organised where EU-funded projects within the topic of thermal energy storage were presented. The different projects that contributed to the workshop are presented next.



**Title of the project: Techno-economical evaluation of different thermal energy storage concepts for CSP plants**

Acronym: CSPplus

Project reference: Cofund ERA-NET Action, N° 838311



CSPplus is a three-year European project that started in March 2021 and is coordinated by University of Lleida (Spain). CSPplus consortium consists of six institutions, from both academia and industry, from three countries: Spain, Israel, and Turkey. The project receives funding under the umbrella of CSP-ERA.NET 1<sup>st</sup> Cofund Joint Call from the European Commission within the EU Framework Programme for Research and Innovation HORIZON 2020. The objective of CSPplus is to reduce 30% the capital expenditure (CAPEX) and 3-4% the operating expenditure (OPEX) in the next generation of CSP plants. This reduction translates into a decrease of the levelized cost of energy (LCOE). Such objective can be achieved by increasing the peak operating temperature of the system, an upgrade that will be exploited by means of specifically designed components. Several storage candidates can theoretically achieve this goal, but there is no single solution when all the boundary system is considered. Therefore, the project aims at developing a new tool capable of fully identify, develop, and compare new storage concepts in an easy manner, providing a reliable and cost-effective solution based on the specific conditions of each possible scenario.

**Title of the project: Efficient Compact Modular Thermal Energy Storage System**

Acronym: ECHO

Project reference: 101096368



Energy storage is one of the key factors to reach EU aims to be climate-neutral by 2050, with a net-zero greenhouse gas (GHG) emissions economy. The decarbonisation and the transition to clean energy sources, together with the improvement of the energy efficiency, will bring to a severe change in the employed energy systems. The potentialities of thermal energy storage (TES) systems, able to provide electricity load shifting by mean of energy conversion and storage, can help in developing flexible energy systems, managing the intrinsically intermittent nature of renewable energy sources. ECHO solutions will be flexible and adaptable to different end-user requests, in terms of charging (and discharging) power, dimension and types of energy sources.

The project's goal is to develop and demonstrate novel modular, compact, high performances and Plug&Play thermal energy storage (TES) solutions for heating, cooling and hot tap water production, able to provide electricity load shifting with meaningful peak shaving of the thermal and electric load demands.

ECHO project will provide a key tool for thermal energy storage in the context of sector coupling and provision of flexibility of demand. ECHO system will be adapted to the different energetic scenarios. Additionally, its modularity will allow to use the concept in different scales, from small apartments to larger buildings.

The developed systems will be adaptable to different energy sources and user demands. They will be feasible to be charged directly by means of an internal heat pump, exploiting the electricity overproduction from the grid, or directly connecting to renewable energy sources installed in the building.

**Title of the project: Development of a medium-high temperature waste heat recovery hybrid thermal energy storage layout, based on red mud, a disregarded and potentially hazardous solid waste of the aluminium industry**

Acronym: REDTHERM

Project reference: ID: 101068507



Europe's industrial sector generates up to 30 % of heat-related CO<sub>2</sub> emissions, with the European industrial thermal processes requiring around 20 % of the European energy demand. Currently, energy-intensive industries make use of waste heat recovery technologies. However, they have grown inefficient. Thermal energy storage (TES) is a technology likely to replace them, utilising phase change materials (PCM) to absorb and release medium-to-high heat. The EU-funded REDTHERM project aims to utilise these findings and Red mud, a hazardous waste material of the aluminium industry, to develop a novel thermal energy storage layout technology. REDTHERM aims to vastly improve recycling but also to contribute to the creation of a circular economy.

**Title of the project: Thermal energy storage solutions to optimally Manage Buildings and Unlock their grid balancing and flexibility Potential**

Acronym: THUMBS UP

Project reference: 101096921



Short summary: THUMBS UP aims to develop and demonstrate thermal energy storage (TES) at daily (based on environmental friendly PCM) and weekly level (based on TCM sorption technology) solutions to be easily integrated in EU buildings (both connected and not-connected to DHN) to increase their energy efficiency as well as to exploit Power-to-Heat (PtH) approaches also to make EU Buildings as grid flexibility actors. THUMBS UP wants to overcome all the limits of state-of-the-art building-integrated PCM and TCM TES technologies, increasing TES energy density and reducing CAPEX. THUMBS UP innovates at different levels, from modelling to materials and enhance heat exchanger solutions, targeting demonstration at TRL 7. High-performance TES solutions part of an EU sustainable economy is a factor at the core of THUMBS UP. The project develops truly i) bio-based PCMs from raw materials currently wasted in the EU food industry, turning them into valuable TES materials and ii) TCMs relying exclusively on non-hazardous materials and on water as working fluid. THUMBS UP TES will be demonstrated in 3 demosites (a single-family building in Spain and 2 multi-family buildings in Sweden/Spain) in different EU climates and energy market contexts also to assess THUMBS UP replication potential in two replication sites (ITA, NL). Via its demonstration and replication campaign, THUMBS UP promotes TES role as key enabling technology to optimize thermal comfort and energy efficiency in buildings as well as to promote PtH as facilitator of RES grid integration in a sector coupling approach, to be studied via innovative modelling tools. THUMBS UP gives specific attention to how to fully integrate TES solutions into buildings and wider smart energy networks by combining the technology advancements with TES-tailored digital innovations. THUMBS UP widens the capability to control, monitor and forecasts how to operate building-integrated TES systems to provide services toward both the H&C and power sector.

**Title of the project: Advanced thermocline concepts for thermal energy storage for CSP**

Acronym: NEWCLINE

Project reference: CSP-ERA.NET 1st Cofund Joint Call (PCI2020-120701-2)



The Newcline project has been conceived with the objective of improving the thermal energy storage in CSP plants, from central receivers to parabolic trough collectors and Frensel linear reflectors. Thermal energy storage plays a key role to assure energy dispatchability. In the Newcline project, new thermocline concepts will be developed using innovative materials, advanced computational simulation tools, and experimentally tested prototypes at both lab-scale and pilot-scale set-ups. The project pursues the successful system integration of the developed thermal energy storage concepts in commercial concentrated solar power plants, allowing significant costs reductions.

**Title of the project: Application of Solar Thermal Energy to Processes**

Acronym: ASTEP

Project reference: LC-SC3-RES-7-2019



Application of Solar Thermal Energy to Processes (ASTEP) will create a new innovative Solar Heating for Industrial Processes (SHIP) concept focused on overcoming the current limitations of these systems. This solution is based on modular and flexible integration of two innovative designs for the solar collector (SunDial) and the Thermal Energy Storage (TES, based on Phase Change Materials, PCM) integrated via a control system which will allow flexible operation to maintain continuous service against the unpredictable nature of the solar source and partially during night operation. ASTEP will demonstrate its capability to cover a substantial part of the heat demand of the process industry at temperatures above 150 °C and for latitudes where current designs are not able to supply it. Its modularity and compactness will also enable easy installation and repair with reduced space requirements, while most of components can be sourced locally. The ASTEP's process integration will allow full compatibility with the existing systems of potential end-users of SHIP. These aspects will provide a very competitive solution to substitute fossil fuel consumption. The developed solar concept will be tested at two industrial sites to prove the objective's target of TRL5. Life Cycle Analysis will be included to validate and demonstrate the efficiency of the proposed technologies. The first Industrial Site of the proposal is the world's leading steel company, ArcelorMittal, with a heating demand above 220 °C for a factory located at a latitude of 47.1 N (Iasi, Romania). The second site is the dairy company MANDREKAS, located at a latitude of 37.93 N (Corinth, Greece) with a heating demand for steam at 175 °C and a cooling demand at 5 °C. These test locations will validate the ASTEP solution for a substantial part of the potential requirements of industrial heating and cooling demand of the European Union (EU28), which is estimated at approximately 72 TWh per year.

**Title of the project: High performance parabolic trough collector and innovative silicone fluid for CSP power plants**

Acronym: Si-CO

Project reference: ERA - 20200007



The Si-CO project aims to techno-economically demonstrate a new optimized and large-scale parabolic trough collector (Si-PTC) design that operates using HELISOL® XLP at 430°C, a siliconebased heat transfer fluid (Si-HTF). This project also pursues to demonstrate and evaluate the exchange of this Si-HTF in existing power plants. The combination proposed (Si-PTC + Si-HTF), enables a cost reduction in the solar field, HTF and TES CAPEX of 12% and a 14% in OPEX for new solar plants. The technology proposed will enhance the annual energy production of a commercial PTC plant by 7.5% and the global capacity factor by 2%. Altogether, this translates in a LCOE reduction of up to 15%. Furthermore, the exchange application of the Si-HTF in existing plants, designed for an operation T of 400°C, has the potential to fix the H<sub>2</sub> permeation issues because HELISOL®XLP shows almost zero formation at 400°C. After the HTF exchange, the use of HELISOL® XLP will avoid any future H<sub>2</sub>-HCE issues increasing its performance while prolonging its service time and reducing power plant down time, presenting clear O&M and environmental advantages for existing plants even if they can't operate at 430°C. This also applies to new power plants with higher working T. Therefore, Si-CO pursues the 2 independent actions above mentioned, both based on the new HELISOL® XLP, which has additional cost reduction and better performance potential with respect to the other 2 commercial existing HELISOL® XLP grades, because it has a lower vapour pressure during operation and can be operated at 430°C. The Si-CO project stands in a row with three international demonstration projects (SING, SITEF, SIMON) that successfully established Si-HTF as a very promising alternative with respect to the state-of-the-art HTF

**Title of the project: INNOvative SOLar micro-TES with high-POWER density**

Acronym: InnoSolPower

Project reference: CSP-ERA.NET 1st Cofund Joint Call.  
CSP-ERA.NET is supported by the European Commission within the EU Framework Programme for Research and Innovation HORIZON 2020 (Cofund ERA-NET Action, N° 838311/ id:12)



InnoSolPower aims to demonstrate a novel concept of an efficient, low-cost, low temperature, high energy density micro-thermal energy storage ( $\mu$ TES) dedicated to concentrated solar power (CSP) systems.

The ultimate goal is to develop and test an efficient “one size fit all”  $\mu$ TES charged with a high temperature heat pump (HTHP) using a solar  $\mu$ CSP for daily local heat capacity demands.

**Title of the project: Solar Facilities for the European Research Area - Third Phase**

Acronym: SFERA-III

Project reference: RIA 823802



SFERA-III Project aims to engage all major European Solar Research Institutes, with relevant and recognized activities in Concentrating Solar Thermal (CST) technology field, into an integrated structure to promote research, improve services offered by CST RI and to train researchers and engineers on the CST technologies. Between these services, a special room is devoted to thermal storage issues, so WP6 is entirely dedicated to enhancing the current services and procedures for reliability of materials and equipment of thermal storage systems. The activities focus on sensible and latent heat storage, paving the way for thermochemical storage. This WP is divided in 4 tasks:

- Task 6.1 Compatibility of molten salt with structural materials
- Task 6.2 Development of testing protocols to demonstrate the feasibility of materials as storage media
- Task 6.3 Development of protocols to test prototypes for storage systems
- Task 6.4 Establishment of standard procedures for the characterization of components for commercial TES (using sensible and molten solar salts)

In this contribution the main challenges and achievements will be presented.

**Title of the project: Solar Hybrid Air-sCO<sub>2</sub> Power Plants**

Acronym: SHARP-sCO<sub>2</sub>

Project reference: Grant Agreement No: 101083899



SHARP-sCO<sub>2</sub> addresses key technological challenges to enable the development of a new generation of highly efficient and flexible CSP plants. Keeping on working with CSP-sCO<sub>2</sub> power cycles (leveraging from previous project experiences) and investigating how to exploit air as operating fluid, SHARP-sCO<sub>2</sub> will develop and validate novel enabling technologies in EU top level CSP labs (TRL5) (including receiver, thermal storage (TES), sCO<sub>2</sub>-air Heat Exchanger (HEX), electric heater (EH), as well as integrated piping and control). SHARP-sCO<sub>2</sub> will attain high temperatures and cycle efficiency, while guaranteeing reliable and flexible operation. Introducing a smart hybridization with PV by means of an innovative EH, SHARP-sCO<sub>2</sub> will maximize sCO<sub>2</sub> operation and remuneration, exploiting PV affordability while counting on the unique energy storage capabilities of CSP via TES.

By developing and validating key components (receiver, storage, HEXs, electric heater), SHARP-sCO<sub>2</sub> will prove the effectiveness and techno-economic viability of air solar-driven/sCO<sub>2</sub> CSP plants able to be efficiently hybridized with PV in order to maximise CSP flexibility, reduce CAPEX and LCOE, and reduce the environmental impact. Four prototypes, one per key component, will be investigated in a cross-fertilizing lab campaign (TRL5) that will serve to validate partners' modeling approach to robustly study replication and upscale strategies. Taking into account EU/extra-EU solar irradiation, electric market perspectives, environmental, safety and regulation aspects, the project will be the first keystone towards the promotion of air-driven/sCO<sub>2</sub> CSP concept as key solution for next-generation EU CSP being instrumental to achieve 2030 EU targets.

**Title of the project: Zero waste Heat vessel towards relevant ENergy savings also thanks to IT technologies**

Acronym: ZHENIT

Project reference: GA 101056801



ZHENIT is a 42 months HEU project, focusing on the exploitation of Waste Heat Recovery on board of vessels as key and “ready-to-scale up” solutions to reach the decarbonization targets by validating different solutions systems at various temperature levels, for different end-product (cooling, power, desalination) and optimizing integration/performance thanks to thermal energy storage (TES).

**Title of the project: Solar based sCO<sub>2</sub> Operating Low-cost plants**

Acronym: SOLARsCO<sub>2</sub>OL

Project reference: GA# 952953



Concentrating Solar Power (CSP) plants are a promising technology for decarbonizing the electricity grid because of their ability to incorporate cost-effective thermal energy storage (TES). However, the commercial development of this technology has been limited due to its higher Levelized Cost of Electricity (LCOE) compared to other energy sources. Hybrid systems that combine CSP with solar photovoltaic (PV) have been identified as a viable solution to reduce the LCOE of CSP plants while maintaining the flexibility and high-capacity factors provided by the TES unit. In addition, the shift from steam cycles to supercritical CO<sub>2</sub> (sCO<sub>2</sub>) cycles has also been identified as a path forward for lowering the LCOE of CSP systems due to its compactness and potential to enable better system efficiencies by allowing higher operating temperatures.

SOLARSCO<sub>2</sub>OL is an EU funded project that aims to demonstrate a first-of-a-kind MW-scale pilot plant comprising a 3.5 MW<sub>t</sub> molten salt CSP loop with two-tank TES, an innovative 3.5 MW<sub>e</sub> molten salt electric heater for PV hybridization, and a 2MW<sub>e</sub> simple-recuperated sCO<sub>2</sub> cycle. This demonstrator is planned to be erected in the premises of the Evora Molten Salt Platform in Évora, Portugal. In doing so the project aims to be the first project in EU that demonstrates an MW-scale sCO<sub>2</sub> cycle at MW-scale, and the first worldwide to connect it to a functioning CSP hybridized with molten salt electric heaters. In addition, the project aims at investigating future up-scale replications of the hybrid system by assessing the techno-economic feasibility of advanced configurations exploiting the use of other heat transfer fluids and storage media that could potentially increase the system efficiency.

SOLARSCO<sub>2</sub>OL is a consortium formed by 18 partners from 8 countries, most of which from industry, under the leadership of Rina Consulting and KTH..

**Title of the project: Hybrid services from advanced thermal energy storage systems**

Acronym: HYSTORE

Project reference: 101096789



The mission of HYSTORE is to develop and validate four innovative sets of TES concepts, based on PCM and TCM solutions. The four novel concepts attain different applications on heating/cooling (H/C), DHW configurations, and further set up optimal conditions for the provision of hybrid – meaning energy and power services thanks to the development of a smart aggregator and an open-source multi-service platform.

The main key features of HYSTORE are:

- Technological advancement of thermal energy storage (TES) with up to +120% energy density and -50% CAPEX compared to state-of-art (SoA).
- Significant lower design and installation effort thanks to pre-defined and standardized guidelines. The abstract shows 150% and the STO1 shows 120%.
- Allow TES to be coupled and integrated with grid-level aggregators that can be federated in the context of both single buildings and local energy communities.
- 4 use case application in different climates both for District Heating/Cooling connected and non DHC-connected buildings with high-impact and replication potential.
- LCOS in line with EU targets from IRENA annual reports and SET-plan. HYSTORE puts TES systems in the path of 0,05€/kW/cycle over around 0,04 €/kWh by 2030, which is competitive with batteries.

To reach these goals, HYSTORE leverages on a consortium of 18 entities from 8 different EU countries, highly qualified and leaders in their sectors of activity. This consortium covers the whole value chain of thermal energy storage, technologies for its interconnection with the grid and its optimal operation by exploiting the flexibility resources.

The final goal for HYSTORE is to realize the paradigmatic shift of thermal storage from an auxiliary service to the HVAC system to a service for the building to provide the needed comfort with high efficiency while supporting the grid for effective electric-thermal sector coupling.

**Title of the project: Photonic Metaconcrete with Infrared Radiative Cooling capacity for Large Energy savings**

Acronym: MIRACLE

Project reference: Grant agreement ID: 964450



Photonics has a broad range of applications, gradually also conquering the building construction industry. The development of multi-functional concrete with improved traditional properties and enhanced novel functionalities is key for sustainable and high-performance solutions. The EU-funded MIRACLE project will construct and test a revolutionary photonic meta-concrete (PMC) whose response to light will be engineered for exhibiting radiative cooling ability. MIRACLE's proposed solution is advantageous and fully scalable, based on simple technologies already used in concrete technology. The PMC innovation aims to drastically contribute to the construction of nearly zero-energy buildings but can also be expanded in multiple fields such as solar cell technology or communication technologies.



**Title of the project: Advanced HYBRID solar plant with PCM storage solutions in sCO<sub>2</sub> cycles**

Acronym: HYBRIDplus

Project reference: HE-101084182



HYBRIDplus aims to pioneer the next generation of concentrated solar plant (CSP) with an advanced innovative high-density and high-temperature thermal energy storage (TES) system capable of providing a high degree of dispatchability at low cost and with much lower environmental burden than the state of the art. This thermal storage is based in the Phase Change Material (PCM) technology, with a cascade configuration that can reproduce the effect of a thermocline and integrates recycled metal wool in its nucleus that provide hybridization possibilities by acting as an electric heater, transforming non-dispatchable renewable electricity such as photovoltaic (PV) into thermal stored energy ready to be dispatched when needed.

HYBRIDplus proposes a novel PV+CSP plant with an electrified PCM thermal energy storage system in cascade configuration coupled with a high temperature supercritical CO<sub>2</sub> power cycle. This new plant is called to form the backbone of the coming energy system thanks to a higher efficiency and lower LCoE than state-of-the-art technology. The enabling hybrid TES developed in the project provides full dispatchability due to its embedded electric heaters, which allow higher shares of variable output renewables in the energy system and increases environmental friendliness (lower CO<sub>2</sub> emissions, minimum water consumption, enhancement life cycle impact).

**Title of the project: Hybrid coupled networks for thermal-electric integrated smart energy Districts**

Acronym: HYPERGRYD

Project reference: Grant Agreement 101036656



HYPERGRYD aims at developing a set of replicable and scalable cost effective technical solutions to allow the integration of RES with different dispatchability and intrinsic variability inside Thermal Grids as well as their link with the Electrical Grids, including the development of innovative key components, in parallel with innovative and integrated ICT services formed by a scalable suite of tools for the proper handling of the increased complexity of the systems from building to Local Energy Community (LEC) levels and beyond, accelerate the sustainable transformation, planning and modernization of District Heating and Cooling (DHC) toward 4th and 5th generation.

In order to reach these goals, a set of technological solutions and dedicated tools are being developed. Among them, there is an integrated heat pump with PCM storage for the smart management of coupled thermal and electric grids at building level, in view of a distributed generation. Moreover, a thermochemical storage for mid to long term applications at building or neighborhood level is being designed and tested, which employs a combination of standard and advanced storage materials.

**Title of the project: Solar-Biomass Reversible energy system for covering a large share of energy needs in buildings**

Acronym: SolBio-Rev

Project reference: 814945



The SolBio-Rev project will develop a flexible energy system suitable for building integration based on renewables for covering a large share of energy demand (heating/cooling/electricity). Its flexibility is derived from the long-term collaboration of key industrial partners with research organisations, having in mind the large variety of EU buildings, especially non-residential (types, uses and sizes).

The overall objective is to develop a configuration based on renewables that allows covering all heating and cooling demand and a variable electricity demand (from zero up to even 100%) in a cost-effective manner. This configuration is based on solar, ambient and bioenergy, while it is suitable to be installed in various building types and sizes without any geographical restriction. The main technologies included have already proven their performance and they are combined with the aim to exploit all possible energy flows/sources, ensuring their cost-effectiveness compared to standard solutions.

The SolBio-Rev concept is based on solar thermal collectors with vacuum tubes combined with thermoelectrics, a cascade thermal chiller with electrical-driven heat pump for very high performance under cooling operation even at extreme hot conditions, a reversible heat pump/ORC for enhancing flexibility and switching operating modes between summer and winter, exploiting all available solar heat, and an advanced biomass boiler coupled with the above ORC for CHP operation. A smart control is also envisaged to manage and optimise the system operation with user-friendly features.

**Title of the project: Collaborative development of renewable/thermally driven and storage-integrated cooling technologies**

Acronym: CO-COOL

Project reference: 101007976



Global climate change and emissions are tightly intertwined. Our last decade was the warmest on record, and we are all aware by now of our need to reduce human activity-related emissions to slow global warming. Unfortunately, warming has increased Europe's reliance on cooling. This has resulted in its emergence to the forefront of areas targeted for decarbonisation. The EU-funded CO-COOL will bring together a large international consortium to develop improved cooling technologies that leverage either renewable electricity/heat or waste heat to keep people and spaces cool without warming our planet. We assemble an international, interdisciplinary consortium from 12 research institutions and 5 industrial companies to collectively accelerate the cooling technology development and deployment, with complementary expertise/skills including composite solids, phase change materials (PCMs), complex fluids, process intensification (heat and mass transfer), cold thermal storage, refrigeration systems, as well as techno-economic analysis (TEA) and life cycle assessment (LCA), marketing analysis, and entrepreneurship skills.

**Title of the project: European ecosystem to advance innovation in energy storage devices**

Acronym: StoRIES

Project reference: 101036910



According to the European Green Deal goals, new energy storage technologies will supply more flexibility and balance in the grid, providing a back-up to intermittent renewable energy and contribute to seasonal energy storage challenges. Above all, the main challenge for energy storage development is economic. In order to achieve more performing, competitive and cost effective energy storage devices, the project fosters a European ecosystem of industry and research organisations on energy storage technologies aimed at developing novel concepts and technologies. StoRIES brings together a consortium of 32 beneficiaries from 17 countries: ESFRI facilities, technology institutes, universities and industrial partners to jointly improve the economic performance of storage technologies. Members of the European Energy Research Alliance and from the industry lead European Association for Storage of Energy are establishing the core of this world-class European ecosystem. The main objectives of StoRIES are linked to the energy storage development by providing access to world-class research infrastructures and services, with a focus on improving materials for devices and optimizing hybrid energy systems with a view to make energy technologies more competitive and reducing costs. In addition, StoRIES focuses on the analysis of socio-technical and environmental aspects of new developments and systems and provides training and education on these issues. By promoting complementary expertise, interdisciplinary cooperation and a broader exchange of knowledge and technologies throughout the academic world and with industry, StoRIES will significantly improve the technological basis for energy storage applications. Furthermore, StoRIES will establish an ecosystem with international peer partners from Research and Industry to foster open science and promote new energy technology standards.

**Title of the project: Sustainable surface treatments of complex shape components for transsectorial industrial innovation**

Acronym: SURE2COAT

Project reference: GA 101091982



Many industries are looking for alternatives to prolong lifetime and improve performance of their metal products. While easily recyclable aluminium (Al) offers a lighter weight option with respect to existing technologies, it is prone to corrosion. Heat transfer of copper (Cu) products also enclose potential for improvement. In this context, the EU-funded SURE2COAT project will enable the use and uptake of Al and Cu in new sectors involving products with complex shapes. New surface treatments (ST) will be developed for parts of electrical engines, water heaters and heat storage units. SURE2COAT aims to increase the energy efficiency by at least 50% and increase the use of recycled Al by 70% by using ST and innovative production technologies.

**Title of the project: Development and Validation of an Innovative Solar Compact Selective-Water-Sorbent-Based Heating System**

Acronym: SWS-HEATING

Project reference: 764025



The SWS-HEATING project will develop an innovative seasonal thermal energy storage (STES) unit with a novel storage material and creative configuration, i.e. a sorbent material embedded in a compact multi-modular sorption STES unit. This will allow to store and shift the harvested solar energy available abundantly during the summer to the less sunny and colder winter period thus covering a large fraction of heating and domestic hot water demand in buildings. The targeted benefit of this next generation solar heating technology is to reach and overcome a solar fraction of 60% in central/north Europe, reaching 80% in the sunnier south of Europe, with a compact and high performing STES system at low cost, realizing solar-active houses throughout EU.

The SWS-heating system is based on a multi-modular sorption seasonal thermal energy storage (STES) unit, using novel sorbent materials of Selective Water Sorbents (SWS) family characterized by superior heat storage density compared to the state of the art, making it possible to drastically decrease the storage volume with negligible thermal

losses. These materials are employed in a sorption module with dedicated heat exchangers. Solar heat is provided to the storage modules by high-efficiency evacuated tube solar thermal collectors. Intensive research activities will deal with an advanced vacuum combi-storage tank, with the aim to further minimize thermal losses. A smart and adaptive control will be developed for efficiently managing heat supply and demand sides, including advanced features aiming at user-friendliness. A building prototype will be commissioned including the SWS-heating system, which will be tested and validated in Germany and Sweden and proof all challenging objectives.

**Title of the project: Dispatchable concentrated Solar-to-X energy solution for high penetration of renewable energy**

Acronym: SOLARX

Project reference: Grant number: 101084158



SOLARX's main goal is to demonstrate the technical, economic and social relevance, at the laboratory scale, of the synergetic efficient production of heat, electricity and H<sub>2</sub> from solar resource in a single facility, considering energy demands and market prices for a wide range of locations and application scenarios. SOLARX global assessment will demonstrate its role as a Game-changing RES within the framework of future implementation in a carbon-negative energy system. SOLARX will also provide power-to-X for larger integration of intermittent energy sources into the electric grid.

SOLARX integrates three high concentration solar technologies and AI-based smart resource management, to produce – either directly with high efficiencies or through storage stages for maximizing revenues – mainly electricity, heat for storage and/or Solar Heat from Industrial Processes (SHIP), and green H<sub>2</sub> or Syngas in a carbon-neutral way.